frontiers | Research Topics

Cellular and molecular factors that drive the behavior of oligodendrocyte progenitor cells in physiological conditions and disease

Edited by
Davide Lecca, Wia Baron and Arthur Morgan Butt

Published in
Frontiers in Cellular Neuroscience

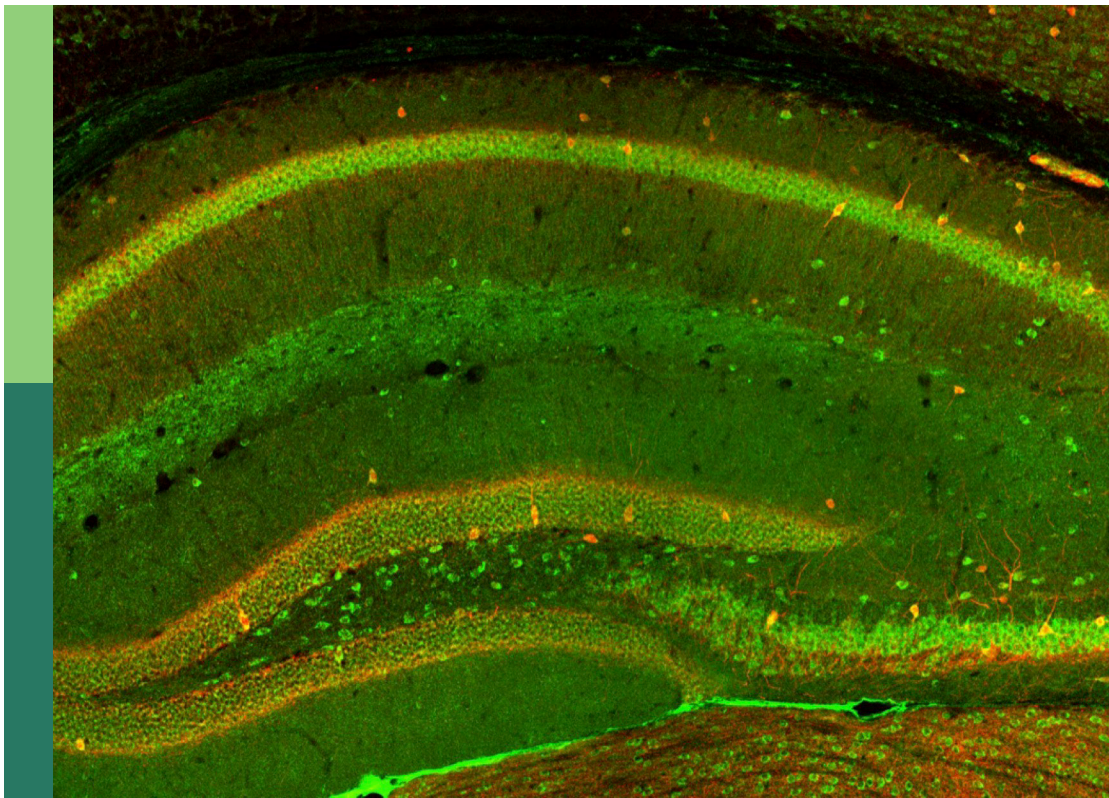

FRONTIERS EBOOK COPYRIGHT STATEMENT

The copyright in the text of individual articles in this ebook is the property of their respective authors or their respective institutions or funders. The copyright in graphics and images within each article may be subject to copyright of other parties. In both cases this is subject to a license granted to Frontiers.

The compilation of articles constituting this ebook is the property of Frontiers.

Each article within this ebook, and the ebook itself, are published under the most recent version of the Creative Commons CC-BY licence. The version current at the date of publication of this ebook is CC-BY 4.0. If the CC-BY licence is updated, the licence granted by Frontiers is automatically updated to the new version.

When exercising any right under the CC-BY licence, Frontiers must be attributed as the original publisher of the article or ebook, as applicable.

Authors have the responsibility of ensuring that any graphics or other materials which are the property of others may be included in the CC-BY licence, but this should be checked before relying on the CC-BY licence to reproduce those materials. Any copyright notices relating to those materials must be complied with.

Copyright and source acknowledgement notices may not be removed and must be displayed in any copy, derivative work or partial copy which includes the elements in question.

All copyright, and all rights therein, are protected by national and international copyright laws. The above represents a summary only. For further information please read Frontiers' Conditions for Website Use and Copyright Statement, and the applicable CC-BY licence.

ISSN 1664-8714
ISBN 978-2-83251-707-9
DOI 10.3389/978-2-83251-707-9

About Frontiers

Frontiers is more than just an open access publisher of scholarly articles: it is a pioneering approach to the world of academia, radically improving the way scholarly research is managed. The grand vision of Frontiers is a world where all people have an equal opportunity to seek, share and generate knowledge. Frontiers provides immediate and permanent online open access to all its publications, but this alone is not enough to realize our grand goals.

Frontiers journal series

The Frontiers journal series is a multi-tier and interdisciplinary set of open-access, online journals, promising a paradigm shift from the current review, selection and dissemination processes in academic publishing. All Frontiers journals are driven by researchers for researchers; therefore, they constitute a service to the scholarly community. At the same time, the *Frontiers journal series* operates on a revolutionary invention, the tiered publishing system, initially addressing specific communities of scholars, and gradually climbing up to broader public understanding, thus serving the interests of the lay society, too.

Dedication to quality

Each Frontiers article is a landmark of the highest quality, thanks to genuinely collaborative interactions between authors and review editors, who include some of the world's best academicians. Research must be certified by peers before entering a stream of knowledge that may eventually reach the public - and shape society; therefore, Frontiers only applies the most rigorous and unbiased reviews. Frontiers revolutionizes research publishing by freely delivering the most outstanding research, evaluated with no bias from both the academic and social point of view. By applying the most advanced information technologies, Frontiers is catapulting scholarly publishing into a new generation.

What are Frontiers Research Topics?

Frontiers Research Topics are very popular trademarks of the *Frontiers journals series*: they are collections of at least ten articles, all centered on a particular subject. With their unique mix of varied contributions from Original Research to Review Articles, Frontiers Research Topics unify the most influential researchers, the latest key findings and historical advances in a hot research area.

Find out more on how to host your own Frontiers Research Topic or contribute to one as an author by contacting the Frontiers editorial office: frontiersin.org/about/contact

Cellular and molecular factors that drive the behavior of oligodendrocyte progenitor cells in physiological conditions and disease

Topic editors

Davide Lecca — University of Milan, Italy

Wia Baron — University Medical Center Groningen, Netherlands

Arthur Morgan Butt — University of Portsmouth, United Kingdom

Citation

Lecca, D., Baron, W., Butt, A. M., eds. (2023). *Cellular and molecular factors that drive the behavior of oligodendrocyte progenitor cells in physiological conditions and disease*. Lausanne: Frontiers Media SA. doi: 10.3389/978-2-83251-707-9

Table of contents

frontiers | Frontiers in Cellular Neuroscience

TYPE Editorial
PUBLISHED 06 February 2023
DOI 10.3389/fncel.2023.1145627

Check for updates

OPEN ACCESS

EDITED AND REVIEWED BY
Marie-Ève Tremblay,
University of Victoria, Canada

*CORRESPONDENCE
Davide Lecca
✉ davide.lecca@unimi.it

SPECIALTY SECTION
This article was submitted to Non-Neuronal Cells, a section of the journal Frontiers in Cellular Neuroscience

RECEIVED 16 January 2023
ACCEPTED 23 January 2023
PUBLISHED 06 February 2023

CITATION
Lecca D, Baron W and Butt AM (2023) Editorial: Cellular and molecular factors that drive the behavior of oligodendrocyte progenitor cells in physiological conditions and disease. *Front. Cell. Neurosci.* 17:1145627. doi: 10.3389/fncel.2023.1145627

COPYRIGHT
© 2023 Lecca, Baron and Butt. This is an open-access article distributed under the terms of the Creative Commons Attribution License (CC BY). The use, distribution or reproduction in other forums is permitted, provided the original author(s) and the copyright owner(s) are credited and that the original publication in this journal is cited, in accordance with accepted academic practice. No use, distribution or reproduction is permitted which does not comply with these terms.

Editorial: Cellular and molecular factors that drive the behavior of oligodendrocyte progenitor cells in physiological conditions and disease

Davide Lecca[1]*, Wia Baron[2] and Arthur M. Butt[3]

[1]Department of Pharmaceutical Sciences, Università degli Studi di Milano, Milan, Italy, [2]Department of Biomedical Sciences of Cells and Systems, University of Groningen, University Medical Center Groningen, Groningen, Netherlands, [3]School of Pharmacy and Biomedical Science, University of Portsmouth, Portsmouth, United Kingdom

KEYWORDS

oligodendrocyte progenitor cell (OPC), remyelination failure, inflammation, myelin, extracellular environment, energy metabolism

Editorial on the Research Topic
Cellular and molecular factors that drive the behavior of oligodendrocyte progenitor cells in physiological conditions and disease

Oligodendrocyte progenitor cells (OPCs) are a subtype of glia giving rise to the myelin producing cells in the central nervous system. OPCs are not passive actors unavoidably committed to become oligodendrocytes (OLs) through a precise intrinsic program. As highlighted in this Research Topic, OPCs are extremely plastic and functionally heterogeneous and adapt their program in response to a multitude of signals both in physiological and pathological conditions (Marisca et al., 2020; Boda et al., 2022).

Local environmental cues drive OPC diversity during embryogenesis, development, and adulthood. Green et al. demonstrate that, in zebrafish, peripheral sensory neurons at the dorsal root entry zone are responsible for the development of a very specific subset of OL lineage cells. These sensory OL lineage cells lack *mbpa* transcripts, wrap around axons, affect the function of peripheral sensory nerves, but behave differently than typical oligodendrocytes.

Fekete and Nishiyama provide an overview of environmental signals that direct OPC fate, differentiation, maturation, and myelination and discuss in detail molecular mechanisms of how neuronal-derived BDNF and L1CAM that share common signaling pathways, control OPC differentiation. Differentiation and myelination are complex physiological processes that take place simultaneously in the same areas, and a relevant set of extrinsic factors often trigger different cellular programs thereby selectively acting in the correct subset of cells. Elucidating how extracellular signals are integrated in OPCs would provide new insights in the pathophysiology of these cells and is a therapeutic goal in regenerative medicine. For example, sonic hedgehog (Shh) has a plethora of effects that regulate both OPC proliferation and differentiation (Ruat et al., 2015). In the canonical Shh signaling, its key effector Smo triggers a downstream cascade through the transcription factor Gli1. Shh/Smo signaling was found to be reactivated in demyelinating lesions during remyelination (Ferent et al., 2013). Clobetasol, an FDA-approved promyelinating drug, modulate Smo in oligodendroglial cells and promote a Gli2-dependent modulatory pathway. For this reason, the identification of novel Smo agonists is a therapeutic goal in regenerative medicine. Del Giovane et al. investigated the activity of

the recently developed Smo-binding compound GSA-10. *In vitro*, GSA-10 treatment increased axonal ensheathment and myelin compaction more efficiently than Clobetasol. Moreover, in mice subjected to lysolecithin-induced demyelination, GSA-10 promoted recruitment and differentiation of OPCs into lesions, supporting its role as a pro-myelinating drug.

Successful differentiation of resident OPCs is a key event to restore damaged circuitry and myelin loss that takes place during chronic inflammation. However, a non-permissive environment negatively affects OPC maturation capabilities (Coppolino et al., 2018). Göttle et al. focused on the endogenous envelope protein (ENV), a negative regulator of OPC maturation acting at the TLR-4 receptor. They investigated how ENV could be neutralized to improve remyelination and identified pharmacological agents acting at TLR-4 that restore oligodendroglial differentiation and fully rescue myelination deficits by counteracting ENV-dependent changes in mitochondrial integrity.

During differentiation, OPCs have to fully rewire their energy metabolism, to support axons in response to environmental cues (Marangon et al., 2022). It is crucial to understand how certain inputs can regulate OL metabolism, and how alterations in cell-to-cell communication can be at the basis of neurodegeneration or remyelination failure. In their review, Narine and Colognato describe OL metabolism and the signaling events that regulate the key steps of differentiation, maturation, and myelination. Extrinsic factors such as drugs and diet can disrupt OL energy metabolism thus altering the homeostasis of the CNS and contributing to the development of neurodegenerative diseases. Along these lines, targeting OL bioenergetic pathways represent a new opportunity to boost their regenerative potential.

The mitochondrial aspartate-glutamate transporter AGC1 is an essential player for correct glucose oxidation. Downregulation of AGC1 in OPCs inhibits proliferation and leads to precocious differentiation, together with a reduction in the levels of *N*-acetyl-aspartate, an important acetate donor for myelin lipid synthesis, and a potential source of acetate in histone acetylation (Profilo et al., 2017). Poeta et al. show that down-regulation of AGC1 affected the balance between acetylation and deacetylation in OPCs. This epigenetic defect could be part of the pathogenetic mechanism underlying AGC1 deficiency, an ultrarare genetic disease characterized by global hypomyelination and brain atrophy.

Epigenetic regulation functionally governs differentiation of OPCs. The epigenetic enzyme PRMT5 is a protein arginine methyl transferase responsible for the symmetric methylation of arginine residues on histone tails. In OPCs, PMRT5 is predominantly localized in the cytosol, where it methylates several RNA-binding proteins involved in RNA processing. Using a mass spectrometry-based proteomic approach and iTRAQ labeling of nuclear and cytosolic protein extracts, Dansu et al. identify new direct interactors of PRMT5 in OPCs and show its potential role in biological processes such as RNA stability, transcription, and migration. HMGB1, the most abundant nuclear non-histone binding protein associated to chromatin, is secreted during cellular stress and senescence, and induces inflammation. Rouillard et al. demonstrate that HMGB1 arrests OPC differentiation through a TLR2-mediated mechanism and contributes to remyelination failure in a model of lysolecithin-induced demyelination. Interestingly, high levels of HMGB1 released by senescent neural precursor cells were previously described within human demyelinated multiple sclerosis lesions (Nicaise et al., 2019), thus suggesting the clinical relevance of this inhibitory factor in pathological conditions.

Considerable myelin loss and consequent progressive cognitive deficit were also found in aging brain (Rivera et al., 2021). Rivera et al. describe the molecular consequences of aging in OPCs and focus on the epidermal growth factor (EGF). Network analysis on the aging myelinating OL transcriptome revealed core genes belonging to the EGF signaling commonly dysregulated in Alzheimer's disease and multiple sclerosis. The identification of drugs that target this signaling pathway could positively influence rejuvenation and myelin regeneration.

The cellular and molecular context makes OPCs highly heterogeneous and plastic both in time and space with mechanisms largely unknown. The articles in this Research Topic contributed to gain insights in the multitude of signals received by OPCs and how these signals are processed to determine OPC behavior. Many, if not all, neurodegenerative diseases are likely to share common pathogenetic mechanisms; deciphering how OPCs rewire their program in response to injury signals may open new therapeutic chances to facilitate CNS homeostasis in disease.

Author contributions

DL wrote the manuscript. AB and WB revised the manuscript. All authors have read, revised, and approved the submitted version.

Acknowledgments

We thank all the authors and reviewers that have contributed to this Research Topic.

Conflict of interest

The authors declare that the research was conducted in the absence of any commercial or financial relationships that could be construed as a potential conflict of interest.

Publisher's note

All claims expressed in this article are solely those of the authors and do not necessarily represent those of their affiliated organizations, or those of the publisher, the editors and the reviewers. Any product that may be evaluated in this article, or claim that may be made by its manufacturer, is not guaranteed or endorsed by the publisher.

References

Boda, E., Lorenzati, M., Parolisi, R., Harding, B., Pallavicini, G., Bonfanti, L., et al. (2022). Molecular and functional heterogeneity in dorsal and ventral oligodendrocyte progenitor cells of the mouse forebrain in response to DNA damage. *Nat. Commun.* 13, 2331. doi: 10.1038/s41467-022-30010-6

Coppolino, G. T., Marangon, D., Negri, C., Menichetti, G., Fumagalli, M., Gelosa, P., et al. (2018). Differential local tissue permissiveness influences the final fate of GPR17-expressing oligodendrocyte precursors in two distinct models of demyelination. *Glia* 66, 1118–1130. doi: 10.1002/glia.23305

Ferent, J., Zimmer, C., Durbec, P., Ruat, M., and Traiffort, E. (2013). Sonic Hedgehog signaling is a positive oligodendrocyte regulator during demyelination. *J. Neurosci.* 33, 1759–1772. doi: 10.1523/JNEUROSCI.3334-12.2013

Marangon, D., Audano, M., Pedretti, S., Fumagalli, M., Mitro, N., Lecca, D., et al. (2022). Rewiring of glucose and lipid metabolism induced by G protein-coupled receptor 17 silencing enables the transition of oligodendrocyte progenitors to myelinating cells. *Cells* 11, 2369. doi: 10.3390/cells11152369

Marisca, R., Hoche, T., Agirre, E., Hoodless, L. J., Barkey, W., Auer, F., et al. (2020). Functionally distinct subgroups of oligodendrocyte precursor cells integrate neural activity and execute myelin formation. *Nat. Neurosci.* 23, 363–374 doi: 10.1038/s41593-019-0581-2

Nicaise, A. M., Wagstaff, L. J., Willis, C. M., Paisie, C., Chandok, H., Robson, P., et al. (2019). Cellular senescence in progenitor cells contributes to diminished remyelination potential in progressive multiple sclerosis. *Proc. Natl. Acad. Sci. U. S. A.* 116, 9030–9039. doi: 10.1073/pnas.1818348116

Profilo, E., Peña-Altamira, L. E., Corricelli, M., Castegna, A., Danese, A., Agrimi, G., et al. (2017). Down-regulation of the mitochondrial aspartate-glutamate carrier isoform 1 AGC1 inhibits proliferation and N-acetylaspartate synthesis in Neuro2A cells. *Biochim. Biophys. Acta Mol. Basis Dis.* 1863, 1422–1435. doi: 10.1016/j.bbadis.2017.02.022

Rivera, A. D., Pieropan, F., Chacon-De-La-Rocha, I., Lecca, D., Abbracchio, M. P., Azim, K., et al. (2021). Functional genomic analyses highlight a shift in Gpr17-regulated cellular processes in oligodendrocyte progenitor cells and underlying myelin dysregulation in the aged mouse cerebrum. *Aging Cell* 20, e13335. doi: 10.1111/acel.13335

Ruat, M., Faure, H., and Daynac, M. (2015). Smoothened, stem cell maintenance and brain diseases. *Top Med. Chem.* 16, 147–171. doi: 10.1007/7355_2014_83

frontiers in Cellular Neuroscience

ORIGINAL RESEARCH
published: 23 November 2021
doi: 10.3389/fncel.2021.777542

TLR4 Associated Signaling Disrupters as a New Means to Overcome HERV-W Envelope-Mediated Myelination Deficits

*Peter Göttle[1], Kira Schichel[1], Laura Reiche[1], Luisa Werner[1], Annika Zink[2], Alessandro Prigione[2] and Patrick Küry[1]**

[1] Department of Neurology, Medical Faculty, Heinrich-Heine-University, Düsseldorf, Germany, [2] Department of General Pediatrics, Neonatology and Pediatric Cardiology, Medical Faculty, Heinrich-Heine-University, Düsseldorf, Germany

OPEN ACCESS

Edited by:
Arthur Morgan Butt, University of Portsmouth, United Kingdom

Reviewed by:
Jelena Skuljec, Essen University Hospital, Germany
Bilal Ersen Kerman, Istanbul Medipol University, Turkey

***Correspondence:**
Patrick Küry
kuery@hhu.de

Specialty section:
This article was submitted to Cellular Neuropathology, a section of the journal Frontiers in Cellular Neuroscience

Received: *15 September 2021*
Accepted: *25 October 2021*
Published: *23 November 2021*

Citation:
Göttle P, Schichel K, Reiche L, Werner L, Zink A, Prigione A and Küry P (2021) TLR4 Associated Signaling Disrupters as a New Means to Overcome HERV-W Envelope-Mediated Myelination Deficits. Front. Cell. Neurosci. 15:777542. doi: 10.3389/fncel.2021.777542

Myelin repair in the adult central nervous system (CNS) is driven by successful differentiation of resident oligodendroglial precursor cells (OPCs) and thus constitutes a neurodegenerative process capable to compensate for functional deficits upon loss of oligodendrocytes and myelin sheaths as it is observed in multiple sclerosis (MS). The human endogenous retrovirus type W (HERV-W) represents an MS-specific pathogenic entity, and its envelope (ENV) protein was previously identified as a negative regulator of OPC maturation—hence, it is of relevance in the context of diminished myelin repair. We here focused on the activity of the ENV protein and investigated how it can be neutralized for improved remyelination. ENV-mediated activation of toll like receptor 4 (TLR4) increases inducible nitric oxide synthase (iNOS) expression, prompts nitrosative stress, and results in myelin-associated deficits, such as decreased levels of oligodendroglial maturation marker expression and morphological alterations. The intervention of TLR4 surface expression represents a potential means to rescue such ENV-dependent deficits. To this end, the rescue capacity of specific substances, either modulating V-ATPase activity or myeloid differentiation 2 (MD2)-mediated TLR4 glycosylation status, such as compound 20 (C20), L48H437, or folimycin, was analyzed, as these processes were demonstrated to be relevant for TLR4 surface expression. We found that pharmacological treatment can rescue the maturation arrest of oligodendroglial cells and their myelination capacity and can prevent iNOS induction in the presence of the ENV protein. In addition, downregulation of TLR4 surface expression was observed. Furthermore, mitochondrial integrity crucial for oligodendroglial cell differentiation was affected in the presence of ENV and ameliorated upon pharmacological treatment. Our study, therefore, provides novel insights into possible means to overcome myelination deficits associated with HERV-W ENV-mediated myelin deficits.

Keywords: myelin repair, multiple sclerosis (MS), oligodendrocyte, toll-like receptor, HERV-W, ENV, mitochondrial dysfunction, endogenous retrovirus

INTRODUCTION

Multiple sclerosis (MS) is an autoimmune disease of the adult central nervous system (CNS) resulting in the loss of mature oligodendrocytes and their myelin sheaths subsequently leading to neurodegeneration (Lassmann, 2018). Efficient remyelination of resulting white matter lesions is rare but can eventually replace lost oligodendrocytes and myelin sheaths as a result of activation and recruitment of resident oligodendroglial precursor cells (OPCs) (Franklin and Ffrench-Constant, 2008; Tripathi et al., 2010). These cells are, therefore, able to restore axonal functions *via* stabilization, protection, electrical insulation, and by providing trophic and metabolic support (Gensert and Goldman, 1997; Simons and Nave, 2015; Franklin and Ffrench-Constant, 2017). Due to the presence of inhibitory regulators within the MS environment, the overall remyelination efficiency remains low and even further declines with disease progression as these precursor cells often fail to generate new oligodendrocytes (Kuhlmann et al., 2008; Kremer et al., 2011). Hence, overcoming differentiation blockades and enhancement of oligodendrogenesis represent a promising strategy for functional recovery (Göttle et al., 2019b; Kremer et al., 2019a; Manousi et al., 2021). Pointing out one specific inhibitor, the envelope (ENV) protein encoded by the human endogenous retrovirus type W (HERV-W) was previously shown by us to interfere with oligodendroglial cell differentiation (Kremer et al., 2013; Göttle et al., 2019a) contributing to the number of MS-related pathological roles of this factor as summarized previously (Küry et al., 2018). Strategies to overcome the negative impact of the ENV protein, activating the toll like receptor 4 (TLR4) signaling pathway on OPCs, have therefore revealed to be potentially interesting in light of the development of specific myelin repair therapies. This was exemplified by the description of KM91104, a vacuolar-ATPase inhibitor, shown to efficiently neutralize ENV-mediated oligodendroglial effects *via* disruption of TLR4 surface expression (Göttle et al., 2019a). Given the widespread expression profile of V-ATPase, a specific (oligodendroglial) prevention of TLR4 activation is difficult to achieve. We therefore addressed to what degree other small molecules are known to modulate TLR4 cell surface expression and activation, e.g., *via* interfering with V-ATPase activity or myeloid differentiation 2 (MD2)-mediated TLR4 glycosylation (Ohnishi et al., 2003; Saitoh and Miyake, 2006), exhibit the capacity to rescue ENV-dependent myelin deficits. The curcumin derivate [1-ethyl-3,5-bis (3,4,5-trimethoxybenzylidene) piperidin-4-one] L48H37, folimycin (concanamycin A) a macrolide antibiotic agent, and the small molecule compound 20 (C20; chalcone derivate that contains the moiety of (E)-4-phenylbut-3-en-2-one) were previously demonstrated to reduce TLR4 cell surface expression in macrophages thus decreasing nitrosative stress reactions and the production of proinflammatory cytokines, respectively (Eswarappa et al., 2008; Wang et al., 2015; Zhang et al., 2016). Applying these substances to OPCs, we indeed found that oligodendroglial cell differentiation and internode formation can be stabilized in the presence of ENV to various degrees. Moreover, as the myelination process is dependent on high metabolic turnover, which is maintained by mitochondria the essential organelles regulating energy production through oxidative phosphorylation (Tepavcevic, 2021), we revealed for the first time unbalanced mitochondrial homeostasis in the presence of the ENV protein likely to contribute to their impaired myelination activity (Barcelos et al., 2019; Maiuolo et al., 2020). Such ENV-dependent changes in mitochondrial integrity/structure could also be counteracted by means of L48H37 or C20. Our study thus sheds light on a plausible correlation between ENV-dependent nitrosative stress inductions affecting oligodendroglial energy homeostasis that can be reversed *via* specific pharmacological stimulation, hence, revealing new subcellular mechanisms that could provide therapeutic targets for upcoming regenerative MS therapies.

MATERIALS AND METHODS

Oligodendroglial Cell Culture

Generation of primary OPCs from postnatal day zero (P0) cerebral rat cortices (Wistar rats of either sex) was performed as previously described (Göttle et al., 2010). The Institutional Review Board (IRB) of the Zentrale Einrichtung für Tierforschung und wissenschaftliche Tierschutzaufgaben (ZETT) at the Heinrich Heine University Düsseldorf has approved all animal procedures under licenses O69/11 and V54/09. Anti-A2B5 staining (Merck Millipore, Darmstadt, Germany; MAB312R RRID:AB_11213098) revealed that the cultures consisted of 98% oligodendroglial cells (data not shown). OPCs were either seeded onto 0.25 mg/ml poly-D-lysine-coated (PDL, Merck Millipore, Darmstadt, Germany) glass coverslips (13 mm) in 24-well plates (for immunocytochemistry; 2.5×10^4 cells/well) or onto 0.25 mg/ml PDL-coated 24-well plates [for quantitative reverse transcription PCR (qRT-PCR); 5×10^4 cells/well] in high-glucose Dulbecco's Modified Eagle Medium (DMEM)-based Sato medium. After 1.5 h, oligodendroglial cell differentiation was initiated by Sato medium supplemented with 0.5% fetal bovine serum (FBS) (Capricorn Scientific, Palo Alto, CA, United States). The medium was exchanged every 3 days. To determine the physiological reaction from OPCs in exposure to the substances, OPCs were treated in a dose-dependent manner using concentrations 0.1, 0.2, 0.5, 1, 2, and 5 μM for L48H37 (Merck Millipore, Darmstadt, Germany; Cat #: SML1443–L48H37) and C20 (Invivochem, Köln, Germany; Cat #: V4032; CAS #: 111797-22-9) and 0.1, 0.2, 0.5, 1, 2, and 5 nM for folimycin (Merck Millipore, Darmstadt, Germany; Cat#: 344085) respectively. Stock concentrations of L48H37 (4.14 mM), folimycin (10 μM), and C20 (10 mM) were prepared using dimethylsulfoxide (DMSO, Merck Millipore, Darmstadt, Germany), and this solvent was also used as control at equal dilutions. Total 500 μl of prepared solutions were added to the cells containing either substances or DMSO, and final concentrations of L48H38 (0.5 μM), folimycin (0.2 nM), and C20 (0.5 μM) were used. Oligodendroglial cells were treated with 100 ng/ml full-length ENV protein in a differentiation medium as previously described (Kremer et al., 2013; Göttle et al., 2019a). Recombinant HERV-W ENV protein was produced

by Protein'eXpert (Grenoble, France) according to quality control specifications of GeNeuro SA (Lyon, France) and kindly provided by Dr. Hervé Perron (GeNeuro SA). Endotoxin levels were below the detection limit (<5 EU = ml) as measured by the Limulus amebocyte lysate test. Control experiments were conducted using recombinant protein buffer preparation [20 mM histidine, 5% (w/v) sucrose, and 0.01% (w/v) polysorbate 20, pH 6.0]. ENV protein and buffer were applied at equal dilutions in the differentiation medium (DMEM-based Sato-medium with 0.5% FCS). The control treatment and the treatment with the substance were only diluted in differentiation medium. The ENV treatment and the combination of ENV with the substances were diluted in the differentiation medium containing ENV. The following combinations were used: (a) recombinant protein buffer; (b) recombinant ENV protein; (c) recombinant ENV and 0.5 μM L48H37; (d) recombinant ENV and 0.2 nM folimycin; and (e) recombinant ENV protein and 0.5 μM C20.

RNA Preparation, cDNA Synthesis, and qRT-PCR

Total RNA purification from cultured cells was lysed using 350 μl RLT lysis buffer (Qiagen, Hilden, Germany) supplemented with β-mercaptoethanol (1:100, Merck Millipore, Darmstadt, Germany), and total RNA was purified using the RNeasy Mini Kit (Qiagen, Hilden, Germany) according to manufacturer instructions, such as DNase digestion. Before qRT-PCR, reverse transcription with 250 ng RNA [measured using a NanoDrop ND 1000 (Peqlab, Erlangen, Germany)] was done using the High-Capacity cDNA Reverse Transcription Kit (ThermoFisher Scientific, Darmstadt, Germany). Gene expression levels were determined on a 7900HT sequence detection system (ThermoFisher Scientific, Darmstadt, Germany) applying SybrGreen universal master mix (ThermoFisher Scientific, Darmstadt, Germany). For sequence detection, the following forward (fwd) and reverse (rev) primers, generated *via* PrimerExpress 2.0 software (Applied Biosystems, Waltham, MA, United States), were used with ornithine decarboxylase (ODC) and glyceraldehyde 3-phosphate dehydrogenase (GAPDH) serving as reference genes: r-iNOS_fwd: CTCAGCACAGAGGGCTCAAAG, r-iNOS_rev: TGCACCCAAACACCAAGGT, r-IL-6_fwd: GTT GTGCAATGGCAATTCTGA, r-IL-6_rev: TCTGACAGTGCAT CATCGCTG, r-IL-1ß_fwd: GAAACAGCAATGGTCGGGAC, r-IL-1ß_rev: AAGACACGGGTTCCATGGTG, r-TNF-α_fwd: AGCCCTGGTATGAGCCCATGTA, r-TNF-α_rev:CCGGACTC CGTGATGTCTAAGT, r-TLR4_fwd: CTGGGTTTCTGCT GTGGACA, r-TLR4_rev: AGGTTAGAAGCCTCGTGCTCC, r-Ldha_fwd: CTGTGTGGAGTGGTGTGAATGTC, r-Ldha_rev: CAGCTGCGGGTTCAGAACT, r-myc_fwd: CTTCCCCTA CCCGCTCAAC, r-myc_rev: GTGGAATCGGACGAGGTACAG, ppargc1a_fwd: TGAAGAGCGCCGTGTGATT, r-ppargc1a_rev: TTCTGTCCGCGTTGTGTCA, r-ppargc1b_fwd: GGAAAAGG CCATCGGTGAA, ppargc1b_rev: GCTCATGTCACCGGA GAGATTT, r-pparg-1_fwd: CCCACCAACTTCGGAATCAG, r-ppar-γ-1_rev: GGAATGGGAGTGGTCATCCA, r-pdpk1-1_ fwd: AATGGTGAGGTCCCAGACTGA, CCTGCTAACACCAC TAGGAATGC, GAPDH_fwd: GAACGGGAAGCTCACTGGC, GAPDH_rev: GCATGTCAGATCCACAACGG ODC_fwd: GGT TCCAGAGGCCAAACATC, ODC_rev: GTTGCCACATTGAC CGTGAC. Relative gene expression levels were determined according to the ΔΔCt method (ThermoFisher Scientific, Darmstadt, Germany). All measurements were done in duplicates; generated from $n = 4$ independent experiments, and data are shown as mean values ± SEM.

Myelinating Co-cultures

Dissociated neuron/oligodendrocyte co-cultures were obtained from embryonic day 16 (E16) rat cerebral cortex (Wistar rats of either sex) according to Pang et al. (2012) and as previously published by us (Göttle et al., 2015). Cortical cells were plated on 15-mm poly-D-lysine (0.1 mg/ml) coated cover slips (65,000 cells per cover slip) and kept in myelination medium consisting of N2 and neurobasal medium (ThermoFisher Scientific, Darmstadt, Germany; ratio 1:1), such as NGF (50 ng/ml) and NT-3 (10 ng/ml) (both R&D Systems, Minneapolis, MN, United States). The day of primary culture was defined as day one *in vitro* (DIV1). After 10 days *in vitro* (DIV10) insulin was excluded, and the ratio of the insulin-free N2 to neurobasal medium, such as B27 supplement (ThermoFisher Scientific, Darmstadt, Germany), was adjusted to 4:1. This myelination medium was further supplemented with 60 ng/ml tri-iodo-thyronine (T3, Merck Millipore, Darmstadt, Germany). Final concentrations of individual N2 medium components (DMEM-F12 based, high glucose; ThermoFisher Scientific, Darmstadt, Germany) were insulin (10 μg/ml), transferrin (50 μg/ml), sodium selenite (5.2 ng/ml), hydrocortisone (18 ng/ml), putrescine (16 μg/ml), progesterone (6.3 ng/ml), biotin (10 ng/ml), *N*-acetyl-L-cysteine (5 μg/ml) (all Merck Millipore, Darmstadt, Germany), bovine serum albumin (0.1%, Roth, Karlsruhe, Germany), and penicillin–streptomycin (50 units/ml, ThermoFisher Scientific, Darmstadt, Germany). At DIV30, cover slips were washed with PBS, fixed with 4% paraformaldehyde, and processed for immunofluorescent staining. At the onset of myelination DIV17, cultures were treated for other 9 days with myelination medium supplemented with ENV in the presence or absence of L48H37, folimycin, or C20 until DIV26 according to Göttle et al. (2015). Myelinating oligodendrocytes were identified as previously described (Göttle et al., 2015, 2018, 2019a).

Immunostaining

Fixed cells were permeabilized with PBS containing 0.01% Triton X-100 (Merck Millipore, Darmstadt, Germany), and unspecific staining was blocked with 10% normal goat serum or donkey serum (Merck Millipore, Darmstadt, Germany) for 40 min as established previously (Göttle et al., 2010). Cells were then incubated with primary antibodies in PBS with 10% normal goat serum or donkey serum overnight at 4°C using the following dilutions: rat anti-myelin basic protein (MBP; 1/250, Bio-Rad, Munich, Germany; Cat# MCA409S RRID:AB_325004), mouse anti-adenomatosis polyposis coli (CC1; 1:250, GeneTex Cat# GTX16794, RRID:AB_422404), rabbit anti-cleaved caspase-3 (CC-3; 1/500, Cell Signaling Technology Cat# 9661, RRID:AB_2341188), and rabbit anti-TLR4 (1/1,000; Abcam

Cambridge, United Kingdom; Cat# ab13556, RRID:AB_300457). Mitochondrial staining was performed by loading alive OPCs, after 24 h treatment, with 50 nM Mitotracker Red CMX-Ros (ThermoFisher Scientific, Darmstadt, Germany) in serum-free Sato medium for 20 min at 37°C, followed by fixation and phalloidin labeling. Thus, cover slips were incubated with 50 μg/ml phalloidin-fluoresceinisothiocyanate (Merck Millipore, Darmstadt, Germany) for visualization of cells. Fixed co-cultures were blocked with PBS containing 0.5% Triton X-100 and 2% normal goat serum and then incubated overnight in 0.1% Triton and 2% normal goat serum containing rat anti-MBP (1/250, Bio-Rad, Munich, Germany; Cat# MCA409S RRID:AB_325004), and rabbit anti-neurofilament (NF, 1:1,000, Abcam, Cambridge, United Kingdom Cat# ab8135, RRID:AB_306298). After 24 h, cover slips were washed with PBS and then incubated with secondary antibodies in PBS (diluted 1/500) for 2 h conjugated to goat anti-rat Alexa Fluor 488 (ThermoFisher Scientific, Darmstadt, Germany; Cat# A-11006 RRID:AB_2534074), goat anti-rabbit Alexa Fluor 405 (ThermoFisher Scientific, Darmstadt, Germany; Cat# A31556 RRID:AB_221605), goat anti-mouse Alexa Fluor 594 (ThermoFisher Scientific, Darmstadt, Germany; Cat# A11005 RRID:AB_10561507), goat anti-rabbit (ThermoFisher Scientific, Darmstadt, Germany; Cat# A11037 RRID:AB_10561549), or goat anti-rat (ThermoFisher Scientific, Darmstadt, Germany; Cat# A-11007, RRID:AB_10561522). Nuclei were stained with 4′,6-diamidin-2-phenylindol (DAPI, Roche, Basel, Switzerland). Images (20×; Zeiss Axionplan2 microscope) were captured using the same light intensity, and filters for all images were compared and processed with Axiovision 4.2 software (Zeiss, Jena, Germany; RRID:SciRes_000111). The analysis was done using Java software (ImageJ, RRID:SCR_003070,467/Wright Cell Imaging Facility, RRID:SCR_003070,471). Immunopositive cells were counted in nine randomly chosen fields per coverslip. Two coverslips were used per condition. The total number of cells per field was determined *via* DAPI staining. For quantification, the number of immune-positive cells was compared to the total cell number and expressed as a percentage [mean ± SEM]. To compare TLR4 surface, expression cells were subjected to confocal laser scanning microscopy using a confocal LSM microscope 510 (CLSM 510, Zeiss, Jena, Germany). The fluorescence intensity across the plasma membrane was detected by using Zen 2012 software (Zeiss) according to Ohgaki et al. (2017).

Proximity Ligation Assay

Direct protein/protein interactions were investigated by means of a proximity ligation assay (PLA) [(Soderberg et al., 2006) using Duolink *in situ* Red Starter Kit Mouse/Rabbit (Merck Millipore, Darmstadt, Germany] as previously described (Göttle et al., 2015). Cells were rapidly washed with ice-cold PBS and then fixed at room temperature for 10 min in 4% PFA. Cells were further rinsed 3 min × 3 min with PBS containing 0.1% Triton X-100 (Merck Millipore, Darmstadt, Germany) and then washed 3 min × 2 min with 0.05% Tween 20 (Merck Millipore, Darmstadt, Germany) in TBS to allow permeabilization. Then one droplet (40 μl) of Duolink II blocking solution was added to each cover slip and incubated in a preheated humidity chamber for 1 h at 37°C. Next, the blocking solution was tapped off, and cells were incubated for 1 h at 37°C with primary antibodies anti-TLR4 (1/1000; ab13556, Abcam Cambridge, United Kingdom; Cat# ab13556, RRID:AB_300457), mouse anti-ENV (1/500; GNmAB03 provided by GeNeuro; and as established in Kremer et al. (2013), Göttle et al. (2019a), and Kremer et al. (2019b). Duolink anti-rabbit PLUS and anti-mouse MINUS secondary antibodies and Red Detection Reagents were used, and antibody incubation, ligation, amplification, and washing steps were performed according to the manual of supplier. Cover slips were then incubated with 50 μg/ml phalloidin-fluoresceinisothiocyanate (Merck Millipore, Darmstadt, Germany) for visualization of cells, dried, mounted using Duolink Mounting Media with DAPI, and analyzed using Axiovision 4.2 software (Zeiss) and image processing and analysis in Java software (ImageJ, Wright Cell Imaging Facility).

Statistical Analysis

Data are presented as mean ± SEM. Graphs and statistical analysis were performed using Excel and the GraphPad Prism 8.0.2 software (GraphPad Prism, San Diego, CA, United States; RRID: SCR_002798). Shapiro–Wilk normality test was used to assess the absence of the Gaussian distribution of all datasets. To determine statistical significance for normally distributed data sets, one-way ANOVA with Turkey post-test for multiple comparisons was applied to compare three or more groups. For data sets not passing the Shapiro–Wilk normality test, Kruskal–Wallis test with Dunn's post-test was applied. Statistical significance thresholds were set as follows: $^{*}p < 0.05$, $^{**}p < 0.01$, $^{***}p < 0.001$ and n represents the number of independent experiments.

RESULTS

Since it was recently demonstrated that L48H37, folimycin (concanamycin A), and C20 are able to interfere with TLR4 signaling (Eswarappa et al., 2008; Wang et al., 2015; Zhang et al., 2016), hence, decreasing stress reaction within macrophages, we hypothesized that these substances could also stabilize and/or rescue oligodendroglial homeostasis and differentiation in the presence of ENV protein. To this end, we investigated the effect of the given substances on purified postnatal primary rat OPCs regarding differentiation dynamics, myelin sheath generation, and mitochondrial integrity.

Tolerated Dosage of L48H37, Folimycin, and C20 for Rat Oligodendroglial Precursor Cells

To determine functionally relevant cell-specific concentrations, cell death of primary cultured OPCs was investigated in a dose-dependent manner by the detection of activated CC-3 expression. Dilution stock concentrations of L48H37 (4.14 mM), folimycin (10 μM), and C20 (10 mM) were performed, and primary OPCs were stimulated with different concentration series regarding L48H37 and C20 (0.1, 0.2, 0.5, 1, 2, and 5 μM) and folimycin (0.1,

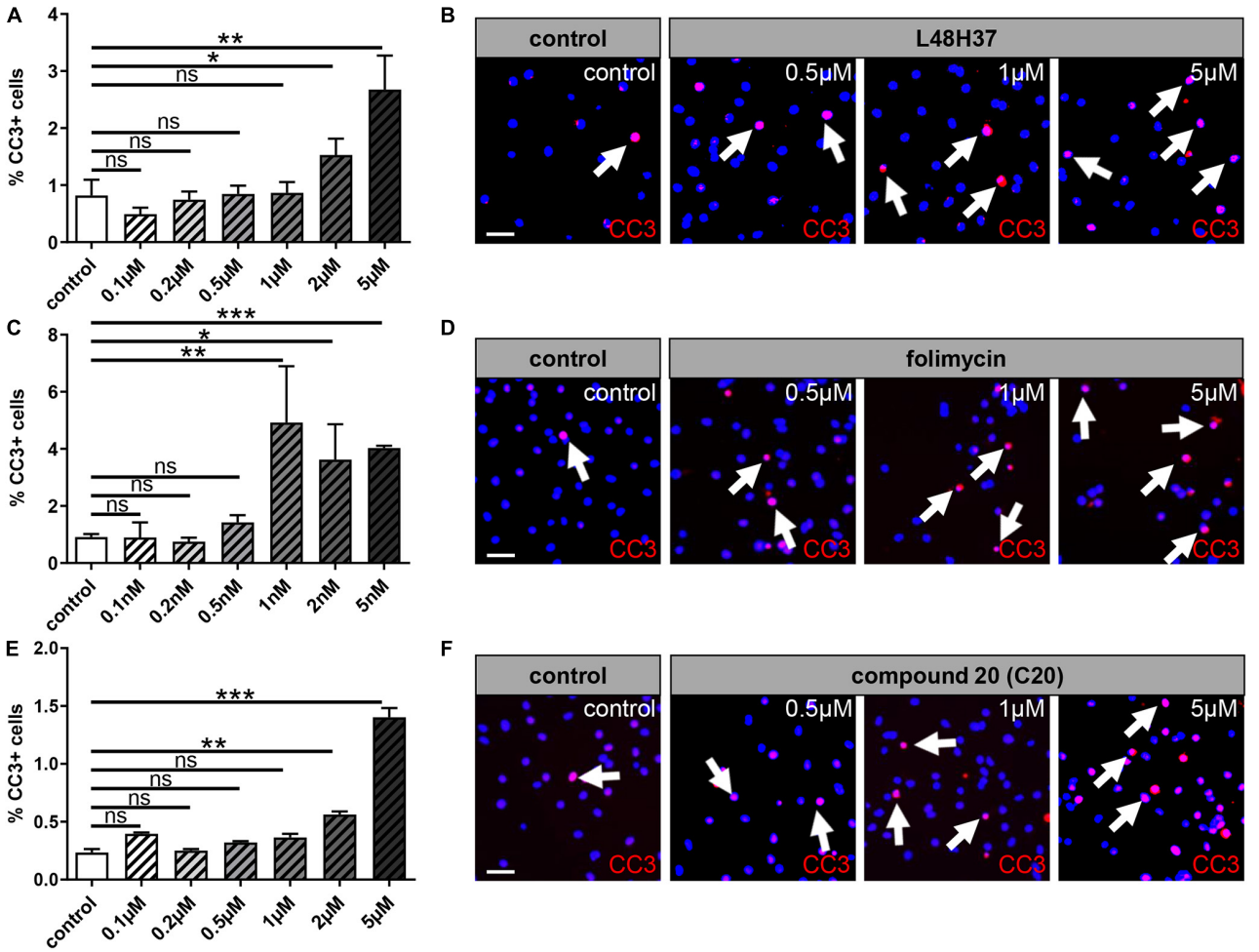

FIGURE 1 | Oligodendroglial cell death rates upon L48H37, compound 20, and folimycin treatment. Immunocytochemical staining by means of cleaved caspase 3 (CC-3) within OPCs after 1 day revealed high doses of L48H37, folimycin, and compound 20 led to an increase in the percentage of apoptotic OPC as judged by the expression of activated CC-3 **(A,C,E)**. DMSO was used as a control and was applied at equal dilutions. Representative pictures show CC3 positive cells marked *via* immunocytochemical staining and DAPI-stained nuclei **(B,D,F)**. Arrows represent CC3 positive cells. Scale bar: 20 μm. Data are shown as mean values (± SEM) and derived from $n = 3$ experiments. Statistical significance was calculated using one-way ANOVA with Tukey post-test (ns, not significant, $^{*}p < 0.05$, $^{**}p < 0.01$, and $^{***}p < 0.001$). DMSO, dimethylsulfoxide; DAPI, 4′,6-diamidin-2-phenylindol.

0.2, 0.5, 1, 2, and 5 nM) for 1 day (**Figure 1**). Immunofluorescent staining for CC-3 revealed that high concentrations (above 0.5 μM for L48H37 and C20; **Figures 1A,B,E,F**) and (above 0.5 nM for folimycin; **Figures 1C,D**) substantially increased the degree of apoptotic OPCs. Therefore, for subsequent stimulation experiments, concentrations with low apoptosis rates were used: 0.5 μM for L48H37 (apoptotic rate $\leq$ 0.85%), 0.2 nM for folimycin (apoptotic rate $\leq$ 0.75%), and 0.5 μM for C20 (apoptotic rate $\leq$ 0.3%).

Envelope Induces the Expression of Proinflammatory Factors and Can Be Reversed by L48H37, Folimycin, and C20

Given that ENV-mediated activation of TLR4 leads to the induction of proinflammatory cytokine expression, nitrosative stress, and a subsequent reduction in myelin protein expression (Kremer et al., 2013, 2015; Göttle et al., 2019a), it was of interest to investigate the capacity of L48H37, folimycin, and C20 to reverse ENV-dependent gene inductions. To this end, gene expression analysis of OPCs 1 day after treatment was conducted by means of qRT-PCR. ENV stimulation led to a proinflammatory reaction, as transcript levels of *inducible nitric oxide synthase* (*iNOS)* and *interleukin-6 (IL-6)* were upregulated (**Figures 2A,B**). Of note, L48H37, folimycin, and C20 were able to repress their expression in the presence of ENV at baseline levels.

Rescue of ENV-Dependent Oligodendroglial Differentiation Deficits by L48H37, Folimycin, and C20

Considering our previous findings demonstrate that the ENV-mediated differentiation/myelination blockade can be overcome by molecules, such as KM91104, which disturbs TLR4 signaling.

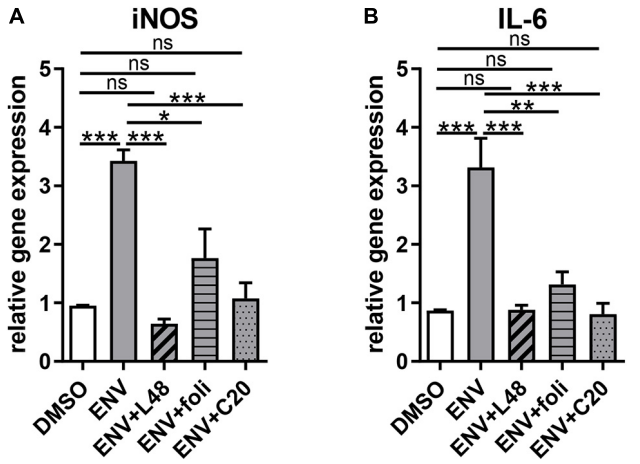

FIGURE 2 | Gene expression alterations due to proinflammatory effects of the recombinant envelope protein (ENV) on cultured rat oligodendroglial precursor cells. **(A,B)** Quantitative RT-PCR after 1d revealed that upon ENV protein stimulation a significant upregulation of *iNOS* and *IL-6* transcript levels occurred, which was compensated to control transcript levels upon L48H37 or compound 20 treatment. Data are shown as mean, and error bars represent SEM. A number of experiments: $n = 4$. Statistical significance was calculated using one-way ANOVA with Tukey post-test (ns, not significant, $^{*}p < 0.05$, $^{**}p < 0.01$, and $^{***}p < 0.001$). iNOS, inducible nitric oxide synthase; IL-6, interleukin-6.

We were wondering whether the substances L48H37, folimycin, and C20, all of which are known to affect macrophage TLR4 signaling (Eswarappa et al., 2008; Wang et al., 2015; Zhang et al., 2016), could also maintain the differentiation capacity of OPC. For functional examination of the selected substances, we treated primary OPCs with L48H37, folimycin, or C20 and determined differentiation-related expression of myelin and late maturation markers, such as MBP and adenomatosis polyposis coli (CC1) protein expression after 3 days by means of immunofluorescent staining (**Figure 3**). Substance treatment alone did not significantly affect MBP- or CC1 positivities, but a clear rescue of the diminished expression in presence of the ENV protein could be observed in cells treated with L48H37 or C20 for both markers MBP (**Figures 3A,C,G,I**) and CC1 (**Figures 3D,F,G,I**) returned to baseline levels. In contrast, no significant rescue reaction was detected in folimycin treated cells.

Rescue of ENV-Dependent Myelination Deficits by L48H37 and C20 but Not by Folimycin

Next, it was important to extend our findings onto the myelination process (**Figure 4**). To this end, mixed rat neuron/glia co-cultures were grown for 17 days and then treated for another 9 days with a myelination medium with or without the addition of recombinant ENV protein. These co-cultures were then co-treated with L48H37, folimycin, C20, or control buffer during the entire myelination period as previously described for KM91104 (Göttle et al., 2019a). After a total duration of 26 days in culture, the percentage of MBP positive oligodendrocytes exhibiting a myelinating phenotype (i.e., featuring internodes) was determined based on the total number of Olig2-positive cells. This analysis revealed a full rescue of the degree of myelinating oligodendrocytes in the presence of ENV protein by L48H37 (**Figure 4A**) and C20 (**Figure 4C**), but not folimycin, indicating that the ENV-mediated deficiency of this critical neuron/glia interaction can be specifically modulated.

L48H37 and C20 Affect TLR4 Surface Presentation on Oligodendroglial Precursor Cells

Given the observed and specific rescue effects of L48H37 and C20 in terms of the ENV-mediated oligodendroglial differentiation blockade, it was of considerable interest to see whether TLR4 surface presentation can be modulated by these three substances (**Figure 5**). TLR4 surface expression was analyzed after 24 h of substance treatment by means of laser scanning microscopy (LSM). Herein, peak/intensity detection across the cell revealed that the fluorescence peak of TLR4 signal is shifted toward the interior compared to DAPI indicating a profound decrease in TLR4 surface expression in presence of ENV in combination with L48H37 (**Figure 5B**) or C20 (**Figure 5C**) as opposed to ENV treatment only (**Figure 5A**), or when folimycin was applied (**Figure 5D**). To further confirm that TLR4 surface localization was abolished, we examined physical interactions between TLR4 and ENV proteins *in situ*, using the PLA (Soderberg et al., 2006; Göttle et al., 2015). To this end, OPCs were stimulated with ENV protein in the absence or presence of either L48H37, folimycin, or C20, fixed and subjected to PLA staining procedure. Upon ENV treatment of control cells, positive PLA events reflecting direct TLR4/ENV binding events on the cells surface (distinct red fluorescent spots) could be observed (**Figure 5A**, right side of the composite Figure). Of note, no direct TLR4/ENV interactions (hence red dots) could be detected in L48H37 and C20 treated cells (**Figures 5B,C**) whereas folimycin-treated cells apparently still allowed a physical ENV/TLR4 interaction (**Figure 5D**).

Envelope Mediated Mitochondrial Changes in Oligodendroglial Cells

Since a balanced mitochondrial function is key for successful oligodendroglial cell differentiation to occur (Schoenfeld et al., 2010) and recent studies associated mitochondrial dysfunction with neurological diseases, such as MS (Lan et al., 2018; Barcelos et al., 2019), we investigated whether ENV exposure affects mitochondria. We treated primary OPCs with L48H37, folimycin, or C20 and determined the expression of genes related to mitochondrial homeostasis after 1 day in the absence and presence of ENV protein (**Figure 5**). A significant downregulation of *peroxisome proliferator-activated receptor gamma coactivator 1 alpha* (*ppargc1a*), *peroxisome proliferator-activated receptor gamma coactivator 1 beta* (*ppargc1b*), and *peroxisome proliferator-activated receptor gamma* (*PPAR-γ*) was determined upon exposure to ENV protein, all of which encode for major regulators of mitochondrial biogenesis (Corona and Duchen, 2016; Yeligar et al., 2018). These transcript levels could essentially be rescued when OPCs were treated with the L48H37

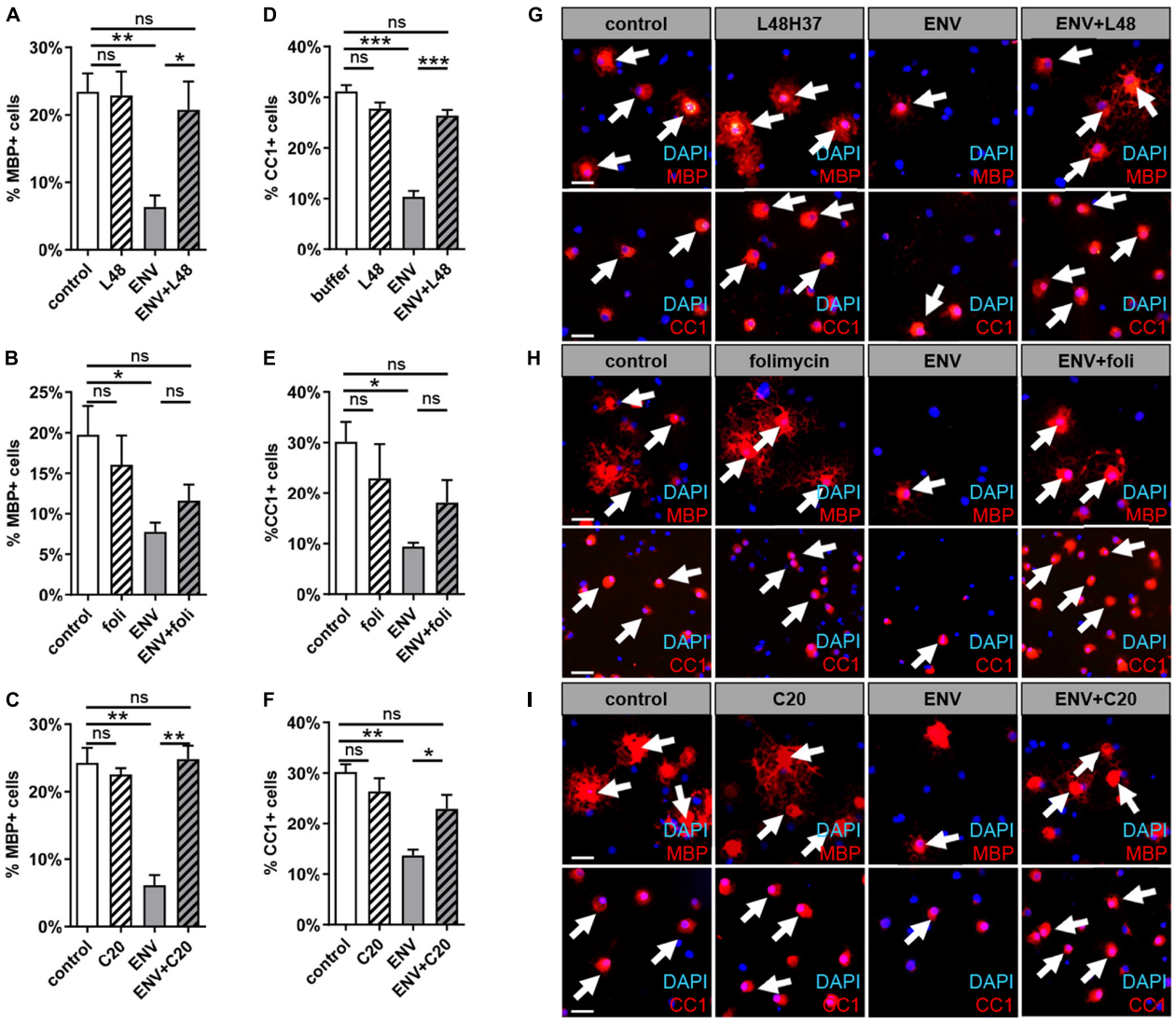

FIGURE 3 | MBP and CC1 expression during spontaneous oligodendroglial precursor cell differentiation upon stimulation with ENV in combination with L48H37, compound 20, or folimycin. **(A–F)** Determination of the percentage of MBP- positive cells upon exposure to protein buffer, to respective substance, to ENV (100 ng/ml) protein or to ENV protein (100 ng/ml) plus respective substance for 3 days. The concentrations for L48H37 (0.5 μM), folimycin (0.2 nM), and C20 (0.5 μM) were determined in the previous CC3 experiment. The protein buffer and the condition with the substance only were diluted in DMSO and were applied at equal dilution. **(G–I)** Representative pictures demonstrate MBP positive OPCs marked *via* immunocytochemical staining (red; indicated through arrows) and DAPI stained nuclei (blue). Scale bar: 50 μm. A number of experiments: $n = 4$. Statistical significance was calculated using one-way ANOVA with Tukey post-test **(A,C,D–F)** and **(B)** Kruskal–Wallis test with Dunn's post-test (ns, not significant, $^{*}p < 0.05$, $^{**}p < 0.01$, and $^{***}p < 0.001$). DAPI, 4′,6-diamidin-2-phenylindol; MBP, myelin basic protein; OPCs, oligodendroglial precursor cells; DMSO, dimethylsulfoxide; ENV, envelope protein.

and C20 generating statistically significant rescue values and with folimycin in failing to do so (**Figures 6A–C**). The expression of genes involved in cellular energy metabolism, such as *lactate dehydrogenase A* (*Ldha-1*), *proto-oncogene MYC Box 6* (*myc*), or *3-phosphoinositide-dependent protein kinase* (*pdpk-1*), was affected neither by the ENV protein nor the three substances (**Figures 6D–F**), suggesting that the observed transcriptional changes of mitochondrial biogenesis were not part of the overall change in cellular metabolism. Given that mitochondrial network morphology correlates with mitochondrial biogenesis in response to environmental cues and has recently emerged as a fundamental feature for neuronal and oligodendroglial cell differentiation (Bertholet et al., 2016; Magalon et al., 2016), we examined changes in the mitochondrial network across the different conditions. It was observed that in OPCs exposed to both ENV proteins only or to ENV protein plus folimycin, mitochondria appeared rather fragmented (**Figures 6H,J**) as compared to buffer-treated (control) cells (**Figure 6G**). Conversely, OPCs exposed to ENV protein in the presence of either L48H37 or C20 (**Figures 6I,K**) exhibited more elongated mitochondria. Altogether, these data indicate that mitochondrial shape is affected by ENV protein and can be stabilized *via* L48H37 and C20.

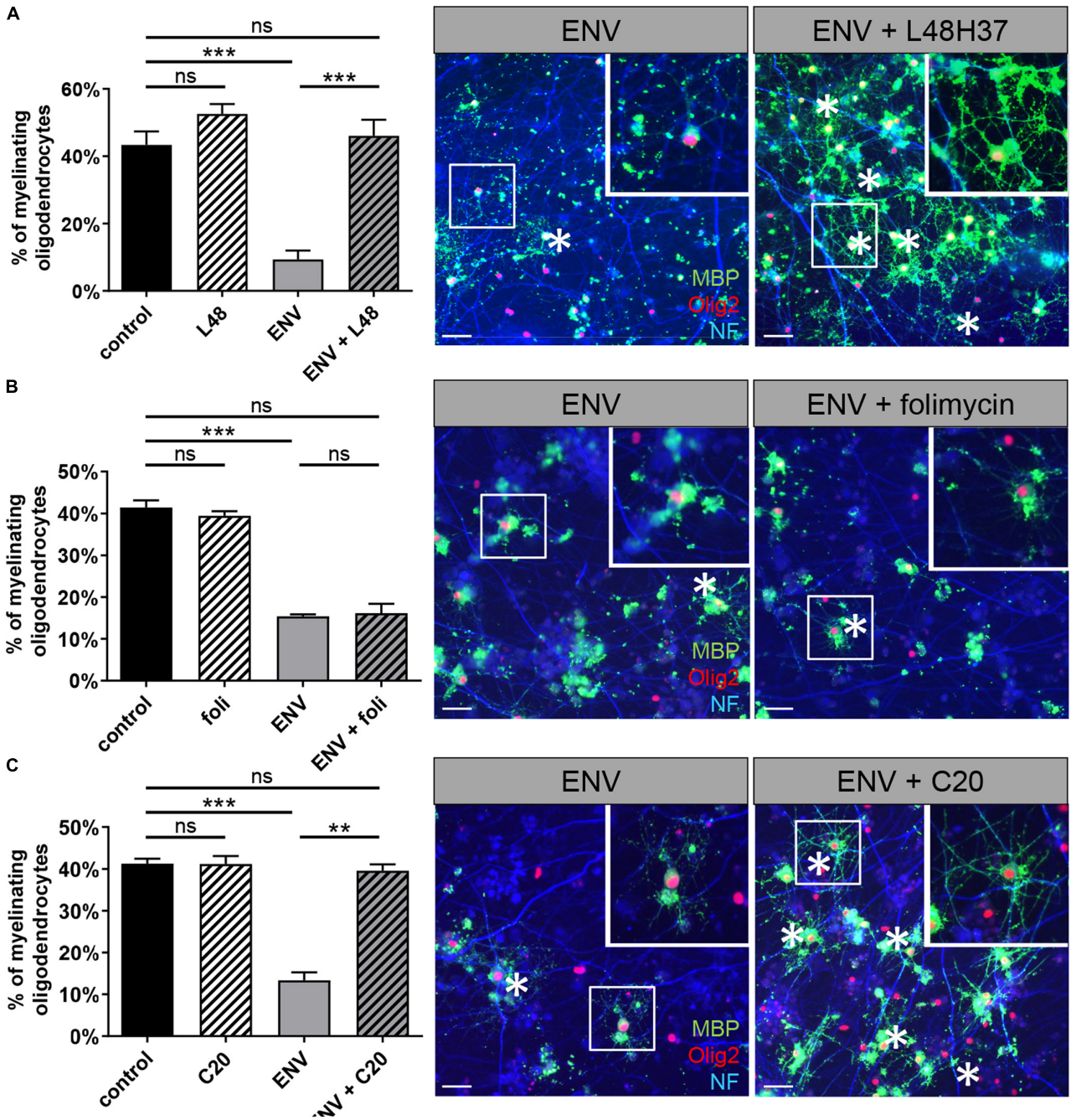

FIGURE 4 | L48H37 and compound 20-mediated rescue of ENV-dependent oligodendroglial myelinating deficits. Quantification of MBP-positive oligodendrocytes (at DIV26) upon ENV protein or ENV protein plus L48H37 **(A)**, folimycin **(B)** or compound 20 **(C)** exposure, starting at DIV17. Representative *in vitro* myelinating co-cultures displaying the rescue of myelinating oligodendrocytes (asterisks; MBP immunostaining signals in green) by means of substance application in presence of ENV protein (axons are visualized by means of NF staining in blue, cell nuclei are marked by Olig2 in red). Scale bars, 50 μM. Inserts in the top right corners correspond to enlarged fields marked by the white squares. Data are shown as mean as values, error bars represent SEM. Number of experiments: $n = 3$. Statistical significance was calculated using one-way ANOVA with Tukey post-test (ns, not significant, $^{**}p < 0.01$, $^{***}p < 0.001$). DAPI, 4′,6-diamidin-2-phenylindol; MBP, myelin basic protein; OPCs, oligodendroglial precursor cells; DMSO, dimethylsulfoxide; ENV, envelope protein.

DISCUSSION

The HERV-W ENV protein has been recognized as an MS-specific pathogenic entity, and functional evidence of its anti-regenerative/remyelinating properties has recently been collected in a clinical trial using the neutralizing antibody GNbAC1/Temelimab (Hartung et al., 2021). Fostering myelin repair in the diseased CNS still represents an unmet clinical need,

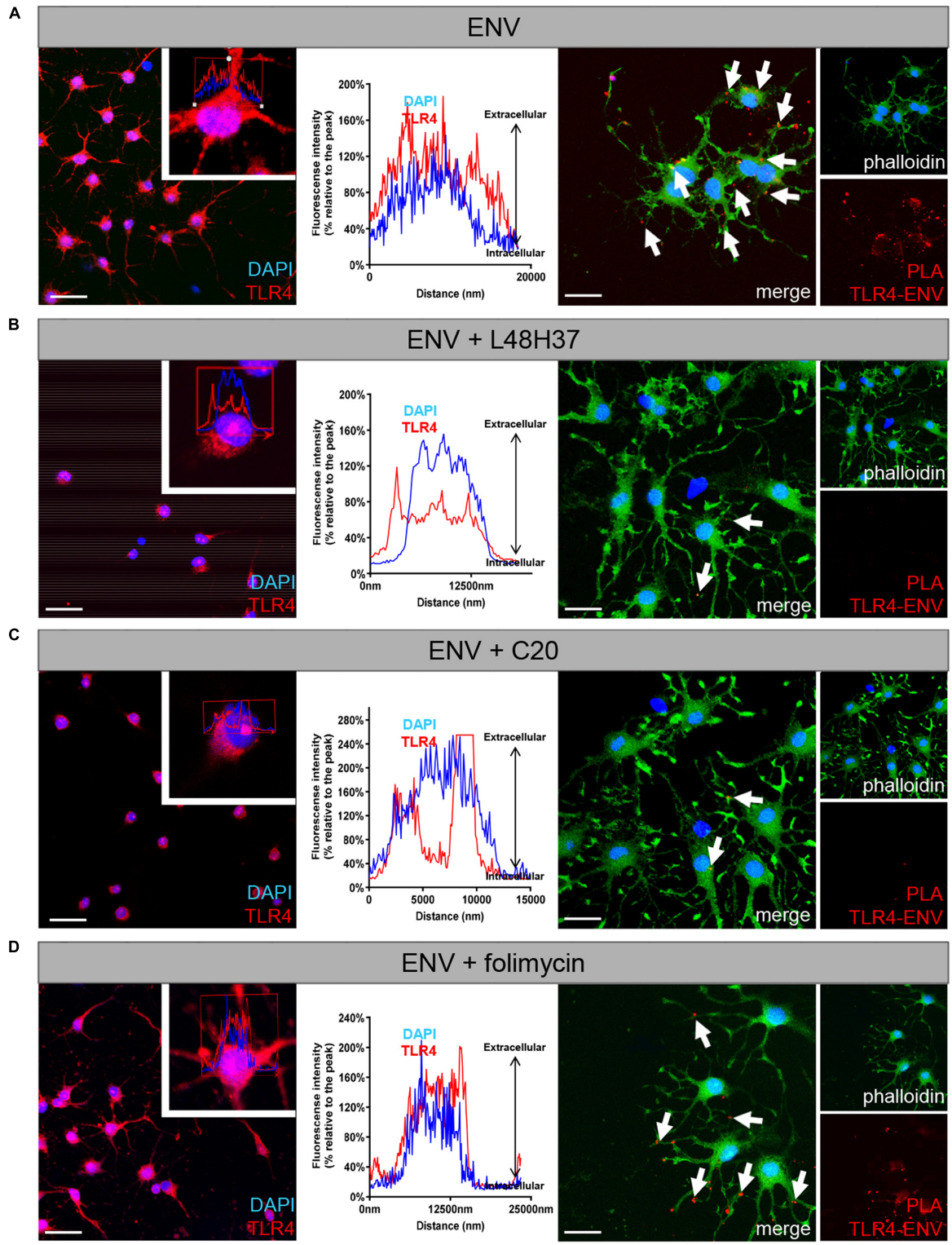

FIGURE 5 | Exposure of L48H37 and compound 20 to oligodendroglial cells affects TLR 4 surface expression. Confocal laser scanning microscopy-based intensity fluorescent peak detection for DAPI (blue) and TLR4 (red) across the cell. Experimental determination of TLR4 surface expression (red) as compared to nuclear DAPI signals following ENV protein exposure only **(A)**, in the presence of L48H37 **(B)**, in the presence of folimycin **(C)** or in the presence of compound 20 **(D)** after 1 day. L48H37 and compound 20 treated cells showed an interior distribution pattern of the receptor molecules, as compared to cells treated with ENV only or in the presence of folimycin where TLR4 was distributed over the entire surface. The normalized fluorescence intensities (% relative to the peak) of TLR4 were plotted

(Continued)

FIGURE 5 | against the distance of the analyzed area. Proximity ligation assay (PLA) of oligodendroglial cells after 1 day in culture, positive PLA events (red dots) are indicated by arrows. Positive events could be detected upon binding of ENV protein to the TLR4 receptor following exposure to recombinant ENV protein. No PLA events were detectable in the presence of ENV accompanied by L48H37 or compound 20 treatment. Phalloidin-fluorescein isothiocyanate was used to visualize cell bodies and processes. Scale bars, 30 μM. DAPI, 4′,6-diamidin-2-phenylindol; ENV, envelope protein; PLA, proximity ligation assay.

and it is therefore evident that overcoming the negative impact of ENV can potentially lead to new therapeutic approaches. We here clearly demonstrated that among the three tested TLR4 modulators, L48H37 and C20 exert potent protective/stabilizing effects regarding the severely diminished differentiation and maturation capacity of HERV-W ENV protein challenged oligodendroglial cells, and that this rescue is accompanied by a preserved mitochondrial integrity. Whereas our observation that L48H37 and C20 efficiently inhibit TLR4 surface localization is in accordance with previous studies on macrophages (Wang et al., 2015; Zhang et al., 2016). We could not detect altered surface expression upon folimycin exposure, as demonstrated within macrophages (Eswarappa et al., 2008). Interestingly, L48H37 and C20 were shown earlier to specifically target MD2, which is crucial for glycosylation, translocation, and cell surface expression of TLR4 and its subsequent activation (Ohnishi et al., 2003; Wang et al., 2015; Zhang et al., 2016). Both substances prevent the interaction of TLR4 with MD2 by binding to the hydrophobic region of the MD2 pockets (Wang et al., 2015; Zhang et al., 2016). Thus the formation of the MD2/TLR4 complex fails. But, folimycin was demonstrated in macrophages to alter intra-Golgi pH by inhibiting V-ATPase activity, which in turn results in defective processing and reduced surface expression of TLR4 (Eswarappa et al., 2008). In contrast to the V-ATPase inhibitor KM91104, which specifically targets the a3-b2 subunits of V-ATPase and found to block TLR4 surface expression in oligodendroglial cells (Göttle et al., 2019a), and folimycin binds to the v0 subunit c of V-ATPase, which apparently does not affect the signaling process to the same extent as KM91104 (Huss et al., 2002). In this respect, previous studies revealed the existence of macrophage- and microglia-specific isoforms of the vascular ATPase protein v0 subunit (Peri and Nusslein-Volhard, 2008; Xia et al., 2019), which could indeed result in cell-type specific effects of folimycin.

Hence, a specific blockade of the MD2/TLR4 complex *via* L48H37 or C20 appears more suitable to reduce TLR4 surface expression and for the desired rescue of ENV-mediated oligodendroglial inhibition than the indirect reduction of TLR4 surface expression by using folimycin-related pH alteration through inhibition of V-ATPase, at least in OPCs—so conferring a certain degree of specificity.

Given the limitations that for the human-specific pathogenic HERV-W element yet no suitable *in vivo* model exists the here presented data are limited to examinations *ex vivo*. Further studies on modulated TLR4 signaling in the context of de- and remyelination *in vivo* will be important to conduct and will depend on the generation of a suitable mouse model mimicking HERV-W activation and expression under inflammatory and demyelinating conditions. Moreover, when it comes to future treatment THAT the blood-brain barrier (BBB) still represents the major obstacle when it comes to the delivery of pharmacological substances into the brain parenchyma and its neural cells. L48H37 is an analog of curcumin, a hydrophobic polyphenol extracted from the dried rhizomes of Curcuma longa, with limited BBB penetrance, promising approaches *via* nano delivery of curcumin were recently reported to improve drug delivery (Askarizadeh et al., 2020; Motavaf et al., 2020). C20, on the other hand, as a chalcone derivate of flavonoids/isoflavonoids, is of small molecular size and its lipophilicity suggests a great BBB permeability (Thapa et al., 2021).

It is of considerable interest to note that both substances L48H37 and C20 have already been shown to exhibit protective effects and a certain therapeutic potential for neurodegenerative diseases including Alzheimer's disease (AD) and Parkinson's disease (PD) and within demyelinating mouse models, such as experimental autoimmune encephalomyelitis (EAE) and cuprizone-induced demyelination (Darvesh et al., 2012; Feng et al., 2014; Wang et al., 2015; Zhang et al., 2016; Motavaf et al., 2020). Of note, upon cuprizone-induced demyelination, Motavaf et al. (2020) suggested side/pleiotropic effects for curcumin in protecting myelinating cells *via* suppression of astrocytes and microglia.

There is increasing relevance of mitochondrial dysfunction as a major driver in neurodegenerative diseases, such as MS (Barcelos et al., 2019; Mari and Colell, 2021; Tepavcevic, 2021). In this context, also OPC differentiation into myelinating oligodendrocytes leading to myelin repair appears to be a metabolically active process (Kirischuk et al., 1995; Schoenfeld et al., 2010) the disturbance of which can contribute to myelin dysfunction, lack of repair, and neurodegeneration (Barcelos et al., 2019). The dynamic nature of their network structure is crucial for mitochondrial integrity. Mitochondria undergo two opposing processes in that they separate and merge using fission and fusion processes in response to changes in energy and stress status (Liu et al., 2020). The imbalance of this dynamic equilibrium can result in cell injury and contribute to developmental and neurodegenerative disorders (Mari and Colell, 2021). Also excessive oxidative and nitrosative stress can mediate neuronal injury, in part *via* mitochondrial fission or fragmentation. In fact, based on the morphological properties of mitochondria i.e., fission resulting in a shorter length and fewer cristae, it has been suggested to result in decreased ATP synthesis levels in oligodendroglial mitochondria (Rinholm et al., 2016). Our here described findings add to a report of cytotoxic stress within chemo-resistant glioblastoma cells mediated by related HERV-WE_1 (syncytin-1) and HERV-FRD_1 (syncytin-2) proteins and shown to trigger large-scale fission of mitochondria (Diaz-Carballo et al., 2017). Consistent with our results, Magalon et al. (2016) demonstrated that a functional interaction between mitochondrial elongation and nitrosative

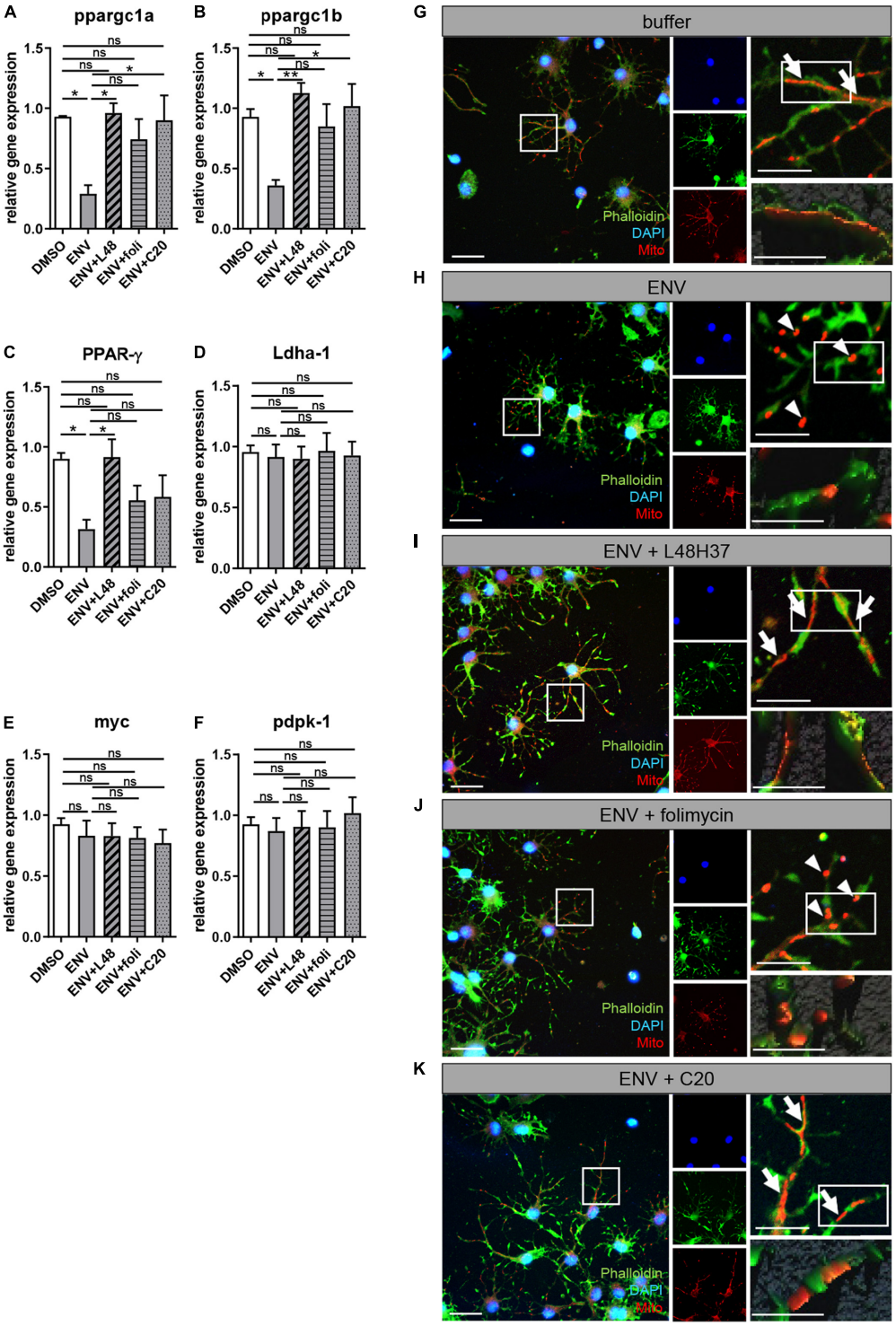

FIGURE 6 | ENV-mediated mitochondrial changes in oligodendroglial cells are rescued upon L48H37 or compound 20 treatment. **(A–F)** Quantitative RT-PCR after 1d of *PPAR-γ*, *ppargc1a*, *ppargc1b, Ldha-1*, *myc*, or *pdpk-1* revealed that ENV protein exposure led to a significant downregulation of genes related to mitochondrial homeostasis that was reversed upon L48H37 or compound 20 treatment **(A–C)**. Data are shown as mean, and error bars represent SEM. The number of experiments: $n = 4$. Statistical significance was calculated using one-way ANOVA with Tukey post-test (ns, not significant, $^{*}p < 0.05$, $^{**}p < 0.01$, and $^{***}p < 0.001$). **(G–K)** fluorescence micrographs of Mitotracker labeled mitochondria (red) in phalloidin (green) stained oligodendroglial cells exposed for 1 day to recombinant buffer **(G)**, ENV protein **(H)**, ENV protein and L48H37 **(I)**, ENV protein and folimycin **(J)** or ENV protein and compound 20 **(K)**. Scale bars for overview and upper images 50 μM. Scale bars for the detailed remaining images 20 μM. Elongated mitochondrial shape **(G,I,K)** is marked by arrows whereas fragmented mitochondrial **(H,J)** is indicated by arrowheads. ENV, envelope protein.

stress exists and contributes to oligodendrocyte maturation, as inhibition of mitochondrial fission/defragmentation led to decreased nitrosative stress levels in OPCs and promoted their maturation.

In addition, gene expression analysis revealed a significant downregulation of genes associated with the peroxisome proliferator- activated receptor gamma (PPAR-γ) signaling pathway upon ENV-protein exposure which could be rescued in presence of L48H37 or C20. Hence, we propose stabilized PPAR-γ signaling as a possible mechanism by which mitochondrial integrity is maintained. This is in accordance with previous studies, pointing to mitochondria as major targets of PPAR-γ signaling shown to protect oligodendroglial cells against nitrosative stress and accelerate oligodendrocyte maturation and maintains mitochondrial function (Bernardo et al., 2009; De Nuccio et al., 2011, 2020). This is further corroborated by the finding that curcumin is able to promote oligodendrocyte differentiation and to protect against nitrosative stress through the activation of the nuclear receptor PPAR-γ (Bernardo et al., 2021).

Collectively, these data highlight two new substances able to counteract the negative impact of HERV-W ENV protein on oligodendroglial homeostasis and suggest mitochondrial fragmentation as an important contributor to blocked OPC differentiation and myelination. Hence, the rescue of mitochondrial homeostasis and morphology following ENV-mediated nitrosative stress induction is a potentially viable and appealing therapeutic strategy in order to promote myelin repair.

CONCLUSION

The here presented study has revealed two new substances stabilizing oligodendroglial differentiation in the presence of the HERV-W ENV protein. Moreover, a completely new context regarding ENV-mediated myelination deficits was discovered and unearthed a link to mitochondrial dysfunction. Hence, despite all the efforts made in recent decades regarding myelin repair strategies, mitochondria-targeted compounds with clinical relevance could present an interesting and novel means, indicating that a deeper knowledge of the mechanisms involved within oligodendroglial homeostasis and maturation is still needed. Herein, the curcumin analog L48H37, featuring great chemical stability and enhanced anti-inflammatory properties (Wang et al., 2015), and the small molecule C20 (Zhang et al., 2016), is exciting therapeutic candidate, however, need to be approved for safety, effectiveness, and manufacturing quality in clinical settings.

DATA AVAILABILITY STATEMENT

The raw data supporting the conclusions of this article will be made available by the authors, without undue reservation.

AUTHOR CONTRIBUTIONS

PG and PK contributed to the conception and design of the study, wrote the manuscript, and contributed to funding acquisition. PG, KS, LW, and LR performed the experiments. PG, AZ, KS, and AP contributed to data analysis and interpretation. PG and KS performed the statistical analysis. PG contributed to the data visualization. AP wrote the sections of the manuscript. PK supervised the project. All authors contributed to the article and approved the submitted version.

FUNDING

The authors have been supported by the Christiane and Claudia Hempel Foundation for clinical stem cell research, Stifterverband/Novartisstiftung and the James and Elisabeth Cloppenburg, Peek and Cloppenburg Düsseldorf Stiftung. AP and AZ acknowledge support from University Hospital Düsseldorf, the German Research Foundation (DFG) (#PR1527/5-1), and the German Federal Ministry of Education and Research (BMBF) (#031L0211 and #01GM2002A).

ACKNOWLEDGMENTS

We would like to thank Brigida Ziegler, Julia Jadasz and Birgit Blomenkamp for their technical assistance. We would also like to thank Hervé Perron for providing recombinant ENV protein.

REFERENCES

Askarizadeh, A., Barreto, G. E., Henney, N. C., Majeed, M., and Sahebkar, A. (2020). Neuroprotection by curcumin: a review on brain delivery strategies. *Int. J. Pharm.* 585:119476. doi: 10.1016/j.ijpharm.2020.119476

Barcelos, I. P., Troxell, R. M., and Graves, J. S. (2019). Mitochondrial dysfunction and multiple sclerosis. *Biology* 8:37. doi: 10.3390/biology8020037

Bernardo, A., Bianchi, D., Magnaghi, V., and Minghetti, L. (2009). Peroxisome proliferator-activated receptor-gamma agonists promote differentiation and antioxidant defenses of oligodendrocyte progenitor cells. *J. Neuropathol. Exp. Neurol.* 68, 797–808. doi: 10.1097/NEN.0b013e3181aba2c1

Bernardo, A., Plumitallo, C., De Nuccio, C., Visentin, S., and Minghetti, L. (2021). Curcumin promotes oligodendrocyte differentiation and their protection against TNF-alpha through the activation of the nuclear receptor PPAR-gamma. *Sci. Rep.* 11:4952. doi: 10.1038/s41598-021-83938-y

Bertholet, A. M., Delerue, T., Millet, A. M., Moulis, M. F., David, C., Daloyau, M., et al. (2016). Mitochondrial fusion/fission dynamics in neurodegeneration and neuronal plasticity. *Neurobiol. Dis.* 90, 3–19. doi: 10.1016/j.nbd.2015.10.011

Corona, J. C., and Duchen, M. R. (2016). PPARgamma as a therapeutic target to rescue mitochondrial function in neurological disease. *Free Radic. Biol. Med.* 100, 153–163. doi: 10.1016/j.freeradbiomed.2016.06.023

Darvesh, A. S., Carroll, R. T., Bishayee, A., Novotny, N. A., Geldenhuys, W. J., and Van der Schyf, C. J. (2012). Curcumin and neurodegenerative diseases: a perspective. *Expert Opin. Investig. Drugs* 21, 1123–1140. doi: 10.1517/13543784.2012.693479

De Nuccio, C., Bernardo, A., De Simone, R., Mancuso, E., Magnaghi, V., Visentin, S., et al. (2011). Peroxisome proliferator-activated receptor gamma agonists accelerate oligodendrocyte maturation and influence mitochondrial functions and oscillatory Ca(2+) waves. *J. Neuropathol. Exp. Neurol.* 70, 900–912. doi: 10.1097/NEN.0b013e3182309ab1

De Nuccio, C., Bernardo, A., Troiano, C., Brignone, M. S., Falchi, M., Greco, A., et al. (2020). NRF2 and PPAR-gamma pathways in oligodendrocyte progenitors: focus on ROS protection, mitochondrial biogenesis and promotion of cell differentiation. *Int. J. Mol. Sci.* 21:7216. doi: 10.3390/ijms2119 7216

Diaz-Carballo, D., Klein, J., Acikelli, A. H., Wilk, C., Saka, S., Jastrow, H., et al. (2017). Cytotoxic stress induces transfer of mitochondria-associated human endogenous retroviral RNA and proteins between cancer cells. *Oncotarget* 8, 95945–95964. doi: 10.18632/oncotarget.21606

Eswarappa, S. M., Basu, N., Joy, O., and Chakravortty, D. (2008). Folimycin (concanamycin A) inhibits LPS-induced nitric oxide production and reduces surface localization of TLR4 in murine macrophages. *Innate Immun.* 14, 13–24. doi: 10.1177/1753425907087349

Feng, J., Tao, T., Yan, W., Chen, C. S., and Qin, X. (2014). Curcumin inhibits mitochondrial injury and apoptosis from the early stage in EAE mice. *Oxid. Med. Cell Longev.* 2014:728751. doi: 10.1155/2014/728751

Franklin, R. J. M., and Ffrench-Constant, C. (2017). Regenerating CNS myelin - from mechanisms to experimental medicines. *Nat. Rev. Neurosci.* 18, 753–769. doi: 10.1038/nrn.2017.136

Franklin, R. J., and Ffrench-Constant, C. (2008). Remyelination in the CNS: from biology to therapy. *Nat. Rev. Neurosci.* 9, 839–855. doi: 10.1038/nrn2480

Gensert, J. M., and Goldman, J. E. (1997). Endogenous progenitors remyelinate demyelinated axons in the adult CNS. *Neuron* 19, 197–203. doi: 10.1016/s0896-6273(00)80359-1

Göttle, P., Förster, M., Weyers, V., Küry, P., Rejdak, K., Hartung, H. P., et al. (2019b). An unmet clinical need: roads to remyelination in MS. *Neurol. Res. Pract.* 1:21. doi: 10.1186/s42466-019-0026-0

Göttle, P., Förster, M., Gruchot, J., Kremer, D., Hartung, H. P., Perron, H., et al. (2019a). Rescuing the negative impact of human endogenous retrovirus envelope protein on oligodendroglial differentiation and myelination. *Glia* 67, 160–170. doi: 10.1002/glia.23535

Göttle, P., Kremer, D., Jander, S., Odemis, V., Engele, J., Hartung, H. P., et al. (2010). Activation of CXCR7 receptor promotes oligodendroglial cell maturation. *Ann. Neurol.* 68, 915–924. doi: 10.1002/ana.22214

Göttle, P., Manousi, A., Kremer, D., Reiche, L., Hartung, H. P., and Küry, P. (2018). Teriflunomide promotes oligodendroglial differentiation and myelination. *J. Neuroinflamm.* 15:76. doi: 10.1186/s12974-018-1110-z

Göttle, P., Sabo, J. K., Heinen, A., Venables, G., Torres, K., Tzekova, N., et al. (2015). Oligodendroglial maturation is dependent on intracellular protein shuttling. *J. Neurosci.* 35, 906–919. doi: 10.1523/JNEUROSCI.1423-14.2015

Hartung, H. P., Derfuss, T., Cree, B. A., Sormani, M. P., Selmaj, K., Stutters, J., et al. (2021). Efficacy and safety of temelimab in multiple sclerosis: results of a randomized phase 2b and extension study. *Mult. Scler.* doi: 10.1177/ 13524585211024997. Online ahead of print.

Huss, M., Ingenhorst, G., Konig, S., Gassel, M., Drose, S., Zeeck, A., et al. (2002). Concanamycin A, the specific inhibitor of V-ATPases, binds to the V(o) subunit c. *J. Biol. Chem.* 277, 40544–40548. doi: 10.1074/jbc.M207345200

Kirischuk, S., Neuhaus, J., Verkhratsky, A., and Kettenmann, H. (1995). Preferential localization of active mitochondria in process tips of immature retinal oligodendrocytes. *Neuroreport* 6, 737–741. doi: 10.1097/00001756-199503270-00008

Kremer, D., Aktas, O., Hartung, H. P., and Küry, P. (2011). The complex world of oligodendroglial differentiation inhibitors. *Ann. Neurol.* 69, 602–618. doi: 10.1002/ana.22415

Kremer, D., Förster, M., Schichel, T., Göttle, P., Hartung, H. P., Perron, H., et al. (2015). The neutralizing antibody GNbAC1 abrogates HERV-W envelope protein-mediated oligodendroglial maturation blockade. *Mult. Scler.* 21, 1200–1203. doi: 10.1177/1352458514560926

Kremer, D., Göttle, P., Flores-Rivera, J., Hartung, H. P., and Küry, P. (2019a). Remyelination in multiple sclerosis: from concept to clinical trials. *Curr. Opin. Neurol.* 32, 378–384. doi: 10.1097/WCO.0000000000000692

Kremer, D., Gruchot, J., Weyers, V., Oldemeier, L., Göttle, P., Healy, L., et al. (2019b). pHERV-W envelope protein fuels microglial cell-dependent damage of myelinated axons in multiple sclerosis. *Proc. Natl. Acad. Sci. U.S.A.* 116, 15216–15225. doi: 10.1073/pnas.1901283116

Kremer, D., Schichel, T., Förster, M., Tzekova, N., Bernard, C., van der Valk, P., et al. (2013). Human endogenous retrovirus type W envelope protein inhibits oligodendroglial precursor cell differentiation. *Ann. Neurol.* 74, 721–732. doi: 10.1002/ana.23970

Kuhlmann, T., Miron, V., Cui, Q., Wegner, C., Antel, J., and Bruck, W. (2008). Differentiation block of oligodendroglial progenitor cells as a cause for remyelination failure in chronic multiple sclerosis. *Brain* 131(Pt .7), 1749–1758. doi: 10.1093/brain/awn096

Küry, P., Nath, A., Creange, A., Dolei, A., Marche, P., Gold, J., et al. (2018). Human endogenous retroviruses in neurological diseases. *Trends Mol. Med.* 24, 379–394. doi: 10.1016/j.molmed.2018.02.007

Lan, M., Tang, X., Zhang, J., and Yao, Z. (2018). Insights in pathogenesis of multiple sclerosis: nitric oxide may induce mitochondrial dysfunction of oligodendrocytes. *Rev. Neurosci.* 29, 39–53. doi: 10.1515/revneuro-2017-0033

Lassmann, H. (2018). Multiple sclerosis pathology. *Cold Spring Harb. Perspect. Med.* 8:a028936. doi: 10.1101/cshperspect.a028936

Liu, Y. J., McIntyre, R. L., Janssens, G. E., and Houtkooper, R. H. (2020). Mitochondrial fission and fusion: a dynamic role in aging and potential target for age-related disease. *Mech. Ageing Dev.* 186:111212. doi: 10.1016/j.mad.2020.111212

Magalon, K., Le Grand, M., El Waly, B., Moulis, M., Pruss, R., Bordet, T., et al. (2016). Olesoxime favors oligodendrocyte differentiation through a functional interplay between mitochondria and microtubules. *Neuropharmacology* 111, 293–303. doi: 10.1016/j.neuropharm.2016.09.009

Maiuolo, J., Gliozzi, M., Musolino, V., Carresi, C., Nucera, S., Scicchitano, M., et al. (2020). Environmental and nutritional "Stressors" and oligodendrocyte dysfunction: role of mitochondrial and endoplasmatic reticulum impairment. *Biomedicines* 8:553. doi: 10.3390/biomedicines8120553

Manousi, A., Göttle, P., Reiche, L., Cui, Q. L., Healy, L. M., Akkermann, R., et al. (2021). Identification of novel myelin repair drugs by modulation of oligodendroglial differentiation competence. *EBioMedicine* 65:103276. doi: 10.1016/j.ebiom.2021.103276

Mari, M., and Colell, A. (2021). Mitochondrial oxidative and nitrosative stress as a therapeutic target in diseases. *Antioxidants* 10:314. doi: 10.3390/antiox10020314

Motavaf, M., Sadeghizadeh, M., Babashah, S., Zare, L., and Javan, M. (2020). Protective effects of a nano-formulation of curcumin against cuprizone-induced demyelination in the mouse corpus callosum. *Iran J. Pharm. Res.* 19, 310–320. doi: 10.22037/ijpr.2020.112952.14033

Ohgaki, R., Teramura, Y., Hayashi, D., Quan, L., Okuda, S., Nagamori, S., et al. (2017). Ratiometric fluorescence imaging of cell surface pH by poly(ethylene glycol)-phospholipid conjugated with fluorescein isothiocyanate. *Sci. Rep.* 7:17484. doi: 10.1038/s41598-017-17459-y

Ohnishi, T., Muroi, M., and Tanamoto, K. (2003). MD-2 is necessary for the toll-like receptor 4 protein to undergo glycosylation essential for its translocation to the cell surface. *Clin. Diagn. Lab. Immunol.* 10, 405–410. doi: 10.1128/cdli.10.3.405-410.2003

Pang, Y., Zheng, B., Kimberly, S. L., Cai, Z., Rhodes, P. G., and Lin, R. C. (2012). Neuron-oligodendrocyte myelination co-culture derived from embryonic rat spinal cord and cerebral cortex. *Brain Behav.* 2, 53–67. doi: 10.1002/brb3.33

Peri, F., and Nusslein-Volhard, C. (2008). Live imaging of neuronal degradation by microglia reveals a role for v0-ATPase a1 in phagosomal fusion in vivo. *Cell* 133, 916–927. doi: 10.1016/j.cell.2008.04.037

Rinholm, J. E., Vervaeke, K., Tadross, M. R., Tkachuk, A. N., Kopek, B. G., Brown, T. A., et al. (2016). Movement and structure of mitochondria in oligodendrocytes and their myelin sheaths. *Glia* 64, 810–825. doi: 10.1002/glia.22965

Saitoh, S., and Miyake, K. (2006). Mechanism regulating cell surface expression and activation of Toll-like receptor 4. *Chem. Rec.* 6, 311–319. doi: 10.1002/tcr.20093

Schoenfeld, R., Wong, A., Silva, J., Li, M., Itoh, A., Horiuchi, M., et al. (2010). Oligodendroglial differentiation induces mitochondrial genes and inhibition of mitochondrial function represses oligodendroglial differentiation. *Mitochondrion* 10, 143–150. doi: 10.1016/j.mito.2009.12.141

Simons, M., and Nave, K. A. (2015). Oligodendrocytes: myelination and axonal support. *Cold Spring Harb. Perspect. Biol.* 8:a020479. doi: 10.1101/cshperspect.a020479

Soderberg, O., Gullberg, M., Jarvius, M., Ridderstrale, K., Leuchowius, K. J., Jarvius, J., et al. (2006). Direct observation of individual endogenous protein complexes in situ by proximity ligation. *Nat. Methods* 3, 995–1000. doi: 10.1038/nmeth947

Tepavcevic, V. (2021). Oligodendroglial energy metabolism and (re)myelination. *Life* 11:238. doi: 10.3390/life11030238

Thapa, P., Upadhyay, S. P., Suo, W. Z., Singh, V., Gurung, P., Lee, E. S., et al. (2021). Chalcone and its analogs: therapeutic and diagnostic applications

in Alzheimer's disease. *Bioorg. Chem.* 108:104681. doi: 10.1016/j.bioorg.2021.104681

Tripathi, R. B., Rivers, L. E., Young, K. M., Jamen, F., and Richardson, W. D. (2010). NG2 glia generate new oligodendrocytes but few astrocytes in a murine experimental autoimmune encephalomyelitis model of demyelinating disease. *J. Neurosci.* 30, 16383–16390. doi: 10.1523/JNEUROSCI.3411-10.2010

Wang, Y., Shan, X., Dai, Y., Jiang, L., Chen, G., Zhang, Y., et al. (2015). Curcumin analog L48H37 prevents lipopolysaccharide-induced TLR4 signaling pathway activation and sepsis via targeting MD2. *J. Pharmacol. Exp. Ther.* 353, 539–550.

Xia, Y., Liu, N., Xie, X., Bi, G., Ba, H., Li, L., et al. (2019). The macrophage-specific V-ATPase subunit ATP6V0D2 restricts inflammasome activation and bacterial infection by facilitating autophagosome-lysosome fusion. *Autophagy* 15, 960–975. doi: 10.1080/15548627.2019.1569916

Yeligar, S. M., Kang, B. Y., Bijli, K. M., Kleinhenz, J. M., Murphy, T. C., Torres, G., et al. (2018). PPARgamma regulates mitochondrial structure and function and human pulmonary artery smooth muscle cell proliferation. *Am. J. Respir. Cell Mol. Biol.* 58, 648–657. doi: 10.1165/rcmb.2016-0293OC

Zhang, Y., Wu, J., Ying, S., Chen, G., Wu, B., Xu, T., et al. (2016). Discovery of new MD2 inhibitor from chalcone derivatives with anti-inflammatory effects in LPS-induced acute lung injury. *Sci .Rep.* 6:25130. doi: 10.1038/srep25130

Conflict of Interest: PK received consulting, travel, congress grants from GeNeuro SA, Sanofi, and Servier. PG performed consultancy work for GeNeuro SA.

The remaining authors declare that the research was conducted in the absence of any commercial or financial relationships that could be construed as a potential conflict of interest.

Publisher's Note: All claims expressed in this article are solely those of the authors and do not necessarily represent those of their affiliated organizations, or those of the publisher, the editors and the reviewers. Any product that may be evaluated in this article, or claim that may be made by its manufacturer, is not guaranteed or endorsed by the publisher.

Copyright © 2021 Göttle, Schichel, Reiche, Werner, Zink, Prigione and Küry. This is an open-access article distributed under the terms of the Creative Commons Attribution License (CC BY). The use, distribution or reproduction in other forums is permitted, provided the original author(s) and the copyright owner(s) are credited and that the original publication in this journal is cited, in accordance with accepted academic practice. No use, distribution or reproduction is permitted which does not comply with these terms.

frontiers in Cellular Neuroscience

ORIGINAL RESEARCH
published: 10 January 2022
doi: 10.3389/fncel.2021.801704

Smoothened/AMP-Activated Protein Kinase Signaling in Oligodendroglial Cell Maturation

Alice Del Giovane[1], Mariagiovanna Russo[2], Linda Tirou[2], Hélène Faure[2], Martial Ruat[2], Sonia Balestri[1], Carola Sposato[1], Francesco Basoli[3], Alberto Rainer[3,4], Abdelmoumen Kassoussi[5], Elisabeth Traiffort[5†] and Antonella Ragnini-Wilson[1*†]*

[1] Department of Biology, University of Rome "Tor Vergata", Rome, Italy, [2] CNRS, Institut des Neurosciences Paris-Saclay, Université Paris-Saclay, Saclay, France, [3] Department of Engineering, Università Campus Bio-Medico di Roma, Rome, Italy, [4] Institute of Nanotechnology (NANOTEC), National Research Council, Lecce, Italy, [5] INSERM, U1195, Université Paris-Saclay, Le Kremlin-Bicêtre, France

OPEN ACCESS

Edited by:
Davide Lecca,
University of Milan, Italy

Reviewed by:
Jinwei Zhang,
University of Exeter, United Kingdom
Greg J. Duncan,
Oregon Health and Science University, United States

***Correspondence:**
Elisabeth Traiffort
elisabeth.traiffort@inserm.fr
Antonella Ragnini-Wilson
antonella.ragnini@uniroma2.it

† These authors share last authorship

Specialty section:
This article was submitted to Non-Neuronal Cells, a section of the journal Frontiers in Cellular Neuroscience

Received: *25 October 2021*
Accepted: *29 November 2021*
Published: *10 January 2022*

Citation:
Del Giovane A, Russo M, Tirou L, Faure H, Ruat M, Balestri S, Sposato C, Basoli F, Rainer A, Kassoussi A, Traiffort E and Ragnini-Wilson A (2022) Smoothened/AMP-Activated Protein Kinase Signaling in Oligodendroglial Cell Maturation. Front. Cell. Neurosci. 15:801704. doi: 10.3389/fncel.2021.801704

The regeneration of myelin is known to restore axonal conduction velocity after a demyelinating event. Remyelination failure in the central nervous system contributes to the severity and progression of demyelinating diseases such as multiple sclerosis. Remyelination is controlled by many signaling pathways, such as the Sonic hedgehog (Shh) pathway, as shown by the canonical activation of its key effector Smoothened (Smo), which increases the proliferation of oligodendrocyte precursor cells *via* the upregulation of the transcription factor Gli1. On the other hand, the inhibition of Gli1 was also found to promote the recruitment of a subset of adult neural stem cells and their subsequent differentiation into oligodendrocytes. Since Smo is also able to transduce Shh signals *via* various non-canonical pathways such as the blockade of Gli1, we addressed the potential of non-canonical Smo signaling to contribute to oligodendroglial cell maturation in myelinating cells using the non-canonical Smo agonist GSA-10, which downregulates Gli1. Using the Oli-neuM cell line, we show that GSA-10 promotes Gli2 upregulation, MBP and MAL/OPALIN expression *via* Smo/AMP-activated Protein Kinase (AMPK) signaling, and efficiently increases the number of axonal contact/ensheathment for each oligodendroglial cell. Moreover, GSA-10 promotes the recruitment and differentiation of oligodendroglial progenitors into the demyelinated corpus callosum *in vivo*. Altogether, our data indicate that non-canonical signaling involving Smo/AMPK modulation and Gli1 downregulation promotes oligodendroglia maturation until axon engagement. Thus, GSA-10, by activation of this signaling pathway, represents a novel potential remyelinating agent.

Keywords: remyelinating drugs, oligodendrocyte, differentiation, multiple sclerosis, hedgehog signaling

INTRODUCTION

Myelin regeneration or remyelination is a fundamental repair process in the central nervous system (CNS) that is activated during pathological demyelinating events in both animal models of demyelination and humans suffering from multiple sclerosis (MS), the most common demyelinating disease of the CNS. Such spontaneous regenerative responses are observed during

the early stages of the disease. However, remyelination ultimately fails in late steps, leading to loss of metabolic support normally provided by myelin to axons and, subsequently, axon degeneration and irreversible neurological disabilities. Therefore, pharmacologically induced remyelination represents great hope for CNS regenerative medicine in the context of demyelinating pathologies (Franklin and Ffrench-Constant, 2017; Plemel et al., 2017; Traiffort et al., 2020; Balestri et al., 2021; Franklin et al., 2021).

Several potential remyelinating drug candidates have been identified and are presently awaiting clinical confirmation. Further development of remyelinating therapies depends on better understanding of the mechanisms and targets that regulate myelin production. The main focus of drug discovery in CNS remyelination, thus far, has been to identify drugs that regulate myelin regenerative processes either at the level of neural progenitor cell (NPC) niches or by promoting the differentiation of oligodendrocyte precursor cells (OPCs) into oligodendrocytes (OLs) (Plemel et al., 2017; Gregath and Lu, 2018; Melchor et al., 2019; Balestri et al., 2021). Indeed, in the mouse dorsal forebrain, myelin regeneration results from OLs arising from both NPCs present in a specific germinative area called the subventricular zone (SVZ), and parenchymal OPCs (Nait-Oumesmar et al., 1999, 2008; Menn et al., 2006; Xing et al., 2014; Brousse et al., 2015). In humans, several lines of evidence also support the existence of different sources of OLs. These include the much higher turnover rate of OLs in normal-appearing white matter from MS patients than in the CNS from healthy subjects (Yeung et al., 2019), and identification of NSCs that may be recruited and fated to the oligodendroglial lineage in the human SVZ (Samanta et al., 2015). The recruitment of these various cell subsets in the site of lesion and their respective contribution to the remyelination process remain to be clarified. Moreover, in addition to the newly generated OPCs, resident OLs also appear to participate in remyelination (Franklin and Ffrench-Constant, 2017; Jäkel et al., 2019; Yeung et al., 2019).

Several promyelinating compounds have been selected in phenotypical screens based on identifying drugs upregulating MBP expression in primary OPC cultures (Deshmukh et al., 2013; Mei et al., 2014; Lariosa-Willingham et al., 2016), in epiblast stem cell-derived OPCs (Najm et al., 2015), and Oli-neuM oligodendroglial cells that stably express the gene encoding the myelin regulatory factor (MyRF) (Porcu et al., 2015). Network analysis and molecular studies have shown that the drugs identified by these screens largely overlap in their target specificity, possibly indicating a limited number of factors regulating remyelination processes (Melchor et al., 2019; Lubetzki et al., 2020; Balestri et al., 2021). Interestingly, the promyelinating drugs identified either inhibit a restricted number of cholesterol biosynthetic enzymes [e.g., emopamil-binding protein (EBP) and TM7F2 (Hubler et al., 2018; Allimuthu et al., 2019], or act *via* other targets including glucocorticoid (GR) and Smoothened (Smo) receptors (Najm et al., 2015; Porcu et al., 2015; Nocita et al., 2019). The recent finding that EBP binds to Smo and inhibits its cholesterylation independently of D8-D7 sterol isomerase activity (Qiu et al., 2021) supports the role for Smo receptor modulation in OPC maturation. However, how such Smo activity might transduce its signal to the OPC differentiation process remains unclear.

The seven-pass transmembrane Smo receptor is a well-characterized component of the Sonic Hedgehog (Shh) signaling pathway involved in both proliferation and differentiation in the embryo and early postnatal tissues (Ruat et al., 2015). In the adult brain, the delivery of exogenous Shh has been shown previously to regulate the number of oligodendroglial cells in the cerebral cortex and corpus callosum (Loulier et al., 2006), while Shh transcription has been detected in a subset of mature oligodendrocytes (Tirou et al., 2020). Smo is the key transducer of Shh signaling that is activated when Shh binds to its receptor Patched (Ptc). In the canonical pathway, Smo activation initiates a complex downstream signaling cascade resulting in the expression of glioma-associated factor 1 (Gli1) and, ultimately, transcription of Shh target genes (Petrova and Joyner, 2014; Ruat et al., 2014; Niewiadomski et al., 2019). Gli factors (Gli1-3) constitute an interconnected network of tightly correlated proteins, such as Gli2 and Gli3, which act both as activators and repressors, regulate Gli1 and each other's expression. Moreover, Gli2 levels have been shown to correlate with decreased levels of Gli1 expression (Schmidt-Heck et al., 2015; Arensdorf et al., 2016), and promyelinating drugs, such as Clobetasol and gefitinib, upregulate Gli2 transcription (Nocita et al., 2019).

During the process of myelin regeneration, Shh/Smo signaling was found to be reactivated in demyelinating lesions. Shh signaling appeared as a positive regulator of parenchymal OPC proliferation and differentiation (Ferent et al., 2013; Sanchez and Armstrong, 2018; Laouarem et al., 2021). On the other hand, the pathway regulates NPC proliferation in the SVZ from healthy adult mice (Ferent et al., 2014; Daynac et al., 2016), whereas blockade of Gli1 is necessary to recruit a subset of NPCs that exclusively differentiate into oligodendroglial cells in mouse models of CNS demyelination (Samanta et al., 2015; Radecki et al., 2020). However, the finding that promyelinating drugs, such as Clobetasol, Halcinonide, and Flurandrenolide (Porcu et al., 2015), target GR (Najm et al., 2015) and, modulate Smo (Wang et al., 2010) and Gli2 activity (Nocita et al., 2019) in oligodendroglial cells raises the question of how Smo modulation might regulate oligodendroglial maturation.

Since Smo has also been reported to transduce Shh signaling *via* non-canonical pathways, mostly unrelated to Gli-mediated transcription (Yam and Charron, 2013; Ruat et al., 2014; Ferent and Traiffort, 2015; Schmidt-Heck et al., 2015; Sharpe et al., 2015; Akhshi and Trimble, 2021), here, we investigated the promyelinating capacity of the recently developed Smo-binding compound GSA-10 [propyl 4-(1-hexyl-4-hydroxy-2-oxo-1,2-dihydroquinoline-3-carboxamido) benzoate] (Gorojankina et al., 2013; Fleury et al., 2016). GSA-10 was previously identified in a Smo pharmacophore-based virtual screen (Gorojankina et al., 2013; Fleury et al., 2016) and belongs to a new family of Smo agonists endowed with non-canonical Shh signaling properties associated with Gli1 inhibition (Gorojankina et al., 2013; Fleury et al., 2016; Manetti et al., 2016). We compared the activity of GSA-10 in Oli-neuM differentiation with the activity of SAG,

the reference Smo agonist (Wang et al., 2010; Kim et al., 2013), and Clobetasol, a GR compound that modulates Smo receptor activity (Wang et al., 2010) and promotes oligodendroglial cell differentiation (Najm et al., 2015; Porcu et al., 2015; Nocita et al., 2019). These compounds were used alone or in combination with Smo gene silencing to determine their Smo-mediated activity in the Oli-neuM cell line. By stably expressing MyRF, Oli-neuM cells differentiate into myelinating cells able to engage artificial axons in the presence of promyelinating stimuli (Porcu et al., 2015; Nocita et al., 2019). Moreover, we performed a stereotactic injection of lysophosphatidylcholine (LPC or lysolecithin) into the corpus callosum of mouse brain to determine GSA-10 efficacy in OPC recruitment toward a demyelinated lesion. Altogether, our data provide evidence that GSA-10 belongs to a novel class of Smo modulators that activate non-canonical signaling leading to Gli2 upregulation and AMPK activation, promoting MBP expression and opening new perspectives in remyelinating therapies.

MATERIALS AND METHODS

Lysophosphatidylcholine Injection

Adult C57Bl/6 mice (Glast-CreERT2R26R-YFP, 10 weeks old) were used. The animal experiments were performed in accordance with the Council Directive 2010/63EU of the European Parliament and approved by the French ethic committees (CEEA59 and CEEA26). LPC-induced demyelination was carried out as previously described (Ferent et al., 2013) under ketamine (100 mg/kg)/xylazine (10 mg/kg)-induced anesthesia. The injection was performed at the following coordinates (to the bregma): anteroposterior (AP) +1 mm, lateral +1 mm, dorsoventral (DV) −2.2 mm. GSA-10 (100 μM) was co-injected with LPC. The mice were sacrificed 5 days post lesion (dpl). The brain was removed and frozen in liquid nitrogen, and cryostat sections (14 μm) were cut.

Immunofluorescence in Lysophosphatidylcholine-Treated Mice

The mice, under deep anesthesia, were perfused with 4% paraformaldehyde. Brain sections were cut in the cryostat (14 μm). For immunostaining, the sections were incubated for 1 h in PBS, 0.25% Triton, and 1% BSA. Primary antibodies were incubated overnight at 4°C: rabbit anti-NG2 (1/300, AB5320; Millipore; Saint-Quentin Fallavier, France), mouse anti-GFAP (1/400, MAB360; Millipore), rabbit anti-Olig2 (1/400, AB9610; Millipore), mouse anti-S100β (1/500, AB66028; Abcam, Amsterdam, The Netherlands), mouse anti-adenomatous polyposis coli (APC) (1/600, clone CC1, OP80; Millipore), rabbit anti-Iba1 (1/500, 234003; Synaptic Systems, Uden, The Netherlands), mouse anti-Ki67 (1/200, 550609; BD Pharmigen, Le Pont de Claix, France), and mouse anti-Sox2 (1/100, MAB2018; R&D Systems, Lille, France). The sections were incubated with appropriate secondary antibody (1/200 to 1/400; Millipore, Jackson IR, Montluçon, France) for 2 h at room temperature. Staining was replicated on three or four mice. Images were acquired with a 40X objective (N.A. 0.75) using a fluorescence microscope (Leica DM2000; Leica, Wetzlar, Germany). The images were analyzed and reconstructed with ImageJ 1.39t (Freeware; NIH, New York, NY, United States).

Cell Counting

Lysophosphatidylcholine-induced demyelination and cell count were evaluated on coronal sections obtained at the level of the lateral ventricles of 3–5 mice. Cells displaying an immunofluorescent-positive signal were counted once the extent of the demyelination had been established based on decrease in CC1 fluorescence (Bin et al., 2016) or high nuclear density. This area has been measured for each lesion and expressed in square millimeters. The quantification of antigen positive cells was expressed as percentage of the total number of DAPI-positive nuclei or as number of cells per square millimeters. The number of counted cells per lesion ranged between 500 and 6000 for DAPI-positive nuclei, 90 and 270 for $Olig2^+$, 65 and 276 for $Sox2^+$, 28 and 134 for $NG2^+$, 9 and 153 for $Ki67^+$, 126 and 278 for $GFAP^+$, 47 and 158 for $S100\beta^+$, and 131 and 359 for $Iba1^+$ cells. Counting of co-localized staining was performed using ROI and multi-point ImageJ tools. Quantitative data were expressed as the mean ± standard error of the mean (SEM). Comparisons between two independent experimental groups were made by unpaired Student's *t*-test, two-tailed. A value of $p < 0.05$ was considered statistically significant. Graphs were drawn using GraphPad Prism 5.2 (GraphPad Software, Inc.).

Cell Culture

The Oli-neuM line (Cellosaurus ExPASy CVCL_VL76) was obtained and cultured as previously described (Porcu et al., 2015; Nocita et al., 2019), and routinely tested for contamination. The cells have been stably transfected with MyrF whose upregulation is routinely checked at each thawing in order to consistently use cells displaying MyrF at comparable levels (Porcu et al., 2015). Growth medium (GM) is based on DMEM (Corning Inc., New York, NY, United States) supplemented with 10% fetal bovine serum (FBS; Corning Inc., New York, NY, United States), 2 mM l-glutamine (Gibco™; Thermo Fisher Scientific, Waltham, MA, United States), 1% pen-strep (Gibco™), 1 mM sodium pyruvate (Gibco™), and 15 mM HEPES (Sigma-Aldrich, Merck KGaA, Darmstadt, Germany). The cells were maintained during growth and differentiation at 37°C in 5% CO2. A differentiation medium (DM) was GM supplemented with 1% N2 supplement (175020–01, Gibco™), 60 nM triiodothyronine (T3; Sigma-Aldrich), and 53.7 ng/ml progesterone (Sigma-Aldrich). The Oli-neuM cells were maintained under antibiotic selection with 500 μg/ml geneticin (G418, Gibco™) during both growth and differentiation.

Compound Treatments

GSA-10 was purchased from Asinex and diluted in dimethyl sulfoxide (DMSO), stock concentration 2.5 mM, and used at a concentration of 10 μM after dose-response selection. Clobetasol (Prestw-781) was purchased from Prestwick Chemical Library®[1].

[1]http://www.prestwickchemical.com/prestwick-chemical-library.html

Drug stock 100 mM was diluted and used at the optimal final concentration of 10 μM (Porcu et al., 2015). SAG, Smo canonical agonist (Wang et al., 2010), was purchased from Sigma Aldrich (566660); stock and final concentrations used were, respectively, 100 and 5 μM. The final concentration was determined by dose-response analysis (data not shown). Dorsomorphin, a potent and selective AMPK inhibitor (Meley et al., 2006), was purchased from Selleckchem.com (S7306), stock concentration was 100 mM, and the concentration used was 3 μM. Dorsomorphin was solubilized in water. To obtain an equal solvent concentration, 0.5% DMSO was added in DM + dorsomorphin treatments to make drugs comparable. All the other drugs were dissolved in DMSO, used as vehicle treatment without exceeding 0.5% of the final volume. Unless otherwise stated, drug treatments were administrated in differentiation media (DM) for 48 h after 24 h from Oli-neuM seeding for fixation (IF); after 48 h from Oli-neuM seeding for protein and RNA extractions (IB and qPCR, respectively). We refer to "vehicle treatment" as the combination of DM and 0.5% DMSO max (DM + DMSO). Culturing and time of drug treatments (48 h) have been established previously to be optimal for MBP expression in Oli-neuM (Porcu et al., 2015; Nocita et al., 2019). For microfiber engage analysis, the cells were treated for 72 h according to previous established growth conditions (Nocita et al., 2019).

Smoothened Silencing and Oli-neuM Infection

Lentiviral particles were produced by a lentivector production facility (SFR BioSciences Gerland; Lyon Sud, UMS3444/US8) from pLKO.1 plasmid-expressing shRNA targeting Smo (TRCN0000026245, MISSION®, Sigma), or a pLKO.1 control vector expressing nonrelevant shRNA (Gorojankina et al., 2013). For lentiviral infection, Oli-neuM cells were seeded into 12-well plates and infected after 24 h with the lentiviral particles at a multiplicity of infection of 5, in the presence of 8 μg/ml polybrene (Sigma). Puromycin (6 μg/ml) was used to select stable Oli-neuM shSmo and shControl clones, which were further allowed to differentiate, as described above. SybrGreen real-time qPCR using primers listed below in qPCR section, and IF image quantitative assay analyzing Smo expression in vehicle-treated or SAG-treated Oli-neuM shSmo vs. ShControl was used to validate knockdown efficiencies in at least 3 independent experiments.

Crude Extract Preparation and Immunoblot Analysis

Typically, 2.75×10^5 Oli-neuM cells were seeded in 6-well plates in GM media, and cells were grown to 70% confluence. Treatments, unless otherwise specified, were performed for 48 h in DM. For immunoblot analyses, the following antibodies diluted in TBS and 4% BSA were used: anti-actin (#A2066, 1:2000; Sigma-Aldrich); AbD Serotec (Bio-Rad Laboratories, Hercules, CA, United States): anti-MBP (MCA409S, 1:200); cell signaling: anti-total Ampkα (CST; #2532; 1:1000); anti-phospho Ampkα (Thr172) (CST; #2535; 1:1000). Cell extract (CE) preparation and immunoblot analyses were performed as previously described (Porcu et al., 2015; Nocita et al., 2019). Band signal intensity was estimated using the ImageJ software (version 1.8.0), and the data were plotted using GraphPad Prism 7.0 (GrahPad Software, San Diego, CA, United States) as fold change versus vehicle, arbitrarily set to 1.

Quantitative Immunofluorescence Analysis

The cells were seeded, fixed, and processed for IF as previously described (Nocita et al., 2019). Acquisition was performed at 20 × magnification (HCX PL FLUOTAR 20 × NA 0.4) using a Leica DMI6000 B epifluorescence inverted microscope (Leica Microsystems, Wetzlar, Germany) equipped with Leica Application Suite X and Matrix Screener software (version 3.0) for automated image acquisition. Micrographs were analyzed with ScanR (version 2.1, Analysis software version 1.1.0.6; Olympus, Tokyo, Japan) for quantification and statistical analyses as previously described (Sacco et al., 2012; Porcu et al., 2015; Nocita et al., 2019). Hoechst 33,342 (Invitrogen, Thermo Fisher Scientific) staining performed used for nucleic acid quantification and nuclei detection. Rat anti-MBP (MCA409S, 1:100; Serotec), Smo [1:500; (Masdeu et al., 2006)]; phalloidin (A12380; 1:40; Thermo Fisher Scientific), and Alexa Fluor 488 or Alexa Fluor 546 conjugated secondary antibodies (Thermo Fisher Scientific) were used as indicated in the text. Image analysis was performed as previously described (Sacco et al., 2012; Porcu et al., 2015; Nocita et al., 2019). Quantitative morphological analysis was performed using either EDGE or INTENSITY module of the ScanR analysis software (Olympus) as previously described (Nocita et al., 2019). We then calculated the percentage of cell population with higher membrane area using the max Feret diameter parameter of the ScanR software. The max Feret diameter is a measure of an object size along its maximal axis. By plotting the max Feret diameter along one axis (y) and the mean intensity FITC on the other axis (X) of a scattered plot, it is possible to visualize cell distribution accordingly. Specifically, the following ScanR analysis software parameters were used for gating the cell population of interest: max Feret diameter > 250 (y)/mean intensity FITC (MBP) (x). This gate identifies the cell population with high membrane extension and MBP levels (FITC or TRITC channel according to the secondary antibody used). Cell population was also analyzed to detect populations with high MBP expression and large area according to the gate: mean intensity FITC (MBP) 130,00-40,000 (y)/area (x). Three wells per sample of three biological replicates were acquired for each experimental condition and tested for statistical significance.

Evaluation of Cell Engagement in PS Microfibers

Cell culture chambers containing electrospun fibers were prepared as indicated in Nocita et al. (2019), UV-sterilized before use, and pre-treated with 10 μg/ml fibronectin (F0895; Sigma-Aldrich). A total of 80,000 Oli-neuM cells were seeded in a growth medium, after 24 h, the medium was changed with either DM supplemented with.5% DMSO (vehicle) or

the indicated treatment(s). The cells were grown for 72 h at 37°C in 5% CO_2. After fixation, the chambers were processed for immunofluorescence using the antibody indicated in the text. Acquisition and engagement analyses were performed as described in Nocita et al. (2019). Nuclei located in fibers characterized also by MBP expression were considered engaged. Nuclei located nearby the fibers were considered not engaged if they were at a distance not longer than 86 μm. Nuclei distant more than 86 μm from any fiber were not considered. When the distance between two fibers was shorter than 86 μm, nuclei located in between the two fibers were considered not engaged. The images were visualized and analyzed with ScanR (Olympus). 86 μm distance was estimated from the empirical observation that cells at this distance from a PS fiber never extend their membrane until to wrap the fiber. To estimate the length of MBP + processes along the fibers and the number of PS fibers associated with each Oli-neuM cell, images of the samples were taken randomly, and analyses were performed on at least 100 engaged cells, which were randomly selected per treatment. After conversion of pixels into μm [(mean pixel length)/22) * 10] (based on the objective used), the mean of the processes length was calculated using Image J tools (1.52a) version.

Total RNA Extraction and qPCR

Following drug administration, total RNA was extracted using RNA-Solv Reagent (R6830-01; VWR) according to the manufacturer's instructions. Typically, 2 μg of the RNA sample was retro-transcribed using the High-Capacity cDNA Reverse Transcription Kit (4368814; Thermo Fisher Scientific) according to the manufacturer's instructions. qPCR was performed using SYBR Green Technology and the QuantStudio® 3 Real-Time PCR System (Applied Biosystems®, Thermo Fisher Scientific). Primer pairs used with StoS Quantitative Master Mix 2X SYBR Green-ROX (GeneSpin Srl, Milan, Italy) were: Gapdh, forward (FW) 5′-CCAATGTGTCCGTCGTGGATCT-3′, reverse (RV) 5′- GTTGAAGTCGCAGGAGACAACC-3′; MBP, FW 5′-TACCCTGGCTAAAGCAGAGC-3′, RV 5′-GAGGTGGTGT TCGAGGTGTC-3′; MAL, FW 5′- CAGATCCCATCATCAGC CCC- 3′, RV 5′- TGGCTGTGTTAAGTGGGCAA-3′; OPALIN, FW 5′- CAGCTGCCTCTCACTCAACATC-3′, RV 5′- TCCCA AAGGCAGACTTCTCTCG-3′; Gli1, FW 5′-GCTGTCGGAAG TCCTATT-3′, RV 5′-ACTGGCATTGCTAAAG-3′; Gli2, FW 5′-CAACGCCTACTCTCCCAGAC-3′, RV 5′-GAGCCTTGATGTA CTGTACCAC-3′; Gli3 5′-GCAACCTCACTCTGCAACAA-3′, RV 5′- CCTTGTGCCTCCATTTTGAT-3′; Ptc, FW 5′- CCTC CTTTACGGTGGACAAA-3′, RV 5′-ATCAACTCCTCCTGCCA ATG-3′; Hip FW 5′- GAAAACGATCCCTCACCCAGCCAGAC-3′, RV 5′- GTGGGGAGAACAGCAGAGATC-3′. GAPDH was used as endogenous control. Typically, 50 ng of cDNA per sample was used per reaction. qPCR was performed in triplicate in MicroAmp Fast Optical 96-Well Reaction Plate (Applied Biosystems®), $n = 3$. The ΔΔCT method of relative quantification was used to determine fold change in expression. This was done by normalizing the resulting threshold cycle (CT) values of the target mRNAs to the CT values of the endogenous control Gapdh in the same samples (ΔCT = CT target–CT GAPDH), and by further normalizing to the control (ΔΔCT = ΔCT–ΔCT vehicle). Fold change in expression was then obtained ($2^{-\Delta\Delta CT}$) and represented in the plots using a log2 scale for ease of visualization of up/down-regulated genes.

Statistical Methods

In studies performed in multiwell plates (immunofluorescence and qPCR), three replicates per sample were spotted in each plate, and mean values obtained from the three samples were considered as one biological replicate. The mean values ± SEM obtained from at least three biological replicates were considered for statistical analyses. Statistical analyses were performed using GraphPad Prism. Effects of each drug treatment versus its internal control (vehicle) in immunofluorescence experiments, WB, and qPCR data were analyzed by paired two-tailed Student's *t*-test, while one-way analysis of variance (ANOVA) with Tukey's tests (as indicated in figure legends) was performed to determine statistically significant differences among multiple single or combined treatments.

RESULTS

GSA-10 Stimulates Oli-neuM Differentiation Until Axon Engagement

The observation that Gli1 downregulation is required for fating NPC cells toward myelinating oligodendrocytes (Samanta et al., 2015) suggests that the non-canonical Smo activation that is able to downregulate Gli1, might stimulate oligodendroglial differentiation. Since GSA-10 belongs to this new class of non-canonical Smo modulators, it was evaluated for its ability to promote MBP expression and Oli-neuM differentiation until axon engagement.

First, we performed a dose-response experiment (0.1, 0.3, 1, 5, 10, and 25 μM of GSA-10) to quantify MBP gene expression by quantitative RT-PCR (qPCR, **Supplementary Figure 1A**). In addition, immunofluorescence microscopy (IF) was used to quantify MBP levels in parallel with morphological changes in the Oli-neuM cells (**Supplementary Figure 1C**), since the switch of OPCs from bipolar or rhomboid morphology (undifferentiated) to enlarged and multipolar cells highly expressing MBP (differentiated) is considered to be a typical sign of OPC maturation to myelinating OLs (Snaidero et al., 2014; Nawaz et al., 2015; Zuchero et al., 2015).

The dose-response curve obtained (**Supplementary Figure 1**) shows that MBP levels increase at both the transcript and protein levels with increasing concentrations of GSA-10. Furthermore, the analysis of cell projections on a two-dimensional surface (gate max Ferret diameter > 250 arbitrary units) showed that high GSA-10 concentrations lead to higher number of Oli-neuM cells displaying enlarged membrane morphology compared to the vehicle condition (**Supplementary Figure 1C**). Altogether, these analyses show that GSA-10 treatment for 48 h promotes a dose-dependent increase in MBP, consistent with morphological changes that characterize OPC differentiation (Nawaz et al., 2015; Zuchero et al., 2015). Unless otherwise specified, a concentration of 10 μM GSA-10 was used for subsequent studies.

The ability of OLs to promote axon engagement is fundamental for a promyelinating drug to be effective *in vivo* (Lee et al., 2012; Espinosa-Hoyos et al., 2018). Therefore, we cultured Oli-neuM cells in chambers containing artificial axons (electrospun aligned polystyrene, PS, microfibers of 2-5 μm diameter) in the presence of GSA-10 or the well-characterized promyelinating molecule Clobetasol. We observed that the percentage of cells engaging the artificial axons was significantly higher in the GSA-10- and Clobetasol-treated cells than in the vehicle-treated cells (**Figures 1A,B**). Importantly, we noted that, compared to Clobetasol, GSA-10 treatment was particularly effective in triggering lateral myelin elongation (**Figures 1A,C**). In addition, we quantified the length of MBP^+ processes along fibers and the number of fibers that were associated with each Oli-neuM cell compared to Clobetasol or vehicle conditions. Both parameters were significantly increased (**Figures 1C,D**), indicating that GSA-10 not only induces increased axonal contact/ensheathment but also rapidly promotes cell differentiation. As mentioned above, GSA-10 was particularly efficient compared to Clobetasol. This might indicate that GSA-10 promotes a further stage of Oli-neuM maturation with respect to Clobetasol by promoting the formation of compact myelin (Snaidero et al., 2014). To corroborate this hypothesis, we analyzed the expression of two markers of compact myelin, MAL and OPALIN (Frank, 2000; Bijlard et al., 2016), in GSA- 10−, Clobetasol-, or Vehicle-treated Oli-neuM cells after a 48-h treatment. MAL is specifically upregulated during the period of active myelination and is expressed later than PLP and MBP (Schaeren-Wiemers et al., 1995; Frank et al., 1999). OPALIN is a paranodal-inner-loop glycoprotein that localizes in compact myelin (Golan et al., 2008). These late myelination markers were both upregulated in the GSA-10- but not in the Clobetasol-treated cells (**Figures 1E,F**).

Thus, GSA-10 not only promotes MBP expression and Oli-neuM differentiation in a dose-dependent manner but also induces Oli-neuM cells to differentiate until the stage of artificial axon engagement and the expression of myelin compaction markers.

Smoothened Modulation by GSA-10, but Not SAG, Promotes Gli2 Upregulation and Oli-neuM Differentiation

To determine how Smo modulation by GSA-10 can promote Oli-neuM differentiation, we compared the effects of GSA-10 and Clobetasol on MBP expression and cell morphology to those of the reference Smo agonist SAG (Chen et al., 2002), which binds the transmembrane-binding domain of Smo (Byrne et al., 2018) and elicits Gli1 activation (Wang et al., 2010; Ruat et al., 2014). The Oli-neuM cells were treated for 48 h with 10 μM GSA-10, 5 μM SAG, or 10 μM Clobetasol and analyzed by IF. As mentioned above, inspection of the Oli-neuM cells showed that GSA-10 and Clobetasol comparably trigger all morphological changes typical of mature OLs, while the SAG-treated cells showed a bipolar morphology, characteristic of immature oligodendroglial cells (**Figure 2A**). Morphological multiparametric analyses were performed by generating histograms of the scattered plot of the entire cell population based on either the mean intensity MBP (y) vs. area (x) (**Figure 2B**) or the max Feret diameter (y) vs. mean intensity MBP (X) (**Figure 2C**), as previously described (Nocita et al., 2019).

We observed that each treatment led to a different percentage of cells falling into these gates (**Figures 2B,C**). Indeed, GSA-10 and Clobetasol increased the percentage of cells expressing high levels of MBP by 2.5- or four-fold compared to the vehicle, respectively. In contrast, the SAG-treated cells decreased this percentage by two-fold. Similarly, we observed that GSA-10 and Clobetasol significantly increased the proportion of cells present in the max Feret diameter gate, and that SAG induced significantly less morphological differentiated cells than the vehicle.

Altogether, these data indicate that GSA-10 and Clobetasol, but not SAG, promote Oli-neuM differentiation. Specifically, GSA-10 and Clobetasol promote Oli-neuM morphological changes that are typical of mature OLs and significantly induce MBP expression, while SAG does not.

Since Smo controls the transcription of Gli1 (the main effector of canonical Hedgehog signaling), Ptc (a physiological repressor of Smo), and Hedgehog-interacting protein (Hip, a physiological repressor of Shh) (Varjosalo and Taipale, 2008; Ruat et al., 2014; Rimkus et al., 2016; Skoda et al., 2018), we further delineated how GSA-10 and SAG regulate these target genes in the Oli-neuM cells. As expected, SAG was found to significantly upregulate Gli1 and Hip expression, but it was not able to regulate Ptc compared to the vehicle (**Figures 3A–C**). In contrast, GSA-10 significantly inhibited all the target genes (**Figures 3A–C**). Moreover, since Gli transcription factors are tightly correlated in an interconnected network and because Gli2 and Gli3 can act both as activators and repressors affecting Gli1 levels in other cell types (Schmidt-Heck et al., 2015), we also analyzed Gli2 and Gli3 expression under GSA-10 and SAG treatments. Gli2 and Gli3 expression was significantly increased by GSA-10 (**Figures 3D,E**). In contrast, SAG had no activity in Gli2, but it stimulated Gli3 expression like GSA-10. These data, thus, suggest that Gli2 upregulation may correlate with the promyelinating activity of GSA-10.

Smoothened Activity Is Necessary for MBP Expression and Oli-neuM Differentiation After Myelin Regulatory Factor Expression

To conclusively establish the requirement of Smo modulation for Oli-neuM differentiation, we performed Smo gene silencing in the Oli-neuM cells and evaluated MBP protein levels, cell differentiation, and late myelin gene expression (MAL and OPALIN) after SAG and GSA-10 treatment. To this end, Oli-neuM cells were stably transfected using pLKO.1 lentiviral Smo shRNA (shSmo) or a nonrelevant shRNA-expressing pLKO.1 vector (shControl; Gorojankina et al., 2013).

SAG has been previously shown to induce Smo internalization that leads to apparent increase in Smo-associated fluorescent staining in the cytoplasm of cultured cells (Chen et al., 2004; Wang et al., 2010). In agreement with this observation, SAG, unlike GSA-10, increased the immunofluorescent Smo signal in

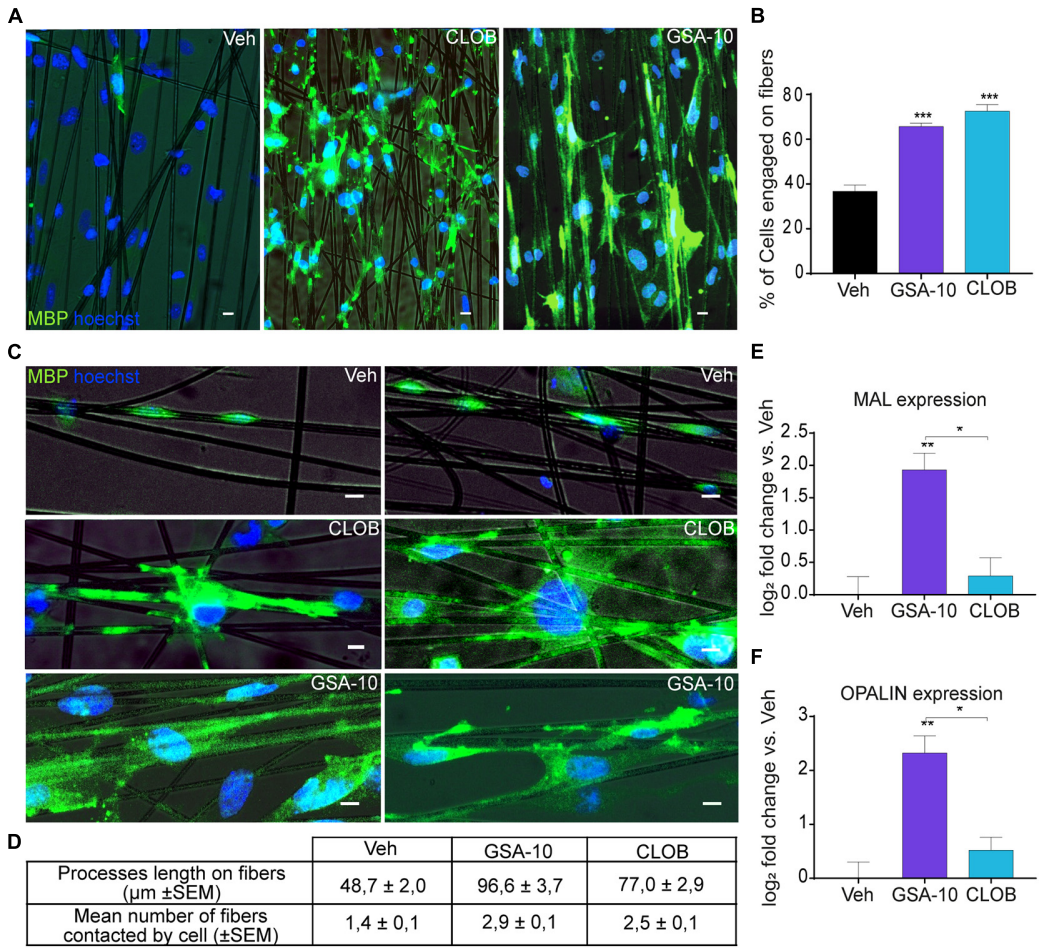

D

	Veh	GSA-10	CLOB
Processes length on fibers (μm ±SEM)	48,7 ± 2,0	96,6 ± 3,7	77,0 ± 2,9
Mean number of fibers contacted by cell (±SEM)	1,4 ± 0,1	2,9 ± 0,1	2,5 ± 0,1

FIGURE 1 | GSA-10 promotes Oli-neuM differentiation until axon engagement and compact myelin marker expression. Oli-neuM was treated with 10 μM GSA-10, 10 μM Clobetasol, or vehicle for 72 h before analysis. **(A)** Representative epifluorescence microscopy images of Oli-neuM cells, treated as indicated, in chambers containing artificial axons (aligned microfibers). Cells were stained with anti-MBP primary and Alexa 488 secondary antibodies (FITC). Hoechst (blue) = nuclei. Scale bar = 10 μm. **(B)** Quantification of fiber engagement was performed by analyzing 75 images per sample for each treatment ($n = 3$). Specifically, the percentage of engaged cells (mean ± standard error of the mean, SEM) was estimated by counting nuclei located in fibers or within a range of 86 μm from the fiber. **(C)** Enlargement of engaged cell morphology under the indicated treatments. Scale bar = 10 μm. **(D)** Quantification of membrane lengthening and number of fiber contacts by engaged cells under the indicated treatments. 100 engaged cells randomly selected per treatment were analyzed. **(E,F)** Quantitative RT-PCR analysis of MAL and OPALIN expression. Data were plotted as log2 fold change versus vehicle (which was set as 0) ± SEM ($n \geq 3$). Two-tailed paired Student's *t* test was performed for statistical significance versus vehicle, one-way analysis of variance (ANOVA) with Tukey's multiple comparison test was performed to analyze statistical significance among different treatments. $^{*}p < 0.05$, $^{**}p < 0.01$, and $^{***}p < 0.001$.

the cytoplasm of Oli-neuM cells. However, our quantifications also revealed an increased amount of Smo protein and transcripts (**Supplementary Figures 2A,B**). Therefore, we used the SAG condition in order to validate the efficiency of shSmo. As expected, after shSmo lentivirus transfection, we observed a significant reduction in Smo protein levels (**Supplementary Figures 3A,B**) and gene expression (**Supplementary Figure 3C**) compared to shControl in both vehicle- and SAG-treated Oli-neuM cells. Thus, these data show that Smo is effectively silenced in this cell line, and that shSmo displays an apparent lower ability to regulate Smo protein than Smo RNA, which might be related to a slow turnover of the protein. To further confirm Smo gene silencing, we analyzed Gli1 gene expression in the shSmo and shControl Oli-neuM cells upon SAG or GSA-10 treatment (**Figure 4A**). As expected, Oli-neuM shControl showed significant upregulation of Gli1 after SAG treatment, while the GSA-10-treated shControl cells displayed significant downregulation of Gli1. SAG-induced increase in Gli1 was blocked by shSmo (**Figure 4A**), indicating effective Smo silencing. Moreover, GSA-10 lost its ability to downregulate Gli1 at a level significantly different from that of the vehicle in the presence of shSmo, showing that GSA-10-mediated inhibition of Gli1 also depends on Smo (**Figure 4A**).

We compared MBP levels in the shSmo vs. shControl Oli-neuM cells under GSA-10, SAG, or vehicle treatment. Quantitative analysis of MBP IF staining (**Figures 4B,C**) showed that under all the treatment conditions, shSmo induced a significant decrease in both MBP^{+} signal and Oli-neuM

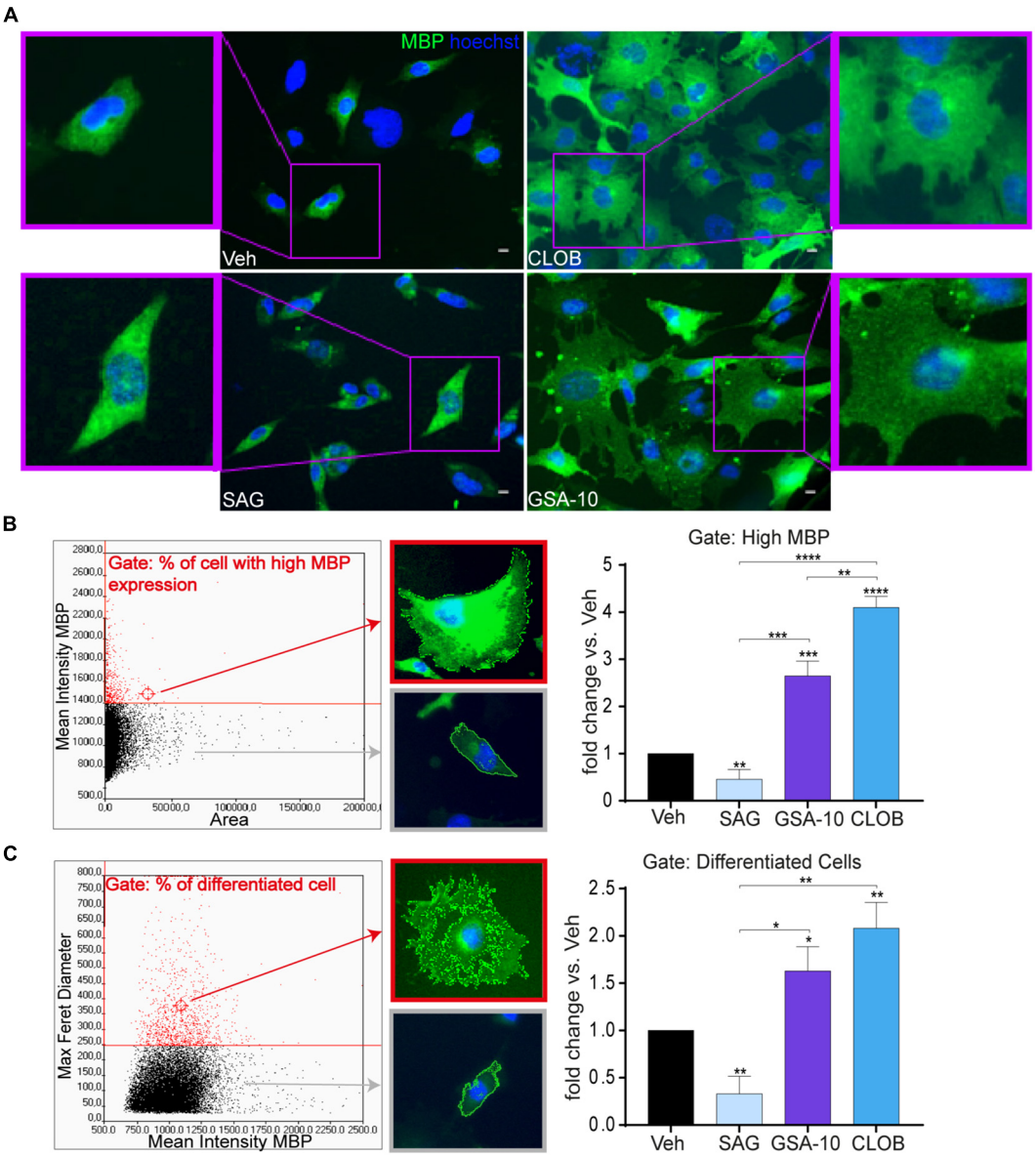

FIGURE 2 | GSA-10 promotes MBP expression and Oli-neuM maturation into myelinating cells, while SAG blocks Oli-neuM differentiation. Oli-neuM was treated for 48 h with 5 μM SAG, 10 μM GSA-10, or 10 μM Clobetasol before IF analysis. **(A)** Representative images of cell morphology showing enlargement of the cell body (boxed areas). Cells were stained with anti-MBP primary and Alexa 488 secondary antibodies (FITC); Hoechst (blue) = nuclei. Scale bar = 10 μm. **(B,C)** Quantification of IF images using ScanR. **(B)** Left panel: ScanR screen detail of the gate considered: % of cells with high MBP expression [mean MBP >1400,00 (y)/area (x)]. Cell morphology in the gate and out of the gate was highlighted by a red box and a gray box, respectively. Right panel: % of the cell population within the gate compared to the vehicle condition. Values are mean ± SEM ($n \geq 3$). **(C)** Left panel: ScanR screen detail of the gate considered: % of cells with differentiated morphology [max Feret diameter (D) > 250 (y)/mean FITC (MBP) (x)]. Fluorescent images show the cell morphology in the gate and out of the gate highlighted by a red box and gray box, respectively. Graph: % of cell population within the gate compared to the vehicle condition. Values are mean ± SEM ($n \geq 3$). Two-tailed paired Student's *t*-test was performed for statistical significance versus vehicle, one-way ANOVA with Tukey's correction multiple comparison test was performed to analyze statistical significance among different treatments. *$p < 0.05$, **$p < 0.01$, ***$p < 0.001$, and ****$p < 0.0001$.

differentiation reflected by the modification of cell morphology (**Figure 4B**). In addition, MAL and OPALIN gene expression was significantly downregulated in the GSA-10-treated shSmo Oli-neuM cells compared to the shControl cells (**Figures 4D,E**). SAG did not stimulate MAL and OPALIN expression either in shSmo or in shControl. Finally, Smo silencing, per se, significantly inhibited the expression of these myelin genes. Moreover, since we showed the capacity of GSA-10 to upregulate Gli2, we finally evaluated how Smo gene silencing influences GSA-10 effect on Gli2 gene expression. GSA-10-induced Gli2 upregulation was completely abrogated in shSmo compared to shControl cells (**Figure 4F**).

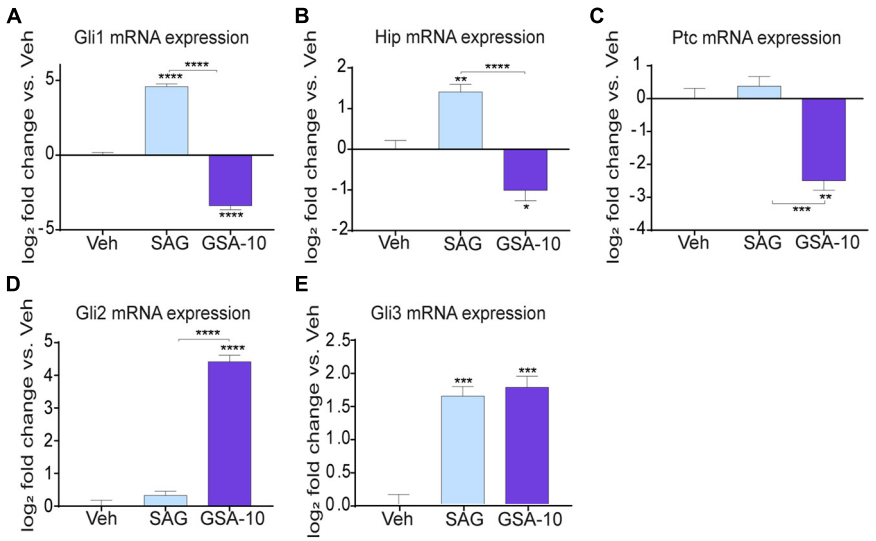

FIGURE 3 | Gli, Hip, and Ptc expression analysis and Smo localization in Oli-neuM. **(A–E)** Gli1, Gli2 Gli3, Hip, and Ptc expression levels in Oli-neuM treated for 48 h with 10 μM GSA-10, 5 μM SAG, or vehicle. Data were normalized and plotted as log2 fold change. Values are mean ± SEM ($n \geq 3$) with respect to vehicle. Two-tailed paired Student's *t*-test was performed for statistical significance versus vehicle. One-way ANOVA with Tukey's multiple comparison test was performed to analyze GSA-10 vs. SAG statistical significance among different treatments. $^{*}p < 0.05$, $^{**}p < 0.01$, $^{***}p < 0.001$, and $^{****}p < 0.0001$.

We conclude that Smo is required for Oli-neuM differentiation into myelinating cells, and that only GSA-10-mediated activation of Smo is able to upregulate myelin proteins such as MBP, MAL, and OPALIN. Furthermore, GSA-10-induced Gli1 and Gli2 gene transcription also requires Smo.

GSA-10-Mediated Smoothened/AMP-Activated Protein Kinase Activation Induces MBP, MAL, and OPALIN Expression

As mentioned above, Smo can modulate Gli1-independent intracellular signals in different cellular systems (Ruat et al., 2014; Rimkus et al., 2016). Here, we focused on the analysis of the AMPK signaling pathway, since this pathway was recently found to restore the capacity of aged OPCs to differentiate (Neumann et al., 2019). Immunoblot analyses of cell extracts from the Oli-neuM cells treated for 48 h with 10 μM GSA-10 or 5 μM SAG showed a significant increase in AMPK phosphorylation under GSA-10 treatment, while SAG significantly decreased the pAMPK/AMPK ratio (**Figure 5A**).

To determine if AMPK phosphorylation depends on Smo activation under our experimental conditions, we evaluated the ability of GSA-10 to induce AMPK phosphorylation in the shSmo cells compared to shControl cells (**Figure 5B**). GSA-10 was unable to promote AMPK phosphorylation in the shSmo cells, while it was still efficient in the shControl cells.

To further investigate AMPK activation and its relevance in MBP induction upon GSA-10 treatment, we used the selective phospho-AMPK inhibitor Dorsomorphin (DRS; **Figure 5A**) (Lo et al., 2019; Sun et al., 2021) in IF (**Figure 5C**) and quantitative RT-PCR analyses (**Figure 5D**) after 48 h treatment. As expected, DRS alone induced decrease in AMPK phosphorylation (**Figure 5A**). Moreover, in the presence of DRS, GSA-10 failed to increase AMPK phosphorylation (**Figure 5A**). Under both conditions, a highly significant reduction in MBP protein (**Figure 5C**) and MBP mRNA (**Figure 5D**) levels was observed. In agreement with these observations, the cells were unable to adopt the morphology characteristic of differentiated cells (**Figure 5C**). Along the same line, DRS prevented GSA-10-mediated MAL and OPALIN upregulation (**Figures 5E,F**), decreased by half GSA-10-induced Gli1 downregulation, and fully abrogated GSA-10-induced Gli2 upregulation (**Figures 5G,H**).

These data indicate that by modulating the Smo/AMPK pathway, GSA-10 promotes Oli-neuM morphological changes typical of mature oligodendroglial cells by stimulating Gli2 gene expression as well as MBP and compact myelin gene expression.

GSA-10 Increases the Recruitment of New Differentiated Oligodendrocytes in Demyelinated Areas *in vivo* After Lysophosphatidylcholine Injection Into the Corpus Callosum

We reasoned that the ability of GSA-10 to activate a non-canonical Smo signaling pathway resulting in Gli1 downregulation and Gli2 upregulation might promote the recruitment of NPCs, as recently shown for the Gli1 antagonist GANT-61 (Samanta et al., 2015; Namchaiw et al., 2019; Radecki et al., 2020). To validate this idea, a stereotactic injection of LPC was performed into the corpus callosum in the presence of GSA-10 in order to determine the effects of non-canonical Smo modulation on the recruitment of oligodendroglial cells

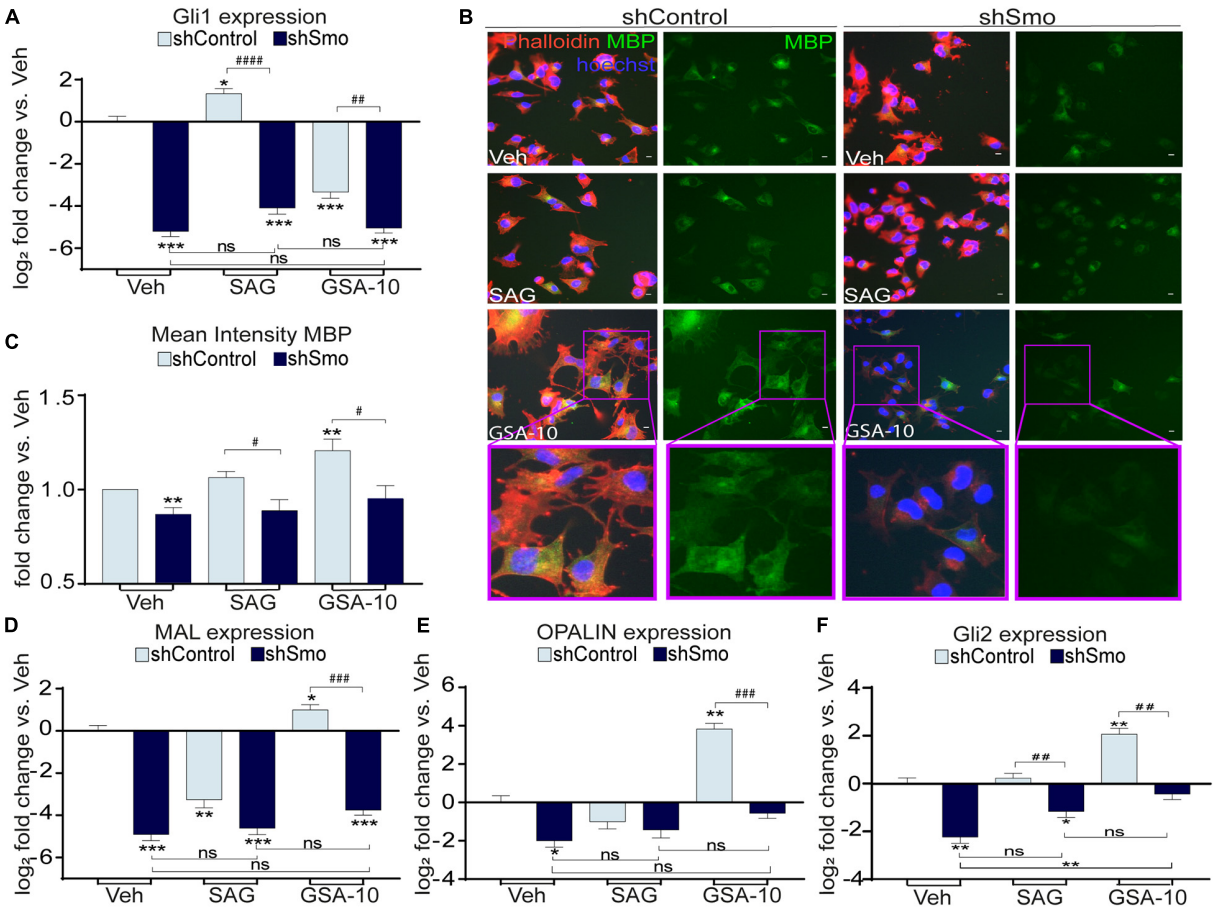

FIGURE 4 | Smo silencing decreases GSA-10-induced MBP, MAL, OPALIN, Gli2 gene expression, and abrogates GSA-10 activity in Oli-neuM differentiation. **(A)** Gli1 gene expression levels. Values were normalized and plotted as log2 fold change and are mean ± SEM ($n \geq 3$) with respect to vehicle shControl. **(B)** Representative IF images of shSmo or shControl cells under the indicated treatments and stained with anti-MBP primary and Alexa 488 secondary antibodies (green); Phalloidin (red); Hoechst (blue) = nuclei. Scale bar = 10 μm. Cell magnifications are shown in boxed area. **(C)** Quantitative analyses of IF cell images. Mean intensity of MBP ± SEM ($n \geq 3$) was plotted as fold change vs. shControl vehicle. **(D–F)** MAL, OPALIN, and Gli2 gene expression levels. Values were normalized and plotted as mean log2 fold change vs. vehicle shControl ± SEM ($n > 3$). Two-tailed paired Student's *t*-test was performed for statistical significance vs. shControl vehicle (* labeled) and to compare shControl vs. shSmo (# labeled) in each treatment. One-way ANOVA with Tukey's multiple comparison test was performed to analyze statistical significance between the different treatments. *$p < 0.05$, **$p < 0.01$, ***$p < 0.001$; #$p < 0.05$, ##$p < 0.01$, ###$p < 0.001$, and ####$p < 0.0001$; ns, non significant.

upon CNS demyelination. GSA-10 or the corresponding vehicle was co-injected with LPC, and the brains were analyzed 5 days post lesion (dpl) to allow for oligodendroglial cell recruitment into the demyelinated area (**Figure 6A**). First, we investigated the effect of GSA-10 on OPC proliferation using an antibody directed against the NG2 proteoglycan and the antibody Ki67 as a marker of cell proliferation (**Figure 6B**). Cell quantification indicated that GSA-10 does not induce any OPC proliferation as shown by the unmodified density of $NG2^+$ cells (386.7 ± 88.7 vs. 277 ± 92.8 cells/mm^2 or 5.2 ± 0.6 vs. 3.9 ± 0.3% of $DAPI^+$ cells; **Figure 6C**), $NG2^+$ proliferation capacity (7.5 ± 4.9 vs. 4.5 ± 3.2% of $Ki67^+$ cells; **Figure 6E**), and whole density of proliferating cells inside the lesion (341.5 ± 77.3 vs. 277 ± 92.8 cells/mm^2 or 5.8 ± 2.3 vs. 4.2 ± 1.6% of DAPI; **Figure 6D**) when compared to the vehicle (**Figures 6C–E**). Along the same line, although the density of cells expressing the transcription factor Sox2, previously reported to play an important role in OPC recruitment by maintaining them in a proliferative state (Zhao et al., 2015), appeared to increase under GSA-10 treatment, but the difference was not significant (680.7 ± 88.8 vs. 432.3 ± 120.7 cells/mm^2 or 18.9 ± 1.3 vs. 12.2 ± 2.8% of $DAPI^+$ cells, **Figures 6F,H**). We further used Olig2, a well-known marker of the whole oligodendroglial lineage. We observed a significant increase in the density of $Olig2^+$ cells inside the lesion in GSA-10- compared to vehicle-treated mice (687 ± 82 vs. 396 ± 47 cells/mm^2, $p = 0.036$ or 15.1 ± 1.3 vs. 9.4 ± 0.8 % of $DAPI^+$ cells, $p = 0.01$; **Figures 6G,I**), indicating that GSA-10 regulates oligodendroglial recruitment toward the lesion independently of cell proliferation. The increase in $Olig2^+$ cells prompted us to investigate a putative increase in the number of differentiated oligodendrocytes in this cell population. Therefore, we analyzed CC1 expression as a marker of the cells in the same animals (**Figures 6J,K**). Cell quantification showed increase in both the density of $CC1^+$ cells and the percentage of $Olig2^+$ cells

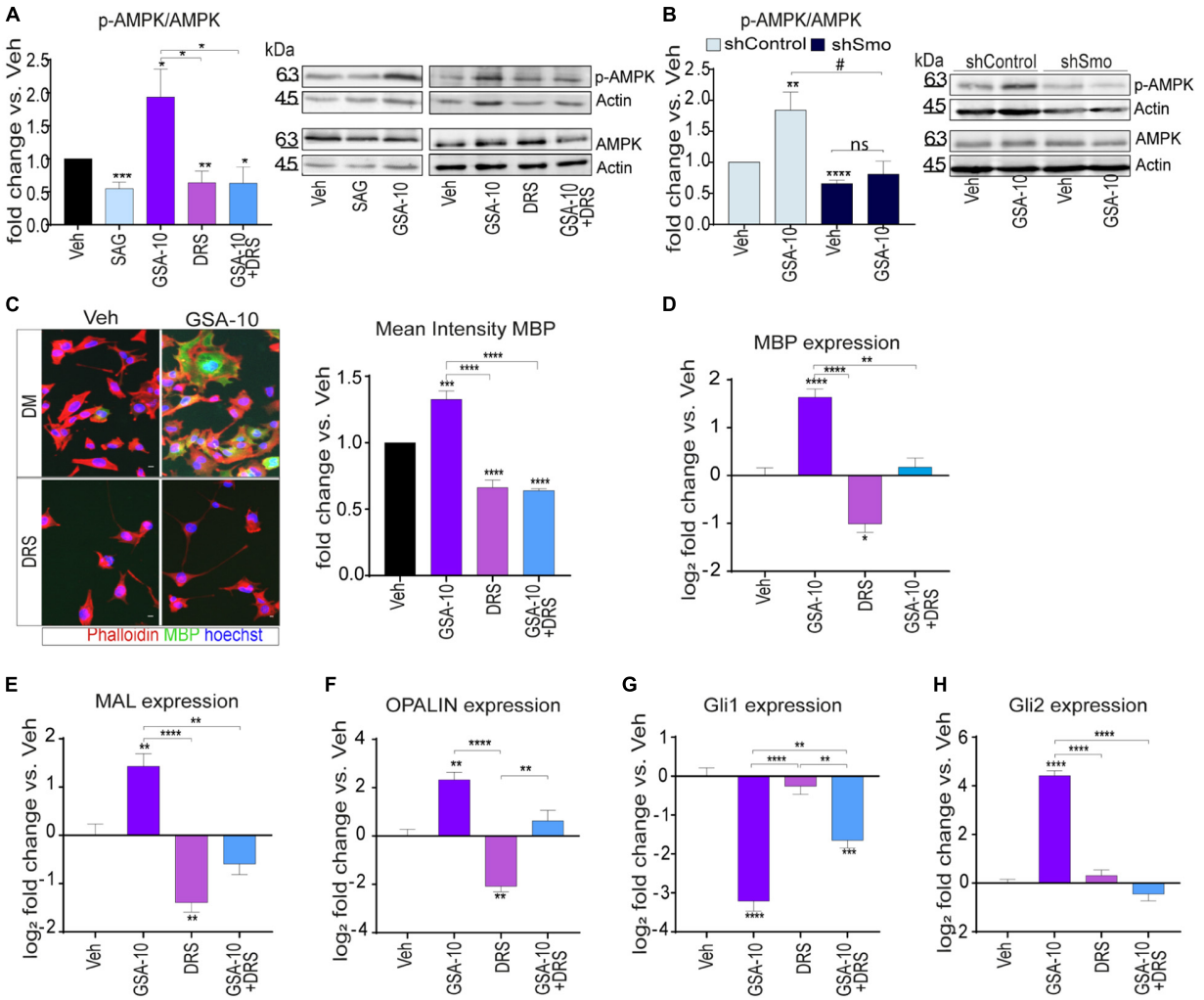

FIGURE 5 | AMPK signaling is required for Oli-neuM differentiation and Gli2 gene expression. **(A)** Immunoblot analysis of Oli-neuM cell extracts after treatment with 5 μM SAG, 10 μM GSA-10, 3 μM Dorsomorphin (DRS), or alone or in combination with GSA-10. Left panel: Quantitative analysis of protein levels: anti-AMPK (AMPK) or phospho-AMPK (pAMPK) antibody. Anti-actin antibody was used to normalize sample loading ($n \geq 3$). Signal intensity was estimated using ImageJ software tools, and values ± SEM were plotted as the fold change of p-AMPK/AMPK. Right panel: representative image of immunoblots used for quantitative analysis. **(B)** Immunoblot analysis of shSmo vs. shControl extracts after treatment with 10 μM GSA-10 or vehicle. Left panel: Quantitative analysis of protein levels: anti-AMPK (AMPK) or phospho-AMPK (pAMPK) antibody. Quantification was performed as in panel **(A)**. Values ± SEM ($n \geq 3$) were plotted as the fold change of p-AMPK/AMPK. Right panel: representative image of immunoblots used for quantitative analysis. **(C)** Quantitative IF images analysis of MBP in Oli-neuM. Left panel: Typical treated cell images, stained with anti-MBP primary and Alexa 488 secondary antibodies (green); Phalloidin (red); Hoechst (blue) = nuclei. Scale bar = 10 μm. Right panel: Mean FITC (MBP) intensity was plotted as mean ± SEM ($n \geq 3$). Data were normalized with respect to vehicle, arbitrarily set to 1, and plotted as fold induction versus vehicle. **(D–H)** Quantitative RT-PCR analysis of MBP, MAL, OPALIN, Gli1, and Gli2 expression under GSA-10, DRS, or their combination. Values ± SEM ($n \geq 3$) were plotted as log2 fold change vs. vehicle (which is equal to 0). Statistical significance: two-tailed Student's *t*-test was performed for treatment vs. vehicle (vs. shControl in panel **(B)**), ANOVA one-way with Tukey's multiple comparison test was performed to determine significance among different treatments. $^{*}p < 0.05$, $^{**}p < 0.01$, $^{***}p < 0.001$, and $^{****}p < 0.0001$; $\#p < 0.05$; ns, non significant.

co-expressing CC1 (122.3 ± 52.5 vs. 226.3 ± 37.7 cells/mm^2 or 16.5 ± 4.1 vs. 29.3 ± 2.6% of Olig2$^+$ cells, $p = 0.03$), indicating that GSA-10 promotes the differentiation of oligodendroglial progenitors (**Figures 6L,M**).

We then asked whether GSA-10 could affect astrogliosis and microgliosis in the lesion. To this end, we analyzed the expression of the astroglial markers GFAP (**Figure 7A**) and cytoplasmic S100β (**Figure 7B**), and the microglial marker Iba1 (**Figure 7C**). GSA-10 did not change the density of either GFAP$^+$ (1029 ± 59.2 vs. 794.3 ± 1 GFAP$^+$ cells/mm^2, or 19.2 ± 1.9 vs. 18.8 ± 1.9% of DAPI$^+$ cells; **Figure 7D**) or S100β$^+$ (335 ± 70.1 vs. 343 ± 80.9 S100β$^+$cells/mm^2, or 9.05 ± 0.7 vs. 10.1 ± 2.5% of DAPI$^+$ cells; **Figure 7E**) astrocytes, or the number of Iba1$^+$ microglia (826.3 ± 134.7 vs. 1254 ± 112.6 cells/mm^2, or 25.6 ± 2.8 vs. 30.5 ± 2.3% of DAPI$^+$ cells; **Figures 7F,G**) when compared to the vehicle condition.

Altogether, the data show that GSA-10 promotes oligodendroglial cell recruitment without inducing progenitor

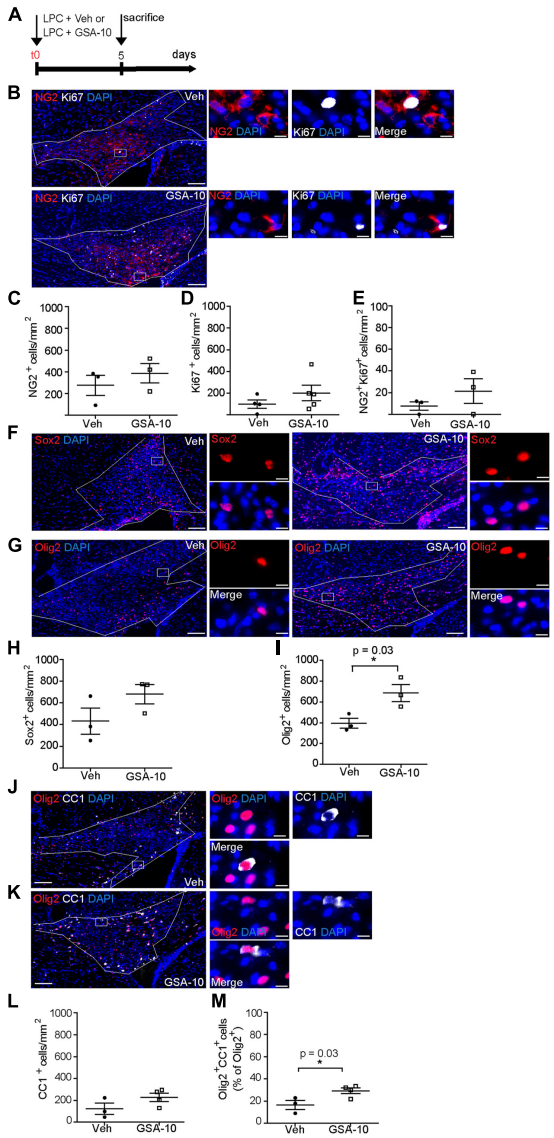

FIGURE 6 | GSA-10 increases Olig2$^+$ cells during remyelination of the corpus callosum. **(A)** Scheme of LPC-induced focal demyelination and GSA-10 treatment. LPC was injected into the corpus callosum of adult mice in the presence of vehicle (Veh) or the quinolinone GSA-10. Mice were perfused 5 days post-lesion to allow OPC recruitment. **(B)** Distribution of Ki67 (white) proliferation marker together with the proteoglycan-NG2 marker (red) inside the lesioned corpus callosum of Veh and GSA-10 treated brains. **(C–E)** GSA-10 does not modify the density of **(C)** NG2$^+$, **(D)** Ki67$^+$, and **(E)** NG2$^+$Ki67$^+$ cells inside the lesion. Mean ± SEM, n = 3–4 experimental replicates. **(F,G)** Distribution of the oligodendroglial markers **(F)** Sox2 and **(G)** Olig2 (red) inside the lesioned corpus callosum of Veh or GSA-10 treated brains. **(H,I)** GSA-10 increases the density of Olig2$^+$ cells **(I)** (p = 0.01) and does not significantly modify the density of Sox2$^+$ **(H)** cells inside the lesion. **(J,K)** Distribution of CC1 (white) marker labeling-differentiated oligodendrocytes together with the Olig2 marker (red), inside the lesioned corpus callosum of Veh and GSA-10-treated brains. **(L,M)** GSA-10 increases the density of CC1$^+$Olig2$^+$ cells and their percentage in the Olig2 population inside the lesion (p = 0.03). Mean ± SEM, n = 3–5 experimental replicates. White squares are magnified on the right **(B,F,G,J,K)** of the main panels, showing positive cells in merge and single channel with the nuclear marker DAPI (blue). Scale bar: **(B,F,G)** = 100 μm; all magnifications = 10 μm. *$p < 0.05$.

proliferation and does not affect the number of astrocytes and microglial cells inside the lesion.

DISCUSSION

Although previously reported arguments have supported the hypothesis that Smo-mediated Shh signaling may control oligodendroglial differentiation, the molecular mechanisms involved are still unclear (Ruat et al., 2014; Del Giovane and Ragnini-Wilson, 2018). Using *in vitro* and *in vivo* complementary approaches, we show here that a non-canonical modulator of the Smo receptor, GSA-10, is a potent activator of the maturation of the oligodendroglial cell line Oli-neuM into myelinating cells, and that it promotes the recruitment and differentiation of Olig2$^+$oligodendroglial cells into the demyelinated CNS areas. Compared to other pharmacological modulators of Smo activity, GSA-10 displays the property of promoting Oli-neuM differentiation up to the stage of engaging artificial axons and the expression of two markers of compact myelin, MAL and OPALIN, by increasing contact with- or ensheathment of the fibers. Importantly, gene silencing experiments clearly indicate that Smo modulation is required during the differentiation of Oli-neuM cells induced by GSA-10. Moreover, we provide evidence for the involvement of Smo-mediated AMPK signaling activation in the capacity of GSA-10 to stimulate morphological changes and increase in MBP, MAL, and OPALIN expression associated with Oli-neuM differentiation. Smo/AMPK signaling involves the ability of GSA-10 to decrease Gli1 and increase Gli2 transcription. Altogether, our data provide arguments supporting a higher level of complexity than initially thought in how Shh signaling may respond to demyelination.

Besides GSA-10, other small molecules are able to activate Smo/Gli signaling and oligodendroglial maturation, such as compounds belonging to the glucocorticoid class, namely Clobetasol, Halcinonide, and Flurandrenolide (Wang et al., 2010; Porcu et al., 2015; Del Giovane and Ragnini-Wilson, 2018). In contrast to these classes of Smo modulators, and to the reference agonist SAG (Wang et al., 2010; Kim et al., 2013), osteogenic quinolone derivatives, represented by the small molecule GSA-10, have not yet been evaluated in the context of myelin regeneration. Quinolone derivatives have been identified previously *via* the generation of a pharmacophoric model of Smo agonists (Gorojankina et al., 2013; Manetti et al., 2016). The use of the selective Smo agonist GSA-10 in the context of this study represents a critical tool to dissect the role of Smo receptor signaling in the last step of oligodendroglial maturation from MyRF expression until axon engagement. The approach also revealed the requirement for Smo-mediated activation of AMPK signaling in oligodendroglial maturation.

At the cellular level, we show that GSA-10 treatment promotes not only a dose-dependent increase in MBP, allowing Oli-neuM cells to mature until the ensheathment of polystyrene microfibers, currently used in drug validation studies as *in vitro* axon surrogates (Lee et al., 2012; Allimuthu et al., 2019; Nocita et al., 2019; Starost et al., 2020; Balestri et al., 2021), but also lateral membrane lengthening and compact myelin

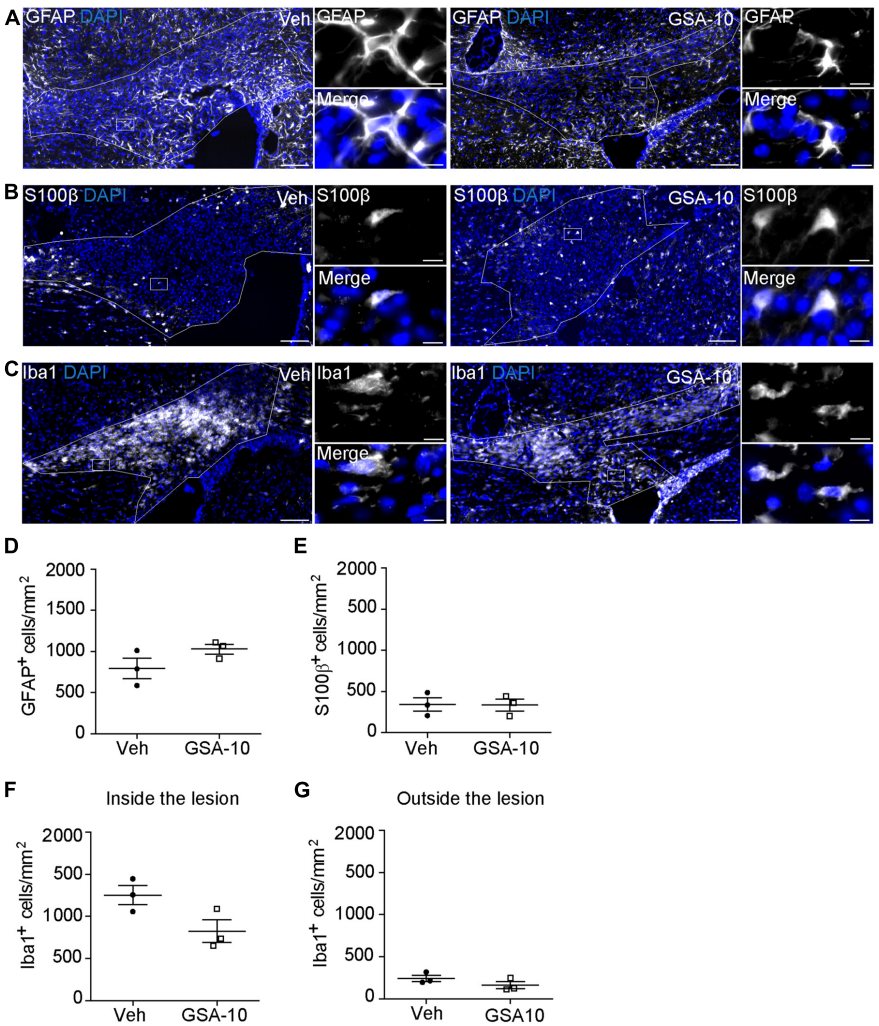

FIGURE 7 | GSA-10 does not affect astrogliosis and microgliosis in the lesioned corpus callosum. **(A–G)** Distribution of **(A)** GFAP and **(B)** S100β astroglial markers or **(C)** Iba1 microglial marker inside the lesioned corpus callosum of vehicle (Veh) and GSA-10 treated mouse brains. GSA-10 does not modify significantly the density of **(D)** GFAP$^+$, **(E)** S100β $^+$, or **(F)** Iba1$^+$ cells inside the lesion. Most S100β$^+$ cells display a cytoplasmic labeling characteristic of astroglial cells. Moreover, as observed inside the lesion, the number of Iba1$^+$ microglia cells was not modified by GSA-10 outside the lesion **(G)**. Mean ± SEM, n = 3–4 experimental replicates. White squares are magnified on the right side of the main panel, showing positive cells in merge and single channel with the nuclear marker DAPI (blue). Scale bar: **(A–C)** = 100 μm; all magnifications = 10 μm.

formation. Importantly, Smo activation by GSA-10, but not by SAG, leads to AMPK phosphorylation and Gli2 upregulation, which together correlate with the increase in MBP expression *via* a pathway that requires Smo, AMPK activation, and Gli1 downregulation. Smo gene silencing demonstrates that AMPK-mediated signaling and Gli2 upregulation are generated by GSA-10 modulation of Smo activity, and that SAG fails to modulate these responses. In addition, our experiments using DRS lead us to propose that GSA-10-mediated Gli2 upregulation requires AMPK activation. Since Gli1 ablation has been proposed previously to increase Gli2 expression *in vivo*, as especially shown in NSCs upon CNS demyelination (Radecki et al., 2020), we may hypothesize that the partial impairment of GSA-10-mediated Gli1 downregulation induced by DRS in Oli-neuM cells may subsequently prevent Gli2 upregulation. This hypothesis would further corroborate the importance of relative expression levels of the two transcription factors in the context of myelin production (Radecki et al., 2020). However, this remains to be verified. Altogether, these data further support the observation that different Smo agonists, presumably by activating Smo at distinct sites, can activate separate Smo-dependent pathways (Gorojankina et al., 2013; Fleury et al., 2016; Akhshi and Trimble, 2021). Clearly, AMPK phosphorylation, following GSA-10-induced Smo activation, is important for both basal MBP expression and morphological changes occurring during Oli-neuM differentiation into myelinating cells, since dorsomorphin-treated Oli-neuM cells display lower MBP expression than cells treated with the vehicle and no differentiated morphology.

Another major finding of our study comes from the comparison of the remyelinating properties of GSA-10 and

Clobetasol, the first glucocorticoid and Smo receptor modulator proposed to enhance remyelination in patients (Najm et al., 2015; Porcu et al., 2015). We observed that GSA-10 not only induces MBP expression as well as Oli-neuM engagement of artificial axons, similarly to Clobetasol (Porcu et al., 2015; Nocita et al., 2019), but also stimulates a further stage of oligodendroglial cell maturation, namely, membrane lateral lengthening. Further confirming the differences between Clobetasol and GSA-10 activity in late maturation stages, only GSA-10 promotes expression of the late markers of myelin compaction MAL and OPALIN. AMPK stimulation by GSA-10 might be the leading event that drives the stimulation of these genes and, thereby, compact myelination.

How GSA-10 promotes selective Smo-mediated AMPK phosphorylation signaling remains to be determined. As previously mentioned, GSA-10 has been identified through the virtual screening of a library of compounds in a pharmacophoric model of Smo agonists, such as SAG. SAG and GSA-10 were proposed to stabilize different active forms of the Smo receptor (Gorojankina et al., 2013). The latter can indeed adopt several conformations in the cell cytoplasm and primary cilium (Rohatgi et al., 2009; Rominger et al., 2009; Wilson et al., 2009; Yang et al., 2009; Belgacem and Borodinsky, 2011; Roudaut et al., 2011; Gorojankina et al., 2013; Ruat et al., 2014). SAG is proposed to stabilize a form addressed to the primary cilium and leads to activation of the Shh pathway *via* transcription of Shh-related genes. In contrast, GSA-10 is suggested to stabilize a form that does not translocate to the cilium (Gorojankina et al., 2013). One possibility is that GSA-10 might stabilize the Smo receptor in early endosomes and, thereby, increase the ability of Smo to interact with the liver kinase b1 (Lkb1), which is known to promote AMPK activation (Teperino et al., 2012, 2014). In agreement with this hypothesis, the Lkb1/AMPK axis was found to act downstream of Smo activation and inhibit adipocyte differentiation (Fleury et al., 2016). In support of the hypothesis that Smo-mediated AMPK pathway modulation is important for CNS remyelination is the finding that metformin, which is able to activate AMPK signaling, has been previously reported to restore the differentiation capacity of aged OPCs (Neumann et al., 2019).

The role of Smo modulation during remyelination processes was previously studied *in vivo*. Specifically, it was shown that the adenovirus-mediated transfer of Shh or its physiological antagonist Hip close to LPC-induced lesions of the corpus callosum accelerated or prevented remyelination, respectively (Ferent et al., 2013). Along the same line, the Smo reference agonist SAG has been reported recently to both directly promote the proliferation of parenchymal OPCs and indirectly induce the differentiation of these progenitors by regulating microglia response to demyelination in the LPC model (Laouarem et al., 2021). On the other hand, the blockade of the main effector of the canonical Shh signaling pathway, Gli1, has been shown to promote the recruitment of a subset of NPCs located in the SVZ bordering the lateral ventricles and exclusively fated to the oligodendroglial lineage (Samanta et al., 2015).

The increase in Olig2-expressing cells induced by GSA-10 when it is concomitantly injected with LPC into the corpus callosum shows the ability of this drug to promote oligodendroglial cell recruitment into demyelinated lesions *in vivo*. Most importantly, GSA-10 appears to accelerate and promote the differentiation of oligodendroglial progenitors into $CC1^+$-differentiated oligodendrocytes, indicating that GSA-10 acts in several steps of the remyelination process, i.e., recruitment of progenitors and their differentiation into oligodendrocytes. In addition, our *in vitro* experiments provide arguments supporting that GSA-10 induces myelin gene expression as well as axon engagement. Although genetic tracing of the recruited progenitors and progeny would be required to accurately delineate the source of the newly generated oligodendrocytes, the present data nevertheless provide arguments supporting the hypothesis that both NPCs and OPCs might be recruited *via* the non-canonical activation of Smo by GSA-10. Indeed, GSA-10 fails to significantly promote parenchymal OPC proliferation as attested by the unmodified number of $NG2^+$ cells detected in the lesion, which may be the result of the accelerated differentiation of OPCs and/or the recruitment of SVZ-derived NSC progeny. The latter hypothesis recalls the activity attributed to the antagonist of the Gli transcription factors, GANT-61. Indeed, GANT-61 was reported to exclusively recruit a subset of SVZ-derived Gli1-expressing NPCs fated to the OL lineage and to be devoid of effects on parenchymal OPCs (Samanta et al., 2015). Like the pharmacological blockade of Gli1, its genetic inhibition was found to be crucial to improve the functional outcome of animals in a relapsing/remitting EAE model and to promote remyelination in the cuprizone model of CNS demyelination (Samanta et al., 2015). Due to the well-characterized capacity of GSA-10 to downregulate Gli1 (Gorojankina et al., 2013; Fleury et al., 2016; Akhshi and Trimble, 2021; and our present data), we hypothesize that GSA-10 may act in the same way as GANT-61 on the recruitment of SVZ-derived NPCs. Consequently, our observation that Sox2 tends to increase, albeit not significantly, upon GSA-10 local administration into the lesion probably may reflect the contribution of Sox2 to the expansion of OPCs and/or its ability to prime oligodendroglial progenitors to eventually undergo differentiation, as previously reported (Zhao et al., 2015).

An additional and original aspect of our study is that GSA-10 stimulates Gli2 and Gli3 expression, and that it downregulates Gli1. GSA-10-induction of Gli2 and Gli3 expression was not observed upon treatment of murine mesenchymal C3H10T1/2 cells (Gorojankina et al., 2013). This suggests a different regulation of Smo-mediated signals in oligodendroglial cells compared to mesenchymal cells.

Two other promyelinating drugs, namely, Clobetasol and Gefitinib, also stimulate Gli2 in Oli-neuM. In this case, we have shown that Gli2 expression depends on RxRγ expression, since RxRγ gene silencing abrogates Gli2 expression in Oli-neuM under Clobetasol or Gefitinib treatments (Nocita et al., 2019). The recent demonstration that Sox17-induced oligodendrocyte regeneration in adult myelin lesions occurs by suppressing lesion-induced Wnt/beta-catenin signaling through an increase in Shh/Smo/Gli2 activity (Ming et al., 2020) supports the importance of Gli2 upregulation for the differentiation program under Gli1 downregulation. Along the same line, Gli2 has been reported to promote the differentiation of Gli1-null NPCs into

OLs in a cuprizone model of demyelination. In addition, the genetic ablation of Gli1 in NPCs was reported to increase Gli2 expression, while the loss of both factors was found to decrease NPC recruitment and the differentiation of their progeny (Radecki et al., 2020). Therefore, we suggest that by downregulating Gli1 and subsequently upregulating Gli2, the non-canonical Smo agonist GSA-10 might open promising perspectives in the context of remyelination by promoting oligodendroglial cell recruitment to the lesion and controlling in an AMPK-dependent manner the maturation of OLs until axon engagement.

Thus, GSA-10 might constitute the first member of a new generation of selective and potent remyelinating agents.

DATA AVAILABILITY STATEMENT

The raw data supporting the conclusions of this article will be made available by the authors, without undue reservation.

ETHICS STATEMENT

The animal experiments were performed in accordance with the Council Directive 2010/63EU of the European Parliament and approved by the French Ethic Committees (CEEA59 and CEEA26). Written informed consent was obtained from the owners for the participation of their animals in this study.

AUTHOR CONTRIBUTIONS

AR-W: conceptualization and supervision: *in vitro* studies. ET and MRa: conceptualization and supervision of animal study. AR-W, ET, and MRa: funding acquisition and project administration. AR-W, ET, MRa, AD, MRs, LT, HF, AK, SB, CS, and FB: design of the experiments and writing of the original draft. AD, AR-W, ET, MRa, MRs, LT, HF, and AK: perform the experiments and analyzed the data. AR and FB: design and produce the microfiber supports. AD, MRs, and AK: visualization. All authors have read and agreed to the published version of the manuscript.

FUNDING

AD Ph.D. fellowship was supported by XXXIV cycle of the Doctorate in Cellular and Molecular Biology of University of Rome Tor Vergata. MRs is a recipient of a doctoral fellowship from the Ministère de la Recherche and Fondation pour la Recherche Médicale. LT and AK were supported by Fondation pour l'Aide à la Recherche sur la Sclérose En Plaque (ARSEP). This study was also supported by grants from ARSEP, Association pour la Recherche contre le Cancer (ARC), and CNRS to MRa, grants from ARSEP (RAK 17128LLA and RAK 19176LLA) to ET, and University of Rome "Tor Vergata": Mission sustainability New Myelin and Beyond the border NAATALS projects of AR-W.

ACKNOWLEDGMENTS

We are deeply indebted to Cathal Wilson for the critical reading and English correction of the text, and Gianni Cesareni and Luisa Castagnoli for their support.

SUPPLEMENTARY MATERIAL

The Supplementary Material for this article can be found online at: https://www.frontiersin.org/articles/10.3389/fncel.2021.801704/full#supplementary-material

REFERENCES

Akhshi, T., and Trimble, W. S. (2021). A non-canonical Hedgehog pathway initiates ciliogenesis and autophagy. *J. Cell. Biol.* 220:e202004179. doi: 10.1083/jcb.202004179

Allimuthu, D., Hubler, Z., Najm, F. J., Tang, H., Bederman, I., Seibel, W., et al. (2019). Diverse chemical scaffolds enhance oligodendrocyte formation by inhibiting CYP51, TM7SF2, or EBP. *Cell Chem. Biol.* 26, 593.e4–599.e4. doi: 10.1016/j.chembiol.2019.01.004

Arensdorf, A. M., Marada, S., and Ogden, S. K. (2016). Smoothened regulation: a tale of two signals. *Trends Pharmacol. Sci.* 37, 62–72. doi: 10.1016/j.tips.2015.09.001

Balestri, S., Del Giovane, A., Sposato, C., Ferrarelli, M., and Ragnini-Wilson, A. (2021). The current challenges for drug discovery in CNS remyelination. *Int. J. Mol. Sci.* 22:2891. doi: 10.3390/ijms22062891

Belgacem, Y. H., and Borodinsky, L. N. (2011). Sonic hedgehog signaling is decoded by calcium spike activity in the developing spinal cord. *Proc. Natl. Acad. Sci. U.S.A.* 108, 4482–4487. doi: 10.1073/pnas.1018217108

Bijlard, M., de Jonge, J. C., Klunder, B., Nomden, A., Hoekstra, D., and Baron, W. (2016). MAL is a regulator of the recruitment of myelin protein PLP to membrane microdomains. *PLoS One* 11:e0155317. doi: 10.1371/journal.pone.0155317

Bin, J. M., Harris, S. N., and Kennedy, T. E. (2016). The oligodendrocyte-specific antibody "CC1" binds Quaking 7. *J. Neurochem.* 139, 181–186. doi: 10.1111/jnc.13745

Brousse, B., Magalon, K., Durbec, P., and Cayre, M. (2015). Region and dynamic specificities of adult neural stem cells and oligodendrocyte precursors in myelin regeneration in the mouse brain. *Biol. Open* 4, 980–992. doi: 10.1242/bio.012773

Byrne, E. F., Luchetti, G., Rohatgi, R., and Siebold, C. (2018). Multiple ligand binding sites regulate the Hedgehog signal transducer Smoothened in vertebrates. *Curr. Opin. Cell Biol.* 51, 81–88. doi: 10.1016/j.ceb.2017.10.004

Chen, J. K., Taipale, J., Young, K. E., Maiti, T., and Beachy, P. A. (2002). Small molecule modulation of Smoothened activity. *Proc. Natl. Acad. Sci. U.S.A.* 99, 14071–14076. doi: 10.1073/pnas.182542899

Chen, W., Ren, X. R., Nelson, C. D., Barak, L. S., Chen, J. K., Beachy, P. A., et al. (2004). Activity-dependent internalization of smoothened mediated by beta-arrestin 2 and GRK2. *Science* 306, 2257–2260. doi: 10.1126/science.1104135

Daynac, M., Tirou, L., Faure, H., Mouthon, M.-A., Gauthier, L. R., Hahn, H., et al. (2016). Hedgehog controls quiescence and activation of neural stem cells in the adult ventricular-subventricular zone. *Stem Cell Rep.* 7, 735–748. doi: 10.1016/j.stemcr.2016.08.016

Del Giovane, A., and Ragnini-Wilson, A. (2018). Targeting smoothened as a new frontier in the functional recovery of central nervous system demyelinating pathologies. *Int. J. Mol. Sci.* 19:3677. doi: 10.3390/ijms19113677

Deshmukh, V. A., Tardif, V., Lyssiotis, C. A., Green, C. C., Kerman, B., Kim, H. J., et al. (2013). A regenerative approach to the treatment of multiple sclerosis. *Nature* 502, 327–332. doi: 10.1038/nature12647

Espinosa-Hoyos, D., Jagielska, A., Homan, K. A., Du, H., Busbee, T., Anderson, D. G., et al. (2018). Engineered 3D-printed artificial axons. *Sci. Rep.* 8:478. doi: 10.1038/s41598-017-18744-6

Ferent, J., Cochard, L., Faure, H., Taddei, M., Hahn, H., Ruat, M., et al. (2014). Genetic activation of Hedgehog signaling unbalances the rate of neural stem cell renewal by increasing symmetric divisions. *Stem Cell Rep.* 3, 312–323. doi: 10.1016/j.stemcr.2014.05.016

Ferent, J., and Traiffort, E. (2015). Hedgehog: multiple paths for multiple roles in shaping the brain and spinal cord. *Neuroscientist* 21, 356–371. doi: 10.1177/1073858414531457

Ferent, J., Zimmer, C., Durbec, P., Ruat, M., and Traiffort, E. (2013). Sonic Hedgehog signaling is a positive oligodendrocyte regulator during demyelination. *J. Neurosci.* 33, 1759–1772. doi: 10.1523/JNEUROSCI.3334-12.2013

Fleury, A., Hoch, L., Martinez, M. C., Faure, H., Taddei, M., Petricci, E., et al. (2016). Hedgehog associated to microparticles inhibits adipocyte differentiation via a non-canonical pathway. *Sci. Rep.* 6:23479. doi: 10.1038/srep23479

Frank, M. (2000). MAL, a proteolipid in glycosphingolipid enriched domains: functional implications in myelin and beyond. *Prog. Neurobiol.* 60, 531–544. doi: 10.1016/s0301-0082(99)00039-8

Frank, M., Schaeren-Wiemers, N., Schneider, R., and Schwab, M. E. (1999). Developmental expression pattern of the myelin proteolipid MAL indicates different functions of MAL for immature Schwann cells and in a late step of CNS myelinogenesis. *J. Neurochem.* 73, 587–597. doi: 10.1046/j.1471-4159.1999.0730587.x

Franklin, R. J. M., and Ffrench-Constant, C. (2017). Regenerating CNS myelin - from mechanisms to experimental medicines. *Nat. Rev. Neurosci.* 18, 753–769. doi: 10.1038/nrn.2017.136

Franklin, R. J. M., Frisén, J., and Lyons, D. A. (2021). Revisiting remyelination: towards a consensus on the regeneration of CNS myelin. *Semin. Cell Dev. Biol.* 116, 3–9. doi: 10.1016/j.semcdb.2020.09.009

Golan, N., Adamsky, K., Kartvelishvily, E., Brockschnieder, D., Möbius, W., Spiegel, I., et al. (2008). Identification of Tmem10/Opalin as an oligodendrocyte enriched gene using expression profiling combined with genetic cell ablation. *Glia* 56, 1176–1186. doi: 10.1002/glia.20688

Gorojankina, T., Hoch, L., Faure, H., Roudaut, H., Traiffort, E., Schoenfelder, A., et al. (2013). Discovery, molecular and pharmacological characterization of GSA-10, a novel small-molecule positive modulator of Smoothened. *Mol. Pharmacol.* 83, 1020–1029. doi: 10.1124/mol.112.084590

Gregath, A., and Lu, Q. R. (2018). Epigenetic modifications-insight into oligodendrocyte lineage progression, regeneration, and disease. *FEBS Lett.* 592, 1063–1078. doi: 10.1002/1873-3468.12999

Hubler, Z., Allimuthu, D., Bederman, I., Elitt, M. S., Madhavan, M., Allan, K. C., et al. (2018). Accumulation of 8,9-unsaturated sterols drives oligodendrocyte formation and remyelination. *Nature* 560:372. doi: 10.1038/s41586-018-0360-3

Jäkel, S., Agirre, E., Mendanha Falcão, A., van Bruggen, D., Lee, K. W., Knuesel, I., et al. (2019). Altered human oligodendrocyte heterogeneity in multiple sclerosis. *Nature* 566, 543–547. doi: 10.1038/s41586-019-0903-2

Kim, J., Aftab, B. T., Tang, J. Y., Kim, D., Lee, A. H., Rezaee, M., et al. (2013). Itraconazole and arsenic trioxide inhibit hedgehog pathway activation and tumor growth associated with acquired resistance to smoothened antagonists. *Cancer Cell* 23, 23–34. doi: 10.1016/j.ccr.2012.11.017

Laouarem, Y., Kassoussi, A., Zahaf, A., Hutteau-Hamel, T., Mellouk, A., Bobé, P., et al. (2021). Functional cooperation of the hedgehog and androgen signaling pathways during developmental and repairing myelination. *Glia* 69, 1369–1392. doi: 10.1002/glia.23967

Lariosa-Willingham, K. D., Rosler, E. S., Tung, J. S., Dugas, J. C., Collins, T. L., and Leonoudakis, D. (2016). A high throughput drug screening assay to identify compounds that promote oligodendrocyte differentiation using acutely dissociated and purified oligodendrocyte precursor cells. *BMC Res. Notes* 9:419. doi: 10.1186/s13104-016-2220-2

Lee, S., Leach, M. K., Redmond, S. A., Chong, S. Y. C., Mellon, S. H., Tuck, S. J., et al. (2012). A culture system to study oligodendrocyte myelination processes using engineered nanofibers. *Nat. Methods* 9, 917–922. doi: 10.1038/nmeth.2105

Lo, M.-C., Chen, J.-Y., Kuo, Y.-T., Chen, W.-L., Lee, H.-M., and Wang, S.-G. (2019). Camptothecin activates SIRT1 to promote lipid catabolism through AMPK/FoxO1/ATGL pathway in C2C12 myogenic cells. *Arch. Pharm. Res.* 42, 672–683. doi: 10.1007/s12272-019-01155-8

Loulier, K., Ruat, M., and Traiffort, E. (2006). Increase of proliferating oligodendroglial progenitors in the adult mouse brain upon Sonic hedgehog delivery in the lateral ventricle. *J. Neurochem.* 98, 530–542. doi: 10.1111/j.1471-4159.2006.03896.x

Lubetzki, C., Zalc, B., Williams, A., Stadelmann, C., and Stankoff, B. (2020). Remyelination in multiple sclerosis: from basic science to clinical translation. *Lancet Neurol.* 19, 678–688. doi: 10.1016/S1474-4422(20)30140-X

Manetti, F., Petricci, E., Gabrielli, A., Mann, A., Faure, H., Gorojankina, T., et al. (2016). Design, synthesis and biological characterization of a new class of osteogenic (1H)-quinolone derivatives. *Eur. J. Med. Chem.* 121, 747–757. doi: 10.1016/j.ejmech.2016.05.062

Masdeu, C., Faure, H., Coulombe, J., Schoenfelder, A., Mann, A., Brabet, I., et al. (2006). Identification and characterization of Hedgehog modulator properties after functional coupling of Smoothened to G15. *Biochem. Biophys. Res. Commun.* 349, 471–479. doi: 10.1016/j.bbrc.2006.07.216

Mei, F., Fancy, S. P. J., Shen, Y.-A. A., Niu, J., Zhao, C., Presley, B., et al. (2014). Micropillar arrays as a high-throughput screening platform for therapeutics in multiple sclerosis. *Nat. Med.* 20, 954–960. doi: 10.1038/nm.3618

Melchor, G. S., Khan, T., Reger, J. F., and Huang, J. K. (2019). Remyelination pharmacotherapy investigations highlight diverse mechanisms underlying multiple sclerosis progression. *ACS Pharmacol. Transl. Sci.* 2, 372–386. doi: 10.1021/acsptsci.9b00068

Meley, D., Bauvy, C., Houben-Weerts, J. H. P. M., Dubbelhuis, P. F., Helmond, M. T. J., Codogno, P., et al. (2006). AMP-activated protein kinase and the regulation of autophagic proteolysis. *J. Biol. Chem.* 281, 34870–34879. doi: 10.1074/jbc.M605488200

Menn, B., Garcia-Verdugo, J. M., Yaschine, C., Gonzalez-Perez, O., Rowitch, D., and Alvarez-Buylla, A. (2006). Origin of oligodendrocytes in the subventricular zone of the adult brain. *J. Neurosci.* 26, 7907–7918. doi: 10.1523/JNEUROSCI.1299-06.2006

Ming, X., Dupree, J. L., Gallo, V., and Chew, L.-J. (2020). Sox17 promotes oligodendrocyte regeneration by dual modulation of Hedgehog and Wnt signaling. *iScience* 23:101592. doi: 10.1016/j.isci.2020.101592

Nait-Oumesmar, B., Decker, L., Lachapelle, F., Avellana-Adalid, V., Bachelin, C., and Baron-Van Evercooren, A. (1999). Progenitor cells of the adult mouse subventricular zone proliferate, migrate and differentiate into oligodendrocytes after demyelination. *Eur. J. Neurosci.* 11, 4357–4366. doi: 10.1046/j.1460-9568.1999.00873.x

Nait-Oumesmar, B., Picard-Riéra, N., Kerninon, C., and Baron-Van Evercooren, A. (2008). The role of SVZ-derived neural precursors in demyelinating diseases: from animal models to multiple sclerosis. *J. Neurol. Sci.* 265, 26–31. doi: 10.1016/j.jns.2007.09.032

Najm, F. J., Madhavan, M., Zaremba, A., Shick, E., Karl, R. T., Factor, D. C., et al. (2015). Drug-based modulation of endogenous stem cells promotes functional remyelination in vivo. *Nature* 522, 216–220. doi: 10.1038/nature14335

Namchaiw, P., Wen, H., Mayrhofer, F., Chechneva, O., Biswas, S., and Deng, W. (2019). Temporal and partial inhibition of GLI1 in neural stem cells (NSCs) results in the early maturation of NSC derived oligodendrocytes in vitro. *Stem Cell Res. Ther.* 27:272. doi: 10.1186/s13287-019-1374-y

Nawaz, S., Sánchez, P., Schmitt, S., Snaidero, N., Mitkovski, M., Velte, C., et al. (2015). Actin filament turnover drives leading edge growth during myelin sheath formation in the central nervous system. *Dev. Cell* 34, 139–151. doi: 10.1016/j.devcel.2015.05.013

Neumann, B., Baror, R., Zhao, C., Segel, M., Dietmann, S., Rawji, K. S., et al. (2019). Metformin restores CNS remyelination capacity by rejuvenating aged stem cells. *Cell Stem Cell* 25, 473.e8–485.e8. doi: 10.1016/j.stem.2019.08.015

Niewiadomski, P., Niedziółka, S. M., Markiewicz, Ł, Uśpieński, T., Baran, B., and Chojnowska, K. (2019). Gli proteins: regulation in development and cancer. *Cells* 8:E147. doi: 10.3390/cells8020147

Nocita, E., Del Giovane, A., Tiberi, M., Boccuni, L., Fiorelli, D., Sposato, C., et al. (2019). EGFR/ErbB inhibition promotes OPC maturation up to axon engagement by Co-regulating PIP2 and MBP. *Cells* 8:844. doi: 10.3390/cells8080844

Petrova, R., and Joyner, A. L. (2014). Roles for Hedgehog signaling in adult organ homeostasis and repair. *Development* 141, 3445–3457. doi: 10.1242/dev.083691

Plemel, J. R., Liu, W.-Q., and Yong, V. W. (2017). Remyelination therapies: a new direction and challenge in multiple sclerosis. *Nat. Rev. Drug Discov.* 16, 617–634. doi: 10.1038/nrd.2017.115

Porcu, G., Serone, E., De Nardis, V., Di Giandomenico, D., Lucisano, G., Scardapane, M., et al. (2015). Clobetasol and halcinonide act as smoothened agonists to promote myelin gene expression and RxRγ receptor activation. *PLoS One* 10:e144550. doi: 10.1371/journal.pone.0144550

Qiu, Z. P., Hu, A., and Song, B. L. (2021). The 3-beta-hydroxysteroid-Delta(8), Delta(7)-isomerase EBP inhibits cholesterylation of Smoothened. *Biochim. Biophys. Acta Mol. Cell Biol. Lipids* 1866:159041. doi: 10.1016/j.bbalip.2021.159041

Radecki, D. Z., Messling, H. M., Haggerty-Skeans, J. R., Bhamidipati, S. K., Clawson, E. D., Overman, C. A., et al. (2020). Relative levels of Gli1 and Gli2 determine the response of ventral neural stem cells to demyelination. *Stem Cell Rep.* 15, 1047–1055. doi: 10.1016/j.stemcr.2020.10.003

Rimkus, T. K., Carpenter, R. L., Qasem, S., Chan, M., and Lo, H.-W. (2016). Targeting the sonic hedgehog signaling pathway: review of smoothened and GLI inhibitors. *Cancers (Basel)* 8:22. doi: 10.3390/cancers8020022

Rohatgi, R., Milenkovic, L., Corcoran, R. B., and Scott, M. P. (2009). Hedgehog signal transduction by Smoothened: pharmacologic evidence for a 2-step activation process. *Proc. Natl. Acad. Sci. U.S.A.* 106, 3196–3201. doi: 10.1073/pnas.0813373106

Rominger, C. M., Bee, W.-L. T., Copeland, R. A., Davenport, E. A., Gilmartin, A., Gontarek, R., et al. (2009). Evidence for allosteric interactions of antagonist binding to the smoothened receptor. *J. Pharmacol. Exp. Ther.* 329, 995–1005. doi: 10.1124/jpet.109.152090

Roudaut, H., Traiffort, E., Gorojankina, T., Vincent, L., Faure, H., Schoenfelder, A., et al. (2011). Identification and mechanism of action of the acylguanidine MRT-83, a novel potent Smoothened antagonist. *Mol. Pharmacol.* 79, 453–460. doi: 10.1124/mol.110.069708

Ruat, M., Faure, H., and Daynac, M. (2015). Smoothened, stem cell maintenance and brain diseases. *Top Med. Chem.* 16, 147–171. doi: 10.1007/7355_2014_83

Ruat, M., Hoch, L., Faure, H., and Rognan, D. (2014). Targeting of Smoothened for therapeutic gain. *Trends Pharmacol. Sci.* 35, 237–246. doi: 10.1016/j.tips.2014.03.002

Sacco, F., Gherardini, P. F., Paoluzi, S., Saez-Rodriguez, J., Helmer-Citterich, M., Ragnini-Wilson, A., et al. (2012). Mapping the human phosphatome on growth pathways. *Mol. Syst. Biol.* 8:603. doi: 10.1038/msb.2012.36

Samanta, J., Grund, E. M., Silva, H. M., Lafaille, J. J., Fishell, G., and Salzer, J. L. (2015). Inhibition of Gli1 mobilizes endogenous neural stem cells for remyelination. *Nature* 526, 448–452. doi: 10.1038/nature14957

Sanchez, M. A., and Armstrong, R. C. (2018). Postnatal Sonic hedgehog (Shh) responsive cells give rise to oligodendrocyte lineage cells during myelination and in adulthood contribute to remyelination. *Exp. Neurol.* 299, 122–136. doi: 10.1016/j.expneurol.2017.10.010

Schaeren-Wiemers, N., Valenzuela, D. M., Frank, M., and Schwab, M. E. (1995). Characterization of a rat gene, rMAL, encoding a protein with four hydrophobic domains in central and peripheral myelin. *J. Neurosci.* 15, 5753–5764.

Schmidt-Heck, W., Matz-Soja, M., Aleithe, S., Marbach, E., Guthke, R., and Gebhardt, R. (2015). Fuzzy modeling reveals a dynamic self-sustaining network of the GLI transcription factors controlling important metabolic regulators in adult mouse hepatocytes. *Mol. Biosyst.* 11, 2190–2197. doi: 10.1039/c5mb00129c

Sharpe, H. J., Wang, W., Hannoush, R. N., and de Sauvage, F. J. (2015). Regulation of the oncoprotein Smoothened by small molecules. *Nat. Chem. Biol.* 11, 246–255. doi: 10.1038/nchembio.1776

Skoda, A. M., Simovic, D., Karin, V., Kardum, V., Vranic, S., and Serman, L. (2018). The role of the Hedgehog signaling pathway in cancer: a comprehensive review. *Bosn. J. Basic Med. Sci.* 18, 8–20. doi: 10.17305/bjbms.2018.2756

Snaidero, N., Möbius, W., Czopka, T., Hekking, L. H. P., Mathisen, C., Verkleij, D., et al. (2014). Myelin membrane wrapping of CNS axons by PI(3,4,5)P3-dependent polarized growth at the inner tongue. *Cell* 156, 277–290. doi: 10.1016/j.cell.2013.11.044

Starost, L., Lindner, M., Herold, M., Xu, Y. K. T., Drexler, H. C. A., Heß, K., et al. (2020). Extrinsic immune cell-derived, but not intrinsic oligodendroglial factors contribute to oligodendroglial differentiation block in multiple sclerosis. *Acta Neuropathol.* 140, 715–736. doi: 10.1007/s00401-020-02217-8

Sun, D., Liu, X., Zhu, L., and Zhang, B. (2021). Zinc-finger E-box-binding homeobox 1 alleviates acute kidney injury by activating autophagy and the AMPK/mTOR pathway. *Mol. Med. Rep.* 23:443. doi: 10.3892/mmr.2021.12082

Teperino, R., Aberger, F., Esterbauer, H., Riobo, N., and Pospisilik, J. A. (2014). Canonical and non-canonical Hedgehog signalling and the control of metabolism. *Semin. Cell Dev. Biol.* 33, 81–92. doi: 10.1016/j.semcdb.2014.05.007

Teperino, R., Amann, S., Bayer, M., McGee, S. L., Loipetzberger, A., Connor, T., et al. (2012). Hedgehog partial agonism drives Warburg-like metabolism in muscle and brown fat. *Cell* 151, 414–426. doi: 10.1016/j.cell.2012.09.021

Tirou, L., Russo, M., Faure, H., Pellegrino, G., Sharif, A., and Ruat, M. (2020). C9C5 positive mature oligodendrocytes are a source of Sonic Hedgehog in the mouse brain. *PLoS One* 15:e0229362. doi: 10.1371/journal.pone.0229362

Traiffort, E., Kassoussi, A., Zahaf, A., and Laouarem, Y. (2020). Astrocytes and microglia as major players of myelin production in normal and pathological conditions. *Front. Cell Neurosci.* 14:79. doi: 10.3389/fncel.2020.00079

Varjosalo, M., and Taipale, J. (2008). Hedgehog: functions and mechanisms. *Genes Dev.* 22, 2454–2472. doi: 10.1101/gad.1693608

Wang, J., Lu, J., Bond, M. C., Chen, M., Ren, X.-R., Lyerly, H. K., et al. (2010). Identification of select glucocorticoids as Smoothened agonists: potential utility for regenerative medicine. *Proc. Natl. Acad. Sci. U.S.A.* 107, 9323–9328. doi: 10.1073/pnas.0910712107

Wilson, C. W., Chen, M.-H., and Chuang, P.-T. (2009). Smoothened adopts multiple active and inactive conformations capable of trafficking to the primary cilium. *PLoS One* 4:e5182. doi: 10.1371/journal.pone.0005182

Xing, Y. L., Röth, P. T., Stratton, J. A. S., Chuang, B. H. A., Danne, J., Ellis, S. L., et al. (2014). Adult neural precursor cells from the subventricular zone contribute significantly to oligodendrocyte regeneration and remyelination. *J. Neurosci.* 34, 14128–14146. doi: 10.1523/JNEUROSCI.3491-13.2014

Yam, P. T., and Charron, F. (2013). Signaling mechanisms of non-conventional axon guidance cues: the Shh, BMP and Wnt morphogens. *Curr. Opin. Neurobiol.* 23, 965–973. doi: 10.1016/j.conb.2013.09.002

Yang, H., Xiang, J., Wang, N., Zhao, Y., Hyman, J., Li, S., et al. (2009). Converse conformational control of smoothened activity by structurally related small molecules. *J. Biol. Chem.* 284, 20876–20884. doi: 10.1074/jbc.M807648200

Yeung, M. S. Y., Djelloul, M., Steiner, E., Bernard, S., Salehpour, M., Possnert, G., et al. (2019). Dynamics of oligodendrocyte generation in multiple sclerosis. *Nature* 566, 538–542. doi: 10.1038/s41586-018-0842-3

Zhao, C., Ma, D., Zawadzka, M., Fancy, S. P. J., Elis-Williams, L., Bouvier, G., et al. (2015). Sox2 sustains recruitment of oligodendrocyte progenitor cells following CNS demyelination and primes them for differentiation during remyelination. *J. Neurosci.* 35, 11482–11499. doi: 10.1523/JNEUROSCI.3655-14.2015

Zuchero, J. B., Fu, M., Sloan, S. A., Ibrahim, A., Olson, A., Zaremba, A., et al. (2015). CNS myelin wrapping is driven by actin disassembly. *Dev. Cell* 34, 152–167. doi: 10.1016/j.devcel.2015.06.011

Conflict of Interest: The authors declare that the research was conducted in the absence of any commercial or financial relationships that could be construed as a potential conflict of interest.

Publisher's Note: All claims expressed in this article are solely those of the authors and do not necessarily represent those of their affiliated organizations, or those of the publisher, the editors and the reviewers. Any product that may be evaluated in this article, or claim that may be made by its manufacturer, is not guaranteed or endorsed by the publisher.

Copyright © 2022 Del Giovane, Russo, Tirou, Faure, Ruat, Balestri, Sposato, Basoli, Rainer, Kassoussi, Traiffort and Ragnini-Wilson. This is an open-access article distributed under the terms of the Creative Commons Attribution License (CC BY). The use, distribution or reproduction in other forums is permitted, provided the original author(s) and the copyright owner(s) are credited and that the original publication in this journal is cited, in accordance with accepted academic practice. No use, distribution or reproduction is permitted which does not comply with these terms.

frontiers in Cellular Neuroscience

ORIGINAL RESEARCH
published: 12 January 2022
doi: 10.3389/fncel.2021.773709

Histone Acetylation Defects in Brain Precursor Cells: A Potential Pathogenic Mechanism Causing Proliferation and Differentiation Dysfunctions in Mitochondrial Aspartate-Glutamate Carrier Isoform 1 Deficiency

Eleonora Poeta[1], Sabrina Petralla[1], Giorgia Babini[1], Brunaldo Renzi[1], Luigi Celauro[1], Maria Chiara Magnifico[2], Simona Nicole Barile[3], Martina Masotti[1], Francesca De Chirico[1], Francesca Massenzio[1], Luigi Viggiano[4], Luigi Palmieri[2,3], Marco Virgili[1], Francesco Massimo Lasorsa[2,3] and Barbara Monti[1]**

[1] Department of Pharmacy and Biotechnology, University of Bologna, Bologna, Italy, [2] Department of Biosciences, Biotechnologies and Biopharmaceutics, University of Bari Aldo Moro, Bari, Italy, [3] CNR Institute of Biomembranes, Bioenergetics and Molecular Biotechnologies, Bari, Italy, [4] Department of Biology, University of Bari Aldo Moro, Bari, Italy

Mitochondrial aspartate-glutamate carrier isoform 1 (AGC1) deficiency is an ultra-rare genetic disease characterized by global hypomyelination and brain atrophy, caused by mutations in the *SLC25A12* gene leading to a reduction in AGC1 activity. In both neuronal precursor cells and oligodendrocytes precursor cells (NPCs and OPCs), the AGC1 determines reduced proliferation with an accelerated differentiation of OPCs, both associated with gene expression dysregulation. Epigenetic regulation of gene expression through histone acetylation plays a crucial role in the proliferation/differentiation of both NPCs and OPCs and is modulated by mitochondrial metabolism. In AGC1 deficiency models, both OPCs and NPCs show an altered expression of transcription factors involved in the proliferation/differentiation of brain precursor cells (BPCs) as well as a reduction in histone acetylation with a parallel alteration in the expression and activity of histone acetyltransferases (HATs) and histone deacetylases (HDACs). In this study, histone acetylation dysfunctions have been dissected in *in vitro* models of AGC1 deficiency OPCs (Oli-Neu cells) and NPCs (neurospheres), in physiological conditions and following pharmacological treatments. The inhibition of HATs by curcumin arrests the proliferation of OPCs leading to their differentiation, while the inhibition of HDACs by suberanilohydroxamic acid (SAHA) has only a limited effect on proliferation, but it significantly stimulates the differentiation of OPCs. In NPCs, both treatments determine an alteration in the commitment toward glial cells. These data contribute to clarifying the molecular and epigenetic mechanisms regulating the proliferation/differentiation of OPCs and NPCs. This will

OPEN ACCESS

Edited by:
Davide Lecca,
University of Milan, Italy

Reviewed by:
Xianshuang Liu,
Henry Ford Hospital, United States
Friederike Pfeiffer,
University of Tübingen, Germany
Josephine Lok,
Massachusetts General Hospital and Harvard Medical School, United States

***Correspondence:**
Francesco Massimo Lasorsa
francesco.lasorsa@uniba.it
Barbara Monti
b.monti@unibo.it

Specialty section:
This article was submitted to Non-neuronal Cells, a section of the journal Frontiers in Cellular Neuroscience

Received: *10 September 2021*
Accepted: *29 November 2021*
Published: *12 January 2022*

Citation:
Poeta E, Petralla S, Babini G, Renzi B, Celauro L, Magnifico MC, Barile SN, Masotti M, De Chirico F, Massenzio F, Viggiano L, Palmieri L, Virgili M, Lasorsa FM and Monti B (2022) Histone Acetylation Defects in Brain Precursor Cells: A Potential Pathogenic Mechanism Causing Proliferation and Differentiation Dysfunctions in Mitochondrial Aspartate-Glutamate Carrier Isoform 1 Deficiency. Front. Cell. Neurosci. 15:773709. doi: 10.3389/fncel.2021.773709

help to identify potential targets for new therapeutic approaches that are able to increase the OPCs pool and to sustain their differentiation toward oligodendrocytes and to myelination/remyelination processes in AGC1 deficiency, as well as in other white matter neuropathologies.

Keywords: white matter disorder, mitochondria, epigenetics, oligodendrocytes, neurons, SLC25A12/aralar1/AGC1 deficiency

INTRODUCTION

Mitochondrial aspartate-glutamate carrier isoform 1 (AGC1) deficiency (DEE39; OMIM #612949; ICD-10 Code: G31.8; ORPHA Nr: ORPHA353217) is an ultra-rare (less than 10 cases known worldwide) developmental and epileptic encephalopathy caused by mutations in *SLC25A12* gene encoding the AGC1, a member of the SLC25 family of transport proteins of the inner mitochondrial membrane. Young patients develop normally during the first months of life, and subsequently begin to have seizures, muscular hypotonia, and psychomotor retardation. MRI showed decreased cerebral volume and hypomyelination with reduced content of N-acetyl aspartate (NAA), which is an acetate donor for myelin lipid synthesis (Wibom et al., 2009; Falk et al., 2014; Pfeiffer et al., 2020). More recent MRI support for the classification of SLC25A12-related disease as leukodystrophy, but this is still debated (Kavanaugh et al., 2019).

In humans, AGC1/SLC25A12 (also named, aralar1) is expressed in the brain and muscles, while the second isoform, AGC2/SLC25A13 (also named, citrin) is mainly expressed in the liver. Both the AGC isoforms catalyze the import of cytosolic glutamate plus a proton in the matrix, in exchange for aspartate, and they are components of the malate-aspartate shuttle (MAS) that allows for the entry of the glycolysis-derived NADH to the mitochondria essential for correct pyruvate oxidation (Llorente-Folch et al., 2013). Different mutations in the *SLC25A12* gene have been identified, all leading to the impairment of AGC1 activity and reduced NAA content in the patients' brain, along with the onset of pathological features similar to other white matter diseases (Wibom et al., 2009; Falk et al., 2014; Pfeiffer et al., 2020). Neurons are the primary producers of NAA in the Central Nervous System (CNS) and they deliver this metabolite to oligodendrocytes as a source of acetyl moieties that are needed to produce myelin-associated lipids. This implies a continuous cross-talk between neurons and oligodendrocytes, with an exchange of NAA to support myelination (Moffett et al., 2007; Nave and Werner, 2014).

Until now, studies have mainly focused to mature neurons in the murine model of AGC1 deficiency, showing profound neuronal metabolic disturbances with a limited NAA production especially affecting the nigrostriatal pathway (Ramos et al., 2011; Llorente-Folch et al., 2013; Juaristi et al., 2017). More recently, it has been demonstrated that the downregulation of AGC1 inhibits proliferation and NAA synthesis in neuronal precursor cells (NPCs), as well as reduces the proliferation of oligodendrocytes precursor cells (OPCs) leading to their spontaneous and precocious differentiation in both *in vitro* and *in vivo* murine models. Interestingly, while the proliferation defects in NPCs are associated with a reduced mitochondrial respiration causing energy fault (Profilo et al., 2017), in OPCs, this appears related to a dysregulation in the expression of trophic factors and receptors involved in the proliferation/differentiation processes (Petralla et al., 2019). Since epigenetic regulation of gene expression through histone acetylation is involved in the proliferation/differentiation of both NPCs and OPCs (Juliandi et al., 2010; Emery and Lu, 2015; Hernandez and Casaccia, 2015) and NAA can act as a source of acetate for histone acetylation (Long et al., 2013; Bogner-Strauss, 2017), a reduced AGC1 activity may be linked to epigenetic/transcriptional changes affecting the OPCs pool maintenance, their differentiation toward oligodendrocytes and, therefore, lead to the myelination/remyelination processes. To test our hypothesis, in this study, we focused on the transcription factors known to be involved in the proliferation/differentiation of OPCs and NPCs, as well as on histone post-translational modifications (PTMs), histone acetyltransferases (HATs), and histone deacetylates (HDACs) in two different *in vitro* models of AGC1 deficiency: a stable clone of immortalized murine OPCs (Oli-Neu) with a partial silencing of AGC1 and the relative control and neurospheres from the sub-ventricular zone (SVZ) of $AGC1^{\pm}$ and $AGC1^{+/+}$ mice, as a model of NPCs (Petralla et al., 2019). Finally, to better clarify HATs and HDACs implication in the unbalance regulation of brain cells in the biological processes, we performed pharmacological inhibitions through the general HDAC inhibitor, suberanilohydroxamic acid (SAHA; Zhou et al., 2011), approved by FDA for cancer therapy, and the natural compound, curcumin, a specific HAT p-300 activity inhibitor (Sunagawa et al., 2018), in both the AGC1 deficiency models of siAGC1 Oli-neu cells and $AGC1^{\pm}$ mice-derived neurospheres.

MATERIALS AND METHODS

Cell Cultures

Oli-Neu cells (kindly provided by Jacqueline Trotter, University of Mainz, Germany, RRID:CVCL_IZ82) stably transfected with a scrambled control, shRNA, or an shRNA targeting the AGC1 coding sequence, which induces a 60% reduction of carrier expression, were obtained as previously published (Petralla et al., 2019). Cells were grown at 37°C and 5% CO_2 on poly-L-lysine (10 μg/ml; Sigma-Aldrich, St Louis, MO, United States) coated Petri dishes in SATO medium [DMEM basal medium, 2 mM of glutamine, 10 μg/ml of insulin, 5.5 μg/ml of transferrin, 38.72 nM of sodium selenite, 100 μM of putrescine, 520 nM of L-thyroxine (T4), 500 nM of triiodo-L-thyronine (T3), 200 nM of progesterone, 25 μg/ml of gentamycin;

all from Sigma-Aldrich, excluding insulin-transferrin-sodium selenite 100X supplement, Thermo Fisher Scientific, Waltham, Massachusetts, United States], supplemented with 1% heat-inactivated Horse Serum (HS; Sigma-Aldrich, St Louis, MO, United States) and 1 μg/ml of puromycin (Sigma-Aldrich, St Louis, MO, United States). Once confluent, the cells were detached with 0.01% trypsin–0.02% ethylenediaminetetraacetic acid (EDTA)-Hank's Balanced Salt Solution (HBSS; Sigma-Aldrich, St Louis, MO, United States).

Oxygen Consumption Rates Measurements

Oxygen consumption rates (OCRs) were measured with an XF^{96} Extracellular Flux analyzer (Agilent Technologies, MA, United States). The 30,000 cells/well were incubated for 1 h in a humidified incubator at 37°C in the presence of unbuffered XF base medium supplemented with 1 g/l glucose, 1 g/l glucose with 1 mM pyruvate, 1 g/l glucose with 2 mM glutamine, or 1 g/l glucose with 1 mM pyruvate and 2 mM glutamine. After incubation, OCRs were measured as previously described (Brand and Nicholls, 2011). More in the detail, basal OCRs were recorded, prior to the sequential injections of 2 μM of oligomycin, as an inhibitor of ATP synthase and indicating the oxygen consumption associated with mitochondrial ATP production (three measurements for total 15 min), 0.5 μM of FCCP, as mitochondrial uncoupler to collapse the mitochondrial membrane potential and to determine the maximal respiratory capacity (four measurements for total 15 min), and 1 μM antimycin A with 1 μM of rotenone, as mitochondrial respiratory chain inhibitors to evaluate the non-mitochondrial oxygen consumption (three measurements for total 15 min).

Extraction and Isolation of Histones

The histone component of Oli-Neu nuclei was isolated and purified by using the acid extraction protocol (Shechter et al., 2007). The 5×10^6 cells were lysed in 1 ml of hypotonic lysis buffer (10 mM of Tris-Cl pH 8.0, 1 mM of KCl, 1.5 mM of $MgCl_2$, 1 mM of DTT, and 1X protease and phosphatase inhibitor cocktails; all from Sigma-Aldrich, St Louis, MO, United States). After 30 min at 4°C in mild shaking to favor hypotonic swelling and lysis, intact nuclei were pelleted 10,000 × g for 10 min at 4°C, resuspended in 400 μL of 0. N H_2SO_4, and incubated for 30 min in rotation. After centrifugation at 16,000 × g for10 min at 4°C, 100% of trichloroacetic acid (TCA; Sigma-Aldrich, St Louis, MO, United States) was added dropwise to the supernatant to allow histones precipitation overnight at 4°C. The following day, the solution was centrifuged at 16,000 × g for 10 min at 4°C and the pellet was washed twice in glacial acetone, dried at room temperature, and resuspended in phosphate-buffered saline (PBS) with 1X protease and phosphatase inhibitor cocktails. All samples were sonicated with a Branson 250 digital sonifier, before quantification for subsequent Western Blot (WB) analysis.

Subcellular Fractionation

Cytosolic, mitochondrial, and nucleic extracts were obtained from a modified Grove BD and Bruckey protocol (Grove and Bruchey, 2001). Oli-Neu cells were lysed with a Potter homogenizer (B. Braun, Melsungen AG) in an isotonic buffer (10 mM of Hepes, 200 mM of mannitol, 70 mM of sucrose, 1 mM of EDTA pH 7.6, 1X protease and phosphatase inhibitor cocktails; all from Sigma-Aldrich, St Louis, MO, United States) and centrifuged at 800 × g for 10 min at 4°C. The supernatant (cytoplasmic fraction; CF) was separated from the pellet (nucleic fraction) that was washed two times with buffer A (2 mM of Hepes pH 7.9, 1 mM of NaCl, 3 mM of $MgCl_2$, 0.1% of NP40, 10% of glycerol, 0.2 mM of EDTA, 1 mM of DTT, 1X protease and phosphatase inhibitor cocktails) and then with buffer B (20 mM of Hepes pH 7.9, 0.2 mM of EDTA, 200 mM of glycerol, 1 mM of DTT, 1X protease and phosphatase inhibitor cocktails). Washed nuclei were resuspended in the extraction buffer with salt (20 mM of Hepes, pH 7.9, 400 mM of NaCl, 2% of sodium dodecyl sulfate (SDS), 0.2 mM of EDTA, 20 mM of glycerol, 1 mM of DTT, 1X protease and phosphatase inhibitor cocktails). To obtain mitochondria, CF was centrifuged at 14,000 × g/20 min/4°C and the pellet (mitochondria) was resuspended in isotonic buffer with 1X protease and phosphatase inhibitor cocktails. The total protein contents were quantified (Lowry et al., 1951) and stored at −80°C until used.

Activities of Histone Acetyltransferase and Histone Deacetylases Assay

To quantify the activities of HATs and HDACs in Oli-Neu cells, the HAT Activity Assay Kit (Abcam, Cambridge, United Kingdom) and the Epigenase HDAC Activity/Inhibition Direct Assay Kit (EpigGenetek, NY, United States) were respectively used, according to the manufacturer's instruction. For HATs activity assays, 50 μg of nuclear extract in 40 μL of water (final volume) were added in a 96-well plate; 40 μL of water instead of samples were used for background reading; 10 μL of cell nuclear extract (NE) were added to 30 μL of water as a positive control. Depending on color development, the plates were incubated 1/4 h at 37°C and read OD440 nm at different times during incubation. To measure the activity of the HDACs, 5 μg of nuclear extracts were diluted with kit-specific reagents up to 50 μL/well (final volume). Only the reagents were used as a blank sample. The signal was detected at 450 nm with a Multiplate Spectrophotometric Reader (Bio-rad Laboratories, Milano, Italy) after 1–2 h of incubation.

Neurospheres Preparation

Neurospheres were initially acquired from the SVZ of 8-months-old C57BL/6N wild-type and heterozygous SLC25A12 male mice (*Mus musculus*), generated by the Texas A&M Institute for Genomic Medicine (Houston, Texas, United States), as previously described (Petralla et al., 2019). Animals were fed *ad libitum* with the 2018 Teklad global diet (Envigo, United States), in a 12/12-h light-dark cycle at 20 ± 2°C and set at humidity; appropriate environmental enrichments were placed to guarantee their well-being. All animal experiments were authorized by a local bioethical committee (Protocol no 3/79/2014) and performed in agreement with the Italian and European Community law (Directive 2010/63/EU) on the use

of animals for experimental purposes, and adherence to the ARRIVE Reporting Guidelines. Neurospheres were obtained through SVZ microdissection on three AGC1$^{+/+}$ and three AGC1$^{\pm}$ mice, respectively, previously anesthetized through intraperitoneal injection of 10 mg/kg xylazine followed by cervical dislocation. Fresh tissue was mechanically dissociated in HBSS, 3.9 mg/ml of N-2-hydroxyethylpiperazine-N-2-ethane sulfonic acid (HEPES), 0.5 mg/ml of $NaHCO_3$, 0.9 mg/ml of glucose, 0.5% penicillin/streptomycin, and centrifuged for 5 min at 1,000 rpm. The pellet was resuspended in papain solution (0.2 mg/ml of EDTA, 0.66 mg/ml of Papain, 0.2 mg/ml of cysteine in HBSS) and placed for 20 min at 37°C shaking at every 5 min. For further dissociation, the tissue was resuspended in HBSS and left for another 10 min at 3°C. Papain reaction was then inhibited by adding DMEM F-12 (Gibco Life Technologies, Waltham, MA, United States), and samples were centrifuged at 100 rpm for 5 min. The cells were plated in 35 mm dishes in a complete culture medium: DMEM-F12 (Gibco Life Technologies, Waltham, MA, United States) was supplemented with 2 mM of glutamine, 10 μg/ml of insulin from bovine pancreas (Sigma-Aldrich, St Louis, MO, United States), 20 ng/ml of epidermal growth factor (EGF; PeproTech EC, London, United Kingdom), 20 ng/ml of fibroblast growth factor-2 (FGF2; PeproTech), 1% of N2 (Thermo Fisher Scientific, Waltham, MA, United States), 1% of B27 (Thermo Fisher Scientific, Waltham, MA, United States), 10 units/ml of penicillin and 10 μg of streptomycin. Neo-formed neurospheres were cultured and passed every week (5/7 days of growth). For this purpose, the cells were collected and pelleted for 5 min at 1,000 rpm, washed in PBS, and centrifuged again for 5 min at 1,000 rpm. The neurospheres were dissociated through 5 min incubation in Accutase (Aurogene Srl, Roma, Italy) at 37°C, and basal DMEM F-12 was added to stop the reaction. Following centrifugation for 5 min at 1,000 rpm, single cells were resuspended in a complete culture medium to proceed with cell count in order to obtain a final cell density of 5×10^3 cells/cm^2 in 35 mm dishes. After passage 3, the neurospheres were stabilized as stable clones to be used for the experiments.

Curcumin and Suberanilohydroxamic Acid Treatments

To act on HATs and HDACs activity, Oli-Neu cells and the neurospheres were treated with the specific HAT p300 inhibitor, curcumin (Sunagawa et al., 2018) and the general HDAC inhibitor, SAHA (Zhou et al., 2011) that has been approved by FDA for cancer therapy, respectively. For WB and microscopy analysis on Oli-Neu cells, 2×10^5 cells/well were plated in a 6-well plate or 24 mm diameter glass coverslips, both previously treated with poly-L-lysine (10 μg/ml). After 2 h, complete SATO medium was replaced with a fresh medium containing SAHA (0.5 μM; 1 μM) or curcumin (10 μM; 20 μM), and the cells were incubated at 37°C in 5% CO_2 for 24 or 48 h depending on the proliferation or differentiation assays. The same dimethyl sulfoxide (DMSO) volume that was required to dissolve the molecules was used as a control. For immunostainings, the cells on glass coverslips were then fixed with 4% of paraformaldehyde (PFA) in PBS 0.1% pH 7.4 for 30 min, washed with PBS, and stored at 4°C in PBS. For WB analysis, the Oli-Neu on dishes were collected with the lysis buffer (50 mM of Tris pH7.4, 1% SDS, 1 mM of EDTA, 1X protease and phosphatase inhibitor cocktails) and kept at −80°C until use. In parallel, to study HATs and HDACs inhibition on neurospheres proliferation, the cells were plated as single stem cells in 96-well plates (5×10^3cells/well) in presence of SAHA (0.5 μM; 1 μM) or curcumin (5 μM; 10 μM) in complete DMEM F-12 culture medium; same DMSO volumes were used as control. Depending on the inhibitor's toxicity after a long-time in culture, the neurospheres were let grown 5 days in the presence of SAHA and 7 days with curcumin. In contrast, to evaluate the differentiation of neurospheres, 75 or 30 spheres were plated on 35 mm Petri dishes or 13 mm glass coverslips in complete DMEM F-12 medium and inhibitors, for subsequent WB or immunofluorescence analysis, respectively. To allow for stem cell adhesion and neuronal differentiation, both the dishes and coverslips previously treated with poly-L-lysine (10 μg/ml) were incubated at 37°C with fibronectin (1 μg/ml) for at least 3 h. After 7 days in culture, the differentiated neurospheres were collected in a lysis buffer and stored at −80°C, or fixed for 30 min with 4% of PFA in PBS 0.1% pH 7.4 and kept at 4°C in PBS.

Western Blot

The samples of oli-Neu cells and neurospheres in lysis buffer (50 mM Tris pH 7.4, 1% of SDS, 1 mM of EDTA, 1X protease and phosphatase inhibitor cocktails), were sonicated with a Branson 250 sonifier. Each sample (20 μg) was resolved in SDS–PAGE with Laemli loading buffer (Sigma-Aldrich, St Louis, MO, United States) and transferred onto a nitrocellulose membrane (GE Healthcare Life Sciences, Little Chalfont, United Kingdom) for the reaction with the following primary antibodies: Anti-acetyl-Histone H3 (Millipore, Burlington, Massachusetts, United States; Cat# 06-599, RRID:AB_2115283), CBP (D6C5) (Cell Signaling Technology, Danvers, Massachusetts; Cat# 7389, RRID:AB_2616020), CNPase (Cell Signaling; Cat# 5664, RRID:AB_10705455), CREB (48H2) (Cell Signaling; Cat# 9197, RRID:AB_331277), c-Myc (N-262) (SantaCruz Biotechnology, Dallas, Texas, United States; Cat# sc-764, RRID:AB_631276), Anti-Doublecortin (Abcam; Cat# ab18723, RRID:AB_732011), GAPDH (SantaCruz Biotechnology, Dallas, Texas, United States; Cat# sc-32233, RRID:AB_627679), GFAP (Dakopatts (Agilent Technologies), Santa Clara, California, United States; Cat# sc-33673, RRID:AB_627673), Histone Deacetylase 1 (HDAC1) (Cell Signaling; Cat# 2062, RRID:AB_2118523), HDAC2 (D6S5P) (Cell Signaling; Cat# 2540, RRID:AB_2116822), Histone Deacetylase 3 (HDAC3) (Cell Signaling; Cat# 2632, RRID:AB_331545), Histone Deacetylase 4 (HDAC4) (Cell Signaling; Cat# 2072, RRID:AB_2232915), Histone H3 (SantaCruz Biotechnology, Dallas, Texas, United States,; Cat# sc-10809, RRID:AB_2115276), HSP60 (Bioss, Woburn, Massachusetts, United States; Cat# bs-0191R-HRP, RRID:AB_11117391), MAX (H-2) (SantaCruz Biotechnology, Dallas, Texas, United States; Cat# sc-8011, RRID:AB_627913), Anti-NG2 (Abcam, Cambridge, United Kingdom; Cat# ab83178, RRID:AB_10672215), NRSF (P-18) (SantaCruz Biotechnology, Dallas, Texas, United States; Cat# sc-15120, RRID:AB_2179628), Olig2 (SantaCruz Biotechnology, Dallas, Texas, United States; Cat#

sc-48817, RRID:AB_2157550), PanMetH3 (MBL International, Woburn, Massachusetts, United States; Cat# LS-A4069, RRID:AB_591306), PDGFRα (SantaCruz Biotechnology, Dallas, Texas, United States; Cat# sc-338, RRID:AB_631064), Phospho-CREB (Ser133) (Cell Signaling; Cat# 9198, RRID:AB_2561044). The following specific HRP-linked secondary antibodies (horseradish peroxidase conjugated) were used: Goat anti-Mouse (Jackson ImmunoResearch, West Grove, Pennsylvania, United States; Cat# 115-035-146, RRID:AB_2307392), Goat anti-Rabbit (Jackson ImmunoResearch; Cat# 111-035-144, RRID:AB_230739), and Mouse anti-Goat (SantaCruz Biotechnology, Dallas, Texas, United States; Cat# sc-2354, RRID:AB_628490). Labeled proteins were then detected by using Clarity^{TM} Western ECL Substrate (Bio-Rad). Densitometric analysis were performed by using Biorad Image Lab software 6.0.0 (RRID:SCR_014210). All primary antibodies were diluted 1:1,000 excl. GAPDH 1:20,000, whereas secondary antibodies were diluted at 1:5,000 in 0.1% Tween-20/PBS.

Immunofluorescence Analysis

Oli-Neu cells and neurospheres fixed on coverslips were permeabilized in 0.1% Triton X-100/PBS and then incubated with the following primary antibodies: AGC1/Aralar1 (SantaCruz Biotechnology, Dallas, Texas, United States; Cat# sc-271056, RRID:AB_10608837), CBP (D6C5) (Cell Signaling T; Cat# 7389, RRID:AB_2616020), CNPase (Cell Signaling; Cat# 5664, RRID:AB_10705455), c-Myc (9E10) (SantaCruz Biotechnology, Dallas, Texas, United States; Cat# sc-764, RRID:AB_631276), Anti-Doublecortin (Abcam; Cat# ab18723, RRID:AB_732011), GFAP (Dakopatts; Cat# sc-33673, RRID:AB_627673), HDAC2 (D6S5P) (Cell Signaling; Cat# 2540, RRID:AB_2116822), Histone Deacetylase 3 (HDAC3) (Cell Signaling; Cat# 2632, RRID:AB_331545), HSP60 (Bioss; Cat# bs-0191R-HRP, RRID:AB_11117391), anti-Ki67 (Abcam Cambridge, United Kingdom; Cat# ab15580, RRID:AB_443209), MAX (H-2) (SantaCruz Biotechnology, Dallas, Texas, United States; Cat# sc-8011, RRID:AB_627913), NRSF (P-18) (SantaCruz; Cat# sc-15120, RRID:AB_2179628), Olig2 (SantaCruz Biotechnology, Dallas, Texas, United States; Cat# sc-48817, RRID:AB_2157550), and Phospho-CREB (Ser133) (Cell Signaling; Cat# 9198, RRID:AB_2561044). The fluorescent secondary antibodies used were as follows: Donkey anti-Mouse IgG Alexafluor 555 (Abcam, Cambridge, United Kingdom; Cat# ab150106, RRID:AB_2857373), Goat anti-Mouse IgG Alexafluor 488 (Abcam Cambridge, United Kingdom; Cat# ab150113, RRID:AB_2576208), Goat anti-Rabbit IgG Alexafluor 488 (Abcam, Cambridge, United Kingdom; Cat# ab150077, RRID:AB_2630356), and Goat anti-Rabbit IgG Alexafluor 555 (Abcam; Cat# ab150078, RRID:AB_2722519). Nuclei were stained with Hoechst 33258 (Sigma-Aldrich) or DAPI (Santa Cruz Biotechnology, Dallas, Texas, United States, Cat#. sc-24941). For cell counting, stained Oli-Neu cells, three randomly selected fields/coverslip were acquired by using the Nikon EZ-C1 microscope (10X or 100X objective); positive cells were counted and the labeling index was expressed as the ratio of positive/total cells using Fiji software (ImageJ2, Fiji; RRID:SCR_002285). The confocal images of the neurospheres were obtained with 10 X or 60 X objective and the z-stack function (40 total stacks), and 3D image reconstruction were performed by using Fiji ImageJ2 software z-project plugin. The fluorescence intensity index was estimated as the ratio of the markers' positive cells intensity/total cells fluorescence intensity stained with DAPI.

Neurospheres Proliferation

To evaluate the growth rate of AGC1$^{+/+}$ and AGC1$^{\pm}$ neurospheres, following HATs and HDACs inhibition, five different images were acquired in bright field mode (10 X objective) for each 96-well (5×10^3 cells/well) by using an Eclipse TE2000-s—Nikon microscope. The images were analyzed with Fiji ImageJ2 using the publicly available colony and cell counting method (Choudhry, 2016) and only aggregates with areas greater than 400 μm^2 were considered.

Oli-Neu Cells Extensions Number and Length Measurement

To analyze the extension number and length of Oli-Neu cells in the presence or absence of inhibitors, five randomly selected fields for each 6-well (2×10^5 cells/well) were acquired (20 × objective) with an Eclipse TS100—Nikon microscope. The length of the processes was measured with Fiji ImageJ2 software. Scale bar distance in pixels and the corresponding distance in micrometers were set by using the reference scale bar and the SET SCALE function (Analyze menu). Each cell process was traced with the segmented-line function and the MEASURE function (Analyze menu) was used to determine the length of the extensions in micrometers. The number of processes was directly determined from individual processes of length measurement.

Statistical Analysis

All results were subjected to statistical analysis by using Student's *t*-test or one-way ANOVA followed by Bonferroni's *post hoc* comparison test. In drug treatments, to evaluate both AGC1 silencing and HATs/HDACs inhibition, two-way ANOVA followed by Dunnett's *post hoc* comparison test, was used. Statistical analysis was performed with GraphPad Prism 4 software (GraphPad Prism, San Diego, CA, United States; RRID:SCR_002798), and only p-values < 0.05 were considered statistically significant.

RESULTS

Expression of Transcription Factors in Aspartate-Glutamate Carrier Isoform 1-Deficient Oligodendrocytes Precursor Cells and Neuronal Precursor Cells

In order to understand whether the dysregulation in trophic factors and receptors involved in the proliferation deficit of OPCs with AGC1 deficiency could be related to a transcriptional alteration, we evaluated the expression of transcription factors that are known to play a role in the proliferation/differentiation of BPCs, such as c-Myc (Magri et al., 2014; Palazuelos et al., 2014) and its co-factor, Max

(Carroll et al., 2018), Olig2 (Meijer et al., 2012), the Repressor element 1 silencing transcription factor/neuron-restrictive silencing factor (REST/NRSF) (Song et al., 2015), as well as the cAMP response element binding protein (CREB) (Yan et al., 2013). We initially performed WB analysis on Oli-Neu (immortalized mouse OPCs) cells, with a stable downregulation of the *SLC25A12* gene (*siAGC1*) and on control cells, as well on the NPCs model of neurospheres, derived from the SVZ of C57BL/6N wild-type (AGC1$^{+/+}$) and AGC1$^{\pm}$ mice, both generated as previously described (Petralla et al., 2019). Oxygen consumption rate (OCR) measurements confirmed that siAGC1 Oli-Neu cells do not exhibit a mitochondrial respiratory deficit compared to the control cells (**Figure 1**). However, siAGC1 Oli-Neu cells revealed an altered transcriptional profile with a significant reduction in both c-Myc and Max, as well as in Olig2 expression, together with a marked increase in CREB activation through its phosphorylation on serine 133. Differently, no significant changes in total CREB and REST/NRSF were observed (**Figures 2A–G**). Similar data were obtained in immunofluorescence experiments with double staining for AGC1 and transcription factors. As shown in **Figure 2H**, we detected lower c-Myc and Olig2 labeling in siAGC1 Oli-Neu

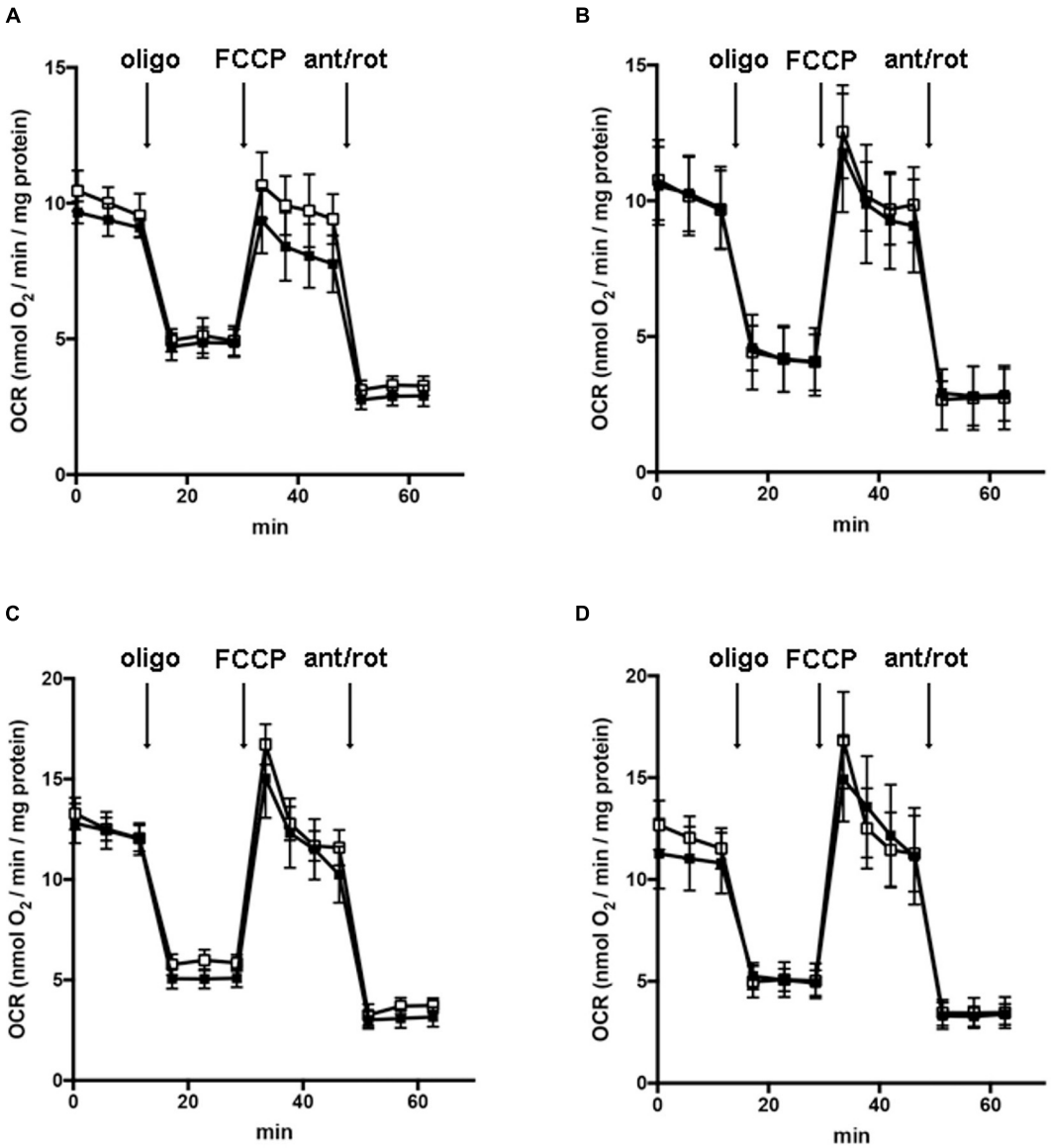

FIGURE 1 | Downregulation of AGC1 does not inhibit mitochondrial respiration in Oli-Neu cells. Oxygen consumption rates (OCRs) were measured with XF^{96} extracellular flux analyzer (SeaHorse; Agilent Technologies, MA, United States) in control (□) and siAGC1 Oli-Neu (■) cells incubated for 1 h in XF base medium supplemented with 1 g/l glucose **(A)**, 1 g/l glucose with 1 mM pyruvate **(B)**, 1 g/l glucose with 2 mM glutamine **(C)**, or 1 g/l glucose with 1 mM pyruvate with 2 mM glutamine **(D)**. Oli-Neu cells were exposed to sequential additions of 2 μM oligomycin, 0.5 μM FCCP, and 1 μM antimycin A with 1 μM rotenone. OCR data were normalized to cell protein content. Mean values ± SD from three independent experiments each including 5–6 replicates per cell type are shown.

cells compared to the control cells, with no relevant differences in REST intensity, whereas phospho-CREB staining resulted increased, thus indicating an altered transcriptional profile when AGC1 is downregulated. Parallel experiments have been carried on neurospheres from AGC1$^{+/+}$ and AGC1$^{\pm}$ mice used as a near-perfect *in vitro* model to provide a consistent and self-renewable source of NSPs, which can lead to neuronal-restricted precursor cells, OPCs, and astrocytes (Tropepe et al., 1999; Petralla et al., 2019). We previously demonstrated that neurospheres from AGC1$^{\pm}$ mice display a reduction in OPCs with a parallel increase in oligodendrocytes, neuronal-restricted progenitors, and astrocytes compared to those from AGC1$^{+/+}$ animals (Petralla et al., 2019). In this study, in AGC1$^{\pm}$ mice neurospheres, we found a reduction in c-Myc, but not in its co-factor Max, and a decrease in Olig2 expression. Instead, no changes were observed in total CREB and REST/NRSF, whereas CREB phosphorylation turned out the significant reduction in AGC1$^{\pm}$ neurospheres compared to AGC1$^{+/+}$ (**Figures 2I–O**).

Taken together, these data pointed out that, in both the models with reduced AGC1 levels, the expression pattern of transcription factors involved in the proliferation/differentiation of BPCs is altered. Olig2 and c-Myc were strongly downregulated, whereas pCREB increases in siAGC1 Oli-Neu cells and decreases in AGC1$^{\pm}$ neurospheres, probably as a consequence of t more heterogeneous cellular composition of the NSCs model.

Histone Acetylation, Histone Deacetylases, and Histone Acetyltransferases in Aspartate-Glutamate Carrier Isoform 1-Deficient Oligodendrocytes Precursor Cells and Neuronal Precursor Cells

It is well known that epigenetic mechanisms related to histone modification may have an impact on the proliferation/differentiation of OPCs and NPCs (Tiane et al., 2019; Zhang et al., 2020). Therefore, in OPCs and NPCs with AGC1 deficiency, we evaluated histone PTMs, as well as the activity and the expression profiles of the two classes of enzymes promoting histone acetylation, i.e., HATs, or deacetylation processes, i.e., HDACs. From WB and immunofluorescence analysis, siAGC1 Oli-Neu cells displayed a significant reduction in both histone H3 acetylation and methylation, with a parallel increase in its phosphorylation (**Figures 3A–D**). In siAGC1 Oli-Neu cells, the resultant HATs activity was not significantly lower than the control cells (**Figure 3E**), whereas the p300/CREB-Binding Protein (CBP), the most important protein of HATs family for brain development (Sheikh, 2014; Lipinski et al., 2019), came out significantly downregulated (**Figures 3F,G**). Differently, the total HDACs activity proved to be significantly reduced in siAGC1 Oli-Neu cells compared to the controls (**Figure 3H**). Therefore, we further investigated the expression of the HDACs isoforms mainly involved in CNS development, i.e., the nuclear isoform 1, 2, and 3 of class I HDAC and the isoform 4 of the class II HDAC (Morris and Monteggia, 2013; D'Mello, 2020; **Figures 3I–N**). The WB analysis demonstrated that HDAC2 (**Figure 3L**) and HDAC3 (**Figure 3K**) levels were significantly lower in siAGC1 Oli-Neu cells compared to the controls, whereas HDAC1 (**Figure 3J**) and HDAC4 (**Figure 3M**) expression remained unchanged. Similar data were obtained in immunofluorescence experiments, where both HDAC2 and HDAC3 costained with AGC1 turned out to be weaker in cells where AGC1 is downregulated (**Figure 3N**), suggesting that AGC1 inhibition affects the balance between acetylation and deacetylation pathways in OPCs.

Histone acetylation and the expression of the related enzymes were also investigated in neurospheres derived from AGC1$^{\pm}$ and AGC1$^{+/+}$ mice (**Figure 4**). In AGC1$^{\pm}$ neurospheres, we observed lower levels of histone H3 acetylation (**Figures 4A,B**) vs. higher levels of histone H3 methylation (**Figures 4A,C**) and phosphorylation (**Figures 4A,D**), while CBP turned out strongly downregulated (**Figures 4E,F**).

Concerning HDAC isoforms, HDAC2 (**Figures 4G,I**), which regulates together with HDAC1 (**Figures 4G,H**) the oligodendorcyte and astrocytes lineage fate switch (Ye et al., 2009), and HDAC4 (**Figures 4G,K**) resulted downregulated in AGC1$^{\pm}$ neurospheres compared to AGC1$^{+/+}$, whereas HDAC3 (**Figures 4G,J**) revealed an opposite expression profile. Data were confirmed through immunofluorescence analysis (**Figure 4L**), where AGC1$^{\pm}$ neurospheres showed lower HDAC2 labeling and higher levels of HDAC3 compared to AGC1$^{+/+}$. Additionally, after subcellular fractionation on Oli-neu cells, no relevant differences were observed for HDAC2 and HDAC3 localization in siAGC1 cells compared to the control, whereas CBP appeared mainly localized in the cytosolic compartment and less represented in the nuclear fraction, probably as part of other different multimeric complexes (**Figure 5**).

Overall, these data revealed that histone PTMs are affected by AGC1 downregulation in both immortalized OPCs and NPCs, in which acetylation appeared reduced with significantly low levels of the HAT CBP. In addition, although HDACs pathways turned out differently impaired in the two distinct models, our data suggest an altered balance of HATs/HDACs expression and activity following AGC1 inhibition.

Histone Acetyltransferases Inhibition Through Curcumin in the Proliferation/Differentiation of Oligodendrocytes Precursor Cells and Neuronal Precursor Cells

In order to clarify the role of histone acetylation in the proliferation/differentiation OPCs and NPCs, and how this biological process is involved in AGC1-deficiency brain cells proliferation defects, we further performed a pharmacological inhibition of either HATs or HDACs in both the control and siAGC1 Oli-Neu cells, as well as AGC1$^{+/+}$ and AGC1$^{\pm}$ neurospheres.

To inhibit HATs activity, we used curcumin, a well-known inhibitor of p300/CBP (Balasubramanyam et al., 2004). In cells, it promotes proteasome-dependent degradation of p300 and the closely related CBP protein without affecting the HATs PCAF or GCN5, in addition to inhibiting the acetyltransferase

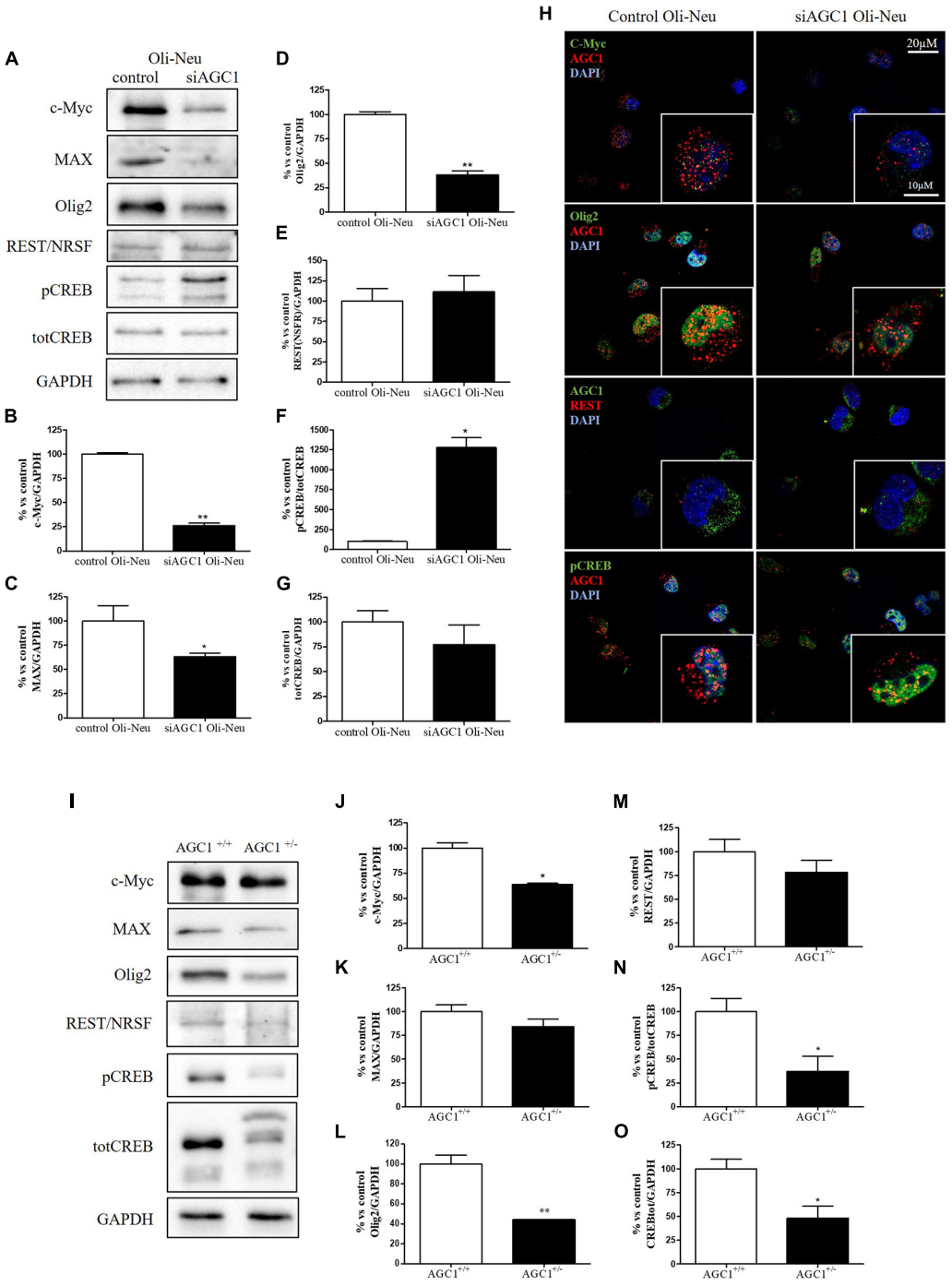

FIGURE 2 | Different expression of proliferation/differentiation transcription factors characterizes both Oli-Neu and neurospheres AGC1 deficiency *in vitro* models. WB and relative densitometries of c-Myc **(A,B)**, MAX **(A,C)**, Olig2 **(A,D)**, REST **(A,E)**, pCREB **(A,F)**, and total CREB **(A,G)** expression in Oli-Neu cells; GAPDH was used for endogenous normalization. Confocal microscopy images (100X) of the transcription factors **(H)** in Oli-Neu cells; nuclei were labeled with DAPI. Scale bars: 20 and 10 μm. WB analysis and relative densitometries of c-Myc **(I,J)**, MAX **(I,K)**, Olig2 **(I,L)**, REST **(I,M)**, pCREB **(I,N)**, and total CREB **(I,O)** expression in neurospheres; GAPDH was used for endogenous normalization. Values are mean ± SD of at least 3 independent experiments; $^{**}p < 0.01$, $^{*}p < 0.05$, compared to controls; Student's *t*-test.

activity of purified p300 as assessed using either histone H3 or p53 as a substrate. Radiolabeled curcumin formed a covalent association with p300, and tetrahydrocurcumin displayed no p300 inhibitory activity, consistent with a Michael reaction-dependent mechanism (Marcu et al., 2006). We first evaluated the curcumin effect on Oli-Neu cells. Cell counting

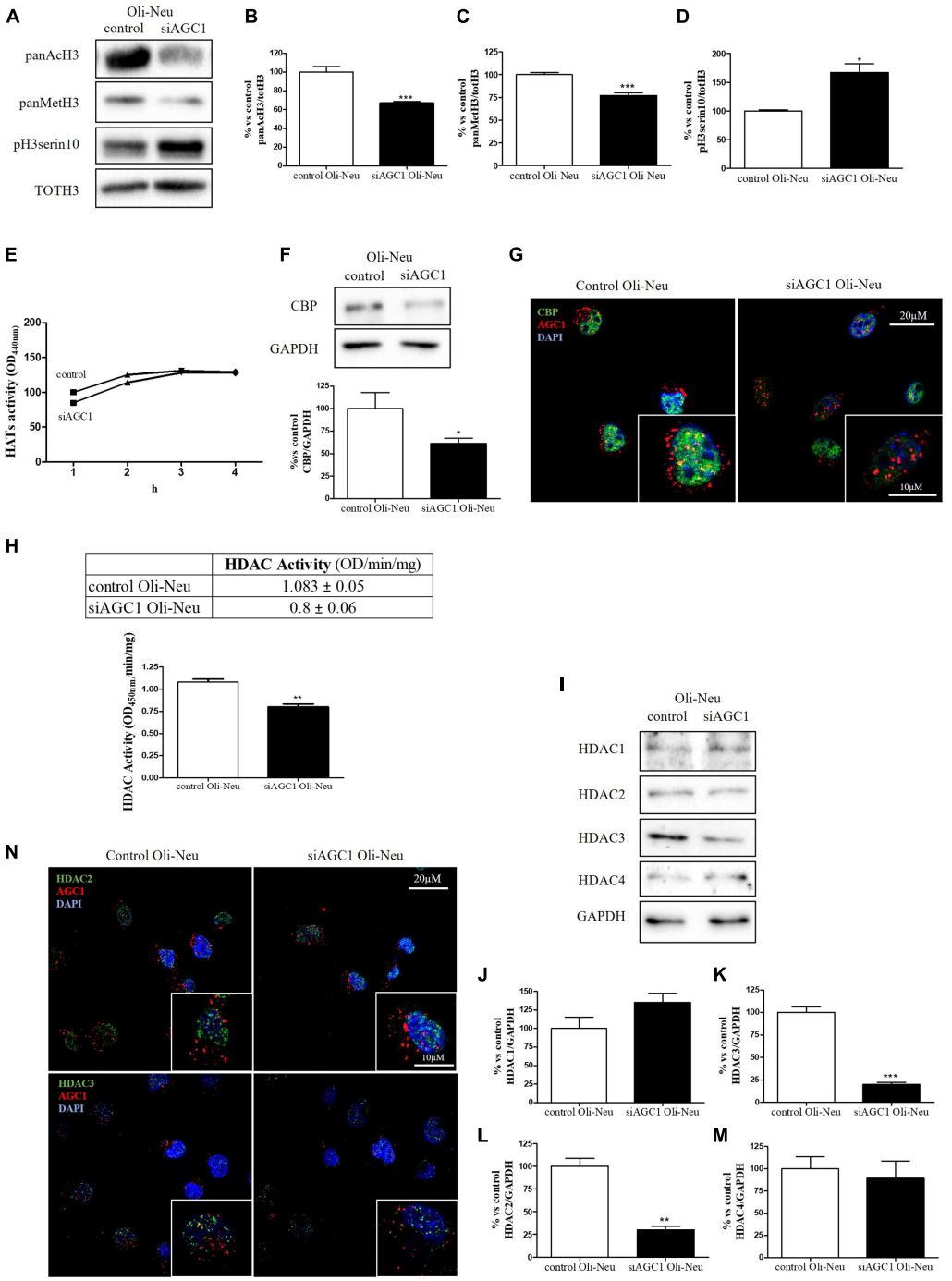

	HDAC Activity (OD/min/mg)
control Oli-Neu	1.083 ± 0.05
siAGC1 Oli-Neu	0.8 ± 0.06

FIGURE 3 | Altered histone PTMs, HAT CBP, and HDAC isoforms expression/activities in AGC1-silenced Oli-Neu cells. WB analysis and relative densitometries of panAcH3 **(A,B)**, panMetH3 **(A,C)**, pH3 **(A,D)**, CBP **(F)**, HDAC1 **(I,J)**, HDAC2 **(I,K)**, HDAC3 **(I,L)** and HDAC4 **(I,M)** expression in Oli-Neu cells; GAPDH was used for endogenous normalization. Activity assay of CBP **(E)** and HDAC **(H)** in Oli-Neu cells. Histone deacetylases (HDACs) activity mean ± SEM of control Oli-neu: 1.083 ± 0.0535, Mean ± SEM of siAGC1 Oli-neu: 0.8000 ± 0.0608, $N = 3$. Difference between means 0.2830 ± 0.04676. Confocal microscopy images (100X) of CBP **(G)** and HDAC2 and HDAC3 **(N)** (green) and AGC1 (red) in Oli-Neu cells; nuclei were labeled with DAPI. 20 and 10 μm scale bar. Values are mean ± SD of at least 3 independent experiments; $^{***}p < 0.001$, $^{**}p < 0.01$, $^{*}p < 0.05$, compared to control; Student's *t*-test.

after staining for the proliferation marker, Ki67 (Gerdes et al., 1991; **Figures 6A,B**) confirmed the lower proliferation rate of siAGC1 Oli-Neu compared to control cells (DMSO treated cells) (Petralla et al., 2019) and demonstrated that 24 h curcumin treatment (used at 10 and 20 μM on the basis of preliminary did not show MTT cytotoxicity assays) induced

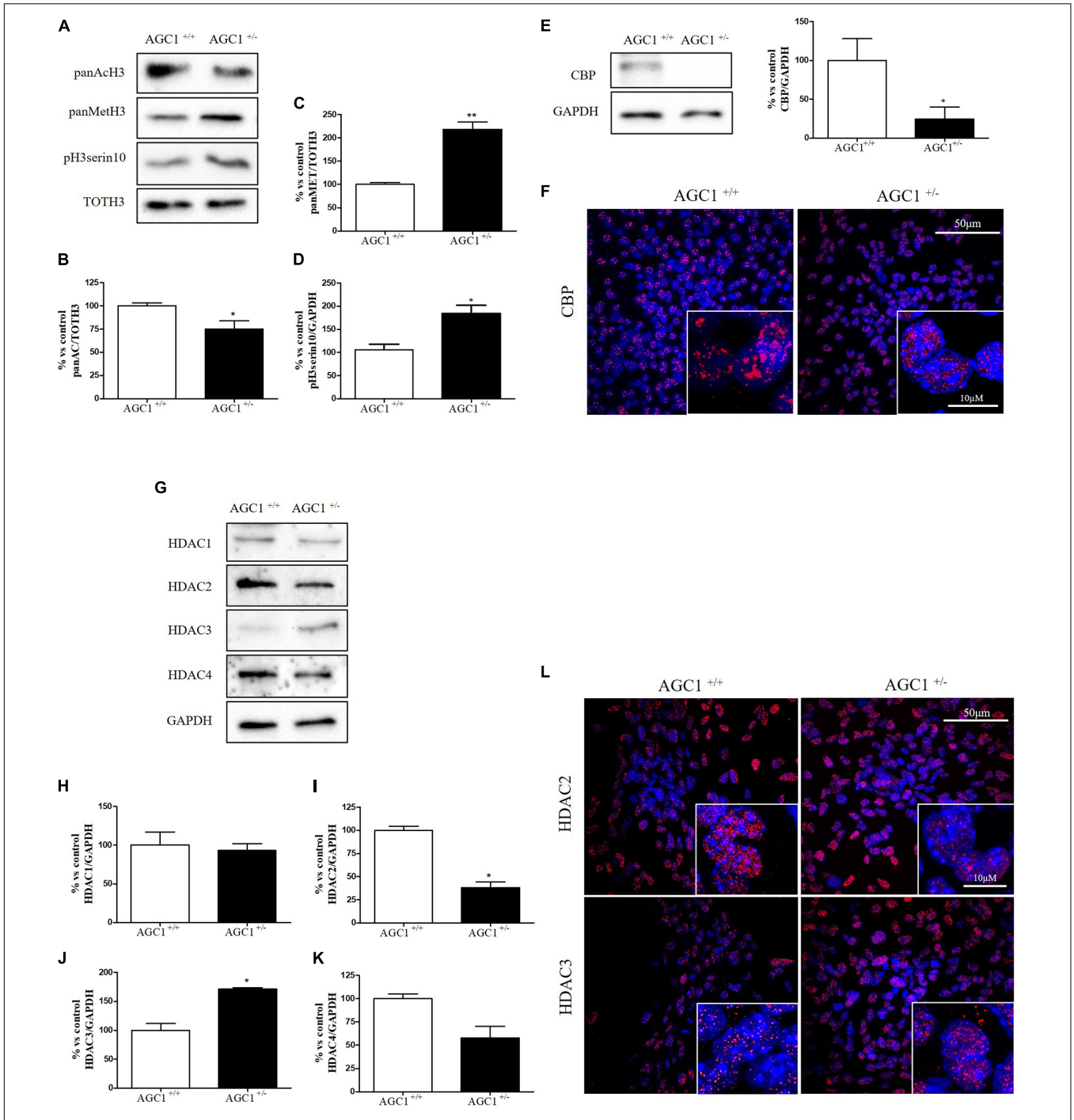

FIGURE 4 | Histone H3 PTMs, HAT, and HDACs expression in AGC1$^{+/+}$ and AGC1$^{\pm}$ neurospheres. WB analysis and relative densitometries of panAcH3 **(A,B)**, panMetH3 **(A,C)**, pH3 **(A,D)**, CBP **(E)**, HDAC1 **(G,H)**, HDAC2 **(G,I)**, HDAC3 **(G,J)**, and HDAC4 **(G,K)** expression in AGC1$^{\pm}$ and AGC1$^{+/+}$ spontaneously differentiated neurospheres; GAPDH was used for endogenous normalizations. Confocal microscopy images (60X and 100X) of CBP **(F)**, HDAC2, and HDAC3 **(L)** in neurospheres; nuclei were labeled with DAPI. 50 and 10 μm scale bar. Values are mean ± SD of at least 3 independent experiments; $^{**}p < 0.01$, $^{*}p < 0.05$, compared to control; Student's *t*-test.

a global reduction in proliferation levels, leading to control cells similar to Oli-Neu cells with AGC1 downregulation. This effect seemed related to HATs inhibition, as curcumin significantly reduced histone H3 acetylation in both control and siAGC1 Oli-Neu cells (**Figures 6C,D**). To better investigate the effect of HATs inhibition on the proliferation/differentiation of OPCs, several markers have been further evaluated after 48 h of curcumin treatment. In particular, platelet-derived

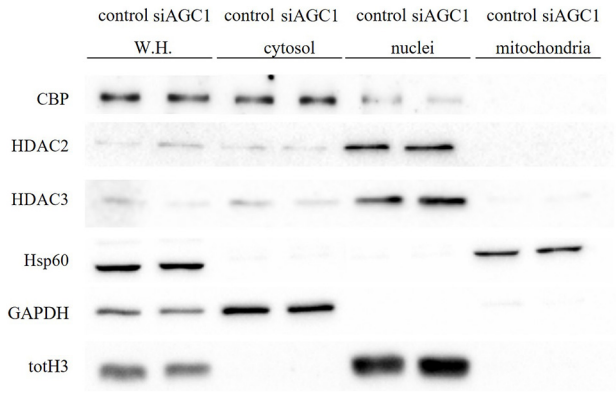

FIGURE 5 | Proliferation factor c-Myc, acetyltransferase CBP and HDAC isoform 2 and 3 do not show alterations in the subcellular localization in siAGC1 Oli-Neu cells. WB analysis of c-Myc, HAT–CBP and HDAC2 and HDAC3 expression in the whole homogenate (WH), cytosolic, nuclear, and mitochondrial fractions from siAGC1 and control Oli-Neu cells; HSP60, GAPDH, and totH3 were used as mitochondrial, cytosolic, and nuclear specific markers, respectively.

growth factor receptor α (PDGFRα; **Figures 6C,E**), a marker of pre-progenitors and oligodendrocytes precursors (Nishiyama et al., 2021b), and the oligodendrocyte-specific transcription factor, Olig2 (**Figures 6C,G**), whose expression decreases during differentiation (Grinspan, 2002), appeared significantly less expressed in the control and siAGC1 Oli-Neu cells treated with curcumin compared to DMSO cells, with no more significant differences among the treated cells. In addition, curcumin significantly decreased the level of neuron glial antigen 2 (NG2; Polito and Reynolds, 2005) in the control and siAGC1 Oli-neu, to suggest a reduction in OPCs pool compared to untreated controls (**Figures 6C,F**). In order to exclude apoptosis and cell death, we then verified through WB analysis, the expression of the pro-apoptotic marker, caspase3 (both precursor and cleaved versions of the enzyme) (Widmann, 2007), and no differences were observed in treated vs. control cells (**Figures 6C,J**). Additionally, we performed WB for the full length PARP1 (116 kDa) and the large fragment (89 kDa) of PARP1 resulting from caspase cleavage (Mashimo et al., 2021; **Figures 6C,I**), as well as for the anti-apoptotic protein, BCL-2 (Chipuk et al., 2010) (data not shown). In parallel, in Oli-Neu cells with AGC1 downregulation, the marker of mature oligodendrocytes CNPase (Scherer et al., 1994) showed higher expression as compared to the control cells and was further induced by curcumin treatment (**Figures 6C,H**). This CNPase over-expression was then confirmed by immunofluorescence and cell counting (**Figures 6K,L**). To deepen the possible induction of differentiation by curcumin, the Oli-Neu cells were also evaluated through the protrusion number and length counting after microscopic morphology analysis. Curcumin 10 μM induced a significant increase in protrusions number both after 24 h (**Figures 7A,B**) and 48 h (**Figures 7A,D**) in control Oli-Neu cells, whereas relevant effects were observed only at 48 h in siAGC1 cells (**Figures 7A,D**). Differently, protrusions length significantly increased only in the control Oli-Neu cells after 48 h of treatment (**Figures 7A,E**). Thus, these data demonstrate that the lower AGC1 expression in immortalized OPCs determines a reduction in histone acetylation probably related to the reduction in CBP expression, as previously shown. Additionally, the pharmacological inhibition of HATs through curcumin affects proliferation, especially in the control Oli-Neu cells, leading to proliferation levels comparable to siAGC1 Oli-Neu.

Similar treatments have been performed on neurospheres from the SVZ of AGC1$^{\pm}$ and AGC1$^{+/+}$ mice. Neurospheres have been allowed to grow in culture for 7 days with 5 or 10 μM curcumin (based on MTT assay, not shown) and their number and diameter have been evaluated (Gil-Perotín et al., 2013). As already demonstrated, AGC1$^{\pm}$ neurospheres appeared smaller, but in greater number compared to AGC1$^{+/+}$ ones (DMSO cells) (Petralla et al., 2019). Curcumin treatments induced a significant reduction in neurospheres diameter in both AGC1$^{\pm}$ and AGC1$^{+/+}$ cells. However, the treatment increased the number of AGC1$^{+/+}$ neurospheres, while it decreased the number of AGC1$^{\pm}$ ones, probably due to an earlier arrest in the proliferation as a consequence of their lower intrinsic proliferation rate (**Figures 8A–C**).

To further study the effect of HAT inhibition on NPCs spontaneous differentiation, AGC1$^{\pm}$ and AGC1$^{+/+}$ neurospheres have been plated on fibronectin and exposed to 5 or 10 μM curcumin for 7 days. Fluorescence quantification after staining with Olig2 (oligodendrocyte lineage marker), CNPase (myelinating oligodendrocytes marker), DCX (neural precursor cells marker; Francis et al., 1999), and GFAP (astrocytes marker; Nolte et al., 2001) confirmed AGC1$^{\pm}$ neurospheres being characterized by reduced Olig2^{+} cells and increased CNPase^{+}, DCX^{+}, and GFAP^{+} cells compared to AGC1$^{+/+}$ neurospheres (**Figures 8D–H**; Petralla et al., 2019). Curcumin treatment-induced almost no change in AGC1$^{+/+}$ neurospheres differentiation, besides a little, but significant reduction in GFAP^{+} cells after 10 μM treatment (**Figure 8H**). Conversely, it leads to a significant reduction in CNPase^{+} (**Figures 8D,F**) and GFAP^{+} (**Figures 8D,H**) cells in AGC1$^{\pm}$ neurospheres, with no relevant changes in both Olig2^{+} (**Figures 8D,E**) and DCX^{+} (**Figures 8D,G**) cells. Further confirmation has been obtained by WB analysis (**Figures 8I–N**). As previously shown, in DMSO-treated controls, the Olig2 expression turned out lower, while CNPase, GFAP, and even DCX resulted in a significant increase in AGC1$^{\pm}$ than in AGC1$^{+/+}$ neurospheres. Curcumin treatment has no significant effect on Olig2 and DCX expression in both AGC1$^{\pm}$ and AGC1$^{+/+}$ neurospheres, but it significantly decreases both CNPase and GFAP expression in AGC1$^{\pm}$ neurospheres.

Altogether, these data demonstrate that HATs inhibition arrests proliferation and stimulates differentiation of immortalized OPCs toward myelinating oligodendrocytes. This pro-differentiating effect is more evident in control cells than after AGC1 downregulation, thus creating a condition similar to AGC1 deficiency. In NPCs represented by neurospheres, AGC1 silencing induces the differentiation toward both differentiated glial and neuronal cells. HATs inhibition has almost no effect on AGC1$^{+/+}$ neurospheres, while it reduces

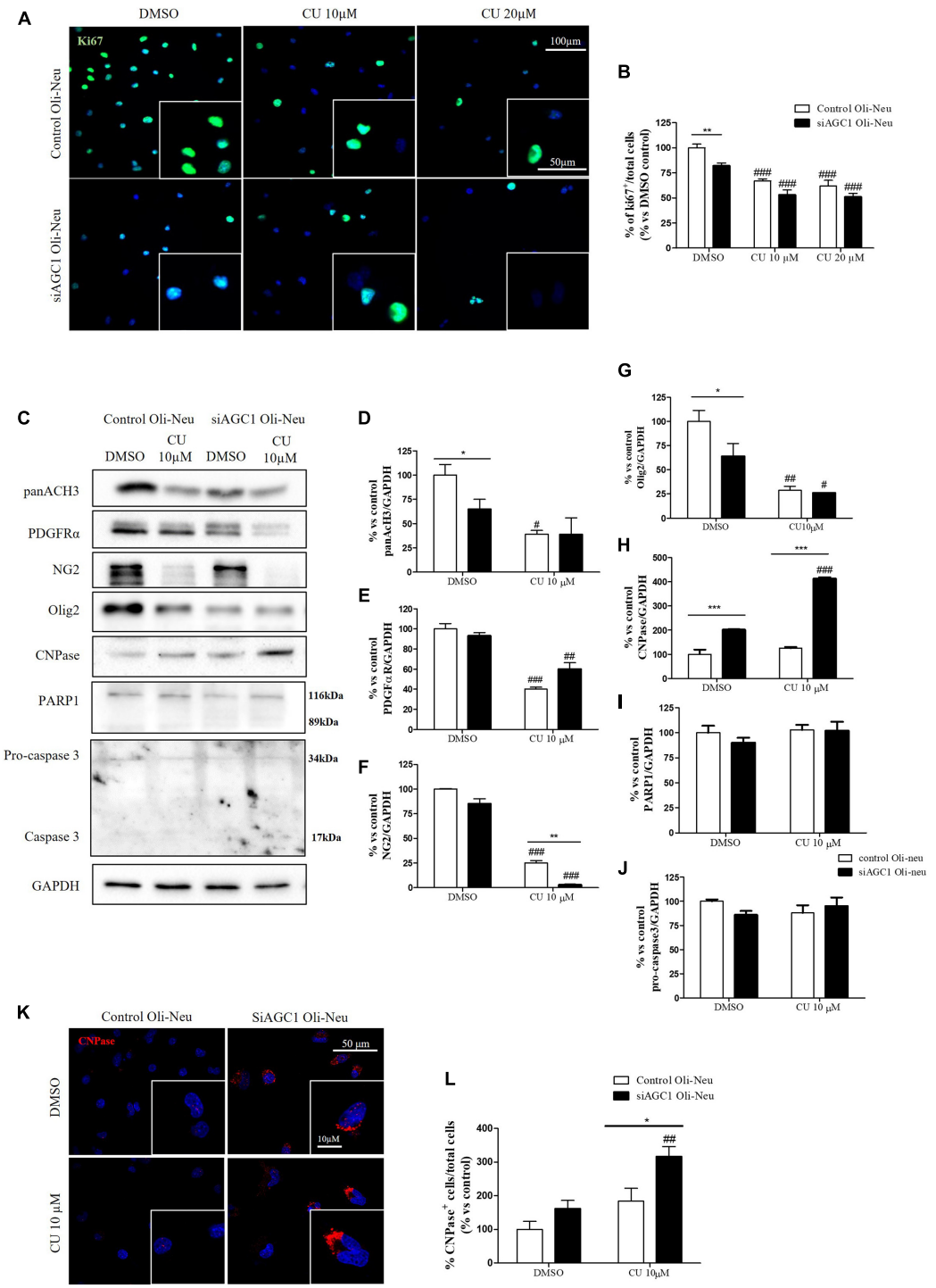

FIGURE 6 | Curcumin-mediated HAT inhibition differentially affects proliferation in both control and siAGC1 Oli-Neu cells. Immunofluorescence staining of Ki67 proliferation marker **(A)** and Ki67^{+} cell count analysis **(B)** in Oli-Neu cells after 24 h treatment with 10 or 20 μM curcumin. Values are expressed as the *ratio* of Ki67^{+} cells (green)/total cells; nuclei were labeled with DAPI. Values are mean ± SD of 3 independent experiments; 3 different fields were acquired for each condition. 40X objective; 50 and 100 μm bar scale. WB and relative densitometries of panAcH3 **(C,D)**, PDGFRα **(C,E)**, NG2 **(C,F)**, Olig2 **(C,G)**, CNPase **(C,H)**, PARP1 **(C,I)**, and pro-caspase3 **(C,J)** expression in OliNeu cells after 48 h treatment with 10 μM curcumin. Immunofluorescence staining of CNPase **(K)** and CNPase^{+} cell count analysis **(L)** in Oli-Neu cells after 48 h treatment with 10 μM curcumin. Values are expressed as the *ratio* of CNPase^{+} cells (red)/total cells; nuclei were labeled with DAPI. Three different fields were acquired for each condition. Values are mean ± D of at least 3 independent experiments. 40X objective; 50 and 10 μm bar scale. $^{\#}p < 0.05$, $^{\#\#}p < 0.01$, $^{\#\#\#}p < 0.001$, compared to DMSO control, respectively; $^{*}p < 0.05$, $^{**}p < 0.01$, $^{***}p < 0.001$, compared to each treated control; two-way ANOVA (Bonferroni's *post hoc* test).

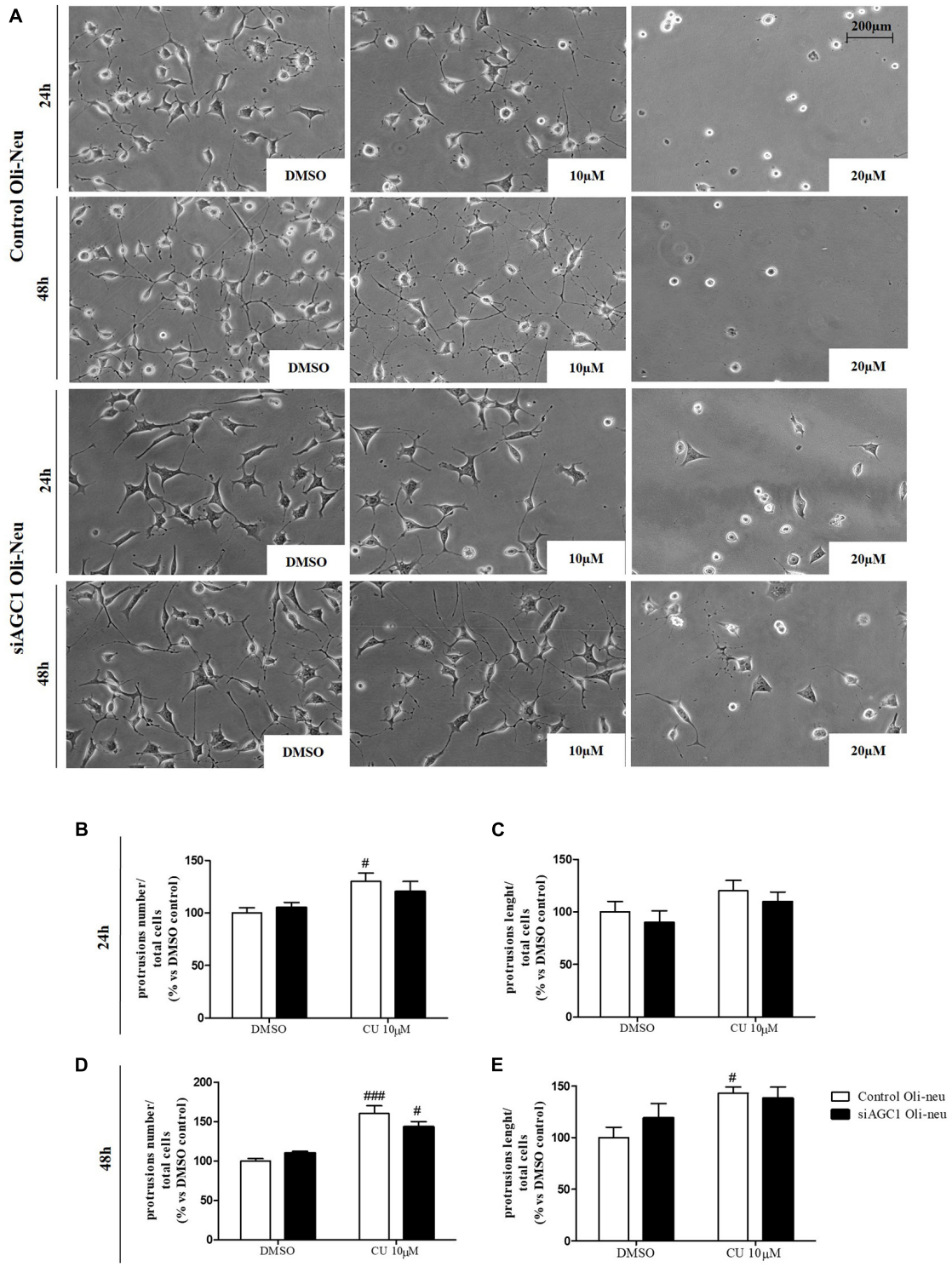

FIGURE 7 | After acetyltransferase CBP inhibition, cells appeared more elongated and branched, index of oligodendrocytes maturation, showing an increase in both processes number and average length compared to DMSO-treated controls. Optical microscope proliferation/differentiation analysis in control and siAGC1 Oli-Neu cells following 24 and 48 h of treatment with curcumin 10 and 20 μM **(A)**. Filaments number and lengths were counted and measured, respectively, and analyses were carried out with Fuji Imagej2 software. Given the potential toxicity of curcumin 20 μM, statistical analyses were executed only at 10 μM **(B–E)**. Values are mean ± SD of 3 independent experiments; 3 different fields were acquired for each condition. 20X objective; 200 μM bar scale. $^{###}p < 0.001$, $^{#}p < 0.05$, compared to DMSO control, respectively; two-way ANOVA (Bonferroni's *post hoc* test).

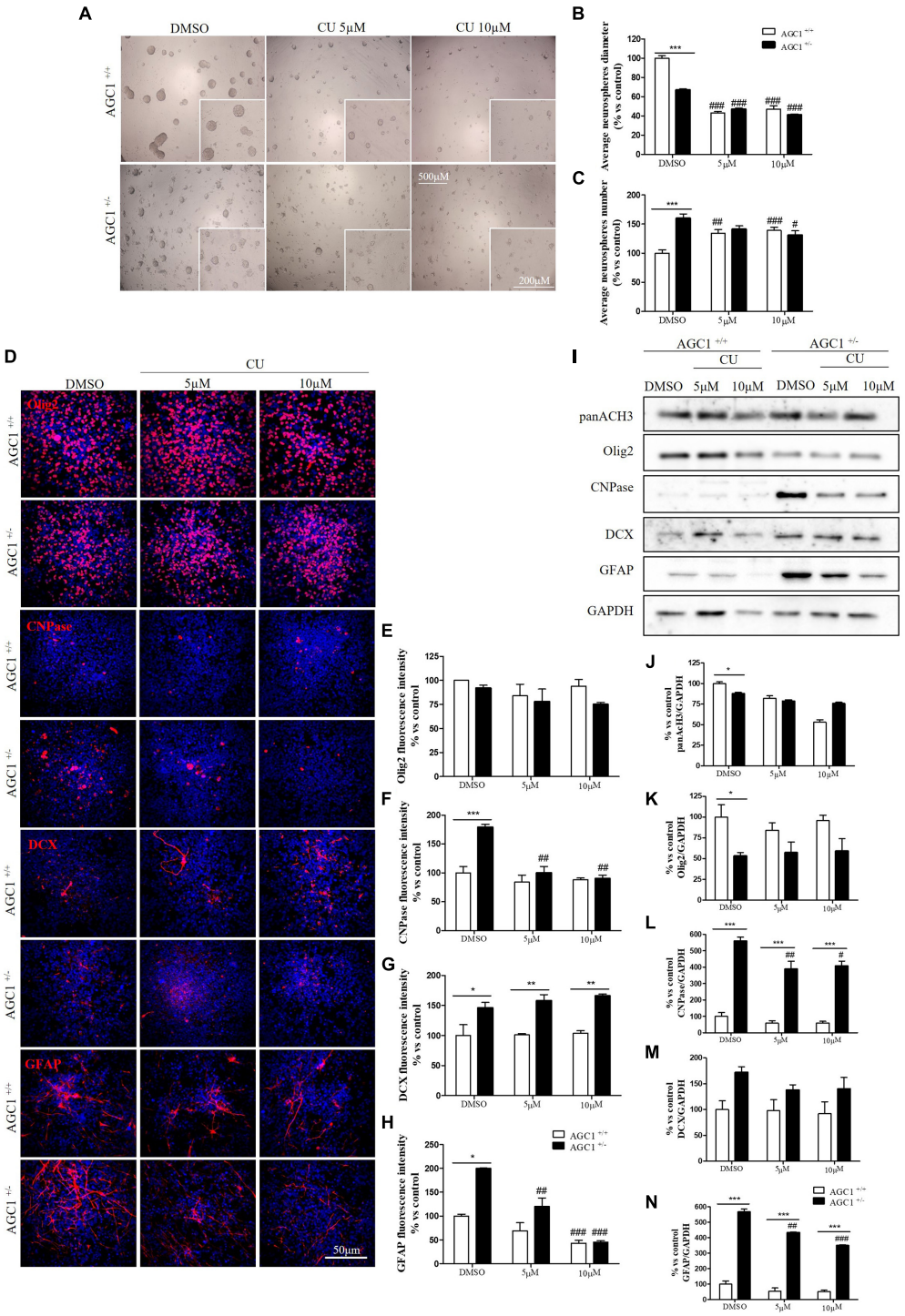

FIGURE 8 | Curcumin-mediated HAT inhibition differentially affects proliferation and glial commitment in spontaneously differentiated AGC1$^{+/+}$ and AGC1$^{\pm}$ neurospheres. Optical microscope images **(A)** and counting of number **(B)**, and diameter **(C)** of neurospheres after 7 days of culture in presence of curcumin 5 and 10 μM. Average number and size were measured with Fuji Imagej2 software using an automated colony and cell counting method; only aggregates bigger than 400 μm^2 were considered. Values are mean ± SD of 5 different fields acquired for each condition. 10X objective; 500 and 200 μm bar scale. Immunofluorescence staining and cell counting of Olig2 **(D,E)**, CNPase **(D,F)**, DCX **(D,G)**, and GFAP **(D,H)** on AGC1$^{+/+}$ and AGC1$^{\pm}$ 7DIV spontaneously differentiated neurospheres following HAT inhibition with curcumin 5 and 10 μM. Values are mean ± SD of 3 different fields acquired for each condition. 60X objective; 50 μm bar scale. WB and relative densitometries of panAcH3 **(I,J),** Olig2 **(I,K)**, CNPase **(I,L)**, DCX **(I,M)**, and GFAP **(I,N)** expression in AGC1$^{+/+}$ and AGC1$^{\pm}$ differentiated neurospheres following HAT inhibition with curcumin 5 and 10 μM. Values are mean ± SD of 3 independent experiments. $^{\#}p < 0.05$, $^{\#\#}p < 0.01$, $^{\#\#\#}p < 0.001$, compared to DMSO control, respectively; $^{*}p < 0.05$, $^{**}p < 0.01$, $^{***}p < 0.001$, compared to each treated control; two-way ANOVA (Bonferroni's *post hoc* test).

the differentiation toward both oligodendrocytes and astrocytes, with no effect on OPCs and the commitment toward neurons in AGC1$^{\pm}$ cells.

Histone Deacetylases Inhibition Through Suberanilohydroxamic Acid in the Proliferation/Differentiation of Oligodendrocytes Precursor Cells and Neuronal Precursor Cells

The role of HDACs in the proliferation/differentiation of OPCs and NPCs, as well as their alteration in AGC1 deficiency, was investigated in Oli-Neu cells and neurospheres treated with SAHA, a broad-spectrum HDAC inhibitor suppressing the family members in multiple HDAC classes (Xu et al., 2007) and approved by FDA for cancer therapy. In cells, SAHA is known to be involved in several processes i.e., it induces the accumulation of acetylated histones and acetylated non-histone proteins in transcription factor TF complexes (e.g., TFIIB), which alter gene expression; it promotes acetylation of proteins regulating cell proliferation (e.g., Rb), protein stability (e.g., Hsp90), apoptosis (e.g., Bcl-2 family of proteins), cell motility (e.g., tubulin), and angiogenesis (HIF-1α); it alters the expression of proteins (e.g., Trx), which modulate the accumulation of reactive oxygen species (ROS) that facilitated cell death (Johnstone and Licht, 2003; Rosato et al., 2003; Shao et al., 2004; Bhalla, 2005; Dokmanovic and Marks, 2005; Minucci and Pelicci, 2006; Yoo and Jones, 2006).

Control and siAGC1 Oli-Neu cells have been treated with SAHA 0.5 and 1.0 μM for 24 h. Counting of Ki67^{+} cells showed lower proliferation in siAGC1 cells compared to the control (DMSO-treated cells), whereas SAHA treatment significantly reduced proliferation in both the cell lines, at both concentrations (**Figures 9A,B**). The WB analysis confirmed a strong induction of histone H3 acetylation following HDACs inhibition, which is more evident in the control Oli-Neu cells than in siAGC1 ones (**Figures 9C,D**). PDGFαR, Olig2, and NG2, as expected, were less expressed in siAGC1 Oli-Neu cells, but only PDGFαR and NG2 significantly decreased after SAHA treatment only in the control cells, indicating a decrease in the OPCs pool (**Figures 9C,E–G**). Conversely, CNPase expression significantly increased in both cell lines following HDACs inhibition (**Figures 9C–H**), as confirmed in immunofluorescence (**Figures 9K,L**), to suggest a stimulated differentiation in OPCs when HDACs is inhibited. Additionally, through WB analysis, no differences were observed for the pro-apoptotic marker, caspase3 (both precursor and cleaved versions of the enzyme) (**Figures 9C,J**), the full length PARP1 (116 kDa), and the large fragment (89 kDa) of PARP1 resulting from caspase cleavage (**Figures 9C,I**), and the anti-apoptotic protein, BCL-2 (data not shown) in treated vs. control cells, excluding apoptosis and cell death in the reduction of OPCs pool. From microscopic morphology analysis, protrusion length, but not the protrusion number, significantly increased in siAGC1 Oli-Neu cells after 24 h with 1.0 μM SAHA (**Figures 10A–C**). However, at 48 h, greater effects were obtained from both cell lines with 0.5 μM SAHA, where protrusion number and length turned out significantly higher compared to DMSO-treated controls, respectively (**Figures 10A,D,E**). These data demonstrated that the inhibition of HDACs, and the consequent increase of histone H3 acetylation, limits the proliferation of OPCs with a parallel increase in their differentiation, being this effect more evident in control cells, where it leads to a condition similar to AGC1 deficiency.

Suberanilohydroxamic acid treatment has been also evaluated on the proliferation/differentiation of AGC1$^{\pm}$ and AGC1$^{+/+}$ neurospheres. AGC1$^{+/+}$ neurospheres treated with the culture of SAHA of 0.5 or 1.0 μM (DMSO as control) for 5 days (not 7 days as for curcumin, because of its toxicity in long-time culture; Zhou et al., 2011), revealed a significant decrease in average diameter, with a parallel increase in number. In the same experimental conditions, DMSO-treated AGC1$^{\pm}$ neurospheres confirmed their higher number and smaller size compared to AGC1$^{+/+}$ controls, and after SAHA treatment, showed a further significant increase in number and decrease in size (**Figures 11A–C**). Therefore, pharmacological HDACs inhibition seems to determine a reduction in the proliferation of NPCs in neurospheres with a more limited effect on AGC1$^{\pm}$ ones compared to AGC1$^{+/+}$, probably due to the pathological reduction in HDACs expression and histone acetylation.

The effect of the inhibition of HDACs by SAHA on the differentiation of NPCs has been then tested on both AGC1$^{\pm}$ and AGC1$^{+/+}$ neurospheres spontaneously differentiated on fibronectin. Unlike AGC1$^{+/+}$, the fewer number of Olig2^{+} cells in AGC1$^{\pm}$ neurospheres were not further reduced by SAHA treatments (**Figures 11D,E**), whereas the higher number of CNPase^{+} cells significantly decreased, with no change in AGC1$^{+/+}$ control (**Figures 11D,F**). Neuronal-restricted progenitors, which express DCX as a specific marker and are more present in AGC1$^{\pm}$ neurospheres compared to AGC1$^{+/+}$ ones (Petralla et al., 2019), did not reveal any change (**Figures 11D,G**). Astrocytes, however, were identified as GFAP^{+} cells and significantly more expressed in AGC1$^{\pm}$ than in AGC1$^{+/+}$ neurospheres$^{+/+}$ (Petralla et al., 2019), showed a strong reduction in treated AGC1$^{\pm}$ but not in the control cells (**Figures 11D,H**).

Western Blot analysis confirmed a significant increase in histone H3 acetylation in NPCs following SAHA treatment (**Figures 11I,J**). As observed through immunostaining, while SAHA did not change Olig2 and DCX expression, the former lower (**Figures 11I,K**) and the latter higher (**Figures 11I,M**) in AGC1$^{\pm}$ neurospheres as compared to AGC1$^{+/+}$, respectively, the pharmacological HDACs inhibition determined a significant reduction in CNPase (**Figures 11I,L**) and GFAP (**Figures 11I,N**) expression in AGC1$^{\pm}$ neurospheres only, where these markers have a basal significant higher level compared to control conditions, as previously demonstrated (Petralla et al., 2019). Therefore, the inhibition of HDACs has only a limited effect on the proliferation of OPCs, while it significantly induces the differentiation of OPCs, both in cells with downregulated AGC1 and in controls, being this effect more evident in the latter ones. The SAHA effect on the proliferation of OPCs has been observed in both Oli-Neu cells and neurospheres. On the contrary, in AGC1$^{\pm}$ neurospheres, in which the number of

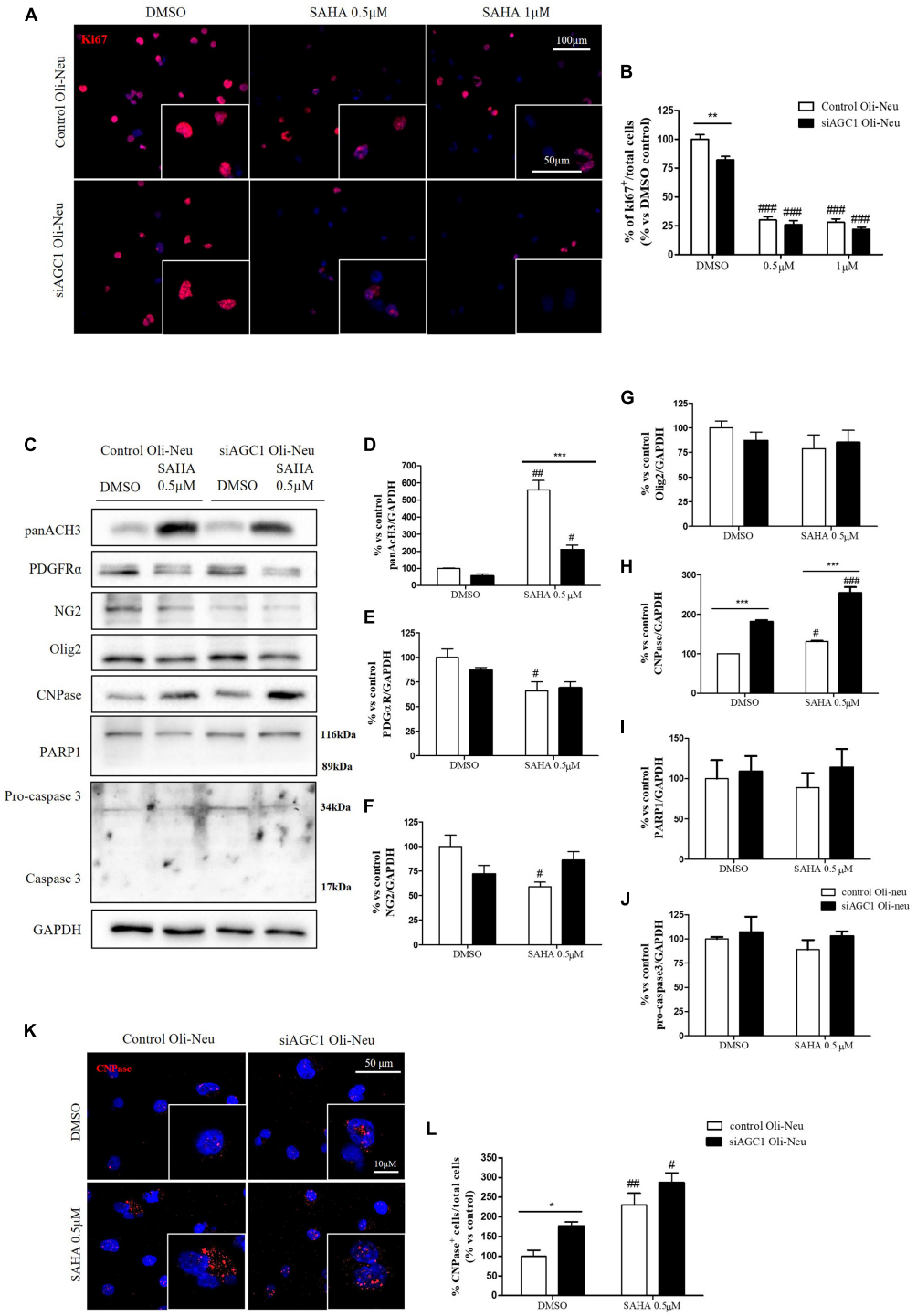

FIGURE 9 | Suberanilohydroxamic acid (SAHA)-mediated HDACs inhibition differentially reduces proliferation and promotes differentiation in control and AGC1-silenced Oli-Neu cells. Immunofluorescence staining of Ki67 proliferation marker **(A)** and Ki67$^+$ cell count analysis **(B)** in Oli-Neu cells after 24 h treatment with 0.5 or 1.0 μM SAHA. Values are expressed as the *ratio* of Ki67$^+$ cells (red)/total cells; nuclei were labeled with DAPI. Values are mean ± SD of 3 independent experiments; 3 different fields were acquired for each condition. 40X objective; 50 and 100 μm bar scale. WB and relative densitometries of panAcH3 **(C,D)**, PDGFRα **(C,E)**, NG2 **(C,F)**, Olig2 **(C,G)**, CNPase **(C,H)**, PARP1 **(C,I)**, and pro-caspase3 **(C,J)** expression in OliNeu cells after 48 h treatment with 0.5 μM SAHA. Immunofluorescence staining of CNPase **(K)** and CNPase$^+$ cell count analysis **(L)** in OliNeu cells after 48 h treatment with 0.5 μM SAHA. Values are expressed as the *ratio* of CNPase$^+$ cells (red)/total cells; nuclei were labeled with DAPI. Three different fields were acquired for each condition. Values are mean ± SD of at least 3 independent experiments. 40X objective; 50 and 10 μm bar scale. $^{\#}p < 0.05$, $^{\#\#}p < 0.01$, $^{\#\#\#}p < 0.001$, compared to DMSO control, respectively; $^{*}p < 0.05$, $^{**}p < 0.01$, $^{***}p < 0.001$, compared to each treated control; two-way ANOVA (Bonferroni's *post hoc* test).

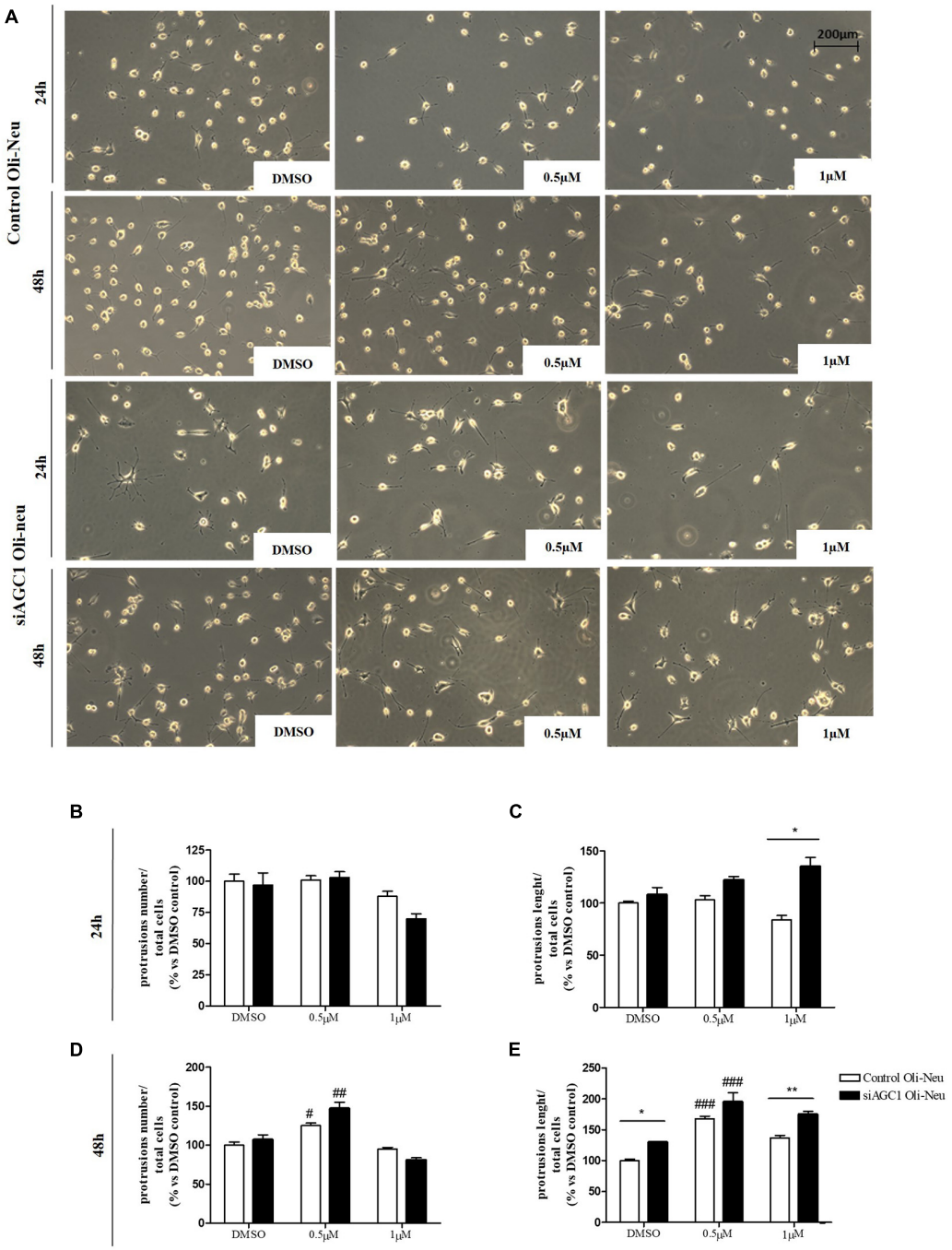

FIGURE 10 | Histone deacetylases inhibition leads to Oli-Neu cells differentiation with a decrease in filament number and increases in filaments length in siAGC1 cells compared to control ones after 48 h SAHA treatment. Optical microscope proliferation/differentiation analysis in siAGC1 and control Oli-Neu cells following 24 and 48 h of SAHA treatment **(A)**. The number and lengths of filaments were counted and measured, respectively, and analyses were carried out with Fuji Imagej2 software **(B–E)**. Analysis was carried out with Fuji Imagej2 software. Values are mean ± SD of 3 independent experiments; 3 different fields were acquired for each condition. 20X objective; 200 μM bar scale. $^{\#}p < 0.05$, $^{\#\#}p < 0.01$, $^{\#\#\#}p < 0.001$, compared to DMSO control, respectively; $^{*}p < 0.05$, $^{**}p < 0.01$, compared to each treated control; two-way ANOVA (Bonferroni's *post hoc* test).

oligodendrocytes and astrocytes is significantly higher than in AGC1$^{+/+}$ cells, the inhibition of HDACs determines a reduction in both differentiated glial cells number, with no effects on the neural progenitors.

DISCUSSION

The deficiency of AGC1 is a mitochondrial disorder manifesting with developmental epileptic encephalopathy, recently defined

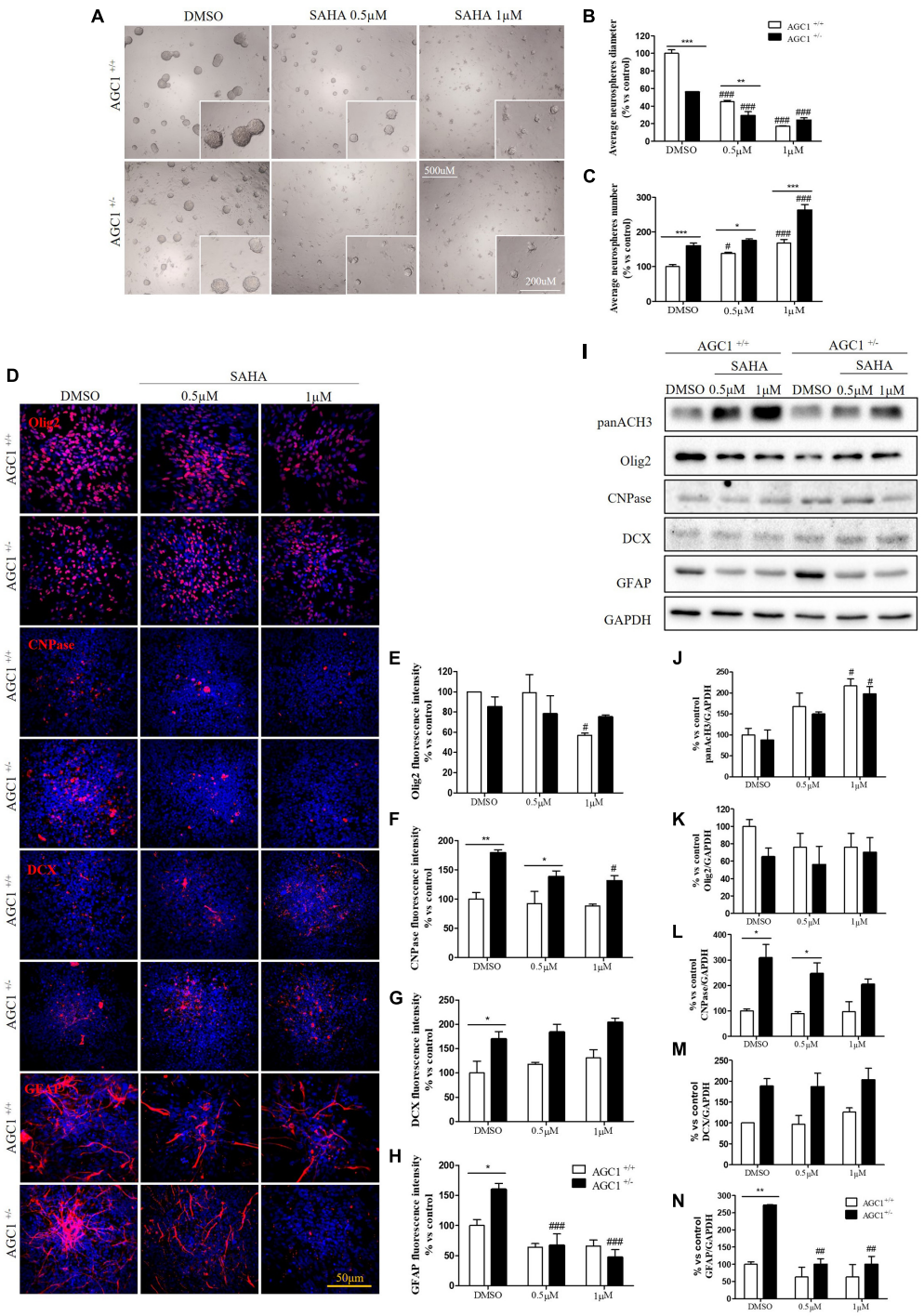

FIGURE 11 | Suberanilohydroxamic acid-mediated HDACs inhibition affects proliferation and commitment through glial cells in spontaneously differentiated AGC1$^{+/+}$ and AGC1$^{\pm}$ neurospheres. Optical microscope images **(A)** and counting of number **(B)** and diameter **(C)** of neurospheres after 7 days of culture in presence of SAHA 0.5 and 1 μM. Average number and size were measured with Fuji Imagej2 software using an automated colony and cell counting method; only aggregates bigger than 400 μm^2 were considered. Values are mean ± SD of 5 different fields acquired for each condition. 10X objective; 500 and 200 μm bar scale. Immunofluorescence staining and cell counting of Olig2 **(D,E)**, CNPase **(D,F)**, DCX **(D,G)**, and GFAP **(D,H)** on AGC1$^{+/+}$ and AGC1$^{\pm}$ 7DIV spontaneously differentiated neurospheres following HDACs inhibition with SAHA 0.5 and 1 μM. Values are mean ± SD of 3 different fields acquired for each condition. 60X objective; 50 μm bar scale. WB and relative densitometries of panAcH3 **(I,J)**, Olig2 **(I,K)**, CNPase **(I,L)**, DCX **(I,M)**, and GFAP **(I,N)** expression in AGC1$^{+/+}$ and AGC1$^{\pm}$ differentiated neurospheres following HDAC inhibition with SAHA 0.5 and 1 μM. Values are mean ± D of 3 independent experiments. $^{\#}p < 0.05$, $^{\#\#}p < 0.01$, $^{\#\#\#}p < 0.001$, compared to DMSO control, respectively; $^{*}p < 0.05$, $^{**}p < 0.01$, $^{***}p < 0.001$, compared to each treated control; two-way ANOVA (Bonferroni's *post hoc* test).

as a leukodystrophy (Kavanaugh et al., 2019). These childhood white matter disorders (WMDs) display neurologic features, such as motor deficits, hypotonia, and epileptic seizures associated with important systemic symptoms, and involve a wide range of heterogeneous genetic and metabolic disorders, also including mitochondrial encephalopathies (Ashrafi and Tavasoli, 2017; Ashrafi et al., 2020). This is the reason why the study of the ultra-rare, genetic AGC1 deficiency can provide useful information to understand the pathogenic mechanisms at the basis of the wide family of leukodystrophies. Besides, WMDs, leukodystrophy, and leukoencephalopathy have been recently involved in dementia (Lok and Kwok, 2021), further increasing the interest in understanding the molecular mechanisms underlying these disorders.

White matter is composed of myelinated neuronal axons and glial cells, mainly OPCs and oligodendrocytes, but astrocytes and microglia are also present. Myelination and remyelination are the main processes that modulate the correct functioning of the white matter, both during development and in adulthood. In CNS, myelin is formed by oligodendrocytes that wrap axons through multiple concentric membranous layers. Oligodendrocytes, derived from the maturation of OPCs, are highly migratory and are actively proliferative glial progenitors, representing about 5% of mouse brain cells. OPCs in turn originates from the gliogenic commitment of NPCs, mostly localized in the SVZ (Goldman and Kuypers, 2015). The NPCs can give rise to different cells in CNS: neurons, astrocytes, and oligodendrocytes, both during brain development and in adulthood (Gage, 2000). Formerly published data from our lab have previously shown a deficit in the proliferation of OPCs with low AGC1 expression (siAGC1 Oli-Neu cells), with no change in their differentiation into oligodendrocytes. This proliferation defect correlated with the dysregulation in the expression of growth factors involved in the proliferation/differentiation of OPCs and these data were confirmed in AGC1$^{\pm}$ mice. Furthermore, in the neurospheres from SVZ of the murine model, we observed a reduced number of OPCs with a parallel increase in oligodendrocytes, astrocytes, and precursor neurons, as well as an imbalance in the proliferation/differentiation pathways (Petralla et al., 2019). It is noteworthy that in our model of OPCs with downregulated AGC1, we do not observe any mitochondrial respiration deficit, thus suggesting that the alterations in the proliferation/differentiation pathways may be not directly due to a bioenergetic dysfunction, but due to a different molecular mechanism (Petralla et al., 2019).

It is widely recognized that transcriptional (Meijer et al., 2012; Yan et al., 2013; Magri et al., 2014; Palazuelos et al., 2014; Song et al., 2015; Carroll et al., 2018) and epigenetic mechanisms, especially histone acetylation (Juliandi et al., 2010; Emery and Lu, 2015; Hernandez and Casaccia, 2015; Tiane et al., 2019; Zhang et al., 2020), are major contributors to OPCs and NPCs proliferation and differentiation and that their dysregulation is involved in demyelinating disorders (Hsieh and Gage, 2004; Podobinska et al., 2017). Acetylation and deacetylation of histones are highly dynamic processes that depend on the activity of two groups of enzymes: HATs and HDACs. HDAC1, 2, 3, and 4 are the most relevant isoforms in CNS (D'Mello, 2020), while, among the HATs, CBP is mainly active in CNS. The CBP, by binding with the transcription factor CREB (Sheikh, 2014; Lipinski et al., 2019), creates a direct link between transcriptional and epigenetic regulation of gene expression in the development, differentiation, and function of the brain cells (Bito and Takemoto-Kimura, 2003). CREB, which is activated by its phosphorylation, is known to be involved in neuronal differentiation and survival, as well as in many other brain functions (Yan et al., 2013).

In both the investigated *in vitro* models of AGC1 deficiency, we observed a strong reduction in the expression of the transcription factors, Olig2 and Myc, which can be related to the reduction in the proliferation of OPCs. Instead, CREB is increased in siAGC1 Oli-Neu cells and reduced in AGC1$^{\pm}$ neurospheres, compared to the controls, experimental evidence that could be explained by the multicellular composition of the NPCs model, in which we previously demonstrated a shift in the spontaneous differentiation of both the neuronal and glial cells (Petralla et al., 2019). Moreover, the altered expression pattern of the TFs, investigated in this study, is accompanied by changes of HATs enzyme and in particular of CBP, found significantly reduced in both OPCs and NPCs with downregulated AGC1. As a consequence, histone acetylation is reduced, and the parallel reduction in HDACs activity and expression appears not sufficient to sustain the necessary histone acetylation and in turn the proliferation of our models of AGC1 deficiency.

The role of histone acetylation/deacetylation in the proliferation deficit of OPCs and NPCs with low AGC1 was then investigated in the presence of the HATs inhibitor, curcumin (Balasubramanyam et al., 2004; Sunagawa et al., 2018), and the HDACs inhibitor, SAHA (Xu et al., 2007; Zhou et al., 2011). Curcumin, by decreasing histone acetylation, reduces the proliferation of OPCs in the control and stimulates their differentiation toward oligodendrocytes, hence mimicking the condition described in siAGC1 Oli-Neu cells. Furthermore, curcumin has greater effects also on NPCs commitment, where it reduces the gliogenic differentiation toward both astrocytes and oligodendrocytes, without changing neurogenesis and the proliferation of OPCs. The data here presented, therefore, suggest that the lower CBP level and in turn HATs activity in OPCs with impaired AGC1 may cause their proliferation deficit, as well as the precocious differentiation of OPCs to mature oligodendrocytes, whereas, in NPCs, it determines an alteration in the commitment toward glial cells and limited effect on NPCs neuronal commitment, in line with what was previously hypothesized (Hernandez and Casaccia, 2015).

The pharmacological inhibition of HDACs by SAHA has only a limited effect on the proliferation of OPCs, inducing a slight differentiation toward oligodendrocytes, especially in the control cells, whereas in NPCs, it produces a strong reduction in differentiated astrocytes with almost no effect on neural progenitors (**Figure 12**).

Overall, our data showed that changes in HATs and HDACs activity and consequently in histone PTMs may underly the altered balance between proliferation and differentiation in the investigated models with downregulated AGC1. On the other hand, and more in general, our data pointed

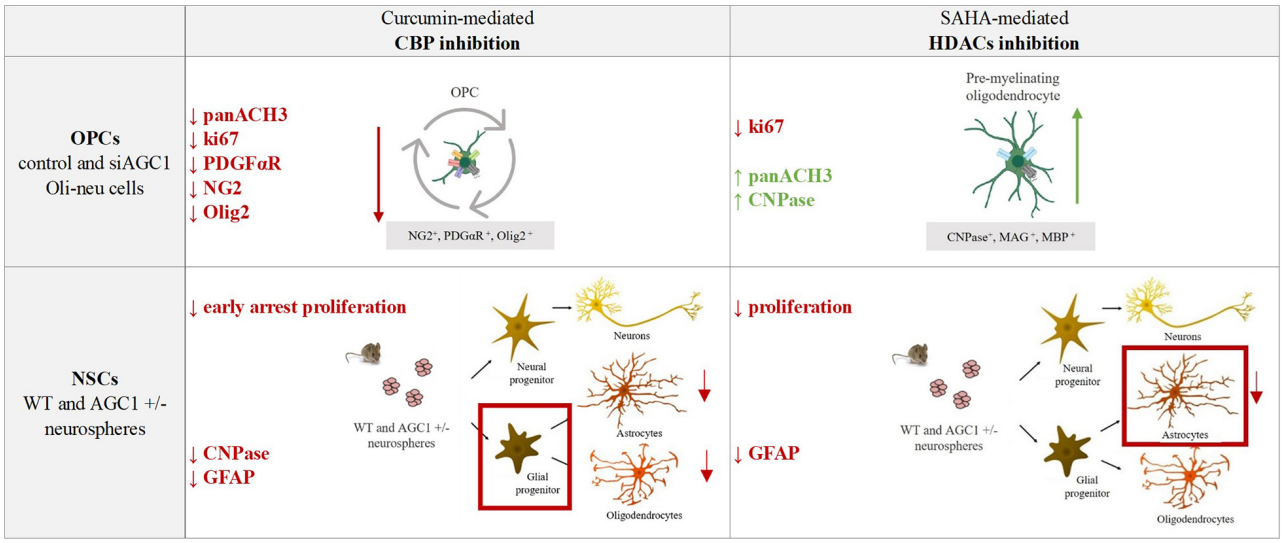

FIGURE 12 | Summary table of increased/decreased markers involved in OPCs and NSCs proliferation/differentiation following curcumin-mediated CBP inhibition and SAHA-mediated HDACs inhibition in control and siAGC1 Oli-neu and WT and AGC1$^{\pm}$ neurospheres.

out that pharmacological inhibition or pathologic conditions impairing histone acetylation could be responsible for the proliferation deficit of brain progenitors with HATs likely more involved in the gliogenic commitment of NPCs and the proliferation/differentiation balance of OPCs, while HDACs may play a later role in the differentiation of glial precursor cells toward astrocytes.

An important issue arising from the data presented here shows the role of mitochondria, and in particular of AGC1, for the generation of acetyl groups. Histone acetylation by HATs requires acetyl-CoA produced by mitochondrial activity, and cellular levels of this metabolite depend on energy status. The AGC1 regulates and preserves mitochondrial pyruvate oxidation through the malate/aspartate, NADH shuttle (Kerkhofs, 2020), a biochemical pathway essential to supply the energy demands of the brain cells by feeding the tricarboxylic acid (TCA) cycle. In addition, the import of pyruvate in the mitochondrial matrix allows for the synthesis of citrate that releases acetyl-CoA *via* citrate lyase once exported to the cytosol. Therefore, AGC1 function may be determinant for histone acetylation, thus representing an important link between mitochondrial metabolism and gene expression (Menzies et al., 2016; Matilainen et al., 2017). It has been previously demonstrated that chronic mitochondrial dysfunction leads to a reduced mitochondrial output of acetyl-CoA, which in turn limits the HATs activity and histone acetylation, overall contributing to the regulation of gene expression in the nucleus (Lozoya et al., 2019; Santos, 2021). This evidence resembles what we have observed in our models of BPCs with AGC1 deficiency. Indeed, our data revealed no significant reduction of mitochondrial respiration in the OPCs model with low AGC1. We can speculate that the residual activity of the carrier is sufficient to sustain the mitochondrial pyruvate oxidation and in turn OXPHOS (Llorente-Folch et al., 2013; Szibor et al., 2020). However, AGC1 silencing may limit the amount of the citrate synthesized in the TCA cycle that is exported in the cytosol, hence providing less acetyl-CoA for the whole OPCs and in turn affecting the histone acetylation. It should also be considered that a further important physiological source of acetyl groups in OPCs is the NAA synthesized in neurons and transaxonally transported to oligodendrocytes (Wibom et al., 2009) for myelin synthesis. In control OPCs here investigated, the AGC1 may compensate for the absence of the neuronal-derived NAA with minor consequences in histone acetylation than in OPCs with silenced AGC1. Whether exogenous NAA may have a role in the proliferation/differentiation of OPCs will deserve further experimentation.

Overall, the data presented in this study suggested a new role for the mitochondrial aspartate-glutamate carrier that links metabolism, epigenetics, and gene expression regulation in the brain precursor cells (BPCs). This connection is particularly remarkable if we take into consideration, the positive effect produced in patients with AGC1 deficiency in which NAA levels and myelination significantly increase (Dahlin et al., 2015; Pérez-Liébana et al., 2020; Broeks et al., 2021). This nutritional intervention is based on a high fat, low-carbohydrate diet that uses lipids and ketone bodies (β-hydroxybutyrate and acetoacetate), rather than glucose, as primary fuels, thus inducing favorable metabolic adaptions. KD is effectively utilized as a metabolic treatment in a wide range of neurological metabolic diseases, as it is neuroprotective and strongly improves myelination in drug-refractory epilepsy, mitochondrial diseases, leukodystrophies, and multiple sclerosis (Finsterer, 2011; Stumpf et al., 2019; Bahr et al., 2020; Norwitz et al., 2020; Rudy et al., 2020). KD may alternatively fulfill the energetic demands of the cells, but its beneficial effects could also be attributed to epigenetic mechanisms, that might be consequential to the increased intracellular acetyl-CoA pool formed by the administration of

ketone bodies and to the debated HDACs inhibitory potential of β-hydroxybutyrate, both sustaining histone acetylation (Chriett et al., 2019; Dąbek et al., 2020). The pro-acetylating effect of KD could also improve the proliferation of BPCs, thus providing cells that can differentiate between oligodendrocytes and support myelination.

Similar to AGC1 deficiency, dysfunctions in OPCs and NSCs are now widely recognized in many neuropathologies. The OPCs have been involved in demyelinating conditions, where these cells are the main source of regenerating oligodendrocytes and the inadequate expansion of the OPCs pool may be a limiting factor for successful remyelination.

Oligodendrocyte precursor cells may also change in response to acute injuries, such as ischemia and trauma, and white matter abnormalities with OPCs changes have been observed in neuropsychiatric disorders, including depression and schizophrenia (Nishiyama et al., 2021a).

In conclusion, our study in models of the ultra-rare genetic disease, AGC1 deficiency provided new information to describe the pathogenetic mechanisms of the disease that could also be useful to clarify the role of histone acetylation in the regulation of gene expression in the BPCs in other neuropathologies affecting white matter. The comprehension of the molecular pathways and epigenetic mechanisms regulating proliferation and/or differentiation of OPCs could lead to the identification of new targets for potential therapeutic approaches acting on histone-modifying enzymes may increase the OPCs pool and adequately sustain their differentiation toward oligodendrocytes for correct myelination/remyelination processes (Monti, 2021) in neurodegenerative, neuropsychiatric, and neurodevelopmental diseases (Ganguly and Seth, 2018; D'Mello, 2020; Gupta et al., 2020).

DATA AVAILABILITY STATEMENT

The raw data supporting the conclusions of this article will be made available by the authors, without undue reservation.

ETHICS STATEMENT

The animal study was reviewed and approved by the University of Bologna Bioethical Committee (Protocol no 3/79/2014).

AUTHOR CONTRIBUTIONS

BM and FL conceptualized the general approach and designed the experiments. EP, SP, GB, BR, LC, MCM, SB, MM, FD, and FM performed the experiments. EP, BM, and FL analyzed and interpreted the data, as well as drafted the manuscript. LV, LP, and MV helped design the experiments and contributed methodology. All authors reviewed and approved the final version of the manuscript.

FUNDING

This study was supported by the Telethon GGP19067.

REFERENCES

Ashrafi, M. R., Amanat, M., Garshasbi, M., Kameli, R., Nilipour, Y., Heidari, M., et al. (2020). An update on clinical, pathological, diagnostic, and therapeutic perspectives of childhood leukodystrophies. *Exp. Rev. Neurother.* 20, 65–84. doi: 10.1080/14737175.2020.1699060

Ashrafi, M. R., and Tavasoli, A. R. (2017). Childhood leukodystrophies: a literature review of updates on new definitions, classification, diagnostic approach and management. *Brain Dev.* 39, 369–385. doi: 10.1016/j.braindev.2017.01.001

Bahr, L. S., Bock, M., Liebscher, D., Bellmann-Strobl, J., Franz, L., Prüß, A., et al. (2020). Ketogenic diet and fasting diet as nutritional approaches in multiple sclerosis (NAMS): protocol of a randomized controlled study. *Trials* 21:3. doi: 10.1186/s13063-019-3928-9

Balasubramanyam, K., Varier, R. A., Altaf, M., Swaminathan, V., Siddappa, N. B., Ranga, U., et al. (2004). Curcumin, a novel p300/CREB-binding protein-specific inhibitor of acetyltransferase, represses the acetylation of histone/nonhistone proteins and histone acetyltransferase-dependent chromatin transcription. *JBC* 279, 51163–51171. doi: 10.1074/jbc.M409024200

Bhalla, K. N. (2005). Epigenetic and chromatin modifiers as targeted therapy of hematologic malignancies. *J. Clin. Oncol.* 23, 3971–3993. doi: 10.1200/JCO.2005.16.600

Bito, H., and Takemoto-Kimura, S. (2003). Ca(2+)/CREB/CBP-dependent gene regulation: a shared mechanism critical in long-term synaptic plasticity and neuronal survival. *Cell Calcium* 34, 425–430. doi: 10.1016/s0143-4160(03)00140-4

Bogner-Strauss, J. G. (2017). N-acetylaspartate metabolism outside the brain: lipogenesis, histone acetylation, and cancer. *Front. Endocrinol.* 8:240. doi: 10.3389/fendo.2017.00240

Brand, M. D., and Nicholls, D. G. (2011). Assessing mitochondrial dysfunction in cells. *JBC* 435, 297–312.

Broeks, M. H., van Karnebeek, C., Wanders, R., Jans, J., and Verhoeven-Duif, N. M. (2021). Inborn disorders of the malate aspartate shuttle. *J. Inherit. Metab. Dis.* 44, 792–808. doi: 10.1002/jimd.12402

Carroll, P. A., Freie, B. W., Mathsyaraja, H., and Eisenman, R. N. (2018). The MYC transcription factor network: balancing metabolism, proliferation and oncogenesis. *Front Med.* 12:412–425. doi: 10.1007/s11684-018-0650-z

Chipuk, J. E., Moldoveanu, T., Llambi, F., Parsons, M. J., and Green, D. R. (2010). The BCL-2 family reunion. *Mol. Cell* 37, 299–310. doi: 10.1016/j.molcel.2010.01.025

Choudhry, P. (2016). High-throughput method for automated colony and cell counting by digital image analysis based on edge detection. *PLoS One* 11:e0148469. doi: 10.1371/journal.pone.0148469

Chriett, S., Dąbek, A., Wojtala, M., Vidal, H., Balcerczyk, A., and Pirola, L. (2019). Prominent action of butyrate over β-hydroxybutyrate as histone deacetylase inhibitor, transcriptional modulator and anti-inflammatory molecule. *Sci. Rep.* 9:742. doi: 10.1038/s41598-018-36941-9

Dąbek, A., Wojtala, M., Pirola, L., and Balcerczyk, A. (2020). Modulation of cellular biochemistry, epigenetics and metabolomics by ketone bodies. implications of the ketogenic diet in the physiology of the organism and pathological states. *Nutrients* 12:788. doi: 10.3390/nu12030788

Dahlin, M., Martin, D. A., Hedlund, Z., Jonsson, M., von Döbeln, U., and Wedell, A. (2015). The ketogenic diet compensates for AGC1 deficiency and improves myelination. *Epilepsia* 56, e176–e181. doi: 10.1111/epi.13193

D'Mello, S. R. (2020). Histone deacetylases 1, 2 and 3 in nervous system development. *Curr. Opin. Pharmacol.* 50, 74–81. doi: 10.1016/j.coph.2019.11.007

Dokmanovic, M., and Marks, P. A. (2005). Prospects: histone deacetylase inhibitors. *J. Cell Biochem.* 96, 293–304. doi: 10.1002/jcb.20532

Emery, B., and Lu, Q. R. (2015). Transcriptional and epigenetic regulation of oligodendrocyte development and myelination in the central nervous system. *CSH Perspect. Biol.* 7:a020461. doi: 10.1101/cshperspect.a020461

Falk, M. J., Li, D., Gai, X., McCormick, E., Place, E., Lasorsa, F. M., et al. (2014). AGC1 deficiency causes infantile epilepsy, abnormal myelination, and reduced N-acetylaspartate. *JIMD Rep.* 14, 77–85. doi: 10.1007/8904_2013_287

Finsterer, J. (2011). Treatment of central nervous system manifestations in mitochondrial disorders. *Eur. J Neurol.* 18, 28–38. doi: 10.1111/j.1468-1331.2010.03086.x

Francis, F., Koulakoff, A., Boucher, D., and Chelly, J. (1999). Doublecortin is a developmentally regulated, microtubule-associated protein expressed in migrating and differentiating neurons. *Neuron* 23, 247–256. doi: 10.1016/s0896-6273(00)80777-1

Gage, F. H. (2000). Mammalian neural stem cells. *Science* 287, 1433–1438. doi: 10.1126/science.287.5457.1433

Ganguly, S., and Seth, S. (2018). A translational perspective on histone acetylation modulators in psychiatric disorders. *Psychopharmacology* 235, 1867–1873. doi: 10.1007/s00213-018-4947-z

Gerdes, J., Li, L., Schlueter, C., Duchrow, M., Wohlenberg, C., Gerlach, C., et al. (1991). Immunobiochemical and molecular biologic characterization of the cell proliferation-associated nuclear antigen that is defined by monoclonal antibody Ki-67. *Am. J. Pathol.* 138, 867–873.

Gil-Perotín, S., Duran-Moreno, M., Cebrián-Silla, A., Ramírez, M., García-Belda, P., and García-Verdugo, J. M. (2013). Adult neural stem cells from the subventricular zone: a review of the neurosphere assay. *Anat. Rec.* 296, 1435–1452. doi: 10.1002/ar.22746

Goldman, S. A., and Kuypers, N. J. (2015). How to make an oligodendrocyte. *Development* 142, 3983–3995. doi: 10.1242/dev.126409

Grinspan, J. (2002). Cells and signaling in oligodendrocyte development. *J. Neuropathol. Exp. Neurol.* 61, 297–306.

Grove, B. D., and Bruchey, A. K. (2001). Intracellular distribution of gravin, a PKA and PKC binding protein, in vascular endothelial cells. *J. Vasc. Res.* 38, 163–175. doi: 10.1159/000051043

Gupta, R., Ambasta, R. K., and Kumar, P. (2020). Pharmacological intervention of histone deacetylase enzymes in the neurodegenerative disorders. *Life Sci.* 243:117278. doi: 10.1016/j.lfs.2020.117278

Hernandez, M., and Casaccia, P. (2015). Interplay between transcriptional control and chromatin regulation in the oligodendrocyte lineage. *Glia* 63, 1357–1375. doi: 10.1002/glia.22818

Hsieh, J., and Gage, F. H. (2004). Epigenetic control of neural stem cell fate. *Curr. Opin. Genet. Dev.* 14, 461–469.

Johnstone, R. W., and Licht, J. D. (2003). Histone deacetylase inhibitors in cancer therapy: is transcription the primary target? *Cancer Cell* 4, 13–18. doi: 10.1016/s1535-6108(03)00165-x

Juaristi, I., García-Martín, M. L., Rodrigues, T. B., Satrústegui, J., Llorente-Folch, I., and Pardo, B. (2017). ARALAR/AGC1 deficiency, a neurodevelopmental disorder with severe impairment of neuronal mitochondrial respiration, does not produce a primary increase in brain lactate. *J. Neurochem.* 142, 132–139. doi: 10.1111/jnc.14047

Juliandi, B., Abematsu, M., and Nakashima, K. (2010). Epigenetic regulation in neural stem cell differentiation. *Dev. Growth Differ.* 52, 493–504. doi: 10.1111/j.1440-169x.2010.01175.x

Kavanaugh, B. C., Warren, E. B., Baytas, O., Schmidt, M., Merck, D., Buch, K., et al. (2019). Longitudinal MRI findings in patient with SLC25A12 pathogenic variants inform disease progression and classification. *Am. J. Med. Genet.* 179, 2284–2291. doi: 10.1002/ajmg.a.61322

Kerkhofs, M. (2020). Cytosolic Ca^{2+} oversees the MASs production of pyruvate for the mitochondrial market. *Cell Calcium* 89:102223. doi: 10.1016/j.ceca.2020.102223

Lipinski, M., Del Blanco, B., and Barco, A. (2019). CBP/p300 in brain development and plasticity: disentangling the KAT's cradle. *Curr. Opin. Neurobiol.* 59, 1–8. doi: 10.1016/j.conb.2019.01.023

Llorente-Folch, I., Sahún, I., Contreras, L., Casarejos, M. J., Grau, J. M., Saheki, T., et al. (2013). AGC1-malate aspartate shuttle activity is critical for dopamine handling in the nigrostriatal pathway. *J. Neurochem.* 124, 347–362. doi: 10.1111/jnc.12096

Lok, H. C., and Kwok, J. B. (2021). The role of white matter dysfunction and leukoencephalopathy/leukodystrophy genes in the aetiology of frontotemporal dementias: implications for novel approaches to therapeutics. *IJMS* 22:2541. doi: 10.3390/ijms22052541

Long, P. M., Moffett, J. R., Namboodiri, A., Viapiano, M. S., Lawler, S. E., and Jaworski, D. M. (2013). N-acetylaspartate (NAA) and N-acetylaspartylglutamate (NAAG) promote growth and inhibit differentiation of glioma stem-like cells. *JBC* 288, 26188–26200. doi: 10.1074/jbc.M113.487553

Lowry, O. H., Rosebrough, N. J., Farr, A. L., and Randall, R. J. (1951). Protein measurement with the Folin phenol reagent. *JBC* 193, 265–275. doi: 10.1016/s0021-9258(19)52451-6

Lozoya, O. A., Wang, T., Grenet, D., Wolfgang, T. C., Sobhany, M., Ganini, et al. (2019). Mitochondrial acetyl-CoA reversibly regulates locus-specific histone acetylation and gene expression. *Life Sci. Alliance* 2:e201800228. doi: 10.26508/lsa.201800228

Magri, L., Gacias, M., Wu, M., Swiss, V. A., Janssen, W. G., and Casaccia, P. (2014). c-Myc-dependent transcriptional regulation of cell cycle and nucleosomal histones during oligodendrocyte differentiation. *Neuroscience* 276, 72–86. doi: 10.1016/j.neuroscience.2014.01.051

Marcu, M. G., Jung, Y. J., Lee, S., Chung, E. J., Lee, M. J., Trepel, J., et al. (2006). Curcumin is an inhibitor of p300 histone acetylatransferase. *Med Chem.* 2, 169–174. doi: 10.2174/157340606776056133

Mashimo, M., Onishi, M., Uno, A., Tanimichi, A., Nobeyama, A., Mori, M., et al. (2021). The 89-kDa PARP1 cleavage fragment serves as a cytoplasmic PAR carrier to induce AIF-mediated apoptosis. *JBC* 296:100046. doi: 10.1074/jbc.RA120.014479

Matilainen, O., Quirós, P. M., and Auwerx, J. (2017). Mitochondria and epigenetics - crosstalk in homeostasis and stress. *Trends Cell Biol.* 27, 453–463. doi: 10.1016/j.tcb.2017.02.004

Meijer, D. H., Kane, M. F., Mehta, S., Liu, H., Harrington, E., Taylor, C. M., et al. (2012). Separated at birth? The functional and molecular divergence of OLIG1 and OLIG2. *Nat. Rev. Neurosci.* 13, 819–831. doi: 10.1038/nrn3386

Menzies, K. J., Zhang, H., Katsyuba, E., and Auwerx, J. (2016). Protein acetylation in metabolism - metabolites and cofactors. *Nat. Rev. Endocrinol.* 12, 43–60. doi: 10.1038/nrendo.2015.181

Minucci, S., and Pelicci, P. G. (2006). Histone deacetylase inhibitors and the promise of epigenetic (and more) treatments for cancer. *Nat. Rev. Cancer* 6, 38–51. doi: 10.1038/nrc1779

Moffett, J. R., Ross, B., Arun, P., Madhavarao, C. N., and Namboodiri, A. M. (2007). N-acetylaspartate in the CNS: from neurodiagnostics to neurobiology. *Prog. Neurobiol.* 81, 89–131. doi: 10.1016/j.pneurobio.2006.12.003

Monti, B. (2021). p57kip2 nuclear export as a marker of oligodendrocytes differentiation: towards an innovative phenotyping screening for the identification of myelin repair drugs. *EBioMedicine* 66:103298. doi: 10.1016/j.ebiom.2021.103298

Morris, M. J., and Monteggia, L. M. (2013). Unique functional roles for class I and class II histone deacetylases in central nervous system development and function. *Int. J. Dev. Neurosci.* 31, 370–381. doi: 10.1016/j.ijdevneu.2013.02.005

Nave, K. A., and Werner, H. B. (2014). Myelination of the nervous system: mechanisms and functions. *Annu. Rev. Cell Dev. Biol.* 30, 503–533. doi: 10.1146/annurev-cellbio-100913-013101

Nishiyama, A., Serwanski, D. R., and Pfeiffer, F. (2021a). Many roles for oligodendrocyte precursor cells in physiology and pathology. *Neuropathology* 41, 161–173. doi: 10.1111/neup.12732

Nishiyama, A., Shimizu, T., Sherafat, A., and Richardson, W. D. (2021b). Life-long oligodendrocyte development and plasticity. *Semin. Cell Dev. Biol.* 116, 25–37. doi: 10.1016/j.semcdb.2021.02.004

Nolte, C., Matyash, M., Pivneva, T., Schipke, C. G., Ohlemeyer, C., Hanisch, U. K., et al. (2001). GFAP promoter-controlled EGFP-expressing transgenic mice: a tool to visualize astrocytes and astrogliosis in living brain tissue. *Glia* 33, 72–86. doi: 10.1002/1098-1136(20010101)33:1<72::aid-glia1007>3.0.co;2-a

Norwitz, N. G., Dalai, S. S., and Palmer, C. M. (2020). Ketogenic diet as a metabolic treatment for mental illness. *Curr. Opin. Endocrinol. Diabetes Obes.* 27, 269–274. doi: 10.1097/MED.0000000000000564

Palazuelos, J., Klingener, M., and Aguirre, A. (2014). TGFβ signaling regulates the timing of CNS myelination by modulating oligodendrocyte progenitor cell cycle exit through SMAD3/4/FoxO1/Sp1. *J. Neurosci.* 34, 7917–7930. doi: 10.1523/JNEUROSCI.0363-14.2014

Pérez-Liébana, I., Casarejos, M., Alcaide, A., Herrada-Soler, E., Llorente-Folch, I., Contreras, L., et al. (2020). βOHB protective pathways in Aralar-KO neurons and brain: an alternative to ketogenic diet. *J. Neurosci.* 40, 9293–9305. doi: 10.1523/JNEUROSCI.0711-20.2020

Petralla, S., Peña-Altamira, L. E., Poeta, E., Massenzio, F., Virgili, M., Barile, S. N., et al. (2019). Deficiency of mitochondrial aspartate-glutamate carrier 1 leads to oligodendrocyte precursor cell proliferation defects both *In vitro* and *In vivo*. *IJMS* 20:4486. doi: 10.3390/ijms20184486

Pfeiffer, B., Sen, K., Kaur, S., and Pappas, K. (2020). Expanding phenotypic spectrum of cerebral aspartate-glutamate carrier isoform 1 (AGC1) deficiency. *Neuropediatrics* 51, 160–163. doi: 10.1055/s-0039-3400976

Podobinska, M., Szablowska-Gadomska, I., Augustyniak, J., Sandvig, I., Sandvig, A., and Buzanska, L. (2017). Epigenetic modulation of stem cells in neurodevelopment: the role of methylation and acetylation. *Front. Cell. Neurosci.* 11:23. doi: 10.3389/fncel.2017.00023

Polito, A., and Reynolds, R. (2005). NG2-expressing cells as oligodendrocyte progenitors in the normal and demyelinated adult central nervous system. *J. Anat.* 207, 707–716. doi: 10.1111/j.1469-7580.2005.00454.x

Profilo, E., Peña-Altamira, L. E., Corricelli, M., Castegna, A., Danese, A., Agrimi, G., et al. (2017). Down-regulation of the mitochondrial aspartate-glutamate carrier isoform 1 AGC1 inhibits proliferation and N-acetylaspartate synthesis in Neuro2A cells. *Biochim. Biophys. Acta Mol. Basis Dis.* 1863, 1422–1435. doi: 10.1016/j.bbadis.2017.02.022

Ramos, M., Pardo, B., Llorente-Folch, I., Saheki, T., Del Arco, A., and Satrústegui, J. (2011). Deficiency of the mitochondrial transporter of aspartate/glutamate aralar/AGC1 causes hypomyelination and neuronal defects unrelated to myelin deficits in mouse brain. *J. Neurosci. Res.* 89, 2008–2017. doi: 10.1002/jnr.22639

Rosato, R. R., Almenara, J. A., Dai, Y., and Grant, S. (2003). Simultaneous activation of the intrinsic and extrinsic pathways by histone deacetylase (HDAC) inhibitors and tumor necrosis factor-related apoptosis-inducing ligand (TRAIL) synergistically induces mitochondrial damage and apoptosis in human leukemia cells. *Mol. Cancer Ther.* 2, 1273–1284.

Rudy, L., Carmen, R., Daniel, R., Artemio, R., and Moisés, R. O. (2020). Anticonvulsant mechanisms of the ketogenic diet and caloric restriction. *Epilepsy Res.* 168:106499. doi: 10.1016/j.eplepsyres.2020.106499

Santos, J. H. (2021). Mitochondria signaling to the epigenome: a novel role for an old organelle. *Free Radic. Biol. Med.* 170, 59–69. doi: 10.1016/j.freeradbiomed.2020.11.016

Scherer, S. S., Braun, P. E., Grinspan, J., Collarini, E., Wang, D. Y., and Kamholz, J. (1994). Differential regulation of the 2',3'-cyclic nucleotide 3'-phosphodiesterase gene during oligodendrocyte development. *Neuron* 12, 1363–1375. doi: 10.1016/0896-6273(94)90451-0

Shao, Y., Gao, Z., Marks, P. A., and Jiang, X. (2004). Apoptotic and autophagic cell death induced by histone deacetylase inhibitors. *PNAS* 101, 18030–18035. doi: 10.1073/pnas.0408345102

Shechter, D., Dormann, H. L., Allis, C. D., and Hake, S. B. (2007). Extraction, purification and analysis of histones. *Nat. Protoc.* 2, 1445–1457.

Sheikh, B. N. (2014). Crafting the brain - role of histone acetyltransferases in neural development and disease. *Cell Tissue Res.* 356, 553–573. doi: 10.1007/s00441-014-1835-7

Song, Z., Zhao, D., Zhao, H., and Yang, L. (2015). NRSF: an angel or a devil in neurogenesis and neurological diseases. *J. Mol. Neurosci.* 56, 131–144. doi: 10.1007/s12031-014-0474-5

Stumpf, S. K., Berghoff, S. A., Trevisiol, A., Spieth, L., Düking, T., Schneider, L. V., et al. (2019). Ketogenic diet ameliorates axonal defects and promotes myelination in Pelizaeus-Merzbacher disease. *Acta Neuropathol.* 138, 147–161. doi: 10.1007/s00401-019-01985-2

Sunagawa, Y., Funamoto, M., Sono, S., Shimizu, K., Shimizu, S., Genpei, M., et al. (2018). Curcumin and its demethoxy derivatives possess p300 HAT inhibitory activity and suppress hypertrophic responses in cardiomyocytes. *J. Pharmacol. Sci.* 136, 212–217. doi: 10.1016/j.jphs.2017.12.013

Szibor, M., Gizatullina, Z., Gainutdinov, T., Endres, T., Debska-Vielhaber, G., Kunz, M., et al. (2020). Cytosolic, but not matrix, calcium is essential for adjustment of mitochondrial pyruvate supply. *JBC* 295, 4383–4397. doi: 10.1074/jbc.RA119.011902

Tiane, A., Schepers, M., Rombaut, B., Hupperts, R., Prickaerts, J., Hellings, N., et al. (2019). From OPC to oligodendrocyte: an epigenetic journey. *Cells* 8:1236. doi: 10.3390/cells8101236

Tropepe, V., Sibilia, M., Ciruna, B. G., Rossant, J., Wagner, E. F., and van der Kooy, D. (1999). Distinct neural stem cells proliferate in response to EGF and FGF in the developing mouse telencephalon. *Dev. Biol.* 208, 166–188. doi: 10.1006/dbio.1998.9192

Wibom, R., Lasorsa, F. M., Töhönen, V., Barbaro, M., Sterky, F. H., Kucinski, T., et al. (2009). AGC1 deficiency associated with global cerebral hypomyelination. *N Engl. J. Med.* 361, 489–495. doi: 10.1056/NEJMoa0900591

Widmann, C. (2007). *Caspase 3. xPharm: The Comprehensive Pharmacology Reference*. Amsterdam: Elsevier, 1–9.

Xu, W. S., Parmigiani, R. B., and Marks, P. A. (2007). Histone deacetylase inhibitors: molecular mechanisms of action. *Oncogene* 26, 5541–5552.

Yan, Y., Li, X., Kover, K., Clements, M., and Ye, P. (2013). CREB participates in the IGF-I-stimulation cyclin D1 transcription. *Dev. Neurobiol.* 73, 559–570. doi: 10.1002/dneu.22080

Ye, F., Chen, Y., Hoang, T., Montgomery, R. L., Zhao, X. H., Bu, H., et al. (2009). HDAC1 and HDAC2 regulate oligodendrocyte differentiation by disrupting the beta-catenin-TCF interaction. *Nat. Neurosci.* 12, 829–838. doi: 10.1038/nn.2333

Yoo, C. B., and Jones, P. A. (2006). Epigenetic therapy of cancer: past, present and future. *Nat. Rev. Drug Discov.* 5, 37–50.

Zhang, M., Zhao, J., Lv, Y., Wang, W., Feng, C., Zou, W., et al. (2020). Histone variants and histone modifications in neurogenesis. *Trends Cell Biol.* 30, 869–880. doi: 10.1016/j.tcb.2020.09.003

Zhou, Q., Dalgard, C. L., Wynder, C., and Doughty, M. L. (2011). Histone deacetylase inhibitors SAHA and sodium butyrate block G1-to-S cell cycle progression in neurosphere formation by adult subventricular cells. *BMC Neurosci.* 12:50. doi: 10.1186/1471-2202-12-50

Conflict of Interest: The authors declare that the research was conducted in the absence of any commercial or financial relationships that could be construed as a potential conflict of interest.

Publisher's Note: All claims expressed in this article are solely those of the authors and do not necessarily represent those of their affiliated organizations, or those of the publisher, the editors and the reviewers. Any product that may be evaluated in this article, or claim that may be made by its manufacturer, is not guaranteed or endorsed by the publisher.

Copyright © 2022 Poeta, Petralla, Babini, Renzi, Celauro, Magnifico, Barile, Masotti, De Chirico, Massenzio, Viggiano, Palmieri, Virgili, Lasorsa and Monti. This is an open-access article distributed under the terms of the Creative Commons Attribution License (CC BY). The use, distribution or reproduction in other forums is permitted, provided the original author(s) and the copyright owner(s) are credited and that the original publication in this journal is cited, in accordance with accepted academic practice. No use, distribution or reproduction is permitted which does not comply with these terms.

frontiers in Cellular Neuroscience

MINI REVIEW
published: 17 March 2022
doi: 10.3389/fncel.2022.838007

Epidermal Growth Factor Pathway in the Age-Related Decline of Oligodendrocyte Regeneration

Andrea D. Rivera[1]*, *Kasum Azim*[2], *Veronica Macchi*[1], *Andrea Porzionato*[1], *Arthur M. Butt*[3†] *and Raffaele De Caro*[1†]

[1]Department of Neuroscience, Institute of Human Anatomy, University of Padua, Padua, Italy, [2]Department of Neurology, Medical Faculty, Heinrich-Heine-University, Düsseldorf, Germany, [3]School of Pharmacy and Biomedical Science, University of Portsmouth, Portsmouth, United Kingdom

Oligodendrocytes (OLs) are specialized glial cells that myelinate CNS axons. OLs are generated throughout life from oligodendrocyte progenitor cells (OPCs) *via* a series of tightly controlled differentiation steps. Life-long myelination is essential for learning and to replace myelin lost in age-related pathologies such as Alzheimer's disease (AD) as well as white matter pathologies such as multiple sclerosis (MS). Notably, there is considerable myelin loss in the aging brain, which is accelerated in AD and underpins the failure of remyelination in secondary progressive MS. An important factor in age-related myelin loss is a marked decrease in the regenerative capacity of OPCs. In this review, we will contextualize recent advances in the key role of Epidermal Growth Factor (EGF) signaling in regulating multiple biological pathways in oligodendroglia that are dysregulated in aging.

Keywords: EGF, EGFR, ErbB, oligodendrocyte, myelin, aging, white matter

OPEN ACCESS

Edited by:
Jason R. Plemel,
University of Alberta, Canada

Reviewed by:
Enrica Boda,
University of Turin, Italy
Feng Mei,
Army Medical University, China

***Correspondence:**
Andrea D. Rivera
andrea.rivera@unipd.it

†*These authors have contributed equally to this work*

Specialty section:
This article was submitted to Non-Neuronal Cells, a section of the journal Frontiers in Cellular Neuroscience

Received: *17 December 2021*
Accepted: *23 February 2022*
Published: *17 March 2022*

Citation:
Rivera AD, Azim K, Macchi V, Porzionato A, Butt AM and De Caro R (2022) Epidermal Growth Factor Pathway in the Age-Related Decline of Oligodendrocyte Regeneration. Front. Cell. Neurosci. 16:838007. doi: 10.3389/fncel.2022.838007

INTRODUCTION

Brain aging is characterized by a slowing down of sensory, cognitive and behavioral processes (Harada et al., 2013). Notably, brain imaging studies in humans have demonstrated shrinkage of white matter that precedes overt loss of neurons and appears to be accelerated in dementia (Bartzokis et al., 2012; Maniega et al., 2015; Cox et al., 2016). White matter is comprised of myelinated axons which are thin protrusions of the neurons that transmit electrical signals between the different parts of the central nervous system (CNS). Myelin is a lipid-rich insulating layer that is wrapped around axons in concentrical lamellae by terminally differentiated glial cells called oligodendrocytes (OLs). Myelin increases the propagation speed of electrical signaling along the length of an axon by saltatory conduction. Moreover, myelin has numerous emerging roles that includes, providing metabolic support (Fünfschilling et al., 2007; Philips and Rothstein, 2017), memory consolidation (Pan et al., 2020; Steadman et al., 2020), task-associated learning experiences (Kato et al., 2020; Wang et al., 2020), and reviewed by (Pan and Chan, 2021), whilst myelin loss renders axons more vulnerable to damage (Smith, 2006). Once developmental myelination is complete, myelin remodeling continues throughout life *via* a reservoir of oligodendrocyte progenitors (OPCs) which are the main proliferating pool of cells in the adult CNS and possess

the stem-cell-like feature of self-renewal (Nishiyama et al., 2021). The life-long generation of OLs from OPCs is essential to produce new myelin required to insulate new brain connections formed in response to new life experiences and to replace myelin lost through natural "wear-tear" or pathology (Rivera et al., 2016). However, the regenerative power of OPCs declines with age leading to impaired oligodendrogenesis and myelin remodeling, and an overall gradual loss of major CNS functions such as spatial learning and memory (Pan et al., 2020; Steadman et al., 2020; Wang et al., 2020). The age-related impairments in OPC differentiation have been discussed in a number of recent reviews (for example, Rivera et al., 2021a; Butt et al., 2019). Moreover, in many age-related neuropathologies such as AD or secondary progressive MS, due to a number of reasons that include and are not limited to the inflammatory environment, excess inhibitory myelin debris, lack of appropriate trophic support, etc, OPC differentiation drastically fails and contributes to the loss in cognitive function (Neumann et al., 2019; Wang et al., 2020; Coelho et al., 2021; Rivera et al., 2021a,b). Currently, the development of treatments to halt these changes is hampered by gaps in fundamental scientific knowledge. Developmental studies propose a positive role of epidermal growth factor (EGF) acting *via* its main receptor, EGFR, as a key regulator of cell survival, proliferation, migration and differentiation which are disrupted in aging (**Figure 1**; Herbst, 2004; Gonzalez-Perez et al., 2009; Galvez-Contreras et al., 2013; Yang et al., 2017). To the best of our knowledge, functional studies of EGF signaling in the context of OL differentiation during later stages of adulthood have yet to be performed. Nevertheless, these are exciting future avenues in the field as a potential therapeutic target in OL pathologies and aging.

OLIGODENDROCYTE AND MYELIN DISRUPTION IN THE AGING BRAIN

Age-related loss of brain connectivity underlies cognitive decline, with a "last in, first out" pattern, whereby white matter tracts associated with cognition are the "last" to be fully myelinated and the first to be lost in aging (Davis et al., 2009; Bartzokis et al., 2012; Gozdas et al., 2020). This process is the result of brain architectural complexity described as heterochronicity and spatial heterogeneity intrinsic in white matter tracts. In addition, it suggests that the latest tracts to develop are the most vulnerable to the deleterious effects of aging (Cox et al., 2016; Kochunov et al., 2016). Post-mortem diffusion magnetic resonance imaging (dMRI) studies indicate ontogenetic differences between early-myelinating projection and posterior callosal fibers in aging (Sexton et al., 2014; Cox et al., 2016; Slater et al., 2019). Although the precise causes of WM shrinkage are currently unresolved, they include metabolic disruption of oligodendroglia, OPC senescence and loss of extracellular trophic factors that support OPCs and OLs which can contribute to the functional decline of brain function including deficits in spatial memory and learning (Rivera et al., 2016, 2021b; Neumann et al., 2019; Kato et al., 2020; Pan et al., 2020; Steadman et al., 2020; Willis et al., 2020). Several studies in both humans and rodents have demonstrated marked changes in the transcriptome of OLs and myelination processes (Soreq et al., 2017; Neumann et al., 2019; Rivera et al., 2021b). Moreover, alterations in OPC densities have been reported in brain aging (Soreq et al., 2017; Rivera et al., 2021b). The age-related disruption of indispensable signaling pathway components hinders myelin remodeling and repair, and ultimately adds to the cumulative loss of myelin, which is aggravated in pathology. Recently, we have demonstrated that the critical OPC protein GPR17 is downregulated in the aged murine brain, together with myelin-related transcripts such as MBP, PLP1, CNP, and UGT8A (Rivera et al., 2021b). Our transcriptomic analysis identified a central role for age-related changes in EGFR signaling in oligodendroglia, consistent with its recognized importance in OLregeneration and myelin repair (Aguirre et al., 2007; Hayakawa-Yano et al., 2007; Ivkovic et al., 2008).

Unraveling Novel Roles of EGFR Signaling in Aged Oligodendroglia

In our network analyses (**Figure 1B**), we identified EGFR association with myelination *via* its interaction with ERBB3 which is required for OL maturation (Schmucker et al., 2003; Makinodan et al., 2012). ERBB3 is coupled to the Ras family member NRAS which has intrinsic GTPase activity and is involved in the control of cell proliferation, regulating microtubule stability and actin polymerization (Fotiadou et al., 2007), and is implicated in cancer pathways (Bronte et al., 2015). Interestingly, NRAS has recently been reported to be elevated in expression in the aging OPC proteome (de la Fuente et al., 2020). NRAS interacts with VCL (vinculin) and CLDN11 (claudin-11) to regulate OL morphogenesis/myelin growth (Nawaz et al., 2015), or the formation of tight junctions (TJs) with ECM-integrin interactions, respectively (Gow et al., 1999; Bronstein et al., 2000; Tiwari-Woodruff et al., 2001). Notably, EGFRs are mechanosensitive (Tschumperlin, 2004; Müller-Deubert et al., 2017), transduced by vinculin (including Talin and similar linker proteins) to regulate the anchoring of the actin cytoskeleton to the ECM through integrin, leading to cytoskeleton regulation and cellular spreading (Rübsam et al., 2017). Our analysis predicted the interaction of vinculin on with the actin cytoskeleton *via* gelsolin (GSN), which is enriched in OLs (Tanaka and Sobue, 1994; Zhang et al., 2014) and is required for myelination (Liu et al., 2003; Zuchero et al., 2015). Intriguingly, vinculin and gelsolin are focal adhesion proteins important for the association of cell-cell and cell-matrix junctions and are critical for controlling cell spreading, cytoskeletal mechanics, and lamellipodia formation (Ciobanasu et al., 2014; Elosegui-Artola et al., 2016; Argentati et al., 2019; Merkel et al., 2019; Muñoz-Lasso et al., 2020). Moreover, the interaction of EGFR and vinculin with CLDN11 is consistent with the evidence that they mediate cell/integrin/ECM interactions (Hagen, 2017). Recent *in vivo* experiments in which CLDN11 was deleted in OLs have shown dysregulation of myelin with subsequent aberrant behavioral changes due to increased latency of signals (Maheras et al., 2018). The ECM plays a pivotal role in OL differentiation (Lourenço and Grãos, 2016) and increased stiffness of the ECM is related to age-related deterioration of OPC function (Segel et al., 2019).

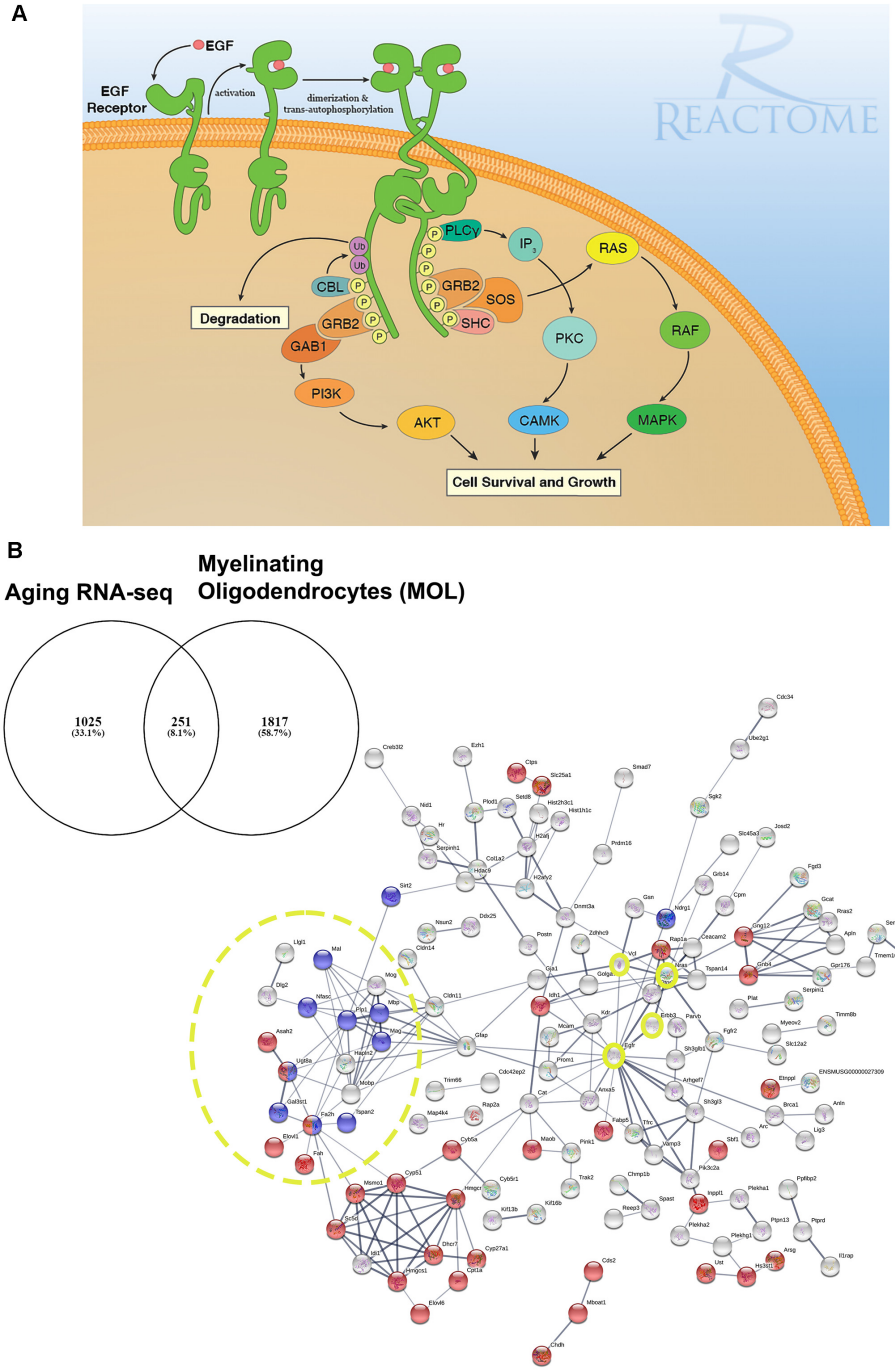

FIGURE 1 | EGF receptor signaling and resolving its dysregulation in aged oligodendroglial *via* protein-protein network analysis. **(A)** EGFR is a member of ERBB receptors that belong to the superfamily of Receptor Tyrosine Kinases (RTKs). The binding of ligands to EGFR induces conformational changes resulting in the receptor homo- or heterodimerization at the cell surface. Dimerization of the extracellular regions of EGFR cascades results in further conformational change at the cytoplasmic region of the receptor, leading to the activation of the catalytic domain. EGFR dimers trans-autophosphorylate on tyrosine residues in the cytoplasmic tail becoming binding sites for the recruitment of intracellular modulator for downstream signaling cascades. Recruitment of complexes containing GRB2 and SOS1 directly through GRB2 or indirectly through SHC1 promotes the activation of RAS/RAF/MAP kinase signaling. The binding of GRB2 and GAB1 to phosphorylated EGFR leads to the activation of PI3K/AKT signaling cascade. Finally, PLCγcan be recruited to the phosphorylated EGFR which, in turn, activates IP3/PKC signaling. Image generated from REACTOME "Signaling by EGFR" (https://reactome.org/PathwayBrowser/#/R-HSA-177929). **(B)** RNA-seq transcriptome analysis of the aging murine brain was compared to a database of genes expressed by myelinating OLs (MOL) and 251 genes were identified as significantly altered in aging (Rivera et al., 2021b). **(B)** Functional protein-protein network analysis identified EGFR as centrally connected with ERBB3, NRAS, VCL, GSN, CLDN11, and the myelination node (yellow circles). Red nodes represent genes associated with Metabolism ($p < 0.000034$) and blue nodes represent genes associated with Myelination ($p < 5.55e\text{-}07$). PPI enrichment p-value < : 2.44e-15. Adapted from Rivera et al. (2021b).

Our data implicate for the first time the EGFR-VINCULIN-GELSOLIN-CLDN11 network as key to age-related changes in oligodendroglial ECM interactions.

EGFR AND THEIR ROLES IN OLIGODENDROGLIA

Overview of EGFR Ligands and Receptors in the CNS

The EGFR, also known as ERBB1 or HER-1, and its family of ligands are widely expressed across the CNS. EGFR, together with ERBB2, ERBB3, ERBB4 belong to the receptor tyrosine kinases (RTKs) superfamily (reviewed extensively elsewhere, for example, Novak et al., 2001; Fu et al., 2003; Galvez-Contreras et al., 2013). Canonical ligands include: epidermal growth factor (EGF), transforming growth factor-α (TGFα), Heparin-binding EGF (HB-EGF) B-cellulin (BTC) and low-affinity binding ligands such as neuregulins (NRG 1–4) amphiregulin (AR) and epiregulin (EPR; **Figure 1A**; Knudsen et al., 2014; Singh et al., 2016). In young adult mice, bulk transcriptomic analysis could resolve their detection across multiple cell types where most of these are expressed by the vasculature, choroid plexus (TGFα), or astrocytes (HB-EGF; Azim et al., 2018). It remains to be determined which of these are altered during aging and are aspects which will be addressed in follow-up studies using the same procedures done in older mice.

The major downstream effectors of EGFR signaling are described in **Figure 1A** illustrating the RAS/RAF/ERK1-2/STAT3-5 and the PI3K/AKT protein complexes are fundamental regulators of many OL biological processes aside from the EGFR signaling pathway (Ishii et al., 2014, 2019; Azim et al., 2017; Sanz-Rodriguez et al., 2018; Rivera et al., 2021b). The precise interaction of these kinases to the newly identified EGFR-VINCULIN-GELSOLIN-CLDN11 network remains to be resolved.

EGFR Signaling in Oligodendroglia and Myelination

Recent transcriptomic studies have shed further light on the expression of EGFR and ERRB2–4 in developmental and adult human OL lineage cells demonstrating elevated expression in OPC compared to other CNS cell types (Zhang et al., 2014; Jäkel et al., 2019). *In vivo* gain- and loss-of-function studies underlined the critical importance of EGFR in OLs (Aguirre et al., 2007, 2010). Specifically, overexpression of EGFR enhanced the densities and maturation state of myelinating oligodendrocytes (MOL; Aguirre et al., 2007), which may be owed to sustained AKT phosphorylation in post-mitotic immature OLs (Flores et al., 2000, 2008) *via* the Src homology 2-containing phosphotyrosine phosphatase (SHP2) which integrates EGFR to AKT signaling (Agazie and Hayman, 2003; Zhu et al., 2010; Nocita et al., 2019). Similarly, the Grb2 associated binder 1 (GAB1) is another modulator of PI3K/AKT signaling capable of directing oligodendrogenesis *via* EGFR (Holgado-Madruga et al., 1996; Hayakawa-Yano et al., 2007). *In vitro* studies indicated that EGF interacts with PDGF-AA and FGF to direct early glial progenitors toward the OL fate, suggesting the combinatorial role for these two pathways towards oligodendrogenesis (Yang et al., 2017). Intriguingly, OPCs cultured with EGF in the absence of PDGF-AA are driven to differentiate into MOLs, suggesting a dual role of EGF in the control of oligodendrogenesis and myelination, depending on the activation of other signaling pathways (Yang et al., 2017). Similarly, intraventricular administration of EGF promotes subventricular progenitors to differentiate into OPCs and MOL *in vivo* (Gonzalez-Perez et al., 2009; Galvez-Contreras et al., 2013). Furthermore, overexpression of human-EGFR (hEGFR) in CNP+ OLs leads to an increase in OL densities and remyelination of the corpus callosum following a lesion (Aguirre et al., 2007). However, persistent overexpression of EGFR in OPCs leads to their dramatic enhancement in densities and white matter hyperplasia, although differentiation appears to be hindered (Hayakawa-Yano et al., 2007; Ivkovic et al., 2008; Gonzalez-Perez et al., 2009). Finally, intranasal administration of exogenous heparin-binding EGF (HB-EGF) in a neonatal hypoxia murine model reduced apoptosis of MOL preserving axonal myelination (Scafidi et al., 2014). These results suggest that the control of oligodendrogenesis and myelination requires temporal and cell-specific interplay of EGFR with other unknown signaling pathways. OL lineage cells also express ERBB2–4 which are required depending on the maturation stage (Flores et al., 2000; Park et al., 2001; Yarden and Sliwkowski, 2001; Kim et al., 2003; Schmucker et al., 2003; Makinodan et al., 2012). For example, ERBB2 regulates OL proliferation and differentiation, while ERBB3 and ERBB4 are necessary for maturation and myelination (Park et al., 2001; Schmucker et al., 2003; Roy et al., 2007; Joubert et al., 2010; Makinodan et al., 2012). However, overexpression or excessive activation of ERBBs in defined stages of OLs can lead to inflammation, demyelination, and cell death (Hu et al., 2021). Taken together, EGFR/ERBB signaling has key roles in the regulation of defined stages of OLs and white matter formation in the CNS.

EGFR AS A POTENTIAL THERAPEUTIC STRATEGY IN AGE-RELATED WHITE MATTER LOSS

Studies on preclinical murine animal models and human post-mortem tissue have demonstrated downregulation of EGFR in the aging brain (Hiramatsu et al., 1988; Werner et al., 1988). Moreover, EGFR signaling is disturbed in aging and gain and loss of function experiments *in vivo* posit the idea of the presence of undiscovered factors in the aging CNS that limit its efficacy in positively regulating biological processes required for proliferation and differentiation of NSCs (Cochard et al., 2021). To further investigate this, we have interrogated the transcriptome of the aging murine brain (Rivera et al., 2021b) with genes associated with Alzheimer's Disease (AD) and Multiple Sclerosis (MS) using the DISGENET database (**Figure 2**; Pinero et al., 2015). These analyses identified 60 AD-associated genes that are altered in aged MOLs, with an apparent EGFR-ANXA5-GSN-APOD axis interconnected with a myelin gene hub; ANXA5 (annexin 5) is involved in pathogenesis through autophagy mechanisms (Iannaccone et al., 2015;

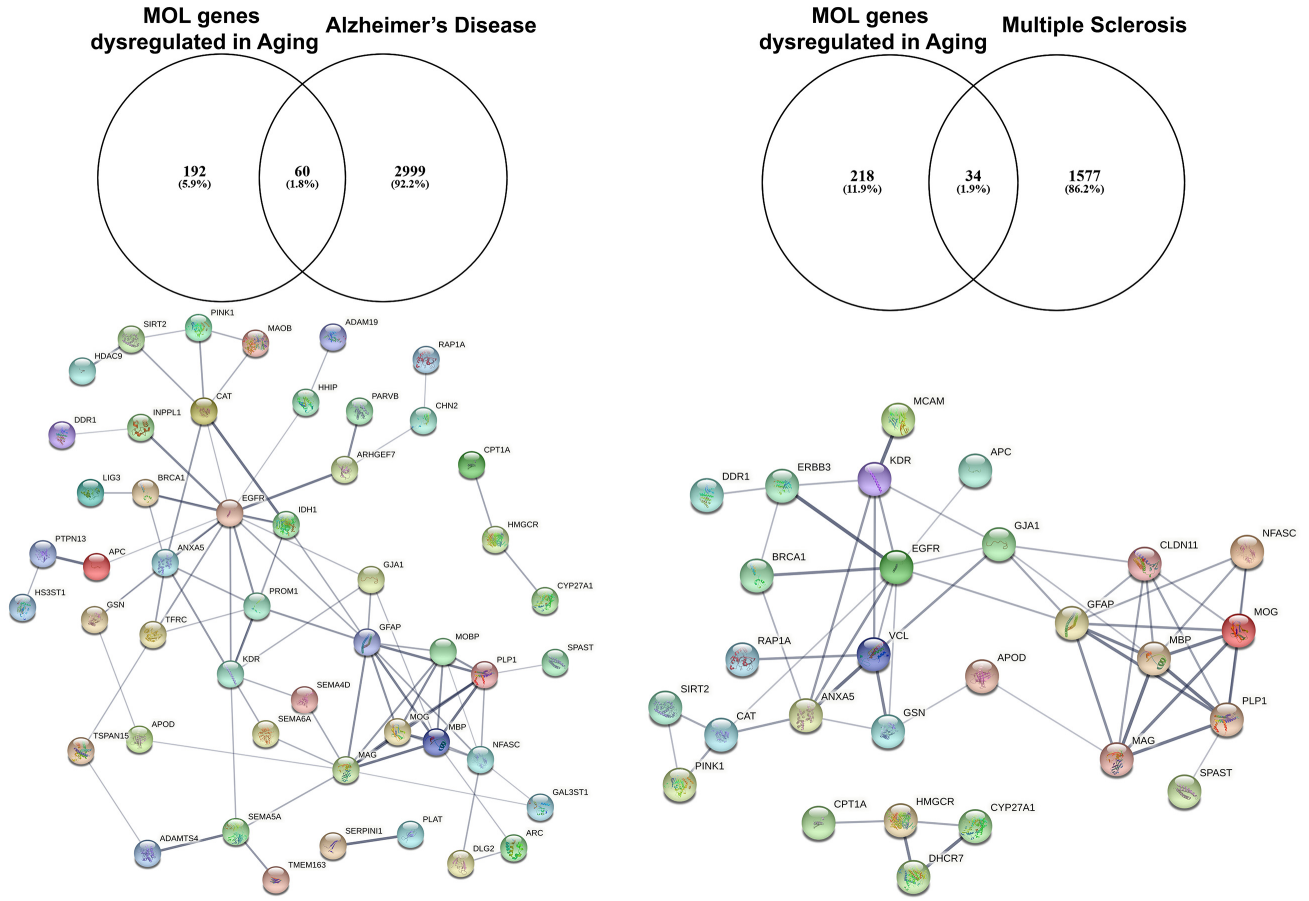

FIGURE 2 | Identification of altered EGFR signaling in aged myelinating oligodendrocytes are further associated as altered genes in Alzheimer's disease and multiple sclerosis. The aging myelinating OLtranscriptome was interrogated to identify novel associations within disease-specific databases for Alzheimer's disease and multiple sclerosis. Functional protein–protein prediction analysis identified EGFR at the core of the networks for Alzheimer's disease and multiple sclerosis (PPI enrichment $p < 0.0001$).

Xi et al., 2020), and APOD (apolipoprotein D) is a secreted glycoprotein involved in lipid transport that is linked to AD, MS and other neuroinflammatory diseases (Reindl et al., 2001; Li et al., 2015). In the same way, analysis of oligodendroglial genes altered in aging and associated with MS revealed 34 highly correlated genes with a conserved EGFR-VCL-GSN-APOD network associated with myelin genes. In MS, APOD levels are decreased in sclerotic plaques and elevated during remyelination (Navarro et al., 2018). Hence, identifying small molecules that target these networks has promising therapeutic potential for rejuvenating OPCs in aging contexts. A novel approach is to use genomics and chemical informatics data, most notably the connectivity map (CMAP) and the Library of Integrated Network-based Cellular Signatures (LINCS), which enables the identification of small molecules that counteract disease-specific transcriptional profiles (Azim et al., 2017; Rivera et al., 2022a). In this way, we recently identified the PI3K-Akt inhibitor LY294002 as a potent driver of OPC rejuvenation and myelin repair *in vivo* (Rivera et al., 2022a,b). Notably, transcriptional profiling and signaling pathway activity assays identified EGFR signaling as a target of LY294002 in OPCs and GO analysis of LY294002-responsive oligodendroglial genes indicated a central role for Rhoa at the core of ERBB3 signaling, which regulates oligodendrogenesis *via* RAF-MAPK and PI3K/Akt (Rivera et al., 2022a). These studies demonstrate that transcript-specific targeting using pharmacogenomics approaches streamlines the identification of drugs to target EGFR signaling, and can be readily adapted to probe genes and transcriptional networks of interest for driving rejuvenation and myelin repair.

CONCLUSION

In summary, EGFR signaling and its subsequent signaling cascade depends on the combination of ERBB receptors activated. EGFR signaling is central for the OPC self-renewal and their differentiation into MOLs. In the aged brain, there is a decline in the regenerative capacity of OPCs and this is highly correlated with changes in EGFR signaling pathways. Moreover, we have recently shown that targeting PI3K/AKT signaling, which is a key downstream mechanism of EGFR, promotes OPC

regeneration and remyelination in an aging context (Rivera et al., 2022a,b). These data support a key role for EGFR as a potential therapeutic target for rejuvenating OPCs and promoting repair in pathologies with age-related contexts, including MS and AD.

AUTHOR CONTRIBUTIONS

AR: conceptualization, formal analysis, investigation, methodology, writing—original draft, writing—review and editing. KA: formal analysis, investigation, writing—review and editing. VM and AP: supervision, writing—review and editing. AB and RD: conceptualization, formal analysis, funding acquisition, project administration, resources, supervision, visualization, writing—original draft, writing—review and editing.

FUNDING

This work was supported by grants from the Biotechnology and Biological Sciences Research Council (BBSRC, UK) (BB/M029379/1), Medical Research Council (MRC, UK) (MR/P025811/1), MSCA Seal of Excellence @ UNIPD and NVIDIA Hardware Grant, German Research Council (AZ/115/1-1; AZ/115/1-3), and Swiss National Funds (P300PA_171224).

REFERENCES

Agazie, Y. M., and Hayman, M. J. (2003). Molecular mechanism for a role of SHP2 in epidermal growth factor receptor signaling. *Mol. Cell Biol.* 23, 7875–7886. doi: 10.1128/MCB.23.21.7875-7886.2003

Aguirre, A., Dupree, J. L., Mangin, J. M., and Gallo, V. (2007). A functional role for EGFR signaling in myelination and remyelination. *Nat. Neurosci.* 10, 990–1002. doi: 10.1038/nn1938

Aguirre, A., Maria Rubio, E., and Vittorio, G. (2010). Notch and EGFR pathway interaction regulates neural stem cell number and self-renewal. *Nature* 467, 323–327. doi: 10.1038/nature09347

Argentati, C., Morena, F., Tortorella, I., Bazzucchi, M., Porcellati, S., Emiliani, C., et al. (2019). Insight into mechanobiology: how stem cells feel mechanical forces and orchestrate biological functions. *Int. J. Mol. Sci.* 20:5337. doi: 10.3390/ijms20215337

Azim, K., Angonin, D., Marcy, G., Pieropan, F., Rivera, A., Donega, V., et al. (2017). Pharmacogenomic identification of small molecules for lineage specific manipulation of subventricular zone germinal activity. *PLoS Biol.* 15:e2000698. doi: 10.1371/journal.pbio.2000698

Azim, K., Rainer, A., Martina, C., Julio, V., Janusz Jadasz, J., and Patrick, K. (2018). Transcriptional profiling of ligand expression in cell specific populations of the adult mouse forebrain that regulates neurogenesis. *Front. Neurosci.* 12:220. doi: 10.3389/fnins.2018.00220

Bartzokis, G., Po Lu, H., Panthea, H., Alexander, C., Grace Lee, J., Greta, K., et al. (2012). Multimodal magnetic resonance imaging assessment of white matter aging trajectories over the lifespan of healthy individuals. *Biol. Psychiatry* 72, 1026–1034. doi: 10.1016/j.biopsych.2012.07.010

Bronstein, J. M., Tiwari-Woodruff, S., Buznikov, A. G., and Stevens, D. B. (2000). Involvement of OSP/claudin-11 in oligodendrocyte membrane interactions, role in biology and disease. *J. Neurosci. Res.* 59, 706–711. doi: 10.1002/(SICI)1097-4547(20000315)59:6<706::AID-JNR2>3.0.CO;2-D

Bronte, G., Silvestris, N., Castiglia, M., Galvano, A., Passiglia, F., Sortino, G., et al. (2015). New findings on primary and acquired resistance to anti-EGFR therapy in metastatic colorectal cancer: do all roads lead to RAS. *Oncotarget* 6, 24780–24796. doi: 10.18632/oncotarget.4959

Butt, A. M., De La Rocha, I. C., and Rivera, A. (2019). Oligodendroglial cells in Alzheimer's disease. *Adv. Exp. Med. Biol.* 1175, 325–333. doi: 10.1007/978-981-13-9913-8_12

Ciobanasu, C., Faivre, B., and Le Clainche, C. (2014). Actomyosin-dependent formation of the mechanosensitive talin-vinculin complex reinforces actin anchoring. *Nat. Commun.* 5:3095. doi: 10.1038/ncomms4095

Cochard, L. M., Louis-Charles, L., Sandra, E., Joppé, F. P., Anne, A., and Karl Fernandes, J. L. (2021). Manipulation of EGFR-induced signaling for the recruitment of quiescent neural stem cells in the adult mouse forebrain. *Front. Neurosci.* 15:621076. doi: 10.3389/fnins.2021.621076

Coelho, A., Henrique Fernandes, M., Ricardo, M., Moreira, P. S., Marques, P., José Soares, M., et al. (2021). Signatures of white-matter microstructure degradation during aging and its association with cognitive status. *Sci. Rep.* 11:4517. doi: 10.1038/s41598-021-83983-7

Cox, S. R., Ritchie, S. J., Tucker-Drob, E. M., Liewald, D. C., Hagenaars, S. P., Davies, G., et al. (2016). Ageing and brain white matter structure in 3,513 UK Biobank participants. *Nat. Commun.* 7:13629. doi: 10.1038/ncomms13629

Davis, S. W., Dennis, N. A., Buchler, N. G., White, L. E., Madden, D. J., and Cabeza, R. (2009). Assessing the effects of age on long white matter tracts using diffusion tensor tractography. *Neuroimage* 46, 530–541. doi: 10.1016/j.neuroimage.2009.01.068

de la Fuente, A. G., Queiroz, R. M. L., Ghosh, T., McMurran, C. E., Cubillos, J. F., Bergles, D. E., et al. (2020). Changes in the oligodendrocyte progenitor cell proteome with ageing. *Mol. Cell. Proteomics* 19, 1281–1302. doi: 10.1074/mcp.RA120.002102

Elosegui-Artola, A., Oria, R., Chen, Y., Kosmalska, A., Pérez-González, C., Castro, N., et al. (2016). Mechanical regulation of a molecular clutch defines force transmission and transduction in response to matrix rigidity. *Nat. Cell Biol.* 18, 540–548. doi: 10.1038/ncb3336

Flores, A. I., Mallon, B. S., Matsui, T., Ogawa, W., Rosenzweig, A., Okamoto, T., et al. (2000). Akt-mediated survival of oligodendrocytes induced by neuregulins. *J. Neurosci.* 20, 7622–7630. doi: 10.1523/JNEUROSCI.20-20-07622.2000

Flores, A. I., Narayanan, S. P., Morse, E. N., Shick, H. E., Yin, X., Kidd, G., et al. (2008). Constitutively active Akt induces enhanced myelination in the CNS. *J. Neurosci.* 28, 7174–7183. doi: 10.1523/JNEUROSCI.0150-08.2008

Fotiadou, P. P., Takahashi, C., Rajabi, H. N., and Ewen, M. E. (2007). Wild-type NRas and KRas perform distinct functions during transformation. *Mol. Cell. Biol.* 27, 6742–6755. doi: 10.1128/MCB.00234-07

Fu, L., Abu-Khalil, A., Morrison, R. S., Geschwind, D. H., and Kornblum, H. I. (2003). Expression patterns of epidermal growth factor receptor and fibroblast growth factor receptor 1 mRNA in fetal human brain. *J. Comp. Neurol.* 462, 265–273. doi: 10.1002/cne.10727

Fünfschilling, U., Saher, G., Xiao, L., Möbius, W., and Nave, K.-A. (2007). Survival of adult neurons lacking cholesterol synthesis *in vivo*. *BMC Neurosci.* 8:1. doi: 10.1186/1471-2202-8-1

Galvez-Contreras, A., Quinones-Hinojosa, A., and Gonzalez-Perez, O. (2013). The role of EGFR and ErbB family related proteins in the oligodendrocyte specification in germinal niches of the adult mammalian brain. *Front. Cell. Neurosci.* 7:258. doi: 10.3389/fncel.2013.00258

Gonzalez-Perez, O., Romero-Rodriguez, R., Soriano-Navarro, M., Garcia-Verdugo, J. M., and Alvarez-Buylla, A. (2009). Epidermal growth factor induces the progeny of subventricular zone type B cells to migrate and differentiate into oligodendrocytes. *Stem Cells* 27, 2032–2043. doi: 10.1002/stem.119

Gow, A., Southwood, C. M., Li, J. S., Pariali, M., Riordan, G. P., Brodie, S. E., et al. (1999). CNS myelin and sertoli cell tight junction strands are absent in Osp/claudin-11 null mice. *Cell* 99, 649–659. doi: 10.1016/s0092-8674(00)81553-6

Gozdas, E., Fingerhut, H., Chromik, L. C., O'Hara, R., Reiss, A. L., and Hadi Hosseini, S. M. (2020). Focal white matter disruptions along the cingulum tract explain cognitive decline in amnestic mild cognitive impairment (aMCI). *Sci. Rep.* 10:10213. doi: 10.1038/s41598-020-66796-y

Hagen, S. J. (2017). Non-canonical functions of claudin proteins: beyond the regulation of cell-cell adhesions. *Tissue Barriers* 5:e1327839. doi: 10.1080/21688370.2017.1327839

Harada, C. N., Natelson Love, M. C., and Triebel, K. L. (2013). Normal cognitive aging. *Clin. Geriat. Med.* 29, 737–752. doi: 10.1016/j.cger.2013.07.002

Hayakawa-Yano, Y., Nishida, K., Fukami, S., Gotoh, Y., Hirano, T., Nakagawa, T., et al. (2007). Epidermal growth factor signaling mediated by grb2 associated binder1 is required for the spatiotemporally regulated proliferation of olig2-expressing progenitors in the embryonic spinal cord. *Stem Cells* 25, 1410–1422. doi: 10.1634/stemcells.2006-0584

Herbst, R. S. (2004). Review of epidermal growth factor receptor biology. *Int. J. Radiat. Oncol. Biol. Phys.* 59, 21–26. doi: 10.1016/j.ijrobp.2003.11.041

Hiramatsu, M., Kashimata, M., Sato, A., Murayama, M., and Minami, N. (1988). Influence of age on epidermal growth factor receptor level in the rat brain. *Experientia* 44, 23–25. doi: 10.1007/BF01960230

Holgado-Madruga, M., Emlet, D. R., Moscatello, D. K., Godwin, A. K., and Wong, A. J. (1996). A Grb2-associated docking protein in EGF- and insulin-receptor signalling. *Nature* 379, 560–564. doi: 10.1038/379560a0

Hu, X., Xiao, G., He, L., Niu, X., Li, H., Lou, T., et al. (2021). Sustained ErbB activation causes demyelination and hypomyelination by driving necroptosis of mature oligodendrocytes and apoptosis of oligodendrocyte precursor cells. *J. Neurosci.* 41, 9872–9890. doi: 10.1523/JNEUROSCI.2922-20.2021

Iannaccone, A., Giorgianni, F., New, D. D., Hollingsworth, T. J., Umfress, A., Alhatem, A. H., et al. (2015). Circulating autoantibodies in age-related macular degeneration recognize human macular tissue antigens implicated in autophagy, immunomodulation and protection from oxidative stress and apoptosis. *PLoS One* 10:e0145323. doi: 10.1371/journal.pone.0145323

Ishii, A., Furusho, M., Dupree, J. L., and Bansal, R. (2014). Role of ERK1/2 MAPK signaling in the maintenance of myelin and axonal integrity in the adult CNS. *J. Neurosci.* 34, 16031–16045. doi: 10.1523/JNEUROSCI.3360-14.2014

Ishii, A., Furusho, M., Macklin, W., and Bansal, R. (2019). Independent and cooperative roles of the Mek/ERK1/2-MAPK and PI3K/Akt/mTOR pathways during developmental myelination and in adulthood. *Glia* 67, 1277–1295. doi: 10.1002/glia.23602

Ivkovic, S., Canoll, P., and Goldman, J. E. (2008). Constitutive EGFR signaling in oligodendrocyte progenitors leads to diffuse hyperplasia in postnatal white matter. *J. Neurosci.* 28, 914–922. doi: 10.1523/JNEUROSCI.4327-07.2008

Jäkel, S., Agirre, E., Falcão, A. M., Bruggen, D. V., Lee, K. W., Knuesel, I., et al. (2019). Altered human oligodendrocyte heterogeneity in multiple sclerosis. *Nature* 566, 543–547. doi: 10.1038/s41586-019-0903-2

Joubert, L., Foucault, I., Sagot, Y., Bernasconi, L., Duval, F., Alliod, C., et al. (2010). Chemical inducers and transcriptional markers of oligodendrocyte differentiation. *J. Neurosci. Res.* 88, 2546–2557. doi: 10.1002/jnr.22434

Kato, D., Wake, H., Lee, P. R., Tachibana, Y., Ono, R., Sugio, S., et al. (2020). Motor learning requires myelination to reduce asynchrony and spontaneity in neural activity. *Glia* 68, 193–210. doi: 10.1002/glia.23713

Kim, J. Y., Sun, Q., Oglesbee, M., and Yoon, S. O. (2003). The role of ErbB2 signaling in the onset of terminal differentiation of oligodendrocytes *in vivo*. *J. Neurosci.* 23, 5561–5571. doi: 10.1523/JNEUROSCI.23-13-05561.2003

Knudsen, S. L., Mac, A. S., Henriksen, L., van Deurs, B., and Grøvdal, L. M. (2014). EGFR signaling patterns are regulated by its different ligands. *Growth Factors* 32, 155–163. doi: 10.3109/08977194.2014.952410

Kochunov, P., Ganjgahi, H., Winkler, A., Kelly, S., Shukla, D. K., Du, X., et al. (2016). Heterochronicity of white matter development and aging explains regional patient control differences in schizophrenia. *Hum. Brain Mapp.* 37, 4673–4688. doi: 10.1002/hbm.23336

Li, H., Ruberu, K., Muñoz, S. S., Jenner, A. M., Spiro, A., Zhao, H., et al. (2015). Apolipoprotein D modulates amyloid pathology in APP/PS1 Alzheimers disease mice. *Neurobiol. Aging* 36, 1820–1833. doi: 10.1016/j.neurobiolaging.2015.02.010

Liu, A., Muggironi, M., Marin-Husstege, M., and Casaccia-Bonnefil, P. (2003). Oligodendrocyte process outgrowth *in vitro* is modulated by epigenetic regulation of cytoskeletal severing proteins. *Glia* 44, 264–274. doi: 10.1002/glia.10290

Lourenço, T., and Grãos, M. (2016). Modulation of oligodendrocyte differentiation by mechanotransduction. *Front. Cell. Neurosci.* 10:277. doi: 10.3389/fncel.2016.00277

Maheras, K. J., Peppi, M., Ghoddoussi, F., Galloway, M. P., Perrine, S. A., and Gow, A. (2018). Absence of claudin 11 in CNS myelin perturbs behavior and neurotransmitter levels in mice. *Sci. Rep.* 8:3798. doi: 10.1038/s41598-018-22047-9

Makinodan, M., Rosen, K. M., Ito, S., and Corfas, G. (2012). A critical period for social experience-dependent oligodendrocyte maturation and myelination. *Science* 337, 1357–1360. doi: 10.1126/science.1220845

Maniega, S. M., Valdes Hernandez, M. C., Clayden, J. D., Royle, N. A., Murray, C., Morris, Z., et al. (2015). White matter hyperintensities and normal-appearing white matter integrity in the aging brain. *Neurobiol. Aging* 36, 909–918. doi: 10.1016/j.neurobiolaging.2014.07.048

Merkel, C. D., Li, Y., Raza, Q., Stolz, D. B., and Kwiatkowski, A. V. (2019). Vinculin anchors contractile actin to the cardiomyocyte adherens junction. *Mol. Biol. Cell* 30, 2639–2650. doi: 10.1091/mbc.E19-04-0216

Müller-Deubert, S., Seefried, L., Krug, M., Jakob, F., and Ebert, R. (2017). Epidermal growth factor as a mechanosensitizer in human bone marrow stromal cells. *Stem Cell Res.* 24, 69–76. doi: 10.1016/j.scr.2017.08.012

Muñoz-Lasso, D. C., Romá-Mateo, C., Pallardó, F. V., and Gonzalez-Cabo, P. (2020). Much more than a scaffold: cytoskeletal proteins in neurological disorders. *Cells* 9:358. doi: 10.3390/cells9020358

Navarro, A., Rioseras, B., del Valle, E., Martínez-Pinilla, E., Astudillo, A., and Tolivia, J. (2018). Expression pattern of myelin-related apolipoprotein D in human multiple sclerosis lesions. *Front. Aging Neurosci.* 10:254. doi: 10.3389/fnagi.2018.00254

Nawaz, S., Sánchez, P., Schmitt, S., Snaidero, N., Mitkovski, M., Velte, C., et al. (2015). Actin filament turnover drives leading edge growth during myelin sheath formation in the central nervous system. *Dev. Cell* 34, 139–151. doi: 10.1016/j.devcel.2015.05.013

Neumann, B., Baror, R., Zhao, C., Segel, M., Dietmann, S., Rawji, K. S., et al. (2019). Metformin restores CNS remyelination capacity by rejuvenating aged stem cells. *Cell Stem Cell* 25, 473–485.e8. doi: 10.1016/j.stem.2019.08.015

Nishiyama, A., Shimizu, T., Sherafat, A., and Richardson, W. D. (2021). Life-long oligodendrocyte development and plasticity. *Semin. Cell Dev. Biol.* 116, 25–37. doi: 10.1016/j.semcdb.2021.02.004

Nocita, E., Giovane, A. D., Tiberi, M., Boccuni, L., Fiorelli, D., Sposato, C., et al. (2019). EGFR/ErbB inhibition promotes OPC maturation up to axon engagement by co-regulating PIP2 and MBP. *Cells* 8:844. doi: 10.3390/cells8080844

Novak, U., Walker, F., and Kaye, A. (2001). Expression of EGFR-family proteins in the brain: role in development, health and disease. *J. Clin. Neurosci.* 8, 106–111. doi: 10.1054/jocn.2000.0799

Pan, S., and Chan, J. R. (2021). Clinical applications of myelin plasticity for remyelinating therapies in multiple sclerosis. *Ann. Neurol.* 90, 558–567. doi: 10.1002/ana.26196

Pan, S., Mayoral, S. R., Sun Choi, H., Chan, J. R., and Kheirbek, M. A. (2020). Preservation of a remote fear memory requires new myelin formation. *Nat. Neurosci.* 23, 487–499. doi: 10.1038/s41593-019-0582-1

Park, S. K., Miller, R., Krane, I., and Vartanian, T. (2001). The erbB2 gene is required for the development of terminally differentiated spinal cord oligodendrocytes. *J. Cell Biol.* 154, 1245–1258. doi: 10.1083/jcb.200104025

Philips, T., and Rothstein, J. D. (2017). Oligodendroglia: metabolic supporters of neurons. *J. Clin. Invest.* 127, 3271–3280. doi: 10.1172/JCI90610

Pinero, J., Queralt-Rosinach, N., Bravo, A., Deu-Pons, J., Bauer-Mehren, A., Baron, M., et al. (2015). DisGeNET: a discovery platform for the dynamical exploration of human diseases and their genes. *Database (Oxford)* 2015:bav028. doi: 10.1093/database/bav028

Reindl, M., Knipping, G., Wicher, I., Dilitz, E., Egg, R., Deisenhammer, F., et al. (2001). Increased intrathecal production of apolipoprotein D in multiple sclerosis. *J. Neuroimmunol.* 119, 327–332. doi: 10.1016/s0165-5728(01)00378-2

Rivera, A. D., Chacon-De-La-Rocha, I., Pieropan, F., Papanikolau, M., Azim, K., and Butt, A. M. (2021a). Keeping the ageing brain wired: a role for purine signalling in regulating cellular metabolism in oligodendrocyte progenitors. *Pflügers Arch.* 473, 775–783. doi: 10.1007/s00424-021-02544-z

Rivera, A. D., Pieropan, F., Chacon-De-La-Rocha, I., Lecca, D., Abbracchio, M. P., Azim, K., et al. (2021b). Functional genomic analyses highlight a shift in Gpr17-regulated cellular processes in oligodendrocyte progenitor cells and underlying myelin dysregulation in the aged mouse cerebrum. *Aging Cell* 20:e13335. doi: 10.1111/acel.13335

Rivera, A. D., Pieropan, F., Williams, G., Calzolari, F., Butt, A. M., and Azim, K. (2022a). Drug connectivity mapping and functional analysis reveal therapeutic small molecules that differentially modulate myelination. *Biomed. Pharmacother.* 145:112436. doi: 10.1016/j.biopha.2021.112436

Rivera, A. D., Butt, A. M., and Azim, K. (2022b). Resolving the age-related decline in central nervous system myelin turnover and drug discovery for oligodendroglial rejuvenation. *Neural Regen. Res.* in press.

Rivera, A., Vanzuli, I., Arellano, J. J., and Butt, A. (2016). Decreased regenerative capacity of oligodendrocyte progenitor cells (NG2-Glia) in the ageing brain: a vicious cycle of synaptic dysfunction, myelin loss and neuronal disruption? *Curr. Alzheimer Res.* 13, 413–418. doi: 10.2174/1567205013666151116125518

Roy, K., Murtie, J. C., El-Khodor, B. F., Edgar, N. S., Sardi, P., Hooks, B. M., et al. (2007). Loss of erbB signaling in oligodendrocytes alters myelin and dopaminergic function, a potential mechanism for neuropsychiatric disorders. *Proc. Natl. Acad. Sci. U S A* 104, 8131–8136. doi: 10.1073/pnas.0702157104

Rübsam, M., Mertz, A. F., Kubo, A., Marg, S., Jüngst, C., Goranci-Buzhala, G., et al. (2017). E-cadherin integrates mechanotransduction and EGFR signaling to control junctional tissue polarization and tight junction positioning. *Nat. Commun.* 8:1250. doi: 10.1038/s41467-017-01170-7

Sanz-Rodriguez, M., Gruart, A., Escudero-Ramirez, J., de Castro, F., Delgado-García, J. M., Wandosell, F., et al. (2018). R-Ras1 and R-Ras2 are essential for oligodendrocyte differentiation and survival for correct myelination in the central nervous system. *J. Neurosci.* 38, 5096–5110. doi: 10.1523/JNEUROSCI.3364-17.2018

Scafidi, J., Hammond, T. R., Scafidi, S., Ritter, J., Jablonska, B., Roncal, M., et al. (2014). Intranasal epidermal growth factor treatment rescues neonatal brain injury. *Nature* 506, 230–234. doi: 10.1038/nature12880

Schmucker, J., Ader, M., Brockschnieder, D., Brodarac, A., Bartsch, U., and Riethmacher, D. (2003). erbB3 is dispensable for oligodendrocyte development *in vitro* and *in vivo*. *Glia* 44, 67–75. doi: 10.1002/glia.10275

Segel, M., Neumann, B., Hill, M. F. E., Weber, I. P., Viscomi, C., Zhao, C., et al. (2019). Niche stiffness underlies the ageing of central nervous system progenitor cells. *Nature* 573, 130–134. doi: 10.1038/s41586-019-1484-9

Sexton, C. E., Walhovd, K. B., Storsve, A. B., Tamnes, C. K., Westlye, L. T., Johansen-Berg, H., et al. (2014). Accelerated changes in white matter microstructure during aging: a longitudinal diffusion tensor imaging study. *J. Neurosci.* 34, 15425–15436. doi: 10.1523/JNEUROSCI.0203-14.2014

Singh, B., Carpenter, G., and Coffey, R. J. (2016). EGF receptor ligands: recent advances. *F1000Res.* 5(F1000 Faculty Rev):2270. doi: 10.12688/f1000research.9025.1

Slater, D. A., Melie-Garcia, L., Preisig, M., Kherif, F., Lutti, A., and Draganski, B. (2019). Evolution of white matter tract microstructure across the life span. *Hum. Brain Mapp.* 40, 2252–2268. doi: 10.1002/hbm.24522

Smith, K. J. (2006). Axonal protection in multiple sclerosis—a particular need during remyelination?. *Brain* 129, 3147–3149. doi: 10.1093/brain/awl323

Soreq, L., Rose, J., Soreq, E., Hardy, J., Trabzuni, D., Cookson, M. R., et al. (2017). Major shifts in glial regional identity are a transcriptional hallmark of human brain aging. *Cell Rep.* 18, 557–570. doi: 10.1016/j.celrep.2016.12.011

Steadman, P. E., Xia, F., Ahmed, M., Mocle, A. J., Penning, A. R. A., Geraghty, A. C., et al. (2020). Disruption of oligodendrogenesis impairs memory consolidation in adult mice. *Neuron* 105, 150–164.e6. doi: 10.1016/j.neuron.2019.10.013

Tanaka, J., and Sobue, K. (1994). Localization and characterization of gelsolin in nervous tissues: gelsolin is specifically enriched in myelin-forming cells. *J. Neurosci.* 14, 1038–1052. doi: 10.1523/JNEUROSCI.14-03-01038.1994

Tiwari-Woodruff, S. K., Buznikov, A. G., Vu, T. Q., Micevych, P. E., Chen, K., Kornblum, H. I., et al. (2001). OSP/claudin-11 forms a complex with a novel member of the tetraspanin super family and beta1 integrin and regulates proliferation and migration of oligodendrocytes. *J. Cell Biol.* 153, 295–305. doi: 10.1083/jcb.153.2.295

Tschumperlin, D. J. (2004). EGFR autocrine signaling in a compliant interstitial space: mechanotransduction from the outside in. *Cell Cycle* 3, 996–997. doi: 10.4161/cc.3.8.1062

Wang, F., Ren, S. Y., Chen, J. F., Liu, K., Li, R. X., Li, Z. F., et al. (2020). Myelin degeneration and diminished myelin renewal contribute to age-related deficits in memory. *Nat. Neurosci.* 23, 481–486. doi: 10.1038/s41593-020-0588-8

Werner, M. H., Nanney, L. B., Stoscheck, C. M., and King, L. E. (1988). Localization of immunoreactive epidermal growth factor receptors in human nervous system. *J. Histochem. Cytochem.* 36, 81–86. doi: 10.1177/36.1.3275713

Willis, C. M., Nicaise, A. M., Bongarzone, E. R., Givogri, M., Reiter, C. R., Heintz, O., et al. (2020). Astrocyte support for oligodendrocyte differentiation can be conveyed *via* extracellular vesicles but diminishes with age. *Sci. Rep.* 10:828. doi: 10.1038/s41598-020-57663-x

Xi, Y., Ju, R., and Wang, Y. (2020). Roles of annexin A protein family in autophagy regulation and therapy. *Biomed. Pharmacother.* 130:110591. doi: 10.1016/j.biopha.2020.110591

Yang, J., Cheng, X., Qi, J., Xie, B., Zhao, X., Zheng, K., et al. (2017). EGF enhances oligodendrogenesis from glial progenitor cells. *Front. Mol. Neurosci.* 10:106. doi: 10.3389/fnmol.2017.00106

Yarden, Y., and Sliwkowski, M. X. (2001). Untangling the ErbB signalling network. *Nat. Rev. Mol. Cell Biol.* 2, 127–137. doi: 10.1038/35052073

Zhang, Y., Chen, K., Sloan, S. A., Bennett, M. L., Scholze, A. R., OKeeffe, S., et al. (2014). An RNA-sequencing transcriptome and splicing database of glia, neurons and vascular cells of the cerebral cortex. *J. Neurosci.* 34, 11929–11947. doi: 10.1523/JNEUROSCI.1860-14.2014

Zhu, Y., Park, J., Hu, X., Zheng, K., Li, H., Cao, Q., et al. (2010). Control of oligodendrocyte generation and proliferation by Shp2 protein tyrosine phosphatase. *Glia* 58, 1407–1414. doi: 10.1002/glia.21016

Zuchero, J. B., Fu, M. M., Sloan, S. A., Ibrahim, A., Olson, A., Zaremba, A., et al. (2015). CNS myelin wrapping is driven by actin disassembly. *Dev. Cell* 34, 152–167. doi: 10.1016/j.devcel.2015.06.011

Conflict of Interest: AR and AB are shareholders of Gliagenesis LTD.

The remaining authors declare that the research was conducted in the absence of any commercial or financial relationships that could be construed as a potential conflict of interest.

Publisher's Note: All claims expressed in this article are solely those of the authors and do not necessarily represent those of their affiliated organizations, or those of the publisher, the editors and the reviewers. Any product that may be evaluated in this article, or claim that may be made by its manufacturer, is not guaranteed or endorsed by the publisher.

Copyright © 2022 Rivera, Azim, Macchi, Porzionato, Butt and De Caro. This is an open-access article distributed under the terms of the Creative Commons Attribution License (CC BY). The use, distribution or reproduction in other forums is permitted, provided the original author(s) and the copyright owner(s) are credited and that the original publication in this journal is cited, in accordance with accepted academic practice. No use, distribution or reproduction is permitted which does not comply with these terms.

frontiers in Cellular Neuroscience

ORIGINAL RESEARCH
published: 17 March 2022
doi: 10.3389/fncel.2022.820226

PRMT5 Interacting Partners and Substrates in Oligodendrocyte Lineage Cells

David K. Dansu[1,2†], Jialiang Liang[3,4†], Ipek Selcen[1,2], Haiyan Zheng[5,6], Dirk F. Moore[7] and Patrizia Casaccia[1,2]*

[1] Neuroscience Initiative, Advanced Science Research Center, CUNY, New York, NY, United States, [2] Graduate Program in Biochemistry, The Graduate Center of the City University of New York, New York, NY, United States, [3] Department of Neuroscience, Icahn School of Medicine at Mount Sinai, New York, NY, United States, [4] Graduate School of Biomedical Sciences, Icahn School of Medicine at Mount Sinai, New York, NY, United States, [5] Center for Advanced Biotechnology and Medicine, Piscataway, NJ, United States, [6] Department of Biochemistry and Molecular Biology, Robert-Wood Johnson Medical School, Rutgers Biomedical and Health Sciences, Piscataway, NJ, United States, [7] Department of Biostatistics, School of Public Health, Rutgers, The State University of New Jersey, Piscataway, NJ, United States

The protein arginine methyl transferase PRMT5 is an enzyme expressed in oligodendrocyte lineage cells and responsible for the symmetric methylation of arginine residues on histone tails. Previous work from our laboratory identified PRMT5 as critical for myelination, due to its transcriptional regulation of genes involved in survival and early stages of differentiation. However, besides its nuclear localization, PRMT5 is found at high levels in the cytoplasm of several cell types, including oligodendrocyte progenitor cells (OPCs) and yet, its interacting partners in this lineage, remain elusive. By using mass spectrometry on protein eluates from extracts generated from primary oligodendrocyte lineage cells and immunoprecipitated with PRMT5 antibodies, we identified 1196 proteins as PRMT5 interacting partners. These proteins were related to molecular functions such as RNA binding, ribosomal structure, cadherin and actin binding, nucleotide and protein binding, and GTP and GTPase activity. We then investigated PRMT5 substrates using iTRAQ-based proteomics on cytosolic and nuclear protein extracts from CRISPR-PRMT5 knockdown immortalized oligodendrocyte progenitors compared to CRISPR-EGFP controls. This analysis identified a similar number of peptides in the two subcellular fractions and a total number of 57 proteins with statistically decreased symmetric methylation of arginine residues in the CRISPR-PRMT5 knockdown compared to control. Several PRMT5 substrates were in common with cancer cell lines and related to RNA processing, splicing and transcription. In addition, we detected ten oligodendrocyte lineage specific substrates, corresponding to proteins with high expression levels in neural tissue. They included: PRC2C, a proline-rich protein involved in methyl-RNA binding, HNRPD an RNA binding protein involved in regulation of RNA stability, nuclear proteins involved in transcription and other proteins related to migration and actin cytoskeleton. Together, these results highlight a cell-specific role of PRMT5 in OPC in regulating several other cellular processes, besides RNA splicing and metabolism.

Keywords: brain, arginine methylation, RNA processing, epigenetics, iTRAQ

OPEN ACCESS

Edited by:
Davide Lecca, University of Milan, Italy

Reviewed by:
Karine Choquet, Harvard Medical School, United States
Constantin Gonsior, Johannes Gutenberg University of Mainz, Germany

****Correspondence:***
Patrizia Casaccia
pcasaccia@gc.cuny.edu

† These authors have contributed equally to this work

Specialty section:
This article was submitted to Non-Neuronal Cells, a section of the journal Frontiers in Cellular Neuroscience

Received: *22 November 2021*
Accepted: *04 January 2022*
Published: *17 March 2022*

Citation:
Dansu DK, Liang J, Selcen I, Zheng H, Moore DF and Casaccia P (2022) PRMT5 Interacting Partners and Substrates in Oligodendrocyte Lineage Cells. Front. Cell. Neurosci. 16:820226. doi: 10.3389/fncel.2022.820226

INTRODUCTION

The protein arginine methyltransferases (PRMTs) family of enzymes catalyzes the transfer of methyl groups from S-adenosyl methionine (SAM) to guanidine nitrogen of peptidyl arginine residues in mammals (Bedford and Clarke, 2009) and their role in oligodendrocyte lineage cells has been recently highlighted (Blanc and Richard, 2017). PRMTs can be grouped into three categories, based on their final methylarginine products. While type III PRMTs (including PRMT-7 and 9) (Feng et al., 2013; Yang Y. et al., 2015) only generate monomethylarginines (MMA) (Zurita-Lopez et al., 2012), type I PRMTs (including PRMT-1, -2, -3, -4/CARM1, -6, and 8) catalyze the conversion of MMA to asymmetric dimethylarginines (ADMA) while type II PRMTs (including PRMT-5 and -9), generate symmetric dimethylarginines (SDMA) (Tewary et al., 2019). The functional importance of the steric localization of methyl groups on specific arginine residues on the tails of histone H3 (H3R2 and H3R8) and that of histone H4 (H4R3), has been highlighted (Wang et al., 2001; Pal et al., 2004). The symmetric or asymmetric deposition on the same histone R residue results in opposing functions, either promoting or repressing transcription, depending on the position of the arginines and of the adjacent amino acids (Bedford and Richard, 2005; Litt et al., 2009). Besides transcriptional regulation (Kleinschmidt et al., 2008), arginine methylated residues have been shown to play important roles in RNA metabolism and DNA repair (Bedford and Clarke, 2009), thereby affecting diverse cellular functions, including survival and proliferation (Hua et al., 2020; Tanaka et al., 2020).

Among the PRMTs, the type II PRMT5 is highly expressed in the brain and enriched in oligodendrocyte lineage cells (Huang et al., 2011; Zhang et al., 2014; Tasic et al., 2016). Previous work from our lab and others has highlighted the importance of post-translational modification of amino acids on histone tails in regulating the behavior of oligodendrocyte progenitors (Liu et al., 2015, 2016; Moyon et al., 2016; Pruvost and Moyon, 2021). For instance, we previously reported the existence of an interesting cross-talk between PRMT5-mediated symmetric dimethylation of arginine residue R3 and acetylation of lysine residue K5 on histone H4, as critical for oligodendrocyte progenitor survival and differentiation (Scaglione et al., 2018). OPCs lacking *Prmt5* failed to differentiate *in vitro* (Huang et al., 2011), an event attributed to the persistent expression of differentiation inhibitors (*Id2* and *Id4*) (Huang et al., 2011) and more recently attributed to broader effects of PRMT5 loss of function on increased histone acetylation and P53-mediated apoptosis leading to defective myelination (Scaglione et al., 2018), a finding independently validated by a different group (Calabretta et al., 2018). However, PRMT5 is predominantly found in the cytoplasm of OPC and of several other cell types, such as cancer cells (Gu et al., 2012) and stem cells (Koh et al., 2015). In these other cell types, cytosolic PRMT5 has been shown to regulate several aspects of RNA metabolism, including spliceosome assembly, through methylation of Sm proteins (Meister and Fischer, 2002; Gonsalvez et al., 2007), RNA splicing, through methylation of the splicing regulator SRSF1 (Radzisheuskaya et al., 2019), ribosome biogenesis, through methylation of RPS10 (Gao et al., 2017) and RNA transport, *via* arginine methylation of hnRNPA1 (Ren et al., 2010). Cytoplasmic PRMT5 has also been shown to methylate several transcription factors including sterol regulatory element-binding transcription factor 1 (SREBP1) and programmed cell death protein 4 (PDCD4), leading to their nuclear translocation and regulation of their targets (Liang et al., 2021).

Therefore, many of the previous studies focused on PRMT5 as critical regulator of RNA biology, while our previous study addressed the nuclear function of PRMT5, despite its predominant cytosolic localization in OPCs. In this study we use mass spectrometry-based proteomic approaches and iTRAQ labeling of nuclear and cytosolic protein extracts, to broaden our understanding of the role of PRMT5 in OPC by identifying its protein interactors and substrates in oligodendrocyte lineage cells.

MATERIALS AND METHODS

Primary Oligodendrocyte Progenitor Cell Isolation

Primary mouse OPCs were generated from the cortices of C57BL/6 mice, purchased from Jackson Laboratories and euthanized at postnatal day 7 according to IACUC approved protocols at Icahn School of Medicine. Progenitors were immunopanned with a rat anti-mouse CD140a antibody (BD Bioscience, 558774), as previously described (J. Liu et al., 2015). The isolated cells were then cultured in SATO medium (Dulbecco's modified Eagle's medium (DMEM), 100 μg/mL BSA, 100 μg/mL apo-transferrin, 16 μg/mL putrescine, 62.5 ng/mL progesterone, 40 ng/mL selenium, 5 μg/mL insulin, 1 mM sodium pyruvate, 5 μg/ml N-acetyl-cysteine, 10 ng/ml biotin, 5 μM forskolin, B27 Supplement and Trace Element B). Progenitors were plated on PDL coated dishes and cultured in SATO medium supplemented either with Platelet-Derived Growth Factor-AA (PDGFA) (10 ng/ml) and basic Fibroblast Growth Factor (bFGF) (20 ng/ml) or supplemented with 60 nM of Triiodothyronine (T3) in the absence of growth factors.

Immortalized Oligodendrocyte Progenitors (Oli-neu)

Immortalized oligodendrocyte progenitors were received as a gift from Jackie Trotter (Jung et al., 1995) and were cultured on poly-D-lysine coated plates in media (Dulbecco's modified Eagle's medium (DMEM), 100 μg/mL BSA, 100 μg/mL apo-transferrin, 16 μg/mL putrescine, 62.5 ng/mL progesterone, 40 ng/mL selenium, 5 μg/mL insulin, 1 mM sodium pyruvate, 5 μg/ml N-acetyl-cysteine, 10 ng/ml biotin, 5 μM forskolin, B27 Supplement, Trace Element B and 1% horse serum).

Lenti-CRISPR/Cas9 Mediated Gene Knockdown System in 293T Cells

The lentiCRISPR-v2 vector was received as a gift from Feng Zhang (Addgene plasmid #52961). Feng Zhang's laboratory

online program[1]was used in designing the sgRNA targets. The two sgRNA target sequences of PRMT5-CRISPR (GAATTGC GTCCCCGAAATAG & CCCGCGTTTCAAGAGGGAGT) used in the study were directed to exon 1 and 2, respectively, of the *Prmt5 gene.* The other two sgRNAs targeted *EGFP* gene (GGG CGAGGAGCTGTTCACCG & GAGCTGGACGGCGACGTA AA) and these were used as controls. Both the *Prmt5 and EGFP* sgRNAs were cloned into the same vector backbone. Cloning was performed according to the Addgene guidelines and as previously described (Shalem et al., 2014; Scaglione et al., 2018). The lenti-CRISPR viruses were generated by transfecting 293T cells with CRISPR/Cas9 plasmids and packing plasmids, psPAX2 and pMD2.G (from Addgene #12260 and #12259). For transfection of every 10-cm dish of 293T cells with polyethylenimine, 10 μg of lenti-CRISPR/Cas9 plasmids, 6 μg of psPAX2 and 2 μg of pMD2.G plasmids were used. The 293T cells were cultured in 293T medium (DMEM, 1mM sodium pyruvate, 2 mM L-glutamine) supplemented with 10% FBS. Tissue culture media were refreshed 15 h post transfection and media containing viruses were harvested 45 h post transfection. Lenti-X^{TM} concentrator kit (Clontech) was used in concentrating viruses.

Prmt5 Knockdown in Immortalized Oligodendrocyte Progenitors

Immortalized oligodendrocyte progenitors (0.5 million cells) were split into each 10-cm dish 24 h prior to viral infection. Concentrated virus was added into the tissue culture medium of the cells to be infected. The culture medium was supplemented with 4 μg/ml of polybrene. Virus-containing media were replaced by fresh media 8 h post infection. To select for transfected cells, 1 μg/ml of puromycin was added to the medium 2 days post transfection. For experimental analysis, the infected cells were harvested 6 days after infection.

Western Blotting

Western blotting was done by sodium dodecyl sulfate–polyacrylamide gel electrophoresis (SDS-PAGE) followed by a wet transfer of the proteins onto a polyvinylidene fluoride (PVDF) membrane. The membranes were blocked for 1 h in 10% milk/0.1% Tween/TBS. Primary antibodies were incubated overnight at 4°C in 5% milk/0.1% Tween/TBS. Primary antibodies used include: rabbit-PRMT5 (Abcam ab109451, 1:5000), mouse-GAPDH (Abcam ab8245, 1:5000), total H3 rabbit-(Abcam ab1791, 1:200000), rabbit anti-symmetric Di-Methyl Arginine Motif (Cell Signaling 13222S, 1:1000) and rabbit anti-asymmetric Di-Methyl Arginine Motif (Cell Signaling 13522S, 1:1000). Membranes were washed with 0.1% Tween/TBS and incubated at room temperature for 1 h with horseradish peroxidase conjugated secondary antibodies (Jackson Immunoresearch, 1:10,000) 5% milk/0.1% Tween/TBS. ECL Prime Wester Blotting Detection Reagent kit (GE Healthcare, RPN2232) were then used to develop the membrane. Ponceau staining was performed with Ponceau S solution (Sigma) according to the manufacturer's instruction. Image J was used to quantify the protein bands.

Subcellular Protein Fractionation

To sperate cellular extracts into cytosolic and nuclear fractions, cell pellets were treated with hypotonic buffer (10 mM HEPES, pH 7.9, 1.5 mM $MgCl_2$, 10 mM KCl) supplemented with 0.5 mM DTT, 1 mM phenylmethylsulfonyl fluoride (PMSF), and protease inhibitor cocktail. After incubation of the re-suspended cells (by rotation at 4°C for 15 min), the membranes of the cells were disrupted by the addition of 0.5% NP40 and vortexed for 10 sec. Cell lysates were centrifuged at 1,500 × *g* for 10 min at 4°C to separate cytoplasmic components (supernatant) from nuclei-enriched fractions (pellets). Cytoplasmic extraction buffer (10×) (0.3 M HEPES, 1.4 M KCl and 30 mM $MgCl_2$) was added to the supernatant and sonicated for 5 min (30 s ON/OFF) at high power in the Bioruptor (Diagenode). The soluble fraction was collected as cytoplasmic extract after centrifugation at 16,000 × *g* for 10 min at 4°C. The nuclei-enriched pellet initially obtained was then washed twice with hypotonic buffer + 0.5% NP40. The washed nuclei pellets were re-suspended in mild salt buffer (20 mM HEPES, pH 7.9, 10% glycerol, 1.5 mM $MgCl_2$, 0.2mM EDTA and 150 mM KCl) supplemented with 0.5 mM PMSF and protease inhibitor cocktail. The re-suspended pellets were rotated in 4°C for 20 min. The solution was centrifuged at 10,000 × *g* for 10 min at 4°C. The soluble fraction was collected as soluble nuclear protein extract.

Immunoprecipitation

Primary oligodendrocyte progenitors kept either in the presence or absence of mitogens supplemented with T3 for 48 h (four preparations) were lysed in NP-40 lysis buffer (50 mM HEPES, pH 7.4, 150 mM NaCl, 10% glycerol, 1 mM EDTA, pH 8 and 1% NP-40) supplemented with protease inhibitor cocktail, PMSF, phosphatase inhibitor and TSA. The re-suspended cells were then incubated and rotated at 4°C for 2 h followed by light sonication at low power for 5 min (30 s ON/OFF). After sonication, the samples were centrifuged at 15,000 × *g* for 10 min at 4°C and the supernatant saved. Protein concentration was measured and diluted (if needed) into 1–2 mg/ml with lysis buffer. For immunoprecipitation, 5 mg of total proteins for each IP reaction were used. The lysates were pre-cleared with 10 μg of normal IgG for 2 h at 4°C, followed by addition of 50 μL of protein-A. Each sample was divided into two aliquots. One aliquot was immunoprecipitated with 10 μg of PRMT5 antibody (Abcam, ab109451) while 10 μg of normal IgG were added to the other aliquot and served as control. The samples were left in rotation at 4°C overnight. Next, 50 μl of protein-A beads were added into each sample and left in rotation for 2 h at 4°C. Following centrifugation at 3,000 × *g* for 30 s at 4°C, the immunoprecipitated complexes were washed with 500 μl of lysis buffer supplemented with the inhibitors for a total of five times. Elution was achieved by boiling the samples at 95°C for 10 min in 50 μl of 5× WB loading buffer supplemented with beta-mercaptoethanol. Upon rapid cooling of the samples on ice followed by centrifugation at 15,000 × *g* for 2 min, the supernatant was used for in gel tryptic digestion and LC-MS/MS.

[1]http://crispr.mit.edu/

In Gel Tryptic Digestion and Liquid Chromatography-Tandem Mass Spectrometry for Interactome Samples

The immunoprecipitated samples were run ∼1 cm into SDS-PAGE (Invitrogen NuPAGE Bis-Tris 1.5 mm 10% gel) and stained with Coomassie R250. Gel plugs were subjected to in-gel reduction, alkylation, tryptic digestion, and peptide extraction as described in Shevchenko et al. (1996) and Sleat et al. (2008). Resulting peptides were analyzed by nano LC-MS/MS (Dionex Ultimate 3000 RLSCnano System interfaced with a Velos-LTQ-Orbitrap (Thermo Fisher Scientific, San Jose, CA, United States) as described in (Sleat et al., 2013).

Interactome Data Analysis

Proteome Discoverer was used to generate mgf files and data were searched against the Ensembl mouse database (Mus_musculus.GRCm37.pep.all.fasta) using an in house version of X!Tandem (GPM cyclone, Beavis Informatics Ltd, Winnipeg, Canada) (Beavis, 2006). Precursor ion mass error tolerance was set to ± 10 ppm and fragment mass error tolerance to ± 0.4 Da. Cysteine carbamidomethylation was set as a complete modification. Acetylation on protein N-termini and oxidation on methionine were set as variable modifications during the first pass search. Deamination of glutamine and asparagine, dioxidation on methionine, oxidation, and dioxidation on tryptophan were set as variable modifications during the search refinement. Trypsin was set for protein cleavage with one or five missed cuts allowed during the initial and refinement searches, respectively. Peptide-spectrum matches with an expectation score of 0.01 were included in the final report. The peptides were grouped into proteins using strict parsimony principle. The spectral counts were analyzed as previously described (Qian et al., 2008). Only proteins with at least two unique peptides detected in the samples immunoprecipitated with PRMT5 antibody, and not in the IgG group, were considered for further analysis. Protein names were converted into gene names and gene ontology analysis was performed using DAVID software. To determine the most abundant molecular functions driven by PRMT5 interactors, we considered categories including at least 1% of the total protein interactors. The percentages were calculated by using only unique proteins in each of the molecular functional categories.

Protein Digestion, Isobaric Tags for Relative and Absolute Quantitation Labeling, and LC-MS/MS

The protein samples included cytosolic and nuclear fractions, which were independently processed and 0.7 mg/sample for cytosolic fractions and 0.9 mg/sample for nuclear fractions were digested with trypsin, labeled with the iTRAQ reagents following manufacturer's instruction (ABSciex). iTRAQ samples from each genotype were pooled together and a small fraction (5%) was initially analyzed by quantitative nanoLC-MS/MS, thereby verifying that similar protein amounts were present in both samples. Total reporter ion intensities for each iTRAQ label were determined to be in a similar range in both samples, further validating the similar protein amounts and used as normalization factors in analysis of enriched methylated peptides. This served as control for minor variations in amounts of protein analyzed along with digestion and labeling efficiency. The rest of the samples from each fraction from PRMT5 silenced cells and controls, were subjected to an affinity enrichment using an immobilized antibody recognizing symmetric dimethyl arginine residues (Cell Signaling, 13563) following manufacturer's standard protocol. At the elution stage, the beads were eluted with 0.15% TFA (trifluroracetic acid) and desalted/concentrated using STAGE trips (Rappsilber et al., 2007). Each of these eluted fractions were analyzed by quantitative LC-MS/MS using a Dionex Ultimate 3000 RLSCnano System interfaced with a QExactive HF (Thermo Fisher Scientific, San Jose, CA) with parameters described in Sleat et al. (2019). The iTRAQ data analysis and statistics were performed using an in-house program described in Sleat et al. (2017). Ontology analysis of the identified non-histone substrates of PRMT5 was performed after converting protein names to gene names using DAVID software. To exclude the inaccurate attribution of substrates due to the effects of PRMT5 knockdown on transcription, we excluded from all the identified substrates those which overlapped with the downregulated transcript list from Scaglione et al. (2018).

Data Availability

Proteomics MS data (interactome and iTRAQ) have been deposited at Mass Spectrometry Interactive Virtual Environment (MassIVE) with accession number MSV000088396. They can be accessed with the following URL: https://massive.ucsd.edu/ProteoSAFe/static/massive.jsp.

RESULTS

Identification of Novel Interactors of PRMT5 in Oligodendrocyte Lineage Cells

To start identifying potential novel interacting proteins of PRMT5 in oligodendrocyte lineage cells we performed an exploratory analysis using LC-MS/MS. Briefly, peptides were obtained by tryptic digestion of eluates from protein lysates that were immunoprecipitated either with a PRMT5 specific antibody or with a non-specific IgG as control (**Figure 1A**). The putative PRMT5 interacting proteins were identified using Ensembl, by analyzing those peptides with at least two counts in the PRMT5 immunoprecipitates but not in the IgG control (**Supplementary Table 1**). After removal of contaminants, the remaining 1196 murine proteins were referred to their relative gene names and further analyzed, using DAVID Gene Ontology analysis to identify functional categories (**Figure 1B**). As internal validation for the analysis, we retrieved several known interactors of PRMT5. Of note, we detected the methylosome protein 50 (MEP50, encoded by *Mep50/Wdr77*), a molecule that forms a complex with PRMT5 and correctly positions substrates for increased binding affinity (Antonysamy et al., 2012; Burgos et al., 2015). Other known PRMT5 interactors identified by our analysis include: the Band 4.1-like protein 3 (E41L3, encoded by *Epb41l3*)

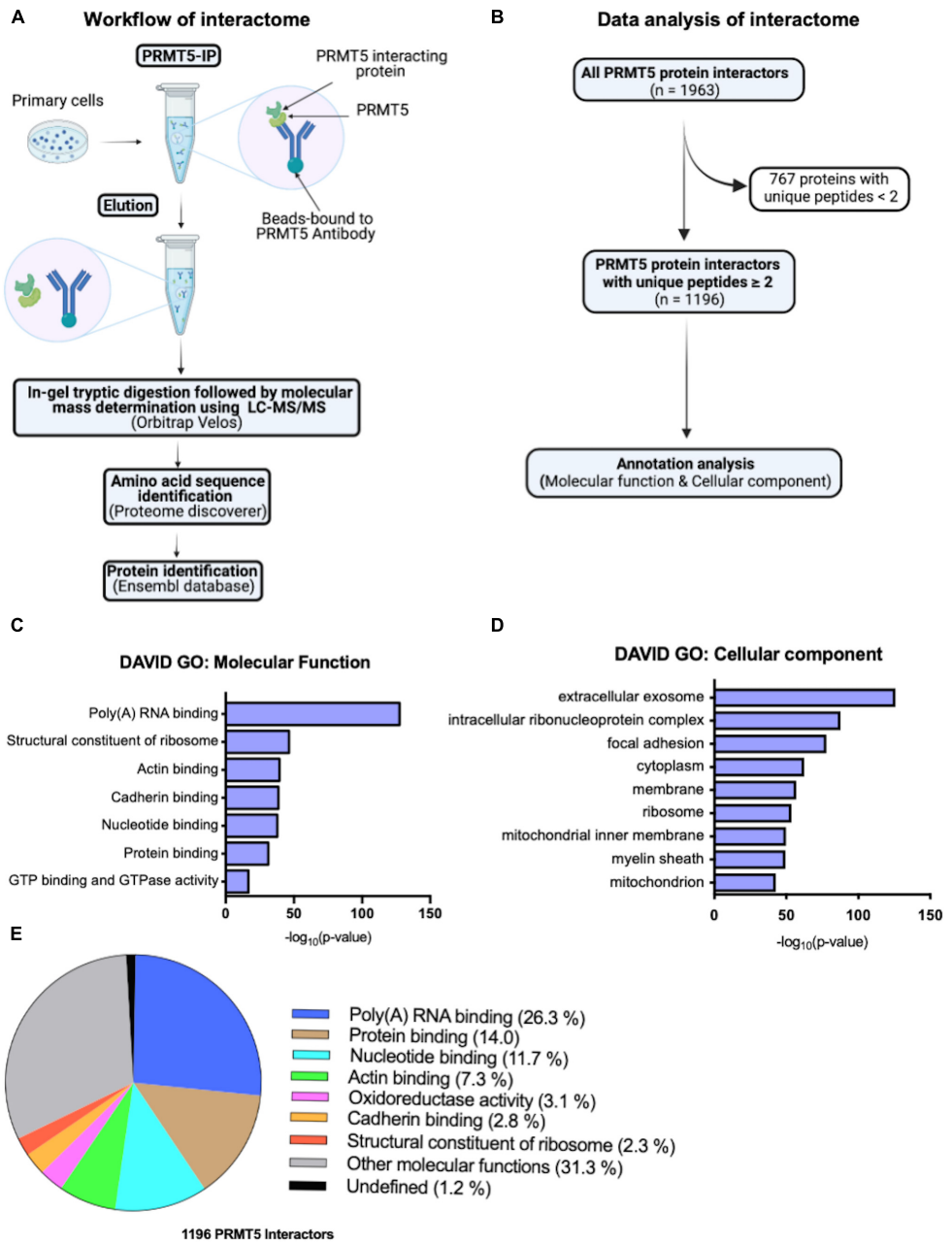

FIGURE 1 | PRMT5 interacting partners in oligodendrocyte lineage cells. **(A)** Schematic diagram of PRMT5 immunoprecipitation (IP) of primary oligodendrocyte lineage cell extracts, followed by mass spectrometry analysis to identifying the interacting partners of PRMT5. **(B)** Summary of the steps involved in the analysis of the interactome data. **(C,D)** Molecular functions **(C)** and cellular localizations **(D)** of PRMT5 interactors in oligodendrocyte lineage cells. Gene ontology analysis was performed using DAVID software. **(E)** The pie-chart shows the proportions of unique proteins involved in the selected molecular functions.

(Jiang et al., 2005), the small nuclear ribonucleoprotein Sm D1 (SMD1, encoded by *Snrpd1*) (Meister et al., 2001; Pesiridis et al., 2009), the TNF receptor-associated factor 4 (TRAF4, encoded by *Traf4*) (Rozan and El-Deiry, 2006; Yang F. et al., 2015), and the zinc-finger protein 326 (ZN326, encoded by *Znf326)* (Rengasamy et al., 2017). In addition, gene ontology analysis of molecular function revealed an enrichment of proteins involved in poly(A)RNA binding, ribosomal structure and nucleotide binding, but also in categories related to cadherin, actin binding and GTPase activity (**Figure 1C** and **Supplementary Table 2**). Gene ontology analysis of cellular localization identified mostly a function of PRMT5 in the extracellular exosomes, cytosol, and also ribosome and membrane organelles (**Figure 1D** and **Supplementary Table 2**). Consistent with previous reports in other cell types (Rengasamy et al., 2017; Radzisheuskaya et al., 2019), the largest proportion

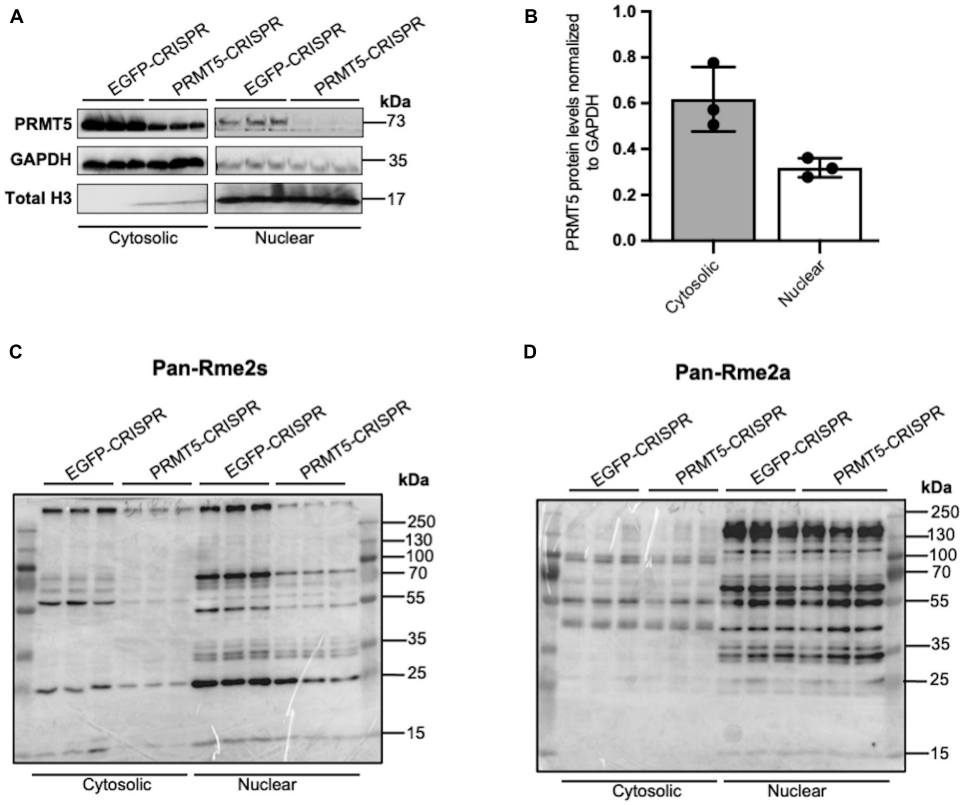

FIGURE 2 | Knockdown of PRMT5 expression using lentiviral CRISPR/Cas9 decreased symmetric but not asymmetric arginine dimethylation in immortalized progenitors. **(A)** Western blots documenting the levels of PRMT5 protein in cytosolic and nuclear protein extracts from immortalized progenitors infected with PRMT5-CRISPR lentiviruses or EGFP-CRISPR as control. **(B)** Quantification of PRMT5 protein levels in cytosolic and nuclear fractions of EGFP-CRISPR control and PRMT5-CRISPR cells. PRMT5 levels in both the cytosolic and nuclear fractions were normalized to GAPDH **(C,D)** Western blot performed with the same protein extracts as **(A)** but probed with antibodies specific for symmetrically dimethylated arginine residues (Rme2s) **(C)** and asymmetrically dimethylated arginine residues (Rme2a) **(D)**.

of the PRMT5 protein interactors was involved in molecular functions related to RNA binding (26.3%), protein binding (14.0%) and nucleotide binding (11.7%), with a minor proportion related to actin (7.3%) or cadherin (2.8%) binding and 31.3% related to other molecular functions (**Figure 1E**). Together, these results suggest that the most prominent function of PRMT5 is conserved in several cell types and is related to RNA processing, although other functions related to actin-dependent events and focal adhesion or cell-cell contacts were also identified in the OPC.

Identification of PRMT5 Non-histone Substrates in Immortalized Oligodendrocyte Progenitors

In order to gain further insights on PRMT5 substrates in the oligodendrocyte lineage, we then used isobaric Tags for Relative and Absolute Quantitation (iTRAQ) of cytosolic or nuclear extracts from immortalized oligodendrocyte progenitors either silenced with lentiviral-mediated PRMT5 CRISPR-Cas9 (PRMT5-CRISPR) or transduced with EGFP-CRISPR, as control. The efficiency of the knockdown was validated using western blot analysis (**Figure 2A**). Decreased levels of PRMT5 in both cytosolic and nuclear extracts were detected in PRMT5-CRISPR cells compared to EGFP-CRISPR controls, although the total number of proteins was shown to be comparable (see section "Materials and Methods") in PRMT5 knockdown cells and controls (**Figure 2B**). As expected, PRMT5 enzymatic activity was decreased in the cytosolic and nuclear extracts from PRMT5 knockdown cells compared to EGFP-CRISPR controls, as indicated by Western-blot analysis, using an antibody recognizing all the proteins with symmetrically dimethylated arginine residues (**Figure 2C**). Multiple immunoreactive bands across a wide range of molecular weights (15–250 kDa) were detected in the EGFP-CRISPR controls, while their signal intensity was either lost or reduced in PRMT5-CRISPR samples (**Figure 2C**), suggesting the existence of several proteins with decreased levels of symmetrically methylated arginine residues in knockdown cells. Importantly, the reduction or absence of proteins with symmetric methylated arginines was not met by increased levels of proteins with asymmetric arginine methylation, suggesting that Type I PRMTs did not compensate for decreased Type II PRMT function (**Figure 2D**). To define the identity of the PRMT5 substrates in immortalized

progenitors, we utilized iTRAQ-based mass spectrometry of cytosolic and nuclear extracts (**Figure 3A**). We digested the cytosolic and nuclear protein samples into peptides and followed by iTRAQ labeling, we then used specific antibodies to enrich for peptides containing symmetric dimethyl arginine residues. Samples were subjected to LC-MS/MS analysis and symmetrically dimethylated arginine levels of each peptide were quantified in cytosolic and nuclear extracts from PRMT5 knockdown cells and controls. Of the peptides with a minimum of three spectral counts in control samples, 307 harbored at least one symmetric dimethyl arginine site (p-value < 0.05) (**Supplementary Table 3**). Of those, 77 peptides were detected as differentially methylated only in the cytosolic fraction, 91 only in the nuclear fraction, and 139 peptides were found in both fractions (**Figure 3B**). Therefore, a similar number of peptides were found to be differentially methylated in either the cytosolic (n = 216) or nuclear fraction (n = 230) of the PRMT5 knockdown cells compared to the EGFP controls. These peptides corresponded to 60 putative protein substrates with significantly different arginine methylation in knockdown cells compared to controls. We then subtracted the proteins whose transcript levels were downregulated by PRMT5 knockdown [as we published in Scaglione et al. (2018)], in order to avoid the potential confounder of the transcriptional effect of PRMT5. The new analysis identified 57 substrates (**Figure 3B**). All the 307 peptides identified in both fractions, with their respective fold changes in knockdown cells and compared to controls and relative p-values are shown in the volcano plot (**Figure 3C** and **Supplementary Table 3**). The identified 57 substrates with 14 proteins detected only in the cytosolic fraction, 11 proteins only in the nuclear fraction and 32 in both (**Figure 3D**). These data do not suggest a preferential methylation of substrate in one fraction versus the other. Substrates were characterized by the presence of symmetrically methylated arginine residues flanked by glycine residues, identifying the RGG or RG motif as previously reported (Thandapani et al., 2013 and **Supplementary Table 4**), with very few exceptions. PRMT5 substrates identified only in the cytosolic fraction of oligodendrocyte lineage cells included: the zinc-finger binding protein CNBP (encoded by *Cnbp*), the temperature responsive mRNA binding protein RBM3 (encoded by *Rbm3*), the mRNA trafficking protein FMR1 (encoded by *Fmr1*), the chromatin remodeling complex BAZ1A (Encoded by *Baz1a)* and the repressor of translation initiation GGYF2 (encoded by *Gigyf2)*. Substrates identified in the nuclear fraction included: the multi-functional ATP binding helicase DHX9 (encoded by *Dhx9)* expressed at high levels in the oligodendrocyte lineage and involved in the positive regulation of nuclear export of constitutive transport element (CTE)-containing unspliced mRNA (Lee and Pelletier, 2016), the histone protein H2Az (encoded by *H2az1),* and the transcription factor ZN658 (encoded by *Zfp658*). Substrates identified in both cytosolic and nuclear fractions included: proteins regulating pre-mRNA splicing (e.g., RSMB encoded by *Snrpb*, SMD3 encoded by *Snrpd3*), brain-specific RNA splicing (e.g., RSMN encoded by *Snrpn*), regulation or packaging of pre-mRNA into hnRNP particles (e.g., HNRH1 encoded by *Hnrnph1*) and transport from the nucleus to the cytoplasm (e.g., ROA1 encoded by *Hnrnpa1*), RNA decay and mRNA turnover (e.g., HNRPD encoded by *Hnrnpd*) as well as the methylated RNA binding proline-rich protein PRC2C (encoded by *Prrc2c)* (**Figure 3D**). Next, we performed gene ontology with the unique substrates detected in the cytosolic or nuclear fraction using DAVID Ontology software (**Figure 3E** and **Supplementary Table 5**). Regardless of the fraction where the proteins were identified, PRMT5 substrates were overwhelmingly represented in categories such as mRNA processing, RNA splicing, regulation of mRNA stability and positive regulation of translation, with the nuclear fraction additionally showing histones and DNA binding proteins. Worth noticing is the fact that some nuclear proteins were found to be methylated in the cytoplasmic fraction, possibly suggesting a role for symmetric arginine methylation in regulating nuclear/cytosolic shuttling and nuclear transport.

Comparative Analysis of PRMT5 Substrates in Immortalized Progenitor Cells and Other Cell Lines

Functional interactions among the 57 PRMT5 substrates were analyzed using Search Tool for the Retrieval of Interacting Genes/Proteins (STRING) and validated the importance of PRMT5 substrates in regulating three main processes: overwhelmingly mRNA splicing and related pathways, but also DNA binding and other cellular processes involved in migration and other functions (**Figure 4A**). We then compared the PRMT5 substrates identified by our study in oligodendrocyte lineage cells to those previously reported in distinct tumors and cell lines (**Supplementary Table 6**). Of the 57 substrates, 18 proteins (31.6%) were in common with the substrates previously identified in HeLa cells (Musiani et al., 2019), 23 proteins (40.3%) were in common with those identified in human AML cells (human acute myeloid leukemia) (Radzisheuskaya et al., 2019), 18 proteins (31.6%) in common with HEK293T cells (Li et al., 2021), and 39 proteins (68.4%) with the MiaPaca2 cells (human pancreatic cancer cell line) (Mulvaney et al., 2021; **Figure 4B**). Among the proteins shared between oligodendrocyte progenitors and the cell lines, we identified the zinc-finger protein ZN326, the RNA binding protein involved in mRNA transport ROA1, and the spliceosome component RSMB, suggesting a common role of PRMT5 in related processes in distinct cell types (**Supplementary Table 6**). Ten PRMT5 substrates were identified only in the oligodendrocyte lineage cells and included HNRPD, a molecule involved in RNA stability and circadian regulation of translation (Fialcowitz et al., 2005; Kojima et al., 2011), the cytoplasmic proline-rich PRC2C substrate, with the ability to bind methylated RNA (Wu et al., 2019), the WASP Like Actin Nucleation Promoting Factor WASL, expressed at high levels in neural tissue (Fukuoka et al., 1997), the nuclear NudE Neurodevelopment protein 1 NDE1, which is involved in microtubule organization and neuronal migration (Feng and Walsh, 2004; Sasaki et al., 2005) and the RNA binding protein DAZP1. Among the oligodendrocyte unique substrates, with atypical

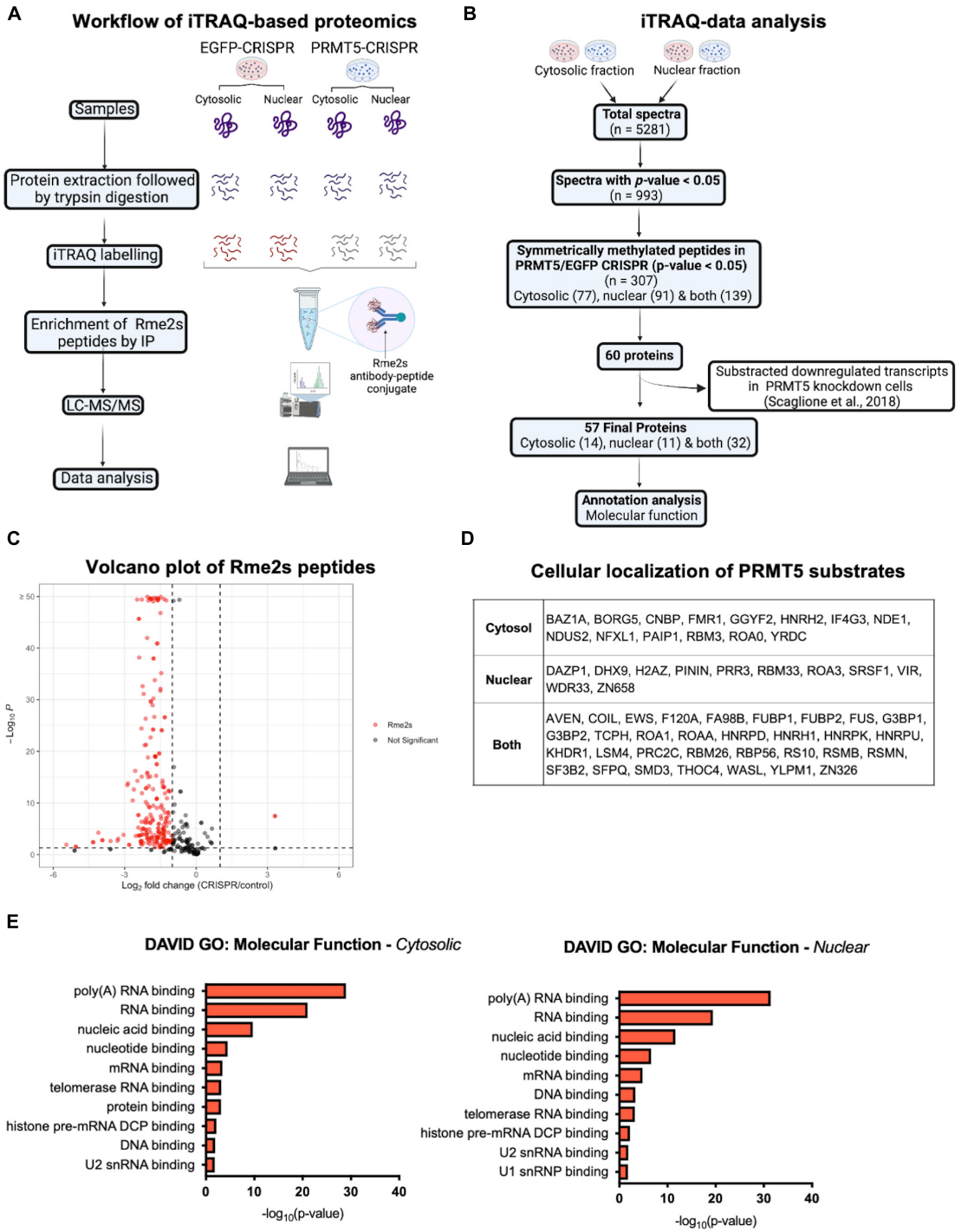

FIGURE 3 | iTRAQ-based proteomics analysis reveals potential substrates of PRMT5 in immortalized progenitors. **(A)** Schematic diagram of the experimental design and workflow of iTRAQ labeling and LC-MS/MS analysis of cytosolic and nuclear extracts from PRMT5 knockdown and EFGP CRISPR controls. **(B)** Flow chart of data analysis after iTRAQ-based proteomic. **(C)** Volcano plot of the 307 immunoaffinity enriched peptides with symmetrically dimethylated arginine residues in control cells, relative to PRMT5-CRISPR cells. On the *X* axis are values of Log_2 (PRMT5-KD/control) and on Y axis are the -log10 (*p*-values). The red dots represent peptides with fold change < -1 or > 1 and with *p*-value < 0.05. The gray dots represent peptides outside these intervals and level of significance. The plot was generated by combining all the peptides detected in nuclear and cytoplasmic fractions. **(D)** List of the PRMT5 substrates identified after analysis of the iTRAQ datasets generated with nuclear and cytosolic extracts from oligodendrocyte lineage cells. **(E)** Molecular functions of PRMT5 non-histone substrates identified in the cytosolic (left) and nuclear (right) fractions. Gene ontology analysis was performed using DAVID software.

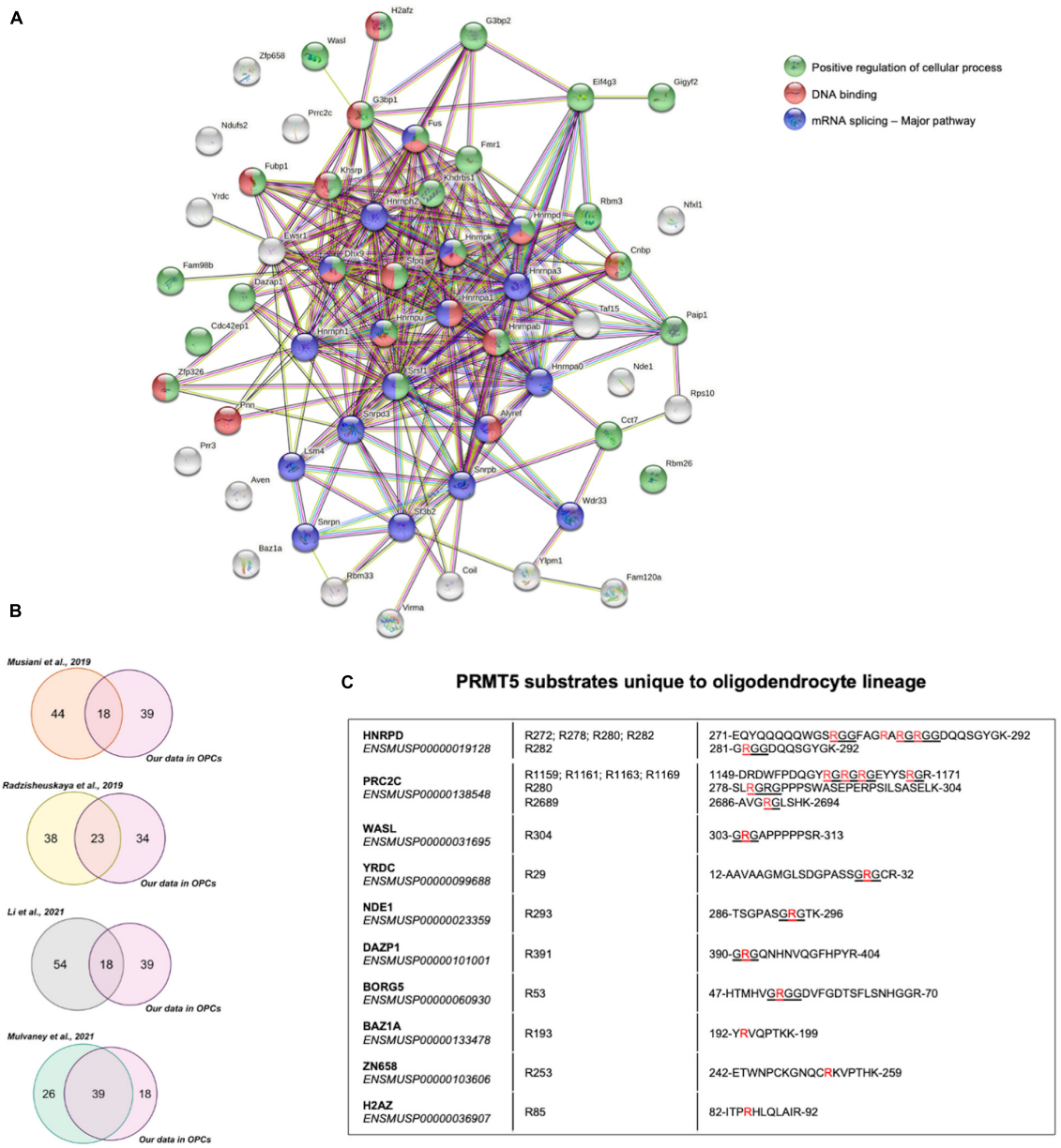

HNRPD *ENSMUSP00000019128*	R272; R278; R280; R282 R282	271-EQYQQQQQWGSRGGFAGRARGRGGDQQSGYGK-292 281-GRGGDQQSGYGK-292
PRC2C *ENSMUSP00000138548*	R1159; R1161; R1163; R1169 R280 R2689	1149-DRDWFPDQGYRGRGRGEYYSRGR-1171 278-SLRGRGPPPSWASEPERPSILSASELK-304 2686-AVGRGLSHK-2694
WASL *ENSMUSP00000031695*	R304	303-GRGAPPPPPSR-313
YRDC *ENSMUSP00000099688*	R29	12-AAVAAGMGLSDGPASSGRGCR-32
NDE1 *ENSMUSP00000023359*	R293	286-TSGPASGRGTK-296
DAZP1 *ENSMUSP00000101001*	R391	390-GRGQNHNVQGFHPYR-404
BORG5 *ENSMUSP00000060930*	R53	47-HTMHVGRGGDVFGDTSFLSNHGGR-70
BAZ1A *ENSMUSP00000133478*	R193	192-YRVQPTKK-199
ZN658 *ENSMUSP00000103606*	R253	242-ETWNPCKGNQCRKVPTHK-259
H2AZ *ENSMUSP00000036907*	R85	82-ITPRHLQLAIR-92

FIGURE 4 | Comparative analysis of PRMT5 protein substrates. **(A)** Functional connections among the 57 PRMT5 substrates identified in oligodendrocyte lineage cells using the STRING protein-protein interaction database (http://string-db.org/), with Medium Confidence (0.400) threshold parameter. Proteins involved in a common pathway are indicated by same-colored nodes (top right). Lines between nodes represent distinct associations between proteins, with line colors indicating different types of relationships: neighborhood (green), gene fusion (red), co-occurrence (dark blue), co-expression (black), experimental evidence (pink), database (turquoise), text mining (light green), and homology (violet). **(B)** Venn diagrams representing the overlaps of PRMT5 substrates between those reported in the indicated studies and the ones identified in our current study. **(C)** List of PRMT5 substrates that are unique to the oligodendrocyte lineage cells. The table shows the detected substrates, their Ensembl IDs, the specific symmetrically methylated arginine residues within the peptide sequences of each substrate. The symmetrically dimethylated arginine residues are in red and the canonical RGG/RG motifs recognized by PRMT5 are underlined.

PRMT5 methylation sites we also identified the zinc-dependent transcriptional repressor ZN658, the histone H2Az previously reported to be involved in gliogenesis (Su et al., 2018) and the component of the ATP-dependent chromatin remodeling complex BAZ1A, which is enriched in the newly formed oligodendrocytes (Sharma et al., 2015; Zeisel et al., 2015).

DISCUSSION

Arginine methylation is an energetically demanding modification, requiring the use of 12 ATP molecules for each methylation event (Gary and Clarke, 1998) resulting in a change of the shape of arginine residues, which lose their ability to bind to hydrogen bond acceptor proteins

(Fuhrmann et al., 2015), while gaining the ability to bind to other proteins (Hughes and Waters, 2006). Methylation is catalyzed by the PRMT family of enzymes, with asymmetric methylation of RxR motifs catalyzed by class I PRMTs (e.g., PRMT1) and symmetric methylation of RGG/RG motifs catalyzed by class II (e.g., PRMT5). Intriguingly PRMT1 deletion in neural stem cells significantly reduced the ability of oligodendrocyte progenitor cells to differentiate into myelin-forming cells while it had no effect on astrocytic and neuronal differentiation (Hashimoto et al., 2016). Oligodendrocyte lineage specific deletion of *Prmt5* impacted survival of newly formed oligodendrocytes and impaired differentiation (Scaglione et al., 2018), thereby suggesting a critical role of PRMT5 in this lineage. PRMT1 has been shown to mostly function as a transcriptional activator by recruiting histone acetyltransferase to the asymmetrically methylated R3 residue in histone H4 (H4R3me2a) and facilitating acetylation of several lysine residues (Huang et al., 2005), while PRMT5 has been characterized as mediating transcriptional repression by competition of H4R3me2s with K5 residue acetylation (Scaglione et al., 2018). However, only a small fraction of the PRMT5 protein displayed nuclear localization in the oligodendrocyte lineage cells and spurred the interest to identify the existence of cell-specific interactors and substrates. The analysis presented in this study provides an initial description of the proteins specifically immunoprecipitated by a PRMT5-specific antibody but not by a non-specific IgG. Of the several interactors, we identified previously reported protein partners (Liang et al., 2021), such as WDR77/MEP50 (Antonysamy et al., 2012; Burgos et al., 2015) and several other molecules reported in other cell types, such as Small nuclear ribonucleoprotein Sm D1 (Meister et al., 2001; Pesiridis et al., 2009), TNF receptor-associated factor 4 (Rozan and El-Deiry, 2006; Yang F. et al., 2015) and transcription factor ZN326 (encoded by *Znf326)* (Rengasamy et al., 2017). At odds with previous reports on the role of PRMT5 in regulating the cell cycle, either by affecting histone methylation (F. Liu et al., 2020) or by direct methylation of P53 and E2F1 in cancer cells (Pastore et al., 2020), we did not detect any cell cycle regulatory molecule in our study. These results are also consistent with the lack of a proliferation-related phenotype in mice with oligodendrocyte lineage specific *Prmt5* knockout (Scaglione et al., 2018) and further reinforce the concept that the physiological role of PRMT5 is distinct from that studied in cancer cells.

We then searched for PRMT5 substrates using iTRAQ analysis of cytosolic and nuclear protein extracts from oligodendrocyte lineage cells with PRMT5 knocked down compared to control cells, immunoprecipitated with antibodies recognizing symmetrically methylated arginine residues. We only analyzed peptides with symmetrically methylated arginine residues in control, but not in PRMT5 knockdown cells. We then obtained the proteins corresponding to those peptides and eliminated from the results any molecule whose transcripts we had previously reported to be downregulated in Prmt5 knockdown cells (Scaglione et al., 2018). This left us with the identification of 57 protein substrates identified in the nuclear and cytosolic extracts. In common with many cell lines (Musiani et al., 2019; Radzisheuskaya et al., 2019; Li et al., 2021; Mulvaney et al., 2021), we detected the majority of PRMT5 substrates involved in RNA splicing and processing. Among the common PRMT5 substrates (Musiani et al., 2019; Radzisheuskaya et al., 2019; Li et al., 2021; Mulvaney et al., 2021), we identified: ROA1, a protein regulating translation at the internal ribosomal entry site (Gao et al., 2017), the ribosomal protein RS10, whose arginine methylation is essential for proper ribosome assembly, and the zinc-finger protein ZN326, enriched in the oligodendrocyte lineage (Zhang et al., 2014; Sharma et al., 2015) and regulated throughout development, with the highest expression in neuronal tissues in E11.5 embryos (Lee et al., 2000). ZN326 complexes with nuclear messenger ribonucleoproteins (mRNPs) and Deleted in Breast Cancer 1 (DBC1) to form the regulatory DBIRD complex. The DBIRD complex binds to RNA polymerase II (RNAPII) and regulates alternative splicing (exon skipping) by facilitating transcriptional elongation at junctions between introns and AT rich exons (Close et al., 2012; Rengasamy et al., 2017). By symmetrically methylating ZN326, PRMT5 ensures the exclusion of AT rich exons as their inclusion has profound destabilizing effects on RNA (Close et al., 2012; Rengasamy et al., 2017). ZN326 has also been reported to positively regulate the WNT pathway and HDAC transcription activities in glioma (Yu et al., 2019), both implicated in timing of oligodendrocyte development in the central nervous system (Marin-Husstege et al., 2002; Conway et al., 2012).

Among the protein substrates uniquely identified in the oligodendrocyte lineage cells we found several proteins enriched in neural tissue, such as chromatin remodeling protein BAZ1A, the ATP-dependent helicase DHX9 and several molecules regulating the microtubule and actin cytoskeleton, including WASL, BORG5, and NDE1. We also detected HNRPD, a component of a family of proteins regulating the maturation of the heterogeneous nuclear RNAs (hnRNAs) into messenger RNAs (mRNA) and their subsequent translation (Geuens et al., 2016). Due to its affinity of for AU-rich mRNA-destabilizing sequence in the 3′-UTR region of mRNA, HNRPD is thought to regulate mRNA decay (Fialcowitz et al., 2005), such as the half-life of immediate-early genes and the circadian regulation of circadian rhythm genes, such as *Cry* and *Per* (Kojima et al., 2011).

PRC2C, an RNA-binding protein seen in few studies (Baltz et al., 2012; Castello et al., 2012, 2016), is an additional PRMT5 substrate that is unique to oligodendrocyte lineage cells. In a recent study in neural cells, PRC2C and PRC2A were both identified as novel readers of N^6-methyladenosine (m^6A), a methylated adenosine modification in mRNA (Wu et al., 2019). While the role of PRC2C protein in oligodendrocyte lineage cells is yet to be investigated, a closely related protein, PRC2A has been shown to control oligodendroglial specification and myelination (Wu et al., 2019).

In summary, our data suggest a critical role of PRMT5 in regulating mRNA metabolism, but also transcription and translation. A potential limitation of our analysis is the focus on PRMT5 substrates in the cytosolic and nuclear fractions of oligodendrocyte lineage cells, thereby leaving out substrates potentially enriched in other subcellular compartments (such as the plasma membranes or internal organelles). A notable example is the membrane associated PDGFRα, previously identified as

PRMT5 target in OPCs (Calabretta et al., 2018). Overall, future studies will be needed to fully elucidate the role of arginine methylation in brain health and in disease states.

DATA AVAILABILITY STATEMENT

The datasets presented in this study can be found in online repositories. The names of the repository/repositories and accession number(s) can be found below: CCMS MassIVE, accession no: MSV000088396.

ETHICS STATEMENT

This animal study was reviewed and approved by IACUC at Icahn School of Medicine.

AUTHOR CONTRIBUTIONS

DD analyzed the data relative to interacting partners and substrates, prepared the figures, wrote the first draft of the text, and edited the manuscript with PC. JL prepared the cell extracts and worked with PC and HZ in experimental design. IS performed the substrate data analysis and comparative analysis with other studies and helped with figure preparation and text editing. HZ and DM helped with the design and performance of the iTRAQ experiment and mass spectrometry, analyzed the raw data, and contributed to manuscript editing. PC worked with JL on the initial experimental design and conceptualization, wrote the text with DD, and supervised the overall workflow. All authors contributed to the article and approved the submitted version.

FUNDING

This project was supported by R35-NS111604 from the National Institute Neurological Disorders and Stroke of Health to PC. Work performed at the Rutgers Biological Mass Spectrometry Facility was partially supported by P30NS046593, S10OD016400, and S10RR024584.

SUPPLEMENTARY MATERIAL

The Supplementary Material for this article can be found online at: https://www.frontiersin.org/articles/10.3389/fncel.2022.820226/full#supplementary-material

Supplementary Table 1 | Interacting partners of PRMT5 in oligodendrocyte lineage cells. List of PRMT5 interactors in oligodendrocyte lineage cells identified by their gene symbols and ranked according to the number of identified unique peptides.

Supplementary Table 2 | Ontology terms of PRMT5 interacting partners in oligodendrocyte lineage cells. Top 50 molecular functions of PRMT5 interactors in oligodendrocyte lineage cells. Gene ontology was performed using DAVID analysis. The GO terms and relative *p*-values are shown.

Supplementary Table 3 | Peptides (n = 307) with differential Rme2s in PRMT5 KD cells compared to EGFP controls. The first column shows the total number of peptides with symmetrically methylated arginine residues that were identified in the control cells as significantly different from the PRMT5 knockdown cells. The corresponding log2foldchange and *p*-values of the significant peptides are shown in the second and third column, respectively.

Supplementary Table 4 | Symmetrically dimethylated arginine residues of PRMT5 substrates in oligodendrocyte lineage cells. List of PRMT5 substrates, their Uniprot Protein Identification Codes and accession numbers, and the specific arginines residues identified as symmetrically dimethylated in the controls but not in PRMT5 knockdown cells.

Supplementary Table 5 | Ontology terms of PRMT5 substrates in oligodendrocyte lineage cells. Molecular functions of PRMT5 substrates identified in cytosolic and nuclear extracts from oligodendrocyte lineage cells. Gene ontology was performed using DAVID analysis. The GO terms and relative *p*-values are shown.

Supplementary Table 6 | PRMT5 substrates in different cell lines. List of PRMT5 substrates identified in our study (immortalized oligodendrocyte progenitors), MiaPaca2 cells (Mulvaney et al., 2021), HeLa cells (Musiani et al., 2019), AML cells (Radzisheuskaya et al., 2019), and HEK293 cells (Li et al., 2021). Highlighted in red are substrates whose transcript levels are downregulated in PRMT5 KD cells (Scaglione et al., 2018).

REFERENCES

Antonysamy, S., Bonday, Z., Campbell, R. M., Doyle, B., Druzina, Z., Gheyi, T., et al. (2012). Crystal structure of the human PRMT5:MEP50 complex. *Proc. Natl. Acad. Sci. U.S.A.* 109, 17960–17965. doi: 10.1073/pnas.1209814109

Baltz, A. G., Munschauer, M., Schwanhäusser, B., Vasile, A., Murakawa, Y., Schueler, M., et al. (2012). The mRNA-bound proteome and its global occupancy profile on protein-coding transcripts. *Mol. Cell* 46, 674–690. doi: 10.1016/j.molcel.2012.05.021

Beavis, R. C. (2006). Using the global proteome machine for protein identification. *Methods Mol. Biol.* 328, 217–228. doi: 10.1385/1-59745-026-x:217

Bedford, M. T., and Clarke, S. G. (2009). Protein arginine methylation in mammals: who, what, and why. *Mol. Cell* 33, 1–13. doi: 10.1016/j.molcel.2008.12.013

Bedford, M. T., and Richard, S. (2005). Arginine methylation: an emerging regulator of protein function. *Mol. Cell* 18, 263–272. doi: 10.1016/j.molcel.2005.04.003

Blanc, R. S., and Richard, S. (2017). Arginine methylation: the coming of age. *Mol. Cell* 65, 8–24. doi: 10.1016/j.molcel.2016.11.003

Burgos, E. S., Wilczek, C., Onikubo, T., Bonanno, J. B., Jansong, J., Reime, U., et al. (2015). Histone H2A and H4 N-terminal tails are positioned by the MEP50 WD repeat protein for efficient methylation by the PRMT5 arginine methyltransferase. *J. Biol. Chem.* 290, 9674–9689. doi: 10.1074/jbc.M115.636894

Calabretta, S., Vogel, G., Yu, Z., Choquet, K., Darbelli, L., Nicholson, T. B., et al. (2018). Loss of PRMT5 promotes PDGFRα degradation during oligodendrocyte differentiation and myelination. *Dev. Cell* 46, 426–440.e5. doi: 10.1016/j.devcel.2018.06.025

Castello, A., Fischer, B., Eichelbaum, K., Horos, R., Beckmann, B. M., Strein, C., et al. (2012). Insights into RNA biology from an atlas of mammalian mRNA-binding proteins. *Cell* 149, 1393–1406. doi: 10.1016/j.cell.2012.04.031

Castello, A., Fischer, B., Frese, C. K., Horos, R., Alleaume, A. M., Foehr, S., et al. (2016). Comprehensive identification of RNA-binding domains in human cells. *Mol. Cell* 63, 696–710. doi: 10.1016/j.molcel.2016.06.029

Close, P., East, P., Dirac-Svejstrup, A. B., Hartmann, H., Heron, M., Maslen, S., et al. (2012). DBIRD complex integrates alternative mRNA splicing with RNA polymerase II transcript elongation. *Nature* 484, 386–389. doi: 10.1038/nature10925

Conway, G. D., O'Bara, M. A., Vedia, B. H., Pol, S. U., and Sim, F. J. (2012). Histone deacetylase activity is required for human oligodendrocyte progenitor differentiation. *Glia* 60, 1944–1953. doi: 10.1002/glia.22410

Feng, Y., and Walsh, C. A. (2004). Mitotic spindle regulation by Nde1 controls cerebral cortical size. *Neuron* 44, 279–293. doi: 10.1016/j.neuron.2004.09.023

Feng, Y., Maity, R., Whitelegge, J. P., Hadjikyriacou, A., Li, Z., Zurita-Lopez, C., et al. (2013). Mammalian protein arginine methyltransferase 7 (PRMT7) specifically targets RXR sites in lysine- and arginine-rich regions. *J. Biol. Chem.* 288, 37010–37025. doi: 10.1074/jbc.M113.525345

Fialcowitz, E. J., Brewer, B. Y., Keenan, B. P., and Wilson, G. M. (2005). A hairpin-like structure within an AU-rich mRNA-destabilizing element regulates trans-factor binding selectivity and mRNA decay kinetics. *J. Biol. Chem.* 280, 22406–22417. doi: 10.1074/jbc.M500618200

Fuhrmann, J., Clancy, K. W., and Thompson, P. R. (2015). Chemical biology of protein arginine modifications in epigenetic regulation. *Chem. Rev.* 115, 5413–5461. doi: 10.1021/acs.chemrev.5b00003

Fukuoka, M., Miki, H., and Takenawa, T. (1997). Identification of N-WASP homologs in human and rat brain. *Gene* 196, 43–48. doi: 10.1016/S0378-1119(97)00184-4

Gao, G., Dhar, S., and Bedford, M. T. (2017). PRMT5 regulates IRES-dependent translation via methylation of hnRNP A1. *Nucleic Acids Res.* 45, 4359–4369. doi: 10.1093/nar/gkw1367

Gary, J. D., and Clarke, S. (1998). RNA and protein interactions modulated by protein arginine methylation. *Prog. Nucleic Acid Res. Mol. Biol.* 61, 65–131. doi: 10.1016/s0079-6603(08)60825-9

Geuens, T., Bouhy, D., and Timmerman, V. (2016). The hnRNP family: insights into their role in health and disease. *Hum. Genet.* 135, 851–867. doi: 10.1007/s00439-016-1683-5

Gonsalvez, G. B., Tian, L., Ospina, J. K., Boisvert, F. M., Lamond, A. I., and Matera, A. G. (2007). Two distinct arginine methyltransferases are required for biogenesis of Sm-class ribonucleoproteins. *J. Cell. Biol.* 178, 733–740. doi: 10.1083/jcb.200702147

Gu, Z., Li, Y., Lee, P., Liu, T., Wan, C., and Wang, Z. (2012). Protein arginine methyltransferase 5 functions in opposite ways in the cytoplasm and nucleus of prostate cancer cells. *PLoS One* 7:e44033. doi: 10.1371/journal.pone.0044033

Hashimoto, M., Murata, K., Ishida, J., Kanou, A., Kasuya, Y., and Fukamizu, A. (2016). Severe hypomyelination and developmental defects are caused in mice lacking protein arginine methyltransferase 1 (PRMT1) in the central nervous system. *J. Biol. Chem.* 291, 2237–2245. doi: 10.1074/jbc.M115.684514

Huang, J., Vogel, G., Yu, Z., Almazan, G., and Richard, S. (2011). Type II arginine methyltransferase PRMT5 regulates gene expression of inhibitors of differentiation/DNA binding Id2 and Id4 during glial cell differentiation. *J. Biol. Chem.* 286, 44424–44432. doi: 10.1074/jbc.M111.277046

Huang, S., Litt, M., and Felsenfeld, G. (2005). Methylation of histone H4 by arginine methyltransferase PRMT1 is essential *in vivo* for many subsequent histone modifications. *Genes Dev.* 19, 1885–1893. doi: 10.1101/gad.1333905

Hua, Z. Y., Hansen, J. N., He, M., Dai, S. K., Choi, Y., Fulton, M. D., et al. (2020). PRMT1 promotes neuroblastoma cell survival through ATF5. *Oncogenesis* 9:50. doi: 10.1038/s41389-020-0237-9

Hughes, R. M., and Waters, M. L. (2006). Arginine methylation in a β-hairpin peptide: implications for Arg-π interactions, ΔCp°, and the cold denatured state. *J. Am. Chem. Soc.* 128, 12735–12742. doi: 10.1021/ja061656g

Jiang, W., Roemer, M. E., and Newsham, I. F. (2005). The tumor suppressor DAL-1/4.1B modulates protein arginine N-methyltransferase 5 activity in a substrate-specific manner. *Biochem. Biophys. Res. Commun.* 329, 522–530. doi: 10.1016/j.bbrc.2005.01.153

Jung, M., Krämer, E., Grzenkowski, M., Tang, K., Blakemore, W., Aguzzi, A., et al. (1995). Lines of Murine oligodendroglial precursor cells immortalized by an activated neu tyrosine kinase show distinct degrees of interaction with axons in vitro and in vivo. *Eur. J. Neurosci.* 7, 1245–1265. doi: 10.1111/j.1460-9568.1995.tb01115.x

Kleinschmidt, M. A., Streubel, G., Samans, B., Krause, M., and Bauer, U. M. (2008). The protein arginine methyltransferases CARM1 and PRMT1 cooperate in gene regulation. *Nucleic Acids Res.* 36, 3202–3213. doi: 10.1093/nar/gkn166

Koh, C. M., Bezzi, M., and Guccione, E. (2015). The where and the how of PRMT5. *Curr. Mol. Biol. Rep.* 1, 19–28. doi: 10.1007/s40610-015-0003-5

Kojima, S., Shingle, D. L., and Green, C. B. (2011). Post-transcriptional control of circadian rhythms. *J. Cell. Sci.* 124, 311–320. doi: 10.1242/jcs.065771

Lee, J. Y., Nakane, Y., Koshikawa, N., Nakayama, K., Hayashi, M., and Takenaga, K. (2000). Characterization of a zinc finger protein ZAN75: nuclear localization signal, transcriptional activator activity, and expression during neuronal differentiation of P19 cells. *DNA Cell Biol.* 19, 227–234. doi: 10.1089/104454900314492

Lee, T., and Pelletier, J. (2016). The biology of DHX9 and its potential as a therapeutic target. *Oncotarget* 7, 42716–42739. doi: 10.18632/oncotarget.8446

Li, W. J., He, Y. H., Yang, J. J., Hu, G. S., Lin, Y. A., Ran, T., et al. (2021). Profiling PRMT methylome reveals roles of hnRNPA1 arginine methylation in RNA splicing and cell growth. *Nat. Commun.* 12:1946. doi: 10.1038/s41467-021-21963-1

Liang, Z., Wen, C., Jiang, H., Ma, S., and Liu, X. (2021). Protein arginine methyltransferase 5 functions via interacting proteins. *Front. Cell. Dev. Biol.* 9:725301. doi: 10.3389/fcell.2021.725301

Cite the following references inside the text.

Lim et al., 2014; Shen et al., 2005; Zhang et al., 2015. J. H., Lee, Y. M., Lee, G., Choi, Y. J., Lim, B. O., Kim, Y. J., et al. (2014). PRMT5 is essential for the eIF4E-mediated 5′-cap dependent translation. *Biochem. Biophys. Res. Commun.* 452, 1016–1021. doi: 10.1016/j.bbrc.2014.09.033

Litt, M., Qiu, Y., and Huang, S. (2009). Histone arginine methylations: their roles in chromatin dynamics and transcriptional regulation. *Biosci. Rep.* 29, 131–141. doi: 10.1042/BSR20080176

Liu, F., Xu, Y., Lu, X., Hamard, P. J., Karl, D. L., Man, N., et al. (2020). PRMT5-mediated histone arginine methylation antagonizes transcriptional repression by polycomb complex PRC2. *Nucleic Acids Res.* 48, 2956–2968. doi: 10.1093/nar/gkaa065

Liu, J., Magri, L., Zhang, F., Marsh, N. O., Albrecht, S., Huynh, J. L., et al. (2015). Chromatin landscape defined by repressive histone methylation during oligodendrocyte differentiation. *J. Neuroscience.* 35, 352–365. doi: 10.1523/JNEUROSCI.2606-14.2015

Liu, J., Moyon, S., Hernandez, M., and Casaccia, P. (2016). Epigenetic control of oligodendrocyte development: adding new players to old keepers. *Curr. Opin. Neurobiol.* 39, 133–138. doi: 10.1016/j.conb.2016.06.002

Marin-Husstege, M., Muggironi, M., Liu, A., and Casaccia-Bonnefil, P. (2002). Histone deacetylase activity is necessary for oligodendrocyte lineage progression. *J. Neurosci.* 22, 10333–10345. doi: 10.1523/JNEUROSCI.22-23-10333.2002

Meister, G., and Fischer, U. (2002). Assisted RNP assembly: SMN and PRMT5 complexes cooperate in the formation of spliceosomal UsnRNPs. *EMBO J.* 21, 5853–5863. doi: 10.1093/emboj/cdf585

Meister, G., Eggert, C., Bühler, D., Brahms, H., Kambach, C., and Fischer, U. (2001). Methylation of Sm proteins by a complex containing PRMT5 and the putative U snRNP assembly factor pICln. *Curr. Biol.* 11, 1990–1994. doi: 10.1016/S0960-9822(01)00592-9

Moyon, S., Liang, J., and Casaccia, P. (2016). Epigenetics in NG2 glia cells. *Brain Res.* 1638, 183–198. doi: 10.1016/j.brainres.2015.06.009

Mulvaney, K. M., Blomquist, C., Acharya, N., Li, R., Ranaghan, M. J., O'Keefe, M., et al. (2021). Molecular basis for substrate recruitment to the PRMT5 methylosome. *Mol. Cell* 81, 3481–3495.e7. doi: 10.1016/j.molcel.2021.07.019

Musiani, D., Bok, J., Massignani, E., Wu, L., Tabaglio, T., Ippolito, M. R., et al. (2019). Proteomics profiling of arginine methylation defines PRMT5 substrate specificity. *Sci. Signal.* 12:eaat8388. doi: 10.1126/scisignal.aat8388

Pal, S., Vishwanath, S. N., Erdjument-Bromage, H., Tempst, P., and Sif, S. (2004). Human SWI/SNF-associated PRMT5 methylates histone H3 arginine 8 and negatively regulates expression of ST7 and NM23 tumor suppressor genes. *Mol. Cell. Biol.* 24, 9630–9645. doi: 10.1128/mcb.24.21.9630-9645.2004

Pastore, F., Bhagwat, N., Pastore, A., Radzisheuskaya, A., Karzai, A., Krishnan, A., et al. (2020). Prmt5 inhibition modulates e2f1 methylation and gene-regulatory networks leading to therapeutic efficacy in jak2v617f-mutant mpn. *Cancer Discov.* 10, 1742–1757. doi: 10.1158/2159-8290.CD-20-0026

Pesiridis, G. S., Diamond, E., and van Duyne, G. D. (2009). Role of pICLn in methylation of Sm proteins by PRMT5. *J. Biol. Chem.* 284, 21347–21359. doi: 10.1074/jbc.M109.015578

Pruvost, M., and Moyon, S. (2021). Oligodendroglial epigenetics, from lineage specification to activity-dependent myelination. *Life (Basel)* 11:62. doi: 10.3390/life11010062

Qian, M., Sleat, D. E., Zheng, H., Moore, D., and Lobel, P. (2008). Proteomics analysis of serum from mutant mice reveals lysosomal proteins selectively

transported by each of the two mannose 6-phosphate receptors. *Mol. Cell. Proteomics* 7, 58–70. doi: 10.1074/mcp.M700217-MCP200

Radzisheuskaya, A., Shliaha, P. V., Grinev, V., Lorenzini, E., Kovalchuk, S., Shlyueva, D., et al. (2019). PRMT5 methylome profiling uncovers a direct link to splicing regulation in acute myeloid leukemia. *Nat. Struct. Mol. Biol.* 26, 999–1012. doi: 10.1038/s41594-019-0313-z

Rappsilber, J., Mann, M., and Ishihama, Y. (2007). Protocol for micro-purification, enrichment, pre-fractionation and storage of peptides for proteomics using StageTips. *Nat. Protoc.* 2, 1896–1906. doi: 10.1038/nprot.2007.261

Ren, J., Wang, Y., Liang, Y., Zhang, Y., Bao, S., and Xu, Z. (2010). Methylation of ribosomal protein S10 by protein-arginine methyltransferase 5 regulates ribosome biogenesis. *J. Biol. Chem.* 285, 12695–12705. doi: 10.1074/jbc.M110.103911

Rengasamy, M., Zhang, F., Vashisht, A., Song, W. M., Aguilo, F., Sun, Y., et al. (2017). The PRMT5/WDR77 complex regulates alternative splicing through ZNF326 in breast cancer. *Nucleic Acids Res.* 45, 11106–11120. doi: 10.1093/nar/gkx727

Rozan, L. M., and El-Deiry, W. S. (2006). Identification and characterization of proteins interacting with Traf4, an enigmatic p53 target. *Cancer Biol. Ther.* 5, 1228–1235. doi: 10.4161/cbt.5.9.3295

Sasaki, S., Mori, D., Toyo-oka, K., Chen, A., Garrett-Beal, L., Muramatsu, M., et al. (2005). Complete Loss of Ndel1 results in neuronal migration defects and early embryonic lethality. *Mol. Cell. Biol.* 25, 7812–7827. doi: 10.1128/mcb.25.17.7812-7827.2005

Scaglione, A., Patzig, J., Liang, J., Frawley, R., Bok, J., Mela, A., et al. (2018). PRMT5-mediated regulation of developmental myelination. *Nat. Commun.* 9:2840. doi: 10.1038/s41467-018-04863-9

Shalem, O., Sanjana, N. E., Hartenian, E., Shi, X., Scott, D. A., Mikkelsen, T. S., et al. (2014). Genome-scale CRISPR-Cas9 knockout screening in human cells. *Science* 343, 84–87. doi: 10.1126/science.1247005

Sharma, K., Schmitt, S., Bergner, C. G., Tyanova, S., Kannaiyan, N., Manrique-Hoyos, N., et al. (2015). Cell type- and brain region-resolved mouse brain proteome. *Nat. Neurosci.* 18, 1819–1831. doi: 10.1038/nn.4160

Shen, S., Li, J., and Casaccia-Bonnefil, P. (2005). Histone modifications affect timing of oligodendrocyte progenitor differentiation in the developing rat brain. *J. Cell Biol.* 169, 577–589. doi: 10.1083/jcb.200412101

Shevchenko, A., Wilm, M., Vorm, O., and Mann, M. (1996). Mass spectrometric sequencing of proteins from silver-stained polyacrylamide gels. *Anal. Chem.* 68, 850–858. doi: 10.1021/ac950914h

Sleat, D. E., Sun, P., Wiseman, J. A., Huang, L., El-Banna, M., Zheng, H., et al. (2013). Extending the mannose 6-phosphate glycoproteome by high resolution/accuracy mass spectrometry analysis of control and acid phosphatase 5-deficient mice. *Mol. Cell. Proteomics* 12, 1806–1817. doi: 10.1074/mcp.M112.026179

Sleat, D. E., Tannous, A., Sohar, I., Wiseman, J. A., Zheng, H., Qian, M., et al. (2017). Proteomic analysis of brain and cerebrospinal fluid from the three major forms of neuronal ceroid lipofuscinosis reveals potential biomarkers. *J. Proteome Res.* 16, 3787–3804. doi: 10.1021/acs.jproteome.7b00460

Sleat, D. E., Valle, M. C. D., Zheng, H., Moore, D. F., and Lobel, P. (2008). The mannose 6-phosphate glycoprotein proteome. *J. Proteome Res.* 7, 3010–3021. doi: 10.1021/pr800135v

Sleat, D. E., Wiseman, J. A., El-Banna, M., Zheng, H., Zhao, C., Soherwardy, A., et al. (2019). Analysis of brain and cerebrospinal fluid from mouse models of the three major forms of neuronal ceroid lipofuscinosis reveals changes in the lysosomal proteome. *Mol. Cell. Proteomics* 18, 2244–2261. doi: 10.1074/mcp.RA119.001587

Su, L., Xia, W., Shen, T., Liang, Q., Wang, W., Li, H., et al. (2018). H2A.Z.1 crosstalk with H3K56-acetylation controls gliogenesis through the transcription of folate receptor. *Nucleic Acids Res.* 46, 8817–8831. doi: 10.1093/nar/gky585

Tanaka, Y., Nagai, Y., Okumura, M., Greene, M. I., and Kambayashi, T. (2020). PRMT5 is required for T cell survival and proliferation by maintaining cytokine signaling. *Front. Immunol.* 11:621. doi: 10.3389/fimmu.2020.00621

Tasic, B., Menon, V., Nguyen, T. N., Kim, T. K., Jarsky, T., Yao, Z., et al. (2016). Adult mouse cortical cell taxonomy revealed by single cell transcriptomics. *Nat. Neurosci.* 19, 335–346. doi: 10.1038/nn.4216

Tewary, S. K., Zheng, Y. G., and Ho, M. C. (2019). Protein arginine methyltransferases: insights into the enzyme structure and mechanism at the atomic level. *Cell. Mol. Life Sci.* 76, 2917–2932. doi: 10.1007/s00018-019-03145-x

Thandapani, P., O'Connor, T. R., Bailey, T. L., and Richard, S. (2013). Defining the RGG/RG Motif. *Mol. Cell* 50, 613–623. doi: 10.1016/j.molcel.2013.05.021

Wang, H., Huang, Z. Q., Xia, L., Feng, Q., Erdjument-Bromage, H., Strahl, B. D., et al. (2001). Methylation of histone H4 at arginine 3 facilitating transcriptional activation by nuclear hormone receptor. *Science* 293, 853–857. doi: 10.1126/science.1060781

Wu, R., Li, A., Sun, B., Sun, J. G., Zhang, J., Zhang, T., et al. (2019). A novel m6A reader Prrc2a controls oligodendroglial specification and myelination. *Cell Res.* 29, 23–41. doi: 10.1038/s41422-018-0113-8

Yang, F., Wang, J., Ren, H. Y., Jin, J., Wang, A. L., Sun, L. L., et al. (2015). Proliferative role of TRAF4 in breast cancer by upregulating PRMT5 nuclear expression. *Tumour Biol.* 36, 5901–5911. doi: 10.1007/s13277-015-3262-0

Yang, Y., Hadjikyriacou, A., Xia, Z., Gayatri, S., Kim, D., Zurita-Lopez, C., et al. (2015). PRMT9 is a Type II methyltransferase that methylates the splicing factor SAP145. *Nat. Commun.* 6:6428. doi: 10.1038/ncomms7428

Yu, X., Wang, M., Wu, J., Han, Q., and Zhang, X. (2019). ZNF326 promotes malignant phenotype of glioma by up-regulating HDAC7 expression and activating Wnt pathway. *J. Exp. Clin. Cancer Res.* 38:40. doi: 10.1186/s13046-019-1031-4

Zeisel, A., Muñoz-Manchado, A. B., Codeluppi, S., Lönnerberg, P., La Manno, G., Juréus, A., et al. (2015). Cell types in the mouse cortex and hippocampus revealed by single-cell RNA-seq. *Science* 347, 1138–1142. doi: 10.1126/science.aaa1934

Zhang, Y., Chen, K., Sloan, S. A., Bennett, M. L., Scholze, A. R., O'Keeffe, S., et al. (2014). An RNA-sequencing transcriptome and splicing database of glia, neurons, and vascular cells of the cerebral cortex. *J. Neurosci.* 34, 11929–11947. doi: 10.1523/JNEUROSCI.1860-14.2014

Zurita-Lopez, C. I., Sandberg, T., Kelly, R., and Clarke, S. G. (2012). Human protein arginine methyltransferase 7 (PRMT7) is a type III enzyme forming ω-N G-monomethylated arginine residues. *J. Biol. Chem.* 287, 7859–7870. doi: 10.1074/jbc.M111.336271

Conflict of Interest: The authors declare that the research was conducted in the absence of any commercial or financial relationships that could be construed as a potential conflict of interest.

Publisher's Note: All claims expressed in this article are solely those of the authors and do not necessarily represent those of their affiliated organizations, or those of the publisher, the editors and the reviewers. Any product that may be evaluated in this article, or claim that may be made by its manufacturer, is not guaranteed or endorsed by the publisher.

Copyright © 2022 Dansu, Liang, Selcen, Zheng, Moore and Casaccia. This is an open-access article distributed under the terms of the Creative Commons Attribution License (CC BY). The use, distribution or reproduction in other forums is permitted, provided the original author(s) and the copyright owner(s) are credited and that the original publication in this journal is cited, in accordance with accepted academic practice. No use, distribution or reproduction is permitted which does not comply with these terms.

frontiers | Frontiers in Cellular Neuroscience

REVIEW
published: 28 April 2022
doi: 10.3389/fncel.2022.892968

Current Insights Into Oligodendrocyte Metabolism and Its Power to Sculpt the Myelin Landscape

Mohanlall Narine[1,2] *and Holly Colognato*[1]*

[1]Department of Pharmacological Sciences, Stony Brook University, Stony Brook, NY, United States, [2]Department of Neurobiology & Behavior, Stony Brook University, Stony Brook, NY, United States

Once believed to be part of the *nervenkitt* or "nerve glue" network in the central nervous system (CNS), oligodendroglial cells now have established roles in key neurological functions such as myelination, neuroprotection, and motor learning. More recently, oligodendroglia has become the subject of intense investigations aimed at understanding the contributions of its energetics to CNS physiology and pathology. In this review, we discuss the current understanding of oligodendroglial metabolism in regulating key stages of oligodendroglial development and health, its role in providing energy to neighboring cells such as neurons, as well as how alterations in oligodendroglial bioenergetics contribute to disease states. Importantly, we highlight how certain inputs can regulate oligodendroglial metabolism, including extrinsic and intrinsic mediators of cellular signaling, pharmacological compounds, and even dietary interventions. Lastly, we discuss emerging studies aimed at discovering the therapeutic potential of targeting components within oligodendroglial bioenergetic pathways.

Keywords: oligodendrocyte, myelin, metabolism, remyelination, glycolysis, lactate, oligodendrocyte progenitor cell (OPC)

OPEN ACCESS

Edited by:
Davide Lecca,
University of Milan, Italy

Reviewed by:
Carmen Sato-Bigbee,
Virginia Commonwealth University, United States
Jacqueline Trotter,
Johannes Gutenberg University Mainz, Germany
Rogelio O. Arellano,
Universidad Nacional Autónoma de México, Mexico

***Correspondence:**
Holly Colognato
Holly.Colognato@stonybrook.edu

Specialty section:
This article was submitted to Non-Neuronal Cells, a section of the journal Frontiers in Cellular Neuroscience

Received: *09 March 2022*
Accepted: *06 April 2022*
Published: *28 April 2022*

Citation:
Narine M and Colognato H (2022) Current Insights Into Oligodendrocyte Metabolism and Its Power to Sculpt the Myelin Landscape. Front. Cell. Neurosci. 16:892968. doi: 10.3389/fncel.2022.892968

INTRODUCTION

The mammalian central nervous system (CNS) is a well-integrated network of cells comprising mostly neurons and glia (astrocytes, microglia, and oligodendrocytes). Neurons are responsible for the bulk of information processing in the CNS as well as complex behaviors and coordinated movements. Glia, on the other hand, designated "nervenkitt" or glue by Virchow and others, was first believed to be cells akin to connective tissue in the CNS with the function of providing structural support (Virchow, 1856). However, the last few decades have evolved our understanding of these specialized cells and has led to a "glial revolution". For example, astrocytes are now known to facilitate neurotransmitter production, modulate synaptic plasticity, and, most recently, mediate neuroinflammation; whereas microglia, the resident immune cells of the CNS, monitor neuronal activity *via* their neurotransmitter surface receptors and in turn alter dendritic spine density to remodel synaptic circuitries (Paolicelli et al., 2011; Colonna and Butovsky, 2017; Weinhard et al., 2018). Oligodendrocytes (OLs), first discovered by Pio del Río Hortega

who correctly purported them to be the Schwann cell equivalent in the brain and spinal cord, are the myelin-producing cells of the CNS (del Río-Hortega, 1921; Boullerne, 2016). Now, more than a century after the term "myelin" was coined by Virchow (Boullerne, 2016), OLs have been implicated in a wide array of white matter dysfunction, including those that have been recognized as contributing to behavioral disorders such as schizophrenia and bipolar disorder (Edgar and Sibille, 2012; Bellani et al., 2016). Recent work has also shown that OLs are involved in learning and memory, remodeling of neuronal circuits, and supporting axonal function and health, all of which rely, at least in part, on OL metabolic functions (Zatorre et al., 2012; Saab et al., 2013; Gibson et al., 2014; Moore et al., 2020). Given the importance of OL metabolism to OL function, in this review, we will describe what is known about the unique energetic demands posited by oligodendroglia, as well as explain how various metabolites can regulate oligodendroglia development and myelination. We then introduce the important role metabolism plays in removing toxic byproducts and how this "waste disposal" is essential for OL health and myelin maintenance. Finally, we conclude by examining the inputs that can regulate these bioenergetic properties, including extrinsic and intrinsic mediators of cellular signaling, pharmacological compounds, and even diet. Together we suggest that the emerging knowledge of OL bioenergetics will provide new ways to develop therapeutics that are beneficial to OL, and hence overall CNS function.

BACKGROUND

Oligodendrogenesis begins as early as E12.5 during the embryonic development of the rodent CNS (Warf et al., 1991). Within the ventricular zone of the neural tube, neuroepithelial cells are transformed into radial glial cells that further differentiate into intermediate progenitor cells, then oligodendrocyte progenitor cells (OPCs; Rowitch and Kriegstein, 2010). Specifically timed waves of OPCs begin to populate the CNS in a caudal to rostral manner, from the spinal cord to the forebrain, using their processes to sample and occupy vacant spaces (Kirby et al., 2006). Upon receiving differentiation-promoting cues, which remain to be fully elucidated, a subset of OPCs then differentiate into OLs that engage in wrapping axons with their lipid-rich myelin membrane (the process known as myelination). Myelin serves both to provide metabolic support and to promote the establishment of saltatory conduction, thus ensuring both neuronal health as well as fast and efficient impulse propagation along axons (Simons and Nave, 2015).

Some of the well-known factors governing OL development stem from transcriptional regulation as well as extracellular signaling mechanisms. For instance, transcription factors *Id2* and *Id4* have been shown to regulate OPC proliferation and differentiation (Kondo and Raff, 2000; Wang et al., 2001). Other transcription factors such as myelin gene regulatory factor (*Myrf*) are essential for CNS myelination such that when the membrane-bound Myrf protein undergoes an activating cleavage event, its cleavage product can localize into the nucleus to bind and enhance the expression of pro-myelin genes such as *Plp1, Mbp, Mag, and Trf* (Bujalka et al., 2013). The extracellular matrix protein laminin, on the other hand, has been shown to regulate OPC survival and the timing of myelination *via* activation of the Fyn kinase pathway as well as promote OPC migration and survival *via* focal adhesion kinase (FAK) mediated signaling (Relucio et al., 2009, 2012; Suzuki et al., 2019). All these events, however, require appropriate resources to support the biosynthetic pathways that are needed for progression through the cell cycle, differentiation, myelination, and interactions with cellular partners. Oligodendroglial metabolism is therefore critical in governing all aspects of key cellular dynamics, with elements such as energy production, lipid metabolites, and the production of reactive oxygen species closely impacting oligodendroglial development.

OLIGODENDROCYTE METABOLISM

Cellular metabolism involves the sum of all biochemical processes involved in producing or consuming energy. Metabolic pathways largely fall into three distinct categories: anabolic, catabolic, or waste disposal. Anabolic pathways are a series of enzyme-catalyzed reactions that require energy inputs and carbon backbones to synthesize complex macromolecules such as proteins, carbohydrates, and lipids, whereas catabolic reactions ultimately produce energy by sequential degradation of large molecules into their smaller constituents: proteins into amino acids, carbohydrates into sugars, and lipids into fatty acids. Waste disposal mechanisms remove toxic byproducts and, together with total cellular metabolism, help to coordinate the optimal energetic balance needed for all cellular activities (Deberardinis and Thompson, 2012).

OLs generate the myelin sheaths that comprise a large fraction of the white matter, which itself is approximately half the total volume of the human brain (Herndon et al., 1998). One OL can myelinate up to 50 axons, with as many as 150 layers of compacted myelin membrane per segment (Baumann and Pham-Dinh, 2001; Fields, 2010). As could be imagined by this large cellular expansion, the energetic demands of OLs are substantial. In white matter, an estimated 82.3% of energy demands are associated with non-signaling activities by glia cells such as protein and lipid synthesis, oligonucleotide turnover, and cytoskeleton remodeling, compared to signaling activities (i.e., action potential firing; Yu et al., 2017; Dienel, 2018). Furthermore, a theoretical minimum of 6.84×10^{21} ATP molecules (the energy currency of the cell) are needed to produce 1 g of total myelin *protein* and 48-fold that per gram *lipid* of the myelin membrane. The benefit of this extensive upfront ATP expenditure is reduced energy usage during action potential propagation, with a predicted 23% savings in overall ATP needed when compared to unmyelinated axons (Harris and Attwell, 2012). Given the critical role that energy production plays in proper OL function and overall brain energy demand, it is important to understand the underlying metabolic components at work

and how they may be used to counter oligodendropathies and demyelinating diseases.

Oxidative Glycolysis in OL

Glucose is the preferred fuel in the brain and is primarily catabolized *via* aerobic glycolysis (Dienel, 2018). During oxidative glycolysis, glucose first enters the cell and is irreversibly phosphorylated by hexokinase to glucose-6-phosphate (G-6-P). The G-6-P metabolite can then continue down the glycolytic pathway, shuttle into the pentose phosphate pathway (PPP), or be stored as glycogen (**Figure 1**). Both the glycolytic and PPP pathways are involved in the production of pyruvate, a critical metabolite that is converted to acetyl coenzyme A (AcCoA) by the pyruvate dehydrogenase (PDH) enzyme complex. AcCoA enters the citric acid cycle (TCA) in the mitochondria to generate the electron carrier metabolites NADH and $FADH_2$ upon cycle completion. Both NADH and $FADH_2$ enter the electron transport chain to produce an estimated net 30 ATP molecules (net amount is lower than theoretical estimates after accounting for proton leak) *via* oxidative phosphorylation (OXPHOS). Notably, the amount of ATP produced by OXPHOS per molecule of glucose is substantially greater than the net 2 ATP molecules generated solely through glycolysis (Dienel, 2018). Remarkably, OLs have been shown to prefer glycolysis over OXPHOS in spite of their high energetic demands. A recent study focused on characterizing the distinct bioenergetic properties of both *human*-derived adult OPCs and OLs, demonstrated that under favorable and nutrient-rich conditions, OPCs and OLs both rely significantly more on glycolysis than OXPHOS to generate ATP (Rone et al., 2016). Additionally, when subjected to stress conditions like those observed in the demyelinating disease, multiple sclerosis (MS), OLs begin retracting their processes to destabilize the compact axonal myelin sheath, which is thought to limit cell death by entering a less-energy intensive, low metabolic state (glycolysis). This response is perhaps favorable in the short-term, preserving existing OLs should they experience conditions conducive for a metabolic rebound. In contrast, OPCs are not capable of sufficiently reducing their metabolic rate as these cells require substantially more ATP. As a result, OPCs begin to rapidly die under stress. Surprisingly, developing *rodent* OPCs have been found to be *more* metabolically active compared to *rodent* OLs, capable of elevating both OXPHOS and glycolysis, with both rodent OPCs and OLs producing more ATP than their human counterparts (Rone et al., 2016).

A central role for glycolysis in OLs was firmly established by studying mice with an inducible knockout for the *Cox10* gene in immature OLs from birth. *Cox10* encodes for cytochrome *c* oxidase (COX—also known as complex IV), which is the terminal electron acceptor in the electron transport chain of the mitochondria that helps to establish the proton gradient needed for ATP generation *via* OXPHOS. Despite confirmed mitochondrial dysfunction, mutant mice ($Cox10^{flox/flox*}Cnp1^{Cre/+}$) displayed no signs of demyelination, oligodendroglial pathology, or white matter abnormalities, even at 9 months of age (Fünfschilling et al., 2012). Lactate levels, however, were found to be significantly increased. Lactate can be generated from the reaction between pyruvate and NADH, catalyzed by lactate dehydrogenase (LDH). Given that the majority of lactate comes from glycolytic pyruvate and that it is secreted from the cell (*via* monocarboxylate transporters, MCTs), lactate is often used as a readout for glycolytic activity (Rogatzki et al., 2015). In other words, OLs were demonstrated to survive and adequately function by using glycolysis to generate their needed energy, although it should be noted that the energy required for mature OL maintenance is lower than developing OLs. Nevertheless, even with lower overall ATP yields, the kinetics of glycolysis is much faster than complete glucose oxidation (glycolysis + OXPHOS; Dienel, 2018). Additionally, the increase in lactate production from enhanced glycolysis can benefit the underlying ensheathed axons since myelin wrapping enables the formation of "myelinic channels" for which lactate and other trophic factors can be shuttled to axons to maintain axonal health (Simons and Nave, 2015). Thus, the high energy needs of neurons during action potential signaling, calculated to be 4.1×10^5 ATP/s for an axon diameter of 0.76 μm and 1.8×10^6 ATP/s for a larger 1.26 μm axon diameter firing at physiological rates of 3 Hz and 8 Hz, respectively (Harris and Attwell, 2012), can be supported by this influx of lactate, which can be readily converted to pyruvate *via* LDH, followed by conversion to AcCoA by pyruvate dehydrogenase. AcCoA can then enter the TCA cycle to ultimately produce the byproducts NADH and $FADH_2$ that will feed into complex 1 and complex 2 of the electron transport chain, respectively, fueling OXPHOS-linked ATP production, ultimately offering a faster way for neurons to produce ATP that bypasses the upstream glycolytic pathway altogether (**Figure 1**). The ability of lactate-derived ATP to meet energy demands in the brain is reminiscent of astrocytic glycogen-derived lactate that has been shown to help maintain ATP in an exhaustive-exercising brain model, thus protecting neurons from cell death (Matsui et al., 2017). Lactate's role in OLs may go beyond supporting neurons as evidence suggests that OLs can also *import* this metabolite through MCT1 transporters, providing a way to support oligodendrocyte development and myelination when glucose concentrations are low (Rinholm et al., 2011). OLs also oxidize lactate at a greater rate than neurons and astrocytes do for lipid synthesis, which may contribute to the preference for glycolysis in these cells (Sánchez-Abarca et al., 2001).

However, it is important to note that other compounds regulate axonal metabolism through their actions within OLs. In particular, sirtuin 2 (SIRT2), a member of the sirtuin family of signaling proteins involved in metabolic regulation, has recently been shown to be present in OL exosomes that readily cross the periaxonal space and enter axons, where the release of SIRT2 (which is undetectable in neurons) acts on mitochondrial proteins to deacetylate them and increase axonal ATP levels, even in the presence of lactate and high glucose containing media (Chamberlain et al., 2021).

Disruption in OL glycolytic activity is also thought to contribute to many diseases, including Alzheimer's disease (AD). Early AD is accompanied by white matter loss, OL death, and axonal degeneration in both human AD patients and AD animal models; these early events have all been linked to mitochondrial dysfunction. Further investigation into

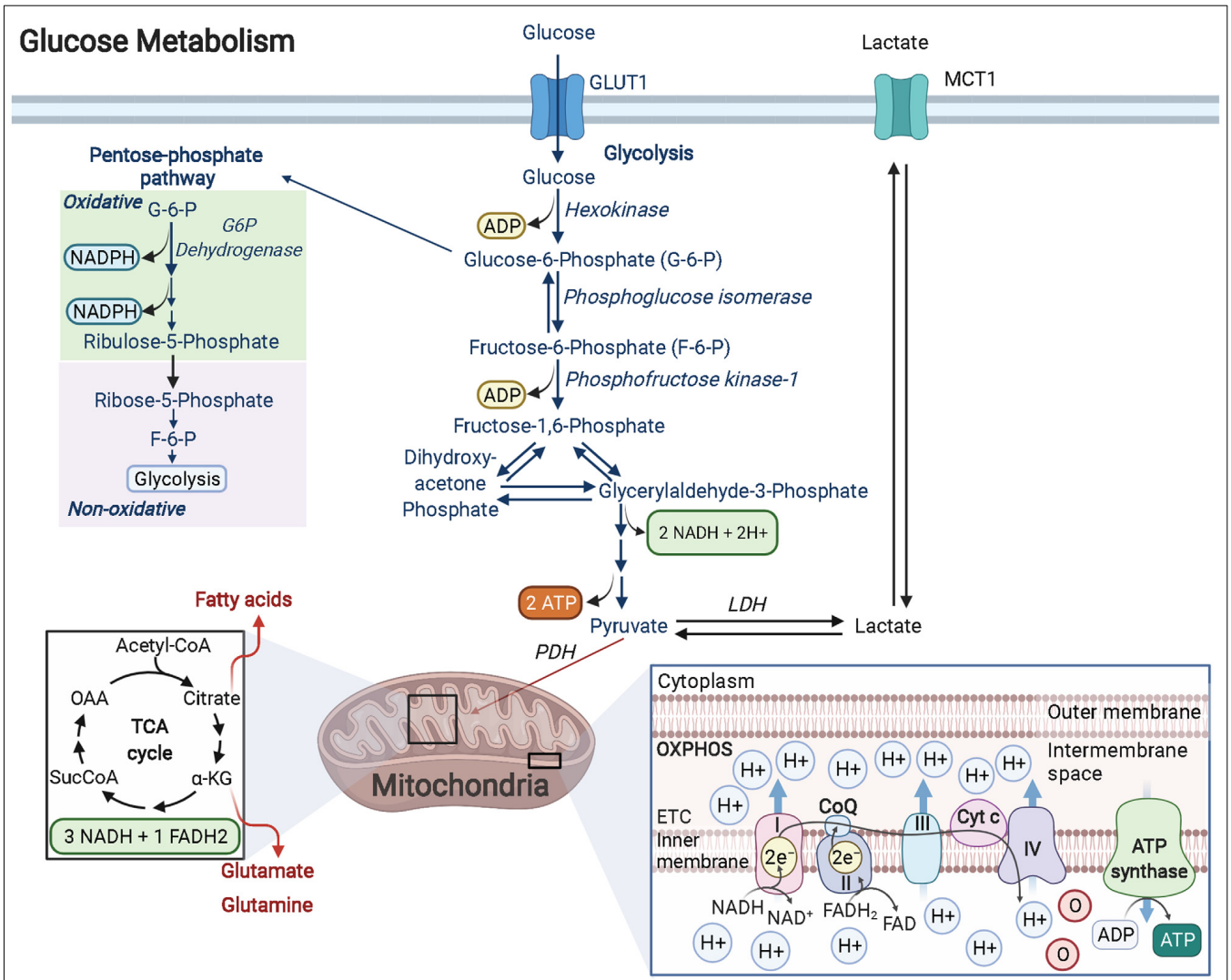

FIGURE 1 | Glucose metabolism in OPCs/OLs. Glucose is imported into the cell by GLUT transporters (GLUT1 is the most abundant GLUT transporter in OLs). Glucose is transformed into G-6-P by the rate-limiting enzyme hexokinase. G-6-P can enter the pentose phosphate pathway (PPP) or continue down the glycolytic pathway. In OPCs and OLs, there is significant PPP activity when compared to other cell types in the brain. The PPP pathway produces NADPH which is essential for cholesterol synthesis (for lipids) and for enhancing antioxidant activity. Furthermore, PPP generates ribose-5-phosphate (R-5-P) which is the backbone used in nucleotide synthesis and is critical in maintaining the proliferative function of cells like OPCs. R-5-P can be converted to F-6-P and enter back into the glycolytic pathway to generate a net of 2 ATP and 2 NADH molecules as well as pyruvate. Pyruvate is then converted to AcCoA by the PDH complex and enters the TCA cycle. The metabolites formed from the TCA cycle become electron donors of the electron transport chain, driving the hydrogen potential difference across the inner mitochondrial membrane to power ATP synthase and produce ATP. Created with BioRender.com.

the role OL stress plays in AD neuropathology determined that dynamin-related protein-1 (Drp1) was activated, leading to mitochondrial fission and fragmentation, causing impaired bioenergetics and suppression of glycolytic activity in OLs *via* inhibition of the rate-limiting enzyme hexokinase-1. In turn, the NLRP3 inflammasome (a multimeric protein complex) was activated, which promotes proinflammatory programmed cell death. However, a genetic knockout of Drp1 restored glycolytic rates in mature OLs of AD mice, which prevented myelin loss, reduced axonal degeneration, and improved cognitive performance. Thus, this study provided strong evidence that correctly regulated OL glycolysis plays an important role in CNS disease (Zhang et al., 2020).

Pentose Phosphate Pathway

The PPP is a biosynthetic pathway (non-ATP producing) in cells that branches from glycolysis after glucose is metabolized to G-6-P by the enzyme hexokinase. Once committed, G-6-P enters the oxidative, irreversible state of the PPP pathway where in a series of stepwise reactions, it forms 6-phosphogluconate, ribulose-5-phosphate (Ru-5-P), and 2 molecules of NADPH. In the non-oxidative, reversible arm of the PPP, Ru-5-P is

converted to ribose-5-phosphate (R-5-P) to provide the carbon backbone needed for nucleotide synthesis (Patra and Hay, 2014). Additionally, other PPP metabolites such as fructose-6-phosphate (F-6-P) and glyceraldehyde-3-phosphate (G-3-P) can shuttle back into the glycolytic pathway or, in the case of F-6-P, can be converted back into G-6-P and replenish oxidative PPP by generating more NADPH (**Figure 1**), which in turn can provide redox power for myelin lipid synthesis or bind with the enzyme catalase to enhance antioxidant activity within the cell (Kirkman et al., 1987; Berg et al., 2002; Kowalik et al., 2017).

The metabolic flux of specific metabolites can be analyzed within cells using 13-carbon (^{13}C) labeling techniques. With this approach, Amaral et al. (2016) assessed [1,2-^{13}C] glucose in differentiated OLs to better understand the metabolic pathways involved in glucose catabolism. They found significant glucose metabolism in OLs, with 10%–15% being metabolized *via* the PPP pathway, a rate similar to that seen in astrocytes. Additionally, they noted that the F-6-P and G-3-P derived from R-5-P of the PPP can enter the glycolytic pathway to produce pyruvate, which gets carboxylated to oxaloacetate (the last metabolite generated in the TCA that forms citrate after condensation with AcCoA) by the enzyme pyruvate carboxylase (PC; Berg et al., 2002; Amaral et al., 2016). The generation of oxaloacetate by pyruvate carboxylation allows alpha-ketoglutarate (α-KG, one of the intermediates in the TCA) to leave the cycle and enter the cytosol to form glutamate, or in the presence of glutamine synthetase (GS), make the amino acid glutamine. This finding has a profound impact on OL metabolic functions as this glutamate-glutamine cycle has previously only been described in astrocytes, where it aids neurons in synthesizing the most abundant excitatory and inhibitory neurotransmitters in the brain, glutamate, and GABA, respectively (Hertz, 2013). Although it is yet to be seen if glutamine release occurs in OLs, it is possible that myelinic channels formed during wrapping can shuttle glutamate/glutamine to neurons and assist in neuronal signaling and more specifically provide feedback for adaptive myelination. It is important to note that in addition to elevated PPP, Amaral et al. (2016) observed high OL mitochondrial activity (TCA activity) but the level of OXPHOS was not reported.

Similar to OLs, OPCs display high glucose catabolism in the PPP pathway. When labeling OPCs with ^{14}Carbon glucose (^{14}C-glucose) to assess the flux of glucose through different metabolic pathways in the postnatal rat brain, the PPP was reported to be two-fold higher than in type 1 astrocytes, 10-fold higher than in type 2 astrocytes, and at least four-fold higher than in neurons (Sánchez-Abarca et al., 2001). This is not surprising given that OPCs are highly proliferative cells, especially during development and in the subventricular zone of adult brains (Spitzer et al., 2019), and thus require ample nutrients for cell cycle progression. This requirement is most pronounced within the late G1/S phase of the cycle, where the non-oxidative branch of the PPP synthesizes R-5-P, the precursor for nucleotides adenine and guanine, to aid in DNA synthesis before mitosis and complete cell division can occur (Khedkar et al., 2016).

Inhibition of PPP in OLs with supra concentration of the G-6-P inhibitor dehydroepiandrosterone (DHEA) compromises NADPH supply and causes significant OL death and decreases in myelin. Similar results are also observed when treating both OPCs and OLs with the NADPH antimetabolite 6-aminonicotinamide (6AN). These findings were attributed to a disruption in NADPH-linked antioxidant activity and treatment with reduced glutathione (a naturally occurring antioxidant) was able to rescue the deficits observed, thereby, highlighting the importance of PPP activity and the many metabolites it produces in oligodendroglia (Kilanczyk et al., 2016).

REACTIVE OXYGEN SPECIES

Reactive oxygen species (ROS) such as superoxide and hydrogen peroxide, are derivatives of molecular oxygen generated from by-products of aerobic metabolism. The majority of ROS (∼90%) come from mitochondrial activity during OXPHOS where electrons can escape the inner mitochondrial membrane to generate free radicals, oxygen molecules with highly reactive unpaired electrons. However, ROS can also be generated by lipid metabolism within peroxisomes, through enzymatic activity within the cytosol, or by plasma membrane proteins such as NADPH oxidase (Lambert and Brand, 2009; del Río-Hortega, 2012; del Río and López-Huertas, 2016; Pizzino et al., 2017; Checa and Aran, 2020). Excess ROS can cause oxidative stress and lead to cellular damage whereas physiological levels have key roles as cell signaling molecules needed for normal biological processes (Pizzino et al., 2017; Sies and Jones, 2020). In the case of excess ROS, cells rely on several mechanisms to eliminate free radicals such as the antioxidant system and scavengers, which are stable molecules that donate electrons to free radicals in order to neutralize them (Lobo et al., 2010). The enzyme superoxide dismutase (SOD) and the tripeptide glutathione (GSH) are among the most abundant endogenous antioxidants of the cell. SOD works by catalyzing the conversion of superoxide to hydrogen peroxide, which further gets converted to water *via* the catalase enzyme, whose activity is enhanced by NADPH (a product of the PPP pathway—see Section "Pentose Phosphate Pathway") binding (Slemmer et al., 2008; Fernandez-Marcos and Nóbrega-Pereira, 2016). NADPH is also used as a cofactor by glutathione reductase to generate reduced GSH that defends against oxidative stress (Slemmer et al., 2008; Gansemer et al., 2020). Interestingly, oligodendroglia express low levels of both manganese SOD (the major detoxifying SOD in the cell) and GSH, making them particularly vulnerable to damage from oxidative stress, a phenomenon that has been observed in multiple white matter pathologies such as spinal cord injury (SCI), MS, schizophrenia (SCZ), Parkinson's disease (PD), and Alzheimer's disease (AD; Thorburne and Juurlink, 1996; Pinteaux et al., 1998; Holley et al., 2011; Spaas et al., 2021). Mutations in the human *SOD1* gene are associated with familial amyotrophic lateral sclerosis (ALS), and result in substantially increased ROS concentrations in the nervous system (Said Ahmed et al., 2000). Recent work has revealed that in ALS, loss of SOD activity in OLs leads to demyelination, downregulation of MCT1 transporters (transporter that shuttles the critical

metabolite lactate to neurons), and subsequent motor neuron degeneration (Kim et al., 2019). Conversely, overexpression of the human *SOD1* gene in transgenic mice reduced oxidative stress-mediated death in OPCs isolated from cerebral cortices. In the same study, OPC proliferation was found to be increased and differentiation was accelerated, with the resulting mature OLs being more resistant to cell death when compared to wild type (WT) controls (Veiga et al., 2011).

Similar to SOD dysfunction, deficits in GSH synthesis resulted in impaired OPC proliferation and maturation in a model of SCZ, where anomalies in white matter integrity have been reported in the patient population (Monin et al., 2015). Intriguingly, trinucleotide repeat polymorphisms in the *GCLC* gene, which encodes the catalytic subunit of glutamine cysteine ligase (GCLC), the rate-limiting enzyme of GSH synthesis, have been observed in SCZ patients (Gysin et al., 2007). Knockdown of *GCLC* in cultured OPCs showed a ∼28% decrease in total GSH levels and a subsequent ∼29 reduction in OPC proliferation compared to WT controls. Additionally, reduced GSH leads to a dramatic decrease of (∼57.2%) in the number of MBP+, mature OLs. Further, an analysis of oligodendroglial dynamics in a mouse that lacks the modifier subunit of glutamine cysteine ligase (GCLM-KO), a mouse model that displays SCZ behavioral phenotypes, presented similar reductions in GSH and OPC proliferation and maturation levels at the peripubertal age (Monin et al., 2015). These and other studies have begun to uncover the key role that oligodendroglial metabolism may play in behavioral disorders.

A fine balance in redox reactions is critical for cell survival and function, as ROS at physiological levels can behave as signaling molecules that mitigate stress responses, DNA damage, and promote cellular differentiation (Sies, 2015; Checa and Aran, 2020). In fact, treatment of the human oligodendroglial cell line MO3.13 (which expresses phenotypic markers of OPCs) with hydrogen peroxide at low levels (200 μM) displayed significant *increases* in MBP RNA and protein levels. Moreover, hydrogen peroxide treatment induced the activation of the extracellular signal-regulated kinase 1–2 (ERK $\frac{1}{2}$) and of cyclic AMP responsive element binding protein-1 (CREB-1), known regulators of OL differentiation (Sato-Bigbee et al., 1999; Fyffe-Maricich et al., 2011; Accetta et al., 2016). NADPH oxidase (NOX), a membrane bound enzyme that generates ROS, also increased MBP mRNA levels when treated with low concentrations of hydrogen peroxide, and silencing of NOX genes (*NOX3* and *NOX5*) in MO3.13 cells inhibited MBP and Olig2 mRNA expression, and OL differentiation. Together these studies have highlighted the important role of redox signaling in oligodendroglia (Accetta et al., 2016; Vilchis-Landeros et al., 2020).

MYELIN LIPID METABOLISM

One result of myelin wrapping (i.e., myelination around axon segments) is the rapid transmission of action potentials along neurons *via* saltatory conduction. Most but not all neurons in white matter tracts of the nervous system eventually become myelinated, enabling fast and reliable information processing for proper circuitry function (Almeida and Lyons, 2017). In the CNS, there is continued myelin sheath remodeling and lipid turnover mediated by OLs, which produce ∼40% of the total lipids synthesized in the human brain, most of which is used for forming myelin membrane (Schmitt et al., 2015). Interestingly, the molecular makeup of the *myelin* membrane itself differs drastically from other cellular membranes in that it contains ∼70% of its dry weight as lipids compared to 25%–50% in other cells (Cooper, 2000; Jahn et al., 2009). While myelin is not unique to the CNS [Schwann cells wrap myelin around axons in the peripheral nervous system (PNS)], the *lipid* composition of myelin throughout the nervous system is remarkably similar. The most abundant lipids of myelin are cholesterol, the glycolipid galactosylceramide (GalC), and the phospholipid ethanolamine plasmalogen (EP), representing approximately 70% of total myelin lipids (**Table 1**, Norton and Poduslo, 1973; Chrast et al., 2011; Schmitt et al., 2015).

TABLE 1 | Estimated lipid composition of the myelin membrane within the mammalian CNS.

Lipid type	% in Myelin membrane
Cholesterol	26%
Galactosylceramide (GalC)	23%
Sulfatide	4%
Ethanolamine Plasmogen (EP)	16%

The table highlights the most common lipids present in myelin (Norton and Poduslo, 1973; Chrast et al., 2011; Schmitt et al., 2015).

Cholesterol

Cholesterol is a critical component of the myelin sheath needed to preserve the complex arrangement of lipids and proteins of the myelin membrane. Along with GalC, cholesterol helps to form specialized domains along the membrane, the so-called "lipid rafts", which contribute to protein trafficking and signaling, as well as myelin fluidity and stability (Decker, 2004; Saher et al., 2011; Montani, 2021). Because the blood-brain barrier prevents the uptake of circulating lipoprotein bound dietary cholesterol, cholesterol synthesis occurs *in situ* (Petrov et al., 2016). The rate of cholesterol synthesis in the CNS is at the highest during the first few weeks to months after birth, when OLs are engaged in active myelination. However, within the myelin membrane, there is long-term stability of cholesterol such that turnover occurs at the relatively slow pace of ∼1 year in the young adult mouse brain and ∼5 years in the human adult brain (Ando et al., 2003; Russell et al., 2009).

OL cholesterol synthesis is reliant on AcCoA generated from either glucose or ketone sources, although OLs show a preference for ketone bodies (Koper et al., 1981). AcCoA is formed from pyruvate (an end product of glycolysis) *via* pyruvate dehydrogenase or, in the case of ketones, the ketone body acetoacetate can be converted back into AcCoA *via* the enzyme β-ketoacyl-CoA. AcCoA then gets transformed into 3-hydroxyl-3-methylglutaryl-coenzyme A (HMG-CoA) and subsequently into mevalonate, which then goes on to produce lanosterol followed by a series of reactions that ultimately generates cholesterol. The intermediary reactions in this process are catalyzed by specific enzymes that require NADPH (a

byproduct of the PPP) as a cofactor. Notably, the formation of mevalonate by HMG-CoA reductase is the irreversible, rate-limiting step for cholesterol biosynthesis (Petrov et al., 2016). HMG-CoA reductase is targeted by statin drugs to lower cholesterol production in the body. Given the widespread use of statins (e.g., simvastatin), several studies have used statins to assess the impact of cholesterol synthesis in OLs. Both OPCs and OLs that underwent prolonged treatment with simvastatin *in vitro* exhibited significant process retraction, increased cell death, and decreased mitochondrial activity whereas treatment with mevalonate or cholesterol itself was able to rescue the simvastatin-induced phenotype (Miron et al., 2007). Furthermore, severe hypomyelination has been observed in both white and gray matter tissue in mice engineered with OL-specific loss of *Fdft1*, the gene encoding squalene synthase, which catalyzes the first step of the cholesterol synthesis pathway. These *Fdft1* conditional knockouts displayed ataxia, tremors, and premature death (Saher et al., 2005). These and other studies have concluded that cholesterol is essential for myelin membrane growth and function, as well as for the survival of OPCs and OLs, which may be possibly mediated through signaling proteins contained within membrane cholesterol-enriched lipid rafts. In the absence of cholesterol, signaling proteins can become decoupled from lipid rafts, suppressing necessary signal transduction that mediates survival and other cellular processes in oligodendroglia (Bryant et al., 2009).

Galactosylceramide

Galactosylceramide (GalC) is synthesized from a sphingolipid ceramide molecule. The UDP-galactose: ceramide galactosyltransferase (CGT) enzyme transfers UDP-galactose (UDP: uridine diphosphate) to ceramide, forming GalC. Interestingly, in CGT global knockout mice, no GalC production was detected and myelin instead contained high levels of *glucocerebroside*. Despite this compensatory mechanism, significant decreases in the number of myelinated axon segments in the spinal cord were observed. Unexpectedly, CGT deficient mice demonstrated a 50% increase in mature OLs, revealing a possible negative regulatory role for GalC in OL differentiation. A reduction in conduction velocity and insulative capacity of the myelin sheath was also noted, which led to progressive hindlimb paralysis, tremors, and even premature death (Coetzee et al., 1996; Bansal et al., 1999; Marcus et al., 2000). Problems with myelin compaction were also reported with the appearance of outward facing paranodal loops, outfolding of the myelin membrane, and incorrect myelin compaction (Bosio et al., 1998; Ishibashi et al., 2002).

The molecular structure of GalC has provided useful insights into its function. GalC and its sulfated form, sulfatide, are the most abundant glycolipids in the myelin membrane, accounting for 23% and 4% respectively, of the total myelin lipid mass (Norton and Cammer, 1984). GalC, like other galactosphingolipids, have longer, more saturated fatty acids than phospholipids and can participate in intermolecular hydrogen bonding, allowing them to form ordered membrane domains (Dicko et al., 2003). In fact, GalC is believed to interact with other sulfur enriched glycolipids such as sulfatide to form "glycosynapses" during the wrapping of the myelin sheath, contributing to the stability of myelin. These glycosynapses can interact with axonal ligands, extracellular matrix proteins, or even with each other across the apposed membranes to facilitate the transmission of transmembrane signals (Hakomori, 2002; Boggs et al., 2010). Liposomes containing GalC and sulfatide were added to OLs in culture to mimic facing pairs of extracellular surfaces of myelin or interactions between OLs processes. These liposomes were able to interact with glycosynapses to cause a disruption in the microtubule network and a concentrated redistribution of GalC on the extracellular side and MBP on the cytosolic side. However, as there is no clear role for the seGalC-MBP rich domains in OL signaling, future work is needed to understand their purpose (Boggs and Wang, 2001).

Ethanolamine Plasmalogen

In the myelin membrane, the most abundant *phospholipid* belongs to the subclass plasmalogen. Plasmalogens are a type of glycerophospholipid that exhibit a vinyl-ether group on the first carbon of the glycerol molecule, with the predominant plasmalogen in OLs being ethanolamine plasmalogen (EP). EP synthesis begins in the peroxisome and is completed in the endoplasmic reticulum (Messias et al., 2018; Montani, 2021). Peroxisomal dihydroxyacetone phosphate acyltransferase (DHAPAT) enzyme is necessary for plasmalogen synthesis and loss of this enzyme results in ethanolamine deficiency, dysmyelination of the cerebellum, reduction in total MBP protein in both cortex and cerebellum, paranode disorganization, as well as a ∼40% decrease in myelinated fibers of the EP deficient corpus callosum (Teigler et al., 2009). Future studies are still needed however to fully decipher the precise role EP has in OLs.

AUTOPHAGY

One of the main ways that cells maintain metabolic homeostasis is through autophagy. During autophagy, cells form a double-membraned vesicle (the autophagosome) around components targeted for removal and reuse. Lysosomes containing degradative enzymes then fuse with the autophagosome to form the autolysosome. In this way, autophagy removes waste such as damaged organelles, proteins, and other cytoplasmic components for which the breakdown products become inputs to various metabolic processes (Eisenstein, 2014). Thus, autophagy is often thought of as the cell's waste removal and recycling program. In terminally differentiated cells such as OLs, autophagy is critical in maintaining cellular health, as damaged components cannot be diluted out by cell replication. Additionally, in times of starvation or nutrient deprivation, autophagy can promote survival by breaking down cellular components to serve as metabolites for critical functions. Defects in autophagy have been connected to liver disease, aging, and neurodegeneration, and, while autophagy is generally considered to be beneficial, it can also contribute to tumorigenesis in nutrient-poor cancers. Thus, modalities aimed at upregulating autophagy should be approached with caution. Nevertheless, recent studies investigating the

role autophagy plays in OL function have pointed to select benefits this "remove and reuse" mechanism can confer (Rabinowitz and White, 2010; Eisenstein, 2014).

To understand the role autophagy plays in OL function, Bankston and colleagues generated WT control and conditional knockout mice with the *Atg5* (Atg5 protein is necessary for the formation of the phagophore—the precursor to the autophagosome) deleted in mouse OPCs and OLs. Firstly, they found that oligodendroglia express autophagy markers at all stages but as OPCs transition to OLs they have substantial increasing levels of ATG5 and LC3B-II and corresponding decreases in p62, a pattern that is in accordance with autophagosome formation and lysosome fusion. Interestingly, the number of autophagic vesicles per area was significantly higher in OL processes than in OPCs, perhaps due to the rapid rate of growth OL processes experience during both differentiation and myelin membrane formation. To confirm this, immunostaining revealed that ATG5 and LC3B were present throughout the corpus callosum and in spinal cord white matter, as well as in myelinating co-cultures where ATG5 colocalized in myelin wrapped axon segments. Additionally, live cell imaging of tagged autophagosomes revealed the ability of OLs to engage in distal autophagosome formation as autophagosomes trafficked from the cell soma to its processes (Bankston et al., 2019).

The increased presence of autophagosomes in OLs and myelin sheaths suggested that autophagy activity may be necessary for myelination. Further experiments were conducted in mutant mice that had the *Atg5* gene selectively removed in OPCs. When compared to control, the *Atg5* mutant mice exhibited significantly fewer OPCs and OLs, with the few surviving OLs producing abnormal myelin that was uncompacted and with multiple myelin outfoldings. The $Atg5^{-/-}$mice also displayed severe tremors by P12 followed by death by P15. Furthermore, a striking 75% reduction in MBP staining in the corpus callosum of the mutant mice was observed followed by a four-fold decrease in the percent of myelinated axons, strongly implicating autophagy as a key player in OL myelination. Similar findings were also observed when using pharmacological inhibitors of autophagy (KU55933 and Verteporfin) whereas, the use of Tat-beclin1, an autophagy *enhancer*, remarkably increased the number of myelin segments by more than two-fold when compared to vehicle controls or KU55933/Verteporfin treated OLs (Bankston et al., 2019). Autophagy has thus emerged as a critical player in OL function and myelinogenesis but additional study is clearly needed to fully understand this requirement.

SIGNALING EVENTS REGULATING OL METABOLISM

Netrin-1 Signaling Promotes Mitochondria Elongation and Glycolysis

Understanding how both intrinsic and extrinsic signaling events can affect oligodendroglial metabolism will be key to the development of therapeutic agents to either enhance metabolic control of oligodendroglial functions or counter metabolic dysregulation. Several recent studies have shed light on some of the signaling pathways impacting OL metabolism. For example, netrin-1, a secreted protein that binds to the transmembrane receptor DCC (deleted in colorectal cancer), has recently been implicated in regulating OL mitochondrial dynamics and bioenergetics. Proteomic analysis and confocal imaging of netrin-coated beads in association with OLs revealed binding to paranodal enriched proteins DCC and neurofascin-1 (NF155). Similarly, binding to the dynein-1 heavy chain and kinesin light chain-1 (two major mitochondrial microtubule motor proteins) was observed, indicating OL netrin-1 may be associated with mitochondria trafficking. Indeed, super-resolution microscopy and transmission electron microscopy confirmed that netrin-1 was involved in mitochondria movement to distal regions of OL processes and paranodes. Furthermore, mitochondria elongation was enhanced by netrin-1 induced src family kinase (SFK) activation, and downstream inactivation of rho-associated protein kinase (ROCK). Mitochondrial elongation results from the fusion of multiple mitochondria organelles and as such can alter the metabolic dynamics of the cell. Live cell metabolic profiling showed that prolonged netrin-1 signaling (through SFK activation and ROCK inhibition) hyperpolarizes the mitochondrial inner membrane and increases glycolysis but not OXPHOS in primary OLs (Nakamura et al., 2021). Whether these netrin-1/SFK induced changes in OL metabolism can be beneficial in a demyelination paradigm with dysfunctional OLs remains to be determined but nevertheless, these findings present new pathways to pursue in the quest for next-generation oligodendroglia therapeutics.

Oligodendrocyte NMDA Receptor Activation Increases Glucose and Lactate

OLs are known to provide trophic and metabolic support to the axons they ensheath, yet variations in synaptic strengths and neuronal firing rates can greatly alter the metabolic demand of axons. Thus, a key unanswered question is how OL adjust their ability to metabolically support axons in response to environmental cues (Mount and Monje, 2017; Bonetto et al., 2020). In a recent study, researchers were able to demonstrate that OLs "sense" neuronal activity through OL NMDA receptors, which can respond to the neurotransmitter glutamate (released upon neuronal firing) and then adjust the OLs ability to regulate axonal energy metabolism (Saab et al., 2016). For instance, stimulation of NMDA receptors with NMDA-acid and glycine (NMDA-A/Gly) in OL cultures triggered an increase in GLUT1 expression and trafficking to the membrane, leading to increased intracellular glucose and lactate concentrations as well as high lactate *release*. Selective deletion of the NR1 subunit [the glycine binding subunit critical to NMDA receptor function (Catts et al., 2015)] from OLs (NR1 cKO) conversely resulted in a strong reduction of GLUT1 transporters in OLs (e.g., an ∼80% reduction in the optic nerve). GLUT1 deficiency in OLs negatively impacted the rate of myelin growth, which is metabolically controlled. Thinner and fewer myelinated axons were observed in the optic nerve of NR1 cKO mice by P18–P20. By adulthood (P70) myelination "caught up", however, in the context of correct circuitry formation, delays in myelination may have detrimental effects on learning and memory in the postnatal

brain by leading to aberrant synapse formation. Additionally, adult NR1 cKO mice (P50–P70) that were subjected to metabolic stress in the form of oxygen-glucose deprivation, had reduced conduction velocity (CV) in the optic nerve by as much as 50% compared to WT control, further demonstrating the role OL metabolism plays in regulating both OL dynamics and axon function. Remarkably, treatment with lactate for reperfusion of the nerve promoted CV similar to control levels, demonstrating axons readily use lactate to generate ATP which in itself can regulate axon CV (Massicotte et al., 2001; Saab et al., 2016).

mTORC1 Signaling Regulates OL Myelination and Lipid Metabolism

All mammalian cells require sufficient nutrients for proper growth and maintenance. A major player in sensing and regulating cellular growth based upon nutritional availability is the mechanistic target of the rapamycin (mTOR) pathway. mTOR consists of two complexes, mTORC1, and mTORC2, both of which are capable of integrating nutrients such as glucose, oxygen, amino acids, and insulin to influence growth and proliferation (Sabatini, 2017). mTORC1 is functionally dependent on the regulatory associated protein of the mTOR (raptor) subunit whereas, mTORC2 activity is modulated by the rapamycin insensitive companion of the mTOR (rictor) subunit (Lebrun-Julien et al., 2014). The mTOR complex interacts with Akt kinase both in upstream and downstream signaling. Interestingly, overexpression of constitutively active Akt in mouse OLs resulted in significant CNS hypermyelination and as expected, elevated mTOR activity. However, when mTOR signaling was inhibited *via* chronic administration of rapamycin, the observed hypermyelination was significantly reduced in young adult mice (Narayanan et al., 2009). Recent findings have been able to further unravel the contributions each mTOR complex plays in CNS myelination with an emphasis being placed on mTORC1 for its part in modulating OL dynamics and myelin lipids (Lebrun-Julien et al., 2014).

Conditional knock-out mice lacking raptor, rictor, or a combination of raptor and rictor (raptor/rictor) in adult OLs were generated to study the effects of mTORC1 (raptor-dependent) and mTORC2 (rictor-dependent) in CNS myelin. *Both* raptor and rictor OL-knockouts resulted in reduced myelination when compared to control but the raptor knockout mice were persistently hypomyelinated into late adulthood whereas, rictor knockout mice underwent transient hypomyelination and restored their spinal cord myelin by p60, partly due to the compensation of raptor-driven mTORC1 activity. In double raptor/rictor knockouts, hypomyelination remained throughout adulthood (6 months) indicating mTORC1 is indeed critical for myelination. However, when analyzing OL dynamics in the raptor knockouts, the number of Olig2+, CC1+Olig2+, and PDGFRa+Olig2+ cells did not differ significantly from control as they did in the rictor knockouts. Interestingly, the double knockout raptor/rictor group did exhibit reductions in OPCs, mature OLs, and late progenitor to pre-myelinating OLs (characterized by Tcf-4+/Olig2+), revealing that the total mTOR complex (mTORC1 and mTORC2) contributes to oligodendroglia maturation. When analyzing levels of known transcription factors involved in OL differentiation (*Sox10* and *Myrf*), both the raptor/rictor and raptor mutant mice displayed strong decreases in transcript levels. In addition, the phosphorylation of 4E-BP1 and S6 kinase (downstream mTOR targets) was drastically reduced in the raptor and raptor/rictor mutants indicating mTORC1 activity is capable of regulating OL dynamics more than mTORC2 (Lebrun-Julien et al., 2014).

Because mTOR has a major role in lipogenesis, it was postulated that mTORC1 could also be in part responsible for controlling proper lipid biosynthesis in adult myelinating OLs (Soliman, 2011; Lamming and Sabatini, 2013). Similar to the hypomyelination phenotype observed during development, tamoxifen-inducible loss of raptor and raptor/rictor mutants in adult OLs displayed a significant reduction in myelin even 12 months post induction. Axon diameter was also reduced in these mutant mice. Although no changes were seen in sterol regulatory element-binding protein-1 (SREB1), transcription factors that regulate gene expression involved in lipid synthesis, the enzymatic activity of their main targets fatty acid synthase (FAS) and stearoyl-CoA desaturase-1 (SCD1), decreased in raptor and raptor/rictor mutants (Lebrun-Julien et al., 2014; Shimano and Sato, 2017). Interestingly, alterations in lipid composition were observed in the raptor mutant group with total levels of cholesterol, ceramide, sphingomyelin, and glycosylceramide (critical component of myelin—see Section "Reactive Oxygen Species") severely reduced in the whole spinal cord (Lebrun-Julien et al., 2014). Taken together, these results indicate that mTORC1 activity of the mTOR complex is predominantly responsible for affecting OL lipid biosynthesis as well as myelin growth and maintenance.

EXOGENOUS MODULATORS OF OL METABOLISM: FROM DRUGS TO DIETARY THERAPIES

Donepezil Promotes OL Differentiation and Increases Brain Glucose Metabolism

The ability to exogenously regulate oligodendroglial metabolism has implications for a host of neurodegenerative diseases. For instance, in sporadic AD, a strong correlation exists between impaired brain glucose metabolism and disease onset and progression (Saito et al., 2021). More specifically, when analyzing gene expression data in post-mortem AD brains *via* RNA sequencing, impairments in both glycolytic and ketolytic genes were observed, more so in OLs than in neurons, astrocytes, or microglia, suggesting that regional OL hypometabolism may contribute much more to disease pathology than originally believed (Saito et al., 2021). In support of a more central role for OL dysfunction in AD, there is evidence that the demyelination precedes the toxic beta-amyloid and tau pathologies that lead to synaptic dysfunction and symptoms of cognitive decline in AD (Papuć and Rejdak, 2018). One drug approved for mild to moderate AD that has been shown to positively influence AD outcomes is donepezil. A potent and selective inhibitor of acetylcholinesterase (AchE), donepezil helps to reduce the

breakdown of acetylcholine in the body thereby, prolonging the activity of cholinergic neurons in the brain and thus slowing down the neuronal loss normally observed in AD (Chen and Mobley, 2019). Recent research has revealed that donepezil might also exert its anti-AD therapeutic effects *via* its impact on OLs. Cui and colleagues conducted experiments on neural progenitor cell (NPC)-derived OPCs treated with varying concentrations of donepezil and found that donepezil promoted OPC-to-OL differentiation in a dose-dependent manner with higher concentrations nearly doubling the number of differentiated OLs relative to those in control cultures. Furthermore, this effect was limited to donepezil as other AchE inhibitors used in AD therapy such as rivastigmine, tacrine, and huperzine A did not result in any significant changes in the number of OLs. When donepezil was administered to mice undergoing active remyelination following cuprizone-mediated demyelination, by 2 weeks the donepezil treated group had a significant increase in the number of myelinated axons per field as well as thicker myelin, as defined by a significant decrease in the *g ratio* (the inner axonal diameter/outer axonal diameter; Cui et al., 2019). Interestingly, in a separate randomized, double-blinded, placebo-controlled study assessing the effect of donepezil in 28 patients with mild to moderate AD over a 24-week period, overall brain glucose metabolism was maintained within 0.5% of baseline levels in the treatment group whereas, the placebo group experienced an average 10.4% decline in brain glucose metabolism. In the parietal, temporal, and frontal lobes (areas where white matter lesions are often observed in AD patients), a slight but significant increase in glucose metabolism was also observed in AD patients on donepezil, which may contribute to the therapeutic effect of the drug (Tune et al., 2003). Whether or not donepezil's pro-myelination effects are mediated through metabolic changes in OLs remains to be seen but the data gathered thus far presents a hypothesis worth investigating.

The Antipsychotic Drug Clozapine Increases Glycolytic Activity and Myelin Synthesis

OL dysfunction in SCZ has recently been linked to cerebral dysconnectivity, where white matter anomalies, decreased OL number, and the breakdown of neuronal circuitry across varying brain regions are observed (Schmitt et al., 2011; Steiner et al., 2014). Moreover, elevated glucose levels and reduced lactate were identified in the cerebrospinal fluid of first onset, drug-naive SCZ patients (Holmes et al., 2006). Additionally, decreased expression in glycolytic and glycogen synthesis enzymes was observed and genetic studies have identified linkages between genes involved in glucose metabolism with an elevated risk of SCZ (Prabakaran et al., 2004; Stone et al., 2004). Taken together, SCZ is a disease closely tied to both OL dysfunction and impaired glucose metabolism of the brain. Clozapine, an atypical antipsychotic drug used to mitigate symptoms in SCZ, has antagonistic effects on serotonin (5-HT) and dopamine receptors, yet new evidence suggests that clozapine's therapeutic efficacy may in part stem from its ability to upregulate key metabolic mediators in OLs, possibly by disinhibiting decreased activation of the MAPK/ERK pathway following 5-HT stimulation (Meltzer, 1994; Masson et al., 2012; Steiner et al., 2014). In support of this idea, clozapine treatment of OLN-93 cells (an OL cell line) led to increased glycolytic activity and lactate production as well as increases in GalC and myelin lipid synthesis (Steiner et al., 2014). A notable and significant increase in intracellular glucose was observed in the clozapine treatment group but the number of GLUT1 transcripts was not changed. Similarly, lactate concentrations were increased in both intracellular homogenates and extracellular media, suggesting upregulation of glycolysis in treated cells. However, no significant changes in mitochondrial oxygen consumption were noted. Interestingly, clozapine treatment led to elevated acetyl-CoA-carboxylase (ACC) activity, a key rate-limiting enzyme that converts AcCoA into the fatty acid malonyl-CoA needed for downstream lipogenesis (Brownsey et al., 2006). Although pre-clinical data with clozapine looks promising for treating white matter pathologies, a recent phase 1, randomized, blinded, placebo controlled clinical trial in patients with progressive MS (pMS), concluded that clozapine was not well tolerated as patients experienced spastic ataxic gait and worsening mobility, which resolved after drug cessation (La Flamme et al., 2020). Thus, additional studies are needed to achieve a better understanding of this promising drug's pharmacodynamics and other parameters in the context of human disease.

Metformin-Induced AMP-Kinase Activation Influences OL Function

The anti-hyperglycemic drug metformin has been used extensively to treat Type-2 Diabetes Mellitus and is globally the most prescribed anti-diabetic drug. Metformin is believed to exert its therapeutic effect by indirectly altering the metabolic state of cells. Due to its polarity, metformin entry into the cell is facilitated by members of the organic cation transporter (OCT) family. Following entry, metformin binds to complex I in the mitochondria to inhibit its function, resulting in decreased ATP output. This causes a shift in the cellular ATP:AMP ratio, which is detected by the enzyme complex AMP-kinase (AMPK; Zhou et al., 2001). In addition to its role as the cells' "metabolic sensor", AMPK is a master regulator of many signaling pathways, including the mTOR pathway (Sabatini, 2017). When activated, AMPK will suppress many energy intensive anabolic processes that require ATP (e.g., gluconeogenesis and protein synthesis) and turn on catabolic processes such as beta-oxidation to liberate more cellular ATP. In the context of type II diabetes, metformin-induced activation of AMPK leads to increased trafficking of GLUT transporters to increase glucose uptake and glycolysis, thereby, lowering blood glucose (Pernicova and Korbonits, 2014). Additionally, AMPK activation also decreases cyclic AMP, which in turn through downstream signaling increases the activity of phosphofructose kinase-1, thus leading to elevated levels of glycolysis to generate ATP and downregulation of gluconeogenesis (Pernicova and Korbonits, 2014). However, it is important to note that metformin's effect on cellular metabolism is only well understood in hepatocytes where a large concentration of OCT1 transporters is localized in the body. Nevertheless, active research is exploring the potential other

uses for metformin in metabolopathies such as cancer. Given the presence of other OCT transporters in the brain, mainly OCT3 (believed to be a functional but less potent transporter of metformin; Shirasaka et al., 2016; Koepsell, 2021), several groups have begun to investigate metformin's effect on the CNS. New findings regarding the relationship between metformin and myelin are discussed below (Rotermund et al., 2018).

Metformin Reduces Degeneration of RGC Neurons and Increases Myelin Thickness

Neurodegenerative diseases such as PD, AD, and glaucoma can lead to the loss of retinal ganglion cells (RGC). Photoreceptor cells convey visual information to RGC neurons whose myelinated axons form the optic nerve responsible for engaging visual cortex processing (Etxeberria et al., 2016; Kim et al., 2021). By using the DNA alkylating agent N-ethyl-*N*-nitrosourea (ENU) to induce retinal photoreceptor degeneration in rats, Eltony et al. (2021) assessed whether metformin was neuroprotective. Daily ENU treated retina developed pronounced photoreceptor degeneration with vacuolations and loss of nuclei, followed by RGC death and a reduction in myelinated axons. Interestingly, when undergoing daily metformin concurrently (metformin given intraperitoneally @ 200 mg/kg), the severity of photoreceptor degeneration was reduced. Additionally, the diameter of the optic nerve fiber and the thickness of its myelin sheath increased significantly by >two-fold when compared to the ENU+ only group, although the metformin+ENU group did not match the levels seen in the untreated controls. Metformin also led to significant reductions in inducible nitric oxide synthase (iNOS), a proinflammatory agent induced by microglia, and the apoptotic marker caspase-3, whose activity is modulated by AMPK (Villanueva-Paz et al., 2016; Eltony et al., 2021). However experiments to measure OL dynamics or its metabolism were not conducted, thus leaving open the question of whether changes in myelin were due to alterations in OL metabolism and possibly myelin repair (Eltony et al., 2021).

Metformin Increases Neurotrophic Factors and Stimulates Remyelination *via* AMPK

Neurotrophic factors (NTFs) are small molecules that help to promote and regulate the survival, growth, and plasticity of cells in the nervous system (Johnson and Tuszynski, 2008). In addition to their known effects on neurons, NTFs such as brain-derived neurotrophic factor (BDNF), ciliary neurotrophic factor (CNTF), and nerve growth factor (NGF) also act upon OLs where they can promote survival and differentiation (Pöyhönen et al., 2019). However, the key effectors involved in OL NTF signaling and the degree to which NTFs can influence repair in diseased OLs remain poorly understood. Using cuprizone (a copper chelating agent that inhibits complex IV of the ETC) to induce demyelination, Houshmand et al. (2019) reported that treatment with metformin-induced upregulation of BDNF, CNTF, and NGF, and downregulated neurite outgrowth inhibitor (NogoA) mRNA in OLs, which led to an increase in OPC proliferation as well as OL differentiation. Interestingly, these pro-OL effects were absent in the combined cuprizone (−) and metformin (+) group, suggesting that the increase observed in these neurotrophic factors may only be linked to periods of OL metabolic dysfunction (Faizi et al., 2016; Houshmand et al., 2019). Neurodegenerative diseases such as PD, HD, and MS all exhibit decreases in the trophic factor BDNF which in part contributes to neuronal loss (Sohrabji and Lewis, 2006; Scalzo et al., 2010; Bathina and Das, 2015). Yet BDNF has also been found to promote OL myelination through its effects on Fyn kinase (a member of the Src family of kinases) signaling, which itself has been proposed to regulate lipid metabolism *via* its upstream effects on AMPK (Vatish et al., 2009; Peckham et al., 2016). Thus, the metformin-to-BDNF axis may have a dual effect in the context of myelin loss, both promoting OL intrinsic repair mechanisms as well as providing needed trophic support to axons.

Metformin Rejuvenates Aged OPCs to Increase CNS Remyelination

Aging is associated with a metabolic decline in the brain. In both human and animal studies, aging has been linked to reduced expression of glucose transporters and altered levels of glycolytic and OXPHOS enzymes in the brain (Camandola and Mattson, 2017). Decreases in ATP levels are also observed in aging white matter and are accompanied by ultrastructural changes in mitochondria (Stahon et al., 2016). In the context of neurodegenerative diseases such as MS, aging contributes to impairments in the endogenous remyelination capacity that wanes during disease progression. For instance, remyelination relies upon the recruitment and differentiation of OPCs at the lesion site, both of which decline with age. A recent study by Neumann et al. (2019) found that, when compared to OPCs from young adult rats (2 to 3 months old), OPCs isolated from adult rats aged 20 to 24 months were largely unable to differentiate into OLs when stimulated with triiodothyronine (T3), a well-known OL differentiation. Thus, employing strategies that can counter the effects of aging may be able to provide aged OPCs with a more "youthful" phenotype that can overcome differentiation deficits. Neumann et al. (2019) focused on alternate day fasting (discussed below) and administration of metformin. In addition to being considered a fasting mimetic (fasting also activates AMPK), metformin is also thought of as a geroprotective agent. A systematic review and meta-analysis study conducted by Campbell et al. (2017) revealed that the use of metformin increased health and lifespan by reducing both all-cause mortality and diseases of aging through either its effect on ROS, mTOR, and AMPK signaling or lowering inflammation and DNA damage. In fact, when Neumann and colleagues treated aged OPCs with 100 μM metformin, they found the aged OPCs reverted to a "younger" state and significantly increased their responsiveness to differentiation factors. They attributed these findings to significant reductions in DNA damage and the senescent marker *Cdkn2a*, as well as demonstrated that metformin's effects required AMPK signaling since

inhibition of AMPK using dorsomorphin or knockout of *Prkaa2* (the gene encoding for the catalytic AMPK α2 subunit) ameliorated the pro-OL effects with metformin treatment (Neumann et al., 2019).

Dietary Changes Influence OL Function

Systemic metabolic changes can also be achieved through alterations in dietary intake. For instance, a diet high in glucose, carbohydrate, and fat can lead to impaired glucose metabolism, dyslipidemia, and hyperinsulinemia, which collectively can cause a metabolic syndrome with symptoms such as hypertension, fibrosis, and inflammation in the heart, liver, and kidneys (Panchal et al., 2011). Brain development is also often affected by dietary changes. In fact, when subjecting piglets to sustained iron deficiency for the first month of life, white matter development was significantly impaired throughout with the greatest reduction seen in the corpus callosum as evident by changes in its fractional anisotropy and anatomical width (Leyshon et al., 2016). In contrast, iron homeostasis is critical for proper CNS function, particularly for OPCs and mature OLs, which have the highest cellular iron in the brain, utilizing iron as a cofactor for enzymes involved in glucose oxidation and lipid and cholesterol synthesis that make up the myelin sheath (e.g., lipid saturases and lipid dehydrogenases (Stephenson et al., 2014; Cheli et al., 2020).

Dietary fasting is also capable of inducing changes in oligodendroglia. In the previously mentioned study (see "Metformin Rejuvenates Aged OPCs to Increase CNS

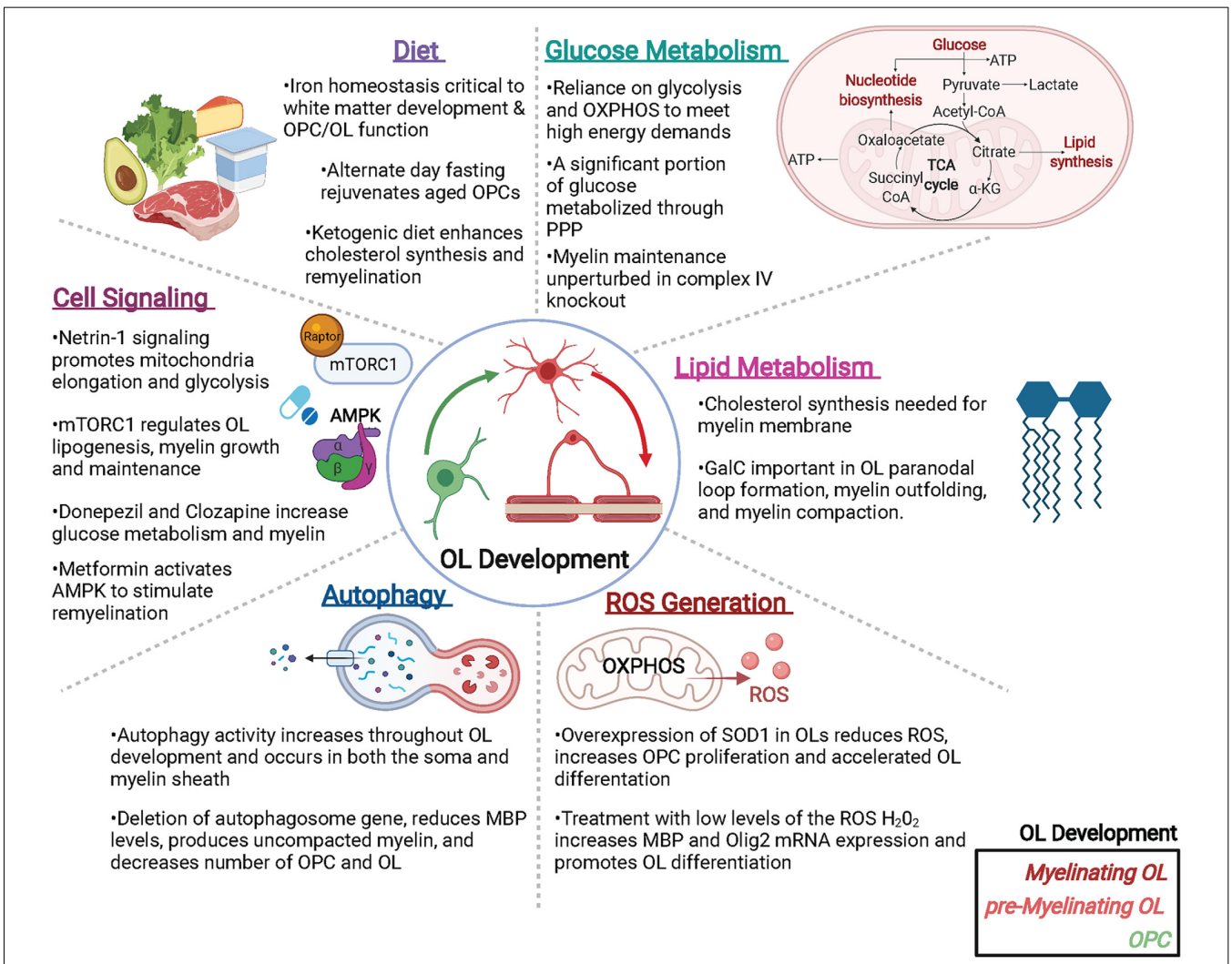

FIGURE 2 | Metabolic factors impacting oligodendroglial development and function. Oligodendrocytes (OLs) are metabolically active cells that both myelinate and provide trophic support to neurons, as well as supply metabolites to neurons and other cells of the CNS. Many metabolic factors can alter OL function including (but not limited to): glucose and lipid metabolism, reactive oxygen species (ROS) that can generate pro- or anti-OL effects, autophagy, cell signaling events, and diet. Abbreviations: PPP, pentose phosphate pathway; OXPHOS, oxidative phosphorylation; SOD, superoxide dismutase; mTORC1, mammalian target of Raptor complex I. Created with BioRender.com.

Remyelination" Section), Neumann and colleagues investigated the potential alternate day fasting (ADF) may have on OPC dynamics. As noted previously, aged OPCs were unable to undergo efficient differentiation as well as have decreased ATP production and basal respiration rates. ADF is capable of altering the aging processes by restricting caloric intake both of which induce changes to the body's metabolism (Heilbronn and Panda, 2019). The ADF group was given access to food on alternate days for 6 months compared to the control group which was able to feed *ad libitum*. Upon cessation of the ADF fasting period, demyelination was induced in cerebellar white matter by means of focal ethidium bromide injection. Immunohistological analysis revealed a two-fold increase in the number of mature myelinating cells (identified with the markers CC1 and MBP) in the ADF group when compared to the "old" controls. This finding supports the idea that ADF may prove to be beneficial for WM deficiencies, but more studies are warranted to fully assess its therapeutic efficacy in humans.

Other dietary therapies such as the ketogenic diet (KD) have been recognized for their positive effects on disease. The KD, first described in 1921, is well known for its antiseizure effects and as such is used to treat intractable epilepsy in both adults and children (Vining, 1999). The traditional KD consists of high fat, low carbohydrate, and limited but adequate protein to allow the body to transition away from using glucose for "fuel" and instead to using ketones from fat. While the exact underlying cellular and molecular mechanisms of the KD remain elusive, it is being explored for treatment in AD, PD, and amyotrophic lateral sclerosis (ALS) because of its positive effects on the brain. Accruing evidence, however, suggests that the KD may mechanistically be working through activation of ATP sensitive potassium channels in cells of the CNS and/or by inhibition of the mTOR pathway which interestingly is linked to myelination and AMPK activity (see Section "mTORC1 Signaling Regulates OL Myelination and Lipid Metabolism"). Therefore, it seems plausible that the KD should be able to alter OL dynamics as well, a concept Stumpf and others set out to investigate using a mouse model of Pelizaeus-Merzbacher disease (PMD), a hereditary leukodystrophy. PMD most often occurs *via* a duplication in the X-linked myelin gene, proteolipid protein 1 (*PLP1*), causing PLP-cholesterol accumulation and subsequently impaired protein-lipid transport to the myelin sheath. As a result, PMD presents with pathological hypomyelination and symptoms of nystagmus, spasticity, ataxia, and impaired cognitive development. Furthermore, late stage PMD is accompanied by progressive loss of OLs, axonal degeneration, and cortical atrophy, some of which were reversed after starting a KD (Stumpf et al., 2019).

PMD and control mice were fed either a high fat/low carbohydrate KD or a standard control diet for 2–12 weeks while monitoring ketone bodies such as beta-hydroxybutyrate, which in the brain helps facilitate cholesterol synthesis and is essential for myelin membrane growth (Koper et al., 1981; Saher et al., 2005). As expected, the mice on the KD saw a five-fold increase in blood ketone levels and a 70% drop in serum glucose in as little as 7 days from KD onset when compared to control mice. Remarkably, PMD mice on the KD significantly increased *PLP1* mRNA expression followed by increases in the number of Olig2+ cells and mature OLs. Furthermore, these changes in OL dynamics also resulted in more myelinated axons in the PMD-KD mice with the *g-ratio* matching that seen in WT control mice. Most importantly, these positive changes in myelination were able to restore normal function in the PMD mice. When assessing motor performance with the elevated beam test and rotarod test, control diet PMD mice exhibited progressive worsening of motor functions over time whereas, the PMD-KD mice retained motor fitness at WT levels. Independent of PMD pathology, the researchers confirmed the pro-OL/pro-myelin effects of the KD diet were also applicable in the cuprizone model of adult remyelination where during the cuprizone off/remyelination phase, mice on a KD diet saw accelerated repair 2 weeks into remyelination, evident by significant increases in mature OLs and reduction in the number of slips on the beam motor test (Stumpf et al., 2019). Hence when taken together, entering into a state of ketosis may prove beneficial for patients coping with WM diseases and in fact several clinical trials are currently underway to determine if the KD diet can reverse and repair WM damage in the CNS (ClinicalTrials.gov Identifier: NCT03718247, NCT04820478, NCT03509571, CT04530032, and NCT04701957).

CONCLUSION

Oligodendroglia are specialized cells whose metabolism is uniquely tuned to support its functions. From developmental myelination to adaptive myelination to myelin repair, OLs regulate a host of metabolic components to meet the energetic demands of both themselves and the axons they support. Disruptions in OL metabolism are likely to contribute to many neurological diseases including SCZ, PD, AD, and MS, all of which may benefit from next generation therapeutics that target or override OL metabolic pathways. Here we have summarized some of the key recent studies that address metabolic elements important to oligodendroglial function, such as the rate of glycolysis, lipid metabolism, ROS generation, and autophagy, as well as the intrinsic and extrinsic signaling pathways that regulate OL metabolism (**Figure 2**). While much has been revealed by these recent exciting advances, a great deal of future research is needed to fill in the gaps in knowledge between OL metabolism and OL function, both in health and in disease.

AUTHOR CONTRIBUTIONS

MN and HC wrote and edited the manuscript. All authors contributed to the article and approved the submitted version.

FUNDING

This work was supported by funding from National Institutes of Health (HC; NS114769), the National Multiple Sclerosis Society (HC; RG-1607-25279), and a Turner Dissertation Fellowship (MN).

REFERENCES

Accetta, R., Damiano, S., Morano, A., Mondola, P., Paternò, R., Avvedimento, E. V., et al. (2016). Reactive oxygen species derived from Nox3 and Nox5 drive differentiation of human oligodendrocytes. *Front. Cell. Neurosci.* 10:146. doi: 10.3389/fncel.2016.00146

Almeida, R. G., and Lyons, D. A. (2017). On myelinated axon plasticity and neuronal circuit formation and function. *J. Neurosci.* 37, 10023–10034. doi: 10.1523/JNEUROSCI.3185-16.2017

Amaral, A. I., Hadera, M. G., Tavares, J. M., Kotter, M. R., and Sonnewald, U. (2016). Characterization of glucose-related metabolic pathways in differentiated rat oligodendrocyte lineage cells. *Glia* 64, 21–34. doi: 10.1002/glia.22900

Ando, S., Tanaka, Y., Toyoda, Y., and Kon, K. (2003). Turnover of myelin lipids in aging brain. *Neurochem. Res.* 28, 5–13. doi: 10.1023/a:1021635826032

Bankston, A. N., Forston, M. D., Howard, R. M., Andres, K. R., Smith, A. E., Ohri, S. S., et al. (2019). Autophagy is essential for oligodendrocyte differentiation, survival, and proper myelination. *Glia* 67, 1745–1759. doi: 10.1002/glia.23646

Bansal, R., Winkler, S., and Bheddah, S. (1999). Negative regulation of oligodendrocyte differentiation by galactosphingolipids. *J. Neurosci.* 19, 7913–7924. doi: 10.1523/JNEUROSCI.19-18-07913.1999

Bathina, S., and Das, U. N. (2015). Brain-derived neurotrophic factor and its clinical implications. *Arch. Med. Sci.* 11, 1164–1178. doi: 10.5114/aoms.2015.56342

Baumann, N., and Pham-Dinh, D. (2001). Biology of oligodendrocyte and myelin in the mammalian central nervous system. *Physiol. Rev.* 81, 871–927. doi: 10.1152/physrev.2001.81.2.871

Bellani, M., Boschello, F., Delvecchio, G., Dusi, N., Altamura, C. A., Ruggeri, M., et al. (2016). DTI and myelin plasticity in bipolar disorder: integrating neuroimaging and neuropathological findings. *Front. Psychiatry* 7:21. doi: 10.3389/fpsyt.2016.00021

Berg, J. M., Tymoczko, J. L., and Stryer, L. (2002). *Biochemistry*. New York: W.H. Freeman.

Boggs, J. M., Gao, W., Zhao, J., Park, H.-J., Liu, Y., and Basu, A. (2010). Participation of galactosylceramide and sulfatide in glycosynapses between oligodendrocyte or myelin membranes. *FEBS Lett.* 584, 1771–1778. doi: 10.1016/j.febslet.2009.11.074

Boggs, J. M., and Wang, H. (2001). Effect of liposomes containing cerebroside and cerebroside sulfate on cytoskeleton of cultured oligodendrocytes. *J. Neurosci. Res.* 66, 242–253. doi: 10.1002/jnr.1217

Bonetto, G., Kamen, Y., Evans, K. A., and Káradóttir, R. T. (2020). Unraveling myelin plasticity. *Front. Cell. Neurosci.* 14:156. doi: 10.3389/fncel.2020.00156

Bosio, A., Büssow, H., Adam, J., and Stoffel, W. (1998). Galactosphingolipids and axono-glial interaction in myelin of the central nervous system. *Cell Tissue Res.* 292, 199–210. doi: 10.1007/s004410051051

Boullerne, A. I. (2016). The history of myelin. *Exp. Neurol.* 283, 431–445. doi: 10.1016/j.expneurol.2016.06.005

Brownsey, R. W., Boone, A. N., Elliott, J. E., Kulpa, J. E., and Lee, W. M. (2006). Regulation of acetyl-coa carboxylase. *Biochem. Soc. Trans.* 34, 223–227. doi: 10.1042/BST20060223

Bryant, M. R., Marta, C. B., Kim, F. S., and Bansal, R. (2009). Phosphorylation and lipid raft association of fibroblast growth factor receptor-2 in oligodendrocytes. *Glia* 57, 935–946).doi: 10.1002/glia.20818

Bujalka, H., Koenning, M., Jackson, S., Perreau, V. M., Pope, B., Hay, C. M., et al. (2013). MYRF is a membrane-associated transcription factor that autoproteolytically cleaves to directly activate myelin genes. *PLoS Biol.* 11:E1001625. doi: 10.1371/journal.pbio.1001625

Camandola, S., and Mattson, M. P. (2017). Brain metabolism in health, aging, and neurodegeneration. *EMBO J.* 36, 1474–1492. doi: 10.15252/embj.201695810

Campbell, J. M., Bellman, S. M., Stephenson, M. D., and Lisy, K. (2017). Metformin reduces all-cause mortality and diseases of ageing independent of its effect on diabetes control: a systematic review and meta-analysis. *Ageing Res. Rev.* 40, 31–44. doi: 10.1016/j.arr.2017.08.003

Catts, V. S., Derminio, D. S., Hahn, C.-G., and Weickert, C. S. (2015). Postsynaptic density levels of the NMDA receptor Nr1 subunit and PSD-95 protein in prefrontal cortex from people with schizophrenia. *NPJ Schizophrenia* 1:15037. doi: 10.1038/npjschz.2015.37

Chamberlain, K. A., Huang, N., Xie, Y., Licausi, F., Li, S., Li, Y., et al. (2021). Oligodendrocytes enhance axonal energy metabolism by deacetylation of mitochondrial proteins through transcellular delivery of SIRT2. *Neuron* 109, 3456–3472.e8. doi: 10.1016/j.neuron.2021.08.011

Checa, J., and Aran, J. M. (2020). Reactive oxygen species: drivers of physiological and pathological processes. *J. Inflamm. Res.* 13, 1057–1073. doi: 10.2147/JIR.S275595

Cheli, V. T., Correale, J., Paez, P. M., and Pasquini, J. M. (2020). Iron metabolism in oligodendrocytes and astrocytes, implications for myelination and remyelination. *ASN Neuro* 12:1759091420962681. doi: 10.1177/1759091420962681

Chen, X.-Q., and Mobley, W. C. (2019). Exploring the pathogenesis of alzheimer disease in basal forebrain cholinergic neurons: converging insights from alternative hypotheses. *Front. Neurosci.* 13:446. doi: 10.3389/fnins.2019.00446

Chrast, R., Saher, G., Nave, K.-A., and Verheijen, M. H. G. (2011). Lipid metabolism in myelinating glial cells: lessons from human inherited disorders and mouse models. *J. Lipid Res.* 52, 419–434. doi: 10.1194/jlr.R009761

Coetzee, T., Fujita, N., Dupree, J., Shi, R., Blight, A., Suzuki, K., et al. (1996). Myelination in the absence of galactocerebroside and sulfatide: normal structure with abnormal function and regional instability. *Cell* 86, 209–219. doi: 10.1016/s0092-8674(00)80093-8

Colonna, M., and Butovsky, O. (2017). Microglia function in the central nervous system during health and neurodegeneration. *Ann. Rev. Immunol.* 35, 441–468. doi: 10.1146/annurev-immunol-051116-052358

Cooper, G. M. (2000). "The cell: a molecular approach," in *Cell Membranes*, 2nd Edn. Sunderland, MA: Sinauer Associates.

Cui, X., Guo, Y.-E., Fang, J.-H., Shi, C.-J., Suo, N., Zhang, R., et al. (2019). Donepezil, a drug for Alzheimer's disease, promotes oligodendrocyte generation and remyelination. *Acta Pharmacol. Sin.* 40, 1386–1393. doi: 10.1038/s41401-018-0206-4

Deberardinis, R. J., and Thompson, C. B. (2012). Cellular metabolism and disease: what do metabolic outliers teach us. *Cell* 148, 1132–1144. doi: 10.1016/j.cell.2012.02.032

Decker, L. (2004). Lipid rafts and integrin activation regulate oligodendrocyte survival. *J. Neurosci.* 24, 3816–3825. doi: 10.1523/JNEUROSCI.5725-03.2004

del Río-Hortega, P. (1921). La glía de escasas radiaciones (oligodendroglía) boletín de la real sociedad española de historia natural. *Estudios Sobre la Neurologia* 21, 63–92.

del Río-Hortega, P. (2012). Studies on neuroglia: Glia with very few processes (oligodendroglia) by Pío del Río-Hortega. *Clin. Neuropathol.* 31, 440–459. doi: 10.5414/NP300999

del Río, L. A., and López-Huertas, E. (2016). Ros generation in peroxisomes and its role in cell signaling. *Plant. Cell Physiol.* 57, 1364–1376. doi: 10.1136/bmjopen-2019-029923

Dicko, A., Heng, Y. M., and Boggs, J. M. (2003). Interactions between glucosylceramide and galactosylceramide I3 sulfate and microstructures formed. *Biochim. Biophys. Acta* 1613, 87–100. doi: 10.1016/s0005-2736(03)00141-x

Dienel, G. A. (2018). Brain glucose metabolism: integration of energetics with function. *Physiol. Rev.* 99, 949–1045. doi: 10.1152/physrev.00062.2017

Edgar, N., and Sibille, E. (2012). A putative functional role for oligodendrocytes in mood regulation. *Trans. Psychiatry* 2, E109–E109. doi: 10.1038/tp.2012.34

Eisenstein, M. (2014). Molecular biology: remove, reuse, recycle. *Nature* 514, S2–S4. doi: 10.1038/514S2a

Eltony, S. A., Mohaseb, H. S., Sayed, M. M., and Ahmed, A. A. (2021). Metformin treatment confers protection of the optic nerve following photoreceptor degeneration. *Anat. Cell Biol.* 54, 249–258. doi: 10.5115/acb.20.320

Etxeberria, A., Hokanson, K. C., Dao, D. Q., Mayoral, S. R., Mei, F., Redmond, S. A., et al. (2016). Dynamic modulation of myelination in response to visual stimuli alters optic nerve conduction velocity. *J. Neurosci.* 36, 6937–6948. doi: 10.1523/JNEUROSCI.0908-16.2016

Faizi, M., Salimi, A., Seydi, E., Naserzadeh, P., Kouhnavard, M., Rahimi, A., et al. (2016). Toxicity of cuprizone a Cu^{2+} chelating agent on isolated mouse brain mitochondria: a justification for demyelination and subsequent behavioral

dysfunction. *Toxicol. Mech. Methods* 26, 276–283. doi: 10.3109/15376516.2016.1172284

Fünfschilling, U., Supplie, L. M., Mahad, D., Boretius, S., Saab, A. S., Edgar, J., et al. (2012). Glycolytic oligodendrocytes maintain myelin and long-term axonal integrity. *Nature* 485, 517–521. doi: 10.1038/nature11007

Fernandez-Marcos, P. J., and Nóbrega-Pereira, S. (2016). NADPH: new oxygen for the ROS theory of aging. *Oncotarget* 7, 50814–50815. doi: 10.18632/oncotarget.10744

Fields, R. D. (2010). Neuroscience. change in the brain's white matter. *Science* 330, 768–769. doi: 10.1126/science.1199139

Fyffe-Maricich, S. L., Karlo, J. C., Landreth, G. E., and Miller, R. H. (2011). The Erk2 mitogen-activated protein kinase regulates the timing of oligodendrocyte differentiation. *J. Neurosci.* 31, 843–850. doi: 10.1523/JNEUROSCI.3239-10.2011

Gansemer, E. R., Mccommis, K. S., Martino, M., King-Mcalpin, A. Q., Potthoff, M. J., Finck, B. N., et al. (2020). NADPH and glutathione redox link TCA cycle activity to endoplasmic reticulum homeostasis. *iScience* 23:101116. doi: 10.1016/j.isci.2020.101116

Gibson, E. M., Purger, D., Mount, C. W., Goldstein, A. K., Lin, G. L., Wood, L. S., et al. (2014). Neuronal activity promotes oligodendrogenesis and adaptive myelination in the mammalian brain. *Science* 344:1252304. doi: 10.1126/science.1252304

Gysin, R., Kraftsik, R., Sandell, J., Bovet, P., Chappuis, C., Conus, P., et al. (2007). Impaired glutathione synthesis in schizophrenia: convergent genetic and functional evidence. *Proc. Natl. Acad. Sci. U S A* 104, 16621–16626. doi: 10.1073/pnas.0706778104

Hakomori, S.-I. (2002). The glycosynapse. *Proc. Natl. Acad. Sci. U S A* 99, 225–232. doi: 10.1073/pnas.012540899

Harris, J. J., and Attwell, D. (2012). The energetics of CNS white matter. *J. Neurosci.* 32, 356–371. doi: 10.1523/JNEUROSCI.3430-11.2012

Heilbronn, L. K., and Panda, S. (2019). Alternate-day fasting gets a safe bill of health. *Cell Metab.* 30, 411–413. doi: 10.1016/j.cmet.2019.08.006

Herndon, R. C., Lancaster, J. L., Giedd, J. N., and Fox, P. T. (1998). Quantification of white matter and gray matter volumes from three-dimensional magnetic resonance volume studies using fuzzy classifiers. *J. Magn. Reson. Imaging* 8, 1097–1105. doi: 10.1002/jmri.1880080515

Hertz, L. (2013). The glutamate-glutamine (GABA) cycle: importance of late postnatal development and potential reciprocal interactions between biosynthesis and degradation. *Front. Endocrinol.* 4:59. doi: 10.3389/fendo.2013.00059

Holley, A. K., Bakthavatchalu, V., Velez-Roman, J. M., and St Clair, D. K. (2011). Manganese superoxide dismutase: guardian of the powerhouse. *Int. J. Mol. Sci.* 12, 7114–7162. doi: 10.3390/ijms12107114

Holmes, E., Tsang, T. M., Huang, J. T.-J., Leweke, F. M., Koethe, D., Gerth, C. W., et al. (2006). Metabolic profiling of CSF: evidence that early intervention may impact on disease progression and outcome in schizophrenia. *PLoS Med.* 3:E327. doi: 10.1371/journal.pmed.0030327

Houshmand, F., Barati, M., Golab, F., Ramezani-Sefidar, S., Tanbakooie, S., Tabatabaei, M., et al. (2019). Metformin-induced AMPK activation stimulates remyelination through induction of neurotrophic factors, downregulation of Nogoa and recruitment of Olig2+ precursor cells in the cuprizone murine model of multiple sclerosis. *Daru* 27, 583–592. doi: 10.1007/s40199-019-00286-z

Ishibashi, T., Dupree, J. L., Ikenaka, K., Hirahara, Y., Honke, K., Peles, E., et al. (2002). A myelin galactolipid, sulfatide, is essential for maintenance of ion channels on myelinated axon but not essential for initial cluster formation. *J. Neurosci.* 22, 6507–6514. doi: 10.1523/JNEUROSCI.22-15-06507.2002

Jahn, O., Tenzer, S., and Werner, H. B. (2009). Myelin proteomics: molecular anatomy of an insulating sheath. *Mol. Neurobiol.* 40, 55–72. doi: 10.1007/s12035-009-8071-2

Johnson, E. M., and Tuszynski, M. H. (2008). "Chapter 4 - Neurotrophic factors," in *CNS Regeneration*, 2nd Edn., eds J. H. M. Kordower and M. H. Tuszynski (San Diego, CA: Academic Press), 95–144.

Khedkar, G. D., Prakash, B., Khedkar, C. D., and Chopade, B. A. (2016). "Nucleic acids," in *Encyclopedia of Food and Health*, eds B. Caballero P. M. Finglas and F. Toldrá (Oxford: Academic Press), 84–92.

Kilanczyk, E., Saraswat Ohri, S., Whittemore, S. R., and Hetman, M. (2016). Antioxidant protection of NADPH-depleted oligodendrocyte precursor cells is dependent on supply of reduced glutathione. *ASN Neuro* 8:1759091416660404. doi: 10.1177/1759091416660404

Kim, S., Chung, A. Y., Na, J. E., Lee, S. J., Jeong, S. H., Kim, E., et al. (2019). Myelin degeneration induced by mutant superoxide dismutase 1 accumulation promotes amyotrophic lateral sclerosis. *Glia* 67, 1910–1921. doi: 10.1002/glia.23669

Kim, U. S., Mahroo, O. A., Mollon, J. D., and Yu-Wai-Man, P. (2021). Retinal ganglion cells—diversity of cell types and clinical relevance. *Front. Neurol.* 12:661938. doi: 10.3389/fneur.2021.661938

Kirby, B. B., Takada, N., Latimer, A. J., Shin, J., Carney, T. J., Kelsh, R. N., et al. (2006). *In vivo* time-lapse imaging shows dynamic oligodendrocyte progenitor behavior during zebrafish development. *Nat. Neurosci.* 9, 1506–1511. doi: 10.1038/nn1803

Kirkman, H. N., Galiano, S., and Gaetani, G. F. (1987). The function of catalase-bound NADPH. *J. Biol. Chem.* 262, 660–666.

Koepsell, H. (2021). "General overview of organic cation transporters in brain," in *Organic Cation Transporters in the Central Nervous System*, ed L. C. Daws (Cham: Springer International Publishing), 1–13.

Kondo, T., and Raff, M. (2000). The Id4 HLH protein and the timing of oligodendrocyte differentiation. *EMBO J.* 19, 1998–2007. doi: 10.1093/emboj/19.9.1998

Koper, J. W., Lopes-Cardozo, M., and Van Golde, L. M. (1981). Preferential utilization of ketone bodies for the synthesis of myelin cholesterol *in vivo*. *Biochim. Biophys. Acta* 666, 411–417. doi: 10.1016/0005-2760(81)90300-3

Kowalik, M. A., Columbano, A., and Perra, A. (2017). Emerging role of the pentose phosphate pathway in hepatocellular carcinoma. *Front. Oncol.* 7:87. doi: 10.3389/fonc.2017.00087

La Flamme, A. C., Abernethy, D., Sim, D., Goode, L., Lockhart, M., Bourke, D., et al. (2020). Safety and acceptability of clozapine and risperidone in progressive multiple sclerosis: a phase I, randomised, blinded, placebo-controlled trial. *BMJ Neurol. Open* 2:e000060. doi: 10.1136/bmjno-2020-000060

Lambert, A. J., and Brand, M. D. (2009). Reactive oxygen species production by mitochondria. *Methods Mol. Biol.* 554, 165–181. doi: 10.1007/978-1-59745-521-3_11

Lamming, D. W., and Sabatini, D. M. (2013). A central role for mTOR in lipid homeostasis. *Cell Metab.* 18, 465–469. doi: 10.1016/j.cmet.2013.08.002

Lebrun-Julien, F., Bachmann, L., Norrmén, C., Trötzmüller, M., Köfeler, H., Rüegg, M. A., et al. (2014). Balanced mTORC1 activity in oligodendrocytes is required for accurate CNS myelination. *J. Neurosci.* 34:8432. doi: 10.1523/JNEUROSCI.1105-14.2014

Leyshon, B. J., Radlowski, E. C., Mudd, A. T., Steelman, A. J., and Johnson, R. W. (2016). Postnatal iron deficiency alters brain development in piglets. *J. Nutr.* 146, 1420–1427. doi: 10.3945/jn.115.223636

Lobo, V., Patil, A., Phatak, A., and Chandra, N. (2010). Free radicals, antioxidants and functional foods: impact on human health. *Pharmacogn. Rev.* 4, 118–126).doi: 10.4103/0973-7847.70902

Marcus, J., Dupree, J. L., and Popko, B. (2000). Effects of galactolipid elimination on oligodendrocyte development and myelination. *Glia* 30, 319–328. doi: 10.1002/(sici)1098-1136(200006)30:4<319::aid-glia10>3.0.co;2-t

Massicotte, C., Barber, D. S., Jortner, B. S., and Ehrich, M. (2001). Nerve conduction and ATP concentrations in sciatic-tibial and medial plantar nerves of hens given phenyl saligenin phosphate. *Neurotoxicology* 22, 91–98. doi: 10.1016/s0161-813x(00)00004-8

Masson, J., Emerit, M. B., Hamon, M., and Darmon, M. (2012). Serotonergic signaling: multiple effectors and pleiotropic effects. *Wiley Interdiscipl. Rev. Membrane Transport Signal.* 1, 685–713. doi: 10.1002/wmts.50

Matsui, T., Omuro, H., Liu, Y.-F., Soya, M., Shima, T., Mcewen, B. S., et al. (2017). Astrocytic glycogen-derived lactate fuels the brain during exhaustive exercise to maintain endurance capacity. *Proc. Natl. Acad. Sci. U S A* 114, 6358–6363. doi: 10.1073/pnas.1702739114

Meltzer, H. Y. (1994). An overview of the mechanism of action of clozapine. *J. Clin. Psychiatry* 55, 47–52.

Messias, M. C. F., Mecatti, G. C., Priolli, D. G., and De Oliveira Carvalho, P. (2018). Plasmalogen lipids: functional mechanism and their involvement in

gastrointestinal cancer. *Lipids Health Dis.* 17:41. doi: 10.1186/s12944-018-0685-9

Miron, V. E., Rajasekharan, S., Jarjour, A. A., Zamvil, S. S., Kennedy, T. E., and Antel, J. P. (2007). Simvastatin regulates oligodendroglial process dynamics and survival. *Glia* 55, 130–143. doi: 10.1002/glia.20441

Monin, A., Baumann, P., Griffa, A., Xin, L., Mekle, R., Fournier, M., et al. (2015). Glutathione deficit impairs myelin maturation: relevance for white matter integrity in schizophrenia patients. *Mol. Psychiatry* 20, 827–838. doi: 10.1038/mp.2014.88

Montani, L. (2021). Lipids in regulating oligodendrocyte structure and function. *Semin. Cell Dev. Biol.* 112, 114–122. doi: 10.1016/j.semcdb.2020.07.016

Moore, S., Meschkat, M., Ruhwedel, T., Trevisiol, A., Tzvetanova, I. D., Battefeld, A., et al. (2020). A role of oligodendrocytes in information processing. *Nat. Commun.* 11:5497. doi: 10.1038/s41467-020-19152-7

Mount, C. W., and Monje, M. (2017). Wrapped to adapt: experience-dependent myelination. *Neuron* 95, 743–756. doi: 10.1016/j.neuron.2017.07.009

Nakamura, D. S., Lin, Y. H., Khan, D., Gothié, J.-D. M., De Faria Jr, O., Dixon, J. A., et al. (2021). Mitochondrial dynamics and bioenergetics regulated by Netrin-1 in oligodendrocytes. *Glia* 69, 392–412. doi: 10.1002/glia.23905

Narayanan, S. P., Flores, A. I., Wang, F., and Macklin, W. B. (2009). Akt signals through the mammalian target of rapamycin pathway to regulate CNS myelination. *J. Neurosci.* 29:6860. doi: 10.1523/JNEUROSCI.0232-09.2009

Neumann, B., Baror, R., Zhao, C., Segel, M., Dietmann, S., Rawji, K. S., et al. (2019). Metformin restores CNS remyelination capacity by rejuvenating aged stem cells. *Cell Stem Cell* 25, 473–485.e8. doi: 10.1016/j.stem.2019.08.015

Norton, W. T., and Cammer, W. (1984). "Isolation and characterization of myelin," in *Myelin*, ed P. Morell (Boston, MA: Springer), 147–195.

Norton, W., and Poduslo, S. E. (1973). Myelination in rat brain: changes in myelin composition during brain maturation 1. *J. Neurochem.* 21, 759–773.

Pöyhönen, S., Er, S., Domanskyi, A., and Airavaara, M. (2019). Effects of neurotrophic factors in glial cells in the central nervous system: expression and properties in neurodegeneration and injury. *Front. Physiol.* 10:486. doi: 10.3389/fphys.2019.00486

Panchal, S. K., Poudyal, H., Iyer, A., Nazer, R., Alam, A., Diwan, V., et al. (2011). High-carbohydrate high-fat diet-induced metabolic syndrome and cardiovascular remodeling in rats. *J. Cardiovasc. Pharmacol.* 57, 611–624. doi: 10.1097/FJC.0b013e31821b1379

Paolicelli, R. C., Bolasco, G., Pagani, F., Maggi, L., Scianni, M., Panzanelli, P., et al. (2011) Synaptic pruning by microglia is necessary for normal brain development. *Science* 333, 1456–1458. doi: 10.1126/science.1202529

Papuć, E., and Rejdak, K. (2018). The role of myelin damage in Alzheimer's disease pathology. *Arch. Med. Sci.* 16, 345–351. doi: 10.5114/aoms.2018.76863

Patra, K. C., and Hay, N. (2014). The pentose phosphate pathway and cancer. *Trends Biochem. Sci.* 39, 347–354. doi: 10.1016/j.tibs.2014.06.005

Peckham, H., Giuffrida, L., Wood, R., Gonsalvez, D., Ferner, A., Kilpatrick, T. J., et al. (2016). Fyn is an intermediate kinase that BDNF utilizes to promote oligodendrocyte myelination. *Glia* 64, 255–269. doi: 10.1002/glia.22927

Pernicova, I., and Korbonits, M. (2014). Metformin—mode of action and clinical implications for diabetes and cancer. *Nat. Rev. Endocrinol.* 10, 143–156. doi: 10.1038/nrendo.2013.256

Petrov, A. M., Kasimov, M. R., and Zefirov, A. L. (2016). Brain cholesterol metabolism and its defects: linkage to neurodegenerative diseases and synaptic dysfunction. *Acta Naturae* 8, 58–73. doi: 10.32607/20758251-2016-8-1-58-73

Pinteaux, E., Perraut, M., and Tholey, G. (1998). Distribution of mitochondrial manganese superoxide dismutase among rat glial cells in culture. *Glia* 22, 408–414.

Pizzino, G., Irrera, N., Cucinotta, M., Pallio, G., Mannino, F., Arcoraci, V., et al. (2017). Oxidative stress: harms and benefits for human health. *Oxid. Med. Cell Longev.* 2017:8416763. doi: 10.1155/2017/8416763

Prabakaran, S., Swatton, J., Ryan, M., Huffaker, S., Huang, J.-J., Griffin, J., et al. (2004). Mitochondrial dysfunction in schizophrenia: evidence for compromised brain metabolism and oxidative stress. *Mol. Psychiatry* 9, 684–697. doi: 10.1038/sj.mp.4001511

Rabinowitz, J. D., and White, E. (2010). Autophagy and metabolism. *Science* 330, 1344–1348. doi: 10.1126/science.1193497

Relucio, J., Menezes, M. J., Miyagoe-Suzuki, Y., Takeda, S., and Colognato, H. (2012). Laminin regulates postnatal oligodendrocyte production by promoting oligodendrocyte progenitor survival in the subventricular zone. *Glia* 60, 1451–1467. doi: 10.1002/glia.22365

Relucio, J., Tzvetanova, I. D., Ao, W., Lindquist, S., and Colognato, H. (2009). Laminin alters Fyn regulatory mechanisms and promotes oligodendrocyte development. *J. Neurosci.* 29, 11794–11806. doi: 10.1523/JNEUROSCI.0888-09.2009

Rinholm, J. E., Hamilton, N. B., Kessaris, N., Richardson, W. D., Bergersen, L. H., and Attwell, D. (2011). Regulation of oligodendrocyte development and myelination by glucose and lactate. *J. Neurosci.* 31, 538–548. doi: 10.1523/JNEUROSCI.3516-10.2011

Rogatzki, M. J., Ferguson, B. S., Goodwin, M. L., and Gladden, L. B. (2015). Lactate is always the end product of glycolysis. *Front. Neurosci.* 9, 22–22. doi: 10.3389/fnins.2015.00022

Rone, M. B., Cui, Q.-L., Fang, J., Wang, L.-C., Zhang, J., Khan, D., et al. (2016). Oligodendrogliopathy in multiple sclerosis: low glycolytic metabolic rate promotes oligodendrocyte survival. *J. Neurosci.* 36:4698. doi: 10.1523/JNEUROSCI.4077-15.2016

Rotermund, C., Machetanz, G., and Fitzgerald, J. C. (2018). The therapeutic potential of metformin in neurodegenerative diseases. *Front. Endocrinol. (Lausanne)* 9:400. doi: 10.3389/fendo.2018.00400

Rowitch, D. H., and Kriegstein, A. R. (2010). Developmental genetics of vertebrate glial-cell specification. *Nature* 468, 214–222. doi: 10.1038/nature09611

Russell, D. W., Halford, R. W., Ramirez, D. M., Shah, R., and Kotti, T. (2009). Cholesterol 24-hydroxylase: an enzyme of cholesterol turnover in the brain. *Annu. Rev. Biochem.* 78, 1017–1040. doi: 10.1146/annurev.biochem.78.072407.103859

Sánchez-Abarca, L. I., Tabernero, A., and Medina, J. M. (2001). Oligodendrocytes use lactate as a source of energy and as a precursor of lipids. *Glia* 36, 321–329. doi: 10.1002/glia.1119

Saab, A. S., Tzvetanova, I. D., and Nave, K.-A. (2013). The role of myelin and oligodendrocytes in axonal energy metabolism. *Curr. Opin. Neurobiol.* 23, 1065–1072. doi: 10.1016/j.conb.2013.09.008

Saab, A. S., Tzvetavona, I. D., Trevisiol, A., Baltan, S., Dibaj, P., Kusch, K., et al. (2016). Oligodendroglial NMDA receptors regulate glucose import and axonal energy metabolism. *Neuron* 91, 119–132. doi: 10.1016/j.neuron.2016.05.016

Sabatini, D. M. (2017). Twenty-five years of mTOR: uncovering the link from nutrients to growth. *Proc. Natl. Acad. Sci. U S A* 114:11818. doi: 10.1073/pnas.1716173114

Saher, G., Brügger, B., Lappe-Siefke, C., Möbius, W., Tozawa, R.-I., Wehr, M. C., et al. (2005). High cholesterol level is essential for myelin membrane growth. *Nat. Neurosci.* 8, 468–475. doi: 10.1038/nn1426

Saher, G., Quintes, S., and Nave, K.-A. (2011). Cholesterol: a novel regulatory role in myelin formation. *Neuroscientist* 17, 79–93. doi: 10.1177/1073858410373835

Said Ahmed, M., Hung, W. Y., Zu, J. S., Hockberger, P., and Siddique, T. (2000). Increased reactive oxygen species in familial amyotrophic lateral sclerosis with mutations in Sod1. *J. Neurol. Sci.* 176, 88–94. doi: 10.1016/s0022-510x(00)00317-8

Saito, E. R., Miller, J. B., Harari, O., Cruchaga, C., Mihindukulasuriya, K. A., Kauwe, J. S. K., et al. (2021). Alzheimer's disease alters oligodendrocytic glycolytic and ketolytic gene expression. *Alzheimer's Dement.* 17, 1474–1486. doi: 10.1002/alz.12310

Sato-Bigbee, C., Pal, S., and Chu, A. K. (1999). Different neuroligands and signal transduction pathways stimulate creb phosphorylation at specific developmental stages along oligodendrocyte differentiation. *J. Neurochem.* 72, 139–147. doi: 10.1046/j.1471-4159.1999.0720139.x

Scalzo, P., Kümmer, A., Bretas, T. L., Cardoso, F., and Teixeira, A. L. (2010). Serum levels of brain-derived neurotrophic factor correlate with motor impairment in parkinson's disease. *J. Neurol.* 257, 540–545. doi: 10.1007/s00415-009-5357-2

Schmitt, S., Cantuti Castelvetri, L., and Simons, M. (2015). Metabolism and functions of lipids in myelin. *Biochim. Biophys. Acta* 1851, 999–1005. doi: 10.1016/j.bbalip.2014.12.016

Schmitt, A., Hasan, A., Gruber, O., and Falkai, P. (2011). Schizophrenia as a disorder of disconnectivity. *Eur. Arch. Psychiatry Clin. Neurosci.* 261, S150–S154. doi: 10.1007/s00406-011-0242-2

Shimano, H., and Sato, R. (2017). Srebp-regulated lipid metabolism: convergent physiology—divergent pathophysiology. *Nat. Rev. Endocrinol.* 13, 710–730. doi: 10.1038/nrendo.2017.91

Shirasaka, Y., Lee, N., Zha, W., Wagner, D., and Wang, J. (2016). Involvement of organic cation transporter 3 (Oct3/Slc22a3) in the bioavailability and pharmacokinetics of antidiabetic metformin in mice. *Drug Metab. Pharmacokinet.* 31, 385–388. doi: 10.1016/j.dmpk.2016.04.005

Sies, H. (2015). Oxidative stress: a concept in redox biology and medicine. *Redox Biol.* 4, 180–183. doi: 10.1016/j.redox.2015.01.002

Sies, H., and Jones, D. P. (2020). Reactive oxygen species (Ros) as pleiotropic physiological signalling agents. *Nat. Rev. Mol. Cell Biol.* 21, 363–383. doi: 10.1038/s41580-020-0230-3

Simons, M., and Nave, K. A. (2015). Oligodendrocytes: myelination and axonal support. *Cold Spring Harb. Perspect. Biol.* 8:a020479. doi: 10.1101/cshperspect.a020479

Slemmer, J. E., Shacka, J. J., Sweeney, M. I., and Weber, J. T. (2008). Antioxidants and free radical scavengers for the treatment of stroke, traumatic brain injury and aging. *Curr. Med. Chem.* 15, 404–414. doi: 10.2174/092986708783497337

Sohrabji, F., and Lewis, D. K. (2006). Estrogen-BDNF interactions: implications for neurodegenerative diseases. *Front. Neuroendocrinol.* 27, 404–414. doi: 10.1016/j.yfrne.2006.09.003

Soliman, G. A. (2011). The integral role of mTOR in lipid metabolism. *Cell Cycle* 10, 861–862. doi: 10.4161/cc.10.6.14930

Spaas, J., Van Veggel, L., Schepers, M., Tiane, A., Van Horssen, J., Wilson, D. M., et al. (2021). Oxidative stress and impaired oligodendrocyte precursor cell differentiation in neurological disorders. *Cell. Mol. Life Sci.* 78, 4615–4637. doi: 10.1007/s00018-021-03802-0

Spitzer, S. O., Sitnikov, S., Kamen, Y., Evans, K. A., Kronenberg-Versteeg, D., Dietmann, S., et al. (2019). Oligodendrocyte progenitor cells become regionally diverse and heterogeneous with age. *Neuron* 101, 459–471.e5. doi: 10.1016/j.neuron.2018.12.020

Stahon, K. E., Bastian, C., Griffith, S., Kidd, G. J., Brunet, S., and Baltan, S. (2016). Age-related changes in axonal and mitochondrial ultrastructure and function in white matter. *J. Neurosci.* 36:9990. doi: 10.1523/JNEUROSCI.1316-16.2016

Steiner, J., Martins-De-Souza, D., Schiltz, K., Sarnyai, Z., Westphal, S., Isermann, B., et al. (2014). Clozapine promotes glycolysis and myelin lipid synthesis in cultured oligodendrocytes. *Front. Cell. Neurosci.* 8:384. doi: 10.3389/fncel.2014.00384

Stephenson, E., Nathoo, N., Mahjoub, Y., Dunn, J. F., and Yong, V. W. (2014). Iron in multiple sclerosis: roles in neurodegeneration and repair. *Nat. Rev. Neurol.* 10, 459–468. doi: 10.1038/nrneurol.2014.118

Stone, W. S., Faraone, S. V., Su, J., Tarbox, S. I., Van Eerdewegh, P., and Tsuang, M. T. (2004). Evidence for linkage between regulatory enzymes in glycolysis and schizophrenia in a multiplex sample. *Am. J. Med. Genet. B Neuropsychiatr. Genet.* 127B, 5–10. doi: 10.1002/ajmg.b.20132

Stumpf, S. K., Berghoff, S. A., Trevisiol, A., Spieth, L., Düking, T., Schneider, L. V., et al. (2019). Ketogenic diet ameliorates axonal defects and promotes myelination in pelizaeus-merzbacher disease. *Acta Neuropathol.* 138, 147–161. doi: 10.1007/s00401-019-01985-2

Suzuki, N., Hyodo, M., Hayashi, C., Mabuchi, Y., Sekimoto, K., Onchi, C., et al. (2019). Laminin α2, α4, and α5 chains positively regulate migration and survival of oligodendrocyte precursor cells. *Sci. Rep.* 9:19882. doi: 10.1038/s41598-019-56488-7

Teigler, A., Komljenovic, D., Draguhn, A., Gorgas, K., and Just, W. W. (2009). Defects in myelination, paranode organization and purkinje cell innervation in the ether lipid-deficient mouse cerebellum. *Hum. Mol. Genet.* 18, 1897–1908. doi: 10.1093/hmg/ddp110

Thorburne, S. K., and Juurlink, B. H. J. (1996). Low glutathione and high iron govern the susceptibility of oligodendroglial precursors to oxidative stress. *J. Neurochem.* 67, 1014–1022. doi: 10.1046/j.1471-4159.1996.67031014.x

Tune, L., Tiseo, P. J., Ieni, J., Perdomo, C., Pratt, R. D., Votaw, J. R., et al. (2003). Donepezil HCl (E2020) maintains functional brain activity in patients with Alzheimer disease: results of a 24-week, double-blind, placebo-controlled study. *Am. J. Geriatr. Psychiatry* 11, 169–177. doi: 10.1097/00019442-200303000-00007

Vatish, M., Yamada, E., Pessin, J. E., and Bastie, C. C. (2009). Fyn kinase function in lipid utilization: a new upstream regulator of AMPK activity. *Arch. Physiol. Biochem.* 115, 191–198. doi: 10.1080/13813450903164348

Veiga, S., Ly, J., Chan, P. H., Bresnahan, J. C., and Beattie, M. S. (2011). Sod1 overexpression improves features of the oligodendrocyte precursor response *in vitro*. *Neurosci. Lett.* 503, 10–14. doi: 10.1016/j.neulet.2011.07.053

Vilchis-Landeros, M. M., Matuz-Mares, D., and Vázquez-Meza, H. (2020). Regulation of metabolic processes by hydrogen peroxide generated by NADPH oxidases. *Processes* 8:1424. doi: 10.3390/pr8111424

Villanueva-Paz, M., Cotán, D., Garrido-Maraver, J., Oropesa-Ávila, M., De La Mata, M., Delgado-Pavón, A., et al. (2016). "AMPK regulation of cell growth, apoptosis, autophagy, and bioenergetics," in *Amp-Activated Protein Kinase*, eds M. D. Cordero and B. Viollet (Cham: Springer International Publishing), 45–71.

Vining, E. P. (1999). Clinical efficacy of the ketogenic diet. *Epilepsy Res.* 37, 181–190. doi: 10.1016/s0920-1211(99)00070-4

Virchow, R. (1856). *Gesammelte Abhandlungen zur Wissenschaftlischen Medizin*. Frankfurt A. M.: Meidinger Sohn & Comp..

Wang, S., Sdrulla, A., Johnson, J. E., Yokota, Y., and Barres, B. A. (2001). A role for the helix-loop-helix protein Id2 in the control of oligodendrocyte development. *Neuron* 29, 603–614. doi: 10.1016/s0896-6273(01)00237-9

Warf, B. C., Fok-Seang, J., and Miller, R. H. (1991). Evidence for the ventral origin of oligodendrocyte precursors in the rat spinal cord. *J. Neurosci.* 11, 2477–2488. doi: 10.1523/JNEUROSCI.11-08-02477.1991

Weinhard, L., Di Bartolomei, G., Bolasco, G., Machado, P., Schieber, N. L., Neniskyte, U., et al. (2018). Microglia remodel synapses by presynaptic trogocytosis and spine head filopodia induction. *Nat. Commun.* 9:1228. doi: 10.1038/s41467-018-03566-5

Yu, Y., Herman, P., Rothman, D. L., Agarwal, D., and Hyder, F. (2017). Evaluating the gray and white matter energy budgets of human brain function. *J. Cereb. Blood Flow Metab.* 38, 1339–1353. doi: 10.1177/0271678X17708691

Zatorre, R. J., Fields, R. D., and Johansen-Berg, H. (2012). Plasticity in gray and white: neuroimaging changes in brain structure during learning. *Nat. Neurosci.* 15, 528–536).doi: 10.1038/nn.3045

Zhang, X., Wang, R., Hu, D., Sun, X., Fujioka, H., Lundberg, K., et al. (2020). Oligodendroglial glycolytic stress triggers inflammasome activation and neuropathology in Alzheimer's disease. *Sci. Adv.* 6:Eabb8680. doi: 10.1126/sciadv.abb8680

Zhou, G., Myers, R., Li, Y., Chen, Y., Shen, X., Fenyk-Melody, J., et al. (2001). Role of AMP-activated protein kinase in mechanism of metformin action. *J. Clin. Invest.* 108, 1167–1174. doi: 10.1172/JCI13505

Conflict of Interest: The authors declare that the research was conducted in the absence of any commercial or financial relationships that could be construed as a potential conflict of interest.

Publisher's Note: All claims expressed in this article are solely those of the authors and do not necessarily represent those of their affiliated organizations, or those of the publisher, the editors and the reviewers. Any product that may be evaluated in this article, or claim that may be made by its manufacturer, is not guaranteed or endorsed by the publisher.

Copyright © 2022 Narine and Colognato. This is an open-access article distributed under the terms of the Creative Commons Attribution License (CC BY). The use, distribution or reproduction in other forums is permitted, provided the original author(s) and the copyright owner(s) are credited and that the original publication in this journal is cited, in accordance with accepted academic practice. No use, distribution or reproduction is permitted which does not comply with these terms.

frontiers | Frontiers in Cellular Neuroscience

ORIGINAL RESEARCH
published: 28 April 2022
doi: 10.3389/fncel.2022.833186

The Cellular Senescence Factor Extracellular HMGB1 Directly Inhibits Oligodendrocyte Progenitor Cell Differentiation and Impairs CNS Remyelination

*Megan E. Rouillard[1], Jingwen Hu[2], Pearl A. Sutter[1], Hee Won Kim[2], Jeffrey K. Huang[2] and Stephen J. Crocker[1]**

[1]Department of Neuroscience, University of Connecticut School of Medicine, Farmington, CT, United States, [2]Department of Biology and Center for Cell Reprogramming, Georgetown University, Washington, DC, United States

HMGB1 is a highly conserved, ubiquitous protein in eukaryotic cells. HMGB1 is normally localized to the nucleus, where it acts as a chromatin associated non-histone binding protein. In contrast, extracellular HMGB1 is an alarmin released by stressed cells to act as a danger associated molecular pattern (DAMP). We have recently determined that progenitor cells from multiple sclerosis patients exhibit a cellular senescent phenotype and release extracellular HMGB1 which directly impaired the maturation of oligodendrocyte progenitor cells (OPCs) to myelinating oligodendrocytes (OLs). Herein, we report that administration of recombinant HMGB1 into the spinal cord at the time of lysolecithin administration resulted in arrest of OPC differentiation *in vivo*, and a profound impairment of remyelination. To define the receptor by which extracellular HMGB1 mediates its inhibitory influence on OPCs to impair OL differentiation, we tested selective inhibitors against the four primary receptors known to mediate the effects of HMGB1, the toll-like receptors (TLRs)-2, -4, -9 or the receptor for advanced glycation end-products (RAGE). We found that inhibition of neither TLR9 nor RAGE increased OL differentiation in the presence of HMGB1, while inhibition of TLR4 resulted in partial restoration of OL differentiation and inhibiting TLR2 fully restored differentiation of OLs in the presence of HMGB1. Analysis of transcriptomic data (RNAseq) from OPCs identified an overrepresentation of NFκB regulated genes in OPCs when in the presence of HMGB1. We found that application of HMGB1 to OPCs in culture resulted in a rapid and concentration dependent shift in NFκB nuclear translocation which was also attenuated with coincident TLR2 inhibition. These data provide new information on how extracellular HMGB1 directly affects the differentiation potential of OPCs. Recent and past evidence for elevated HMGB1 released from senescent progenitor cells within demyelinated lesions in the MS brain suggests that a greater understanding of how this molecule acts on OPCs may unfetter the endogenous remyelination potential in MS.

Keywords: cellular senescence, myelin, multiple sclerosis, lysolecithin (LPC), microglia, TLR2, spinal cord

OPEN ACCESS

Edited by:
Davide Lecca,
University of Milan, Italy

Reviewed by:
Niels Hellings,
University of Hasselt, Belgium
Jessica Louise Fletcher,
University of Tasmania, Australia

****Correspondence:***
Stephen J. Crocker
crocker@uchc.edu

Specialty section:
This article was submitted to Non-Neuronal Cells, a section of the journal Frontiers in Cellular Neuroscience

Received: *10 December 2021*
Accepted: *23 March 2022*
Published: *28 April 2022*

Citation:
Rouillard ME, Hu J, Sutter PA, Kim HW, Huang JK and Crocker SJ (2022) The Cellular Senescence Factor Extracellular HMGB1 Directly Inhibits Oligodendrocyte Progenitor Cell Differentiation and Impairs CNS Remyelination. Front. Cell. Neurosci. 16:833186. doi: 10.3389/fncel.2022.833186

INTRODUCTION

Multiple sclerosis (MS) is a debilitating autoimmune disease affecting myelination of the central nervous system (CNS). Worsening disability among MS patients with progressive forms of disease is attributable to chronic loss of oligodendrocytes (OLs) and myelin, as well as the failure of oligodendrocyte progenitor cells (OPCs) to differentiate into mature OLs to replace lost myelin (Nicaise et al., 2019). This differentiation failure occurs even as OPCs populate the demyelinated lesions in the MS brain, indicating the presence of anti-differentiation factors or the loss of pro-differentiation factors (Wolswijk, 1998, 2002; Chang et al., 2002). It is hypothesized that manipulating these factors may offer a mechanism to halt disease progression and restore neurological function by promoting myelination in the brain and spinal cord (Brück et al., 2013; Faissner and Gold, 2019).

Neural progenitor cells (NPCs) are an early progenitor cell type with the capability to differentiate into neurons, astrocytes, or OLs, depending on the environmental cues they encounter (Chang et al., 2002; Gudi et al., 2014). Previous work in our lab determined that induced pluripotent stem cells (iPSCs) obtained from primary progressive MS (PPMS) patients and subsequently differentiated to NPCs were deficient in supporting myelin regeneration both *in vitro* and *in vivo* when compared to iPS-derived NPCs from age matched controls (Nicaise et al., 2017). It was initially reported, and recently independently confirmed by others (Mutukula et al., 2021), that NPCs from PPMS samples *in vitro* exhibit a senescent phenotype, and validated the finding that Sox2+ progenitor cells in progressive MS brain tissues expressed elevated levels of cellular p16, p21, p53, and other markers (Nicaise et al., 2019). This finding indicated that the conditioned media (CM) from iPS-derived NPCs from PPMS patients represents a disease-associated senescent secretory phenotype. A proteomic analysis of the NPC secretome was conducted and PPMS NPCs were found to secrete high levels of high mobility group box 1 (HMGB1) that control NPCs did not secrete high levels of HMGB1 (Nicaise et al., 2019). HMGB1 was also found to colocalize to Sox2+ cells within the white matter lesions in autopsy pathology. Moreover, when a function blocking antibody against HMGB1 was applied to the CM derived from PPMS patient iPS-derived NPCs, maturation of OPCs increased significantly. This indicates an important role for HMGB1 in the influence of senescence on limiting OL-mediated remyelination (Nicaise et al., 2019).

HMGB1, also known as amphoterin, is a highly conserved, ubiquitous protein found in nearly all eukaryotic cells. It is highly conserved between rodents and humans, with the sequence homology exceeding 98% (Ellerman et al., 2007). HMGB1 is recognized as the prototypical alarmin, or danger/damage associated molecular pattern (DAMP). This class of proteins have functions in the unstressed cell but are actively secreted following stress or damage, provoking an innate immune response (Robinson et al., 2013). Under normal circumstances, HMGB1 remains in the cell, acting in the nucleus as the most abundant chromatin associated non-histone binding protein, stabilizing nucleosomes and regulating the transcription of many genes (O'Connor et al., 2003; Ellerman et al., 2007). In contrast, extracellular HMGB1 has been found to be a mediator of both sterile inflammation and infection associated responses (Yang and Tracey, 2010), which can induce proinflammatory cytokine release from cells. HMGB1 has been implicated in a variety of inflammatory conditions including sepsis, inflammatory bowel disease, pancreatitis, acute lung injury, rheumatoid arthritis, hemorrhagic shock lacking infection, traumatic brain injury, stroke, depression, and ischemia-reperfusion injury (Wang et al., 1999; O'Connor et al., 2003; Yang and Tracey, 2010; Lian et al., 2017). Importantly, treatment of animal models of diseases with anti-HMGB1 antibodies has been shown to be effective in reducing the impact of these conditions (O'Connor et al., 2003; Robinson et al., 2013). While HMGB1 is considered a cytokine when released from immune cells, our data indicates that HMGB1 acts on OPCs, suggesting a direct receptor-mediated function. Extracellular HMGB1 has several identified receptors, including the toll-like receptors (TLRs) TLR2, TLR4, and TLR9 and the receptor for advanced glycation end products (RAGE; Hori et al., 1995; Hoarau et al., 2011). TLRs belong to a family of pattern recognition receptors capable of recognizing a large range of pathogen or danger associated molecular patterns (PAMPs or DAMPs), both of which can trigger an immune response. HMGB1 has been found to promote production of inflammatory factors by binding to TLRs (Andersson et al., 2000) and promote inflammation by binding to RAGE (Watanabe and Son, 2021). It is currently unknown which of these receptors and subsequent pathways HMGB1 acts on in OPCs to prevent maturation.

Herein we report that the HMGB1 suppresses OPC maturation by a TLR2mediated mechanism and co-application of recombinant HMGB1 to spinal cord lysolecithin (LPC) lesions significantly impairs remyelination. Taken together, these data demonstrate a potentially important extracellular role for HMGB1 as a factor involved in impaired remyelination in the multiple sclerosis brain.

MATERIALS AND METHODS

Animals

Rat pups used in this study were the offspring of WT Sprague Dawley rats purchased from Charles River. C57BL/6J wild-type mice of both sexes were purchased from the Jackson Laboratory. Mice were accommodated for a week after receiving and were maintained on a 12-h light/12-h dark cycle with food and water *ad libitum* throughout the experiments. All experiments were performed in accordance with protocols approved by either the University of Connecticut School of Medicine or Georgetown University Institutional Animal Care and Use Committees. Procedures were also conducted following the guidelines set forth by the National Research Council of the National Academies *Guide for the Care and Use of Laboratory Animals*.

Lysolecithin Lesions

Focal demyelinated lesions were induced by injecting 1 μl of 1.0% LPC (Sigma-Aldrich, MA, USA) in PBS into the spinal cord ventral funiculus of 11-week-old mice as previously described

(Psachoulia et al., 2016). For the treatment group, 1 μl of 1 mg/ml recombinant human HMGB1 protein (Abcam, Cambridge, UK) in water was co-injected along with 1.0% LPC into the ventral spinal cord. For the control group, 1 μl of 1 mg/ml recombinant human HMGB1 protein (Abcam, Cambridge, UK) in water was co-injected with the vehicle, sterile phosphate buffered saline (PBS).

Sample Processing

Mice were perfused intracardially with 4% fresh paraformaldehyde (PFA, Sigma-Aldrich, MA, USA) at 10 days post lesion. Spinal cords were dissected and post-fixed with 4% PFA before being cryoprotected in 30% (w/v) sucrose solution (Sigma-Aldrich, MA, USA) in PBS at 4°C overnight. The tissue was then frozen in O.C.T. (Fisher Scientific, MA, USA) on dry ice and stored at −80°C. Spinal cord demyelinated lesions were serially collected on SuperFrost® Plus slides (VWR International, PA, USA) using a cryostat (CM1900; Leica, Wetzlar, Germany). Sections were cut to 12 μm, and were dried for 30 min at room temperature before storing at −80°C.

Immunohistochemistry

Spinal cord demyelinated sections were dried for 1 h at room temperature before performing immunohistochemistry as previously described (Baydyuk et al., 2019). Antigen retrieval was performed for Olig2 staining. Sections were washed with 0.05% Tween 20 in TBS (Sigma-Aldrich, MA, USA) followed by TBS to remove O.C.T. on the slides. For permeabilization, sections were washed with 1% Triton X-100 (Sigma-Aldrich, MA, USA) in TBS for 15 min. The samples were then incubated in blocking solution (5% normal goat serum, 5% donkey serum, and 0.25% Triton X in TBS) for 1 h at room temperature, followed by mouse-on-mouse IgG blocking solution according to the manufacturer's instructions (Vector Laboratories, CA, USA) when using mouse primary antibodies. Subsequently, the sections were incubated at 4°C overnight in primary antibodies diluted in blocking solution (1:300 rabbit anti-Olig2, EMD Millipore; clone CC-1, EMD Millipore; 1:100 mouse anti-Nkx2.2, Developmental Studies Hybridoma Bank; 1:400 rabbit anti-Iba1, Wako Chemicals USA, Inc. ANTI; 1:100 mouse Anti-iNOS/NOS Type II, BD Biosciences; 1:500 rat anti-myelin basic protein, Millipore). On the following day, slides were washed with 0.05% Tween 20 in TBS followed by TBS, then incubated in secondary antibody solution (1:1,000 Cy3-conjugated AffiniPure donkey anti-rabbit IgG (H + L), Jackson ImmunoResearch; 1:500 Alexa Fluor 488 goat anti-mouse IgG (H + L), Thermo Fisher; 1:500 Alexa Flour 594 donkey anti-rat IgG (H + L), Thermo Fisher, 1:1,000 Hoechst 33342, Thermo Fisher, MA, USA) for 1 h at room temperature. Sections were then washed again with 0.05% Tween 20 in TBS followed by TBS to remove excessive secondary antibodies before mounting. To avoid variable staining quality among different batches, slides from all groups were stained on the same day for each type of staining. Images were taken with Zeiss LSM800 confocal microscope (Zeiss, Oberkochen, Germany). To avoid image differences due to laser stability, images from all groups were taken on the same day with the same confocal settings for each type of staining. DAPI intensity was referred to ensure the staining quality was consistent throughout the slides. For Olig2, CC1, Nkx2.2, Iba1, and iNOS staining, cells were counted in the lesioned area defined by Hoechst staining and then normalized to the lesion area (mm^2) of each section. Spinal meninges are excluded from the counts. For myelin basic protein (MBP) staining, the percentage of MBP+ area coverage in lesions was determined by Image J. The results of 2–6 spinal cord sections from each mouse were used for quantification, 3–5 mice were examined in each group.

Isolation of Rat OPCs and Treatment With HMGB1 and Inhibitors

OPCs were isolated from the cerebral cortices of neonatal rat pups (postnatal day 0–3) as previously described (Moore et al., 2011). Cells were plated on poly-l-ornithine (Sigma-Aldrich, MA, USA) coated glass coverslips, as previously described (Moore et al., 2011). OPCs were treated with 500 μl of differentiation media [neurobasal media; Gibco, 2% B27, 1% L-glutamine (2 mM) and 0.3% T3 (10 ng/ml)] containing recombinant human HMGB1 (0.5 μg/ml; Abcam, Cambridge, UK) or recombinant human HMGB1 (0.5 μg/ml) and the indicated concentration of each inhibitor. All tests were performed with HMGB1 and the inhibitor in differentiation media, with differentiation media alone serving as the control. Concentrations were determined from the manufacturer provided IC50. The following drugs were used: CU CPT22 (TLR2/1 specific inhibitor; 0.5 and 1 μM; Tocris), C34 (TLR4 specific inhibitor, 5 and 10 μM; Tocris), Hydroxychloroquine sulfate (HQS; TLR9 specific inhibitor, 1 and 2 μM; Tocris, Bristol, UK), and FPS-ZM1 (RAGE specific inhibitor; 3 and 6 μM; Tocris, Bristol, UK). All drugs were reconstituted in accordance with the manufacturer instructions. Coverslips were treated for 72 h.

Immunocytochemistry

Following treatment, coverslips were gently washed with PBS before fixation with 4% PFA. Following fixation, cells were permeabilized using 5% goat serum (Thermo Fisher Scientific, MA, USA) and 0.01% Tween20 (Sigma-Aldrich, MA, USA). Cells were stained using 4'6-diamidino-2-phenylindole (DAPI) to identify nuclei, as well as the indicated primary antibodies, including MBP (1:500; Abcam, Cambridge, UK), Olig2 (1:500; Abcam, Cambridge, UK), and NFκB (1:200; Thermo Fisher Scientific, MA, USA). Conjugated secondary antisera directed against the species of the primary were used according to manufacturer instructions (1:1,000, Abcam, Cambridge, UK). Coverslips were then affixed to slides (Denville Ultraclear, MA, USA) with fluromount-G (Invitrogen, MA, USA) and imaged (Olympus 1X71, CellSens Software; Olympus, MA, USA). Five fields of view at 20× magnification using identical image capture settings were assessed by an experimenter blinded to treatments. To analyze the amount of OPC differentiation, Olig2+ cells and MBP+ cells were counted and the percent MBP+ cells was calculated. Olig2+ was also used to distinguish astrocytes in the cultures to

refine the cell counts to only MBP+/Olig2+ OL-lineage cells. Data are presented as the percentage of MBP+/Olig2+ cells relative to the control, differentiation media only, condition set as 100%.

Gene Ontology (GO) Enrichment Analysis of NFκB Target Genes

Gene expression analyses using our previously reported RNAseq datasets were used to identify HMGB1-specific transcriptional changes across OPCs under defined treatment conditions, as previously described (Nicaise et al., 2019). Significantly up or downregulated genes in PPMS vs. PPMS+αHMGB1 were generated ($p < 0.05$, LogFoldChange $> \pm 1$). Differentially expressed genes (DEGs) were then cross-referenced with a list of known NFκB genes (Rouillard et al., 2016) to determine which DEGs were also known to be NFκB regulated. These filtered gene lists were then analyzed using the PANTHER Pathway analysis tool[1] linked through the Gene Ontology Consortium's online database[2] (Mi et al., 2013). Gene names were copied into the PANTHER Pathway analysis tool, where we selected organism (*Rattus norvegicus)*, specific enrichment analysis (*Biological* or *Reactome*), statistical test type and correction (*Fisher's Exact* with *calculation of FDR)*. Significant results were identified by filtering by *false discovery rate (FDR < 0.05)* and *P*-value (p value < 0.01). We reported significant findings using a 3D representation showing the *P*-value and fold enrichment for each significantly enriched pathway.

Statistical Analysis

Statistics for ICC were performed using GraphPad Prism 8 (La Jolla, CA, USA). Statistics for IHC were performed using GraphPad Prism 9 (La Jolla, CA, USA). Data are represented as mean ± SEM. Significance was determined using one-way ANOVA. Statistical significance is reported as not significant (n.s.) $P > 0.05$, $^{*}P \leq 0.05$, $^{**}P \leq 0.01$, $^{***}P \leq 0.001$, $^{****}P \leq 0.0001$.

RESULTS

HMGB1 Inhibits Oligodendrocyte Differentiation in a LPC Model of Demyelination

HMGB1 has been shown to be detrimental to OPC differentiation *in vitro* (Nicaise et al., 2019) and has been found to be significantly elevated in MS patient plasma (Bucova et al., 2020). Higher levels of HMGB1 have also been linked with active lesions as well as an association between HMGB1 levels and disability (Bucova et al., 2020). To determine whether HMGB1 introduced into an active lesion *in vivo* would impact remyelination, we co-injected recombinant human HMGB1 with LPC into mouse spinal cords and assessed lesion volume 10 days later (data post lesion, dpl). Animals that had been co-injected with LPC and HMGB1 were found to have significantly fewer mature Olig2+/CC1+ OLs compared to those co-injected with LPC and vehicle (H_2O; **Figure 1**). The lack of mature oligodendrocytes in the lesion environment was not due to insufficient numbers of early stage oligodendrocyte lineage cells because we also found that the numbers of Olig2+/Nkx2.2+ cells, which identifies activated OPCs during remyelination (Fancy et al., 2004), were present at the same levels in the LPC lesions whether co-injected with HMGB1 or vehicle (PBS; **Figure 2**). These findings indicated that HMGB1 effectively impaired the differentiation of oligodendrocytes when introduced into the LPC lesion environment. To determine if administration of HMGB1 into the LPC lesion affected the degree of remyelination, as indicated by production of myelin basic protein (MBP+), we also assessed the amount of MBP+ immunostaining in each treatment condition and found reduced MBP+ levels in mice that had been LPC lesioned and also treated with HMGB1 (**Figure 1**). To determine if the reduced numbers of mature OLs (CC1+) and myelin (MBP+) in LPC/HMGB1-treated animals was attributed to an overall loss of oligodendrocyte lineage cells in the lesion environment, we then analyzed Olig2+/Nkx2.2+ OPCs in the lesions of each treatment group. This analysis determined that the HMGB1 did not reduce the numbers of OPCs in LPC-treated animals relative to LPC-Vehicle (H_2O) treated subjects (**Figure 2**). We did note that when compared with non-LPC + HMGB1 injected animals, the number of OPCs was higher than in LPC-lesioned animals which indicated that HMGB1 alone did not impact the survival of OL-lineage cells. This was consistent with previous findings that LPC kills nearly all oligodendroglial cells around the injection site, and new OPCs migrating in from outside the lesion are needed for remyelination (Baydyuk et al., 2019). To futher define and compare the state of the demyelinated lesions in each treatment group at this 10 dpl timepoint, we also examined iNOS + /Iba1+ microglia/macrophages as an indicator of active demyelination. This analysis determined that there were no significant differences in the numbers of Iba1+ activated microglia or iNOS + /Iba1+ cells in either LPC treatment group at the timepoint analyzed (**Figure 3**). Hence, these data indicate that a single bolus injection of HMGB1 introduced into an active lesion environment was sufficient to effectively impair the recovery and remyelination of an LPC lesion.

TLR2/1 Inhibitor CU CPT22 Rescued Differentiation in Oligodendrocyte Progenitor Cells Treated With HMGB1

Our previous and current data indicate that HMGB1 can directly inhibit the differentiation of OPCs both *in vivo* and *in vitro*. To understand how extracellular HMGB1 influences OPCs, we examined whether any known HMGB1 receptors were involved and also examined which intracellular signaling pathway it was likely activating. Based on what is known about the action of extracellular HMGB1 in other cell types and disease models, we hypothesized that HMGB1 was likely acting through one of four receptors: TLR2, TLR4, TLR9 or RAGE (Hori et al., 1995;

[1]http://pantherdb.org/
[2]http://www.geneontology.org/

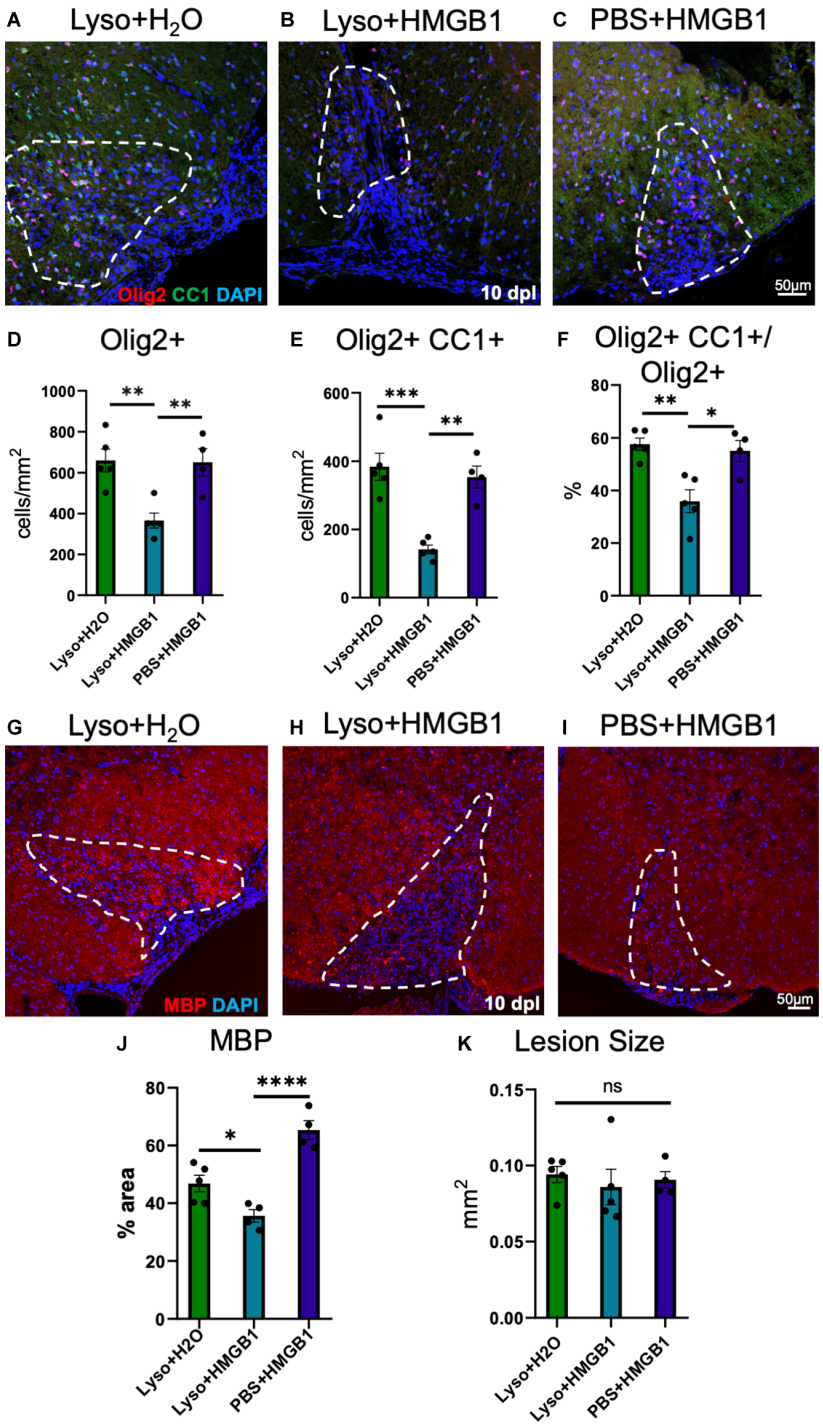

FIGURE 1 | HMGB1 reduced evidence for myelination after LPC-induced demyelination. **(A)** A representative IHC image of mouse spinal cord injected with 1 μl LPC (1.0%) and water control 10 days post lesion (dpl) stained with Olig2, CC1, and DAPI. **(B)** A representative IHC image of mouse spinal cord co-injected with 1 μl LPC (1.0%) and 1 μl rhHMGB1 (1 mg/ml in water) at 10 dpl stained with Olig2, CC1, and DAPI. **(C)** A representative IHC image of mouse spinal cord injected with PBS and 1 μl rhHMGB1 (1 mg/ml in water) at 10 days post injection stained with Olig2, CC1, and DAPI. **(D)** Quantification of the number of Olig2+ cells. **(E)** Quantification of the Olig2+ and CC1+ cells. **(F)** Percent of Olig2+ cells that were also CC1+. **(G)** Representative image of mouse spinal cord injected with 1 μl LPC (1.0%) and water control 10 dpl stained for myelin basic protein (MBP) and DAPI. **(H)** A representative IHC image of mouse spinal cord co-injected with LPC and rhHMGB1 at 10 dpl stained for myelin basic protein (MBP) and DAPI. **(I)** A representative IHC image of mouse spinal cord injected with PBS and 1 μl rhHMGB1 (1 mg/ml in water) at 10 days post injection stained for myelin basic protein (MBP) and DAPI. **(J)** Percent of the lesion area that was MBP+. **(K)** Quantification of the area of the lesion in mm^2. White dashed lines indicate lesion/injection site. Two to six spinal cord sections from each mouse were used for quantification, 3–5 mice per condition. $^{****}P \leq 0.0001$; $^{***}P \leq 0.001$; $^{**}P \leq 0.01$; and $^{*}P \leq 0.05$. ns when $P > 0.05$. Scale bar = 50 μm.

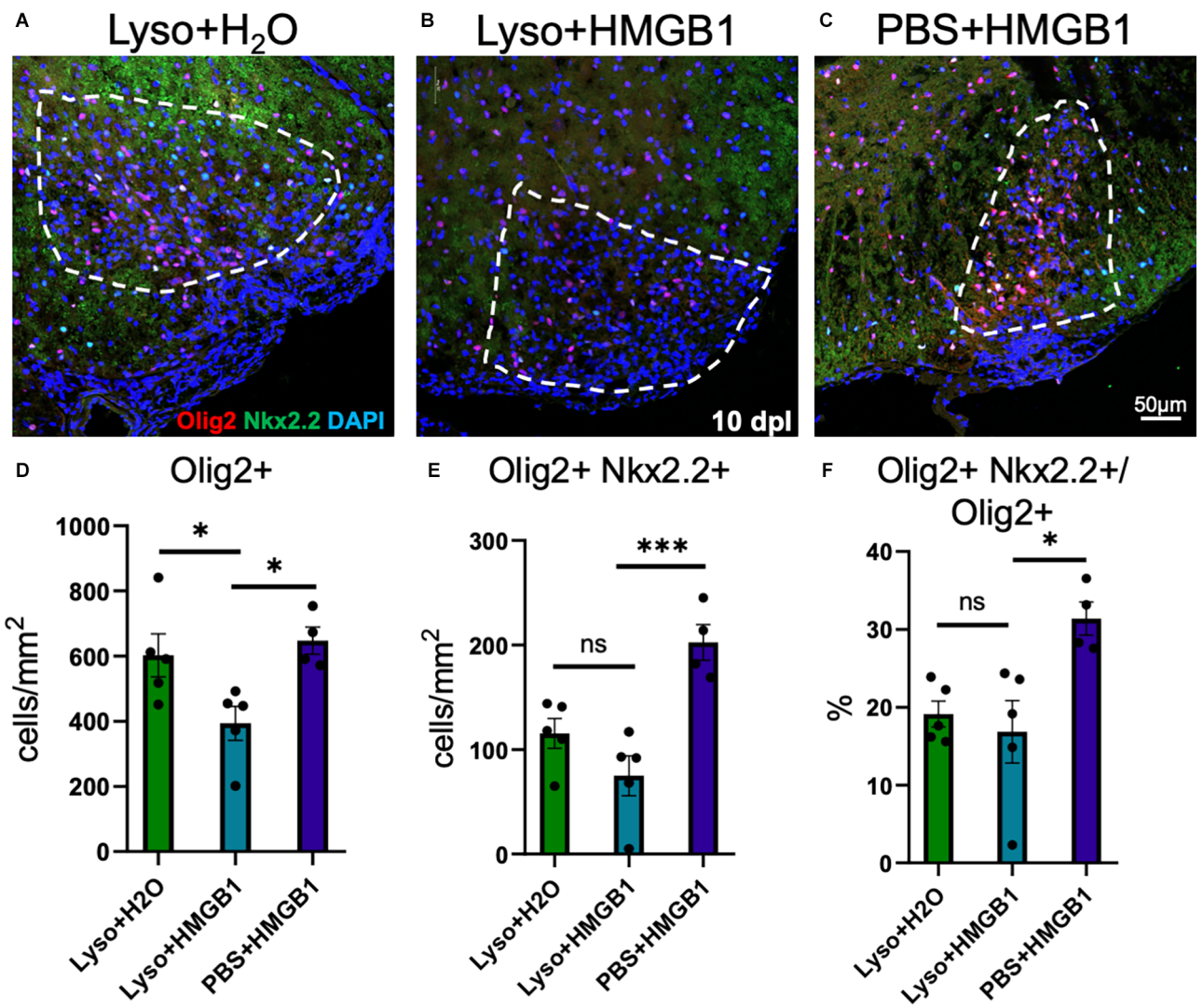

FIGURE 2 | HMGB1 delayed maturation of oligodendrocytes *in vivo*. **(A)** A representative IHC image of mouse spinal cord injected with 1 µl LPC (1.0%) and water control 10 dpl stained for Olig2, Nkx2.2, and DAPI. **(B)** A representative IHC image of mouse spinal cord co-injected with 1 µl LPC (1.0%) and 1 µl rhHMGB1 (1 mg/ml in water) at 10 dpl stained for Olig2, Nkx2.2, and DAPI. **(C)** A representative IHC image of mouse spinal cord injected with 1 µl rhHMGB1 (1 mg/ml in water) 10 days post injection stained for Olig2, Nkx2.2, and DAPI. **(D–F)** Quantification of lesions, including Olig2+ cells, Olig2+, and Nkx2.2+ cells and the percent of Olig2+ cells that were also Nkx2.2+. White lines indicate lesion/injection site. Two to six spinal cord sections from each mouse were used for quantification, 3–5 mice per condition. $^{***}P \leq 0.001$ and $^{*}P \leq 0.05$. ns when $P > 0.05$. Scale bar = 50 µm.

Park et al., 2004; Hoarau et al., 2011). To test this hypothesis, we utilized receptor-specific inhibitors to determine which receptor HMGB1 was acting through in OPCs.

OPC cultures obtained from wild type (WT) Sprague Dawley rat pups (P0–P3) were treated for 72 h with each receptor inhibitor and 0.5 µg/ml HMGB1 in differentiation media. Consistent with prior research (Nicaise et al., 2019), adding HMGB1 to differentiation media significantly diminished the amount of MBP produced by oligodendroglial lineage cells when compared to differentiation media alone. This indicated a failure of OPCs to differentiate into mature, myelinating OLs in the presence of HMGB1 *in vitro*. Treatment with the inhibitors of TLR4 (C34), TLR9 (hydroxychloroquine sulfate) or RAGE (FPS-ZM1) in the presence of HMGB1 was unable to restore differentiation to control levels. However, the TLR4 and TLR9 inhibitors were able to produce significantly more differentiation than the HMGB1 only condition. In contrast, treatment of OPCs with CU CPT22 (1 µM, a TLR2/1 specific inhibitor) in the presence of HMGB1 (0.5 µg/ml) resulted in a significant increase in the percentage of mature OL lineage cells (Olig2+/ MBP+). HMGB1 and CU CPT22 co-treated cultures exhibited no significant differences in differentiation when compared to differentiation media only control conditions (**Figure 4**), suggesting that HMGB1-mediated inhibition of OPC differentiation is mediated, at least in part, by TLR2/1.

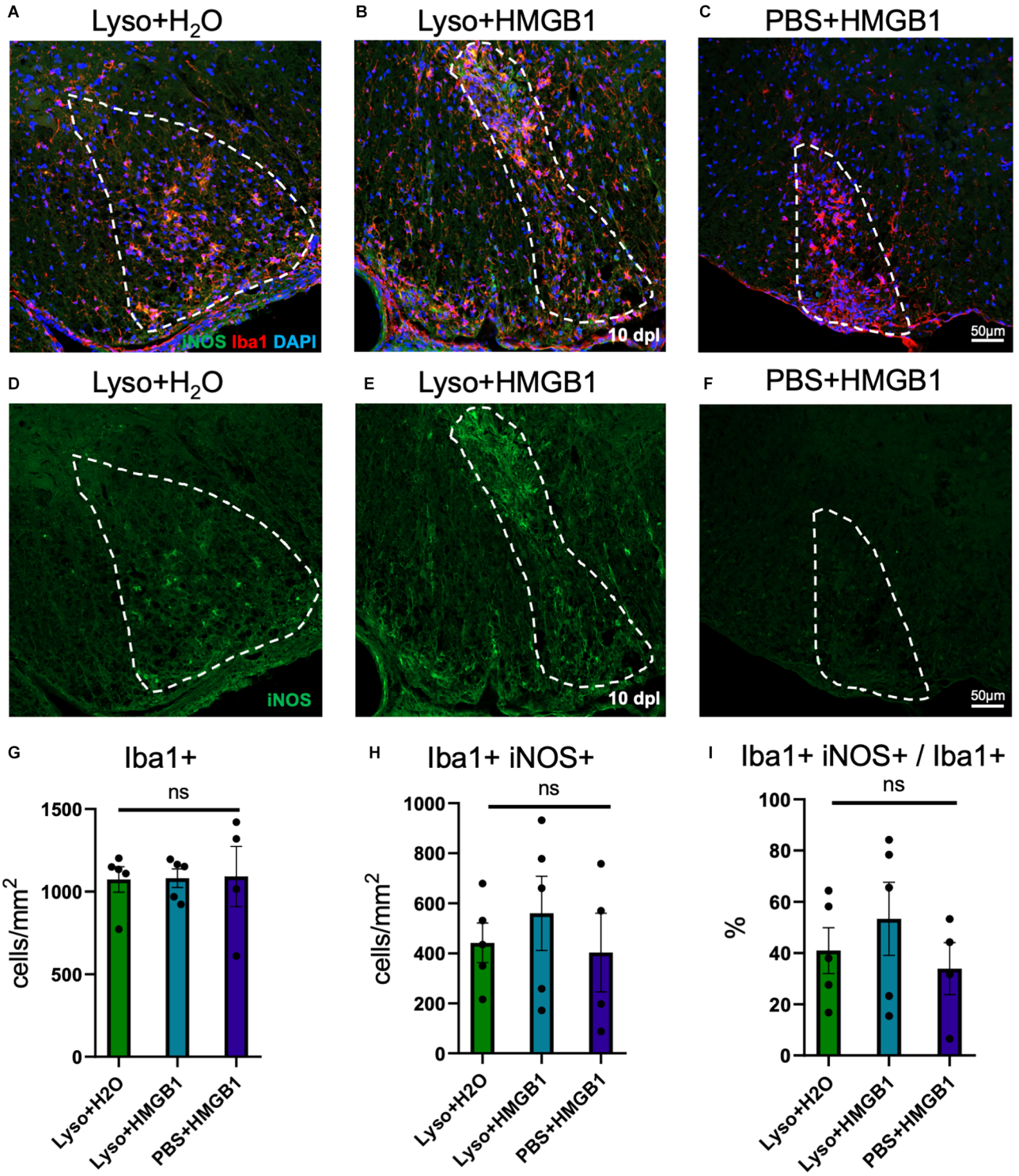

FIGURE 3 | HMGB1 treatment did not increase inflammation within demyelinated lesions. **(A)** A representative IHC image of mouse spinal cord injected with 1 µl LPC (1.0%) and water control 10 dpl stained with iNOS, Iba1, and DAPI. **(B)** A representative IHC image of mouse spinal cord co-injected with 1 µl LPC (1.0%) and 1 µl rhHMGB1 (1 mg/ml in water) at 10 dpl stained with iNOS, Iba1, and DAPI. **(C)** A representative IHC image of mouse spinal cord injected with 1 µl rhHMGB1 (1 mg/ml in water) 10 days post injection stained with iNOS, Iba1, and DAPI. **(D–F)** Single channel images of iNOS immunostaining of samples represented in panels **(A–C)**. Lesion areas are represented by dashed white lines. **(G)** Quantification of Iba1+ cells. **(H)** Quantification of Iba1+ and iNOS+ cells. **(I)** Percent of Iba1+ cells that were also iNOS + . White dashed lines indicate lesion/injection site. Two to six spinal cord sections from each mouse were used for quantification, 3–5 mice per condition. ns when $P > 0.05$. Scale bar = 50 µm.

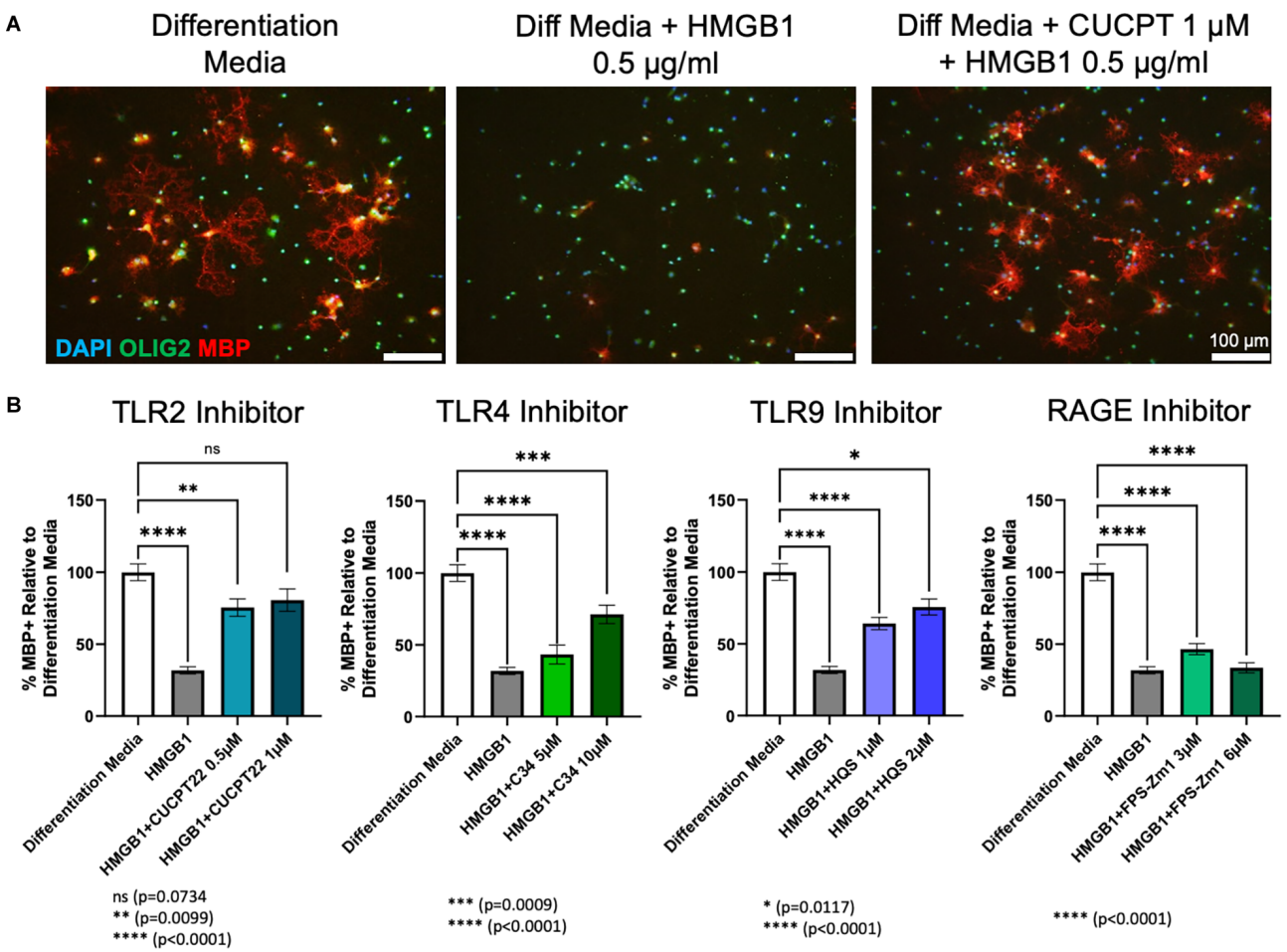

FIGURE 4 | HMGB1 inhibited OPC differentiation *via* TLR2/1 receptors. **(A)** Differentiation of rat OPC cultures after 72 h of treatment with differentation media, differentiation media plus HMGB1 or differentiation media plus HMGB1 and CU CPT22. **(B)** Quantification of the amount of differentiation, as measured by the percent of MBP+ cells, normalized to differentiation media using each receptor inhibitor [Not shown: all conditions are significantly different from HMGB1 ($p < 0.0001$), except FPS-Zm1 3 µM and 6 µM (ns)]. Analyzed by one-way ANOVA, where $^{****}P \leq 0.0001$; $^{***}P \leq 0.001$; $^{**}P \leq 0.01$; and $^{*}P \leq 0.05$. ns when $P > 0.05$. Scale bar = 100 µm.

HMGB1 Regulates NFκB Signaling in OPCs

To define how HMGB1 may regulate the transcriptional responses of OPCs, we noted that NFκB is a common downstream target of TLR2/1 signaling. Nuclear factor κB (NFκB) is a well-established downstream target of TLR2/1 and has also been found to be activated in chronic MS lesions in OLs (Bonetti et al., 1999). NFκB is a transcription factor comprised of at least five cytoplasmic proteins [RelB, c-Rel, p50, p52, and p65 (RelA)] and is inhibited by IκB, which sequesters NFκB in the cytoplasm where it is inactive. Activating NFκB requires degradation of IκB, allowing NFκB to translocate into the nucleus where the Rel subunits can bind target genes and begin transcription (Bonetti et al., 1999). To evaluate the effects of HMGB1 on the intracellular localization of NFκB in OPCs, we treated OPCs with HMGB1 and fixed at various timepoints, then immunostained for NFκB to determine if subcellular localization was influenced by HMGB1. In HMGB1-treated OPCs we found 80% of cells exhibited nuclear localization of NFκB after 1-, 2- and 4-h of treatment (**Figure 5**). This was in contrast to cells treated with only differentiation media, where less than 20% of the OPCs had any notable nuclear NFκB localization. Thus, the nuclear translocation of NFκB in response to HMGB1 suggests that this pathway may represent a means by which HMGB1 could influence gene transcription and OPC differentiation.

To evaluate whether regulation of TLR2/1 signaling also impacted the nuclear localization of NFκB in response to HMGB1, we examined the subcellular localization of NFκB in HMGB1 treated OPCs with and without the TLR2/1 inhibitor CU CPT22. We observed CU CPT22 and HMGB1 co-treated cells did not exhibit significant nuclear localization of NFκB and that the proportion of cells with nuclear NFκB did not differ significantly from OPCs cultured in differentiation media alone (**Figure 5**). These results suggest that HMGB1 activation of NFκB regulated nuclear transcription can be regulated or mediated by TLR2. Hence, identification of NFκB target genes that are transcribed in response to HGMB1 may represent

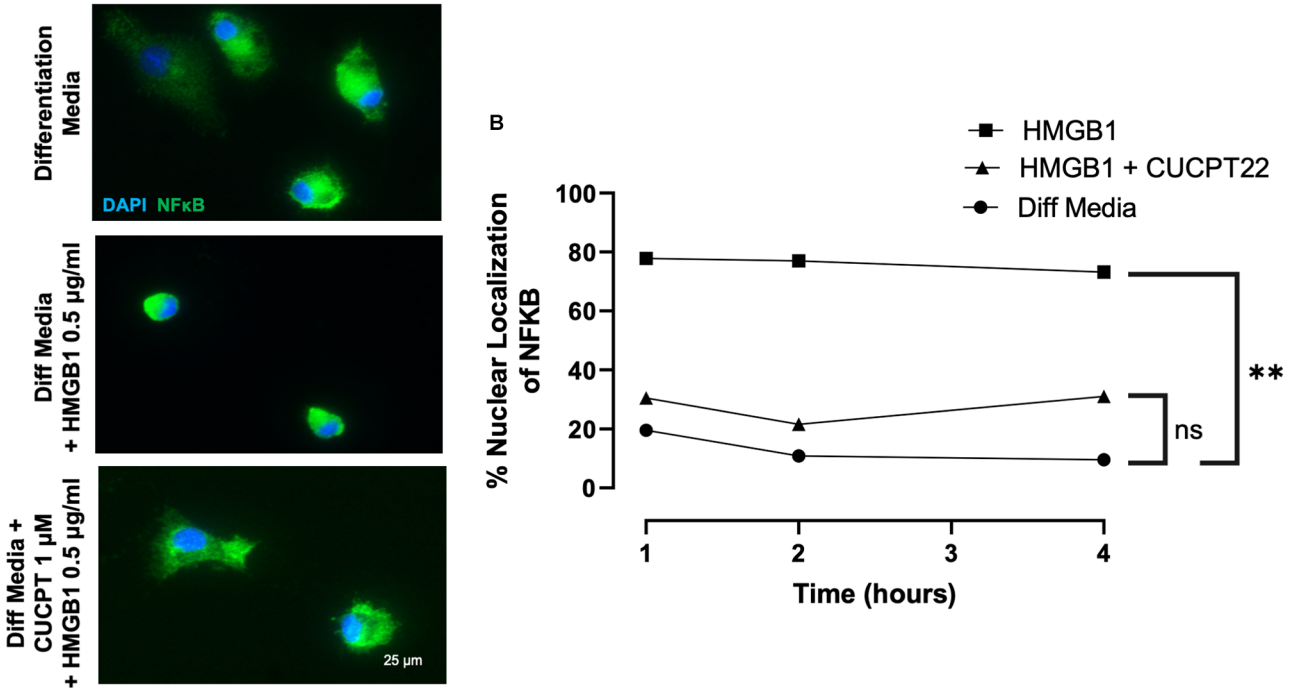

FIGURE 5 | HMGB1 promoted nuclear localization of NFκB after HMGB1 treatment. **(A)** Immunocytochemical detection of NFκB in primary OPC cultures identified NFκB to be predominantly in the cytoplasm of control, differentiating cells, but was observed to be rapidly localized to the nucleus when exposed to HMGB1. Addition of the TLR2 inhibitor, CU CPT22, prevented the nuclear localization of NFκB in HMGB1-treated OL lineage cells. **(B)** Quantification of the percent of OL lineage cells with nuclear localization of NFκB over time. Analyzed by repeated measures ANOVA, where $^{**}P \leq 0.01$; and ns when $P > 0.05$. Scale bar = 20 μm.

future candidates for mediating the arrest of OPC differentiation by HMGB1.

Lastly, to interrogate the downstream effects of HMGB1 on OPC behavior, RNAseq datasets we generated previously (Nicaise et al., 2019) were used to identify HMGB1 regulated genes. We analyzed the differentially expressed genes (DEGs) which exhibited upregulation in the presence of HMGB1, and also downregulation in HMGB1 inhibited conditions, and cross-referenced DEG lists against lists of known NFκB regulated genes (Rouillard et al., 2016). This analysis of transcriptional datasets determined that NFκB target genes represented 35.7% of all significantly upregulated DEGs and also 24.5% of all downregulated DEGs in OPCs. Gene ontology analysis revealed that these NFκB regulated DEGs represented processes of cellular proliferation and differentiation that were consistent with HMGB1-induced impairment of OPC differentiation demonstrated both *in vivo* (**Figure 1**) and in our previous study (Nicaise et al., 2019). Together, these data strongly implicate NFκB-regulated transcription in impaired OPC-mediated remyelination and as a pathway directly regulated by HMGB1 (**Figure 6**).

DISCUSSION

Previous work in our lab has shown that HMGB1 was preferentially expressed by progenitor cells in progressive forms of MS and that this was coincident with these progenitors displaying a cellular senescent phenotype. This led to the hypothesis that elevated HMGB1 in progressive MS may be both an indicator and mediator of chronic demyelination. To further test the possibility that HMGB1 can negatively impact OPC-mediated remyelination, results of this study have shown that a single injection of HMGB1 given at the time of the LPC lesion is sufficient to significantly impair OPC differentiation and thus attenuated the degree of remyelination. However, this failure is not due to a lack of OPCs, as we saw comparable levels of OPCs in the non-HMGB1 and HMGB1 lesions. This observation that OPCs persist in lesions but fail to differentiate has been widely observed and documented in MS (Skaper, 2019). Herein, we have tested this hypothesis and our results show that HMGB1 can negatively impact remyelination *in vivo*, and we have identified TLR-NFκB signaling as a possible signaling mechanism in OPCs that mediates the effects of extracellular HMGB1 *in vitro*.

Since TLRs are known receptors for HMGB1, we had also tested the possibility that TLR-signaling may contribute to the effects of HMGB1 on OPCs. HMGB1 is not the first putative ligand reported for TLR2 as a means of affecting OLs. Indeed, TLR2 has previously been implicated as a receptor for hyaluronan and has been shown to block OPC maturation and remyelination (Sloane et al., 2010). The high molecular weight form of hyaluronan that is secreted by astrocytes has

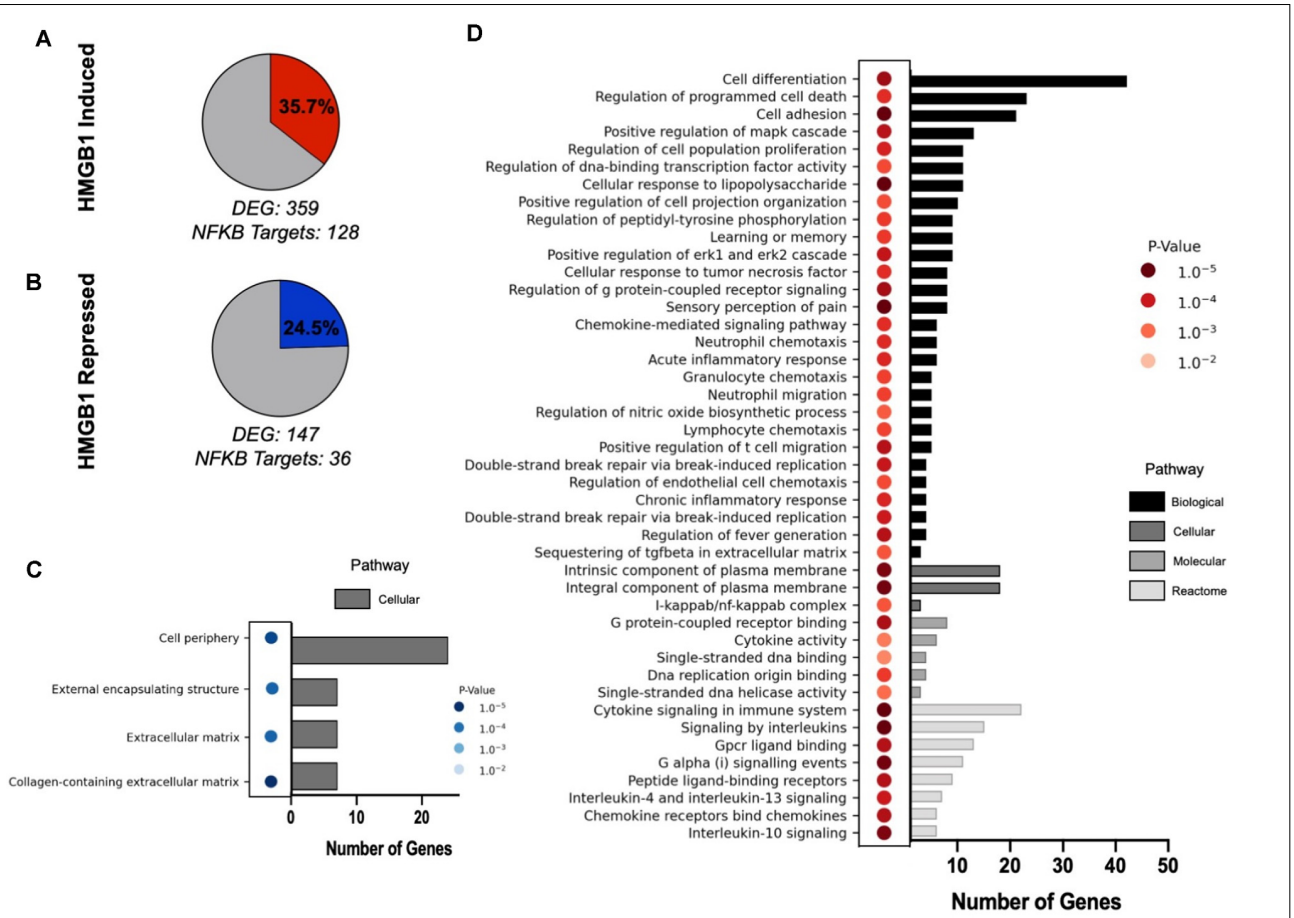

FIGURE 6 | Gene ontology enrichment analysis of HMGB1 regulated NFκB gene pathways. Analysis of HMGB1 regulated transcriptional responses in OPCs identified differentially expressed NFκB target genes which reflected both induced **(A)** and repressed **(B)** patterns of gene expression. **(C)** GO analysis of repressed cellular processes in OPCs treated with HMGB1 as defined by NFκB-regulated transcriptional targets. No pathways in this analysis other than those listed had significant differences from control. **(D)** GO analysis of processes induced by HMGB1 identified biological pathways which emphasized cellular periphery as a major influence of HMGB1 on OPC activity. These data confirm the pathophysiological actions of HMGB1 *in vitro* and *in vivo* and provide a template for understanding of how HMGB1 potently affects OPC differentiation potential. P values depicted in **(C** and **D)** are indicated by color and the number of genes in each pathway category are indicated by a bar graph on the X axis for each panel.

been shown to accumulate in chronically demyelinated lesions in both MS patients and mice with experimental autoimmune encephalomyelitis (EAE), and has also been shown to inhibit remyelination in LPC lesions (Back et al., 2005). It is an interesting possibility that these two significantly different molecules may be acting in similar ways on the same pathway to similar effect. It is important to qualify that although HMGB1 is recognized as a ligand for TLRs, inhibition of TLR2 by itself is known to promote OPC differentiation (Sloane et al., 2010). Thus, our findings cannot conclusively establish that TLR2 is the only receptor for HMGB1 because there remains the possibility that inhibiting TLR2 may have offset the effects of HMGB1 in a manner unrelated to direct ligand-receptor interaction. From this perspective HMGB1 and regulation of TLR2 signaling on OPCs may act as competing physiological antagonists in the regulation of OPC fate.

Our data indicate that extracellular HMGB1 may act *via* TLRs expressed on OPCs to induce activation of NFκB signaling. This finding is consistent with previous work by others on the expression of TLR2 by OPCs and for a negative role for TLR2 activation on OPC differentiation potential (Sloane et al., 2010; Wasko et al., 2019). Interestingly, our work also pointed to a significant influence of HMGB1 on NFκB signaling, both as indicated by the rapid nuclear translocation of NFκB in HMGB1 treated OPCs and in terms of gene ontology analysis of pathways and transcriptional targets in OPCs regulated by HMGB1. Herein we report that extracellular HMGB1, which is also a factor found abundantly in the inflammatory milieu of the demyelinated lesion in the MS brain, is a potential inducer of NFκB signaling resulting in perturbed OPC remyelinating potential (**Figure 7**). Our *in vitro* studies which are corroborated by *in vivo* findings in the LPC lesion model, are in contrast to prior *in vivo* work implicating IFNγ as a driver of NFκB activity in OL (Stone et al., 2017). In the previous study, it was reported that blocking NFκB activation in OLs using cell-specific expression of IκBαΔN resulted in OL death and a

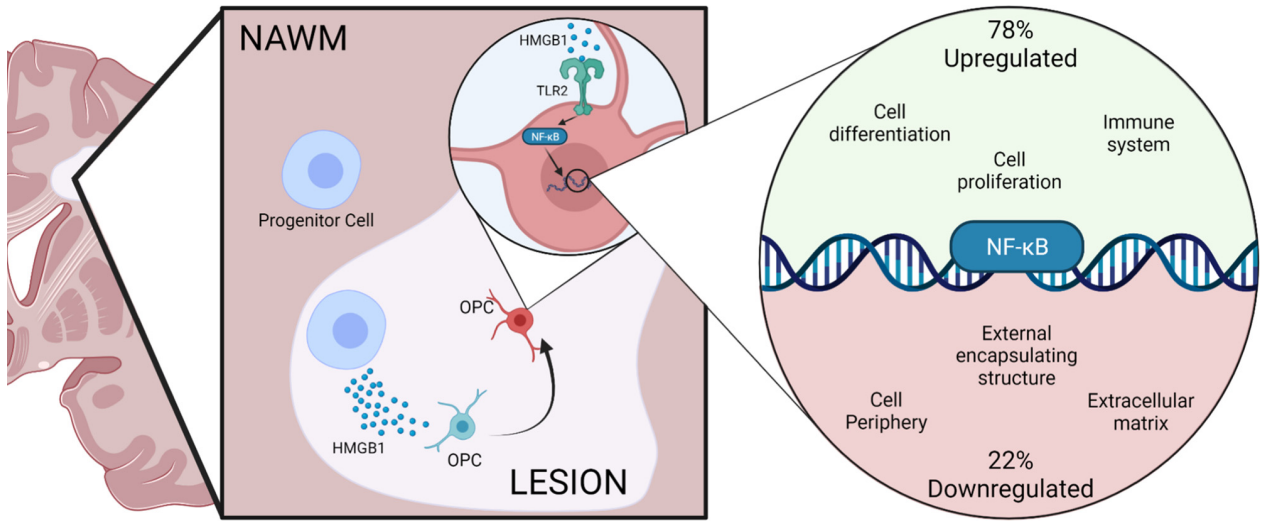

FIGURE 7 | Hypothesized model of HMGB1 inhibitory activity on OPCs in the MS demyelinated lesion environment. Graphical representation of a demyelinated lesion in the MS brain and how expression of HMGB1 negatively impacts the remyelinating potential of OPCs. The stepwise progression from the MS brain (right) to the demyelinated lesion environment (middle panel) where HMGB1 is expressed at higher concentrations, to the intracellular response of OPCs (right panel) depicting a transcriptional influence of HMGB1 on NFκB gene expression regulation. Results from this study implicate TLR2-mediated receptor activation of NFκB gene target pathways as putative negative regulators of HMGB1 in the MS brain lesion environment. Created with BioRender.

hypomyelination phenotype during murine development (Stone et al., 2017), suggesting a positive function for NFκB signaling in promoting myelination. Whereas based on our findings, we consider NFκB signaling *via* TLR2 activation by HMGB1 to be an impediment to OL differentiation and remyelination. Indeed, our analysis of transcriptional changes in OPCs that are regulated by HMGB1 support these findings that blocking HMGB1 results in activation of gene pathways associated with myelination and OL maturation and these data provide a new perspective on regulatory pathways governing the fate potential of OPCs.

HMGB1 has been shown to activate NFκB downstream signaling through TLR2, TLR4, TLR9, and RAGE in several disease contexts (Lohani and Rajeswari, 2016). In diabetic neuropathy, HMGB1 increases NFκB activity (Alomar et al., 2021), while in diabetic retinopathy, HMGB1 has been shown to upregulate NFκB specifically by inhibiting the activity of IKB-α (Liang et al., 2020). IKB-α is a protein responsible for NFκB sequestration in the cytoplasm, where it is unable to perform its transcriptional functions (Liu et al., 2017). In cuprizone studies, drugs found to increase IκB levels were protective (Khaledi et al., 2021), while in developmental studies of the inflammatory molecule S100B, delays in maturation of OPCs were observed concordant to NFκB activation, albeit through the RAGE pathway (Santos et al., 2018).

The present findings and our past work point to a disease-relevant role for extracellular HMGB1 as a factor contributing to remyelination failure in MS. At present, it is unclear if the extracellular (secreted) form of HMGB1 is derived from a separate pool of HMGB1 in progenitor cells, or if the stressful conditions of MS cause nuclear HMGB1 to be modified and exported to the extracellular environment. Since it is known that HMGB1 has nuclear localization and export signals (Bonaldi et al., 2003) that facilitate its movement between the cytoplasm and the nucleus, it is plausible that erroneous signaling could contribute to the redirection of HMGB1 to the extracellular space. Curiously, HMGB1 has no secretory signal peptide, and is not known to be secreted through the Golgi apparatus. Yet, HMGB1 is released, at least by monocytes, after concentrations of cytosolic HMGB1 lead to translocation into secretory lysosomes (Bonaldi et al., 2003). Understanding these fundamental properties of intracellular management of HMGB1 protein could provide important insights into how to affect the release of HMGB1 from progenitor cells in the context of disease. On that point, we know that HMGB1 is expressed and produced by progenitor cells in the MS brain (Nicaise et al., 2019; Absinta et al., 2021) but we do not yet know why progenitor cells in the MS brain seem to acquire a cellular senescent phenotype related to excessive expression and production of HMGB1. Future studies may explore salient questions regarding identifying the critical signals that trigger generation of HMGB1 by a senescent cell in this disease, and how intracellular HMGB1 protein is managed/modified for extracellular release.

The focus of our study was the role of extracellular HMGB1 within demyelinated lesions within the MS brain. While we employed a reductionist approach to refine our understanding of how HMGB1 acts on primary OLs in culture, we recognize that there are other physiological activities attributed to how extracellular HMGB1 may impact the brain that were not examined in this study. For instance, HMGB1 has also been implicated in the breakdown of the BBB (Zhang et al., 2011; Nishibori et al., 2020), an integral component

of MS pathophysiology (Balasa et al., 2021) and studies in MS patients corroborate this; serum levels of HMGB1 in MS patients are significantly higher than healthy controls (Bucova et al., 2020). Additionally, serum HMGB1 levels are also elevated in EAE. Blocking extracellular HMGB1 significantly lessens disease severity by attenuating *T* cell extravasation into the CNS (Robinson et al., 2013). Interestingly, HMGB1 is also a well-known mediator of inflammation (Gorgulho et al., 2019; Wang et al., 2019; Ciprandi et al., 2020; Liu et al., 2020; Nishibori et al., 2020; Yang et al., 2021). We had analyzed the degree of activated microglia/macrophages in HMGB1-LPC and control-LPC lesioned animals as a means to discern whether the impaired recovery in the HMGB1-treated animals was also reflective of an ongoing, active lesion. Our analysis from 10 dpl suggest that at this late timepoint the inflammatory response did not differ in between LPC-treated groups. It is important to point out that since this study did not characterize earlier post-lesion timepoints, we cannot exclude the possibility that HMGB1 may have had an effect on microglial responses within the lesion environment prior to our analysis. Nevertheless, the consequence of HMGB1 administration by 10 dpl suggests that microglia do not remain activated when significantly impaired remyelination was noted (**Figure 7**). We also recognize that the role of microglia in demyelination and MS is complex, potentially playing both beneficial and harmful roles (Voet et al., 2019). In particular, in this LPC model, proinflammatory microglia have been found to be robustly active and present in the earlier stages post-lesion (Baydyuk et al., 2019), and a transition from a pro-inflammatory (iNOS+ TNFα+ CCL2+) to a more regenerative phenotype (Arg-1+ CD206+ IGF-1+) has been associated with initiation of remyelination in the LPC model (Lloyd et al., 2019). Additional study will be required to test whether HMGB1 impairs remyelination through direct actions on OPCs, or engages microglial cells, or both, *in vivo*. When considered together, our findings in this study are distinct but complementary to these previous studies and serve to highlight that extracellular HMGB1 likely contributes to manifold pathological changes associated with demyelination and autoimmunity related to complex, multi-system diseases like MS.

Multiple sclerosis is not the only instance where extracellular HMGB1 may negatively impact white matter. In animal models of stroke, extracellular HMGB1 has been found to stimulate inflammation, albeit through TLR4 signaling (Yang et al., 2011) instead of TLR2, as we showed here. Patients with cerebral and myocardial ischemia have also been found to have elevated levels of HMGB1 in their blood serum (Goldstein et al., 2006), much in the same way MS patients have elevated blood serum levels of HMGB1 (Bucova et al., 2020). HMGB1 has also been implicated in the periphery, with its release from neurons linked to localized inflammation in animal models of nerve injury and arthritis (Yang et al., 2021). Furthermore, we have studied HMGB1 in the context of MS on account of its excessive expression and production of HMGB1 from progenitor cells which exhibit a cellular senescent phenotype (Davalos et al., 2013; Nicaise et al., 2019). Yet, our findings that HMGB1 can directly impair OL maturation may also have implications for Alzheimer's disease and frontotemporal dementia, where HMGB1 released from astrocytes has been reported to promote senescence in addition to neuropathology (Gaikwad et al., 2021). In these cases, perturbation of mitochondrial function may contribute to the development of a cellular senescent state that is also characterized by elevated HMGB1 expression and extracellular release (Wiley et al., 2016). If HMGB1 is also promoting senescence in the MS brain, there is the potential for a positive feedback loop which could exacerbate the disease condition by having the dual consequence of promoting inflammation while blocking remyelination.

Present treatments for MS are immunomodulatory in nature, suppressing inflammation and inhibiting immune infiltration into the CNS, however, this does not fully protect patients from demyelination and eventual axonal loss (Brück et al., 2013). We propose that through advancing our understanding on the potential mechanism(s) by which HMGB1 functions in the context of limiting CNS remyelination, we may exploit this knowledge as a novel means to stimulate endogenous remyelination in the MS brain.

DATA AVAILABILITY STATEMENT

The datasets presented in this study can be found in online repositories. The names of the repository/repositories and accession number(s) can be found below: BioProject accession no. PRJNA524718.

ETHICS STATEMENT

The animal study was reviewed and approved by Institutional Animal Care and Use Committees from UConn Health and Georgetown University.

AUTHOR CONTRIBUTIONS

Experimental design was conceived by MR and SC. *In vitro* studies were performed by MR and PS. *In vivo* studies were conceived by SC and JKH. *In vivo* studies were performed and analyzed by JH and HK. RNAseq analyses were performed by PS and MR. Manuscript was written by MR and SC with editorial contributions from all authors. All authors contributed to the article and approved the submitted version.

FUNDING

This work was supported, in part, by funding from the National Multiple Sclerosis Society (RG-1802-30211 to SC), Harry Weaver Neuroscience Scholar Award (JF-1806-31381 to JKH), and the National Institutes of Health (R01NS107523 to JKH).

ACKNOWLEDGMENTS

We thank Drs. Rosa Guzzo and Jaime Imitola for insightful comments and feedback on this study.

REFERENCES

Absinta, M., Maric, D., Gharagozloo, M., Garton, T., Smith, M. D., Jin, J., et al. (2021). A lymphocyte-microglia-astrocyte axis in chronic active multiple sclerosis. *Nature* 597, 709–714. doi: 10.1038/s41586-021-03892-7

Alomar, S. Y., Gheit, R. E. A. E., Enan, E. T., El-Bayoumi, K. S., Shoaeir, M. Z., Elkazaz, A. Y., et al. (2021). Novel mechanism for memantine in attenuating diabetic neuropathic pain in mice via downregulating the spinal HMGB1/TRL4/NF-kB inflammatory axis. *Pharmaceuticals (Basel)* 14:307. doi: 10.3390/ph14040307

Andersson, U., Wang, H., Palmblad, K., Aveberger, A. C., Bloom, O., Erlandsson-Harris, H., et al. (2000). High mobility group 1 protein (HMG-1) stimulates proinflammatory cytokine synthesis in human monocytes. *J. Exp. Med.* 192, 565–570. doi: 10.1084/jem.192.4.565

Back, S. A., Tuohy, T. M. F., Chen, H., Wallingford, N., Craig, A., Struve, J., et al. (2005). Hyaluronan accumulates in demyelinated lesions and inhibits oligodendrocyte progenitor maturation. *Nat. Med.* 11, 966–972. doi: 10.1038/nm1279

Balasa, R., Barcutean, L., Mosora, O., and Manu, D. (2021). Reviewing the significance of blood-brain barrier disruption in multiple sclerosis pathology and treatment. *Int. J. Mol. Sci.* 22:8370. doi: 10.3390/ijms22168370

Baydyuk, M., Cha, D. S., Hu, J., Yamazaki, R., Miller, E. M., Smith, V. N., et al. (2019). Tracking the evolution of CNS remyelinating lesion in mice with neutral red dye. *Proc. Natl. Acad. Sci. U S A* 116, 14290–14299. doi: 10.1073/pnas.1819343116

Bonaldi, T., Talamo, F., Scaffidi, P., Ferrera, D., Porto, A., Bachi, A., et al. (2003). Monocytic cells hyperacetylate chromatin protein HMGB1 to redirect it towards secretion. *EMBO J.* 22, 5551–5560. doi: 10.1093/emboj/cdg516

Bonetti, B., Stegagno, C., Cannella, B., Rizzuto, N., Moretto, G., and Raine, C. S. (1999). Activation of NF-κB and c-*jun* transcription factors in multiple sclerosis lesions. Implications for oligodendrocyte pathology. *Am. J. Pathol.* 155, 1433–1438. doi: 10.1016/s0002-9440(10)65456-9

Brück, W., Gold, R., Lund, B. T., Oreja-Guevara, C., Prat, A., Spencer, C. M., et al. (2013). Therapeutic decisions in multiple sclerosis: moving beyond efficacy. *JAMA Neurol.* 70, 1315–1324. doi: 10.1001/jamaneurol.2013.3510

Bucova, M., Majernikova, B., Durmanova, V., Cudrakova, D., Gmitterova, K., Lisa, I., et al. (2020). HMGB1 as a potential new marker of disease activity in patients with multiple sclerosis. *Neurol. Sci.* 41, 599–604. doi: 10.1007/s10072-019-04136-3

Chang, A., Tourtellotte, W. W., Rudick, R., and Trapp, B. D. (2002). Premyelinating oligodendrocytes in chronic lesions of multiple sclerosis. *N. Engl. J. Med.* 346, 165–173. doi: 10.1056/NEJMoa010994

Ciprandi, G., Bellussi, L. M., Passali, G. C., Damiani, V., and Passali, D. (2020). HMGB1 in nasal inflammatory diseases: a reappraisal 30 years after its discovery. *Expert Rev. Clin. Immunol.* 16, 457–463. doi: 10.1080/1744666X.2020.1752668

Davalos, A. R., Kawahara, M., Malhotra, G. K., Schaum, N., Huang, J., Ved, U., et al. (2013). p53-dependent release of Alarmin HMGB1 is a central mediator of senescent phenotypes. *J. Cell Biol.* 201, 613–629. doi: 10.1083/jcb.201206006

Ellerman, J. E., Brown, C. K., De Vera, M., Zeh, H. J., Billiar, T., Rubartelli, A., et al. (2007). Masquerader: high mobility group box-1 and cancer. *Clin. Cancer Res.* 13, 2836–2848. doi: 10.1158/1078-0432.CCR-06-1953

Faissner, S., and Gold, R. (2019). Progressive multiple sclerosis: latest therapeutic developments and future directions. *Ther. Adv. Neurol. Disord.* 12:1756286419878323. doi: 10.1177/1756286419878323

Fancy, S. P., Zhao, C., and Franklin, R. J. (2004). Increased expression of Nkx2.2 and Olig2 identifies reactive oligodendrocyte progenitor cells responding to demyelination in the adult CNS. *Mol. Cell. Neurosci.* 27, 247–254. doi: 10.1016/j.mcn.2004.06.015

Gaikwad, S., Puangmalai, N., Bittar, A., Montalbano, M., Garcia, S., Mcallen, S., et al. (2021). Tau oligomer induced HMGB1 release contributes to cellular senescence and neuropathology linked to Alzheimer's disease and frontotemporal dementia. *Cell Rep.* 36:109419. doi: 10.1016/j.celrep.2021.109419

Goldstein, R. S., Gallowitsch-Puerta, M., Yang, L., Rosas-Ballina, M., Huston, J. M., Czura, C. J., et al. (2006). Elevated high-mobility group box 1 levels in patients with cerebral and myocardial ischemia. *Shock* 25, 571–574. doi: 10.1097/01.shk.0000209540.99176.72

Gorgulho, C. M., Romagnoli, G. G., Bharthi, R., and Lotze, M. T. (2019). Johnny on the spot-chronic inflammation is driven by HMGB1. *Front. Immunol.* 10:1561. doi: 10.3389/fimmu.2019.01561

Gudi, V., Gingele, S., Skripuletz, T., and Stangel, M. (2014). Glial response during cuprizone-induced de- and remyelination in the CNS: lessons learned. *Front. Cell. Neurosci.* 8:73. doi: 10.3389/fncel.2014.00073

Hoarau, J. J., Krejbich-Trotot, P., Jaffar-Bandjee, M. C., Das, T., Thon-Hon, G. V., Kumar, S., et al. (2011). Activation and control of CNS innate immune responses in health and diseases: a balancing act finely tuned by neuroimmune regulators (NIReg). *CNS Neurol. Disord. Drug Targets* 10, 25–43. doi: 10.2174/187152711794488601

Hori, O., Brett, J., Slattery, T., Cao, R., Zhang, J., Chen, J. X., et al. (1995). The receptor for advanced glycation end products (RAGE) is a cellular binding site for amphoterin. Mediation of neurite outgrowth and co-expression of rage and amphoterin in the developing nervous system. *J. Biol. Chem.* 270, 25752–25761. doi: 10.1074/jbc.270.43.25752

Khaledi, E., Noori, T., Mohammadi-Farani, A., Sureda, A., Dehpour, A. R., Yousefi-Manesh, H., et al. (2021). Trifluoperazine reduces cuprizone-induced demyelination via targeting Nrf2 and IKB in mice. *Eur. J. Pharmacol.* 909:174432. doi: 10.1016/j.ejphar.2021.174432

Lian, Y. J., Gong, H., Wu, T. Y., Su, W. J., Zhang, Y., Yang, Y. Y., et al. (2017). Ds-HMGB1 and fr-HMGB induce depressive behavior through neuroinflammation in contrast to nonoxid-HMGB1. *Brain Behav. Immun.* 59, 322–332. doi: 10.1016/j.bbi.2016.09.017

Liang, W. J., Yang, H. W., Liu, H. N., Q32an, W., and Chen, X. L. (2020). HMGB1 upregulates NF-kB by inhibiting IKB-α and associates with diabetic retinopathy. *Life Sci.* 241:117146. doi: 10.1016/j.lfs.2019.117146

Liu, T., Son, M., and Diamond, B. (2020). HMGB1 in systemic lupus erythematosus. *Front. Immunol.* 11:1057. doi: 10.3389/fimmu.2020.01057

Liu, T., Zhang, L., Joo, D., and Sun, S. C. (2017). NF-κB signaling in inflammation. *Signal Transduct. Targeted Ther.* 2:17023. doi: 10.1038/sigtrans.2017.23

Lloyd, A. F., Davies, C. L., Holloway, R. K., Labrak, Y., Ireland, G., Carradori, D., et al. (2019). Central nervous system regeneration is driven by microglia necroptosis and repopulation. *Nat. Neurosci.* 22, 1046–1052. doi: 10.1038/s41593-019-0418-z

Lohani, N., and Rajeswari, M. R. (2016). Dichotomous life of DNA binding high mobility group box1 protein in human health and disease. *Curr. Protein Pept. Sci.* 17, 762–775. doi: 10.2174/1389203717666160226145217

Mi, H., Muruganujan, A., and Thomas, P. D. (2013). PANTHER in 2013: modeling the evolution of gene function and other gene attributes, in the context of phylogenetic trees. *Nucleic Acids Res.* 41, D377–D386. doi: 10.1093/nar/gks1118

Moore, C. S., Milner, R., Nishiyama, A., Frausto, R. F., Serwanski, D. R., Pagarigan, R. R., et al. (2011). Astrocytic tissue inhibitor of metalloproteinase-1 (TIMP-1) promotes oligodendrocyte differentiation and enhances CNS myelination. *J. Neurosci.* 31, 6247–6254. doi: 10.1523/JNEUROSCI.5474-10.2011

Mutukula, N., Man, Z., Takahashi, Y., Iniesta Martinez, F., Morales, M., Carreon-Guarnizo, E., et al. (2021). Generation of RRMS and PPMS specific iPSCs as a platform for modeling multiple sclerosis. *Stem Cell Res.* 53:102319. doi: 10.1016/j.scr.2021.102319

Nicaise, A. M., Banda, E., Guzzo, R. M., Russomanno, K., Castro-Borrero, W., Willis, C. M., et al. (2017). iPS-derived neural progenitor cells from PPMS patients reveal defect in myelin injury response. *Exp. Neurol.* 288, 114–121. doi: 10.1016/j.expneurol.2016.11.012

Nicaise, A. M., Wagstaff, L. J., Willis, C. M., Paisie, C., Chandok, H., Robson, P., et al. (2019). Cellular senescence in progenitor cells contributes to diminished remyelination potential in progressive multiple sclerosis. *Proc. Natl. Acad. Sci. U S A* 116, 9030–9039. doi: 10.1073/pnas.1818348116

Nishibori, M., Wang, D., Ousaka, D., and Wake, H. (2020). High mobility group Box-1 and blood-brain barrier disruption. *Cells* 9:2650. doi: 10.3390/cells9122650

O'Connor, K. A., Hansen, M. K., Rachal Pugh, C., Deak, M. M., Biedenkapp, J. C., Milligan, E. D., et al. (2003). Further characterization of high mobility group box 1 (HMGB1) as a proinflammatory cytokine: central nervous system effects. *Cytokine* 24, 254–265. doi: 10.1016/j.cyto.2003.08.001

Park, J. S., Svetkauskaite, D., He, Q., Kim, J. Y., Strassheim, D., Ishizaka, A., et al. (2004). Involvement of toll-like receptors 2 and 4 in cellular activation by high mobility group box 1 protein. *J. Biol. Chem.* 279, 7370–7377. doi: 10.1074/jbc.M306793200

Psachoulia, K., Chamberlain, K. A., Heo, D., Davis, S. E., Paskus, J. D., Nanescu, S. E., et al. (2016). IL4I1 augments CNS remyelination and axonal protection by modulating T cell driven inflammation. *Brain* 139, 3121–3136. doi: 10.1093/brain/aww254

Robinson, A. P., Caldis, M. W., Harp, C. T., Goings, G. E., and Miller, S. D. (2013). High-mobility group box 1 protein (HMGB1) neutralization ameliorates experimental autoimmune encephalomyelitis. *J. Autoimmun.* 43, 32–43. doi: 10.1016/j.jaut.2013.02.005

Rouillard, A. D., Gundersen, G. W., Fernandez, N. F., Wang, Z., Monteiro, C. D., Mcdermott, M. G., et al. (2016). The harmonizome: a collection of processed datasets gathered to serve and mine knowledge about genes and proteins. *Database (Oxford)* 2016:baw100. doi: 10.1093/database/baw100

Santos, G., Barateiro, A., Gomes, C. M., Brites, D., and Fernandes, A. (2018). Impaired oligodendrogenesis and myelination by elevated S100B levels during neurodevelopment. *Neuropharmacology* 129, 69–83. doi: 10.1016/j.neuropharm.2017.11.002

Skaper, S. D. (2019). Oligodendrocyte precursor cells as a therapeutic target for demyelinating diseases. *Prog. Brain Res.* 245, 119–144. doi: 10.1016/bs.pbr.2019.03.013

Sloane, J. A., Batt, C., Ma, Y., Harris, Z. M., Trapp, B., and Vartanian, T. (2010). Hyaluronan blocks oligodendrocyte progenitor maturation and remyelination through TLR2. *Proc. Natl. Acad. Sci. U S A* 107, 11555–11560. doi: 10.1073/pnas.1006496107

Stone, S., Jamison, S., Yue, Y., Durose, W., Schmidt-Ullrich, R., and Lin, W. (2017). NF-κB activation protects oligodendrocytes against inflammation. *J. Neurosci.* 37, 9332–9344. doi: 10.1523/JNEUROSCI.1608-17.2017

Voet, S., Prinz, M., and Van Loo, G. (2019). Microglia in central nervous system inflammation and multiple sclerosis pathology. *Trends Mol. Med.* 25, 112–123. doi: 10.1016/j.molmed.2018.11.005

Wang, H., Bloom, O., Zhang, M., Vishnubhakat, J. M., Ombrellino, M., Che, J., et al. (1999). HMG-1 as a late mediator of endotoxin lethality in mice. *Science* 285, 248–251. doi: 10.1126/science.285.5425.248

Wang, M., Gauthier, A., Daley, L., Dial, K., Wu, J., Woo, J., et al. (2019). The role of HMGB1, a nuclear damage-associated molecular pattern molecule, in the pathogenesis of lung diseases. *Antioxid. Redox Signal.* 31, 954–993. doi: 10.1089/ars.2019.7818

Wasko, N. J., Kulak, M. H., Paul, D., Nicaise, A. M., Yeung, S. T., Nichols, F. C., et al. (2019). Systemic TLR2 tolerance enhances central nervous system remyelination. *J. Neuroinflammation* 16:158. doi: 10.1186/s12974-019-1540-2

Watanabe, H., and Son, M. (2021). The immune tolerance role of the HMGB1-RAGE axis. *Cells* 10:564. doi: 10.3390/cells10030564

Wiley, C. D., Velarde, M. C., Lecot, P., Liu, S., Sarnoski, E. A., Freund, A., et al. (2016). Mitochondrial Dysfunction induces senescence with a distinct secretory phenotype. *Cell Metab.* 23, 303–314. doi: 10.1016/j.cmet.2015.11.011

Wolswijk, G. (1998). Chronic stage multiple sclerosis lesions contain a relatively quiescent population of oligodendrocyte precursor cells. *J. Neurosci.* 18, 601–609. doi: 10.1523/JNEUROSCI.18-02-00601.1998

Wolswijk, G. (2002). Oligodendrocyte precursor cells in the demyelinated multiple sclerosis spinal cord. *Brain* 125, 338–349. doi: 10.1093/brain/awf031

Yang, H., Andersson, U., and Brines, M. (2021). Neurons are a primary driver of inflammation *via* release of HMGB1. *Cells* 10:2791. doi: 10.3390/cells10102791

Yang, Q. W., Lu, F. L., Zhou, Y., Wang, L., Zhong, Q., Lin, S., et al. (2011). HMBG1 mediates ischemia-reperfusion injury by TRIF-adaptor independent Toll-like receptor 4 signaling. *J. Cereb. Blood Flow Metab.* 31, 593–605. doi: 10.1038/jcbfm.2010.129

Yang, H., and Tracey, K. J. (2010). Targeting HMGB1 in inflammation. *Biochim. Biophys. Acta* 1799, 149–156. doi: 10.1016/j.bbagrm.2009.11.019

Zhang, J., Takahashi, H. K., Liu, K., Wake, H., Liu, R., Maruo, T., et al. (2011). Anti-high mobility group box-1 monoclonal antibody protects the blood-brain barrier from ischemia-induced disruption in rats. *Stroke* 42, 1420–1428. doi: 10.1161/STROKEAHA.110.598334

Conflict of Interest: The authors declare that the research was conducted in the absence of any commercial or financial relationships that could be construed as a potential conflict of interest.

Publisher's Note: All claims expressed in this article are solely those of the authors and do not necessarily represent those of their affiliated organizations, or those of the publisher, the editors and the reviewers. Any product that may be evaluated in this article, or claim that may be made by its manufacturer, is not guaranteed or endorsed by the publisher. All authors contributed to the article and approved the submitted version.

Copyright © 2022 Rouillard, Hu, Sutter, Kim, Huang and Crocker. This is an open-access article distributed under the terms of the Creative Commons Attribution License (CC BY). The use, distribution or reproduction in other forums is permitted, provided the original author(s) and the copyright owner(s) are credited and that the original publication in this journal is cited, in accordance with accepted academic practice. No use, distribution or reproduction is permitted which does not comply with these terms.

frontiers | Frontiers in Cellular Neuroscience

ORIGINAL RESEARCH
published: 06 June 2022
doi: 10.3389/fncel.2022.893629

A Subset of Oligodendrocyte Lineage Cells Interact With the Developing Dorsal Root Entry Zone During Its Genesis

Lauren A. Green[1,2†], Robert M. Gallant[1†], Jacob P. Brandt[1], Ev L. Nichols[1] and Cody J. Smith[1,2]*

[1] Department of Biological Sciences, University of Notre Dame, Notre Dame, IN, United States, [2] Center for Stem Cells and Regenerative Medicine, University of Notre Dame, Notre Dame, IN, United States

Oligodendrocytes are the myelinating cell of the CNS and are critical for the functionality of the nervous system. In the packed CNS, we know distinct profiles of oligodendrocytes are present. Here, we used intravital imaging in zebrafish to identify a distinct oligodendrocyte lineage cell (OLC) that resides on the dorsal root ganglia sensory neurons in the spinal cord. Our profiling of OLC cellular dynamics revealed a distinct cell cluster that interacts with peripheral sensory neurons at the dorsal root entry zone (DREZ). With pharmacological, physical and genetic manipulations, we show that the entry of dorsal root ganglia pioneer axons across the DREZ is important to produce sensory located oligodendrocyte lineage cells. These oligodendrocyte lineage cells on peripherally derived sensory neurons display distinct processes that are stable and do not express *mbpa*. Upon their removal, sensory behavior related to the DRG neurons is abolished. Together, these data support the hypothesis that peripheral neurons at the DREZ can also impact oligodendrocyte development.

Keywords: zebrafish, glia, oligodendrocyte, sensory neuron, development, DRG

OPEN ACCESS

Edited by:
Wia Baron,
University Medical Center Groningen, Netherlands

Reviewed by:
Hirohide Takebayashi,
Niigata University, Japan
Fernando C. Ortiz,
Autonomous University of Chile, Chile
Lisbeth Schmidt Laursen,
Aarhus University, Denmark

***Correspondence:**
Cody J. Smith
csmith67@nd.edu

† These authors have contributed equally to this work

Specialty section:
This article was submitted to Non-Neuronal Cells, a section of the journal Frontiers in Cellular Neuroscience

Received: *10 March 2022*
Accepted: *11 May 2022*
Published: *06 June 2022*

Citation:
Green LA, Gallant RM, Brandt JP, Nichols EL and Smith CJ (2022) A Subset of Oligodendrocyte Lineage Cells Interact With the Developing Dorsal Root Entry Zone During Its Genesis. Front. Cell. Neurosci. 16:893629. doi: 10.3389/fncel.2022.893629

INTRODUCTION

Oligodendrocytes are the myelinating glial cell-type of the central nervous system. We know this myelination is essential for the classically described role of insulation that aids in saltatory conductance of neuronal information throughout the body (Nave and Werner, 2014; Allen and Lyons, 2018). Single-cell RNA sequencing approaches have now clearly demonstrated the heterogeneity among such oligodendrocytes (Marques et al., 2016). For example, scRNA sequencing of mature oligodendrocytes (OLs) in the mouse CNS defined 13 distinct populations of mature OLs (Marques et al., 2016). This data, and others, further identifies heterogeneity within subsets of mature OLs enriched in specific regions of the CNS (Marques et al., 2016; Spitzer et al., 2019; Marisca et al., 2020). In zebrafish, immature oligodendrocyte cells have also been described as heterogeneous in the spinal cord (Marisca et al., 2020). While it is now generally accepted that oligodendrocytes display some heterogeneity, the properties of such heterogeneous populations are less understood.

What we do know is that oligodendrocyte heterogeneity in the spinal cord and forebrain can be driven by distinct progenitors (Cai et al., 2005; Vallstedt et al., 2005; Kessaris et al., 2006; Richardson et al., 2006; Tripathi et al., 2011; Crawford et al., 2016; Naruse et al., 2016). In the spinal cord of mice most OPCs originate from common progenitors in the pMN but a subset of

OPCs also arise from *dbx*$^+$ cells that are positioned more dorsally in the spinal cord (Spassky et al., 1998; Cai et al., 2005; Fogarty et al., 2005; Vallstedt et al., 2005). The recent model of progenitor recruitment during oligodendrocyte specification, in zebrafish, may update the theory of dorsal versus ventral derived oligodendrocytes, indicating they both may migrate from the pMN domain but at temporally distinct times (Ravanelli and Appel, 2015). These studies may support origin and temporal derivation as drivers of heterogeneity. It is also clear that environmental events that OPCs experience while navigating to their mature location could impact heterogeneity. We know tiling, activity-dependent mechanisms and a plethora of signaling cascades impact oligodendrocyte differentiation, sheath production and survival (Kirby et al., 2006; Emery, 2010; Hughes et al., 2013; Nave and Werner, 2014; Hines et al., 2015; Mensch et al., 2015; Koudelka et al., 2016; Allen and Lyons, 2018). However, these developmental events have mostly been studied without the heterogeneity of oligodendrocytes as a focus.

Here, we utilize time-lapse imaging of zebrafish to characterize a distinct population of oligodendrocyte lineage cells (OLCs) that reside on sensory neurons in the spinal cord. Using this approach, we visualize a subpopulation of OPCs that migrate toward peripheral sensory neurons as their axons enter the spinal cord. These migrating OPCs contact the dorsal root entry zone (DREZ) and immediately migrate dorsally to associate specifically with CNS-located sensory nerves. These sensory-related OLCs exhibit and maintain unique molecular and process profiles and display a distinct response to OLCs tiling. In the absence of sensory-related OLCs, we observed an elimination of a behavioral response to a noxious stimulus. The identification of a population of sensory-associated OLCs with anatomical, developmental and functional heterogeneity from classically described oligodendrocytes adds insight to the heterogeneity of oligodendrocyte populations in the nervous system.

RESULTS

Profiling of *sox10*$^+$-Spinal Cord Cell Dynamics Reveals a Sensory Associated OLC

To investigate OLC heterogeneity, we used time-lapse imaging of OLCs in the spinal cord of intact *Tg(sox10:mrfp)* zebrafish (Kirby et al., 2006). We considered that the migration of distinct OL progenitor cells could reveal heterogeneous OL populations. To explore this, we tracked individual oligodendrocyte progenitor cells (OPC) within 40 μm spinal cord z-projections spanning 200 μm in zebrafish from anterior/posterior as they migrated from their precursor domain to when they halted migration to produce oligodendrocyte sheathes. In this profiling, we measured the directional changes and total distance traveled of single oligodendrocytes (**Figure 1A**) ($n = 6$ animals, $n = 20$ OLCs). Even with just two parameters, *k*-means clustering analysis showed at least three clusters of distinct populations of OLCs, one of which includes cells that migrate less than 100 μm with less than 2 directional changes, a second that includes cells migrating a similar distance but with 3–5 directional changes and a third cluster that migrated with distances that varied from 165 to 350 μm and greater than 3 directional changes (**Figure 1A**) ($n = 6$ animals, $n = 20$ OLCs).

To determine if these distinct migration patterns dictate potential heterogeneity of OLs we determined if such clusters corresponded with specific anatomically distinct populations. We noted that a cluster of migrating cells resided on the dorsal side of the spinal cord. To determine if they are associated with a specific neuronal population we marked subsets of neurons with specific transgenes. We first scored the location of the OLCs in *Tg(sox10:megfp); Tg(nbt:dsred)* animals which use regulatory sequences of *sox10* to mark oligodendrocytes and their progenitors and *nbt* to panneuronally label axons (**Figures 1B,C**) ($n = 19$ animals total) (Peri and Nüsslein-Volhard, 2008; Smith et al., 2014). In this analysis, 100% of the direct-migration cluster resided on dorsally located *nbt*$^+$ tracts, indicating their association with neurons (**Figure 1C**) ($n = 10$ animals with *nbt*). The location of these dorsal OLCs corresponded near the dorsal longitudinal fasciculus which contains Rohon Beard sensory neurons and DRG sensory neurons in zebrafish. To test if they resided on DRG sensory neurons we similarly scored their association in *Tg(ngn1:gfp); Tg(sox10:mrfp)* animals (Kirby et al., 2006; Prendergast et al., 2012), which mark DRG sensory neurons at 72 hpf as *ngn1*$^+$*; sox10*$^+$. Rohon Beard neurons, in contrast, do not express *sox10* (**Figures 1B,C**). 100% of the direct-migration cluster generated OLCs that reside on the DRG sensory neurons (**Figure 1C**) ($n = 9$ animals with *ngn1*). Throughout the manuscript, we define sensory-related OLCs as *sox10*$^+$ cells that reside on the DRG sensory neurons and non-sensory-related OLCs as *sox10*$^+$ cells that are not located on the sensory neurons.

We further explored the anatomical positioning of sensory-related OLCs by scoring their location in the spinal cord. To do this, we created images that tiled the entirety of the right side of the spinal cord in *Tg(sox10:mrfp);Tg(ngn1:gfp)* animals, allowing us to identify the sensory neurons and the sensory associated OLCs. In this analysis, sensory associated OLCs were distinctly concentrated in two locations in the zebrafish spinal cord. These locations corresponded with DRGs 5–10 and 13–18, with each area having one sensory associated OLC per side of the spinal cord (**Figure 1D**) ($n = 9$ animals). All our analysis below was completed at DRGs 6–10 to maximize our likelihood of visualizing these cells. Collectively, these data led us to further characterize at least one small subpopulation of anatomically distinct OLCs.

Sensory-Related OLCs Are Not Replaced by Surrounding OPC Populations Following Ablation

It is well documented that OPCs intrinsically replenish damaged or apoptotic OLs to fill the newly vacant space following OL death (Kirby et al., 2006; Hughes et al., 2013). We therefore next asked if surrounding non-sensory-related OLC populations could replace an ablated sensory-related OLC. To test this, we ablated individual sensory-related OLCs in *Tg(sox10:mrfp)* animals and

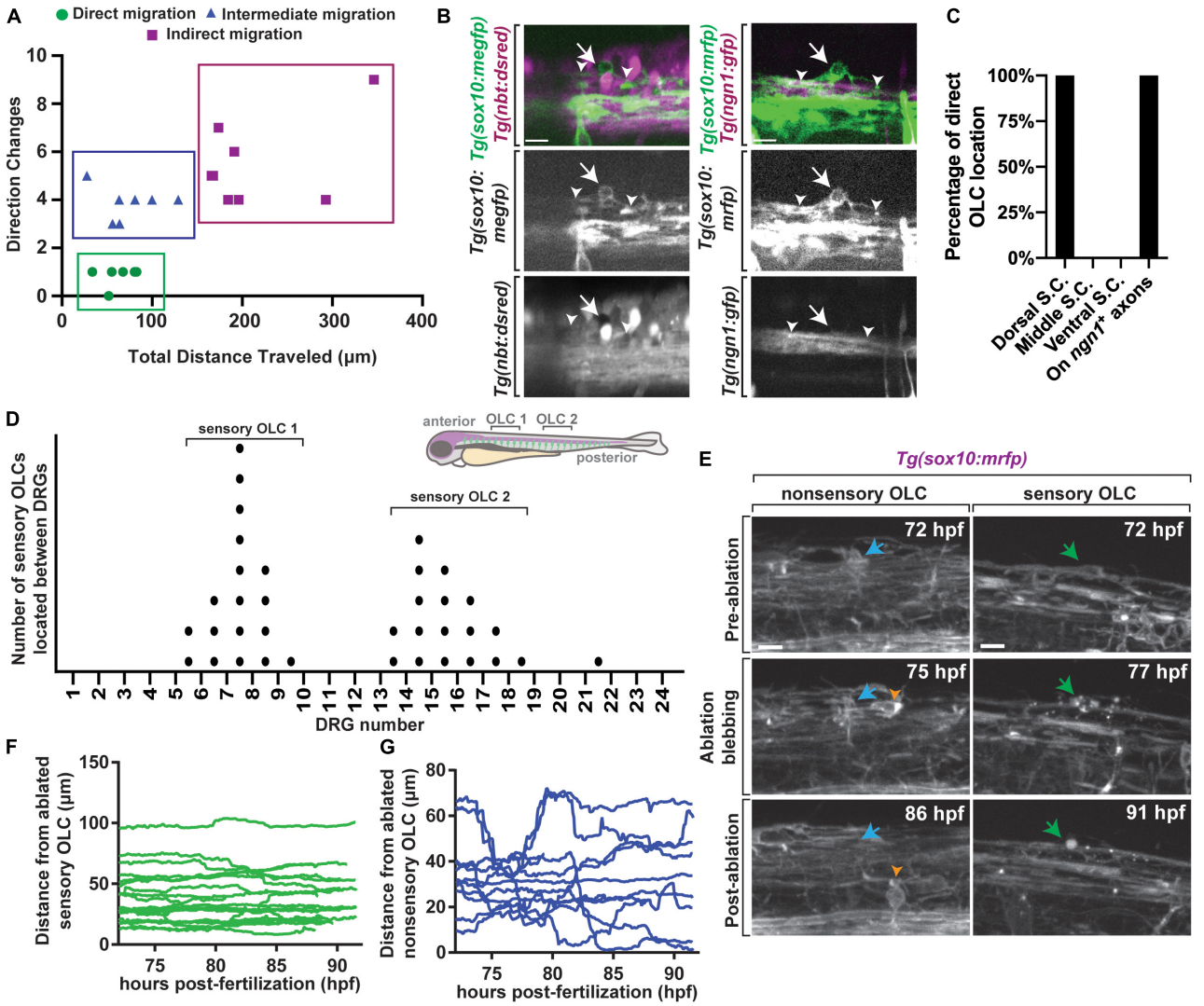

FIGURE 1 | A distinct population of OPCs associates with sensory nerves. **(A)** Plot of individual OPCs with less direct migration versus individual OPCs with a more direct migration. Green dots denote OPC that migrate less and directly. Blue dots denote OPC with longer distances of migration. **(B)** Confocal z-stack images from *Tg(sox10:megfp);Tg(nbt:dsred)* and *Tg(ngn1:gfp);Tg(sox10:mrfp)* animals at 72 hpf showing that dorsal migrating oligodendrocytes associate specifically with sensory neurons. White arrow represents oligodendrocyte associated with sensory neurons and white arrowheads represent sensory axons. **(C)** Quantification of the percentage of OLCs located across specific regions in the spinal cord. **(D)** Quantification of the number of sensory OLs located between specific DRGs. Each point represents one individual sensory OL. Zebrafish diagram in the upper right represents locations of OLC 1 and 2 along the spinal cord. **(E)** Images from a 24 h time-lapse starting at 72 hpf in *Tg(sox10:mrfp)* animals showing the ablation of sensory and non-sensory OLs and surrounding OPC response. Blue arrow represents a non-sensory OL. Green arrow represents a sensory OL. Orange arrowheads represent a responding OPC following non-sensory OL ablation. **(F)** Quantification of the distance surrounding OPCs traveled over time immediately following sensory OL ablation. **(G)** Quantification of the distance surrounding OPCs traveled over time immediately following non-sensory ablation. Scale bar equals 10 μm **(B,E)**. All images are orientated anterior to left, posterior to right, dorsal up and ventral down.

imaged surrounding OL and OPC response from 72 to 96 hpf (**Figure 1E**) (n = 32 animals) (Green et al., 2019). As a control for this, we also ablated individual non-sensory-related OLCs and imaged the surrounding OL response from 72 to 96 hpf. In cases of sensory-related OLC ablation, no surrounding *sox10*$^+$ cell responded to the site of ablation (**Figure 1F**) (n = 19 animals). In cases of non-sensory OL ablation, surrounding *sox10*$^+$ cells immediately responded to the site of ablation as previously reported (**Figure 1G**) (n = 13 animals). These data demonstrate a difference between the sensory subpopulation of OLCs and non-sensory associated OLCs, as they are not replaced by surrounding OLCs.

Sensory-Related OLCs Have Distinct Sheathes

We next tested if these sensory-related OLCs have other distinct structural properties by first measuring their cellular processes. We compared these processes to other classically described OLCs. To investigate this, we imaged sensory-related OLCs in

Tg(nkx2.2a:gfp);Tg(sox10:mrfp) animals at 72 hpf and measured the sheath width and sheath length of both sensory and classically described non-sensory-related OLCs (**Figure 2A**; Kirby et al., 2006). The average process length of sensory-related OLC was 187.78 ± 15.20 μm compared to an average of 94.67 ± 9.88 μm ($p < 0.0001$) for non-sensory OLs, indicating sensory-related OLCs exhibit longer and thinner processes/sheathes than non-sensory OLs (**Figure 2B**) ($n = 12$ sensory-related OLC, 11 non-sensory-related OLC, $p > 0.0001$). Additionally, the average width of sensory-related OLCs process was 5.01 ± 0.23 μm

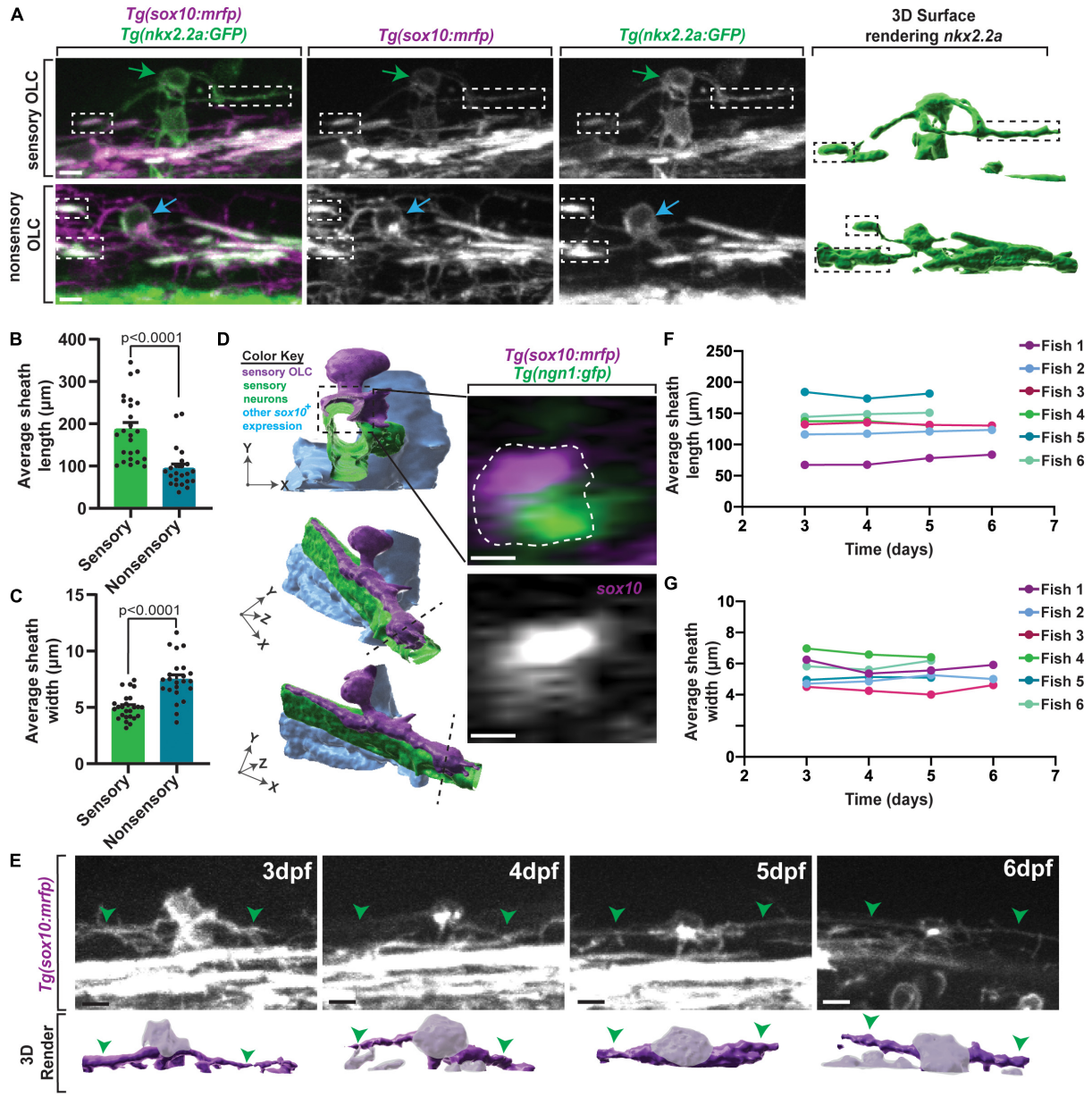

FIGURE 2 | Sensory OLs maintain a distinct sheath profile. **(A)** Confocal z-stack still images of *Tg(nkx2.2a:gfp);Tg(sox10:mrfp)* animals at 72 hpf showing the distinct sheath profile of sensory OLs compared to non-sensory OLs. Green arrows represent a sensory OL. Blue arrows represent a non-sensory OL. White and black boxes represent examples of sheathes. **(B)** Quantification of the average sheath length of sensory OLs compared to non-sensory OLs ($p < 0.0001$). **(C)** Quantification of the average sheath width of sensory OLs compared to non-sensory OLs ($p < 0.0001$). **(D)** 3D IMARIS surface rendering (left) of a sensory-related OLC in *Tg(sox10:mrfp);Tg(ngn1:gfp)* animals from a confocal z-stack image (right) represented at three different angles to show ensheathment of sensory axons. White dashed line represents the cross section view. **(E)** Confocal z-stack images (top row) and IMARIS 3D surface rendering (bottom row) of an individual sensory OL in the same *Tg(sox10:mrfp)* animal at 3dpf, 4dpf, 5dpf, and 6dpf (top row). Green arrowheads represent the sensory axon. Grayed out regions on surface rendering represent sensory OL cell body. **(F)** Quantification of the average sheath length of the same OL in the same animal over time. **(G)** Quantification of the average sheath width of the same OL in the same animals over time. Scale bar equals 10 μm **(A,D,E)**. All images are orientated anterior to left, posterior to right, dorsal up and ventral down.

compared to an average of 7.49 ± 0.41 μm for non-sensory OLs, demonstrating that sensory-related OLCs have a distinct process profile compared to other non-sensory OLs (**Figure 2C**) (n = 12 sensory-related OLC, 11 non-sensory-related OLC, $p > 0.0001$).

Oligodendrocytes ensheath axonal domains whereas precursor and progenitor populations do not (Nave and Werner, 2014; Allen and Lyons, 2018). To determine if these unique processes ensheath, similar to other oligodendrocyte populations, we imaged *Tg(ngn1:gfp); Tg(sox10:mrfp)* animals at 3 dpf. These animals label sensory neurons in GFP and mRFP and sensory-related OLC in mRFP. We then reconstructed the surfaces of the cells and digitally rotated the images. In these images, mRFP cell membrane can be visualized outside and ensheathed around GFP; mRFP axons, likely indicating ensheathment of the axon. These data indicate the sensory-related OLC at 3 dpf have at least initiated ensheathment of axons, likely designating them as oligodendrocytes, albeit by current definitions (**Figure 2D**). Furthermore, time-lapse imaging with *Tg(sox10:mrfp)* animals revealed that oligodendrocyte lineage cells located on sensory axons do not divide, at least during our 24 h imaging windows, potentially arguing again against them representing an immature progenitor or precursor cell.

It is possible that the difference in processes was an indication of immaturity, where sensory-associated OLC represent less mature cells. In zebrafish, classically described oligodendrocytes do not change the number of myelin sheathes after the first 3 h of ensheathment (Watkins et al., 2008; Czopka et al., 2013). We therefore asked if this distinct cellular process profile in sensory-associated OLCs is maintained over time. To test this, we located one sensory-related OLC in individual *Tg(nkx2.2a:gfp);Tg(sox10:mrfp)* animals at 3 dpf. We then imaged that same sensory-related OLC per animal at 4 dpf, 5 dpf, and 6 dpf, far exceeding the published 3-h window of sheath dynamics (**Figure 2E**) (n = 6 animals) (Watkins et al., 2008; Czopka et al., 2013). To ask if individual cellular processes themselves were stable, we measured the length and width of the individual processes. These measurements showed the average process length per sensory-related OLC per animal was maintained from 3 to 6 dpf (**Figure 2F**) (fish 1 $p = 0.8621$, fish 2 $p = 0.9969$, fish 3 $p = 0.9988$, fish 4 $p = 0.9217$, fish 5 $p = 0.9604$, fish 6 $p = 0.9562$). Similarly, these measurements also showed the average process width per sensory-related OLC per animal was maintained from 3 to 6 dpf (**Figure 2G**) (fish 1 $p = 0.7275$, fish 2 $p = 0.9834$, fish 3 $p = 0.9207$, fish 4 $p = 0.9375$, fish 5 $p = 0.9890$, fish 6 $p = 0.9574$). While the length and width of the sheathes did not change overtime, a flattening of the cell body could be visualized (**Figure 2E**). Overall, this data shows that sensory-related OLCs have a cell-process profile that is maintained over time.

Sensory Associated OLCs Are Produced From the Same Spinal Domain as Other OLCs

To uncover potential events that impact sensory-related OLCs production we first considered the possibility that sensory-related OLCs were produced from different oligodendrocyte precursors or progenitors that precedes their arrival to the sensory neurons. In the spinal cord, current literature states that the majority of oligodendrocytes are produced from the *olig2*$^+$ pMN with a subset potentially produced from a more dorsal *dbx*$^+$ pMN domain (Richardson et al., 2006). To determine if these cells are derived from progenitors from different domains we used transgenic markers consistent with different regions of the spinal cord (**Supplementary Figure 1A**). In this analysis, 100% of the sensory associated OLCs expressed *Tg(sox10:mrfp)* and *Tg(sox10:megfp)* that label OPCs and oligodendrocyte (**Supplementary Figure 1B**) (n = 25 animals total). *Tg(dbx:gfp)* labeled 0% of sensory-associated OLCs, indicating that these sensory oligodendrocytes unlikely directly originated from the *dbx*$^+$ region of the spinal cord (n = 7 animals) (Briona and Dorsky, 2014). *Tg(nkx2.2a:gfp)* labeled 50% of the sensory-associated OLC indicating a subset originated from the area around the floor plate region of the spinal cord (n = 8 animals). All the sensory-associated OLCs were labeled with *Tg(olig2:dsred)* specifying they originated from the pMN domain of the spinal cord like other oligodendrocyte populations (n = 7 animals) (Park et al., 2002). These data, in conjunction with previous literature, support the conclusion that both sensory and non-sensory-related OLC are derived from the same spinal domain.

If these sensory-related OLCs are derived from the pMN domain like other oligodendrocytes, then their migration should originate from those ventral spinal domains. We tested this possibility with a second complementary assay by photoconverting OPCs in the ventral spinal region. To trace the direct migration of a single cell to the sensory axon from the ventral spinal cord region, we used *Tg(sox10:eos)* to photoconvert all ventral OPCs and imaged migration from 48 to 72 hpf (**Supplementary Figure 1C**) (n = 3 animals) (McGraw et al., 2012; Green and Smith, 2018). We observed photoconverted (red) cells migrate dorsally from the ventral spinal cord directly to the sensory axon (**Supplementary Figure 1D**). These data are inconsistent with the conclusion that the sensory-related OLCs are a result of production from different spinal cord precursor/progenitor domains, at least defined by current spinal domain literature.

Sensory-Related OLCs Interact With the Dorsal Root Entry Zone

We next considered the hypothesis that their migration exposed them to unique spatiotemporal experience. We noted in timelapse movies that these directed OPCs migrated dorsally and halted their migration in the dorsal spinal cord, close to the dorsal root entry zone (DREZ) (Smith et al., 2017). We therefore asked if this cluster of OPCs contact the DREZ during migration. To test this, we imaged *Tg(sox10:gal4;uas:lifeact-gfp)* zebrafish which allow us to visualize thin projections from the OPCs and sensory neurons during pioneer axon entry (Hines et al., 2015; Nichols and Smith, 2019a,b; Zhang et al., 2019). Since axon entry occurs between 48 and 72 hpf we also quantified the number of OPCs located on sensory nerves from 36 to 96 hpf (**Figures 3A,B**) (n = 20 animals). No OPCs were present on sensory axons from 36 to 48 hpf, however, an average of 0.57 ± 0.291 OPCs were present on sensory axons from 48 to 72 hpf and an average of

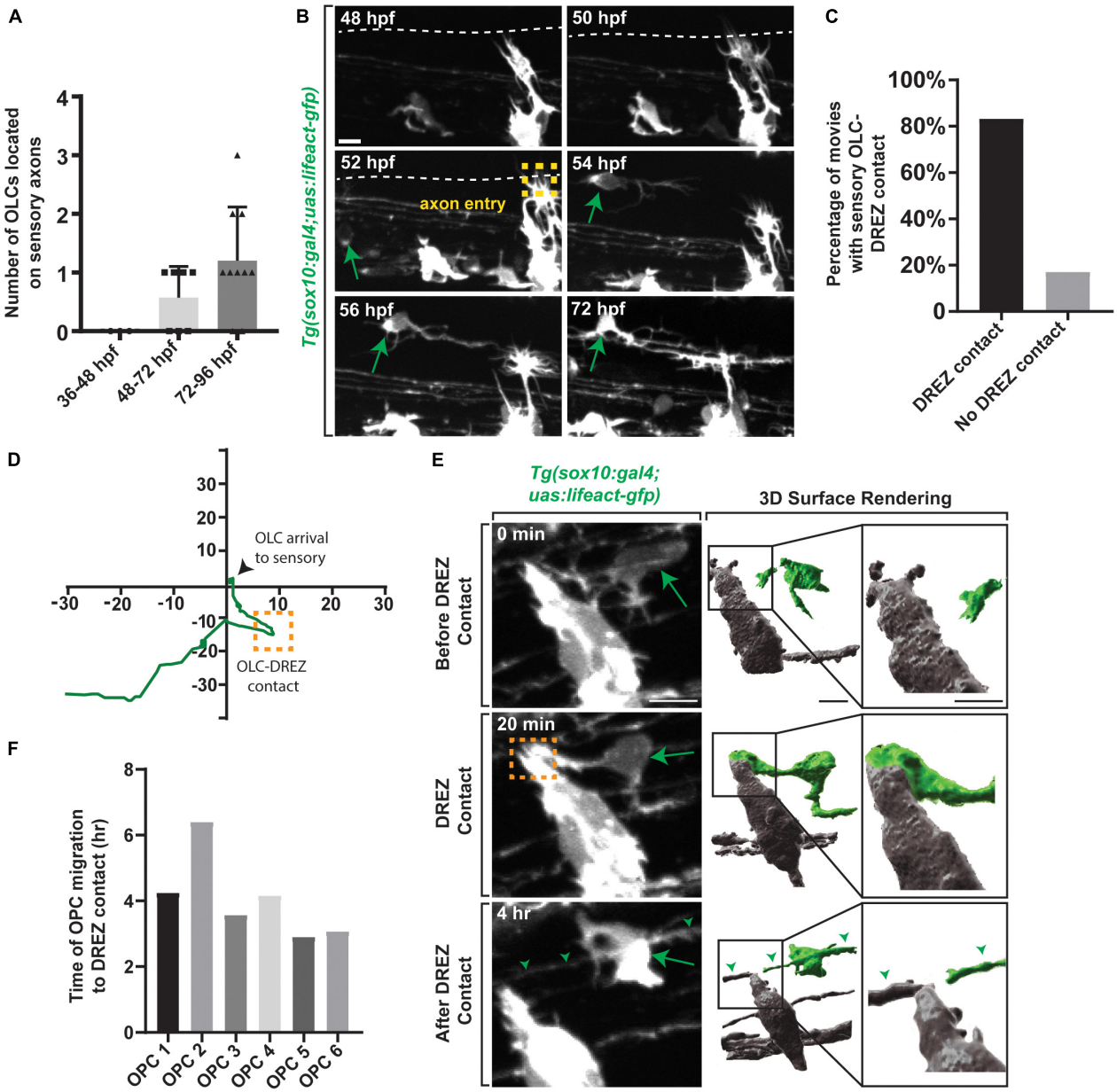

FIGURE 3 | Oligodendrocyte progenitor cells contact the DREZ immediately following axon entry. **(A)** Quantification of the number of OPCs located with DRG sensory nerves from 36 to 96 hpf. **(B)** Images from a 24 h time-lapse movie starting at 48 hpf in *Tg(sox10:gal4; uas:lifeact-gfp)* zebrafish showing OPC migration initiation following axon entry. Green arrow represents migrating OPC. Yellow box represents axon entry. **(C)** Quantification of the percentage of movies where oligodendrocytes arrived to the sensory with or without DREZ contact. **(D)** Migration plot of the path an oligodendrocyte traveled from the ventral spinal cord region to sensory axons. Orange box represents DREZ contact. **(E)** Images from a 24 h time-lapse movie starting at 48 hpf in *Tg(sox10:gal4; uas:lifeact-gfp)* zebrafish showing an oligodendrocyte extending a cellular process that contacts the DREZ. Green arrow represents OPC projection that contacts the DREZ. Orange box indicates OPC-DREZ contact. Green arrowheads represent the sensory axon. IMARIS 3D surface rendering of the 20 min confocal image in showing an OLC cellular process contacting the DREZ. Gray cells are DRG and peripherally located. Green cell is the sensory OL. **(F)** Quantification of the time it takes for an individual OPC to initiate migration post-axon entry and contact the DREZ. Scale bar equals 10 μm **(B,E)**. All images are orientated anterior to left, posterior to right, dorsal up and ventral down.

1.2 ± 0.202 OPCs were present from 72 to 96 hpf (**Figures 3A,B**) (n = 20 animals). Our data further indicate that 80% of OPCs in the directed cluster contacted the DREZ before they halted their migration and produced sheathes on sensory axons (**Figure 3C**) (n = 6 animals). After DREZ contact, these OPCs migrated an average of 17.10 μm dorsally until they halted further migration (**Figure 3D**) (n = 6 animals).

Unlike other events that have been identified to promote oligodendrocyte development, the DREZ is composed of peripheral nervous system components (Golding et al., 1997;

Smith et al., 2017), making it somewhat surprising that it could influence CNS development. To begin to address the role of the DREZ in sensory-related OLCs we assessed when the DREZ-directed OPCs contact the DREZ. For this study, we define the genesis of the DREZ as the time in development when the peripheral nervous system derived pioneer DRG axons enter the spinal cord from their peripheral location (Nichols and Smith, 2019a). In zebrafish, this occurs between 48 and 72 hpf. The precise spatiotemporal location of pioneer axon entry and DREZ genesis can be identified by the formation of actin-based invasive structures in pioneer axons (Nichols and Smith, 2019a,b; Zhang et al., 2019; Kikel-Coury et al., 2021). To ask if DREZ-directed OPCs contact the DREZ during this process we collected z-stacks every 5 min from 48 to 72 hpf in *Tg(sox10:gal4; uas:lifeact-GFP)* animals (**Figures 3E,F**) (n = 6 animals). In these animals, both oligodendrocytes and sensory neurons are labeled with Lifeact-GFP but separated spatially, with OLCs in the spinal cord and sensory neurons in the periphery. We imaged the spinal section where one sensory-related OLC is present per animal. In these movies, 100% of the DREZ-directed OPCs contacted the DREZ after the axons had entered the spinal cord, contacting the peripheral portion of the cells at the DREZ (**Figure 3E** and **Supplementary Figure 2A**) (n = 6 animals). Collectively in the movies, OPC DREZ-contact occurred 4.06 h after pioneer axon entry at the DREZ (**Figure 3F**) (Average time of OPC migration to DREZ per OPC: OPC 1 = 4.25, OPC 2 = 6.40, OPC 3 = 3.58, OPC 4 = 4.16, OPC 5 = 2.91, OPC 6 = 3.08). These results led us to the hypothesis that formation of the DREZ could impact the migration of OPCs from their ventral progenitor.

Formation of the DREZ Is Required to Produce Sensory-Related OLCs

If the genesis of the DREZ directs sensory-related OLCs, then perturbing DREZ formation should alter the production of these sensory-related OLCs. To test this, we altered DREZ formation by disrupting DRG pioneer axons from entering the spinal cord as previously reported (Nichols and Smith, 2019a,b; Zhang et al., 2019). We first did this by blocking DRG pioneer axon entry components using SU6656, an inhibitor of Src that is required for pioneer axons to enter the spinal cord (Nichols and Smith, 2019a). In this experiment *Tg(sox10:mrfp); Tg(ngn1:gfp)* animals were treated with SU6656 or DMSO from 36 to 72 hpf to block axon entry (**Figures 4A,B**) (n = 27 animals total) (Nichols and Smith, 2019a). We imaged a spinal region in these animals that spanned DRGs at somites 6–10 in which we know sensory-related OLCs are located and scored the number of sensory-related OLCs present (**Figure 4C**) (n = 8 animals). In DMSO-treated spinal segments, an average of 0.875 ± 0.085 sensory-related OLCs were present by 72 hpf (n = 16 animals). This was in contrast to an average of 0.091 ± 0.090 sensory OLs that were present in SU6656-treated spinal segments where DREZ formation was perturbed (n = 11 animals) (**Figure 4C**, $p < 0.0001$). These results support the conclusion that failure to form the DREZ could result in reduced migration of OPCs to the sensory axons.

Since this pharmacological treatment is not cell-specific and therefore could impact OPC migration, we also used complementary physical manipulations to test the requirement of DREZ formation to drive sensory-related OLCs. In this paradigm, pioneer axon entry was prevented by ablating the DRG neurons before they produce their pioneer axons and imaged as in our pharmacological experiments (**Figures 4D,E**) (n = 19 animals total). In control spinal segments where the DRG pioneer neuron was not ablated, an average of 0.93 ± 0.077 sensory-related OLCs were present at intact spinal segments (n = 13 animals). This was a stark contrast to spinal segments where the pioneer neurons were ablated, in which we could not detect any sensory-related OLCs (n = 6 animals) (**Figure 4F**, $p < 0.0001$). We could identify the centrally-located DRG axon in DRG ablated animals because adjacent regions to the four-ablated nerves still entered and produced spinal projections.

We extended this analysis by altering the DREZ formation with a third complementary approach. Rac1 activation drives the disassembly of invasive structures and thus by mosaically expressing photoactivatable Rac1 in pioneer neurons and photo activating them during DREZ formation, we can block entry of pioneer axons into the spinal cord (Nichols and Smith, 2019a; Zhang et al., 2019). We injected animals with photoactivatable Rac1 protein at the single-cell stage and imaged *Tg(uas:lifeact-gfp); Tg(sox10:gal4) uas:PA-Rac-mcherry* animals from 48 to 72 hpf (**Figures 4G,H**) (n = 18 animals total) (Nichols and Smith, 2019a; Zhang et al., 2019; Kikel-Coury et al., 2021). Mosaic animals that were selected for this experiment contained PA-Rac-mcherry in the DRG neurons but not sensory-related OLCs, allowing us to manipulate the sensory ingrowth without impacting OLCs directly with Rac1 (**Figure 4I**). In control animals where the PA-Rac protein was injected, but not photoactivated with 445 nm, an average of 1.0 ± 0.111 sensory-related OLCs could be detected in spinal segments (n = 9 animals). In contrast, sensory-related OLCs could not be identified in spinal segments with photoactivated Rac1 (n = 9 animals) (**Figure 4I**, $p < 0.0001$). The simplest explanation for the data from these three manipulations of DREZ formation is consistent with the possibility that DREZ formation is important to produce sensory associated OLCs.

If the formation of the DREZ drives production of distinct OLCs, then altering the timing of DREZ formation should also change the timing of DREZ-directed OPCs and formation of sensory-related OLCs. To address this possibility, we induced early entry of pioneer axons by forcing the formation of invasive structures in pioneer DRG axons as previously noted (**Figure 5A**) (n = 8 animals). To do this, we treated *Tg(sox10:gal4; uas:lifeact-gfp)* animals with paclitaxel, a potent activator of invasive structures, from 36 to 72 hpf, then imaged them from 48 to 72 hpf (**Figures 5A,C,D**) (n = 8 animals) (Nichols and Smith, 2019a,b; Kikel-Coury et al., 2021). To first confirm that pioneer axons entered the spinal cord early we scored the timing of pioneer axon entry. We normalized these time points in DMSO and Paclitaxel treated animals by scoring the time of entry compared to the initiation of the pioneer axon. Consistent with previous reports (Nichols and Smith, 2019a,b; Kikel-Coury et al., 2021), paclitaxel-treated animals had early genesis of the DREZ of 2.33 ± 0.439 h on average compared to DMSO-treated animals where DREZ genesis occurred at

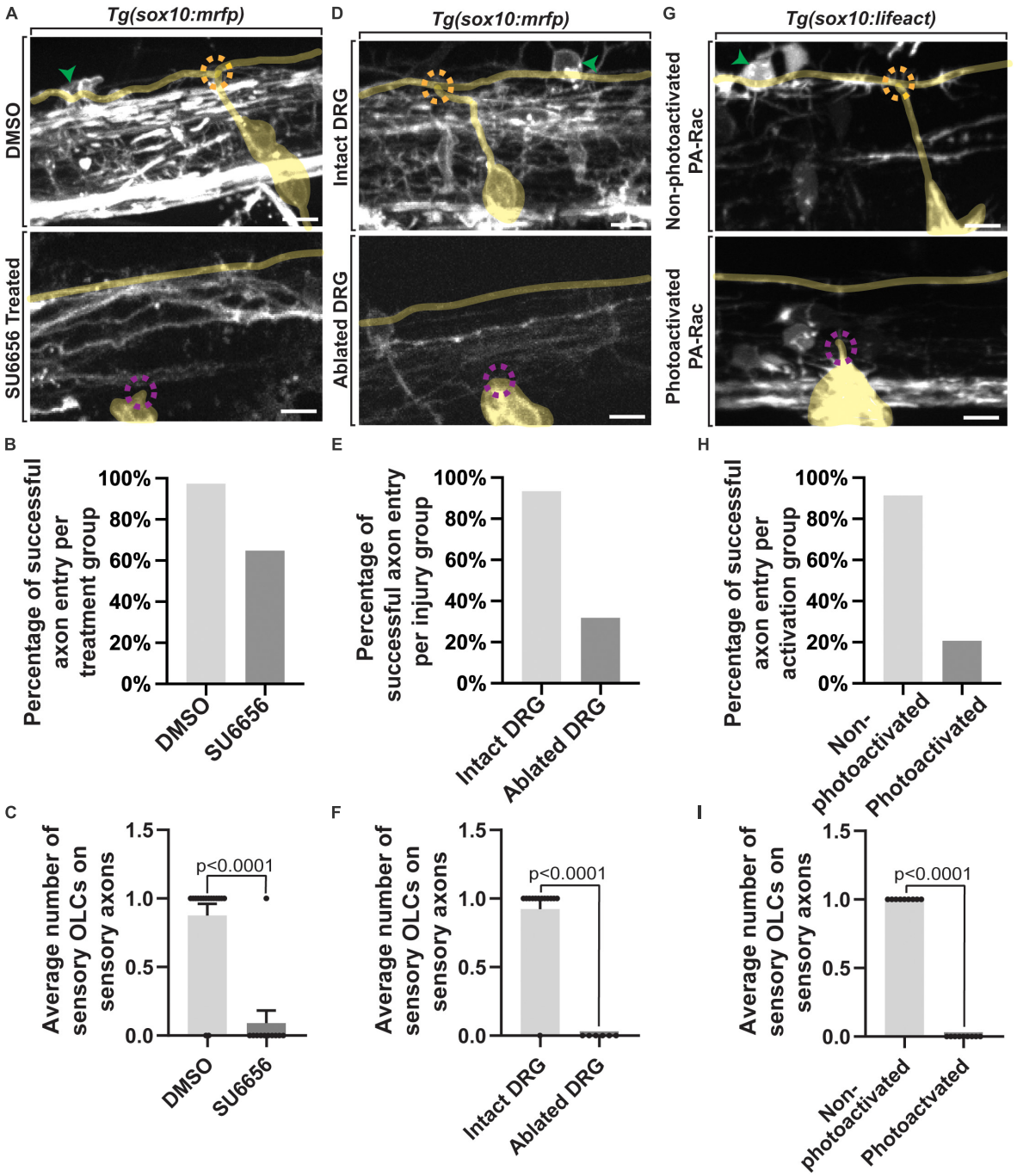

FIGURE 4 | Failed axon entry does not result in sensory-related OLCs. **(A)** Confocal z-stack images of *Tg(sox10:mrfp);Tg(ngn1:gfp)* zebrafish at 3 dpf showing axon entry and the presence or absence of a sensory-related OLC in DMSO control animals compared to SU6656 treated animals. **(B)** Quantification representing the percentage of successful axon entry events per DMSO group versus SU6656 treatments. **(C)** Quantification of the average number of sensory-related OLCs on sensory axons in DMSO versus SU6656 treated animals ($p < 0.0001$). **(D)** Confocal z-stack images of *Tg(sox10:mrfp); Tg(ngn1:gfp)* zebrafish at 3 dpf showing axon entry and the presence or absence of a sensory OL in intact animals compared to animals with ablated DRGs. **(E)** Quantification representing the percentage of successful axon entry events per intact group versus ablated DRGs. **(F)** Quantification of the average number of sensory OCLs on sensory axons in intact DRGs versus ablated DRGs ($p < 0.0001$). **(G)** Confocal z-stack images of *Tg(sox10:gal4; uas:lifeact-gfp)* animals injected with PA-Rac1 at 3 dpf showing axon entry and the presence or absence of a sensory-related OLC in non-photoactivated animals compared to photoactivated animals. **(H)** Quantification representing the percentage of successful axon entry events per non-photoactivated group versus the photoactivated group. **(I)** Quantification of the average number of sensory-related OLCs on sensory axons in non-photoactivated versus photoactivated animals ($p < 0.0001$). All green arrowheads represent sensory-related OLCs. All dashed orange circles represent successful axon entry. All dashed magenta circles represent failed axon entry. Yellow tracing overlays highlight the DRG and sensory axons **(A,D,G)**. Scale bar equals 10 μm **(A,D,G)**. All images are orientated anterior to left, posterior to right, dorsal up and ventral down.

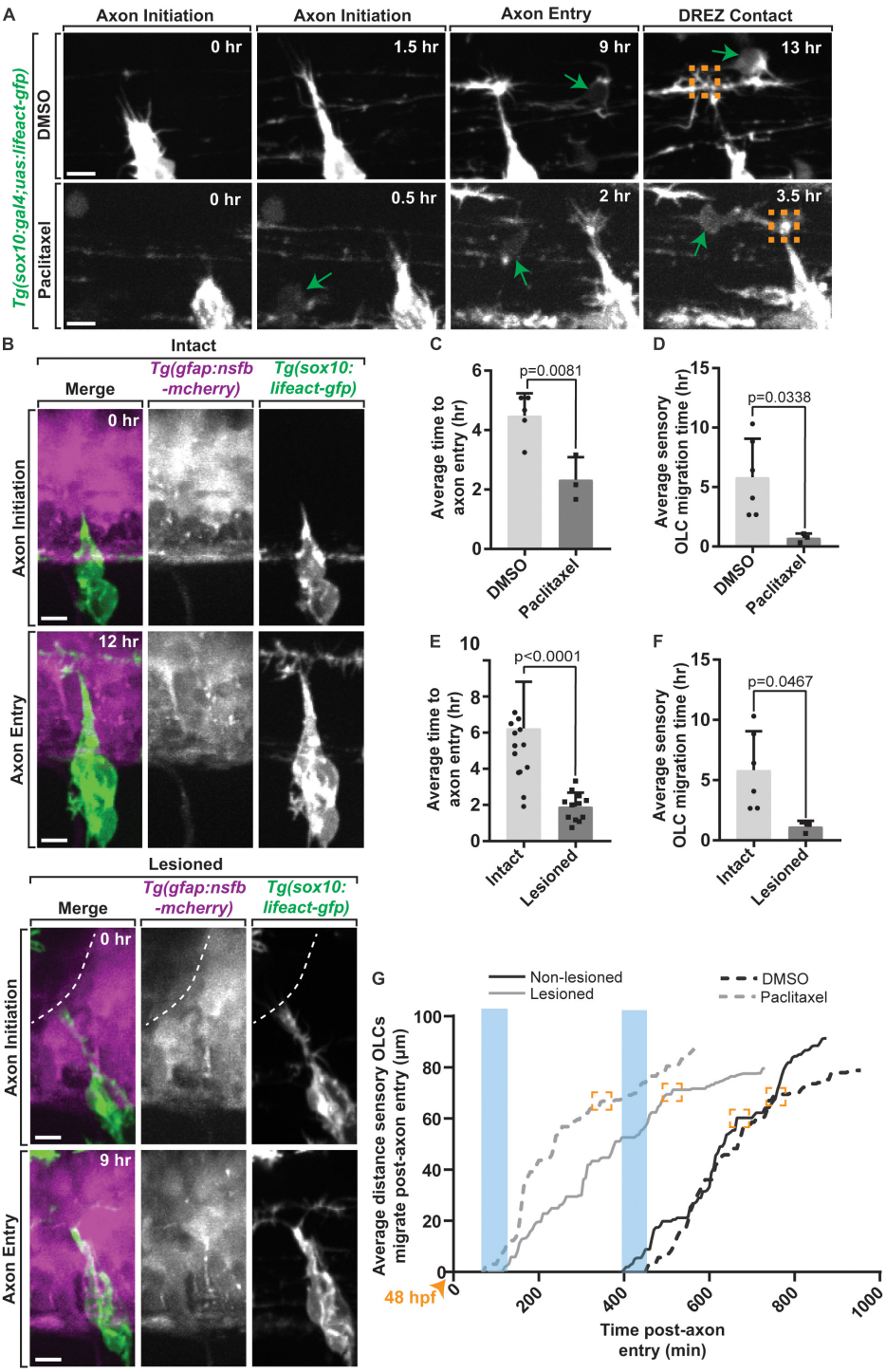

FIGURE 5 | Early axon entry promotes early OPC migration to sensory nerves. **(A)** Images from a 24 h time-lapse movie starting at 48 hpf in *Tg(sox10:gal4;uas:lifeact-gfp)* zebrafish treated with Paclitaxel showing axon initiation and sensory-related OLC and DREZ contact earlier than typical axon entry. Green arrows represent migrating sensory-related OLC. **(B)** Still Images from a 24 h time-lapse movie starting at 48 hpf in intact and lesioned *Tg(sox10:gal4;uas:lifeact-gfp);Tg(gfap:nsfb-mcherry)* zebrafish also showing axon initiation and successful axon entry earlier than typical axon entry. White dashed line indicates lesion site. **(C)** Quantification of average time to axon entry in DMSO and Paclitaxel treated animals ($p = 0.0081$). **(D)** Quantification of the average time to sensory-related OLC migration post-axon entry in DMSO and Paclitaxel treated animals ($p = 0.0338$). **(E,F)** Paralleled quantifications of C-D in Lesioned and Non-lesioned animals ($D = p < 0.0001$, $E = p = 0.0467$). **(G)** Quantification of the average distance and time three OLCs migrated post-axon entry in DMSO and Paclitaxel treated animals and lesioned and non-lesioned animals. Orange arrowhead indicates start of timelapse at 48 hpf. Blue rectangles highlight the time of axon entry. Orange boxes indicate OLC-DREZ contact. Scale bar equals 10 µm **(A,B)**. All images are orientated anterior to left, posterior to right, dorsal up and ventral down.

4.48 ± 0.338 h on average (**Figure 5C**, $p = 0.0081$) ($n = 8$ animals). In support of the hypothesis that DREZ formation drives the production of sensory-related OLCs, paclitaxel-treated animals formed DREZ-directed OPCs at 0.71 ± 0.217 h compared to DMSO that formed at 5.71 ± 1.322 h on average (**Figures 5D,G**) ($p = 0.0338$, $n = 8$ animals). As an argument against the possibility that this accelerated OPC migration was a result of increased velocity of OPCs, we tracked individual DREZ-directed OPCs as they migrated. The velocity of OPC migration in DMSO treated animals was 0.15 ± 0.037 on average compared to 0.08 ± 0.030 in paclitaxel-treated animals (**Supplementary Figure 2B**, $p = 0.3001$, $n = 8$ animals). The duration of time between initiation of OPC migration and arrival to the DREZ in DMSO-treated animals was 4.50 ± 0.936 h on average compared to 1.58 ± 0.096 h in paclitaxel-treated animals (**Supplementary Figure 2C**, $p = 0.0710$, $n = 8$ animals). Both the velocity and time of OPC migration were statistically indistinguishable. Together, these data support the possibility that OPCs migrate earlier when the DRG pioneer axons enter the DREZ early.

We next considered the possibility that the peripherally derived sensory pioneer axon itself could provide a cue to drive sensory-related OLCs. Alternatively, the actual act of the sensory axon breaching the radial glial limitans to cross into the spinal cord could drive the formation of these sensory-related OLCs. To provide insight into these two possibilities, we sought to mimic this potential breach by creating a break in the radial glial limitans with a physical manipulation (Nichols and Smith, 2019a). In this paradigm, we created a lesion of the radial glial limitans in a 10–12 μm region of the spinal cord directly dorsal to the motor exit point where the DREZ consistently forms, prior to pioneer axon initiation in *Tg(sox10:megfp); Tg(gfap:mcherry)* animals at 48 hpf (Nichols and Smith, 2019a). After ablation, we imaged the radial glia lesion site from 48 to 72 hpf and quantified the time of axon initiation to axon entry, or DREZ formation in lesioned and non-lesioned animals (**Figures 5B,E–G**) ($n = 9$ animals total). On average, axons enter in non-lesioned animals at 6.24 ± 0.712 h compared to 1.90 ± 0.225 h in lesioned animals (**Figure 5E**, $p < 0.0001$). We then compared the timing of sensory-related OLC formation and DREZ contact of the OPC. Tracing DREZ directed OPC-cells in these movies revealed that creating an artificial breach of the spinal cord induced OPC-directed migration at an average of 2.0 ± 0.282 h compared to non-lesioned regions that migrated at an average of 6.0 ± 1.322 h (**Figure 5F**, $p = 0.0467$). Arguing against the possibility that this expedited OPC migration was from increased velocity of the OPCs in the control versus experimental paradigm, the time for OPC migration from its initiation to the DREZ or velocity during that time was not significantly different (**Supplementary Figures 2D,E**, $p = 0.5592$ and $p = 0.5445$). Collectively, we observed accelerated OPC initiation of migration was in both Paclitaxel-treated and physically breached animals compared to DMSO-treated and non-breached animals (**Figure 5G**). Although we cannot distinguish between the possibility that sensory OPCs are instructed by sensory neurons versus triggered by the disruption of the glial limitans, we did quantify additional behaviors of sensory and non-sensory OPCs in taxol treated and physically breached animals. In lesioned animals, an average of 2.25 ± 2.0 non-sensory OPCs migrated within 50 μm of the DREZ compared to intact, DMSO treated, and Paclitaxel treated animals (**Supplementary Figures 2F,G**, $p = 0.0203$, $p > 0.9999$). This data suggests the physical breach of the DREZ does elicit an increase in non-sensory OLC migration, however, we did not observe any differences in the number of sensory OLCs. To test whether the physical breaching of the glial limitans may influence the behavior of migrating OPCs, we also quantified the maximum number of dynamic projections created by individual sensory and non-sensory OPCs during their migration to the DREZ in both lesioned animals and Paclitaxel treated animals. We did not detect any changes when compared to their respective intact or DMSO treated controls (**Supplementary Figures 2H–J**, $p = 0.5370$, $p = 0.6433$, $p = 0.2134$, $p = 05801$). The simplest explanation for this data is that the act of pioneer axon entry impacts DREZ-directed OPCs.

Sensory-Related OLCs Have Distinct Molecular Properties to Non-sensory-related OLCs

Given the distinct sheath profile and development of sensory-related OLCs, we next asked whether these cells express myelin-associated factors distinct of other mature myelinating oligodendrocyte (Nave and Werner, 2014). To test this, we imaged *Tg(mbpa:gfp); Tg(sox10:mrfp)* animals at 5 dpf and 15 dpf and scored the number of sensory-associated OLCs that were $mbpa^+$ (**Figure 6A**) ($n = 55$ animals total) (Koudelka et al., 2016). We observed 100% of sensory-related OLCs at 5 dpf animals were $sox10^+$, but 0% were $mbpa^+$ at 5 dpf (**Figure 6B**, $n = 9$, 5 dpf animals). To argue against the possibility that these cells presented immature $mbpa^+$ cells, we also imaged the same *Tg(mbpa:gfp); Tg(sox10:mrfp)* animal at 5 dpf and 15 dpf, which again extends past the typical differentiation period of an oligodendrocyte in zebrafish (Czopka et al., 2013). At 15 dpf, we observed 100% sensory-related OLCs that were $sox10^+$ and 0% sensory-related OLCs that were $mbpa^+$, matching the *mbpa* expression in 5 dpf sensory-related OLCs (**Figure 6B**, $n = 9$, 15 dpf animals). We also quantified the marked *mbpa* expression in non-sensory-related OLCs (**Figure 6C**, $n = 18$ animals total). We observed 25% of non-sensory-related OLCs were $mbpa^-$ while 75% of non-sensory-related OLCs were $mbpa^+$ at 5 dpf ($n = 9$, 5 dpf animals). Similarly at 15 dpf we observed 30% of non-sensory-related OLCs were $mbpa^-$ while 70% of non-sensory-related OLCs were $mbpa^+$ ($n = 9$, 15 dpf animals). To test that the lack of *mbpa* expression in sensory-related OLCs was not specific to the transgene, we also stained animals at 15 dpf with anti-MBPa (**Figure 6D**). At 15 dpf, there were an average of 0.0 ± 0 sensory-related OLCs expressing MBPa (per imaging window) compared to an average of 6.2 ± 1.2 non-sensory-related OLCs that were $MBPa^+$ (per imaging window) (**Figure 6E**, $n = 4$ animals total, $p = 0.0026$). These data are consistent with the possibility that sensory-related OLCs do not express myelin-associated factors at 5 dpf or 15 dpf, past the typical initiation period of ensheathment (Watkins et al., 2008; Czopka et al., 2013). It is important to note that although they do not express myelination components, it is unlikely that these cells

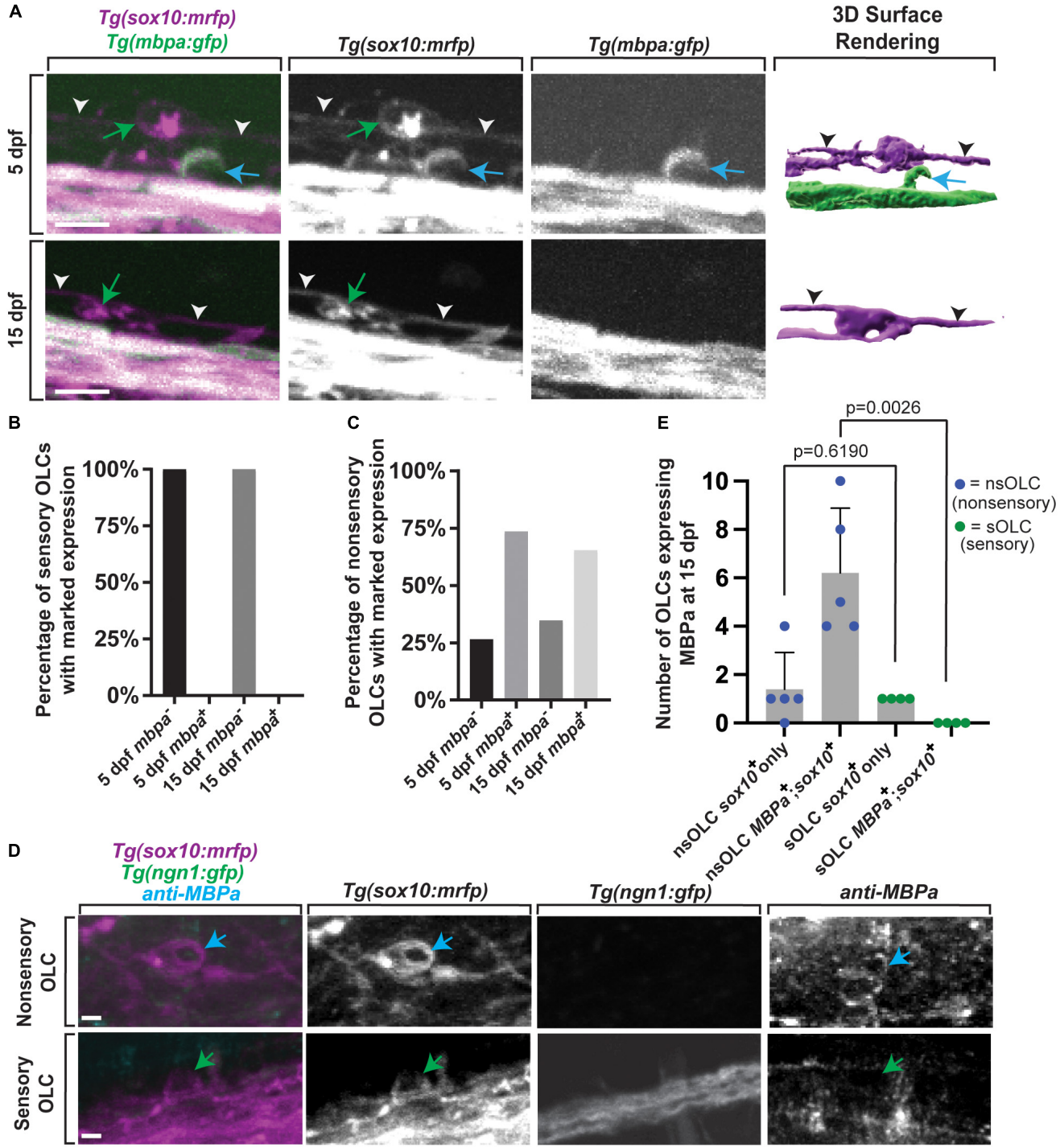

FIGURE 6 | Sensory-related OLCs do not express typical OLC *mbpa* expression. **(A)** Confocal *z*-stack still images of *Tg(mbpa:gfp);Tg(sox10:mrfp)* animals at 5 and 15 dpf showing the lack of *mbpa*$^{+}$ expression in sensory oligodendrocytes. Blue arrows represent non-sensory-related OLCs. Green arrows represent sensory-related OLCs. White and black arrowheads indicate sensory axons. **(B)** Quantification of the percentage of *mbpa*$^{-}$*;sox10*$^{+}$ and *mbpa*$^{+}$*;sox10*$^{+}$ sensory OLs at 5 and 15 dpf. **(C)** Quantification of the percentage of *mbpa*$^{-}$*;sox10*$^{+}$ and *mbpa*$^{+}$*;sox10*$^{+}$ non-sensory OLs at 5 and 15 dpf. **(D)** Confocal *z*-stack still images of *Tg(sox10:mrfp);Tg(ngn1:gfp)* animals at 15 dpf stained with an anti-MBPa antibody showing the lack of anti-MBPa in sensory-related OLCs. Blue arrows represent non-sensory-related OLCs and green arrows represent sensory-related OLCs. **(E)** Quantification of the number of non-sensory-related OLCs (nsOLCs) and sensory-related OLCs (sOLCs) expressing *sox10*$^{+}$ only or at 15 dpf. Scale bar equals 10 μm **(A,E)**. All images are orientated anterior to left, posterior to right, dorsal up and ventral down.

represent NG2 cells because of their expression of *nkx2.2*, which NG2 cells do not express (Hughes and Appel, 2016).

Sensory-Related OLCs Display Distinct Ca^{2+} Transients Than Non-sensory-related OLCs

Oligodendrocytes have been shown to have both spontaneous and evoked Ca^{2+} transients. We next investigated such transients in sensory-related OLCs. DRG neurons can respond to a multitude of stimuli (Lumpkin and Caterina, 2007) and previous literature indicated DRG neurons could be active after exposure to 4°C (Fosque et al., 2015; Nichols and Smith, 2020). We first tested this by imaging *Tg(neurod:gal4); Tg(uas:GCaMP6s)* and measured calcium transients in DRG neurons after exposure to 4 or 23°C water at 3 dpf (n = 21 DRG cells). *Tg(neurod:gal4); Tg(uas:GCaMP6s)* animals were anesthetized for mounting purposes then transferred back into 23°C water without anesthesia before the beginning of the assay (n = 5 animals). Unanesthetized animals were imaged at 2 s intervals, imaged for 1 min, exposed to 23°C water, and then imaged for an additional 1 min, after which 4°C water was added followed by another 1 min of imaging (**Figure 7A**) (n = 21 DRG cells). In this analysis, the Z score of DRG neuron integral densities were measured and used to assess significant changes in GCaMP6s intensity. If GCaMP6s integral density Z score was 2 or greater, this was marked as an active firing event (**Figure 7B**) (n = 5 animals). To verify that this activation was consistent across multiple DRG, we created heat maps of each DRG neuron and their change in GCaMP6s intensity Z score at each timepoint (**Figure 7C**) (n = 5 animals). Using a strict threshold to create a binary assessment of DRG activation, animals exposed to 4°C water resulted in a significant change in the percent of active DRG neurons at an average of 96% as compared to 6.6% activation in 23°C water (**Figure 7D**, $p < 0.0001$, n = 5 animals). These results are consistent with the hypothesis that zebrafish DRG neurons respond to 4°C.

We therefore next tested if sensory-related OLCs display Ca^{2+} characteristics like non-sensory-related OLCs in both spontaneous and evoked scenarios (Krasnow et al., 2018; Marisca et al., 2020). We first asked if sensory-related OLCs display spontaneous activity like those described in previous reports (Hines et al., 2015; Mensch et al., 2015; Baraban et al., 2017; Krasnow et al., 2018; Marisca et al., 2020). To do this *Tg(sox10:gal4); Tg(uas:GCaMP6s)* animals at 3 dpf were imaged. We first imaged baseline Ca^{2+} at 100 ms for 2 min in sensory-related OLCs at 23°C. These movies displayed full cell or sheath Ca^{2+} transients that could be detected in non-sensory OL but not sensory-related OLC (**Figure 7E**) (n = 9 animals total). These data demonstrate that in homeostatic conditions, sensory-related OLC do not display spontaneous Ca^{2+} transients like non-sensory-related OLCs. We may, at the least, expect Ca^{2+} transients to be detectable upon evoking the sensory circuit. To test this we exposed animals to 4°C then measured GCaMP6s intensity in both sensory and non-sensory-related OLCs. Non-sensory-related OLCs displayed an immediate spike in Ca^{2+} transient activity upon exposure to 4°C (**Figure 7F**) (n = 5 non-sensory-related OLCs). Alternatively, sensory-related OLCs did not display full cell/sheath Ca^{2+} transients after exposure to 4°C compared to 23°C (**Figure 7G**) (n = 4 sensory-related OLCs). The average number of peaks with a Z score above 2 was significantly different from 2.0 ± 0.548 in non-sensory-related OLCs compared to 0.25 ± 0.25 in sensory-related OLCs (**Figure 7H**) (n = 9 animals). We then compared the average number of peaks in sensory-related OLCs with a Z score above 2 in 23°C versus 4°C animals and there was no change and the Z scores remained at an average of 0.25 ± 0.25 peaks above threshold, or a Z score below 2 (**Figures 7G,I**) ($p > 0.9999$). These data demonstrate an additional distinct property of sensory-related OLCs from non-sensory-related OLCs.

Sensory-Related OLCs Are Important for Somatosensory Responses

Our results indicate that sensory-related OLCs are located at specific locations in the spinal cord at 5–10 and 13–18 DRGs (**Figure 1D**). We, therefore, next considered the hypothesis that sensory-related OLCs may be required somehow in the sensory response. The DRG neurons fire upon immersion in 4°C, resulting in a hypothermic shivering behavior (Nichols and Smith, 2020; Kikel-Coury et al., 2021). To explore if sensory-related OLCs function in behavior, all detectable sensory-related OLCs on the right side of the animal were ablated at 3 dpf. Following ablation, animals were recovered for 24-h. All animals that were tested displayed an intact sensory axon. Animals with ablated sensory-related OLCs were compared to animals with no ablations. As an additional control that the ablation laser itself did not elicit a change in behavior, the exact laser parameters used to ablate sensory-related OLCs were exposed to a region 10 μm from a sensory-related OLCs (n = 24 animals total). These animals were then immersed in 4°C for 10 sec and the percent of time shivering was calculated. Intact animals displayed a stereotypical shivering for 57.5% of time (intact versus ablation control p = 0.7803) (n = 8 intact animals) (**Figures 8A,B**). A similar phenotype was observed with ablation controls displaying shivering for 53.75% of time (intact versus ablation control p = 0.7803) (n = 8 ablation control animals). This was in contrast to animals in which sensory-related OLCs were removed, which significantly reduced the shiver behavior to 2.5% of time spent shivering (intact versus ablated sensory $p < 0.0001$, ablation control versus ablation sensory $p < 0.0001$) (n = 8 ablated sensory-related OLC animals) (**Figures 8A,B**). To test if this eliminated other somatosensory responses, we performed an assay to determine an intact tactile response by touching the head of the animal with a pipette tip (Kikel-Coury et al., 2021; **Figure 8C**). Following this tactile assay, we could not detect differences in the percentage of intact, ablation control and sensory-related OLC ablated animals exhibiting a tactile response. 87.5% of intact control animals, 100% of ablation control animals, and 100% of ablated sensory-related OLC animals responded to the tactile assay (**Figure 8C**) (n = 24 animals total). In zebrafish at 4 dpf, Rohon Beard and trigeminal neurons detect tactile responses while the DRG

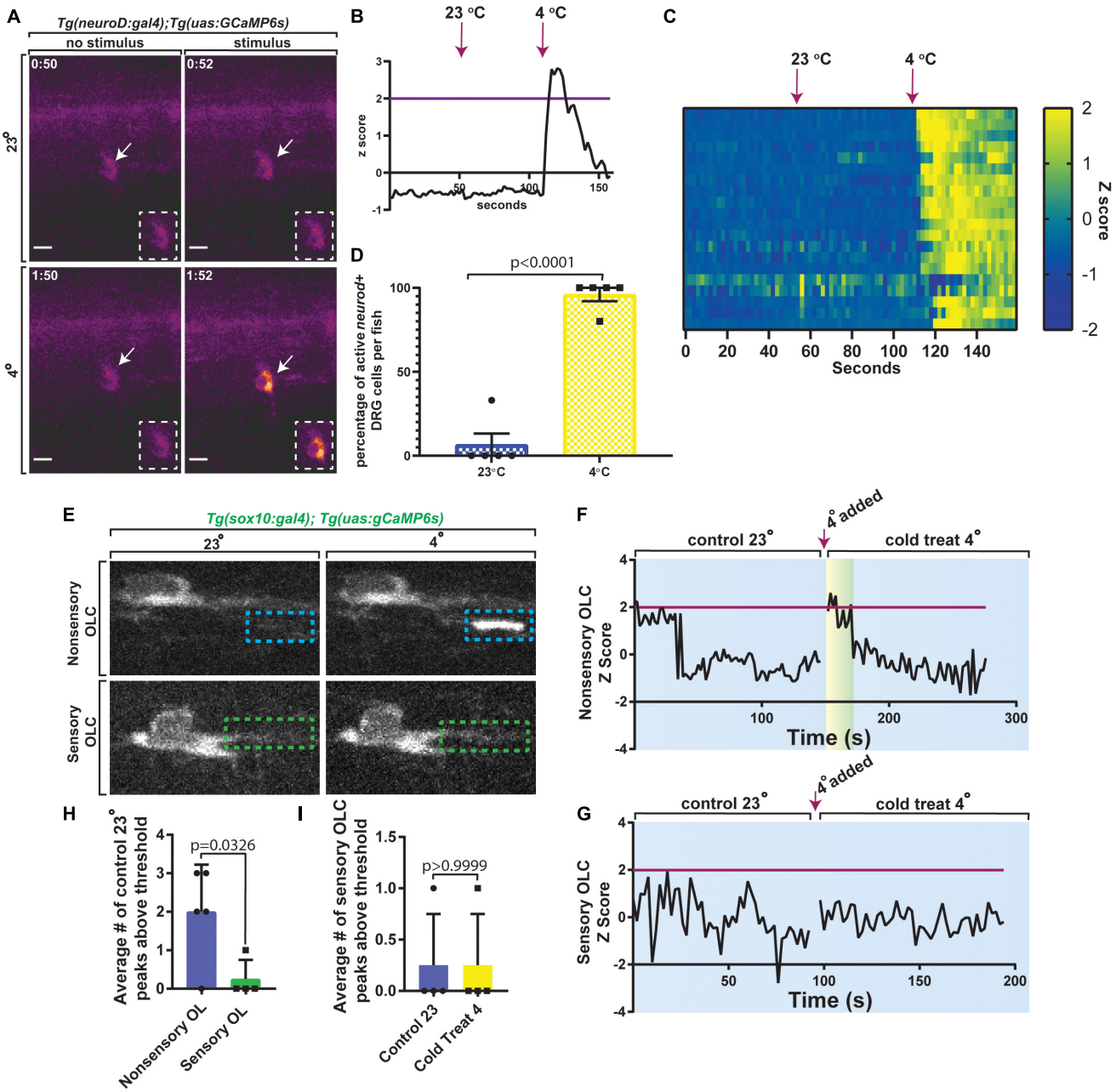

FIGURE 7 | Sensory-related OLCs display distinct Ca^{2+} transients compared to non-sensory-related OLCs. **(A)** Images of *Tg(neurod:gal4); Tg(uas:gCaMP6s)* at 3 dpf showing calcium transients in DRG neurons after exposure to 23 or 4°C water. **(B)** Quantification of the *Z* Score of gCaMP6s intensity over time. Magenta line indicates *Z* score threshold above 2. Magenta arrow indicates the point at which 23 or 4°C water was added. **(C)** Heatmap representing each DRG neuron and the relative change in gCaMP6s intensity between exposure of 23 or 4°C water over time. **(D)** Quantification of the percentage of active DRG *neuroD*$^{+}$ cells per animal in 23°C control temperature compared to 4°C water ($p < 0.0001$). **(E)** Images from a 3 min time-lapse in *Tg(sox10:gal4); Tg(uas:gCaMP6s)* zebrafish showing calcium transients in non-sensory-related OLCs compared to sensory-related OLCs upon exposure to 4°C water. Blue dashed boxes indicate the region of Ca^{2+} transient activity in non-sensory-related OLCs. Green dashed boxes indicate lack of Ca^{2+} transient activity in sensory-related OLCs. **(F)** Quantification of *Z* Score representing Ca^{2+} transient activity in non-sensory-related OLCs upon exposure to 4°C water. **(G)** Quantification of *Z* Score representing the lack of Ca^{2++} transient activity in sensory-related OLCs upon exposure to 4°C water. Magenta line indicates standard deviation threshold above 2 and magenta arrow indicates the point at which 4°C water was added in both F and G. Any peak above this magenta line indicates a positive peak value for calcium expression. **(H)** Quantification of the average number of control 23°C peaks above threshold in sensory-related OLCs versus non-sensory-related OLCs ($p = 0.0326$). **(I)** Quantification of the average number of sensory-related OLCs peaks above the threshold in control 23°C versus 4°C water animals ($p > 0.9999$). Scale bar equals 10 μm **(A,E)**. All images are orientated anterior to left, posterior to right, dorsal up and ventral down.

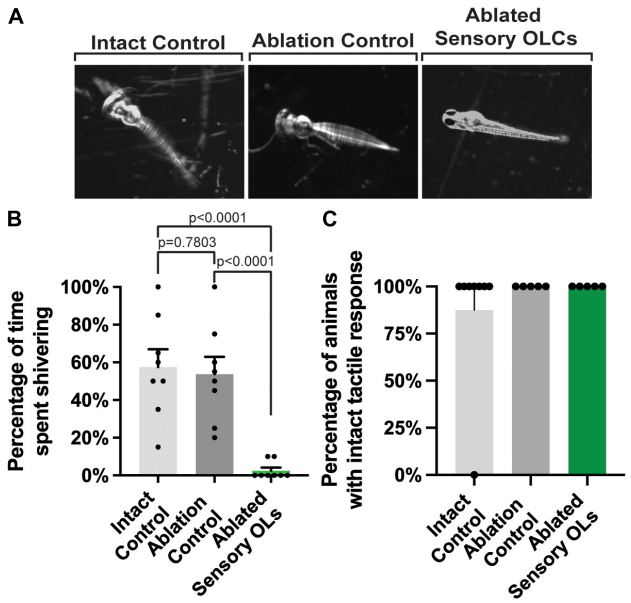

FIGURE 8 | Sensory-related OLC ablation disrupts sensory behavior. **(A)** Images of three timepoints from a 20 s movies overlayed as a maximum projection in intact, ablation control, and ablated sensory OL animals showing the change in twitching behavior in sensory OL ablated animals upon exposure to cold water treatment. **(B)** Quantification of the percentage of time intact, ablated control, and sensory OL ablated animals spent shivering upon exposure to cold water treatment ($p < 0.0001$, $p = 0.7803$, $p < 0.0001$). **(C)** Quantification of the percentage of intact, ablated, or sensory-related OLC ablated animals the exhibited a tactile response. All images are orientated anterior to left, posterior to right, dorsal up and ventral down.

do not (Ribera and Nuslein-Volhard, 1998). This indicates sensory-related OLCs could have a critical function in the DRG-specific behavioral circuit.

DISCUSSION

Oligodendrocytes are essential for brain and spinal cord functionality (Nave and Werner, 2014; Allen and Lyons, 2018). In this study we demonstrate an OLC subpopulation that resides on the DRG axons in the spinal cord of zebrafish. These peripheral derived neurons provide a link between the CNS and PNS (Golding et al., 1997; Lumpkin and Caterina, 2007). Manipulations of DREZ genesis, where these DRG neurons cross from the periphery to the spinal cord, alters sensory-located OLCs. Artificial lesions that mimic a spinal cord axonal invasion supports the hypothesis that DREZ formation could be sufficient to impact these OLCs. Supporting a role of sensory-related OLCs in circuit function, ablation of sensory-related OLCs eliminates a DRG-specific somatosensory behavior (Nichols and Smith, 2020; Kikel-Coury et al., 2021). Together these data reveal a role for the DREZ in producing a unique OLCs population that functions in somatosensory neurons.

The traditional description of a mature oligodendrocyte is that it myelinates (Nave and Werner, 2014; Allen and Lyons, 2018). By the traditional definition, MBP-negative oligodendrocytes are simply immature. For this reason, we conservatively refer to the cells we uncovered as sensory-related OLCs instead of mature OLs. Although this is one interpretation, another is that MBPa-negative oligodendrocytes are themselves mature oligodendrocytes with distinct functions. Pio del Rio Hortega proposed such a possibility, describing cells associated with blood vessels and neuronal somata as non-myelinating oligodendrocytes (Río-Hortega et al., 1921a; Sierra et al., 2016). Single-cell sequencing of oligodendrocyte cells also demonstrate subpopulations of cells that express myelin markers at undetectable levels (Marques et al., 2016). Schwann cells, which myelinate the PNS, also present in non-myelinating mature forms (Jessen and Mirsky, 1997, 2005). Nonetheless, non-myelinating oligodendrocytes remain poorly understood. Our data supports the possibility that *mbpa*-negative OLC could be present in the spinal cord of zebrafish, albeit in low abundance and at very specific locations. In zebrafish, studies have shown heterogeneity of *mbpa*-negative OLCs with one population representing a subgroup that has less complexity like we visualize (Marisca et al., 2020). The potential functional role of sensory-related OLCs in a DRG-specific circuit within that circuit underscores their importance, regardless if they are a mature oligodendrocyte or an immature, long-lived progenitor. It also remains a possibility that sensory-related OLCs do not express *mbpa* but do express *mbpb,* or other myelin proteins.

The results above demonstrate the DREZ is important to produce a subpopulation of OLCs in the zebrafish of the spinal cord. Although our data supports the model that sensory and non-sensory-related OLCs are derived from a similar population of precursors cells in the spinal cord, our experiments do not distinguish between the possibilities that sensory-related OLCs are generated from a progenitor population that is unspecified until the DREZ forms or if a population is pre-determined to arrive to the DREZ once it is formed. It is clear, however, that sensory-related OLCs are derived from the ventral spinal cord region, likely the pMN domain. In mice, the presence of oligodendrocytes that are labeled with traditional myelin markers inhibits synaptic presence in ectopically located somatosensory axons in Semaphorin 6D mutants, suggesting that oligodendrocytes can inhibit synapses and thereby could be hypothesized to be required for somatosensory behaviors (Leslie et al., 2011).

Although our study reveals an interesting interaction between the DREZ and OLCs, it opens a gap in what molecular components at the DREZ drive such events. Discovering such molecules will help to further delineate myelinating oligodendrocytes from those that do not express typical myelin markers. Given that breach alone was sufficient to induce such a sensory-related OLC state, it seems possible the molecules released after injury could be involved. We also identified that sensory-related OLCs contact the DREZ, indicating that both secreted and short-range cues could be involved in the development of sensory-related OLCs. Studies that outline oligodendrocyte responses to injury will also be important guides for such discovery of the DREZ cue.

Our results also indicate an interesting change in sensory-induced behavior when sensory-related OLCs are reduced. This

result was surprising given such a small number of ablated cells had such a profound impact on behavior. At the moment, our interpretation of that result is limited given the potential caveats of cell ablation in the intact spinal cord; although the control animals showed normal behavior. We also cannot explain why sensory-related OLCs appear at two areas of the spinal cord, especially given that spinal cord development should occur similarly on the anterior/posterior axis. However, the location of these cells in limited regions and the change in behavioral responses after their ablation could be linked. One possibility is that these cells function in synapse maturity of the sensory circuit and thus are located at regions where two neurons must be connected. It will be imperative to have a detailed and careful mapping of the sensory circuit in order to investigate such a possibility. Another possibility is that sensory-related OLCs tune the conduction velocity of DRG sensory neurons, akin to what is proposed in the auditory brainstem axons (Ford et al., 2015). However, we do not see changes in sheath length over 4 days. Regardless, it will be important in the future to further investigate the presumed impact on somatosensory driven behaviors. Our work demonstrates that sensory-related OLCs are MBPa^{-} and have distinct Ca^{2+} transients compared to non-sensory-related OLCs. Such data does not completely rule out the possibility that the sensory-related OLCs are in a different stage of differentiation compared to non-sensory-related OLCs. However, tracking sensory-related OLCs over a 4 day period did not show changes in sheathes, consistent to increased differentiation. We also did not see sensory-related OLCs express MBPa by 15 dpf. Investigation of the molecular determinants or markers of sensory-related OLCs will help to address the question of their differentiation state.

Our study establishes the role of PNS development in connectivity and function of the spinal cord, expanding the potential mechanisms that regulate OLC development. Collectively, the OLC heterogeneity in this study includes anatomical, structural, developmental and functional attributes.

MATERIALS AND METHODS

Ethics Statement

All animal studies were approved by the University of Notre Dame Institutional Animal Care and Use Committee.

Contact for Reagent and Resource Sharing

Further information and requests for resources and reagents should be directed to the Lead Contact, CS. All of the data for this study is included in the figures.

Experimental Model and Subject Details

All animal studies were approved by the University of Notre Dame IACUC as noted above. The following zebrafish strains were used in this study: AB, *Tg(sox10:mrfp* (Kucenas et al., 2008), *Tg(sox10:megfp*) (Smith et al., 2014), *Tg(nkx2.2a:gfp)* (Kirby et al., 2006), *Tg(sox10:eos*) (McGraw et al., 2012), *Tg(sox10:gal4;uas:lifeact-gfp)* (Helker et al., 2013; Hines et al., 2015), *Tg(gfap:nsfb-mcherry)* (Johnson et al., 2016; Smith et al., 2016), *Tg(olig2:dsred)* (Park et al., 2002), *Tg(dbx:gfp)* (Briona and Dorsky, 2014), *Tg(nbt:dsred)* (Peri and Nüsslein-Volhard, 2008), *Tg(ngn1:gfp)* (Prendergast et al., 2012), and *Tg(mbpa:gfp)* (Czopka et al., 2013). All germline transgenic lines used in this study were stable unless otherwise noted. Pairwise matings were used to produce embryos and raised at 28°C in egg water in constant darkness. Animals were staged by hours or days post fertilization (hpf and dpf) (Kimmel et al., 1995). Embryos of either sex were used for all experiments.

Method Details

In vivo Imaging

Animals were anesthetized using 3-aminobenzoic acid ester (Tricaine), covered in 0.8% low-melting point agarose. Animals were then mounted laterally on their right side in glass-bottomed 35 mm petri dishes (Nichols et al., 2018). Images were acquired on a spinning disk confocal microscope custom built by 3i technology (Denver, CO) that contains: Zeiss Axio Observer Z1 Advanced Mariana Microscope, X-cite 120LED White Light LED System, filter cubes for GFP and mRFP, a motorized X, Y stage, piezo Z stage, 20X Air (0.50 NA), 63X (1.15NA), 40X (1.1NA) objectives, CSU-W1 T2 Spinning Disk Confocal Head (50 μm) with 1X camera adapter, and an iXon3 1Kx1K EMCCD camera, dichroic mirrors for 446, 515, 561, 405, 488, 561,640 excitation, laser stack with 405 nm, 445 nm, 488 nm, 561 nm, and 637 nm with laser stack FiberSwitcher, photomanipulation from vector high speed point scanner ablations at diffraction limited capacity, Ablate Photoablation System (532 nm pulsed laser, pulse energy 60J @ 200 HZ). Images in time-lapse microscopy were collected every 5 min for 24 h or from 24 to 72 h depending on the experiment. Adobe Illustrator, ImageJ, and IMARIS were used to process images. Only brightness and contrast were adjusted and enhanced for images represented in this study. All fluorescence quantifications were normalized to the background value of each image.

IMARIS Reconstructions

The surface renderings represented in this study were reconstructed using IMARIS version 9.6. We used the surfaces tool within IMARIS to generate surface renderings of raw volume confocal z-stack images (all 30 μm stacks for all reconstructed images). A smoothing detail of 0.200 μm within the surfaces feature was selected and kept consistent across all reconstructed images and no raw volume background values were adjusted when creating reconstructions. The threshold value for each experimental imaging group was selected to remove surface rendered background artifacts and include as much of the rendered OLCs as possible in the reconstructed image. Each threshold cutoff value was manually selected per experimental imaging group and kept consistent within each imaging group. These manual threshold values were set as 182.697 (**Figure 2A**), 298.637 (**Figure 2D**), 222.863 (**Figure 2E**), 376.059 (**Figure 3E**), and 358.236 (**Figure 6A**).

To create the cross sectional view represented in **Figure 2D**, we rotated the raw volume view of our image 90 degrees into the *z*-plane and set our slice position to visualize the right projection of a sensory related OLC. We then used the Ortho Slicer tool in the YZ plane with a slice step size of 1 μm to obtain the slice view of that 1 μm plane.

To create the surface rendering in **Figure 2D**, we created individual surfaces channels for the *Tg(ngn1:gfp)* and *Tg(sox10:mrfp)* channels. Following reconstruction, since the OLC and other *sox10* expression was labeled in the same channel, we grouped the reconstructed surface pixels that coincided with the raw volume view of the sensory related OLC and also grouped the reconstructed surface pixels that were not associated with the sensory related OLC. We then pseudo colored the two groups within the reconstructed *Tg(sox10:mrfp)* channel. Cyan represented the $sox10^{+}$ non-sensory related OLC and magenta represented the sensory related OLC. Similarly, we grouped the reconstructed surface pixels that coincided with the raw volume view of the sensory related OLC contacting the DREZ and grouped the pixels coinciding with the DRG in *Tg(sox10:gal4;uas:lifeact-gfp)* represented in **Figure 3E**. Here we pseudo colored the DRG in gray and pseudo colored the sensory related OLC in green. The surface renderings represented in **Figures 2A,E**, **6A** were also reconstructed using the surfaces tool in IMARIS following the noted smoothing details and thresholding values detailed above, however; no OLCs or structures were present within the same transgenic channel so no pixels were grouped or pseudo colored for these channels.

We did not perform any quantitative analysis using IMARIS software, instead we strictly used this software as a tool to allow for better visualization of small sensory related OLCs and their related structures. All quantifications were performed using ImageJ or Microsoft Excel described below in our quantitative analysis section.

Single-Cell Ablations

Tg(sox10:mrfp), and *Tg(sox10:megfp)* animals were anesthetized using 0.02% 3-aminobenzoic acid ester (Tricaine) in egg water. Fish were then mounted in 0.8% low-melting point agarose solution, arranged laterally on a 10 mm glass-coverslip bottom petri dish, and placed on the microscope anterior to posterior. Confocal *z*-stack images of sensory and non-sensory-related OLCs in individual transgenic animals at 72 hpf were taken pre-ablation. Confirmed sensory and non-sensory cells were brought into a focused ablation window. Upon focusing the confirmed cell, we double-clicked on the center of the cell body using a 4 μm cursor tool to fire the laser (Nichols et al., 2018; Green et al., 2019). All laser parameters used are specific to our confocal microscope. Specific parameters include Laser Power (2), Raster Block Size (4), Double-Click Rectangle Size (8), and Double-Click Repetitions (4). 30 μm z-stack images taken at a 1 μm step size were then collected using time-lapse confocal microscopy every 5 min for 24 h or from 72 to 96 h.

Single OL Imaging Over Multiple Days

Confocal z-stack images of *Tg(nkx2.2a:gfp);Tg(sox10:mrfp)* animals at 3 dpf were taken to locate and confirm the presence of sensory-related OLCs. After locating a sensory-related OLC, we counted DRGs anteriorly from the DRG most adjacent to the sensory-related OLC. We also counted the somites of the animal anteriorly from the somite number most adjacent to the location of the sensory-related OLC. At 4 dpf, we used the DRG number and somite number to locate the same sensory-related OLC within the same animal. Upon locating the sensory-related OLC we took a confocal z-stack image. We repeated the location and imaging process at 5 dpf and 6 dpf. We quantified the length and width of sheaths of individual sensory-related OLCs over a 4-day period using ImageJ. We reconstructed these 30 μm confocal z-stack images of sensory-related OLCs at each timepoint using the surfaces feature using IMARIS. We created individual surfaces channels for the green *Tg(nkx2.2a:gfp)* and pseudocolored cyan *Tg(sox10:mrfp)* channels. Following reconstruction we pseudocolored the sensory related OLC in magenta. All surfaces channels used a surface detail of 0.200 μm and we did not adjust the background values within the surfaces feature.

Chemical Treatments

The chemical treatments used for this study include SU6656 (Santa Cruz Biotechnology) and paclitaxel (Acros) (Nichols and Smith, 2019a). Stock solutions of both reagents were kept at 20°C. SU6656 was kept at a concentration of 375 μM. Paclitaxel was kept at a concentration of 2.2 mM (Nichols and Smith, 2019a). All embryos were dechorionated at 36 hpf and incubated with 3 μM (SU6656) and 22 μM (paclitaxel) in egg water until imaging (Nichols and Smith, 2019a). All control animals were incubated with 1% DMSO in egg water.

Dorsal Root Ganglia Ablations

Tg(sox10:mrfp);Tg(ngn1:gfp) 48 hpf animals were anesthetized using 0.02% 3-aminobenzoic acid ester (Tricaine) in egg water. Fish were then mounted in 0.8% low-melting point agarose solution, arranged laterally on a 10 mm glass-coverslip bottom petri dish, and placed on the microscope anterior to posterior. Following the formation of pioneer axons from the DRG, we selected an 8 μm area between the DRG and the pioneer axon and double-clicked to fire the lesion laser (Nichols et al., 2018; Green et al., 2019). All laser parameters used are specific to our confocal microscope. Specific parameters include Laser Power (3), Raster Block Size (2), Double-Click Rectangle Size (8), and Double-Click Repetitions (4). Following DRG ablations, 30 μm z-stack images taken at a 1 μm step size were then collected using time-lapse confocal microscopy every 5 min for 24 h from 48 to 72 hpf.

PA-Rac1

A *tol2–4xnr UAS-PA Rac1-mcherry* plasmid was diluted to 12 ng/μl in water along with 25 ng/μl of *transposase* mRNA. The injection solution was injected into *Tg(sox10:gal4); Tg(uas:lifeact-GFP)* embryos. Embryos were screened for *mcherry* expression via confocal microscopy at 48 hpf. Mature PA-Rac1 photoactivates upon exposure to 445 nm light. We imaged $mcherry^{+}$ DRGs for 24 h with exposure to 445 nm light. As a control we imaged $mcherry^{+}$ DRGs for 24 h without exposure to 445 nm light. *tol2–4xnr UAS-PA Rac1-mcherry* was a gift from

Anna Huttenlocher (Addgene plasmid #41878) (Yoo et al., 2010). Light stimulation in non-paRac1 animals has no measurable impact (Yoo et al., 2010). Following PA-Rac1 treatment, 30 μm z-stack images taken at a 1 μm step size were then collected using time-lapse confocal microscopy every 5 min for 24 h from 48 to 72 hpf.

Radial Glia Focal Lesion

Focal lesions of the radial glia membrane to mimic a DREZ injury were created using the Ablate!TM© Photoablation System described above (Nichols and Smith, 2019a). Two laser induced lesions were created at 48 hpf. Each focal lesion ranged from 10 to 12 μm in size and was created 10 μm from the ventral radial glial membrane. This area best represented the location of the DREZ. Non-lesioned DREZ areas of adjacent nerves served as controls. Following laser induced focal lesioning, time-lapse images of the nerves were taken as described above for 24 h. Following radial glia focal lesion ablations, 30 μm z-stack images taken at a 1 μm step size were then collected using time-lapse confocal microscopy every 5 min for 24 h from 48 to 72 hpf.

Immunohistochemistry

The primary antibody used to determine mature myelination was anti-mbpa (1:500, rabbit, Appel Lab) (Kucenas et al., 2009). The secondary antibody used was Alexa Fluor 647 goat anti-rabbit (1:600; Invitrogen). 15 dpf animals were fixed in 4% PFA in PBST (PBS, 0.1% Triton X-100) at 25°C for 3 h. Fixed animals were washed with PBST, DWT (dH_20, 0.1% Triton X-100), and acetone for 5 min each. Next, the animals were incubated in −30°C acetone for 10 min and then washed three times with PBST for 5 min each. Animals were then incubated with 5% goat serum in PBST for 1 h at 25°C, then the primary antibody solution was added for 1 h at 25°C. After 1 h, animals were transferred to 4°C overnight. Fixed animals were washed three times with PBST for 30 min each and once more for 1 h. Animals were then incubated with secondary antibody solution for 1 h at 25°C, then transferred to 4°C overnight. Fixed animals were washed three times with PBST for 1 h and immediately imaged. Animals were mounted, and confocal images were taken using the protocol above for *in vivo* imaging. 50 μm still *z*-stack images taken at a 1 μm step size were then collected using confocal microscopy.

Calcium Imaging

Tg(sox10:gal4);Tg(uas:gCaMP6s) and *Tg(neurod:gal4);Tg(uas:gCaMP6s)* 3 dpf animals were mounted in 0.8% low-melting point agarose solution, arranged laterally on a 10 mm glass-coverslip bottom petri dish, and placed on the microscope anterior to posterior. Animals were not anesthetized. For neuronal imaging, spinal cord *z*-stacks were collected that spanned 10 μm (1 μm steps) and imaged for 3 min with 2 s intervals. For OLC imaging, confocal z-stack images of the spinal cord in individual transgenic animals at 3 dpf were taken to confirm the presence of sensory and non-sensory-related OLCs. Upon confirmation, sensory-related OLCs were imaged every 2 s for 2 min to capture Ca^{2+} transients in room temperature (23 degree) egg water. After imaging baseline Ca^{2+} activity, room temperature egg water was removed and 3 mL of 4 degree cold egg water was added. Animals were then imaged immediately following the addition of 4 degree egg water and after refocusing. Non-sensory-related OLCs were also imaged every 2 s for 2 min as a control. The exposure was set to 100 ms.

Animal Behavior After Sensory-Related OLC Ablations

Tg(sox10:mrfp) animals at 72 hpf were anesthetized using 0.02% 3-aminobenzoic acid ester (Tricaine) in egg water. Fish were then mounted in 0.8% low-melting point agarose solution, arranged laterally on a 10 mm glass-coverslip bottom petri dish, and placed on the microscope anterior to posterior. Confocal z-stack images of *Tg(sox10:mrfp)* animals at 72 hpf were taken to locate and confirm the presence of sensory-related OLCs. We ablated sensory-related OLCs using the Ablate!TM© Photoablation Laser following the single-cell ablation methods described above. Following successful ablation, we unmounted individual animals from the agarose solution. We then placed individual animals into a small petri dish containing 4°C egg water and recorded their twitching response to cold water treatment for a 20 s period using an AxioZoom Observer microscope with ZenPro Image Acquisition software. As a control for the ablation, we ablated a small 4 μm region above the sensory axon where a typical sensory OL would reside. As another control, we imaged a separate set of intact control animals that had unablated sensory-related OLCs. The ablated, ablated control, and intact control animals were each exposed to 4°C egg water and their twitching response to cold water treatment was recorded over a 20 s period using Zeiss ZenPro image acquisition software on a Zeiss Axio Observer microscope.

Quantitative Analysis

Quantification and Statistical Analysis

To generate composite z-images for the cell, 3i Slidebook software (Denver, CO, United States) was used. Individual z-images were sequentially observed to confirm composite accuracy. All graphically presented data represent the mean of the analyzed data unless otherwise noted. Cell tracking was performed using the MTrackJ plugin for ImageJ[1]. GraphPad Prism software (San Diego, CA, United States) was used to determine statistical analysis. Full detail of the statistical values can be found in **Supplementary Table S1**.

Quantification of Direction Changes

To track the direction changes of OLCs, we imaged *Tg(sox10:mrfp)* and *Tg(sox10:gal4;uas:lifeact-gfp)* animals from 48 to 72 hpf. We then tracked single $sox10^{+}$ OLCs in each animal throughout the 24 time-lapse movie using the MTrackJ plugin of ImageJ. We quantified the total distance an individual OLC traveled as well as the amount of direction changes an individual OLC experienced throughout the 24-h imaging window.

Quantification of Migration

To track the individual paths of sensory and non-sensory-related OLCs, the MTrackJ plugin on ImageJ was used. The center of

[1]https://imagescience.org/meijering/software/mtrackj/ (Bethesda, MD)

each cell body was traced over time, and quantitative data were collected by ImageJ. Resulting x and y coordinates of each cell were overlaid to create migration plots. All distance and time points were calculated by the MTrackJ software and further quantified using Microsoft Excel (Redmond, WA).

K-Means Analysis

Oligodendrocyte lineage cells were clustered into three groups clustered based on their migration distance and number of direction changes from 48 to 72 hpf using *k*-means analysis in R. The *k* value was determined by the elbow method. Code is available in **Supplementary File 1**.

Quantification of Sheath Length and Width

To determine the length and width of sensory and non-sensory OL sheaths, we used the freehand tracing tool in ImageJ. We traced the ensheathed area longitudinally and laterally and used the Analyze feature within ImageJ to obtain quantitative results.

Quantification of Velocity

To obtain the velocity of an individual OLC traveling, we tracked individual paths of sensory and non-sensory-related OLCs throughout the timelapse imaging window using the MTrackJ plugin on ImageJ. We tracked the center of each cell body over time and used the quantitative distance and time collected by ImageJ to calculate velocity. We calculated the velocity using Microsoft Excel (Redmond, WA, United States).

Quantification of OLC Projections

To determine the number of both sensory and non-sensory related OLC projections, we tracked individual OLCs throughout the 24-h timelapse imaging window from 48 to 72 hpf and counted the maximum number of extended projections each individual OLC created after migrating to the DREZ.

Quantification of Calcium Imaging

We imaged *Tg(sox10:gal4);Tg(uas:gCaMP6s)* 3 dpf animals every 2 s for 2 min to visualize Ca^{2+} transient waves in sensory and non-sensory OLCs exposed to 4 and 23°C degree egg water. Later, we enlarged the movies to visualize one sensory or non-sensory-related OLC at a time. We used the line tool in ImageJ to trace individual projections of OLCs and then measured the integrated density along the projection using the integrated density tool within ImageJ. In order to assess changes in integrated density, we then used Microsoft Excel to calculate the *Z* score of the integrated density for each projection. Any *Z* score $>$ or $=$ 2 were noted as positive for Ca^{2+} transient activity. Any *Z* score $<$ 2 were not recognized as positive for Ca^{2+} transient activity. We first tested this by imaging *Tg(neurod:gal4); Tg(uas:GCaMP6s)* and measured calcium transients in DRG neurons after exposure to 4 or 23°C water. We imaged *Tg(neurod:gal4); Tg(uas:gCaMP6s)* 3dpf animals every 2 s for 3 min to assess changes in gCaMP6s fluorescence of DRG neurons in response to 23 and 4°C egg water. Movies were analyzed in ImageJ by tracing individual DRG neuron somas and measuring integrated density for each timepoint. In this analysis, the *Z* score of DRG neuron integral densities were measured and used to assess changes in integral density. If gCaMP6s integral density *Z* score was 2 or greater, this was marked as an active firing event.

Quantification of Animal Behavior

We recorded the behavior of sensory ablated, ablation control, and intact animals for 20 s immediately following exposure to 4°C egg water. Any movies longer than 20 s were normalized to 20 s. We recorded the amount of time each animal spent shivering in cold water treatment. We divided the total time an animal spent shivering over the total time recorded. All calculations were performed using Microsoft Excel (Redmond, WA, United States).

DATA AVAILABILITY STATEMENT

The original contributions presented in this study are included in the article/**Supplementary Material**, further inquiries can be directed to the corresponding author.

ETHICS STATEMENT

The animal study was reviewed and approved by all animal studies were approved by the University of Notre Dame IACUC.

AUTHOR CONTRIBUTIONS

LG, RG, JB, and EN conducted all experiments. LG, RG, JB, and CS analyzed all experiments. LG and CS wrote the manuscript with input from RG and JB. CS and LG conceived the project. All authors contributed to the article and approved the submitted version.

FUNDING

This work was funded by the Alfred P. Sloan Foundation (CS) and the NIH (DP2NS117177). Further support was provided by the University of Notre Dame, the Elizabeth and Michael Gallagher Family, Garibaldi Family Endowment for Excellence in Adult Stem Cell Research, Center for Zebrafish Research at the University of Notre and Center of Stem Cells and Regenerative Medicine at the University of Notre Dame.

ACKNOWLEDGMENTS

We thank David Lyons, Bruce Appel, and Ethan Scott for transgenic zebrafish lines, Bruce Appel, Jacob Hines, and members of the Smith and Wingert labs for their helpful comments. We also thank Sara Cole and the Notre Dame Imaging Core for their help using IMARIS software.

SUPPLEMENTARY MATERIAL

The Supplementary Material for this article can be found online at: https://www.frontiersin.org/articles/10.3389/fncel.2022.893629/full#supplementary-material

REFERENCES

Allen, N. J., and Lyons, D. A. (2018). Glia as architects of central nervous system formation and function. *Science* 185, 181–185.

Baraban, M., Koudelka, S., and Lyons, D. A. (2017). Ca 2+ activity signatures of myelin sheath formation and growth in vivo. *Nat. Neurosci.* 21, 19–23. doi: 10.1038/s41593-017-0040-x

Briona, L. K., and Dorsky, R. I. (2014). Radial glial progenitors repair the zebrafish spinal cord following transection. *Exp. Neurol.* 256, 81–92. doi: 10.1016/j.expneurol.2014.03.017

Cai, J., Qi, Y., Hu, X., Tan, M., Liu, Z., Zhang, J., et al. (2005). Generation of oligodendrocyte precursor cells from mouse dorsal spinal cord independent of Nkx6 regulation and Shh signaling. *Neuron* 45, 41–53.

Crawford, A. H., Tripathi, R. B., Richardson, W. D., and Franklin, R. J. M. (2016). Developmental origin of oligodendrocyte lineage cells determines response to demyelination and susceptibility to age-associated functional decline. *Cell Rep.* 15, 761–773. doi: 10.1016/j.celrep.2016.03.069

Czopka, T., Ffrench-Constant, C., and Lyons, D. A. (2013). Individual oligodendrocytes have only a few hours in which to generate new myelin sheaths in vivo. *Dev. Cell* 25, 599–609. doi: 10.1016/j.devcel.2013.05.013

Emery, B. (2010). Regulation of oligodendrocyte differentiation. *Trends Neurosci.* 330, 359–362.

Fogarty, M., Richardson, W., and Kessaris, N. (2005). A subset of oligodendrocytes generated from radial glia in the dorsal spinal cord. *Development* 132, 1951–1959. doi: 10.1242/dev.01777

Ford, M. C., Alexandrova, O., Cossell, L., Stange-Marten, A., Sinclair, J., Kopp-Scheinpflug, C., et al. (2015). Tuning of Ranvier node and internode properties in myelinated axons to adjust action potential timing. *Nat. Commun.* 6:8073.

Fosque, B. F., Sun, Y., Dana, H., Yang, C. T., Ohyama, T., Tadross, M. R., et al. (2015). Labeling of active neural circuits in vivo with designed calcium integrators. *Science* 347, 755–760. doi: 10.1126/science.1260922

Golding, J., Shewan, D., and Cohen, J. (1997). Maturation of the mammalian dorsal root entry zone - from entry to no entry. *Trends Neurosci.* 20, 303–308. doi: 10.1016/S0166-2236(96)01044-1042

Green, L. A., Nebiolo, J. C., and Smith, C. J. (2019). Microglia exit the CNS in spinal root avulsion. *PLoS Biol.* 17:e3000159. doi: 10.1371/journal.pbio.3000159

Green, L., and Smith, C. J. (2018). Single-cell photoconversion in living intact zebrafish. *J. Vis. Exp.* e57024. doi: 10.3791/57024

Green, L., and Smith, C. J. (2018). Single-cell photoconversion in living intact zebrafish. *J. Vis. Exp.* 57024. doi: 10.3791/57024

Helker, C. S. M., Schuermann, A., Karpanen, T., Zeuschner, D., Belting, H.-G., Affolter, M., et al. (2013). The zebrafish common cardinal veins develop by a novel mechanism: lumen ensheathment. *Development* 140, 2776–2786. doi: 10.1242/dev.091876

Hines, J. H., Ravanelli, A. M., Schwindt, R., Scott, E. K., and Appel, B. (2015). Neuronal activity biases axon selection for myelination in vivo. *Nat. Neurosci.* 18, 683–689. doi: 10.1038/nn.3992

Hughes, E. G., and Appel, B. (2016). The cell biology of CNS myelination oligodendrocyte precursors and their distribution. *Curr. Opin. Neurobiol.* 39, 93–100. doi: 10.1016/j.conb.2016.04.013

Hughes, E. G., Kang, S. H., Fukaya, M., and Bergles, D. E. (2013). Oligodendrocyte progenitors balance growth with self-repulsion to achieve homeostasis in the adult brain. *Nat. Neurosci.* 16, 668–676. doi: 10.1038/nn.3390

Jessen, K. R., and Mirsky, R. (1997). Embryonic Schwann cell development: the biology of Schwann cell precursors and early Schwann cells. *J. Anat.* 191, 501–505. doi: 10.1017/S0021878297002434

Jessen, K. R., and Mirsky, R. (2005). The origin and development of glial cells in peripheral nerves. *Nat.Rev.Neurosci.* 6, 671–682. doi: 10.1038/nrni746

Johnson, K., Barragan, J., Bashiruddin, S., Smith, C. J., Tyrrell, C., Parsons, M. J., et al. (2016). Gfap-positive radial glial cells are an essential progenitor population for later-born neurons and glia in the zebrafish spinal cord. *Glia* 64, 1170–1189. doi: 10.1002/glia.22990

Kessaris, N., Fogarty, M., Iannarelli, P., Grist, M., Wegner, M., and Richardson, W. D. (2006). Competing waves of oligodendrocytes in the forebrain and postnatal elimination of an embryonic lineage. *Nat. Neurosci.* 9, 173–179. doi: 10.1038/nn1620

Kikel-Coury, N. L., Green, L. A., Nichols, E. L., Zellmer, A. M., Pai, S., Hedlund, S. A., et al. (2021). Pioneer axons utilize a Dcc signaling-mediated invasion brake to precisely complete their pathfinding odyssey. *J. Neurosci.* 41, 6617–6636. doi: 10.1523/JNEUROSCI.0212-21.2021

Kimmel, C. B., Ballard, W. W., Kimmel, S. R., Ullmann, B., and Schilling, T. F. (1995). Stages of embryonic development of the zebrafish. *Dev. Dynam.* 203, 253–310. doi: 10.1002/aja.1002030302

Kirby, B. B., Takada, N., Latimer, A. J., Shin, J., Carney, T. J., Kelsh, R. N., et al. (2006). In vivo time-lapse imaging shows dynamic oligodendrocyte progenitor behavior during zebrafish development. *Nat. Neurosci.* 9, 1506–1511. doi: 10.1038/nn1803

Koudelka, S., Voas, M. G. G., Almeida, R. G. G., Baraban, M., Soetaert, J., Meyer, M. P. P., et al. (2016). Individual neuronal subtypes exhibit diversity in CNS myelination mediated by synaptic vesicle release. *Curr. Biol.* 26, 1447–1455. doi: 10.1016/j.cub.2016.03.070

Krasnow, A. M., Ford, M. C., Valdivia, L. E., Wilson, S. W., and Attwell, D. (2018). Regulation of developing myelin sheath elongation by oligodendrocyte calcium transients in vivo. *Nat. Neurosci.* 21, 24–30. doi: 10.1038/s41593-017-0031-y

Kucenas, S., Takada, N., Park, H. C., Woodruff, E., Broadie, K., and Appel, B. (2008). CNS-derived glia ensheath peripheral nerves and mediate motor root development. *Nat. Neurosci.* 11, 143–151. doi: 10.1038/nn2025

Kucenas, S., Wang, W.-D., Knapik, E. W., and Appel, B. (2009). A selective glial barrier at motor axon exit points prevents oligodendrocyte migration from the spinal cord. *J. Neurosci.* 29, 15187–15194.

Leslie, J. R., Imai, F., Fukuhara, K., Takegahara, N., Rizvi, T. A., Friedel, R. H., et al. (2011). Ectopic myelinating oligodendrocytes in the dorsal spinal cord as a consequence of altered semaphorin 6D signaling inhibit synapse formation. *Development* 138, 4085–4095. doi: 10.1242/dev.066076

Lumpkin, E. A., and Caterina, M. J. (2007). Mechanisms of sensory transduction in the skin. *Nature* 445, 858–865. doi: 10.1038/nature05662

Marisca, R., Hoche, T., Agirre, E., Hoodless, L. J., Barkey, W., Auer, F., et al. (2020). Functionally distinct subgroups of oligodendrocyte precursor cells integrate neural activity and execute myelin formation. *Nat. Neurosci.* 23, 363–374. doi: 10.1038/s41593-019-0581-582

Marques, S., Zeisel, A., Codeluppi, S., Bruggen, D., Van, Falcão, A. M., et al. (2016). Oligodendrocyte heterogneity in the mouse juvenile and adult central nervous system. *Science* 352, 1326–1329. doi: 10.1126/science.aaf6463

McGraw, H. F., Snelson, C. D., Prendergast, A., Suli, A., and Raible, D. W. (2012). Postembryonic neuronal addition in Zebrafish dorsal root ganglia is regulated by Notch signaling. *Neural Dev.* 7:23. doi: 10.1186/1749-8104-7-23

Mensch, S., Baraban, M., Almeida, R., Czopka, T., Ausborn, J., El Manira, A., et al. (2015). Synaptic vesicle release regulates myelin sheath number of individual oligodendrocytes in vivo. *Nat. Neurosci.* 18, 628–630. doi: 10.1038/nn.3991

Naruse, M., Ishino, Y., Kumar, A., Ono, K., Takebayashi, H., Yamaguchi, M., et al. (2016). The dorsoventral boundary of the germinal zone is a specialized niche for the generation of cortical oligodendrocytes during a restricted temporal window. *Cereb. Cortex* 26, 2800–2810.

Nave, K. A., and Werner, H. B. (2014). Myelination of the nervous system: mechanisms and functions. *Annu. Rev. Cell Dev. Biol.* 30, 503–533.

Nichols, E. L., and Smith, C. J. (2019a). Pioneer axons employ Cajal's battering ram to enter the spinal cord. *Nat. Commun.* 10:562. doi: 10.1038/s41467-019-08421-8429

Nichols, E. L., and Smith, C. J. (2019b). Synaptic-like vesicles facilitate pioneer axon invasion. *Curr. Biol.* 29, 2652–2664.e4.

Nichols, E. L., and Smith, C. J. (2020). Functional regeneration of the sensory root via axonal invasion. *Cell Rep.* 30, 9–17.e3. doi: 10.1016/j.celrep.2019.12.008.

Nichols, E. L., Green, L. A., and Smith, C. J. (2018). Ensheathing cells utilize dynamic tiling of neuronal somas in development and injury as early as neuronal differentiation. *Neural Dev.* 13:19. doi: 10.1186/s13064-018-0115-118

Park, H., Mehta, A., Richardson, J. S., and Appel, B. (2002). olig2 is required for zebrafish prim ary motor n euron and oligodendrocyte development. *Dev. Biol.* 368, 356–368.

Peri, F., and Nüsslein-Volhard, C. (2008). Live imaging of neuronal degradation by microglia reveals a role for v0-ATPase a1 in phagosomal fusion in vivo. *Cell* 133, 916–927. doi: 10.1016/j.cell.2008.04.037

Prendergast, A., Linbo, T. H., Swarts, T., Ungos, J. M., McGraw, H. F., Krispin, S., et al. (2012). The metalloproteinase inhibitor Reck is essential for zebrafish DRG development. *Development* 139, 1141–1152. doi: 10.1242/dev.072439

Ravanelli, A. M., and Appel, B. (2015). Motor neurons and oligodendrocytes arise from distinct cell lineages by progenitor recruitment. *Genes Dev.* 29, 2504–2515. doi: 10.1101/gad.271312.115

Ribera, A. B., and Nuslein-Volhard, C. (1998). Zebrafish touch-insensitive mutants reveal an essential role for the developmental regulation of sodium current. *J. Neurosci.* 18, 9181–9191.

Richardson, W. D., Kessaris, N., and Pringle, N. (2006). Oligodendrocyte wars. *Nat. Rev. Neurosci.* 7, 11–18. doi: 10.1038/nrn1826

Río-Hortega, P. (1921a). Estudios sobre la neuroglía. La glía de escasas radiaciones (oligodendroglí). *Bol. Soc. Esp. Hist. Nat.* 21, 63–92.

Sierra, A., de Castro, F., del Río-Hortega, J., Rafael Iglesias-Rozas, J., Garrosa, M., and Kettenmann, H. (2016). The "Big-Bang" for modern glial biology: translation and comments on Pío del Río-Hortega 1919 series of papers on microglia. *Glia* 64, 1801–1840. doi: 10.1002/glia.23046

Smith, C. J., Johnson, K., Welsh, T. G., Barresi, M. J. F., and Kucenas, S. (2016). Radial glia inhibit peripheral glial infiltration into the spinal cord at motor exit point transition zones. *Glia* 64, 1138–1153. doi: 10.1002/glia.22987

Smith, C. J., Morris, A. D., Welsh, T. G., and Kucenas, S. (2014). Contact-Mediated inhibition between oligodendrocyte progenitor cells and motor exit point glia establishes the spinal cord transition zone. *PLoS Biol.* 12:e1001961. doi: 10.1371/journal.pbio.1001961

Smith, C. J., Wheeler, M. A., Marjoram, L., Bagnat, M., Deppmann, C. D., and Kucenas, S. (2017). TNFa/TNFR2 signaling is required for glial ensheathment at the dorsal root entry zone. *PLoS Genet.* 13:e1006712. doi: 10.1371/journal.pgen.1006712

Spassky, N., Goujet-Zalc, C., Parmantier, E., Olivier, C., Martinez, S., Ivanova, A., et al. (1998). Multiple restricted origin of oligodendrocytes. *J. Neurosci.* 18, 8331–8343. doi: 10.1523/jneurosci.18-20-08331.1998

Spitzer, S. O., Sitnikov, S., Kamen, Y., Faria, O., De, Agathou, S., et al. (2019). Oligodendrocyte progenitor cells become regionally diverse and heterogeneous with age article oligodendrocyte progenitor cells become regionally diverse and heterogeneous with age. *Neuron* 101, 459–471.e5. doi: 10.1016/j.neuron.2018.12.020.

Tripathi, R. B., Clarke, L. E., Burzomato, V., Kessaris, N., Anderson, P. N., Attwell, D., et al. (2011). Dorsally and ventrally derived oligodendrocytes have similar electrical properties but myelinate preferred tracts. *J. Neurosci.* 31, 6809–6819. doi: 10.1523/JNEUROSCI.6474-10.2011

Vallstedt, A., Klos, J. M., and Ericson, J. (2005). Multiple dorsoventral origins of oligodendrocyte generation in the spinal cord and hindbrain. *Neuron* 45, 55–67.

Watkins, T. A., Emery, B., Mulinyawe, S., and Barres, B. A. (2008). Distinct stages of myelination regulated by γ-Secretase and astrocytes in a rapidly myelinating CNS coculture system. *Neuron* 60, 555–569. doi: 10.1016/j.neuron.2008.09.011

Yoo, S. K., Deng, Q., Cavnar, P. J., Wu, Y. I., Hahn, K. M., and Huttenlocher, A. (2010). Differential regulation of protrusion and polarity by PI(3)K during neutrophil motility in live zebrafish. *Dev. Cell* 18, 226–236. doi: 10.1016/j.devcel.2009.11.015

Zhang, Y., Nichols, E. L., Zellmer, A. M., Guldner, I. H., Kankel, C., Zhang, S., et al. (2019). Generating intravital super-resolution movies with conventional microscopy reveals actin dynamics that construct pioneer axons. *Development* 146:dev171512. doi: 10.1242/DEV.171512

Conflict of Interest: The authors declare that the research was conducted in the absence of any commercial or financial relationships that could be construed as a potential conflict of interest.

Publisher's Note: All claims expressed in this article are solely those of the authors and do not necessarily represent those of their affiliated organizations, or those of the publisher, the editors and the reviewers. Any product that may be evaluated in this article, or claim that may be made by its manufacturer, is not guaranteed or endorsed by the publisher.

Copyright © 2022 Green, Gallant, Brandt, Nichols and Smith. This is an open-access article distributed under the terms of the Creative Commons Attribution License (CC BY). The use, distribution or reproduction in other forums is permitted, provided the original author(s) and the copyright owner(s) are credited and that the original publication in this journal is cited, in accordance with accepted academic practice. No use, distribution or reproduction is permitted which does not comply with these terms.

frontiers | Frontiers in Cellular Neuroscience

TYPE Review
PUBLISHED 14 November 2022
DOI 10.3389/fncel.2022.1041853

Check for updates

OPEN ACCESS

EDITED BY
Wia Baron,
University Medical Center Groningen, Netherlands

REVIEWED BY
Ethan Hughes,
University of Colorado Anschutz Medical Campus, United States
Enrica Boda,
University of Turin, Italy

*CORRESPONDENCE
Akiko Nishiyama
akiko.nishiyama@uconn.edu

SPECIALTY SECTION
This article was submitted to Non-Neuronal Cells, a section of the journal Frontiers in Cellular Neuroscience

RECEIVED 11 September 2022
ACCEPTED 17 October 2022
PUBLISHED 14 November 2022

CITATION
Fekete CD and Nishiyama A (2022) Presentation and integration of multiple signals that modulate oligodendrocyte lineage progression and myelination.
Front. Cell. Neurosci. 16:1041853.
doi: 10.3389/fncel.2022.1041853

COPYRIGHT
© 2022 Fekete and Nishiyama. This is an open-access article distributed under the terms of the Creative Commons Attribution License (CC BY). The use, distribution or reproduction in other forums is permitted, provided the original author(s) and the copyright owner(s) are credited and that the original publication in this journal is cited, in accordance with accepted academic practice. No use, distribution or reproduction is permitted which does not comply with these terms.

Presentation and integration of multiple signals that modulate oligodendrocyte lineage progression and myelination

Christopher D. Fekete and Akiko Nishiyama*

Department of Physiology and Neurobiology, University of Connecticut, Storrs, CT, United States

Myelination is critical for fast saltatory conduction of action potentials. Recent studies have revealed that myelin is not a static structure as previously considered but continues to be made and remodeled throughout adulthood in tune with the network requirement. Synthesis of new myelin requires turning on the switch in oligodendrocytes (OL) to initiate the myelination program that includes synthesis and transport of macromolecules needed for myelin production as well as the metabolic and other cellular functions needed to support this process. A significant amount of information is available regarding the individual intrinsic and extrinsic signals that promote OL commitment, expansion, terminal differentiation, and myelination. However, it is less clear how these signals are made available to OL lineage cells when needed, and how multiple signals are integrated to generate the correct amount of myelin that is needed in a given neural network state. Here we review the pleiotropic effects of some of the extracellular signals that affect myelination and discuss the cellular processes used by the source cells that contribute to the variation in the temporal and spatial availability of the signals, and how the recipient OL lineage cells might integrate the multiple signals presented to them in a manner dialed to the strength of the input.

KEYWORDS

oligodendrocyte, OPC, NG2, neuron-glia communication, trafficking, Fyn, BDNF, L1

Introduction

In the central nervous system (CNS) oligodendrocyte precursor cells (OPCs) are the lineage committed precursor cells that generate myelinating oligodendrocytes (OLs) and enable saltatory conduction of action potentials. Recent studies show that myelin is not merely a static stack of OL membranes but continues to undergo dynamic remodeling in the adult CNS (Bonetto et al., 2021; Nishiyama et al., 2021). Consistently, OPCs persist throughout the life of the animal, beyond the stage of developmental myelination. Several key steps must occur in order for myelin to be synthesized (**Figure 1**). First, OPCs must be generated by OL commitment and differentiation from neural precursor cells (NPCs) that reside in discrete areas of the germinal zones and by self-renewal of existing OPCs in the CNS parenchyma. Subsequently, OPCs must proliferate and migrate to occupy their final destination and undergo terminal

differentiation into OLs. Terminal OL differentiation is an asynchronous process. Thus, OPCs that undergo self-renewal co-exist with those that terminally differentiate or OLs that are beginning their myelination process. Furthermore, the temporal dynamics of OL appearance and myelination differ in different tracts (Lynn et al., 2021). Finally, newly generated OLs must find target axons and initiate the process of myelination.

Each of these steps is subject to regulation by intrinsic and extrinsic factors. A large body of literature exists on the role of individual factors and the stage at which they regulate OL development and myelination. However, it is less clear how the relevant set of extrinsic factors are presented to OL lineage cells at the correct time and location, and how a response is elicited only in a subset of OL lineage cells and not in others nearby. Moreover, the same single signaling molecule is often used to initiate different cellular programs. In this review, we will first describe the key stages in OL lineage progression that are influenced by the external environment and identify areas where we have a limited understanding of the sources of these external signals and how OL lineage cells integrate them to trigger a specific program. Following a short review of how macromolecules, particularly proteins, are trafficked and released externally, we provide examples of the pleiotropic effects of some proteins that affect OL lineage cells and ways in which their availability can be modulated.

Dynamic regulation from NPCs to myelination

From NPCs to OPCs

NPCs exist in different germinal zones throughout the neuraxis, where they are specified by different transcription factors in a region- and age-specific manner (Woodruff et al., 2001). In the spinal cord, OLs are initially specified in the pMN and P3 domains of the ventral ventricular zone defined by transcription factors Olig1, Olig2, and Nkx2.2 (Sun et al., 2001; Fu et al., 2002). In the forebrain, early OL specification occurs ventrally in the medial and lateral ganglionic eminences defined by the homeodomain transcription factors Nkx2.1 and Gsx2, respectively (Kessaris et al., 2006). Olig1 and Olig2 are induced in these domains, and this lineage is shared with interneurons (Petryniak et al., 2007). Subsequently, OPCs are generated from the dorsal germinal zones in both the spinal cord and telencephalon. The earlier ventrally generated OL lineage cells migrate dorsally and become intermingled with dorsally generated cells.

In the forebrain, the dorsal wall of the lateral ventricles continues to produce OPCs in the corpus callosum in the adult (Ortega et al., 2013). Newly produced OPCs gradually migrate dorsally and lose the stem cell/pluripotent transcription factor Sox2 as they mature (Kondo and Raff, 2004; Dai et al., 2015), although the role of Sox2 in the oligodendrocyte lineage is age- and context-dependent (Zhao et al., 2015; Zhang et al., 2018). How external signals within the SVZ niche induce OL commitment in a subset of NPCs remains poorly understood. Dynamic oscillation in the intracellular concentration of basic helix-loop-helix transcription factors such as Olig2 (Imayoshi et al., 2013) would provide an explanation of the seemingly stochastic nature in which OPCs are committed from NPCs. Neurofibromin, whose mutation leads to Neurofibromatosis type 1, is encoded by the *NF1* gene and is a Ras-GTPase-activating protein. It negatively regulates OPC proliferation (Bennett et al., 2003) and suppresses OL specification from NPCs in the SVZ (Wang et al., 2012; **Figure 1A**, NPC). Biallelic deletion of *Nf1* in NPCs switches the fate of NPCs from neurons to OPCs, leading to an increased density of OLs in the developing and adult SVZ. This can be reversed by inhibiting the extracellular signal-regulated kinase Erk1/2, which is a downstream effector of Ras (Wang et al., 2012). It remains unclear what the specific extracellular signal is that directs NPCs to follow an OPC fate and how the signal is transduced in NPCs to activate the OPC program. Paradoxically, Erk1/2 signaling in differentiated OLs is essential for myelination (Ishii et al., 2019) but is dispensable for OPC proliferation (Hill et al., 2013).

OPC expansion and "maturation"

Once NPCs become committed to the OL lineage, they begin the transcriptional program of pre-OPCs and weakly upregulate platelet-derived growth factor receptor alpha (PDGFRα; Marques et al., 2018; Weng et al., 2019). They subsequently become more permanently committed to OPCs by robustly upregulating the signature OPC transcripts *Pdgfra* and *Cspg4* encoding NG2. As OPCs mature and migrate away from the germinal zone, they lose the expression of NPC molecules such as Sox2 and become fully committed to the OL lineage. This process occurs gradually as they migrate through the parenchyma with a lag period following the initial OL commitment in the SVZ.

Developmental OPCs proliferation is dependent on platelet-derived growth factor AA (PDGF AA), which is a critical mitogen for OPCs and activates PDGFRα on OPCs (van Heyningen et al., 2001; Hill et al., 2013). There are mechanisms that modulate the mitogenic effects of PDGF AA. For example, entrapment of PDGF AA in the extracellular matrix could alter their availability to cells (Pollock and Richardson, 1992) and its co-receptors, such as neuropilin-1 expressed by activated/amoeboid microglia, can trans-activate PDGFRα on neighboring OPCs (Sherafat et al., 2021). In organotypic slice cultures, parenchymal OPCs no longer proliferate in response to other mitogens such as fibroblast growth factor-2 (FGF2)

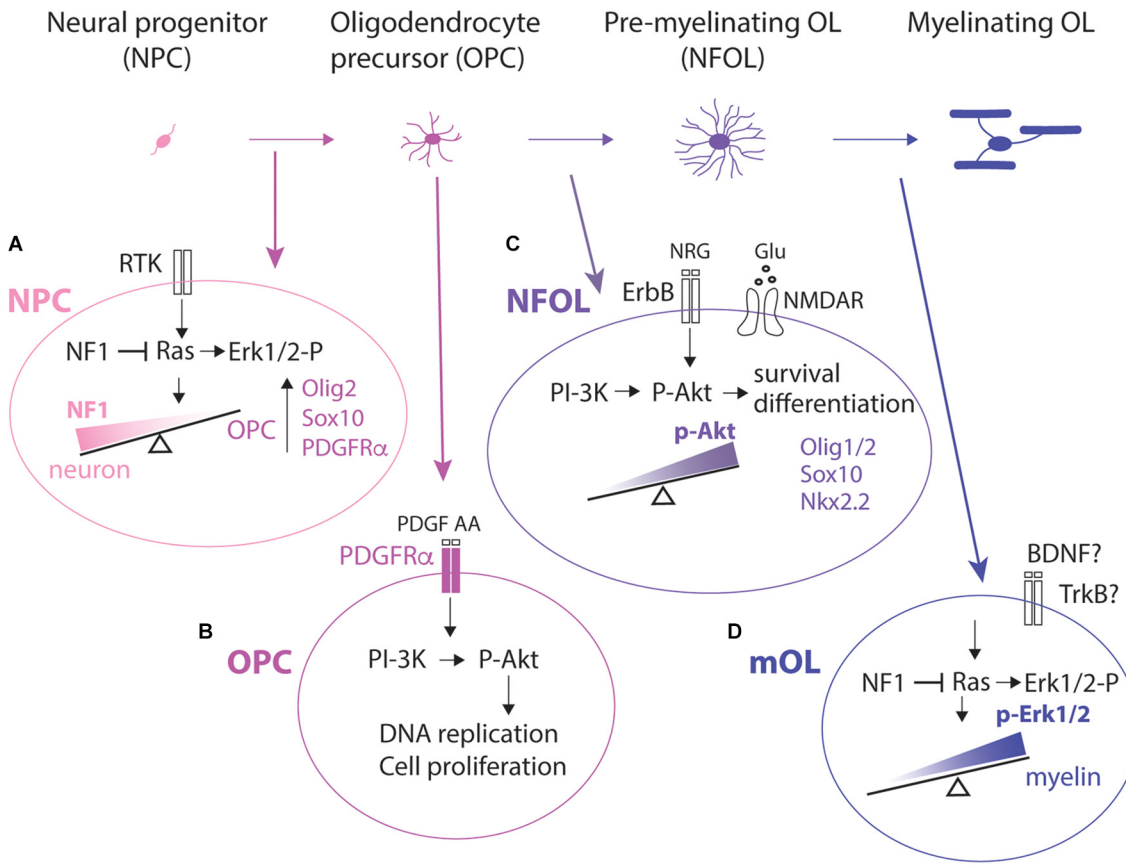

FIGURE 1
Lineage progression from an NPC to a myelinating OL and examples of key signaling pathways at each stage. **(A)**: NPC. OPCs are specified from NPCs in the ventricular and subventricular zones. Reduction in NF1 leading to enhanced activation of Ras-Mapk-Erk1/2 pathway shifts the fate of NPCs to an OPC fate and suppresses the neuronal fate. Committed OPCs upregulate Olig2 and Sox10 which in turn turns on Pdgfra transcription. **(B)**: OPC. OPC proliferation is dependent on PDGFRα and is mediated by PI-3K activating Akt and not through Mapk activating Erk1/2. **(C)**: NFOL. In NFOLs, PI-3K activating Akt is primarily responsible for their terminal differentiation, survival, and initiation of myelination, possibly *via* the transcription factor FoxO1. HDAC1/2 activity, Myrf, and upregulation of Sox10, and Nkx2.2 are also critical for terminal differentiation. **(D)**: mOL. In myelinating OLs (mOLs), activation of the Ras-Erk1/2 pathway is critical for maintaining myelination. NF1, neurofibromin; RTK, receptor tyrosine kinase; Erk1/2-P, phosphorylated Erk1/2; PDGF, platelet-derived growth factor; PDGFRα, platelet-derived growth factor receptor alpha; PI-3K, phosphatidyl inositol-3-kinase; P-Akt, phospho-Akt; BDNF, brain-derived neurotrophic factor; NFOL, newly formed OLs; HDAC1/2, histone deacetylase 1 and 2; Myrf, myelin regulatory factor; NRG, neuregulin.

or epidermal growth factor (EGF; Hill et al., 2013). While OPC production in the embryonic spinal cord is dependent on Erk1/2 signal (Newbern et al., 2011), PDGF-dependent OPC proliferation in slice cultures and OPC proliferation *in vivo* are mediated by Akt activation and not by Erk1/2 signal (Ishii et al., 2012; Hill et al., 2013; **Figure 1B**, OPC). Erk1/2 appears to play a more prominent role in OPC proliferation in dissociated cultures (McKinnon et al., 1990), suggesting the importance of the pericellular microenvironment in regulating signal transduction from PDGFRα in OPCs.

OPCs remain proliferative throughout life. However, as the animal matures, OPCs become more "OL-like" by acquiring a low level of expression of OL-specific genes (Moyon et al., 2015; Marques et al., 2018). These OL-like OPCs are more prevalent in the spinal cord than in the brain (Marques et al., 2018). Besides the signature proteins PDGFRα and NG2 on their surface, OPCs also express voltage-dependent ion channels and neurotransmitter receptors, including AMPA and GABA receptors (Larson et al., 2016), which are essential for their depolarizations at neuron-OPC synapses. There have been a number of studies on whether and how activation of ionotropic glutamate and GABA receptors on OPCs affects their proliferation or OL differentiation (Gallo et al., 1996; Kougioumtzidou et al., 2017; Chen et al., 2018), but the findings vary, and we do not yet fully understand how the signal is transduced following synaptic stimulation of OPCs. While cumulative labeling of cycling cells with thymidine analogs indicates that almost all OPCs are cycling (Psachoulia et al., 2009; Kang et al., 2010; Young et al., 2013), single cell RNA-seq data indicate that cycling OPCs represent

only a subset of OPCs (less than 25% of the cells in the total OPC cluster; Marques et al., 2018). *In vivo* multi-color cell fate mapping has revealed that some isolated clones of OPCs undergo a burst of expansion later in adulthood (Garcia-Marquez et al., 2014), suggesting considerable heterogeneity in the mitotic activity of individual OPCs. It remains unknown whether the mitotic competence of individual OPCs is determined intrinsically, for example by the number of cell divisions, or whether it is influenced by the microenvironment surrounding OPCs in specific regions.

Terminal OL differentiation

The mechanisms that dictate whether individual OPCs differentiate into OLs or continue to self-renew are not fully understood. The signal must be local to their pericellular microenvironment, as OPCs that generate OLs are intermixed with OPCs that self-renew. However, there are some differences in different neuroanatomical regions. In regions where large numbers of myelinating OLs must be generated over a relatively short period of time, such as the white matter in early postnatal CNS, OPCs are more likely to differentiate symmetrically into two OLs, whereas those in gray matter and in older animals are more likely to undergo self-renewing divisions to produce one OL and one OPC or two OPC progeny (Zhu et al., 2011). Many extrinsic signals regulate OL differentiation when tested individually *in vitro* or *in vivo* (Emery, 2010; Huang et al., 2013). However, it remains a major challenge to understand which of the individually tested signals are available to differentiation-competent OPCs at the right time and right place, and what enables them to trigger a response in OPCs that activates specific intracellular signal transducers, transcription factors, and chromatin/DNA regulators to elicit specific outcomes (Huang et al., 2013).

Upon terminal differentiation, OPCs permanently exit the cell cycle, lose PDGFRα and NG2 from the cell surface, and begin the program to terminally differentiate into postmitotic OLs. This process is initiated by the downregulation of PDGFRα and subsequent upregulation of *Nkx2.2* (Zhu et al., 2014). These events, along with upregulation of the myelin regulatory factor (*Myrf*) and transcription factor *Sox10* as well as the function of histone deacetylases HDAC1 and 2, are required for OL differentiation and subsequent upregulation of myelin genes (Emery and Lu, 2015; Liu et al., 2016; Sock and Wegner, 2021). Specific miRNAs downregulate PDGFRα (Budde et al., 2010; Dugas et al., 2010; Zhao et al., 2010), but PDGFRα downregulation and cessation of OPC proliferation are not necessarily coupled with OL differentiation. For example, guanidine compounds that repress *Pdgfra* transcription and OPC proliferation do not stimulate OL differentiation (Medved et al., 2021). Activation of Akt (Protein kinase B) and mammalian target of rapamycin (mTOR) is critical for OL differentiation (Bercury et al., 2014; Ishii et al., 2019), and the effect is mediated by FoxO1 (Wang et al., 2021; **Figure 1C**, NFOL).

From newly formed OLs (NFOLs) to myelinating OLs

Pre-myelinating OLs

NFOLs have a transcriptomic signature that distinguishes them from mature myelinating OLs (Marques et al., 2016; Tasic et al., 2016). Morphologically they have numerous fine radially oriented processes that appear different from the smaller number of thicker, straight myelinating processes characteristic of mature myelinating OLs. These postmitotic NFOLs that are not yet myelinating OLs are often referred to as premyelinating OLs (Trapp et al., 1997; Hughes and Stockton, 2021) or "lacy OLs" (Zerlin et al., 2004). During the premyelinating stage, NFOLs actively make contacts with target axons before they begin the program of myelination (Hughes and Stockton, 2021). They express the DM20 splice variant of the myelin tetraspanin protein proteolipid protein (PLP; Trapp et al., 1997). NFOLs in white matter tracts differentiate quickly into myelinating OLs, whereas those in gray matter stall in the premyelinating stage longer (Zerlin et al., 2004).

NFOLs seem to be particularly sensitive to their local environment for their survival, and as many as 50% of them die (Barres et al., 1992). When OPC production is increased by increasing the amount of available PDGF, supernumerary OLs die (Calver et al., 1998). Conversely, increasing the number of axons in the optic nerve leads to increased OL numbers (Burne et al., 1996), suggesting that axonal signals regulate the survival of NFOLs as a part of a strong homeostatic mechanism that maintains a constant density of OLs optimized to the local neural circuit function.

In the early postnatal forebrain, terminal OL differentiation occurs within a temporal window of 3–4 days after the last OPC division in both gray and white matter, and the fate of NFOLs is influenced by their microenvironment (Hill et al., 2014). For example, reduction of myelin accelerates terminal OL differentiation after the final OPC mitosis, while loss of whisker sensory input reduces the number of NFOLs that survive (Hill et al., 2014). Conversely, in adults, whisker stimulation increases the survival of NFOLs (Hughes et al., 2018). Direct electrical stimulation of cultures containing OPCs and axons promotes the survival of OLs (Gary et al., 2012). Loss of GRIA2 (*GluR2*) and GRIA3 (*GluR3*) AMPA receptor subunits compromises OL survival (Kougioumtzidou et al., 2017). Interestingly, *Nfatc4* (nuclear factor of activated T-cells cytoplasmic 4),

which is activated by the Ca^{2+}-dependent protein phosphatase calcineurin, de-represses *Olig2* and *Nkx2.2* in a *Sox10*-dependent manner (Weider et al., 2018). Thus, neuron-derived signals could change $[Ca^{2+}]_i$ and trigger the signals that downregulate *Pdgfra* mRNA and upregulate *Nkx2.2* and subsequent progression toward myelinating OLs. These events likely depend on the pattern of neuronal activity (Nagy et al., 2017), and thus they are likely to differ in different regions (Etxeberria et al., 2016) and expression of voltage-dependent Ca^{2+} channels (Cheli et al., 2016; Pitman et al., 2020).

Myelination

Interestingly, the process of myelin ensheathment itself requires no extrinsic input from other CNS cell types. *In vitro*, primary OLs have been shown to contact and wrap inert nanofibers mimicking the 3D structure of axons but lacking any signaling cues that would normally be present during myelination (Lee et al., 2012). *In vivo*, however, the process of axonal selection and myelination is still highly regulated, and external factors exert a major influence over both the timing and extent of myelination.

Nkx2.2 is re-upregulated as myelination proceeds (He et al., 2009). The process of myelin ensheathment requires active axons undergoing regulated exocytosis (Hines et al., 2015; Mensch et al., 2015). While PI3K-Akt signal through mTORC1 is critical for OL differentiation and the initiation of myelination, Erk1/2 alone plays a critical role in maintaining myelin. For the process of generating myelin sheath, both Akt and Erk1/2 pathways are needed to effect mTORC1 (Ishii et al., 2019; **Figure 1D**, mOL).

In addition to playing a major role in regulating the survival of NFOLs, neuronal activity has also been shown to influence myelination and OL maturation. Pharmacological stimulation of individual neurons increases the probability of their axons being myelinated (Mitew et al., 2018), and repeated photostimulation, but not a single 3-h stimulation, of cortical association neurons, promotes remyelination of callosal axons and improves conduction (Ortiz et al., 2019). Single photostimulation, which robustly induces OPC proliferation (Gibson et al., 2014), may result in a moderate increase in OLs but may not be sufficient to allow progression to trigger the myelination program. Enhanced sensory experience has also been shown to promote OL maturation and differentiation (Forbes et al., 2020; Goldstein et al., 2021). How changes in neuronal activity are detected by NFOLs remains to be solved. Synapses that are present in OPCs are quickly disassembled at the onset of differentiation (De Biase et al., 2010; Kukley et al., 2010). However, the vesicular release of ATP and glutamate from axons has been shown to evoke Ca^{2+} transients in OPCs (Ziskin et al., 2007; Hamilton et al., 2010), and both have been suggested to play a role in regulating OL differentiation and myelination, suggesting that NFOLs may also utilize extra-synaptic mechanisms to sense neuronal activity (Agresti et al., 2005; De Biase et al., 2010; Kukley et al., 2010; Wake et al., 2011, 2015).

Trafficking of cell surface and secreted molecules

OL lineage cells at different stages of development integrate and respond to the variety of autocrine and paracrine signals presented to them in distinct ways. Their ability to respond, and the nature of their response, are largely determined by the complement of cell surface proteins and secreted signaling molecules present in each stage. Moreover, some signals are tonically or diffusely present in their microenvironment, while others are only made available in a spatially restricted manner. Thus, precisely regulated trafficking and secretion of key signaling factors are essential for proper OL lineage development. **Figure 2** summarizes the major components of the secretory pathways involved in trafficking protein cargo to the cell surface.

In most cases, proteins that are destined for the cell surface, either to be incorporated into the membrane or released into the extracellular space, are first synthesized in the endoplasmic reticulum before being transported to the Golgi apparatus. Following passage through the Golgi, vesicles carrying protein cargo are trafficked through the trans-Golgi network (TGN) where they are sorted into transport vesicles targeting them to appropriate subcellular destinations. After leaving the TGN, vesicles carrying protein cargo can either be transported directly to the plasma membrane for exocytosis or be targeted to the endosomal pathway for further sorting.

Exocytosis can occur either constitutively, where vesicles carrying protein cargo fuse immediately upon arriving at the plasma membrane, or in a regulated fashion, where transport vesicles are stored and only released in response to a defined stimulus (Stöckli et al., 2016). During regulated secretion, the stimulus involved often results in a rise in intracellular Ca^{2+}, which acts as a second messenger to trigger the fusion of primed secretory vesicles with the plasma membrane. Distinct pools of these vesicles have been observed with differing degrees of Ca^{2+} sensitivity, depending on their complement of associated regulatory proteins. Although constitutive exocytosis requires no stimulus to occur, the rate of constitutive secretory processes can still be regulated at the cellular level *via* changes in gene or protein expression. This occurs in B lymphocytes, which are stimulated to produce large amounts of antibody which is then secreted constitutively (Borghesi and Milcarek, 2006).

Proteins that exert specific effects on OL lineage cells can be exocytosed from the cell of origin by a variety of mechanisms. Where they are ultimately targeted determines the mode of

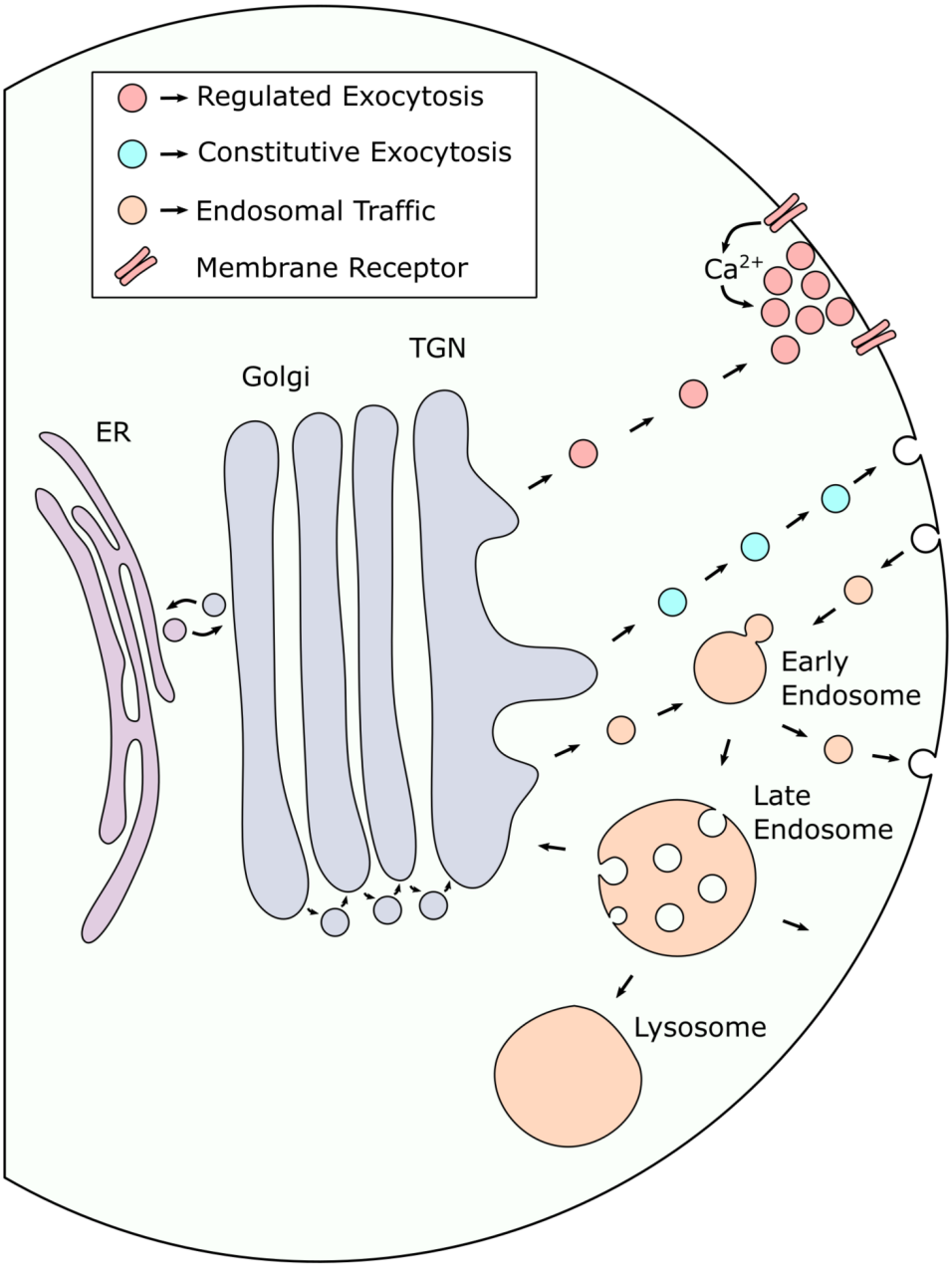

FIGURE 2
Secreted proteins are trafficked to the cell surface *via* multiple distinct pathways. After synthesis in the endoplasmic reticulum (ER), proteins destined for exocytosis undergo processing in the Golgi before being sorted into intracellular transport vesicles in the trans-Golgi network (TGN). Transport vesicles leaving the TGN can either be targeted directly to the plasma membrane to undergo regulated or constitutive exocytosis or be transported to the endosomal pathway, either for further sorting prior to exocytosis or to deliver endosome specific cargo. Proteins that are retrieved from the cell surface are targeted to early endosomes (EE) which act as sorting platforms in endosomal traffic to and from the membrane. EEs can mature into late endosomes (LE) which act as a final sorting station for proteins destined for lysosomal degradation. LEs can also mature into multi-vesicular bodies (MVB) which can alternatively fuse with the plasma membrane to facilitate exosome release. Small arrowheads indicate the direction of vesicle traffic.

activation. The availability of secreted proteins is dependent on whether they are freely available to bind to receptors on OPCs, need a co-receptor to activate the receptor on OPCs, or whether they become sequestered in the extracellular matrix and require an additional mechanism to encounter the receptor on OPCs. The duration of the effect is determined by the half-life of the protein outside the cell and the rate of reuptake, if it occurs. In the case of cell surface proteins, the duration of the availability

is additionally influenced by the rate of their endocytosis. For example, PDGFRα is rapidly internalized in the presence of the ligand in 5–30 min, whereas its half-life is longer than 2 h in resting cells (Kazlauskas, 2017).

SNARE proteins in exocytosis

Soluble N-ethylmaleimide-Sensitive Factor Attachment Protein (Fretto et al., 1993) receptors (SNAREs) are a highly conserved family of small membrane-anchored proteins which comprise the minimal molecular machinery required for membrane fusion involved in exocytosis and endosomal trafficking (Jahn and Scheller, 2006; Galli et al., 2013). The mechanism of SNARE-mediated exocytosis has been most extensively studied in the context of regulated exocytosis at the neuronal presynapse, where the local influx of Ca^{2+} can trigger vesicle fusion on the order of 1 ms. The discovery of a core SNARE complex in neurons, consisting of Syntaxin 1 (STX1), SNAP-25, and vesicle-associated membrane protein 2 (VAMP2), ultimately led to the development of the SNARE hypothesis, which proposed that membrane fusion is mediated by the binding of vesicle-associated SNAREs (v-SNAREs) to cognate target membrane-associated SNAREs (t-SNAREs).

SNARE proteins are required for both regulated and constitutive exocytosis, and although SNARE proteins themselves are not the primary drivers of vesicle targeting, specific combinations of SNARE proteins in a cell type are often linked to specific secretory pathways or processes (Kasai et al., 2012). Therefore, experimental modulation of defined SNARE proteins can serve as a tool to better understand the role of specific secretory processes in a particular cell type. The light chains of different clostridial neurotoxins, which include tetanus toxin and botulinum neurotoxins, cleave distinct sets of SNARE proteins with a high degree of specificity (Schiavo et al., 2000). Cell-type specific expression of these toxins has primarily been employed as a means of disrupting SNARE-mediated exocytosis in different neuron subtypes, though it has also been used to investigate the role of gliotransmission in Müller cells of the retina (Slezak et al., 2012). The time course of SNARE-dependent release in response to a stimulus differs among different cell types, with synaptic vesicles representing the fastest type of release on the order of milliseconds, while release from dense core vesicles at some synapses and neuroendocrine cells are 2–5 orders of magnitude slower (Kasai et al., 2012). Stimulated SNARE-dependent release from astrocytes is three orders of magnitude slower than that of presynaptic vesicle release from axons (Schwarz et al., 2017). Thus, proteins released from both astrocytes and neurons, such as brain-derived neurotrophic factor (BDNF; Zhang et al., 2014), could be presented to OPCs by different dynamics and could lead to the activation of distinct signaling pathways. Another example is PDGF AA, which is produced by neurons, OLs, and microglia (Zhang et al., 2014), and could lead to differential activation of the downstream intracellular signaling pathway from PDGFRα on OPCs depending on the cellular source, mechanism of release, and the quantity of release from the different cells surrounding OPCs.

SNARE-mediated exocytosis in OL lineage cells

OL lineage cells employ SNARE-mediated membrane fusion to enable secretion, vesicle, and membrane trafficking, as well as targeting and sorting of membrane proteins, which provide crucial functions at each of the different stages in OL development (Feldmann et al., 2011). Recently, we and others have shown that genetic expression of Vamp1, 2, and 3-specific B type botulinum toxin (BoNT/B), in OPCs using *Cspg4-cre* (Fekete et al., 2022) or *Pdgfra-creERT* (Pan et al., 2022) or in newly differentiated OLs using *Cnp-cre* (Lam et al., 2022) leads to severe hypomyelination due to inability of the Vamp2/3-cleaved OLs to produce myelin membranes. These findings suggest that a critical autocrine factor that is either secreted from newly generated OLs or is inserted into the plasma membrane of new OLs plays a critical role in myelination.

SNARE-mediated processes in the OL lineage have also been shown to regulate the transcription of myelin basic protein (MBP), a peripheral membrane protein localized at the cytoplasmic surface that is critical for myelin compaction (Bijlard et al., 2015). *Mbp* mRNA is translated locally at the plasma membrane after being transported from the soma to the myelin membranes in RNA granules (Ainger et al., 1997; Barbarese et al., 1999). When the t-SNARE gene *Stx4* is knocked down or overexpressed, *Mbp* transcription is severely reduced, with no apparent effects on OL viability or the expression and trafficking of the other myelin proteins PLP and CNP (2',3'-cyclic nucleotide phosphodiesterase; Bijlard et al., 2015). Knocking down *Stx4* in mature OLs after MBP is translated has no effect on the level of MBP in the myelin. Knockdown of *Vamp3* encoding the v-SNARE partner for STX4 does not alter the trafficking of *Mbp* mRNA. Intriguingly, the conditioned medium of normal developing OLs restores *Mbp* transcription in *Stx4*-downregulated cells, suggesting that STX4 is critical for the release of an autocrine factor that is necessary for initiating *Mbp* transcription.

Myelin proteolipid protein (PLP), a major tetraspanin membrane protein in myelin, is synthesized in the endoplasmic reticulum and is trafficked *via* two distinct SNARE-dependent processes: (1) mediated by VAMP3 and its cognate t-SNARE partner STX4 *via* recycling endosomes; and (2) mediated by VAMP7 and its partner STX3 *via* late endosomes and lysosomal compartments (Feldmann et al., 2011). Compromised

VAMP3 or VAMP7 function in cultured OLs leads to loss of PLP from the cell surface and its accumulation in the soma, but these manipulations do not affect the total expression level of PLP. During OL maturation, endocytic turnover of PLP decreases as the level of PLP at the myelin membrane surface increases, and this is accelerated in the presence of neurons *via* cAMP (Trajkovic et al., 2006).

What triggers SNARE-mediated exocytosis in OL lineage cells remains unknown. When OPCs receive synaptic inputs from neurons, they respond to vesicularly released glutamate through their AMPA receptors, which consist of Ca^{2+}-permeable subunits (Bergles et al., 2000; Ge et al., 2006). Voltage-gated Ca^{2+} channels and Na^{+} /Ca^{2+} -exchanger also contribute to an increase in $[Ca^{2+}]_i$ in OPCs (Tong et al., 2009; Cheli et al., 2016). While an increase in $[Ca^{2+}]_i$ can be readily detected after direct stimulation of AMPA receptors on OPCs, or by activating DRG neurons in a DRG-OPC coculture (Wake et al., 2011), demonstration of a local rise in $[Ca^{2+}]_i$ in response to physiological synaptic stimulation of OPCs has not been achieved (Haberlandt et al., 2011; Sun et al., 2016). Regardless of the nature of the extracellular stimulus that elicits a rise in $[Ca^{2+}]_i$ in OPCs, the importance of Ca^{2+} signal in OPCs is evident. For example, the deletion of voltage-dependent Ca^{2+} channels $Cav_{1.2}$ and $Cav_{1.3}$ in OPCs reduces OL differentiation and myelination in white matter (Cheli et al., 2016) and reduces OPC proliferation in the cortex (Zhao et al., 2021). Furthermore, Nfat proteins, which are activated by the Ca^{2+}-dependent phosphatase calcineurin, cooperate with Sox10 to activate Nkx2.2, which is critical for OL differentiation (Weider et al., 2018). One could thus hypothesize whether depolarization and Ca^{2+} entry into OPCs at neuron-OPC synapses could trigger specific SNARE proteins in OPCs and trigger them to release molecules that are critical for OL lineage progression and possibly those that in turn affect neurons in a paracrine fashion.

Dynamic modulation of extracellular signal availability

Many signaling molecules exert a wide range of effects depending on the context in which they are presented to the target cell. Their effects depend on their temporal and spatial availability and the distribution of their receptors. In this section, we will use brain-derived neurotrophic factor (BDNF) and L1CAM (L1 cell adhesion molecule) as examples to illustrate the different ways in which soluble and integral membrane proteins might be delivered to OL lineage cells. We chose to discuss these proteins in detail because their expression and availability are regulated in different ways, including neuronal activity, and they exhibit pleiotropic cellular effects. While their functions have been described extensively for neurons, some of these regulatory mechanisms may also be applied to how they regulate OL differentiation and myelination. We also discuss the role of the intracellular Src family kinase Fyn as an integrator of multiple signals to OL lineage cells and its potential role as a filter for eliciting specific responses in newly differentiated OLs.

Pleiotropic effects of the soluble protein BDNF

Diverse effects of BDNF on neurons

BDNF belongs to the family of neurotrophins. Nerve growth factor (NGF) was the first member of the family, which was discovered as a target-derived trophic factor for sympathetic and sensory neurons in the periphery (reviewed in Levi-Montalcini, 1987). Subsequently, BDNF was isolated and characterized from the pig brain in search for a neurotrophic factor that functions in the CNS (Barde et al., 1982; Leibrock et al., 1989). In most cases BDNF is proteolytically cleaved from pro-BDNF inside the cell to generate mature BDNF, which is secreted (**Figure 3A**). The binding of mature BDNF to the high-affinity tropomyosin receptor kinase B (TrkB) receptor activates phospholipase C gamma (PLC-γ), PI-3K, and Erk1/2, and exerts a wide range of effects on target neurons such as survival, axon growth, synaptogenesis, and synaptic plasticity (Thoenen, 1995). Under some conditions, pro-BDNF can also be released from the cell. Secreted pro-BDNF binds preferentially to p75 low-affinity neurotrophin receptor ($p75^{NTFR}$) and elicits effects such as apoptosis and long-term depression, which are distinct from the effects of TrkB activation by mature BDNF (Chao, 2003). The cellular effects of BDNF depend on the duration of its availability, the distribution of TrkB receptors, and the subcellular region of the target cell to which BDNF is made available.

The temporal and spatial availability of BDNF is influenced by several factors (**Figure 3A**). For example, constitutive release provides a tonic level of extracellular BDNF, whereas release regulated by neuronal activity leads to a pulsatile elevation in local BDNF concentration (Balkowiec and Katz, 2002). In the developing callosal axons, BDNF secretion is mediated by the vesicular and membrane SNAREs VAMP2 and SNAP25/47, respectively, and the function of these SNARE proteins is critical for BDNF-mediated axonal differentiation (Shimojo et al., 2015). Once secreted, BDNF has a limited ability to diffuse, since it has a tendency to become embedded in the extracellular matrix because of its positive charge (Park and Poo, 2013). In neuronal culture, different effects of BDNF on spine development are elicited by different temporal patterns of elevated local BDNF concentrations (Wang et al., 2022).

At the synapse, BDNF modulates synaptic plasticity *via* specific pre- and postsynaptic mechanisms (**Figure 3A**). TrkB receptors at pre- and postsynaptic membranes differentially contribute to long-term potentiation (LTP) in hippocampal neurons (Lin et al., 2021). BDNF binding to TrkB increases $[Ca^{2+}]_i$ by activating PLC-γ. Activated TrkB also activates Fyn, which in turn increases the open probability of NMDA receptors, additionally contributing to Ca^{2+} influx (Xu et al., 2006; Bjarnadottir et al., 2007; Hildebrand et al., 2016). Increased presynaptic NMDA receptor activity in turn increases $[Ca^{2+}]_i$, which promotes BDNF release (Lituma et al., 2021). At postsynaptic spines, increased activity increases the release of BDNF, which activates TrkB on the same spine in an autocrine manner and promotes LTP (Wang et al., 2022). Furthermore, neuronal activity increases the number of TrkB receptors on the postsynaptic membrane. BDNF, like NGF, is internalized by clathrin-mediated endocytosis. Signaling endosomes containing endocytosed TrkB-BDNF complex are transported from the internalized site on the axon back to the soma where they promote survival *via* Akt (Grimes et al., 1996).

Effects of BDNF on OL lineage cells

BDNF exerts different effects on OPCs and OLs, with a more prominent effect at later stages during myelination. *Bdnf*−/− mice survive up to 4 weeks and show severe hypomyelination with reduced *Mbp* and *Plp1* mRNA in the developing optic nerves (Korte et al., 1995; Cellerino et al., 1997). Heterozygous *Bdnf*+/− mice also exhibit reduced myelin and a transient reduction in OL lineage cell density in the optic nerves (Vondran et al., 2010; Nicholson et al., 2018). Exogenously applied BDNF has no effect on OPC proliferation or OL survival (Barres et al., 1993), although there seems to be some regional heterogeneity in their response to BDNF (Du et al., 2003). However, knockdown of TrkB in purified OPC cultures increases OPC proliferation (Wong et al., 2013), suggesting a suppressive role for TrkB in OPC proliferation. Paradoxically, *Bdnf*+/− mice exhibit impaired OPC proliferation after cuprizone-induced demyelination (Tsiperson et al., 2015; Huang et al., 2020), which could be secondary compensatory proliferation of TrkB-expressing OPCs that occurs in response to myelin defects (Wong et al., 2013). BDNF also increases OPC process extension, especially in the presence of inhibitory proteoglycans (Siebert and Osterhout, 2021). Overall, these effects of BDNF on OPCs are limited and appear only in culture or are reversed as development proceeds.

BDNF exerts a more prominent and long-lasting pro-myelinating effect in OLs *via* TrkB (Barres et al., 1993; Xiao et al., 2010). Conditional knockout of TrkB in postmitotic OLs reduces myelin thickness without affecting OL production or axonal contact (Wong et al., 2013). As described above in section "From newly formed OLs (NFOLs) to myelinating OLs", myelination occurs in two phases. The first phase does not require neuronal activity. Neuregulin (NRG) increases NMDA receptor currents in OLs, thereby switching to an activity-dependent mode of myelination (Lundgaard et al., 2013). BDNF has a similar effect of enabling activity-dependent myelination by increasing NMDAR currents in OLs. BDNF stimulation of OL TrkB leads to Erk1/2 phosphorylation, and manipulating the strength of Erk1/2 activity directly affects the level of myelin protein expression and myelination *in vitro* (Xiao et al., 2012). Consistently, Erk1/2 knockout reduces developmental myelination (Ishii et al., 2019).

Fyn kinase as a transducer of BDNF signal

According to RNA-sequencing datasets, TrkB mRNA is more abundant in OPCs than in OLs (Zhang et al., 2014; Marques et al., 2018). Why then is the effect of BDNF more prominent during myelination and not at the earlier OPC stage? One could speculate that OLs but not OPCs have the critical intracellular mechanism that endows them with a high sensitivity of detecting BDNF to elicit a sustained Erk1/2 response necessary to promote myelination. One candidate for such a stage-specific transducer BDNF/TrkB signal is Fyn kinase (**Figures 3B**, **4**). Fyn is a member of the Src family non-receptor tyrosine kinases. Tyrosine phosphorylation at Y420 increases its kinase activity, whereas tyrosine phosphorylation on Y531 in the C-terminal regulatory region inhibits kinase activity (Matrone et al., 2020). Fyn is marginally expressed in OPCs but robustly upregulated in NFOLs (Colognato et al., 2004; Zhang et al., 2014; Marques et al., 2018). It is sustained at a high level during active developmental myelination (Krämer et al., 1999) and is downregulated by the end of the first postnatal month after the peak of myelination. *Fyn*−/− mice exhibit hypomyelination apparent at 4 weeks (Umemori et al., 1994). In zebrafish, the number of myelin sheaths made by each OL is dependent on Fyn kinase activity (Czopka et al., 2013). In OLs, the ability of BDNF to phosphorylate and activate Erk1/2 is mediated by Fyn (Peckham et al., 2016). Thus, the differential response of OPCs and OLs to BDNF could in part be attributed to the greater expression and activity of Fyn. Since OPCs and OLs coexist in the white and gray matter, the specific effects of BDNF must be determined by how BDNF is made available specifically to individual OPCs or OLs and the temporal and spatial pattern of TrkB expression and downstream effectors in OL lineage cells at different stages. Similar fine-tuning mechanisms are likely to shape the response of OL lineage cells to a variety of other soluble factors such as PDGF, FGF, and Wnt (Emery, 2010; Adams et al., 2021).

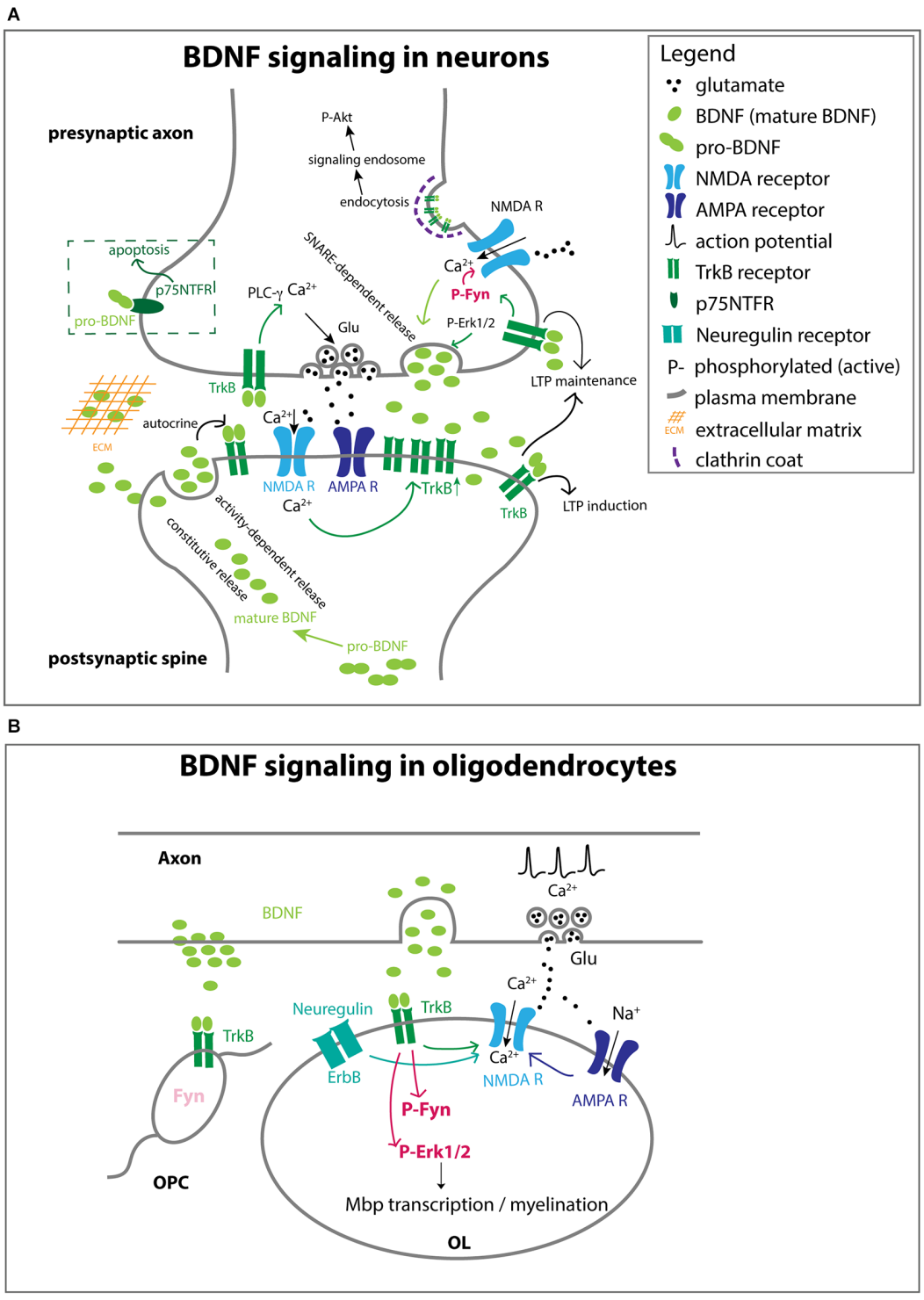

FIGURE 3
Different ways in which BDNF acts on cells **(A)**. BDNF-TrkB function at the neuronal synapse. BDNF from the target neuron or other cells in the target area mediates the survival and axon growth of the presynaptic neuron. Some of the effect is local, while other effects may be mediated by clathrin-dependent endocytosis of BDNF-TrkB complex that could be transported retrogradely by signaling endosomes, analogous to what has been reported for NGF and its high-affinity receptor TrkA. Mature BDNF can be secreted constitutively or in a regulated manner *via* SNARE-dependent mechanisms. BDNF may not be immediately available to the receptor if it becomes embedded in the extracellular matrix. While the majority of the effects are mediated by mature BDNF, pro-BDNF can also be secreted and act on p75NTFR to elicit a cell death response. BDNF acting on presynaptic and postsynaptic membranes can promote LTP. At the presynaptic terminal, axon depolarizations increase Ca^{2+} entry
(*Continued*)

FIGURE 3 (Continued)
through NMDA receptors, which in turn activates the SNARE-dependent release of BDNF. The neuronal activity also increases the level of TrkB at the presynaptic surface, and TrkB activation increases Ca^{2+} *via* PLC-γ activation, leading to enhanced glutamate release from presynaptic vesicles. At the postsynaptic membrane, BDNF acting on TrkB also contributes to LTP by increasing NMDA current. BDNF is secreted in an activity-dependent manner and acts in an autocrine fashion on TrkB on the same spine, which is necessary for LTP. Some of the processes indicated in one compartment also apply to the other compartment. The concept of signaling endosomes has been used to explain the function of endocytosed TrkB-BDNF complex that is transported from the internalized site on the axon back to the soma where it exerts developmental effects (Grimes et al., 1996), similar to what had been reported earlier for TrkA-NGF (Grimes et al., 1996). **(B)** BDNF-TrkB function at axon and OL interface. Neuronal activity triggers BDNF release and glutamate release. BDNF binds to TrkB on OLs and activates Fyn and Erk1/2, which promotes the transcription of myelin genes and myelination. NRG acting on the ErbB receptor and BDNF activating TrkB both increase Ca^{2+} permeation through NMDA receptors. Fyn is much less abundant in OPCs than in OLs, even though OPCs express TrkB.

Integral membrane and extracellular matrix proteins that promote myelination *via* Fyn

The importance of axonal activity in myelination has been a subject of intense investigation. Early studies have shown that dark-rearing reduces the number of myelinated axons in the optic nerve (Gyllensten and Malmfors, 1963), and conversely, myelination is accelerated by artificial eye opening (Tauber et al., 1980). Many other studies have also shown that neuronal activity promotes myelination (Barres and Raff, 1993; Demerens et al., 1996; Stevens et al., 2002), but the molecular and cellular mechanisms by which different patterns of neuronal activity initiates the myelination program in OLs is less clear. In this section, we will use the L1 cell adhesion molecule as an example of an extracellular signal that activates Fyn and highlight the multiple ways in which its presentation to OLs can be modulated.

L1 cell adhesion molecule functions *via* Fyn in myelination

One proposed mechanism for axon-OL signaling in regulating myelination is an interplay between cell surface adhesion molecules on axons and the adjacent OL processes. L1CAM belongs to the immunoglobulin superfamily of calcium-independent cell adhesion molecules (IgCAM) and is predominantly expressed on developing axons. L1 contains six Ig-like domains (Ig1–6) followed by five fibronectin type III-like domains (FN1–5) in the extracellular domain and a short cytoplasmic domain at the C-terminus (**Figure 4A**). It engages in both homophilic and heterophilic interactions in cis and trans and is involved in a variety of developmental processes including neurite growth, cell survival, migration, myelination, and synaptic plasticity (Sytnyk et al., 2017).

Binding partners of L1 on NFOLs include contactin-1 (Cntn1), which is structurally related to L1, and integrins (Laursen et al., 2009). Cntn1 is a glycosylphosphatidyl-inositol (GPI)-anchored protein that consists of six Ig domains and four FN type III-like domains. The binding of L1 to Cntn1 promotes myelination through transient activation of Fyn kinase (**Figure 4A**), and the interaction occurs specifically in lipid rafts (Krämer et al., 1999; Laursen et al., 2009). Lipid rafts are microdomains in the plasma membrane that are enriched in sphingolipids and cholesterol, as well as GPI-anchored proteins, where integral membrane proteins such as cell adhesion molecules and growth factor receptors form detergent-insoluble glycolipid-enriched complexes and function as a platform for cell signaling (Simons and Ikonen, 1997). Lipid rafts are prominent in NFOLs but are not commonly detected in OPCs (Krämer et al., 1999). When Fyn is complexed with Cntn1 and L1 in lipid rafts, its kinase activity is enhanced (Zisch et al., 1995; Krämer et al., 1999). Conversely, outside lipid rafts, Fyn is not complexed with Cntn1 or L1, and it is phosphorylated on the regulatory tyrosine at Y531, which makes it inactive (**Figure 4A**). One downstream consequence of Fyn activation is the local translation of *Mbp* mRNA (White et al., 2008; Kramer-Albers and White, 2011), leading to MBP accumulation at the inner plasma membrane leaflet, where it plays a critical role in myelin compaction.

Activity-dependent neuronal expression of L1

The expression of L1 is dynamically regulated. In cultures of dorsal root ganglion (DRG) neurons, L1 expression is tightly regulated by the frequency of action potential firing (**Figure 4B**). L1 expression is significantly reduced when axons are stimulated at 0.1 Hz but remains unaltered when stimulated at 1 Hz (Itoh et al., 1995). Stimulation of neuron-OL cocultures at 10–20 Hz increases the number of MBP+ myelin sheaths and reduces apoptotic OLs, whereas 1 Hz stimulation has no change (Stevens et al., 2002; Gary et al., 2012). Furthermore, the effect of the 10–20 Hz stimulation is mediated by cAMP (Gary et al., 2012; Malone et al., 2013). These observations provide evidence that axons, and consequently OLs, have a molecular mechanism to detect and transduce different levels of neuronal activity. Additional studies are needed to obtain a more complete understanding of intensity-dependent signaling.

Proteolytic cleavage of L1

L1 is highly expressed on unmyelinated axons before and at the time of contact with OL processes but is quickly downregulated from the entire axon when one or more axon segments become ensheathed by OLs (Bartsch et al., 1989;

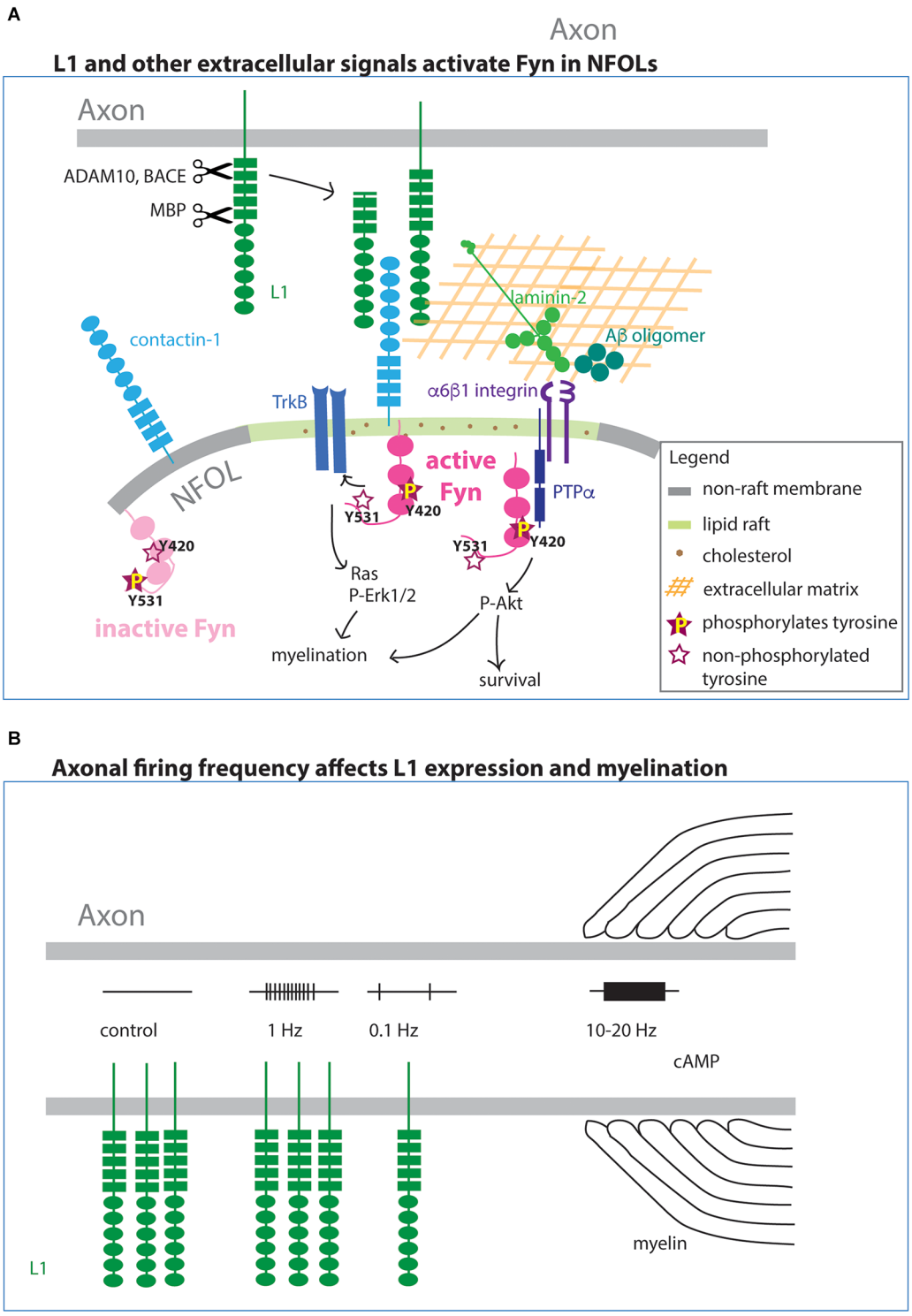

FIGURE 4
Integral membrane and extracellular matrix affecting myelination *via* Fyn **(A)**. Axonal L1 forms a complex with contactin-1 on OLs. The complex becomes preferentially localized to lipid rafts, where they complex with and activate Fyn by phosphorylated Y420. Fyn in the non-raft membrane is not active (not phosphorylated on Y420 but phosphorylated on the regulatory Y531 site). In addition to the membrane-bound form, cleaved L1 also interacts with contactin-1. In addition to L1, the extracellular molecules laminin-2 and Aβ oligomer also activate Fyn on OLs. Activated Fyn also promotes TrkB function. **(B)** The level of L1 expression on the surface of the axon is regulated by the frequency of action potential firing. High-frequency firing increases myelination, and this effect in some cases is mediated by cAMP.

Barbin et al., 2004). It is not known how myelination signals to axons to mediate this downregulation. It is possible that the rapid loss of L1 immunoreactivity from the surface of axons is caused by the shedding of L1. Some proteolytically cleaved forms migrate away from the site of cleavage, whereas other cleaved forms are retained at the membrane (Kleene et al., 2021). Notably, soluble L1 interacting with Cntn1 can activate Fyn in OLs (White et al., 2008).

L1 is proteolytically cleaved by a number of different enzymes including ADAM10 and 17 (a distintegrin and metalloproteinase domain-containing protein 10 and 17), BACE1 (β-site amyloid precursor protein-cleaving enzyme), and externally released MBP (**Figure 4A**; reviewed in Kiefel et al., 2012), eliciting distinct cellular responses. BACE1, which is a type 1 transmembrane aspartic protease, cleaves amyloid precursor protein (APP) to generate Aβ peptide. In mice, *Bace1* transcript is most abundantly detected in NF OLs (Zhang et al., 2014; Marques et al., 2018). When BACE1 is inhibited in primary neuronal cultures, there is a significant reduction of L1 and other cell adhesion molecules in the secretome, including the close homolog of L1 (CHL1), which is expressed on OPCs as well as neurons (Zhou et al., 2012; Zhang et al., 2014). BACE1 interacts with ADAM10, and ADAM10 enhances the catalytical activity of BACE1 to cleave CHL1 (Wang et al., 2018). *Bace1* knockout mice exhibit hypomyelination in the adult hippocampus (Hu et al., 2006) but not in the corpus callosum (Treiber et al., 2012), suggesting a potential role for BACE1 in axon-OL interaction, perhaps through its ability to regulate the amount of L1 available to interact with Cntn1 and stimulate Fyn on OLs. L1 is also cleaved by extracellular MBP. In addition to its well-known intracellular role in myelin compaction, MBP can be released out of the cell as a fusion with the C-terminal region of dynamin 1 or dynamin 1-related protein. Extracellular MBP cleaves L1 at a site in the FN1 domain and affects L1-mediated neurite growth and cell survival (Lutz et al., 2014; Kleene et al., 2021).

Knockdown of the l1cam-b in zebrafish significantly reduces the number of myelinated fibers and oligodendrocytes (Linneberg et al., 2019). In DRG-OL cocultures soluble L1 extracellular domain (ECD) promotes myelination. L1 ECD rescues the myelination defects caused by metalloproteinase inhibitors, suggesting that the shedding of L1 enhances myelination (Linneberg et al., 2019). In addition to the cleaved products, L1 is also found in exosomes, which suggests that it could function at remote sites away from its site of synthesis and surface expression.

Other extracellular signals that activate Fyn

Several extracellular matrix proteins are known to activate Fyn in OLs. The amyloid Aβ oligomer promotes OL maturation and transport of *Mbp* mRNA to the distal processes by interacting with integrins and subsequently activating Fyn (Quintela-López et al., 2019). In neurons, Fyn targets TrkB to lipid rafts (Pereira and Chao, 2007). A similar lateral movement within the plasma membrane could contribute to converging the effects of L1, laminin, and BDNF in NFOLs.

Fyn is also involved in transducing the signal presented to NFOLs by laminin-2 (merosin), which is a large extracellular matrix molecule whose reduction causes delayed OL maturation and muscular dystrophy (Relucio et al., 2009). Laminin-2 binds to α6β1 integrin on NFOLs, which interacts with and activates Fyn (Colognato et al., 2004; Relucio et al., 2009). NRG promotes the survival of NFOL, and this effect is amplified when the cell interacts with laminin-2 (Colognato et al., 2004). Engagement with laminin-2 reduces phosphorylation at Y531 in the regulatory subunit of Fyn, leading to increased Fyn kinase activity. Without laminin-2, the survival effect of NRG is mediated by PI-3K, whereas engagement of the cells with laminin-2 switches the signaling to the MAPK-Erk1/2 pathway. The cell surface protein tyrosine phosphatase alpha (PTPα) binds to integrin β1 subunit and can also activate Fyn and phosphorylate Akt to promote myelination (Ly et al., 2018). Thus, Fyn can be considered an integrator of axon-OL signals that control myelination. The activity of Fyn is transient, and it declines in stably myelinating OLs, but we do not yet understand the mechanism of its downregulation.

Other examples extracellular mechanism suggestive of fine-tuning myelination

Mechanisms that inhibit myelination

Most initial OL-axon contacts appear to result in process retraction, with only a minority becoming stable contacts (Snaidero and Simons, 2017). Below we provide a brief description of cell surface factors that negatively impact myelination.

PSA (polysialic acid)-NCAM (neural cell adhesion molecule)

PSA is a long α2, 8-linked polymer of sialic acid. In the nervous system, it is most frequently attached to the extracellular portion of NCAM, another cell adhesion molecule related to L1 (Rutishauser and Landmesser, 1996). During development when axons navigate to their destination, they are fasciculated *via* adhesion molecules on the surface. The tight bundle facilitates their rapid phase of growth through a permissive terrain established by the pioneer axon. NCAM on these migrating axons does not carry PSA. Once the axons reach their destination, they must defasciculate to find their synaptic

targets. In the target region, the PSA moiety is added to NCAM by the function of polysialyltransferases. The addition of PSA not only adds the bulk of the carbohydrate on NCAM, but the highly negative charge on PSA attracts water, which causes steric hindrance and weakens the homophilic cell adhesion of parallel axons *via* NCAM. PSA also inhibits the adhesion of other adhesion molecules such as L1. Beyond development, PSA is also implicated in synaptic plasticity and remodeling in the adult. Like L1, PSA-NCAM is downregulated concomitant with the onset of myelination (Charles et al., 2000). Removable of PSA with endoneuroaminidase N enhances myelination, though it is not clear whether this occurs by increased adhesion between the axon and the myelinating OL. Since PSA levels on developing axons appear to be influenced by synaptic activity (Rutishauser and Landmesser, 1991), PSA could be another possible mechanism for relaying the "readiness" of the axon to be myelinated.

LINGO1

LINGO1 (Leucine-rich repeat and immunoglobulin domain-containing-1), a transmembrane protein expressed in neurons and OL lineage cells, also acts to negatively regulate the onset of myelination through downstream activation of the small GTPase RhoA, which inhibits the morphological differentiation of OLs (Mi et al., 2005). Interestingly, it was shown that the extracellular domain of LINGO1 expressed by other cell types can act as its own ligand, binding to OL-expressed LINGO1 and inhibiting differentiation and myelination (Jepson et al., 2012). It was also shown that independently modulating the expression of LINGO1 in either neurons or OLs is sufficient to produce effects on differentiation and myelination (Lee et al., 2007). Therefore, it has been proposed that the inhibitory effect of LINGO1 on OL differentiation is mediated by the trans-interaction of LINGO1 at OL-axon contact sites (Jepson et al., 2012).

Arf6-mediated trafficking in neurons affects myelination

Studies on cell type-specific roles of ADP-ribosylation factor 6 (Arf6) provide an interesting example of how specific secretory mechanisms affect OL differentiation in a cell non-autonomous manner. Arf6 is the sole member of class III Arf gene products and is expressed by many cell types in the CNS. While Arfs 1–5 play a role in vesicular trafficking between the ER and Golgi compartments, Arf6 is localized to the plasma membrane and endosomal compartments and regulates endocytosis of the plasma membrane, endosomal recycling, and exocytosis. Arf6 conditional knockout using *Nestin*-cre results in severe hypomyelination specifically in the corpus callosum and hippocampal fimbria (Akiyama et al., 2014). Since *Nestin*-cre causes the deletion of Arf6 from both neurons and OL lineage cells, the authors further generated conditional Arf6 knockout mice in which Arf6 is deleted specifically from neurons or from OLs. Interestingly, hypomyelination is observed in neuronal Arf6 knockout mice but not in OL-specific Arf6 knockout mice. The defect appears to be in OPC migration due to a defect in neuronal secretion of FGF2, which could be rescued by exogenous FGF2 added to the neuronal compartment in a Boyden chamber migration assay with wt OPCs and Arf6-deleted neurons. This illustrates how specific trafficking mechanism in non-OL lineage cells can severely affect OL-mediated myelination in an axon tract-specific manner.

Concluding remarks

A large body of literature exists on how individual molecules or signaling pathways affect OL development and myelination. Much of the knowledge has been obtained by applying specific molecules to OL lineage cells in culture or manipulating them individually *in vivo* and analyzing the phenotype of the cells or mice as a consequence of such an all-or-none type of manipulation. However, we understand little about the mechanisms that integrate multiple signals arriving at OL lineage cells in various strengths and forms to produce the desired effect on myelination. The recent surge of interest in adaptive myelination has revealed that OLs are highly sensitive to subtle network changes, and that their intracellular program to generate myelin is dynamically modulated throughout adult life. To obtain an integrated understanding of how neuronal activity and other factors in their microenvironment influence OL dynamics, there is a need to reevaluate the mechanism of action of various oligodendrogliogenic and myelinogenic factors by taking into consideration the dynamic ways in which these factors are made available to OL lineage cells.

To illustrate the diverse ways in which extracellular signals can be delivered to OL lineage cells, we have provided examples in the soluble and integral membrane proteins, BDNF and L1, respectively, often drawing from their mechanism of action studied in neurons. Additionally, we have reviewed the evidence that suggests that the non-receptor intracellular tyrosine kinase Fyn serves as a converging node of multiple extracellular signals during myelination. An integrated view of how multiple factors dynamically activate appropriate signaling pathways in OLs to produce a specific effect will require not only identification of what the specific signals are but also a way to multidimensionally assess the temporo-spatial profiles of the signals and their volume/intensity. This will require new approaches to manipulating multiple variables in a physiologically relevant and graded manner and new

quantitative approaches to detect the responses in OL lineage cells.

Author contributions

CF and AN wrote the manuscript. Both authors contributed to the article and approved the submitted version.

Funding

This work was supported by National Institutes of Health (NIH; R01NS116182, PI: AN), SNARE complex-mediated exocytosis in oligodendrocyte differentiation and survival NIH (2R01NS073425, PI: AN), homeostatic regulation of NG2 cell dynamics.

Conflict of interest

The authors declare that the research was conducted in the absence of any commercial or financial relationships that could be construed as a potential conflict of interest.

Publisher's note

All claims expressed in this article are solely those of the authors and do not necessarily represent those of their affiliated organizations, or those of the publisher, the editors and the reviewers. Any product that may be evaluated in this article, or claim that may be made by its manufacturer, is not guaranteed or endorsed by the publisher.

References

Adams, K. L., Dahl, K. D., Gallo, V., and Macklin, W. B. (2021). Intrinsic and extrinsic regulators of oligodendrocyte progenitor proliferation and differentiation. *Semin. Cell Dev. Biol.* 116, 16–24. doi: 10.1016/j.semcdb.2020.10.002

Agresti, C., Meomartini, M. E., Amadio, S., Ambrosini, E., Volonté, C., Aloisi, F., et al. (2005). ATP regulates oligodendrocyte progenitor migration, proliferation and differentiation: involvement of metabotropic P2 receptors. *Brain Res. Brain Res. Rev.* 48, 157–165. doi: 10.1016/j.brainresrev.2004.12.005

Ainger, K., Avossa, D., Diana, A. S., Barry, C., Barbarese, E., and Carson, J. H. (1997). Transport and localization elements in myelin basic protein mRNA. *J. Cell Biol.* 138, 1077–1087. doi: 10.1083/jcb.138.5.1077

Akiyama, M., Hasegawa, H., Hongu, T., Frohman, M. A., Harada, A., Sakagami, H., et al. (2014). Trans-regulation of oligodendrocyte myelination by neurons through small GTPase Arf6-regulated secretion of fibroblast growth factor-2. *Nat. Commun.* 5:4744. doi: 10.1038/ncomms5744

Balkowiec, A., and Katz, D. M. (2002). Cellular mechanisms regulating activity-dependent release of native brain-derived neurotrophic factor from hippocampal neurons. *J. Neurosci.* 22, 10399–10407. doi: 10.1523/JNEUROSCI.22-23-10399.2002

Barbarese, E., Brumwell, C., Kwon, S., Cui, H., and Carson, J. H. (1999). RNA on the road to myelin. *J. Neurocytol.* 28, 263–270. doi: 10.1023/a:1007097226688

Barbin, G., Aigrot, M. S., Charles, P., Foucher, A., Grumet, M., Schachner, M., et al. (2004). Axonal cell-adhesion molecule L1 in CNS myelination. *Neuron Glia Biol.* 1, 65–72. doi: 10.1017/S1740925X04000092

Barde, Y. A., Edgar, D., and Thoenen, H. (1982). Purification of a new neurotrophic factor from mammalian brain. *EMBO J.* 1, 549–553. doi: 10.1002/j.1460-2075.1982.tb01207.x

Barres, B. A., Hart, I. K., Coles, H. S., Burne, J. F., Voyvodic, J. T., Richardson, W. D., et al. (1992). Cell death and control of cell survival in the oligodendrocyte lineage. *Cell* 70, 31–46. doi: 10.1016/0092-8674(92)90531-g

Barres, B. A., Schmid, R., Sendnter, M., and Raff, M. C. (1993). Multiple extracellular signals are required for long-term oligodendrocyte survival. *Development* 118, 283–295. doi: 10.1242/dev.118.1.283

Barres, B. A., and Raff, M. C. (1993). Proliferation of oligodendrocyte precursor cells depends on electrical activity in axons. *Nature* 361, 258–260. doi: 10.1038/361258a0

Bartsch, U., Kirchhoff, F., and Schachner, M. (1989). Immunohistological localization of the adhesion molecules L1, N-CAM, and MAG in the developing and adult optic nerve of mice. *J. Comp. Neurol.* 284, 451–462. doi: 10.1002/cne.902840310

Bennett, M. R., Rizvi, T. A., Karyala, S., McKinnon, R. D., and Ratner, N. (2003). Aberrant growth and differentiation of oligodendrocyte progenitors in neurofibromatosis type 1 mutants. *J. Neurosci.* 23, 7207–7217. doi: 10.1523/JNEUROSCI.23-18-07207.2003

Bercury, K. K., Dai, J., Sachs, H. H., Ahrendsen, J. T., Wood, T. L., and Macklin, W. B. (2014). Conditional ablation of raptor or rictor has differential impact on oligodendrocyte differentiation and CNS myelination. *J. Neurosci.* 34, 4466–4480. doi: 10.1523/JNEUROSCI.4314-13.2014

Bergles, D. E., Roberts, J. D., Somogyi, P., and Jahr, C. E. (2000). Glutamatergic synapses on oligodendrocyte precursor cells in the hippocampus. *Nature* 405, 187–191. doi: 10.1038/35012083

Bijlard, M., Klunder, B., Nomden, A., and Tyagi, S. (2015). Transcriptional expression of myelin basic protein in oligodendrocytes depends on functional syntaxin 4: a potential correlation with autocrine signaling. *Mol. Cell Biol.* 35, 675–687. doi: 10.1128/MCB.01389-14

Bjarnadottir, M., Misner, D. L., Haverfield-Gross, S., Bruun, S., Helgason, V. G., Stefansson, H., et al. (2007). Neuregulin1 (NRG1) signaling through Fyn modulates NMDA receptor phosphorylation: differential synaptic function in $NRG1^{+/-}$ knock-outs compared with wild-type mice. *J. Neurosci.* 27, 4519–4529. doi: 10.1523/JNEUROSCI.4314-06.2007

Bonetto, G., Belin, D., and Káradóttir, R. T. (2021). Myelin: a gatekeeper of activity-dependent circuit plasticity? *Science* 374:eaba6905. doi: 10.1126/science.aba6905

Borghesi, L., and Milcarek, C. (2006). From B cell to plasma cell: regulation of V(D)J recombination and antibody secretion. *Immunol. Res.* 36, 27–32. doi: 10.1385/IR:36:1:27

Budde, H., Schmitt, S., Fitzner, D., Opitz, L., Salinas-Riester, G., and Simons, M. (2010). Control of oligodendroglial cell number by the miR-17-92 cluster. *Development* 137, 2127–2132. doi: 10.1242/dev.050633

Burne, J. F., Staple, J. K., and Raff, M. C. (1996). Glial cells are increased proportionally in transgenic optic nerves with increased numbers of axons. *J. Neurosci.* 16, 2064–2073. doi: 10.1523/JNEUROSCI.16-06-02064.1996

Calver, A. R., Hall, A. C., Yu, W. P., Walsh, F. S., Heath, J. K., Betsholtz, C., et al. (1998). Oligodendrocyte population dynamics and the role of PDGF *in vivo*. *Neuron* 20, 869–882. doi: 10.1016/s0896-6273(00)80469-9

Cellerino, A., Carroll, P., Thoenen, H., and Barde, Y. A. (1997). Reduced size of retinal ganglion cell axons and hypomyelination in mice lacking brain-derived neurotrophic factor. *Mol. Cell Neurosci.* 9, 397–408. doi: 10.1006/mcne.1997.0641

Chao, M. V. (2003). Neurotrophins and their receptors: a convergence point for many signalling pathways. *Nat. Rev. Neurosci.* 4, 299–309. doi: 10.1038/nrn1078

Charles, P., Hernandez, M. P., Stankoff, B., Aigrot, M. S., Colin, C., Rougon, G., et al. (2000). Negative regulation of central nervous system myelination by polysialylated-neural cell adhesion molecule. *Proc. Natl. Acad. Sci. U S A* 97, 7585–7590. doi: 10.1073/pnas.100076197

Cheli, V. T., González, D. A. S., Lama, T. N., Spreuer, V., Handley, V., Murphy, G. G., et al. (2016). Conditional deletion of the L-type calcium channel Cav1.2 in oligodendrocyte progenitor cells affects postnatal myelination in mice. *J. Neurosci.* 36, 10853–10869. doi: 10.1523/JNEUROSCI.1770-16.2016

Chen, T. J., Kula, B., Nagy, B., Barzan, R., Gall, A., Ehrlich, I., et al. (2018). *In vivo* regulation of oligodendrocyte precursor cell proliferation and differentiation by the AMPA-receptor subunit GluA2. *Cell Rep.* 25, 852–861.e7. doi: 10.1016/j.celrep.2018.09.066

Colognato, H., Ramachandrappa, S., Olsen, I. M., and ffrench-Constant, C.. (2004). Integrins direct Src family kinases to regulate distinct phases of oligodendrocyte development. *J. Cell Biol.* 167, 365–375. doi: 10.1083/jcb.200404076

Czopka, T., Ffrench-Constant, C., and Lyons, D. A. (2013). Individual oligodendrocytes have only a few hours in which to generate new myelin sheaths *in vivo*. *Dev. Cell.* 25, 599–609. doi: 10.1016/j.devcel.2013.05.013

Dai, J., Bercury, K. K., Jin, W., and Macklin, W. B. (2015). Olig1 acetylation and nuclear export mediate oligodendrocyte development. *J. Neurosci.* 35, 15875–15893. doi: 10.1523/JNEUROSCI.0882-15.2015

De Biase, L. M., Nishiyama, A., and Bergles, D. E.. (2010). Excitability and synaptic communication within the oligodendrocyte lineage. *J. Neurosci.* 30, 3600–3611. doi: 10.1523/JNEUROSCI.6000-09.2010

Demerens, C., Stankoff, B., Logak, M., Anglade, P., Allinquant, B., Couraud, F., et al. (1996). Induction of myelination in the central nervous system by electrical activity. *Proc. Nat. Acad. Sci. U S A* 93, 9887–9892. doi: 10.1073/pnas.93.18.9887

Du, Y., Fischer, T. Z., Lee, L. N., Lercher, L. D., and Dreyfus, C. F. (2003). Regionally specific effects of BDNF on oligodendrocytes. *Dev. Neurosci.* 25, 116–126. doi: 10.1159/000072261

Dugas, J. C., Cuellar, T. L., Scholze, A., Ason, B., Ibrahim, A., Emery, B., et al. (2010). Dicer1 and miR-219 Are required for normal oligodendrocyte differentiation and myelination. *Neuron* 65, 597–611. doi: 10.1016/j.neuron.2010.01.027

Emery, B. (2010). Regulation of oligodendrocyte differentiation and myelination. *Science* 330, 779–782. doi: 10.1126/science.1190927

Emery, B., and Lu, Q.R. (2015). Transcriptional and epigenetic regulation of oligodendrocyte development and myelination in the central nervous system. *Cold Spring Harb Perspect. Biol.* 7:a020461. doi: 10.1101/cshperspect.a020461

Etxeberria, A., Hokanson, K. C., Dao, D. Q., Mayoral, S. R., Mei, F., Redmond, S. A., et al. (2016). Dynamic modulation of myelination in response to visual stimuli alters optic nerve conduction velocity. *J. Neurosci.* 36, 6937–6948. doi: 10.1523/JNEUROSCI.0908-16.2016

Fekete, C. D., Horning, R. Z., Doron, M. S., and Nishiyama, A. (2022). Regulation of oligodendrocyte lineage development by VAMP2/3 in the developing mouse spinal cord. *BioRxiv* [Preprint]. doi: 10.1101/2022.09.10.507429

Feldmann, A., Amphornrat, J., Schönherr, M., Winterstein, C., Möbius, W., Ruhwedel, T., et al. (2011). Transport of the major myelin proteolipid protein is directed by VAMP3 and VAMP7. *J. Neurosci.* 31, 5659–5672. doi: 10.1523/JNEUROSCI.6638-10.2011

Forbes, T. A., Goldstein, E. Z., Dupree, J. L., Jablonska, B., Scafidi, J., Adams, K. L., et al. (2020). Environmental enrichment ameliorates perinatal brain injury and promotes functional white matter recovery. *Nat. Commun.* 11:964. doi: 10.1038/s41467-020-14762-7

Fretto, L. J., Snape, A. J., Tomlinson, J. E., Seroogy, J. J., Wolf, D. L., LaRochelle, W. J., et al. (1993). Mechanism of platelet-derived growth factor (PDGF) AA, AB and BB binding to a and b PDGF receptors. *J. Biol. Chem.* 268, 3625–3631.

Fu, H., Qi, Y., Tan, M., Cai, J., Takebayashi, H., Nakafuku, M., et al. (2002). Dual origin of spinal oligodendrocyte progenitors and evidence for the cooperative role of Olig2 and Nkx2.2 in the control of oligodendrocyte differentiation. *Development* 129, 681–693. doi: 10.1242/dev.129.3.681

Galli, T., Kuster, A., and Tareste, D. (2013). (Nobel prize in physiology and medicine 2013 - an award for the discovery of the actors and fundamental molecular mechanisms of intracellular vesicle trafficking). *Med. Sci. (Paris).* 29, 1055–1058. doi: 10.1051/medsci/20112713024

Gallo, V., Zhou, J. M., McBain, C. J., Wright, P., Knutson, P. L., and Armstrong, R. C. (1996). Oligodendrocyte progenitor cell proliferation and lineage progression are regulated by glutamate receptor-mediated K^+ channel block. *J. Neurosci.* 16, 2659–2670. doi: 10.1523/JNEUROSCI.16-08-02659.1996

Garcia-Marquez, M. A., Shimabukuro-Vornhagen, A., Theurich, S., Kochanek, M., Weber, T., Wennhold, K., et al. (2014). A multimerized form of recombinant human CD40 ligand supports long-term activation and proliferation of B cells. *Cytotherapy* 16, 1537–1544. doi: 10.1016/j.jcyt.2014.05.011

Gary, D. S., Malone, M., Capestany, P., Houdayer, T., and McDonald, J. W.. (2012). Electrical stimulation promotes the survival of oligodendrocytes in mixed cortical cultures. *J. Neurosci. Res.* 90, 72–83. doi: 10.1002/jnr.22717

Ge, W. P., Yang, X. J., Zhang, Z., Wang, H. K., Shen, W., Deng, Q. D., et al. (2006). Long-term potentiation of neuron-glia synapses mediated by Ca^{2+}-permeable AMPA receptors. *Science* 312, 1533–1537. doi: 10.1126/science.1124669

Gibson, E. M., Purger, D., Mount, C. W., Goldstein, A. K., Lin, G. L., Wood, L. S., et al. (2014). Neuronal activity promotes oligodendrogenesis and adaptive myelination in the mammalian brain. *Science* 344:1252304. doi: 10.1126/science.1252304

Goldstein, E. Z., Pertsovskaya, V., Forbes, T. A., Dupree, J. L., and Gallo, V. (2021). Prolonged environmental enrichment promotes developmental myelination. *Front. Cell Dev. Biol.* 9:665409. doi: 10.3389/fcell.2021.665409

Grimes, M. L., Zhou, J., Beattie, E. C., Yuen, E. C., Hall, D. E., Valletta, J. S., et al. (1996). Endocytosis of activated TrkA: evidence that nerve growth factor induces formation of signaling endosomes. *J. Neurosci. Dec.* 16, 7950–7964. doi: 10.1523/JNEUROSCI.16-24-07950.1996

Gyllensten, L. and Malmfors, T. (1963). Myelinization of the optic nerve and its dependence on visual function—a quantitative investigation in mice. *J. Embryol. Exp. Morphol.* 11, 255–266.

Haberlandt, C., Derouiche, A., Wyczynski, A., Haseleu, J., Pohle, J., Karram, K., et al. (2011). Gray matter NG2 cells display multiple Ca^{2+}-signaling pathways and highly motile processes. *PLoS One* 6:e17575. doi: 10.1371/journal.pone.0017575

Hamilton, N., Vayro, S., Wigley, R., and Butt, A. M. (2010). Axons and astrocytes release ATP and glutamate to evoke calcium signals in NG2-glia. *Glia* 58, 66–79. doi: 10.1002/glia.20902

He, Y., Cai, W., Wang, L., and Chen, P. (2009). A developmental study on the expression of PDGFalphaR immunoreactive cells in the brain of postnatal rats. *Neurosci. Res.* 65, 272–279. doi: 10.1016/j.neures.2009.07.011

Hildebrand, M. E., Xu, J., Dedek, A., Li, Y., Sengar, A. S., Beggs, S., et al. (2016). Potentiation of synaptic GluN2B NMDAR currents by Fyn kinase is gated through BDNF-mediated disinhibition in spinal pain processing. *Cell Rep.* 17, 2753–2765. doi: 10.1016/j.celrep.2016.11.024

Hill, R. A., Patel, K. D., Goncalves, C. M., Grutzendler, J., and Nishiyama, A.. (2014). Modulation of oligodendrocyte generation during a critical temporal window after NG2 cell division. *Nat. Neurosci.* 17, 1518–1527. doi: 10.1038/nn.3815

Hill, R. A., Patel, K. D., Medved, J., Reiss, A. M., and Nishiyama, A. (2013). NG2 cells in white matter but not gray matter proliferate in response to PDGF. *J. Neurosci.* 33, 14558–14566. doi: 10.1523/JNEUROSCI.2001-12.2013

Hines, J. H., Hines, J. H., Ravanelli, A. M., Schwindt, R., Scott, E. K., Appel, B., et al. (2015). Neuronal activity biases axon selection for myelination *in vivo*. *Nat. Neurosci.* 18, 683–689. doi: 10.1038/nn.3992

Hu, X., Hicks, C. W., He, W., Wong, P., Macklin, W. B., Trapp, B. D., et al. (2006). Bace1 modulates myelination in the central and peripheral nervous system. *Nat. Neurosci.* 9, 1520–1525. doi: 10.1038/nn1797

Huang, Y., Song, Y. J., Isaac, M., Miretzky, S., Patel, A., McAuliffe, W. G., et al. (2020). Tropomyosin receptor kinase B expressed in oligodendrocyte lineage cells functions to promote myelin following a demyelinating lesion. *ASN Neuro* 12:1759091420957464. doi: 10.1177/1759091420957464

Huang, H., Zhao, X. F., Zheng, K., and Qiu, M. (2013). Regulation of the timing of oligodendrocyte differentiation: mechanisms and perspectives. *Neurosci. Bull.* 29, 155–164. doi: 10.1007/s12264-013-1314-2

Hughes, E. G., Orthmann-Murphy, J. L., Langseth, A. J., and Bergles, D. E. (2018). Myelin remodeling through experience-dependent oligodendrogenesis in the adult somatosensory cortex. *Nat. Neurosci.* 21, 696–706. doi: 10.1038/s41593-018-0121-5

Hughes, E. G., and Stockton, M. E. (2021). Premyelinating oligodendrocytes: mechanisms underlying cell survival and integration. *Front. Cell Dev. Biol.* 9:714169. doi: 10.3389/fcell.2021.714169

Imayoshi, I., Isomura, A., Harima, Y., Kawaguchi, K., Kori, H., Miyachi, H., et al. (2013). Oscillatory control of factors determining multipotency and fate in mouse neural progenitors. *Science* 342, 1203–1208. doi: 10.1126/science.1242366

Ishii, A., Furusho, M., Macklin, W., and Bansal, R. (2019). Independent and cooperative roles of the Mek/ERK1/2-MAPK and PI3K/Akt/mTOR pathways during developmental myelination and in adulthood. *Glia* 67, 1277–1295. doi: 10.1002/glia.23602

Ishii, A., Fyffe-Maricich, S. L., Furusho, M., Miller, R. H., and Bansal, R. (2012). ERK1/ERK2 MAPK signaling is required to increase myelin thickness independent of oligodendrocyte differentiation and initiation of myelination. *J. Neurosci.* 32, 8855–8864. doi: 10.1523/JNEUROSCI.0137-12.2012

Itoh, K., Stevens, B., Schachner, M., and Fields, R. D. (1995). Regulated expression of the neural cell adhesion molecule L1 by specific patterns of neural impulses. *Science* 270, 1369–1372. doi: 10.1126/science.270.5240.1369

Jahn, R., and Scheller, R. H. (2006). SNAREs–engines for membrane fusion. *Nat. Rev. Mol. Cell. Biol.* 7, 631–643. doi: 10.1038/nrm2002

Jepson, S., Vought, B., Gross, C. H., Gan, L., Austen, D., Frantz, J. D., et al. (2012). LINGO-1, a transmembrane signaling protein, inhibits oligodendrocyte differentiation and myelination through intercellular self-interactions. *J. Biol. Chem.* 287, 22184–22195. doi: 10.1074/jbc.M112.366179

Kang, S. H., Fukaya, M., Yang, J. K., Rothstein, J. D., and Bergles, D. E. (2010). NG2$^+$ CNS glial progenitors remain committed to the oligodendrocyte lineage in postnatal life and following neurodegeneration. *Neuron* 68, 668–681. doi: 10.1016/j.neuron.2010.09.009

Kasai, H., Takahashi, N., and Tokumaru, H. (2012). Distinct initial SNARE configurations underlying the diversity of exocytosis. *Physiol. Rev.* 92, 1915–1964. doi: 10.1152/physrev.00007.2012

Kazlauskas, A. (2017). PDGFs and their receptors. *Gene* 614, 1–7. doi: 10.1016/j.gene.2017.03.003

Kessaris, N., Fogarty, M., Iannarelli, P., Grist, M., Wegner, M., and Richardson, W. D. (2006). Competing waves of oligodendrocytes in the forebrain and postnatal elimination of an embryonic lineage. *Nat. Neurosci.* 9, 173–179. doi: 10.1038/nn1620

Kiefel, H., Bondong, S., Hazin, J., Ridinger, J., Schirmer, U., Riedle, S., et al. (2012). L1CAM: a major driver for tumor cell invasion and motility. *Cell Adhes. Migr.* 6, 374–384. doi: 10.4161/cam.20832

Kleene, R., Lutz, D., Loers, G., Bork, U., Borgmeyer, U., Hermans-Borgmeyer, I., et al. (2021). Revisiting the proteolytic processing of cell adhesion molecule L1. *J. Neurochem.* 157, 1102–1117. doi: 10.1111/jnc.15201

Kondo, T., and Raff, M. (2004). Chromatin remodeling and histone modification in the conversion of oligodendrocyte precursors to neural stem cells. *Genes Dev.* 18, 2963–2972. doi: 10.1101/gad.309404

Korte, M., Carroll, P., Wolf, E., Brem, G., Thoenen, H., and Bonhoeffer, T. (1995). Hippocampal long-term potentiation is impaired in mice lacking brain-derived neurotrophic factor. *Proc. Natl. Acad. Sci. U S A* 92, 8856–8860. doi: 10.1073/pnas.92.19.8856

Kougioumtzidou, E., Shimizu, T., Hamilton, N. B., Tohyama, K., Sprengel, R., Monyer, H., et al. (2017). Signalling through AMPA receptors on oligodendrocyte precursors promotes myelination by enhancing oligodendrocyte survival. *eLife* 6:e28080. doi: 10.7554/eLife.28080

Krämer, E.-M., Klein, C., Koch, T., Boytinck, M., and Trotter, J. (1999). Compartmentation of Fyn kinase with glycosylphosphatidylinositol-anchored molecules in oligodendrocytes facilitates kinase activation during myelination. *J. Biol. Chem.* 274, 29042–29049. doi: 10.1074/jbc.274.41.29042

Kramer-Albers, E. M., and White, R. (2011). From axon-glial signalling to myelination: the integrating role of oligodendroglial Fyn kinase. *Cell. Mol. Life Sci.* 68, 2003–2012. doi: 10.1007/s00018-010-0616-z

Kukley, M., Nishiyama, A., and Dietrich, D. (2010). The fate of synaptic input to NG2 glial cells: neurons specifically downregulate transmitter release onto differentiating oligodendroglial cells. *J. Neurosci.* 30, 8320–8331. doi: 10.1523/JNEUROSCI.0854-10.2010

Lam, M., Takeo, K., Almeida, R. G., Cooper, M. H., Wu, K., Iyer, M., et al. (2022). CNS myelination requires VAMP2/3-mediated membrane expansion in oligodendrocytes. *Nat. Commun.* 13:5583. doi: 10.1038/s41467-022-33200-4

Larson, V. A., Zhang, Y., and Bergles, D. E. (2016). Electrophysiological properties of NG2$^+$ cells: matching physiological studies with gene expression profiles. *Brain Res.* 1638, 138–160. doi: 10.1016/j.brainres.2015.09.010

Laursen, L. S., Chan, C. W., and ffrench-Constant, C. (2009). An integrin-contactin complex regulates CNS myelination by differential Fyn phosphorylation. *J. Neurosci.* 29, 9174–9185. doi: 10.1523/JNEUROSCI.5942-08.2009

Lee, S., Leach, M. K., Redmond, S. A., Chong, S. Y., Mellon, S. H., Tuck, S. J., et al. (2012). A culture system to study oligodendrocyte myelination processes using engineered nanofibers. *Nat. Methods* 9, 917–922. doi: 10.1038/nmeth.2105

Lee, X., Yang, Z., Shao, Z., Rosenberg, S. S., Levesque, M., Pepinsky, R. B., et al. (2007). NGF regulates the expression of axonal LINGO-1 to inhibit oligodendrocyte differentiation and myelination. *J. Neurosci.* 27, 220–225. doi: 10.1523/JNEUROSCI.4175-06.2007

Leibrock, J., Lottspeich, F., Hohn, A., Hofer, M., Hengerer, B., Masiakowski, P., et al. (1989). Molecular cloning and expression of brain-derived neurotrophic factor. *Nature* 341, 149–152. doi: 10.1038/341149a0

Levi-Montalcini, R. (1987). The nerve growth factor: thirty-five years later. *EMBO J.* 6, 1145–1154. doi: 10.1002/j.1460-2075.1987.tb02347.x

Lin, P. Y., Ma, Z. Z., Mahgoub, M., Kavalali, E. T., and Monteggia, L. M. (2021). A synaptic locus for TrkB signaling underlying ketamine rapid antidepressant action. *Cell Rep.* 36:109513. doi: 10.1016/j.celrep.2021.109513

Linneberg, C., Toft, C. L. F., Kjaer-Sorensen, K., and Laursen, L. S. (2019). L1cam-mediated developmental processes of the nervous system are differentially regulated by proteolytic processing. *Sci. Rep.* 9:3716. doi: 10.1038/s41598-019-39884-x

Lituma, P. J., Kwon, H. B., Alviña, K., Luján, R., and Castillo, P. E. (2021). Presynaptic NMDA receptors facilitate short-term plasticity and BDNF release at hippocampal mossy fiber synapses. *eLife* 10:e66612. doi: 10.7554/eLife.66612

Liu, J., Moyon, S., Hernandez, M., and Casaccia, P. (2016). Epigenetic control of oligodendrocyte development: adding new players to old keepers. *Curr. Opin. Neurobiol.* 39, 133–138. doi: 10.1016/j.conb.2016.06.002

Lundgaard, I., Luzhynskaya, A., Stockley, J. H., Wang, Z., Evans, K. A., Swire, M., et al. (2013). Neuregulin and BDNF induce a switch to NMDA receptor-dependent myelination by oligodendrocytes. *PLoS Biol.* 11:e1001743. doi: 10.1371/journal.pbio.1001743

Lutz, D., Loers, G., Kleene, R., Oezen, I., Kataria, H., Katagihallimath, N., et al. (2014). Myelin basic protein cleaves cell adhesion molecule L1 and promotes neuritogenesis and cell survival. *J. Biol. Chem.* 289, 13503–13518. doi: 10.1074/jbc.M113.530238

Ly, P. T. T., Stewart, C., and Pallen, C. J. (2018). PTPalpha is required for laminin-2-induced Fyn-Akt signaling to drive oligodendrocyte differentiation. *J. Cell Sci.* 131:jcs212076. doi: 10.1242/jcs.212076

Lynn, J. D., Anand, C., Arshad, M., Homayouni, R., Rosenberg, D. R., Ofen, N., et al. (2021). Microstructure of human corpus callosum across the lifespan: regional variations in axon caliber, density and myelin content. *Cereb. Cortex* 31, 1032–1045. doi: 10.1093/cercor/bhaa272

Malone, M., Gary, D., Yang, I. H., Miglioretti, A., Houdayer, T., Thakor, N., et al. (2013). Neuronal activity promotes myelination via a cAMP pathway. *Glia* 61, 843–854. doi: 10.1002/glia.22476

Marques, S., van Bruggen, D., Vanichkina, D. P., Floriddia, E. M., Munguba, H., Väremo, L., et al. (2018). Transcriptional convergence of oligodendrocyte lineage progenitors during development. *Dev. Cell* 46, 504–517.e7. doi: 10.1016/j.devcel.2018.07.005

Marques, S., Zeisel, A., Codeluppi, S., van Bruggen, D., Falcão, A. M., Xiao, L., et al. (2016). Oligodendrocyte heterogeneity in the mouse juvenile and adult central nervous system. *Science* 352, 1326–1329. doi: 10.1126/science.aaf6463

Matrone, C., Petrillo, F., Nasso, R., and Ferretti, G. (2020). Fyn tyrosine kinase as harmonizing factor in neuronal functions and dysfunctions. *Int. J. Mol. Sci.* 21:4444. doi: 10.3390/ijms21124444

McKinnon, R. D., Matsui, T., Dubois-Dalcq, M., and Aaronson, S. A. (1990). FGF modulates the PDGF-driven pathway of oligodendrocyte development. *Neuron* 5, 603–614. doi: 10.1016/0896-6273(90)90215-2

Medved, J., Wood, W. M., van Heyst, M. D., Sherafat, A., Song, J. Y., Sakya, S., et al. (2021). Novel guanidine compounds inhibit platelet-derived growth factor receptor alpha transcription and oligodendrocyte precursor cell proliferation. *Glia* 69, 792–811. doi: 10.1002/glia.23930

Mensch, S., Baraban, M., Almeida, R., Czopka, T., Ausborn, J., Manira, A. E., et al. (2015). Synaptic vesicle release regulates myelin sheath number of individual oligodendrocytes *in vivo*. *Nat. Neurosci.* 18, 628–630. doi: 10.1038/nn.3991

Mi, S., Miller, R. H., Lee, X., Scott, M. L., Shulag-Morskaya, S., Shao, Z., et al. (2005). LINGO-1 negatively regulates myelination by oligodendrocytes. *Nat. Neurosci.* 8, 745–751. doi: 10.1038/nn1460

Mitew, S., Gobius, I., Fenlon, L. R., McDougall, S. J., Hawkes, D., Xing, Y. L., et al. (2018). Pharmacogenetic stimulation of neuronal activity increases myelination in an axon-specific manner. *Nat. Commun.* 9:306. doi: 10.1038/s41467-017-02719-2

Moyon, S., Dubessy, A. L., Aigrot, M. S., Trotter, M., Huang, J. K., Dauphinot, L., et al. (2015). Demyelination causes adult CNS progenitors to revert to an immature state and express immune cues that support their migration. *J. Neurosci.* 35, 4–20. doi: 10.1523/JNEUROSCI.0849-14.2015

Nagy, B., Hovhannisyan, A., Barzan, R., Chen, T. J., and Kukley, M. (2017). Different patterns of neuronal activity trigger distinct responses of oligodendrocyte precursor cells in the corpus callosum. *PLoS Biol.* 15:e2001993. doi: 10.1371/journal.pbio.2001993

Newbern, J. M., Li, X., Shoemaker, S. E., Zhou, J., Zhong, J., Wu, Y., et al. (2011). Specific functions for ERK/MAPK signaling during PNS development. *Neuron* 69, 91–105. doi: 10.1016/j.neuron.2010.12.003

Nicholson, M., Wood, R. J., Fletcher, J. L., van den Buuse, M., Murray, S. S., Xiao, J., et al. (2018). BDNF haploinsufficiency exerts a transient and regionally different influence upon oligodendroglial lineage cells during postnatal development. *Mol. Cell. Neurosci.* 90, 12–21. doi: 10.1016/j.mcn.2018.05.005

Nishiyama, A., Shimizu, T., Sherafat, A., and Richardson, W. D. (2021). Life-long oligodendrocyte development and plasticity. *Semin. Cell Dev. Biol.* 116, 25–37. doi: 10.1016/j.semcdb.2021.02.004

Ortega, F., Gascón, S., Masserdotti, G., Deshpande, A., Simon, C., Fischer, J., et al. (2013). Oligodendrogliogenic and neurogenic adult subependymal zone neural stem cells constitute distinct lineages and exhibit differential responsiveness to Wnt signalling. *Nat. Cell Biol.* 15, 602–613. doi: 10.1038/ncb2736

Ortiz, F. C., Habermacher, C., Graciarena, M., Houry, P. Y., Nishiyama, A., Nait Oumesmar, B., et al. (2019). Neuronal activity *in vivo* enhances functional myelin repair. *JCI Insight* 5:e123434. doi: 10.1172/jci.insight.123434

Pan, L., Trimarco, A., Zhang, A. J., Fujimori, K., Urade, Y., Sun, L. O., et al. (2022). Oligodendrocyte-lineage cell exocytosis and L-type prostaglandin D synthase promote oligodendrocyte differentiation and myelination. *bioRxiv* [Preprint]. doi: 10.1101/2022.02.14.480339

Park, H., and Poo, M. M. (2013). Neurotrophin regulation of neural circuit development and function. *Nat. Rev. Neurosci.* 14, 7–23. doi: 10.1038/nrn3379

Peckham, H., Giuffrida, L., Wood, R., Gonsalvez, D., Ferner, A., Kilpatrick, T. J., et al. (2016). Fyn is an intermediate kinase that BDNF utilizes to promote oligodendrocyte myelination. *Glia* 64, 255–269. doi: 10.1002/glia.22927

Pereira, D. B., and Chao, M. V. (2007). The tyrosine kinase Fyn determines the localization of TrkB receptors in lipid rafts. *J. Neurosci.* 27, 4859–4869. doi: 10.1523/JNEUROSCI.4587-06.2007

Petryniak, M. A., Potter, G. B., Rowitch, D. H., and Rubenstein, J. L. (2007). Dlx1 and Dlx2 control neuronal versus oligodendroglial cell fate acquisition in the developing forebrain. *Neuron* 55, 417–433. doi: 10.1016/j.neuron.2007.06.036

Pitman, K. A., Ricci, R., Gasperini, R., Beasley, S., Pavez, M., Charlesworth, J., et al. (2020). The voltage-gated calcium channel CaV1.2 promotes adult oligodendrocyte progenitor cell survival in the mouse corpus callosum but not motor cortex. *Glia* 68, 376–392. doi: 10.1002/glia.23723

Pollock, R. A., and Richardson, W. D. (1992). The alternative-splice isoforms of the PDGF A-chain differ in their ability to associate with the extracellular matrix and to bind heparin *in vitro*. *Growth Factors* 7, 267–277. doi: 10.3109/08977199209046409

Psachoulia, K., Jamen, F., Young, K. M., and Richardson, W. D. (2009). Cell cycle dynamics of NG2 cells in the postnatal and ageing brain. *Neuron Glia Biol.* 5, 57–67. doi: 10.1017/S1740925X09990354

Quintela-López, T., Ortiz-Sanz, C., Serrano-Regal, M. P., Gaminde-Blasco, A., Valero, J., Baleriola, J., et al. (2019). Aβ oligomers promote oligodendrocyte differentiation and maturation via integrin β1 and Fyn kinase signaling. *Cell Death Dis.* 10:445. doi: 10.1038/s41419-019-1636-8

Relucio, J., Tzvetanova, I. D., Ao, W., Lindquist, S., and Colognato, H. (2009). Laminin alters fyn regulatory mechanisms and promotes oligodendrocyte development. *J. Neurosci.* 29, 11794–11806. doi: 10.1523/JNEUROSCI.0888-09.2009

Rutishauser, U., and Landmesser, L. (1991). Polysialic acid on the surface of axons regulates patterns of normal and activity-dependent innervation. *Trends Neurosci.* 14, 528–532. doi: 10.1016/0166-2236(91)90006-g

Rutishauser, U., and Landmesser, L. (1996). Polysialic acid in the vertebrate nervous system: a promoter of plasticity in cell-cell interactions. *Trends Neurosci.* 19, 422–427. doi: 10.1016/0166-2236(96)10041-2

Schiavo, G., Matteoli, M., and Montecucco, C. (2000). Neurotoxins affecting neuroexocytosis. *Physiol. Rev.* 80, 717–766. doi: 10.1152/physrev.2000.80.2.717

Schwarz, Y., Zhao, N., Kirchhoff, F., and Bruns, D. (2017). Astrocytes control synaptic strength by two distinct v-SNARE-dependent release pathways. *Nat. Neurosci.* 20, 1529–1539. doi: 10.1038/nn.4647

Sherafat, A., Pfeiffer, F., Reiss, A. M., Wood, W. M., and Nishiyama, A. (2021). Microglial neuropilin-1 promotes oligodendrocyte expansion during development and remyelination by trans-activating platelet-derived growth factor receptor. *Nat. Commun.* 12:2265. doi: 10.1038/s41467-021-22532-2

Shimojo, M., Courchet, J., Pieraut, S., Torabi-Rander, N., Sando, R., Polleux, F., et al. (2015). SNAREs controlling vesicular release of BDNF and development of callosal axons. *Cell Rep.* 11, 1054–1066. doi: 10.1016/j.celrep.2015.04.032

Siebert, J. R., and Osterhout, D. J. (2021). Select neurotrophins promote oligodendrocyte progenitor cell process outgrowth in the presence of chondroitin sulfate proteoglycans. *J. Neurosci. Res.* 99, 1009–1023. doi: 10.1002/jnr.24780

Simons, K., and Ikonen, E. (1997). Functional rafts in cell membranes. *Nature* 387, 569–572. doi: 10.1038/42408

Slezak, M., Grosche, A., Niemiec, A., Tanimoto, N., Pannicke, T., Münch, T. A., et al. (2012). Relevance of exocytotic glutamate release from retinal glia. *Neuron* 74, 504–516. doi: 10.1016/j.neuron.2012.03.027

Snaidero, N., and Simons, M. (2017). The logistics of myelin biogenesis in the central nervous system. *Glia* 65, 1021–1031. doi: 10.1002/glia.23116

Sock, E., and Wegner, M. (2021). Using the lineage determinants Olig2 and Sox10 to explore transcriptional regulation of oligodendrocyte development. *Dev. Neurobiol.* 81, 892–901. doi: 10.1002/dneu.22849

Stevens, B., Porta, S., Haak, L. L., Gallo, V., and Fields, R. D. (2002). Adenosine: a neuron-glial transmitter promoting myelination in the CNS in response to action potentials. *Neuron* 36, 855–868. doi: 10.1016/s0896-6273(02)01067-x

Stöckli, J., Piper, R. C., and James, D. E. (2016). Regulated versus constitutive secretion-a major form of intercellular communication. *Encyclopedia Cell Biol.* 2, 376–383. doi: 10.1016/B978-0-12-394447-4.20037-0

Sun, T., Echelard, Y., Lu, R., Yuk, D. I., Kaing, S., Stiles, C. D., et al. (2001). Olig bHLH proteins interact with homeodomain proteins to regulate cell fate acquisition in progenitors of the ventral neural tube. *Curr. Biol.* 11, 1413–1420. doi: 10.1016/s0960-9822(01)00441-9

Sun, W., Matthews, E. A., Nicolas, V., Schoch, S., and Dietrich, D. (2016). NG2 glial cells integrate synaptic input in global and dendritic calcium signals. *eLife* 5:e16262. doi: 10.7554/eLife.16262

Sytnyk, V., Leshchyns'ka, I., and Schachner, M. (2017). Neural cell adhesion molecules of the immunoglobulin superfamily regulate synapse formation, maintenance and function. *Trends Neurosci.* 40, 295–308. doi: 10.1016/j.tins.2017.03.003

Tasic, B., Menon, V., Nguyen, T. N., Kim, T. K., Jarsky, T., Yao, Z., et al. (2016). Adult mouse cortical cell taxonomy revealed by single cell transcriptomics. *Nat. Neurosci.* 19, 335–346. doi: 10.1038/nn.4216

Tauber, H., Waehneldt, T. V., and Neuhoff, V. (1980). Myelination in rabbit optic nerves is accelerated by artificial eye opening. *Neurosci. Lett.* 16, 235–238. doi: 10.1016/0304-3940(80)90003-8

Thoenen, H. (1995). Neurotrophins and neuronal plasticity. *Science* 270, 593–598. doi: 10.1126/science.270.5236.593

Tong, X.-P., Li, X.-Y., Zhou, B., Shen, W., Zhang, Z.-J., Xu, T.-L., et al. (2009). Ca^{2+} signaling evoked by activation of Na^{+} channels and Na^{+}/Ca^{2+} exchangers is required for GABA-induced NG2 cell migration. *J. Cell Biol.* 186, 113–128. doi: 10.1083/jcb.200811071

Trajkovic, K., Dhaunchak, A. S., Goncalves, J. T., Wenzel, D., Schneider, A., Bunt, G., et al. (2006). Neuron to glia signaling triggers myelin membrane exocytosis from endosomal storage sites. *J. Cell Biol.* 172, 937–948. doi: 10.1083/jcb.200509022

Trapp, B. D., Nishiyama, A., Cheng, D., and Macklin, W. (1997). Differentiation and death of premyelinating oligodendrocytes in developing rodent brain. *J. Cell Biol.* 137, 459–468. doi: 10.1083/jcb.137.2.459

Treiber, H., Hagemeyer, N., Ehrenreich, H., and Simons, M. (2012). BACE1 in central nervous system myelination revisited. *Mol. Psychiatry* 17, 237–239. doi: 10.1038/mp.2011.140

Tsiperson, V., Huang, Y., Bagayogo, I., Song, Y., VonDran, M. W., DiCicco-Bloom, E., et al. (2015). Brain-derived neurotrophic factor deficiency restricts proliferation of oligodendrocyte progenitors following cuprizone-induced demyelination. *ASN Neuro* 7:1759091414566878. doi: 10.1177/1759091414566878

Umemori, H., Sato, S., Yagi, T., Aizawa, S., and Yamamoto, T. (1994). Initial events of myelination involve Fyn tyrosine kinase signalling. *Nature* 367, 572–576. doi: 10.1038/367572a0

van Heyningen, P., Calver, A. R., and Richardson, W. D. (2001). Control of progenitor cell number by mitogen supply and demand. *Curr. Biol.* 11, 232–241. doi: 10.1016/s0960-9822(01)00075-6

Vondran, M. W., Clinton-Luke, P., Honeywell, J. Z., and Dreyfus, C. F. (2010). $BDNF^{+/-}$ mice exhibit deficits in oligodendrocyte lineage cells of the basal forebrain. *Glia* 58, 848–856. doi: 10.1002/glia.20969

Wake, H., Lee, P. R., and Fields, R. D. (2011). Control of local protein synthesis and initial events in myelination by action potentials. *Science* 333, 1647–1651. doi: 10.1126/science.1206998

Wake, H., Ortiz, F. C., Woo, D. H., Lee, P. R., Angulo, M. C., and Fields, R. D. (2015). Nonsynaptic junctions on myelinating glia promote preferential myelination of electrically active axons. *Nat Commun.* 6:7844. doi: 10.1038/ncomms8844

Wang, C. S., Kavalali, E. T., and Monteggia, L. M. (2022). BDNF signaling in context: from synaptic regulation to psychiatric disorders. *Cell* 185, 62–76. doi: 10.1016/j.cell.2021.12.003

Wang, Y., Kim, E., Wang, X., Novitch, B. G., Yoshikawa, K., Chang, L.-S., et al. (2012). ERK inhibition rescues defects in fate specification of Nf1-deficient neural progenitors and brain abnormalities. *Cell* 150, 816–830. doi: 10.1016/j.cell.2012.06.034

Wang, H., Liu, M., Ye, Z., Zhou, C., Bi, H., Wang, L., et al. (2021). Akt regulates Sox10 expression to control oligodendrocyte differentiation via phosphorylating FoxO1. *J. Neurosci.* 41, 8163–8180. doi: 10.1523/JNEUROSCI.2432-20.2021

Wang, X., Wang, C., and Pei, G. (2018). α-secretase ADAM10 physically interacts with β-secretase BACE1 in neurons and regulates CHL1 proteolysis. *J. Mol. Cell Biol.* 10, 411–422. doi: 10.1093/jmcb/mjy001

Weider, M., Kim, E., Wang, X., Novitch, B. G., Yoshikawa, K., Chang, L. S., et al. (2018). Nfat/calcineurin signaling promotes oligodendrocyte differentiation and myelination by transcription factor network tuning. *Nat. Commun.* 9:899. doi: 10.1038/s41467-018-03336-3

Weng, Q., Wang, J., Wang, J., He, D., Cheng, Z., Zhang, F., et al. (2019). Single-cell transcriptomics uncovers glial progenitor diversity and cell fate determinants during development and gliomagenesis. *Cell Stem Cell.* 24, 707–723.e8. doi: 10.1016/j.stem.2019.03.006

White, R., Gonsior, C., Krämer-Albers, E. M., Stöhr, N., Hüttelmaier, S., Trotter, J., et al. (2008). Activation of oligodendroglial Fyn kinase enhances translation of mRNAs transported in hnRNP A2-dependent RNA granules. *J. Cell Biol.* 181, 579–586. doi: 10.1083/jcb.200706164

Wong, A. W., Xiao, J., Kemper, D., Kilpatrick, T. J., and Murray, S. S. (2013). Oligodendroglial expression of TrkB independently regulates myelination and progenitor cell proliferation. *J. Neurosci.* 33, 4947–4957. doi: 10.1523/JNEUROSCI.3990-12.2013

Woodruff, R. H., Tekki-Kessaris, N., Stiles, C. D., Rowitch, D. H., and Richardson, W. D. (2001). Oligodendrocyte development in the spinal cord and telencephalon: common themes and new perspectives. *Int. J. Dev. Neurosci.* 19, 379–385. doi: 10.1016/s0736-5748(00)00083-6

Xiao, J., Ferner, A. H., Wong, A. W., Denham, M., Kilpatrick, T. J., and Murray, S. S. (2012). Extracellular signal-regulated kinase 1/2 signaling promotes oligodendrocyte myelination *in vitro*. *J. Neurochem.* 122, 1167–1180. doi: 10.1111/j.1471-4159.2012.07871.x

Xiao, J., Wong, A. W., Willingham, M. M., van den Buuse, M., Kilpatrick, T. J., and Murray, S. S. (2010). Brain-derived neurotrophic factor promotes central nervous system myelination via a direct effect upon oligodendrocytes. *Neurosignals* 18, 186–202. doi: 10.1159/000323170

Xu, F., Plummer, M. R., Len, G. W., Nakazawa, T., Yamamoto, T., Black, I. B., et al. (2006). Brain-derived neurotrophic factor rapidly increases NMDA receptor channel activity through Fyn-mediated phosphorylation. *Brain Res.* 1121, 22–34. doi: 10.1016/j.brainres.2006.08.129

Young, K. M., Psachoulia, K., Tripathi, R. B., Dunn, S. J., Cossell, L., Attwell, D., et al. (2013). Oligodendrocyte dynamics in the healthy adult CNS: evidence for myelin remodeling. *Neuron* 77, 873–885. doi: 10.1016/j.neuron.2013.01.006

Zerlin, M., Zerlin, M., Milosevic, A., and Goldman, J. E. (2004). Glial progenitors of the neonatal subventricular zone differentiate asynchronously, leading to spatial dispersion of glial clones and to the persistence of immature glia in the adult mammalian CNS. *Dev. Biol.* 270, 200–213. doi: 10.1016/j.ydbio.2004.02.024

Zhang, Y., Chen, K., Sloan, S. A., Bennett, M. L., Scholze, A. R., O'Keeffe, S., et al. (2014). An RNA-sequencing transcriptome and splicing database of glia, neurons and vascular cells of the cerebral cortex. *J. Neurosci.* 34, 11929–11947. doi: 10.1523/JNEUROSCI.1860-14.2014

Zhang, S., Rasai, A., Wang, Y., Xu, J., Bannerman, P., Erol, D., et al. (2018). The stem cell factor Sox2 is a positive timer of oligodendrocyte development in the postnatal murine spinal cord. *Mol. Neurobiol.* 55, 9001–9015. doi: 10.1007/s12035-018-1035-7

Zhao, X., He, X., Han, X., Yu, Y., Ye, F., Chen, Y., et al. (2010). MicroRNA-mediated control of oligodendrocyte differentiation. *Neuron* 65, 612–626. doi: 10.1016/j.neuron.2010.02.018

Zhao, N., Huang, W., Cătălin, B., Scheller, A., and Kirchhoff, F. (2021). L-type Ca^{2+} channels of NG2 glia determine proliferation and NMDA receptor-dependent plasticity. *Front. Cell Dev. Biol.* 9:759477. doi: 10.3389/fcell.2021.759477

Zhao, C., Ma, D., Zawadzka, M., Fancy, S. P., Elis-Williams, L., Bouvier, G., et al. (2015). Sox2 sustains recruitment of oligodendrocyte progenitor cells following CNS demyelination and primes them for differentiation during remyelination. *J. Neurosci.* 35, 11482–11499. doi: 10.1523/JNEUROSCI.3655-14.2015

Zhou, L., Barão, S., Laga, M., Bockstael, K., Borgers, M., Gijsen, H., et al. (2012). The neural cell adhesion molecules L1 and CHL1 are cleaved by BACE1 protease *in vivo*. *J. Biol. Chem.* 287, 25927–25940. doi: 10.1074/jbc.M112.377465

Zhu, X., Hill, R. A., Dietrich, D., Komitova, M., Suzuki, R., and Nishiyama, A. (2011). Age-dependent fate and lineage restriction of single NG2 cells. *Development* 138, 745–753. doi: 10.1242/dev.047951

Zhu, Q., Zhao, X., Zheng, K., Li, H., Huang, H., Zhang, Z., et al. (2014). Genetic evidence that Nkx2.2 and Pdgfra are major determinants of the timing of oligodendrocyte differentiation in the developing CNS. *Development* 141, 548–555. doi: 10.1242/dev.095323

Zisch, A. H., Alessandri, L., Amrein, K., Ranscht, B., Winterhalter, L., and Vaughan, K. H. (1995). The glypiated neuronal cell adhesion molecule contactin/F11 complexes with src-family protein tyrosine kinase Fyn. *Mol. Cell. Neurosci.* 6, 263–279. doi: 10.1006/mcne.1995.1021

Ziskin, J. L., Nishiyama, A., Rubio, M., Fukaya, M., and Bergles, D. E. (2007). Vesicular release of glutamate from unmyelinated axons in white matter. *Nat. Neurosci.* 10, 321–330. doi: 10.1038/nn1854

Frontiers in
Cellular Neuroscience

Leading research in cellular mechanisms underlying brain function and development

Part of the world's most cited neuroscience journal series that advances our understanding of the cellular mechanisms underlying cell function in the nervous system across all species.

Discover the latest Research Topics

See more →

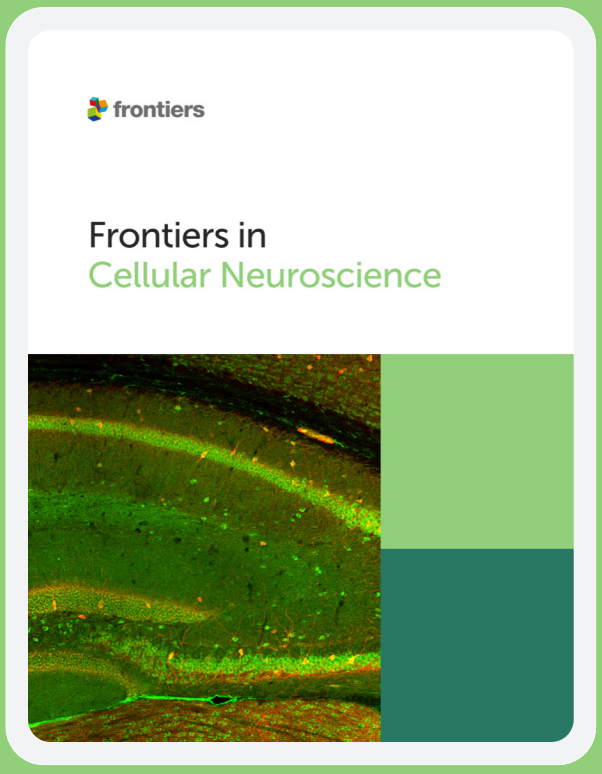

Frontiers

Avenue du Tribunal-Fédéral 34
1005 Lausanne, Switzerland
frontiersin.org

Contact us

+41 (0)21 510 17 00
frontiersin.org/about/contact